TOWARDS A COMPLETE DESIGN OF THE MANOEUVRING AREAS ADDITIONAL FACTORS INVOLVED IN THE DETAILED DESIGN

by

Ismael Verdugo[1], Raul Atienza[1], Carlos Cal[1], Jose R. Iribarren[1], Lourdes Pecharroman[1], Carmen Ayuso[1]

ABSTRACT

In order to establish the dimensions of approach channels and manoeuvring areas, PIANC guidelines consider two phases: **Concept Design** and **Detailed Design**.

The **Concept Design Stage** includes preliminary design of channel width, depth and alignment using empirical formulae, together with limited data related to ships and environmental conditions. Only rough estimates of the dimensions of the proposed channel (width, depth and alignment) are determined. The results are conservative sometimes, because general guidelines cannot assess all case-specific features and conditions.

The **Detailed Design Stage** is a more rigorous process intended to validate, develop and refine the Concept Design. The operational aspects are checked, referred to weather conditions, ship size and manoeuvring capacity, tug assistance, piloting, etc. If the conditions are relatively simple and all the design criteria are easily fulfilled, there may be no need to make significant adjustments to the Concept Design. But in most cases additional analyses are necessary to determine a **more accurate design** that will definitely be safe and usable without unnecessary expense. In this case, much more detailed information is needed regarding fairway geometry, weather and current conditions, ship characteristics, manoeuvring strategies, etc.

Real-time Manoeuvring Simulation is the most advanced tool to be used in this process. A realistic, detailed, complete representation of the port and its particular physical conditions is built. Ship behavior in shallow waters and restricted channels can be accurately reproduced, together with the assistance of specific tugs. Moreover, Pilots and Captains can take part in the analysis, so their expertise and the perception and decision-making factors are incorporated to the design.

Real-time simulation, if properly defined and executed, can absolutely help to define a more accurate design and operation conditions of a port area. A detailed approach based on specific local conditions (geometrical and environmental), specific ships (dimensions, propulsion and steering capacity), AtoN and tug assistance will provide complete, accurate and detailed indications on the execution of manoeuvres, both in normal and emergency conditions. Therefore, precise **operation limits, manoeuvring strategies** and **contingency plans** can be elaborated also involving human factor.

In some cases, the analysis of **new scenarios** is outstanding, such as the access of new larger ship classes to existing ports (container vessels, LNG carriers, cruise vessels, …). The limitation in space and therefore the reduction of the manoeuvring areas becomes a **critical factor**. The final design will depend not only on the dimensions obtained from the statistical analysis of the simulation results but also on many other factors involved. These concern mainly **Change Management** (adaptation to key factors of the project in their new configuration) as well as the creation of a **Confidence Building Process**.

For this purpose, a **technical committee** representing the main experts in the project (Port Authority, Operators, Designers, Maritime Authority, Shipowners, Pilots, Tug Companies, ...) is recommended to be created to participate in common workshops during the design process, in order to check input data and assumptions, survey the simulations, contribute to the discussions and finally **validate** the simulation results and include their opinions.

[1] Siport21 siport21@siport21.com
Chile, 8. 28290 Las Rozas (Madrid, SPAIN) +34-916307073

This process is considered decisive in relevant projects involving such new scenarios, where important changes are proposed (increase in the size of vessels or significant changes in the geometry of the manoeuvring areas, especially if additional dredging is required).

In this way, the **management of the change of all relevant factors** by seafarers in charge of the manoeuvre (detailed knowledge of the behaviour of the **new vessels**, modified operational limits, training process of the new manoeuvring strategy, detailed knowledge of the modified manoeuvring areas and new AtoN, definition of communication procedures between Pilots and Tug operators, definition of operation procedures, ...) is totally connected with the proposed design. This process will finally conclude with the definition of a **detailed procedure** describing all relevant factors to take into account so as to operate the design vessel in the port.

Consequently, in most cases, the **final manoeuvring areas** (geometry and dimensions) are directly related to the manoeuvring skills and **confidence level** that Local Pilots are able to transmit to the main stakeholders of the project.

1. INTRODUCTION

During years of port design studies related to navigable areas, the experience is that it is quite often necessary to explain why the manoeuvring areas obtained are sometimes so optimized in dimensions. From the point of view of the nautical advisor and port designer, it is important to highlight that the final design does not only consist of a set of dimensions to be defined, but also a detailed procedure to be fulfilled. This allows to, step by step, reach the final goal, which consists of operating the Design Vessel in the Port under the limiting conditions using the optimum required navigable areas. So, this complete design concept includes not only a geometrical description of the manoeuvring areas but also the consideration of a relevant set of nautical factors and human behaviour.

Operations of vessels at port are the result of the interaction of three main factors:

1. The vessel (with her propulsion and steering characteristics, capacity, onboard equipment ...)
2. The physical environment (vertical and horizontal dimensions of fairways and basins, meteorological and maritime conditions)
3. The human factor (Masters and Officers, Pilots, Tug Masters, Vessel Traffic Systems...)

Figure 1: General view of a Real-time Full Mission Ship Simulator (Siport21)

Thus, in the design process of port infrastructures or in the definition of operational conditions all three elements must be taken into account. It will only be possible to reach an adequate safety and operability level if all three factors are integrated. Nowadays advanced simulation tools are available allowing for a precise assessment of these aspects. Among them there are moored ship dynamic models, ship to ship interactions models, traffic flow simulation models, and real time manoeuvring simulators.

This paper describes these tools and their application in the complete design process of port terminals (infrastructure and equipment), establishment of operational rules (access, towing, load/unload, ...), risk assessment and contingency plans (dangerous goods terminals) and the transfer of this information to the stakeholders through education and training.

2. MAIN OBJECTIVES

The design of a port terminal of any kind (oil, containers, LNG, passengers, etc.) has to take into account the nautical aspects related to piers, mooring equipment, fenders, fairways and manoeuvring areas (geometry and vertical and horizontal dimensions), met-ocean analysis and operational procedures (access and mooring of design vessels, access of larger vessels, operational limits, traffic analysis, tug requirements, mooring analysis, passing ships, ...).

A detailed nautical risk assessment is required for hazardous goods such as crude oil, refined or chemical products and LNG. This assessment should also include a HAZID/HAZOP procedure.

At last, it is therefore highly recommendable to carry out education and training programmes for Pilots, Captains/Officers and Tug Masters by using real-time simulators.

3. TOOLS AND METHODOLOGY

Several advanced software tools are available to support the accuracy of the analysis:

3.1. Moored/anchored ship dynamic models

The objective of these models is the assessment of the berthing conditions of a vessel in operational (loading/unloading) or survival conditions. These models reproduce the behaviour of a specific ship at berth under the combined action of wind, waves and current. The system solves the equations of ship motion in 6 degrees of freedom (surge, sway, yaw, heave, pitch, roll) in the time domain, without limitations on the motion amplitudes. The simulation results assess the motion amplitudes of the ship and the loads transmitted to the fenders and the mooring lines under the combined action of typical environmental factors (tidal levels, currents, waves, wind).

The main application of these models is the design and optimization of mooring layout and equipment in maritime terminals.

Figure 2: Mooring equipment for specialized LNG terminal

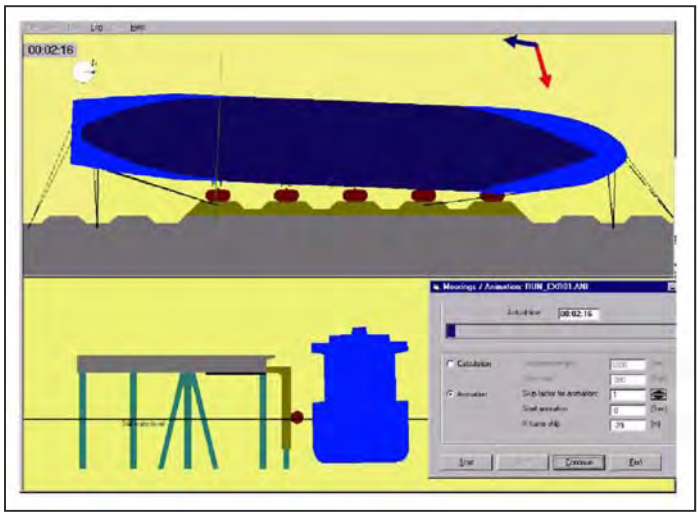

Figure 3: Dynamic Mooring Analysis (DMA) numerical model (Ship-Moorings, Alkyon-Arcadis)

3.2. Passing ships

The objective of these models is to evaluate the hydrodynamic interaction (forces and moments) that one or more passing vessels generate, through a narrow navigation channel, on one or more moored vessels on the specified area, as well as over the mooring structures present on the channel in terminals exposed to navigation fairways (access channels, inner channels, rivers ...), especially in narrow areas and under constrained depth.

The model takes into account the specific hull forms of each vessel, considering the effects of bathymetry changes and lateral restrictions (navigation channels, vertical structures, slopes, ...). This way, and due to the suction forces and moments generated by the “passing vessels” it is possible to assess the transmitted loads to fenders and mooring elements of the terminal by the moored vessels, identifying risk situations and establishing traffic control proceedings (allowable passing speed and distance for ships of different types and dimensions).

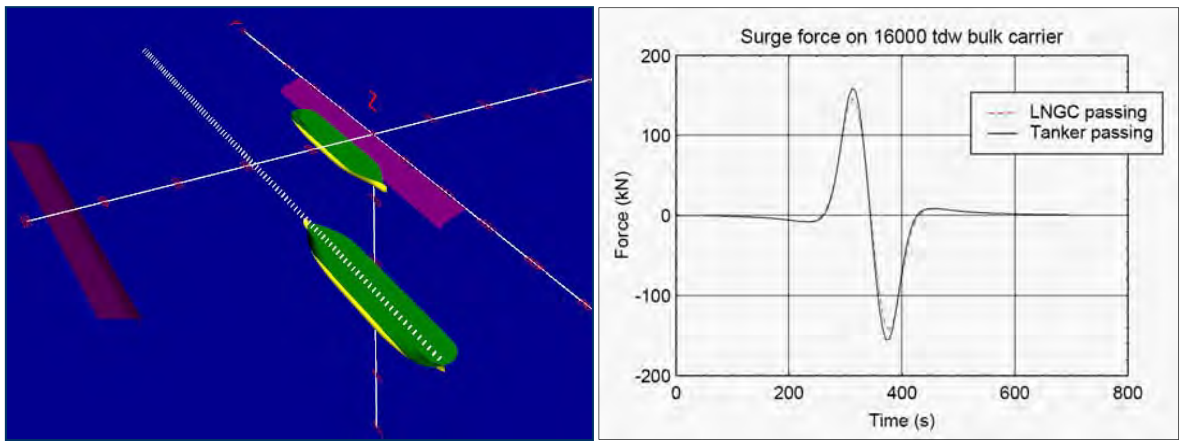

Figure 4: Passing ship analysis numerical model

3.3. Traffic simulation

The objective of these models is to assess the port capacity in order to verify the design requirements in terms of port facilities and forecasted traffic (anchorage areas, number of pilots, number of tugs, channel and quay dimensions, ...).

These numerical models provide ways of identifying possible bottlenecks and of establishing response measures. These simulation models cover the navigation and manoeuvring areas of the port and simulate the ships movements in the area. The objective is to assess the capacity of those areas

considering different alternatives or development phases. Usually, the port capacity will depend on the navigation and manoeuvring area dimensions, on the met-ocean conditions and the traffic distribution.

This capacity index should be certified with the admissible values according to the safety and service levels. The level of service is stated by: waiting times of vessels in the different facilities, both for channels occupation and terminals occupation, tug usage, Pilots usage, anchorage occupation ... These models also allow to express the safety level as a function of the potential number of ship encounters (overtaking and meeting) that could lead to risky situations.

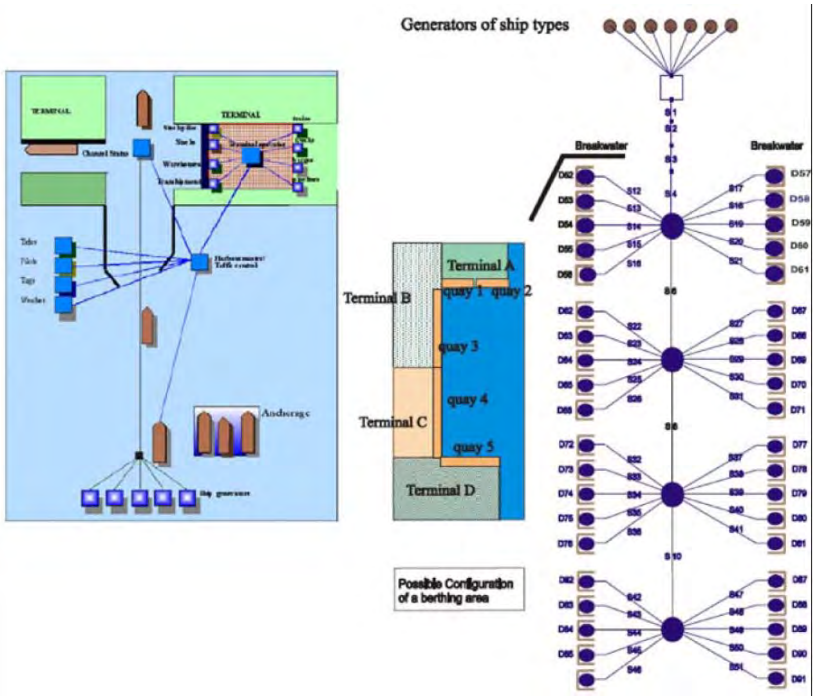

Figure 5: Block diagram of a Traffic Flow Simulation model (HARBOURSIM)

3.4. Ship manoeuvring simulation

The "Fast-Time" manoeuvring models and real time manoeuvring simulators allow reproducing the behaviour of specific vessels in particular areas under the control of an autopilot or a real Captain/Pilot respectively.

Real-Time Simulation incorporates human factor in the development of ship manoeuvres. Therefore, accurate and reliable results are obtained, which incorporate most of the relevant factors involved in real manoeuvres. As a consequence, this way of working is most adequate for the detailed analysis of complex manoeuvring conditions, when human factor (perception and decision making) becomes more important.

Figure 6: Ship Bridge in a real-time simulator

The autopilot mathematical model computes the track of the centre of gravity of the vessels, the course angle and rudder actions. Rudder, engine and tug control is effectuated by a track-keeping auto-pilot that anticipates deviations from the desired track defined by the user and changes in currents. This allows assessing the feasibility of a particular access or departure manoeuvres under different meteorological conditions, orientations about the manoeuvre strategy and defining the tug requirements (number, type and power). In this process wind, waves, currents, shallow waters, and bank suction are also taken into consideration.

In an autopilot numerical model the initial position and the desired track are fixed. The autopilot acts sequentially over the propeller and rudder in order to track-keep the desired fixed trajectory. By removing the human factor it is possible to compare objectively different manoeuvre conditions (different alternatives on the project, different type/dimensions of vessels, different meteorological conditions, ...).

A Real Time Manoeuvre Simulator is characterized by the interactivity of a professional (Captain, Pilot) with the system. The Captain operates on a bridge mock-up and works immersed on an environment similar to reality. Real instruments, ECDIS and a radar screen are available, and the movements of the ship and the image of the port are perceived in a screen with large dimensions. It is possible to interconnect several manoeuvring simulators in the same scenario in order to emulate traffic situations (ships meeting or overtaking) and interaction with other vessels (tugs assisting the sailing vessel), operated as well by Captains, Pilots or Tug Masters.

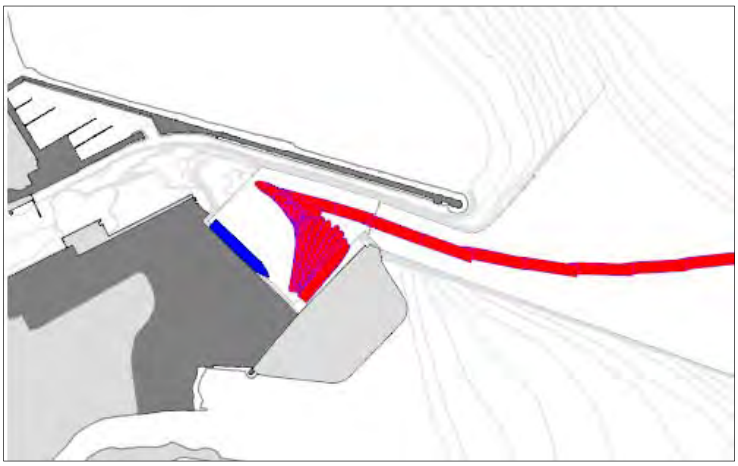

Figure 7: Manoeuvring numerical model (simulated trackplot)

Figure 8: Combined Simulation: Containership (Pilot on board) in bridge A and tugs (Tug Masters) on bridges B and C

4. INFRASTRUCTURE DESIGN

In the Project stage different alternatives for the development of a terminal are considered. Each type of terminal will have standard requirements of space and distribution, both inshore and offshore. Therefore, special attention is paid to the access fairways, navigable and manoeuvring areas, turning basins and quays and jetties (both in dimensions and position).

Horizontal and vertical dimensions of navigable areas and fairways are usually designed following different guidelines such as PIANC (World Association for Waterborne Transport Infrastructure). The definition of the UKC (Under Keel Clearance) is also a basic issue in this stage. These results can be optimized trough the usage of the real time simulator, which will also allow establishing safer access conditions for vessels at the terminals.

Designing the mooring equipment should be done carefully and following guidelines such as PIANC, SIGTTO (Society of International Gas Tanker and Terminal Operators) and OCIMF (Oil Companies International Marine Forum). Again, the numerical models allow optimizing the standard designs and adapting them to the specific conditions of each terminal.

Figure 9: Verification of fairway and basin for Valemax bulkcarrier. Simulator image

5. OPERATIONAL PROCEDURES

Before vessels can access terminals and port areas, operational limits for access and loading/unloading operations should be defined. International rules and regulations are quite demanding for specific traffics (oil and gas mainly) where safety issues are essential. In this way tide and current limits, wind and waves thresholds and visibility should be fixed, depending on the type and size of the vessel.

Tug requirements (number, type, power and bollard pull) need to be clearly defined as a function of vessel dimensions and met-ocean conditions, taking into account the efficiency when working on wave conditions, ... In particular tug usage for approach manoeuvres (eventually escorting), berthing operations and stand-by tugs.

Limits and preliminary requirements are derived from publications and existing guidelines. Nevertheless, the use of more precise tools, such as numerical models or real time simulators, allows for a better definition of those factors.

Figure 10: Tugs assisting a LNG carrier

In the same way, the design of vessels' mooring layout should take into account local conditions (wind, waves, currents…). Depending on the capacity and dimensions of the vessels and the admissible motions limits (cranes tolerances, loading arms limits, …), the optimization of the mooring system can provide a sensitive increase of the availability (reduction of downtime) of the Terminal. Cost-benefit relation of this type of analysis is highly profitable and allows calculating and verifying fenders, bollards and quick release hooks, as well as specific and optimum mooring layouts for every type of vessel. This type of studies is specially recommended for exposed terminals, which require a highly accurate definition of local waves.

The assessment of traffic, mainly in congested ports or with limited resources will define requirements such as safety distances, single or double lane fairways, priority use of the fairway, safety areas surrounding dangerous goods terminals or passing distances for vessels in transit.

6. ACCESS OF LARGER SHIPS

The strong tendency to the increase of vessel capacity is well known, mainly during recent years and in specific traffics. It is due, naturally, to the scale economy in all different transport phases. This has happened with LNG carriers, large container vessels and cruise ships as outstanding traffics.

Port infrastructure is designed for an operational life time that lasts more than vessels life time. Therefore, it is frequent that ports and terminals have to accommodate vessels with dimensions over those initially planned. Appearance of new types of vessels forces to review the capacity of navigable and manoeuvring areas, as well as the terminals. Therefore, it is essential to develop a feasibility study for the access and operation of these new vessels in already existing ports.

This work is focused in nautical aspects (navigation, manoeuvring, safety, mooring, …) even though there are many other aspects to be assessed (loading/unloading equipment, tank storage capacity, container storage areas, facilities for reception and transport of passengers, electricity and provisioning supply, ...). From this point of view, it is necessary to verify the applicability of the current nautical regulations (meteorological or tidal conditions, towing requirements, emergency procedures, …) as well as the capacity of the facilities and the equipment (fenders, bollards, loading/unloading systems compatibility, …).

Figure 11: 3E Maersk containership access manoeuvre. Simulator image

This assessment will lead to an adaptation of the regulations, to updates in equipment, or even to the reinforcement of port structures. In the extreme side, it will be necessary to perform relevant construction works to increase the capacity of access channels (deepening and widening dredging works) and terminals or even build new quays. In all these analyses, the use of advanced simulation methods is already an established, required and useful procedure.

It is crucial to count on the join participation of several stakeholders: Port Authorities, Terminal Operators, Pilots, Tug Masters, Captains and shipping companies, port designers, ... Therefore, all parties have to reach an agreement on updated operational procedures, which might include defining training programs for Masters, Officers and Pilots prior to the access of new vessels.

Figure 12: Access manoeuvre of "Oasis of the Seas" cruise vessel. Simulator image

7. NAUTICAL RISK ASSESSMENT

All possible risk scenarios (grounding, collision, …) have to be assessed as well, emphasizing those cases when transport of dangerous goods is involved. The consequences of these types of events can be estimated by using the abovementioned tools, which will allow defining adequate preventive and corrective measures.

Once all navigation and manoeuvring conditions have been defined, the possible consequences of extraordinary incidents should be assessed, such as propulsion or steering systems failure, tugs failure (breakage of towing line), reduced visibility, positioning errors, sudden increase of wind speed, breakage

of mooring lines, … The assessment of these events has to be done independently if these incidents are caused by the vessel itself or vessels operating nearby the project vessel. These types of events are beyond the usual difficulties in steering the vessel under normal manoeuvres.

Figure 13: LNG carrier manoeuvre in a FSRU Terminal

Therefore, the objective of these studies is the identification, analysis and evaluation of the different risk assumptions that might be expected during the development of the access and loading/unloading operations. As a result, actions and preventive and corrective measures will be defined and their effectiveness evaluated. The starting point is IMO (International Maritime Organization) recommendations related to risk scenarios. This information will be used as a starting point for the definition of the restricted navigable areas as well as the elaboration of contingency plans. It will be a critical aspect in all HAZID/HAZOP processes, that will be developed under a global view and coordinating the information with all the stakeholders (Terminals, Port Authorities, Operators, ...). Clear criteria to be adopted for operations, both for normal and emergency operations, will thus be defined.

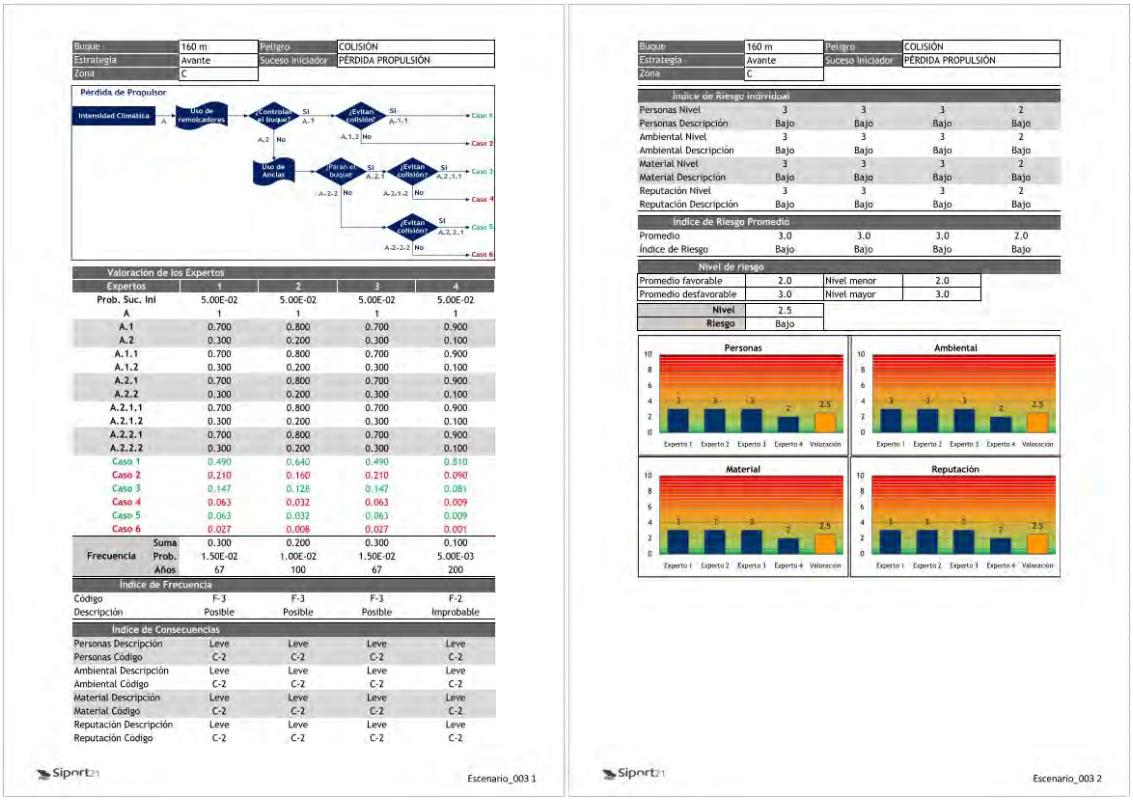

Figure 14: Risk evaluation sheet (FSA Methodology)

8. EDUCATION AND TRAINING

Familiarization with the new vessels and the new manoeuvring areas (meteorological scenarios, bathymetry, manoeuvre strategies, AtoN, and other relevant aspects) is an essential activity. In order to end up with familiarization and training processes it is very important to perform a detailed assessment of all the available data in the preliminary stages of the study, the selection and modeling of the main representative scenarios as well as the definition of an adequate simulation program to cover the objectives of the project.

This type of training sessions will allow the participants (Master, Officers, …) to have a better knowledge of the local conditions and the manoeuvre strategies (new in most cases), as well as better communication procedures with the rest of the technicians involved (Pilots, Tug Masters, Harbour Masters, …).

Figure 15: Masters/Officers and Pilots in the real time Simulator Bridge during training sessions

9. CONCLUSIONS

This paper describes the different simulation tools and techniques used for port planning, design and optimization, from the establishment of the operational rules to the transfer of this information to the stakeholders based on education and training.

Several simulation tools with different objectives have been assessed for the evaluation of port design. Among them there are moored ship dynamic models, ship to ship interaction models, traffic flow simulation models, and fast-time and real-time manoeuvring simulators.

Some of these tools can be used in combination with other simulation tools in order to increase the accuracy and reliability of the results, by including more complex parameters in the simulations. As an example, results of some simulation tools such as ship to ship interaction can be used as input parameters for moored ship dynamic models (to take into account passing effects over the mooring arrangements of vessels) or real-time manoeuvre simulations (to take into account bank suction and blockage effects, of the interaction between two meeting vessels).

Nevertheless, there is a relevant fact to be taken into account: operations of vessels at ports are the result of the interaction of three main factors:

1. The vessel (with her propulsion and steering characteristics, capacity, onboard equipment ...)
2. The physical environment (vertical and horizontal dimensions of fairways and basins, meteorological and maritime conditions)
3. The human factor (Masters and Officers, Pilots, Tug Masters, Vessel Traffic Systems...)

In the design process of port infrastructures or in the definition of operational conditions all three elements must be carefully taken into account. It will only be possible to reach an adequate safety and operability level if all three factors are integrated. This integration is made possible by the available advanced simulation tools that allow for a precise assessment of these aspects.

10. REFERENCES

PIANC Report WG20 “Capability of ship maneuvering simulation models for approach channels and fairways in harbors” (1992)

PIANC Report WG24 “Criteria for Movements of Moored Ships in Harbours” (1995)

PIANC-IAPH Report WG30 “Approach Channels. A Guide for Design” (1997)

PIANC Report 121 “Harbour Approach Channels Design Guidelines” (2014)

PIANC Report WG116 “Safety Aspects Affecting the Berthing Operations of Tankers to Oil and Gas Terminals” (2012)

ROM 3.1 “Maritime Recommendations for the Design of Port Access and Manoeuvring Areas” (1999). Spanish Port Authority

SIGTTO “Site Selection and Design for LNG Ports and Jetties” (1997-2000)

SIGTTO “Liquified Gas Handling Principles on Ships and in Terminals” (2016)

SIGTTO “LNG Operations in Port Areas” (2003)

SIGTTO “Simulation Information Paper”

OCIMF “Ship to Ship transfer guide” (2013)

OCIMF “International Safety Guide for Oil Tankers and Terminals” (2006)

OCIMF “Recommendations for ship’s fittings for use with tugs” (2002)

ISO 28460: “Ship-to-shore interface and port operations”

AVV TRC “Admittance Policy Tidal Bound Ships” Design of a probabilistic computer model for determination of channel transit risk to a seaport” (2005)

IMO Code “Formal Safety Assessment (FSA) MSC- MEPC.2/Cic.12- 8 july 2013"

MASTERING LATENT DEFECTS IN MARITIME AND PORT ENGINEERING THROUGH TECHNICAL RISK MANAGEMENT

Fabián BARBATO[1], David MARTINEZ[2] and Wim VAN ALBOOM[3]

INTRODUCTION

Linear maritime engineering structures are exposed to the highest levels of risk in the construction industry, because of the serial work involved in their design and construction. Systematic design or execution errors can turn these constructions into vulnerable artefacts. At the same time, the economic drive is pushing the long linear structures towards limited levels of redundancy, where failure of individual elements can generate progressive collapse. A global approach to risk is therefore indispensable in the management of coastal engineering projects, in addition to the organization of appropriate quality control systems. The intervention of an independent organization within the framework of this risk management – a well-known traditional concept in many European countries – is an added value in a global risk management of maritime structures.

Awareness has indeed grown that a second performance layer on top of the classic quality control systems is needed to cope with these challenges. Apart from the help that can be expected from working at the level of standardization, progress is mostly expected from measures which instigate project professionalism and collaboration between the different building partners.

QUALITY CONTROL SYSTEMS

During the nineties the construction industry has been criticised for its poor performance and productivity in relation to other industries. Many of the management practices used to organize construction companies have then been challenged. Their clients, active in other industrial sectors demanded improved service quality, faster building and innovations in technology. It was logical that the construction industry has turned to the manufacturing sector as a point of reference and source of innovation. Quality management have since then become increasingly adopted and have nowadays become mainstream in construction companies. The quality that is the subject of these systems is the degree to which the needs of the final customer are being met (customer satisfaction).

However, the implementation of quality control principles and structures has proven to be difficult in the construction sector, mainly due to a number of reasons.

The first one seems to be the nature of the construction process itself. Projects are often multidisciplinary, each project is again a prototype and projects are hardly ever repeated in the same location. The construction process is an environment in which several participants, each with their own interests and perspectives, are brought together to complete a project plan that is typical heavily subject to changes during construction, while each of the parties tries to manage their individual challenges. The construction industry is therefore characterized more by confrontation than by real collaboration between the different parties involved. Even though a common project goal should be shared, participants differ in what they seek to win from their participation in the process. The owner typically strives to spend as little as possible to get the project completed up to the standard they require. Contractors try to provide a product, designed by an engineering office, with an interpretation that allows them to maximize their profit. Designers provide a service to one of them, but not always necessarily to the benefit of the quality of the project. Less can be expected when one descends to the level of the subcontractors (and their subcontractors).

[1] ANP National Port Administration, Uruguay
[2] SECO BELGIUM S.A., Belgium
[3] SECO BELGIUM S.A., Belgium

Another barrier is the lack of standardization. The prototype character of many projects makes it difficult to apply universal standard specifications, that could be expected to lead to the same quality of the result of their application. Changes to the details of a design or a construction method are typical for a standard construction process.

RISK MANAGEMENT

Notwithstanding all of the quality control efforts in an attempt to reach client satisfaction, damage in construction still persists in the 21st century. Some recent bridge collapses are there to testify. We continue to see great losses in construction, which is why over the latest decades an alternative definition of project quality has won grounds, namely its ability to be free from hidden defects. In particular those defects which may give rise to future damages are then being envisaged.

In order to achieve that level of quality, the building team should inevitably engage in a thorough risk management exercise. Although familiarity with risk management principles has risen considerably during the past years, the approach is still very often static and a collaborative approach is missing. One individual aspect of a construction project is covered at the benefit of one intervening party and at one particular stage in the project (one point in time). The designer wants to master his design risks, the contractor his construction risks, the client his financial risks during the investment or during the maintenance period, etc. A traditional linear approach to risk management is represented in figure 1.

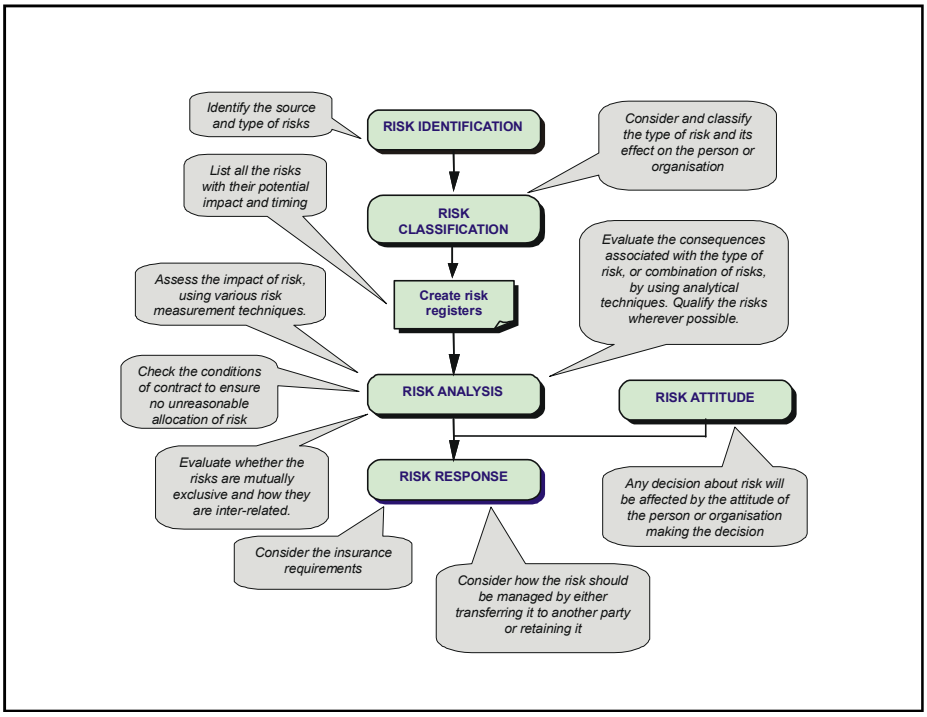

Figure 1: Steps in traditional risk management

A comprehensive risk management programme does not only deal with the individual risks of each intervening party, but tries to comprise the whole project and aims at finding the most economic yet technically perfectly viable answers to the project's strategic brief. Sharing this objective, a technical control agency, independent from the building actors, but actively involved within the preparation and the construction of the project functions as the ideal engine for a continuous project risk exercise. Risk management is turned into a dynamic concept, driven by the active participation of an independent technical inspection service (TIS) from the earliest stages in the project up to the maintenance period. The risk management exercise will profit from the assistance of the TIS at every stage thanks to the experience that they have gained in similar or consecutive projects, turning them into an effective knowledge center for the project. The verification of the design and execution of the works is no longer a systematic, sterile check on the application of specific codes or prescriptions for all construction elements. It is well focused and aims at those aspects that have proven to be crucial for a successful

risk reduction. A global risk management is therefore much more efficient than the implementation of a traditional quality system in avoiding damages.

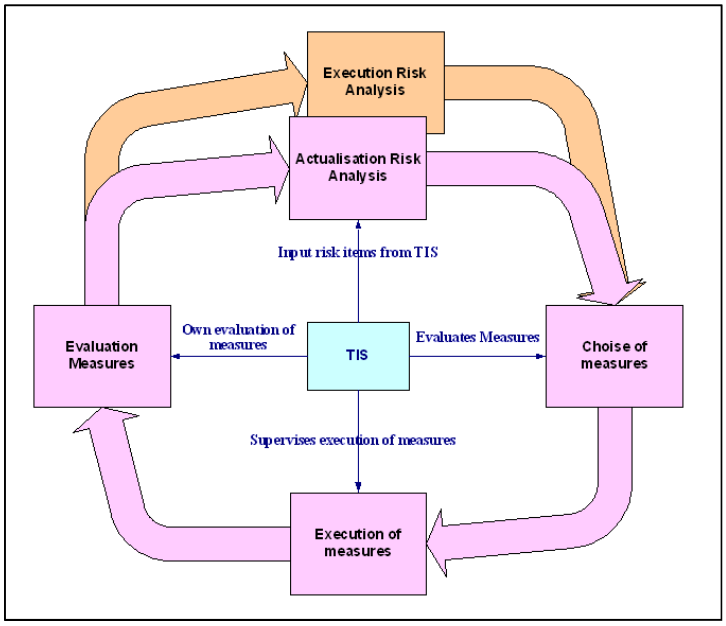

Figure 2: Dynamic risk management with TIS (Technical Inspection Services)

Although a qualitative analysis has become a common tool when dealing with risks in an explicit way, it can - whenever feasible - be combined with a quantitative probabilistic approach to structural failure. In this case the risks involved are evaluated in relation to a well defined 'reliability function'. A typical reliability function compares the likely strength of the design of an element or a construction with the anticipated loading on that element or that construction, taking into account the variation of strength and loading around their most likely values. The numerical possibilities in this respect have become mainstream.

Basic parameters when evaluating the risk of failure are the design conditions and the acceptable damage criteria agreed upon. The introduction of a Life Cycle Management (LCM) policy is indispensable. On the one hand, the design probabilities of failure are influenced by the degree of quality control during the construction works. On the other hand, the real failure probability is defined by the effectiveness of a specific monitoring and maintenance program after construction.

Coastal engineering projects are known to be exposed to the highest level of risks, not only because of the systematics involved in their design and construction processes, but also because of the uncertainty of the environmental actions involved (as well as their effects on the structures and their project environment). A large benefit can therefore be expected from the application of risk management principles.

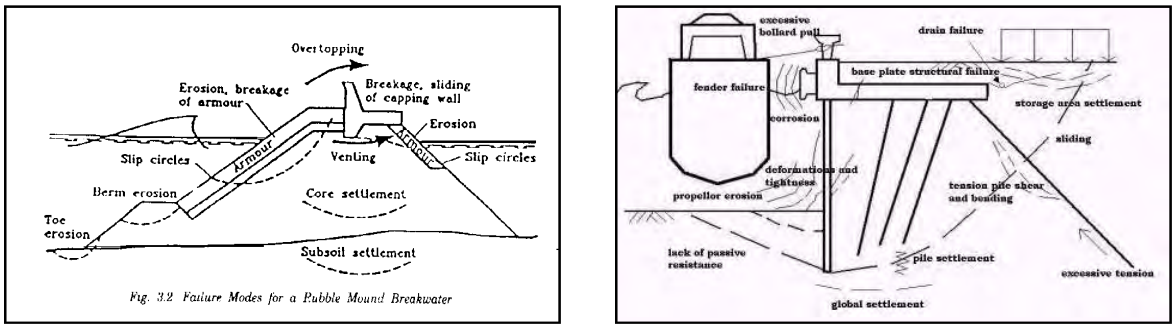

Figure 3: Results of a risk brainstorm exercise for a rubble mound breakwater and a quay wall

4. SOME EUROPEAN PROJECTS AND CONSTRUCTION TYPES REVISITED

Linear structures such as quay walls, seawalls, dikes etc. are very much exposed to risk because of the repetition involved in their construction. Systematic design or execution errors can turn these constructions very vulnerable. At the same time, the economic drive is pushing long linear structures towards limited levels of redundancy. Failure of individual elements can generate progressive collapse. A thorough risk management exercise for these structures is absolutely essential.

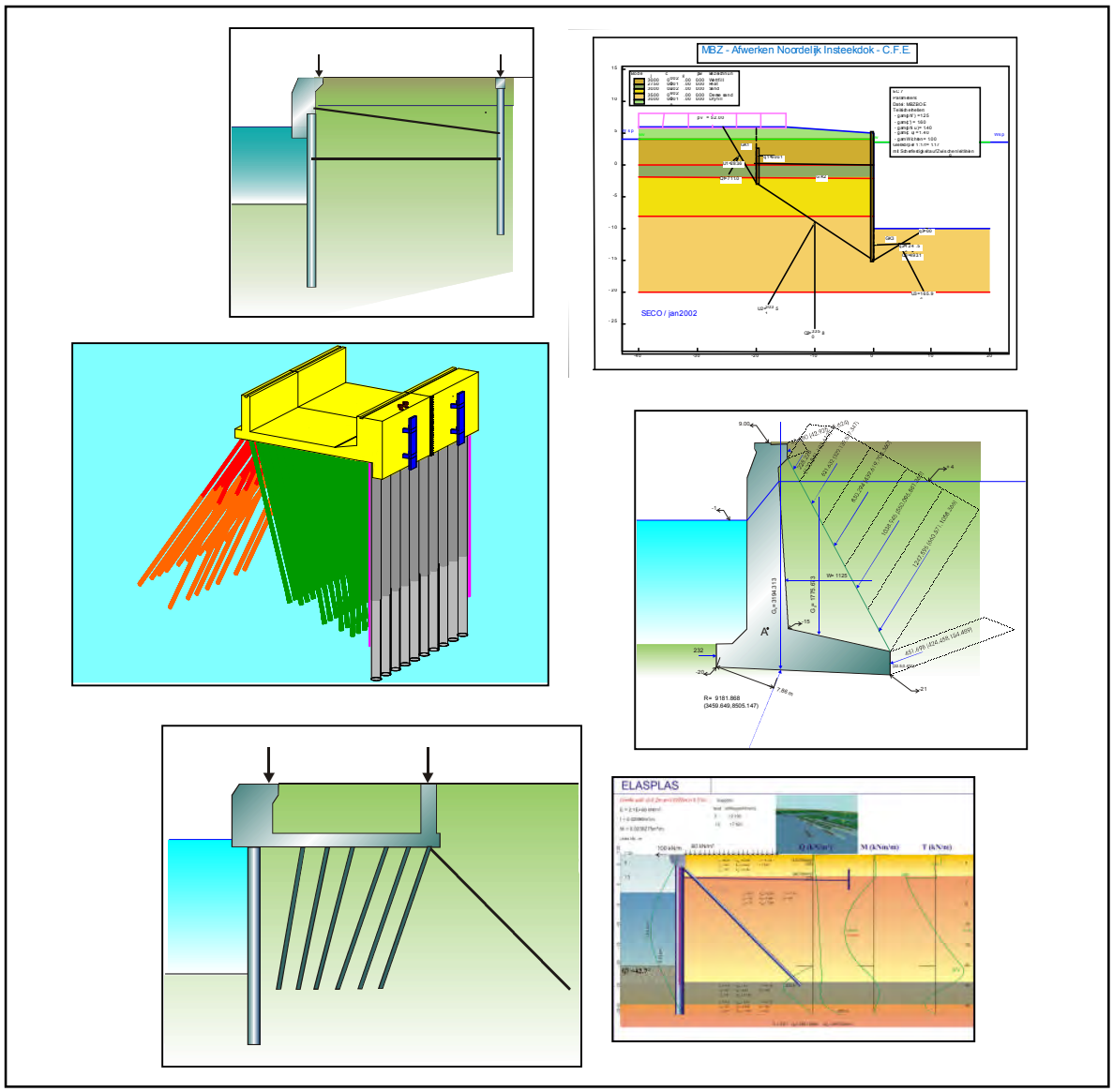

Figure 4: Classification of different types of quay walls

Quay walls can be subdivided in three categories according to two of their main aspects: their level of redundancy and their vulnerability to lack of tightness of the joints (related to the degree of complexity to check these joints). Type 1 structures provide excellent redistribution capacity and complete visual verification of the soil tightness of the joints in the system prior to their service life. Type 3 structures provide none of that. Type 2 quay walls are characterized by only one of the above characteristics. Some examples of quay walls are given in figure 4. A traditional piled platform usually provides excellent redistribution capacity in case of malfunctioning of one of the (numerous) piles. A gravity wall provides complete ability to verify the joints during the construction process. A simple anchored wall is a typical example of a class 3 quay wall. Its redundancy is usually very limited, the possibility to verify the joints is rather limited (although techniques are evolving) and the consequences of soil loss on global stability may be immediate.

The failure of one of the quay wall anchors can lead to the progressive collapse of adjacent stretches. A damage case like this occurred in the harbour of Antwerp in Belgium, where the subsequent zipper effect led to the complete collapse of a stretch of simple anchored wall. Anchors in such wall systems are becoming more and more slender due to the introduction of high yield, but at the same time less ductile steel. Demands for corrosion protection are more stringent for these kinds of anchors, but not always compatible with traditional, rough building practices. Vulnerability of the anchors to ship collisions may also be considerable.

During the latest years a risk management philosophy has developed to verify the design stability of the structure in case of failure of one of the anchors. Even in slender anchored wall types, redundancy e.g. can be attributed to a concrete coping beam on top of the wall. Figure 5 is an example of the verification of the effect of anchor failure on the internal forces in such a coping beam and the forces in the adjacent anchors.

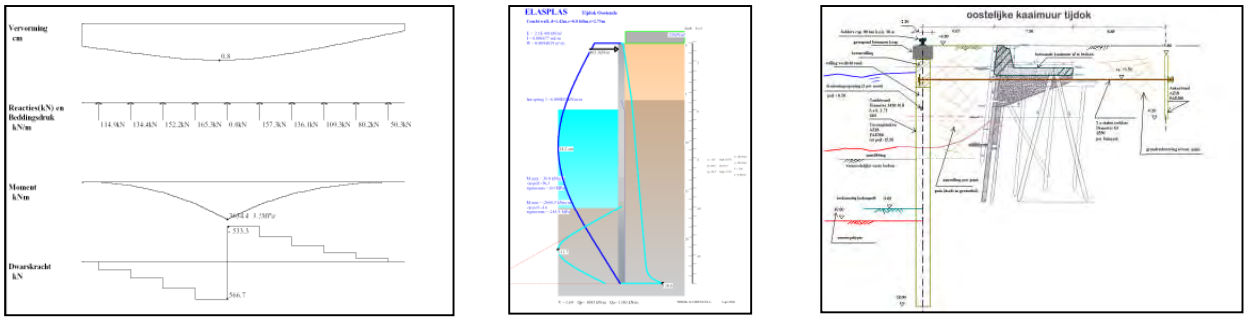

Figure 5: 2D simulation of a stretch of a coping beam on top of an anchored wall with failure of one anchor in the middle of the stretch

In creating redundancy, the existence of ductility may be of the utmost importance. Elastic and plastic elongation has to be generated to mobilise the required redistribution. In France, the extension of a container quay wall in the tidal zone has been covered for decennial liability. A risk identification at the very basis of the technical control led to a successful rectification of fabrication quality problems with respect to the connection principle of transportable lengths of anchors. A picture of a typical section of the project is represented in figure 6. The project comprised a combi-wall anchored at two distinct levels. The level of redundancy is again quite low, although some redistribution capacity is present at the deepest anchor level where a longitudinal steel beam had been installed just behind the wall. A systematic problem occurred at the connections of these passive anchors. The requirement set out upfront -that the connections in the system should be stronger than the standard section of the anchors, permitting ductile behaviour of the anchor – was finally successfully met after corrective measures had been taken.

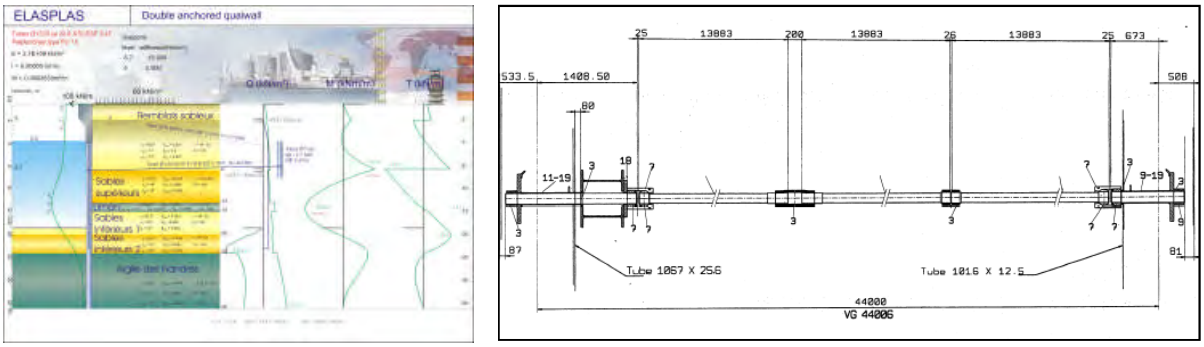

Figure 6: Double anchored wall and principle of the anchor connection system

In Ostend, at the Belgian coast, a new sea defense structure has been built, comprising a series of breakwaters. For the design of these new constructions, hydrodynamic boundary conditions (waves and water levels) had to be determined at different locations near Ostend. The interaction between water level and wind direction had not been examined until recently. This is important as some

constructions can only be attacked by a restricted range of wave directions. Since only a limited number of near shore data were available, extreme value distributions at deep water were examined. These were transformed to the Ostend situation with a numerical wave model. The results were interpreted in order to get directional wave and water level distributions. The numerical model was calibrated with the wave data from a local buoy in Ostend.

The redundancy level provided by a double armour layer on the breakwaters was seriously under discussion within the building team. Single layer systems were tested for extreme conditions to provide the extra reliability required for their use. In the model tests some consideration was also given to breakage of elements.

An important aspect of the study was the analysis of all possible uncertainties and their effect on the uncertainty of the final result. There were mainly two types of uncertainties: those of the deep-water statistics and those of the transformation occurring from deep to shallow water in the vicinity of the new constructions. It became clear that the last mentioned uncertainties were the highest – despite the sophistication of the model used and the elaborate simulation exercises being performed.

With the uncertainties in mind, Monte Carlo analyses were performed on the reliability formulae associated with the failure mechanisms (overtopping, hydraulic instability of the armour layers, …). The use of these kinds of statistical models allowed the building team to make a technically justified and financially sound decision on investment and maintenance, not only based on mean (50% reliable) values, but also on the probability of extreme values.

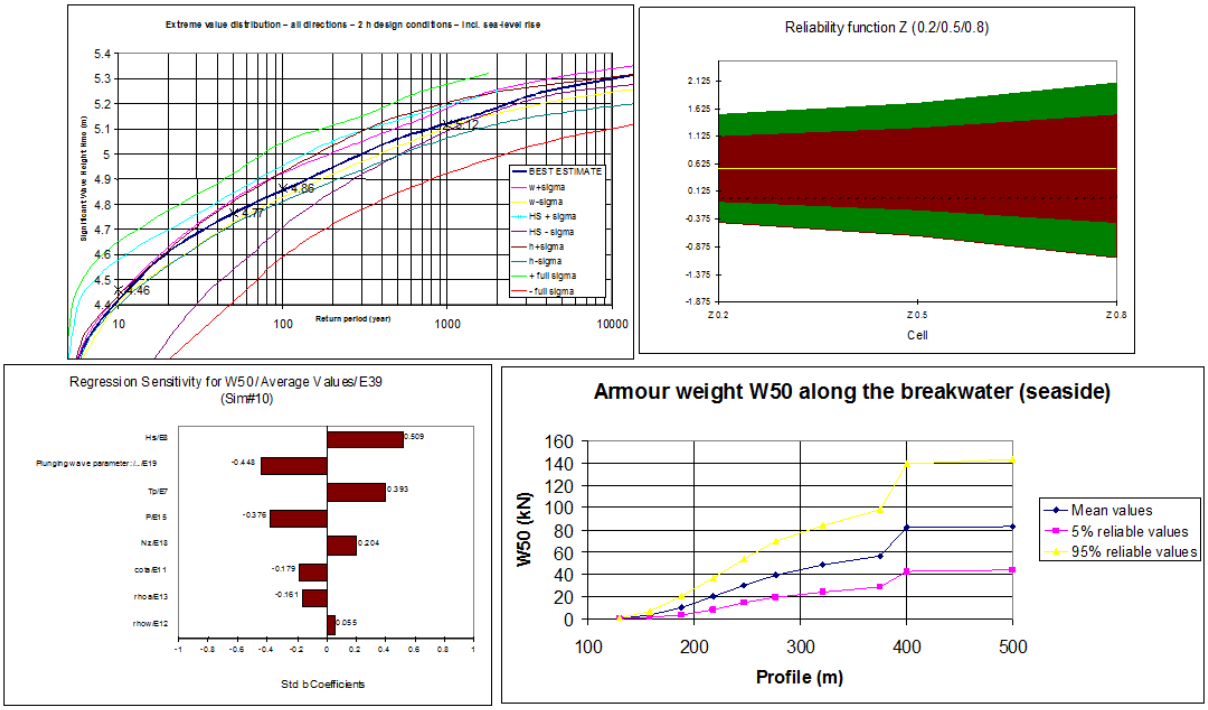

Figure 7: Representation of the significant wave height at an Ostend location after transformation, its use in hydraulic stability formulae and indication of the influence of uncertainty on the main parameters

FOCUS ON A PROJECT IN LATIN AMERICA

The present paragraph will focus on the introduction of this traditional European concept of risk management in the Latin American environment, through a case study of a quay wall project in the port of Montevideo, Uruguay. An alternative calculation model set up independently from the black box model used by the designers, has been used as part of the technical inspection services to establish the sensitivity of the deck-on-pile structure to different sets of load combinations. A representation of the alternative calculation model has been represented in figure 8. Geotechnically, the site consists of an extensive package of mud (typical for the Rio de la Plata estuary) deposited over a number of more

consistent clay and sand layers, all on top of a rock horizon (going from fragmented rock to sound massive substance). It has been confirmed that the resistance to the horizontal loads for these type of structures can relatively easily be increased and tuned to the requirements, primarily by efficiently intervening in the connection node of the landward pile row (the one with the most limited free length) at marginal cost.

The alternative model has been used as part of a risk analysis, which has been able to identify and prioritize technical risks, as well as list mitigation measures for each of them, allowing for assistance in the technical management of the project.

The reanalysis of the structure, taking into account the geotechnical uncertainty of the conglomerate subsoil, also showed that a redistribution of the total projected concrete volume of the piles over the 4 pile rows, without any additional concrete consumption, could contribute to an important relief of the geotechnical risk, based on the information available at the start of construction.

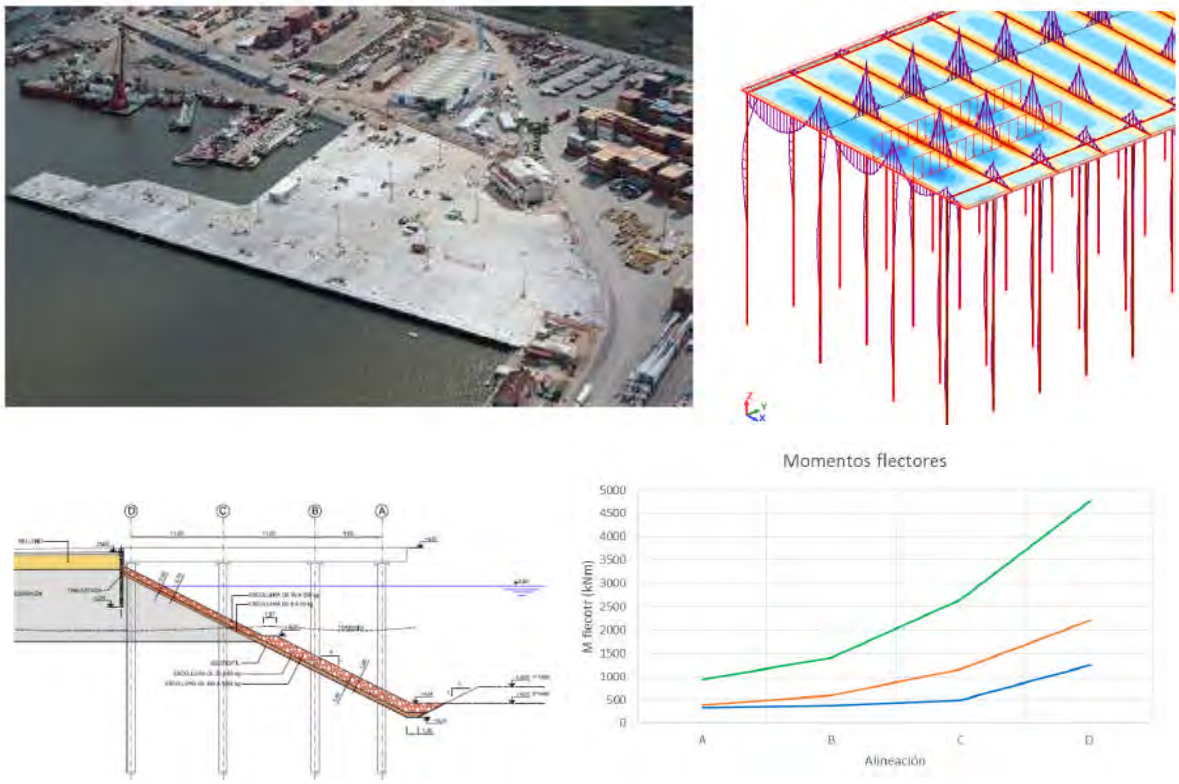

Figure 8: The location of the project, some parallel calculation model output and an overview of the top bending moments in the different piles rows A,B,C,D acc. to different hypotheses

Apart from a sound independent desktop analysis, a complete dynamic risk management process also necessarily includes inspection of the site construction process, an exercise which has proven to be beneficial in demonstrating the need for standardization in the construction methodology and in the specification.

The construction methodology used for the execution of the bored piles for the project has been questioned thoroughly after the detection of probable artesian water in the project area. The artesian water had shown itself at the end of the concreting of the first piles, as if it was an effect of concrete segregation/bleeding. Subsequent sonic testing and coring unfortunately confirmed a specific deterioration of the quality of the concrete executed. Finally, a site specific dedicated execution principle has been developed, as a result of the technical sparring of a series of possible solutions, brought up by the project participants, including the TIS. The finally withheld execution principle tries to take into account an increased respect of standard construction principles (as suggested in applicable construction standards), in connection with a more stringent monitoring campaign as well as a more intensive post-construction quality evaluation (including increased levels of sonic testing and dynamic testing).

CONCLUSION

The intervention of an independent organization within the framework of technical risk management – a well-known traditional concept in many European countries – is an added value in a global risk management of maritime structures. A typical principle that has arisen from this approach is the strife for structural redundancy, even in the most slender and economic of structures. Dealing with uncertainty in an explicit way is another. The TIS (Technical Inspection Services) can play a driving role in the constant review of the risk level within the dynamic risk management environment of a construction project. This can be done in a qualitative or in a quantitative way, depending on the nature and the severity of the risk. The externalization and independency of the service can make for a practical tool to assist in managing the technical project risks and transfer to all parties around the table the necessary confidence in the design and construction process, as well as promote dispute resolution around acceptable technical solutions and innovative alternatives within projects.

RECOMMENDATIONS FOR INCREASED DURABILITY AND SERVICE LIFE OF NEW MARINE CONCRETE INFRASTRUCTURE

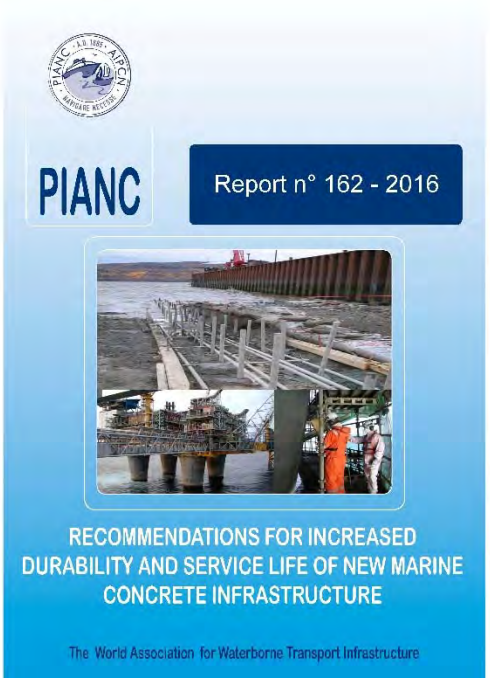

Report of Working Group 162 of the MARITIME NAVIGATION COMMISSION

Boy-Arne BUYLE - Bygg & Anleggslaboratoriet UIT – Narvik - NORWAY

Pascal COLLET – TOTAL SA – Paris – France

In Memory of Odd E Gjørv. Chairman of WG 162

Born 5. februar 1935

Deceased 16. februar 2016, Trondheim

Odd was working on the report when he had a heart attack and sadly did not get to see the finished result.

This proceeding addresses the work done by the PIANC Working Group 162 dedicated to provide recommendations for increased durability and service life of new marine concrete infrastructure.

The durability of concrete structures in the marine environment is not only related to design and materials but also to construction.

As a basis for the durability design and production of new major concrete infrastructure, all minimum requirements in existing concrete codes and standards as well as all established recommendations and guidelines for good construction practice must be strictly followed.

In recent years, many owners of existing concrete infrastructure have experienced a significant and rapidly increasing proportion of their limited construction budgets being spent on repairs and maintenance of the structures, many owners are showing an increasing interest to invest somewhat more at the outset of their new projects in order to obtain a better controlled and enhanced durability of the structures.

A better durability design and quality assurance for new concrete infrastructure can be achieved, and documentation of as-built construction quality and compliance with the durability specification can be obtained.

In the report, some additional recommendations and guidelines to existing concrete standards for durability and service life are provided, the objective of which has been to obtain a better controlled and enhanced durability of new marine concrete infrastructure, beyond what is possible when based only on existing concrete standards. This guidance is given with emphasis upon durability design and quality assurance as well as condition assessment and preventive maintenance during the operational life of the structures.

RECOMMENDATIONS FOR INCREASED DURABILITY AND SERVICE LIFE OF NEW MARINE CONCRETE INFRASTRUCTURE

Report of Working Group 162 of the MARITIME NAVIGATION COMMISSION

Boy-Arne BUYLE - Bygg & Anleggslaboratoriet UIT – Narvik - NORWAY

Pascal COLLET – TOTAL SA – Paris - FRANCE

Historical background – Definition of the problem

Deterioration and repair of marine concrete infrastructures has merged as a challenge for the owners of structures. In all deteriorating processes, extensive experience demonstrates that steel corrosion is still the most critical and greatest threat to the durability and long-term performance of the structures. Although current standards have been improved in recent years, still an uncontrolled penetration of salt with subsequent steel corrosion can take place on relatively new important marine concrete structures. As soon as the corrosion starts, the owner has a p a cost problem but later on also develops into a more difficult safety problem.

The durability and service life of the structure is dependent upon preventing the initiation of electrochemical corrosion. This is typically done by ensuring a quality concrete (low permeability, free of chlorides, reactive aggregates, high temperatures during curing, etc.), concrete resistant to environmental attack (freeze thaw, alkali-aggregate reaction, sulfate attack, carbonation, chlorides, etc.), and concrete cover. Additional measures can be undertaken to extend the life of a structure, such as sealers, coatings, corrosion resistant materials and cathodic protection systems.

The durability of a structure is dependent upon the system of cementitious materials, aggregates, water, admixtures, and reinforcing.

The durability of concrete structures in the marine environment is not only related to design and materials but also to construction.

Although all minimum durability requirements stated by existing standards must always be followed and fulfilled for new concrete structures, some owners are willing to invest somewhat more in order to obtain an increased and more controlled durability and service life beyond what is possible - more than 100 years - when only based on current standards. New recommendations and guidelines for increased durability, service life and service life modeling of new and important marine concrete infrastructure should be developed.

With the environmental constraints placed on the construction of new facilities in many countries, it may be easier or more economical to extend the service life of an existing structure. Guidance should also be developed for mitigation measures to extend the service life of existing structures.

Objective of the report

This report provides guidance to owners and designers of marine concrete infrastructure worldwide, in order to provide a safe, efficient and cost-effective design and construction of these structures, with emphasis upon:

- Durability design
- Quality assurance and achieved construction quality
- Condition assessment and preventive maintenance

The report of the WG is only to be considered as a guidance in addition to existing standards for concrete durability and service life. It should also be considered as an additional document for improved quality assurance during concrete construction as well as the regular condition assessment and preventive maintenance during operation of the structures.

Agenda of the report

Readers will find after an introduction on the topic and a state of art of the way to address the durability (Chapter 2), two approaches to deals with durability over the codes and standards(Chapter 3).

Additional strategies through protective measures and material are addressed (chapter 4) before to focus on quality assurance and achieved construction quality feedbacks (Chapter 5)

Report contains also assessment methods and preventive maintenance and repairs technics (Chapter 6)

CHAPTER 1: INTRODUCTION

CHAPTER 2: DURABILITY AND SERVICE LIFE

2.1 DETERIORATING PROCESSES

2.2 CODES AND PRACTICE

2.3 QUALITY INSURANCE AND ACHIEVED CONSTRUCTION QUALITY

2.4 CONDITION ASSESSMENT AND PREVENTIVE MAINTENANCE

2.5 LIFE CYCLE COSTING (LCC)

2.6 LIFE CYCLE ASSESSMENT (LCA)

CHAPTER 3: DURABILITY DESIGN

3.1 PROBABILITY APPROACH

3.2 PERFORMANCE BASED APPROACH

CHAPTER 4: ADDITIONAL STRATEGIES AND PROTECTIVE MEASURES

4.1 GENERAL

4.2 STAINLESS STEEL REINFORCEMENT

4.3 NON METALLIC REINFORCEMENT

Overview of the durability subject

With all the recent standards requirements focusing on concrete mix and design, the observed durability problems on marine concrete structures can be ascribed to lack of proper quality assurance during concrete construction and poorly achieved construction quality.

Upon completion of new concrete structures, the achieved construction quality typically shows a high scatter and variability, and during the operation of the structures, any weaknesses and deficiencies will soon be revealed whatever durability specifications and materials have been applied. To a certain extent, a probability approach to the durability design can accommodate the high scatter and variability of quality. However, a numerical approach alone is insufficient for ensuring the durability; greater control and improvements in durability also require the specification of performance-based durability requirements which can be verified and controlled during concrete construction in order to practically achieve quality assurance.

As a basis for the durability design and production of new major concrete infrastructure, all minimum requirements in existing concrete codes and standards as well as all established recommendations and guidelines for good construction practice must be strictly followed.

For concrete structures in the marine environment, many different deterioration processes can affect the durability. The mains processes had been summarize, typically the corrosion of steel by chloride or carbonatation ingress thought the concrete cover or in cracks. Environmental context (freeze-thaw process) and intrinsic concrete phenomena (alkali silica reaction of delayed ettringite formation) may be involved in the deterioration process.

Codes and standards address all minimum requirements according the durability specifications but primarily based on prescriptive requirements to composition of the concrete mixture such as upper levels for water/binder ratio and minimum levels for binder content.

Although a low water/binder ratio also reflects a high density and low permeability of the concrete providing both a high resistance to chloride ingress and good durability, extensive investigations demonstrate that selecting a proper binder system may be much more important for obtaining a high resistance to chloride ingress. As a result, the old and very simple terms “water/cement ratio” or “water/binder ratio” for characterizing and specifying concrete quality have successively lost their meaning. As a consequence, there is need for performance-based definitions and specifications for concrete quality; in particular this is true for characterizing and specifying concrete durability (Bjegović et al., 2014).

It is well established that many durability problems for concrete structures in the marine environment can be ascribed to lack of proper quality assurance during concrete construction and poorly achieved construction quality. In order to accommodate the potential high scatter and variability of quality, a probability approach to the durability design as briefly outlined and discussed in Chapter 3 can be applied. However, since none of the models for such design take into account the effect of cracks or other defects also typically occurring during concrete construction, some additional strategies and protective measures can be considered (Chapter 4).

With the probability approach to the durability design described in Chapter 3, however, performance-based requirements both to concrete quality and concrete cover are Figure 3.1. The DURACON Model as a basis for durability design, quality assurance and operation of new major concrete infrastructure in marine environments (PIANC Norway/NAHE, 2009). established which later on provide a basis for quality assurance and documentation of achieved construction quality (Chapter 5). A performance-based durability design without any probability calculations can also be applied as that described in Chapter 3.

Documentation of achieved construction quality and compliance with the durability specification should be very important for the owner since such documentation may have implications both for the obtained durability and expected service life of the structure. Experience from recent years has shown that where such documentation has been required, it has typically clarified the responsibility of the contractor for the quality of the construction process.

Despite the best compliance to the achieved construction quality both from specification and construction quality assurance, a service manual for regular monitoring and control of the real chloride ingress taking place during the operation of the structure should be required (Chapter 6). It is such a service manual that

helps provide the ultimate basis for obtaining a controlled and enhanced service life of the concrete structure in its environment.

In chapter 4, additional strategies and prospective measures are addressing. Whatever approach to the durability design taken, they all have some limitations, since none of them takes into account the effects of cracks or other defects that also typically occur during the production of concrete structures. Therefore, for all new marine concrete infrastructure where high durability and service life are of special importance, additional strategies and protective measures such as those outlined in the following should also be considered.

The report address folowing options:

- Stainless steel reinforcement
- Non metallic reinforcement
- Concrete surface protection
- Concrete hydrophobation
- Protective Skin Systems
- Cathodic prevention systems
- Corrosion inhibitors
- Structural shape
- Prefabricated Structural Elements

For most operational concrete structures, maintenance and repairs are mostly reactive, and the need to take appropriate repair or preventive measures is only identified at an advanced stage of deterioration. Although general condition assessment and preventive maintenance are already part of the established Life Cycle Managment systems for structures, additional regular control of the chloride ingress during operation of marine concrete structures is very important. The general basis for this is briefly outlined and discussed in the chapter 6, and a brief outline of current repair experience is also included.

ON THE CAPACITY OF ESTUARINE ACCESS CHANNELS: A WESTERN SCHELDT CASE STUDY

by

Kevin Delecluyse, Sarah Doorme, Tim Vandenbroucke, Roeland Adams[1] *and Youri Meersschaut*[2]

ABSTRACT

As the demand in maritime traffic increases, so does the need for traffic flow models that can study the nautical accessibility and the capacity of the access channel and port basin to accommodate larger vessels. IMDC has developed such a model for estuarine channels by taking a traffic model for waterway networks and expanding it with a planning module for the destination harbour and including logical rules and maneuvers to translate the typical, complex sailing behaviour of ships on an estuarine channel. The model was then tailored to the case study of the Western Scheldt, an estuarine channel that brings vessels from the North Sea to the port of Antwerp. After calibrating and validating the model to ensure its capabilities of simulating present conditions, the model is being used to investigate the effect of increasing traffic on the channel capacity, and to estimate whether the prognosis for traffic in the year 2030 would lead to congestion issues or capacity problems in the Western Scheldt and/or the port facilities. It can be concluded that with some additional modifications the model can be made fit to simulate traffic flow of ships on estuarine channels.

1. INTRODUCTION

The increase in demand in maritime traffic leads to changes in ship size, charge and draft, leading to more challenging operational conditions of maritime ports, particularly more inland situated ports such as Antwerp. Real time nautical models have been developed and used to study the nautical accessibility and to study the conditions for maneuvering to and in the ports (Verwilligen et al., 2008). Such models are limited to the study of the behaviour of one ship and its interaction with other ships and the shallow water conditions in the port basin and the access channel. Useful and necessary information for pilots is deduced from such simulations to improve the safety of the port entry. However, other instruments are required to deduce information on the capacity of the access channel and port basin to accommodate larger vessels in a context of increasing traffic.

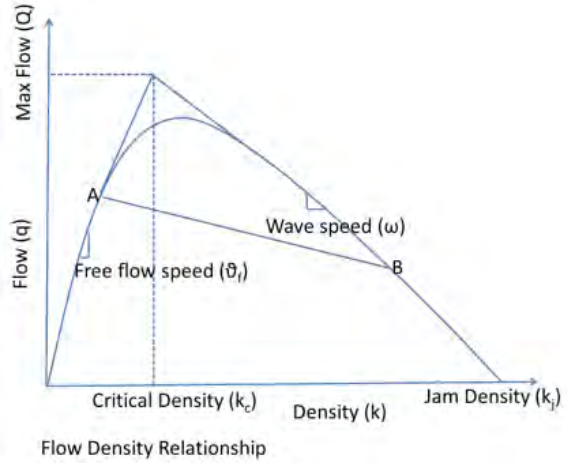

Figure 1: Relationship between traffic flow and traffic density (source: http://www.lorenzopareschi.com/2010/07/research-activity-kinetic-and-mean.html)

[1] International Marine and Dredging Consultants (IMDC), Van Immerseelstraat 66, BE2018 Antwerp, Belgium
[2] Departement Mobiliteit en Openbare Werken, Afdeling Maritieme Toegang

As in all traffic situations, an continuous increase in traffic density (number of vessels), will at first lead to an increase in traffic flow (cargo), before reaching a maximum value and finally decreasing to zero (standing still). This is illustrated in Figure 1.

Figure 1 does not take into account the complexity of the infrastructure or the multimodality of traffic, yet it does illustrate the basic principle that capacity is equal to the maximum traffic flow. The rounded nature of the tipping point indicates that, prior to reaching the maximum capacity, the traffic flow no longer increases proportional to the traffic intensity. In other words, the transport efficiency decreases. Plans to increase the port capacity related to the expected traffic increase led to a prior demand to investigate traffic flow. IMDC developed a new traffic model capable of investigating the flow and potential saturation point of the access channel and port basin.

2. THE STUDY AREA

The Western Scheldt, shown in Figure 2, is the estuary of the Scheldt river that lies completely within Dutch borders. As such, it is an estuarine, intertidal channel that is bordered by the North Sea at its downstream end and the Belgian border (also the location of measuring point CP, used throughout this study) at its upstream end. From there on out, the river is renamed the Lower Sea Scheldt and – even further – the Upper Sea Scheldt.

Figure 2: Aerial view of the Scheldt delta showing the North Sea, the Western Scheldt and the port of Antwerp.

The port of Antwerp, shown in Figure 3, is located just upstream of the Dutch-Belgian border. It consist of two large harbour areas: Linkeroever (also known as Waaslandhaven) at the left bank of the Scheldt, and Rechteroever at the right bank. The Linkeroever harbour can be reached through two locks: the Kieldrechtsluis and the Kallosluis. Rechteroever has four locks, in two groups of two: the Berendrechtsluis and the Zandvlietsluis at the downstream end, and the Boudewijnsluis and the Van Cauwelaertsluis at the upstream end. Besides the two harbours, the port also consists of three tidal terminals. From downstream to upstream these are the Noorzeeterminal, the Europaterminal and Deurganckdok (separated into Deurganckdok Oost and Deurganckdok West), which is actually a dock leading to and from the Kieldrechtsluis.

3. THE NAUTICAL MODEL

IMDC-Waterways (Adams et al., 2014) is a traffic model for waterway networks. It provides insight into the fluidity of traffic as a function of traffic intensity, the bottlenecks in the network and the capacity of the network and its subzones to process current as well as future traffic intensities.

Study areas are divided into a network of homogeneous units or links (e.g. channels, lock complexes) connected by nodes. Fairway properties such as depth, width and angle of curvature can alter between links, but stay the same inside the link. The actions and interactions in the waterways occur on a mesoscopic scale. At the starting node of a link, a prediction is made of the arrival time at the end node of the link, based on the present ship velocity and the path length of the link.

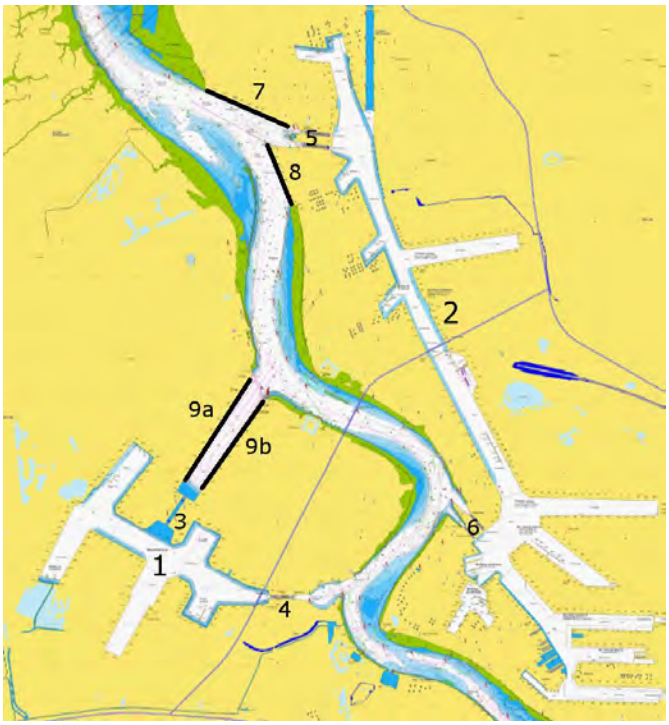

Figure 3: The port of Antwerp, with Linkeroever (1), Rechteroever (2), Kieldrechtsluis (3), Kallosluis (4), Berendrechtsluis and Zandvlietsluis (5), Boudewijnsluis and Van Cauwelaertsluis (6), Noordzeeterminal (7), Europaterminal (8), Deurganckdok West and Deurganckdok Oost (9a and 9b).

When the ship arrives in the end node, the maneuvers of the ship in the link are processed and the real arrival time is calculated. The transfer between links is processed on a microscopic scale. Vessels that want to enter a next link are assigned a departure time that depends on the traffic already present in the link and the other vessels that are queueing at the link entrance. This could cause an extra adjustment to the arrival time at the end node of the previous link.

This combination of microscopic treatment with schematization at different abstraction levels allows to shed light on certain aspects without going into detail too much.

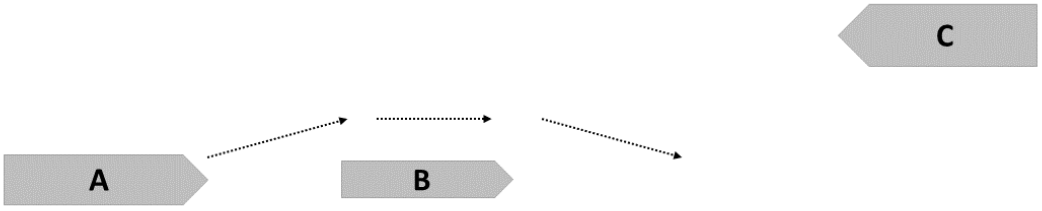

Figure 4: Schematic representation of an overtake maneuver. Ship A = overtaking ship, ship B = overtaken ship, ship C = oncoming ship.

The IMDC-Waterways model was expanded in a number of different ways to suit the purposes of the current study. As a precursor to the actual network model, a new planning module is used to simulate the effect of the quay terminals and access locks in and around the two destination harbours. For each vessel type, the tidal windows are calculated based on the water levels registered during the period of interest, the ship draught and the ship sailing speed. These tidal windows are then matched to the generated ship entry times into the network, the sailing time of the ship route and the availability of a

lock when the ship arrives at its destination. If the ship has to wait for a lock or quay becomes available, this waiting time is added to the ship entry time into the network. If necessary, the entry time is postponed to a later tidal window and the search continues until the ship is finally planned into a lock or quay. Ultimately, the ship gets assigned an Attributed time Slot (ATS) and an ATS window, i.e. a time window during which the ship may arrive at its destination. This ATS window is determined based on the length of the vessel's tidal window and the closing of the destination lock.

The time delay a ship might suffer while sailing on the Western Scheldt constitutes a group of changes introduced to the network model. These delays are caused by two kinds of maneuvers the ship could undertake on its route: overtake maneuvers and swing maneuvers.

Overtake maneuvers occur when a vessel encounters another vessel sailing in the same direction at a lower speed, as shown schematically in Figure 4. Only under certain specific circumstances is the faster vessel A allowed to overtake the slower vessel B:

- The vessel velocity difference is larger than 2 knots.
- The available excess channel width– i.e. the part of the channel that isn't blocked by ship B - is larger than the sum of the width of ship A and the lateral safety distance that needs to be guaranteed between ship A and any vessel it encounters during the maneuver.
- In case the excess channel width does not allow the overtaking of ship B, ship A continues to sail behind ship B and decreases its speed accordingly, until ship A reaches the next network link, thus suffering a delay.
- In case the excess channel width does not allow the oncoming of ship A and an opposing ship C, one of these ships should decrease its speed such that the ship trajectories no longer cross. The selection of the ship that should slow down depends on the time margin the ships have with respect to their respective ATS. In case ship A should slow down, the overtaking maneuver is cancelled and the ship A suffers a delay, similar to the delay discussed above.

Swing maneuvers occur when a ship reaches its destination and needs to turn around before mooring onto a quay or sailing further (as is the case in Deurganckdok). As the swing maneuver takes place, the ship's turning circle blocks part of the main channel, possibly causing a delay for other ships that need to sail past the swinging ship but cannot due to the excess channel width being too narrow to provide enough lateral safety distance between ships.

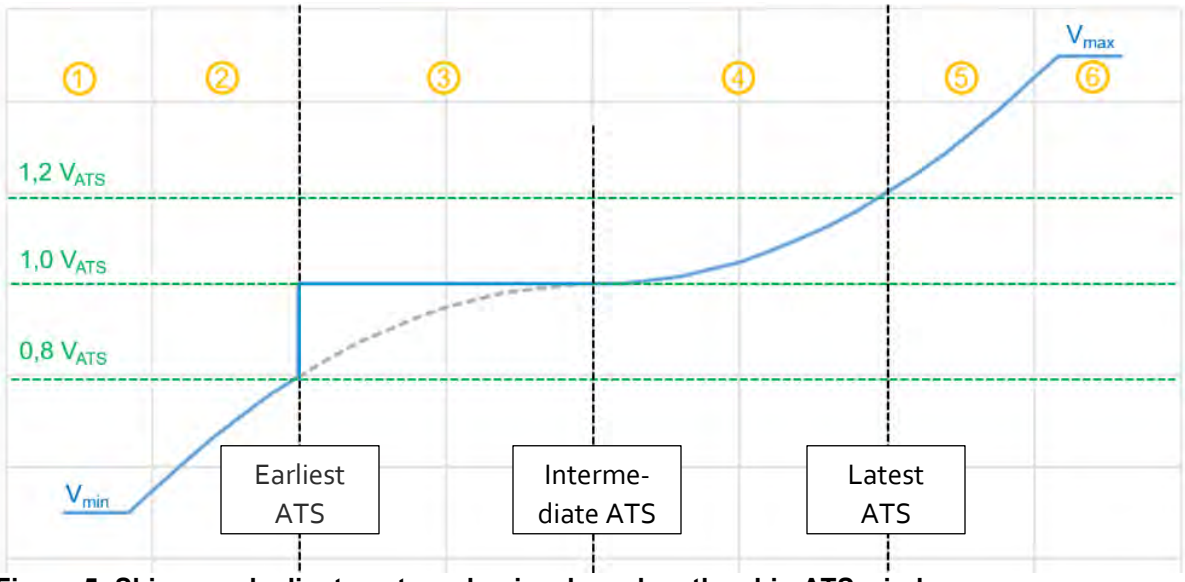

Figure 5: Ship speed adjustment mechanism based on the ship ATS window.

The ATS is one of the key elements in modelling the realistic behaviour of vessels, which want to make up for lost time by increasing their speed if the delay caused by the aforementioned maneuvers become too large, or have to decrease their speed when the destination lock isn't ready. The governing process behind this automatic self-adjustment of vessel speed during the simulation of a ship trajectory is shown in Figure 5.

When a ship arrives at a node of the network, the projected arrival time at its destination is calculated based on the remaining travelling distance and the ship speed. If the ship would arrive too early, i.e. earlier than the earliest RTA, which is the lower limit of the ATS interval, the ship velocity is multiplied by a factor determined by the blue curve in zone 1 and 2 in Figure 5. Alternatively, should a ship arrive later than the middle of the RTA interval, the multiplication factor is determined by the blue curve in zones 4, 5 and 6. Finally, I the ship would end up somewhere tween the earliest RTA and the middle of the RTA interval, the ship is allowed to keep on sailing at its current speed. At no time can the ship sail at a speed higher than its maximum speed and lower than its minimum speed, as shown in zones 6 and 1, respectively.

4. TRAFFIC

In order to investigate the capacity of the study area to process increasing traffic, a traffic generator is required that can generate an artificial series of traffic that acts as a best guess of the expected traffic. To this end, the present traffic needs to be analysed and discretized into a number of 'type vessels'. This analysis is done on a 2016 extract of the APICS (Antwerp Port Information and Control System) database, an integrated system of part related processes that enables the port authority and its partners to plan and follow up the traffic to, from and inside the harbour. It contains all registered journeys of seaworthy vessels to and from the port of Antwerp, together with some properties of the vessel and the journey itself. For the current model, the vessel types in the APICs dataset are rearranged into a new set of vessel types, namely container vessels, tankers, dry bulk carriers, general cargo and roll-on-roll-offs. The ships are then further categorised based on their origin and destination, retention time in the harbour, sailing velocity, dimensions and draught.

After analysis of the APICS traffic and determination of the vessel types, the artificial traffic series is generated using a stochastic process that is best described by a non homogeneous Poisson process (NHPP). This is carried out while taking into account the following, study area specific conditions:

- Tidebound vessels are stochastically generated, yet can only enter the network during a suitable tidal window
- The lock complexes in the port of Antwerp aren't accessed freely, yet carefully planned (cf. section 3) and codirect the traffic flow on the river Scheldt.
- As the study area is connected to the Lower Sea Scheldt through a narrow passage, access to the Lower Sea Scheldt isn't free yet is dependent on traffic conditions. Despite the stochastically generated inter-arrival times, vessels are only allowed entry into the model when this is physically possible.

5. SENSITIVITY ANALYSIS

Given the complicated nature of both the planning of quays and locks in the harbour and the sailing behaviour of actual vessels on a river such as the Scheldt, a sensitivity analysis was carried out to get a sense of the variation that can be expected on the results when changing certain parameters. As for the planning module, parameters such as the available percentage of quay length, maximum filling percentage of the locks, the opening and closing times of the lock doors and the availability window of a lock were a wide range of values. The simulations were carried out using the registered traffic and their actual harbour retention times as pulled from the APICS dataset, and feeding this traffic to the planning module. For each simulation, the simulated quay and lock occupancy percentages were compared to the results calculated from the APICS dataset for the same period.

Figure 6 and Figure 7 show the comparison of quay and lock occupancy percentages, respectively, for the best combination of parameters. The figures show that the quay occupancy aligns very well with that drawn from the APICS dataset. The lock occupancy percentage for the harbour of Linkeroever shows a slight discrepancy between the two locks, meaning that more ships are entering the harbour through the Kieldrechtsluis than the Kallosluis. Still, the numbers are within the same order of magnitude as those registered in APICS. Meanwhile, the occupancy percentage of the locks giving access to the Rechteroever harbour show a very good agreement with the APICS data.

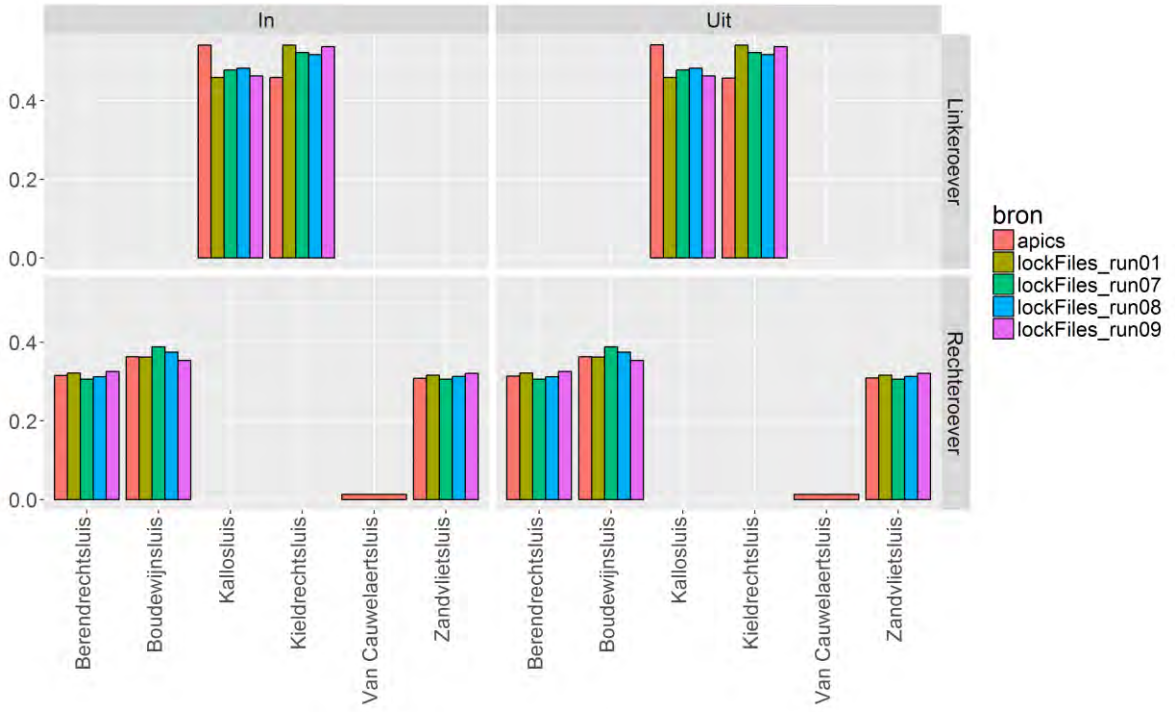

Figure 6: Lock occupancy percentage for in- and outbound traffic (left and right frames, respectively) and Linkeroever and Rechteroever (top and bottom frame, respectively).

The main parameter that was changed in the network model is the coefficient used for calculating the lateral safety distance between two ships, typically expressed as C.B, with B the width of the largest of the two ships and C the coefficient in question. The sensitivity analysis was carried out by calculating the excess channel width that remains in all of the network links when two ships of different dimensions meet each other there. This results in passable and non-passable sections of the network for every ship combination, which was then compared to a similar sort of 'passability chart' created from the expert knowledge gather during pilot interviews. In the end a coefficient of 1.3 was retained, making the safety distance SD = 1.3 B.

6. VALIDATION

The APICS output for a model period of 17/06/2017 – 20/08/2017 was compared to the model output for three different simulations. The final goal of the validation is to determine the ability of the model – i.e. the combination of traffic generator, planning module and network model – to simulate the sailing behaviour and interactions of a real fleet of ships. Only when the agreement is good enough will the model be able to be used with confidence to simulate future traffic flows and do assessments of waterway capacity.

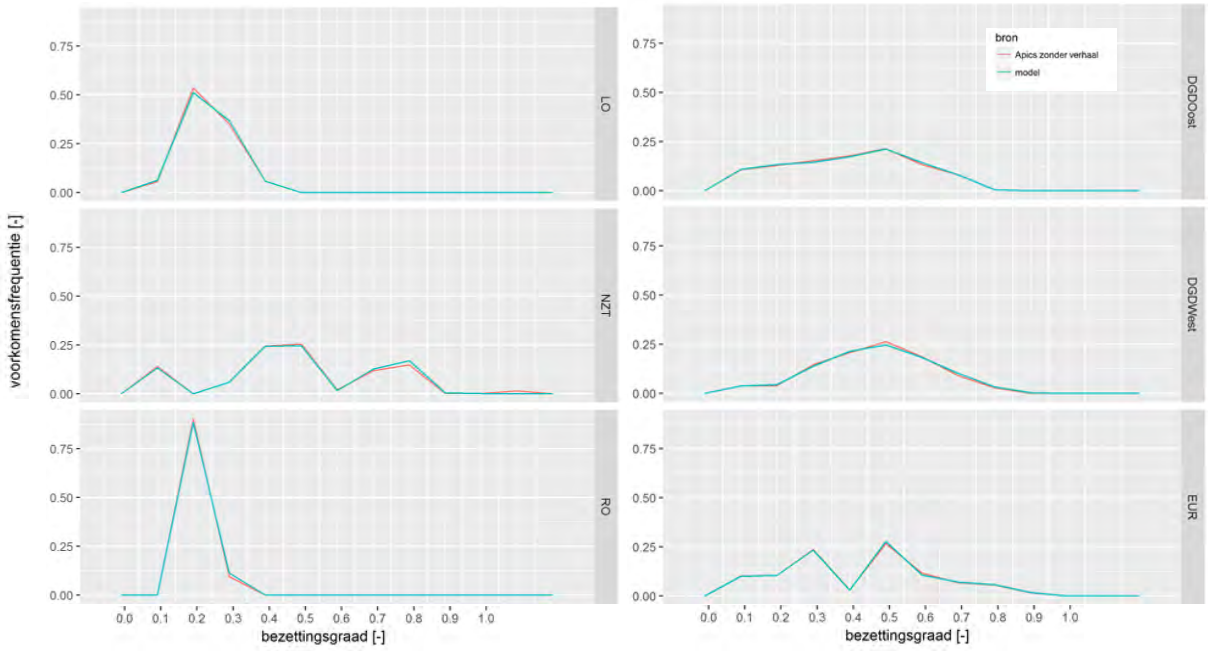

Figure 7: Quay occupancy percentages (abscissa) and their frequency of occurrence (ordinate) for quays at Deurganckdok Oost (DGDOost), Deurganckdok West (DGDWest), Europaterminal, Linkeroever port (LO), Noordzeeterminal (NZT) and Rechteroever port (RO)

In a first simulation (denoted 'registratie enkel'), the APICS traffic is recreated as faithfully as possible by simply having the ships from the APICS dataset enter the model and leave the harbour at their registered times. This simulation circumvents the planning module and focuses on the ability of the network model to recreate realistic ship behaviour.

A second simulation (denoted 'registration retour') takes the registration times from APICS and uses them as input for the planning module such that the vessels' effective departure and arrival times are determined by the availability of the locks and quays and the modelled minimal retention time for each ship type. Finally, a third simulation includes the traffic generator and carries out a simulation (including planning) using an artificial traffic series determined as described in section 4.

Comparison between model and measurements is achieved through two parameters: the vessel velocity and the amount of overtake maneuvers a ship is involved in. The first parameter is displayed in Figure 8 as a velocity per vessel type and per model section (three sections are defined: the coastal region, the river itself and the harbour) for both up and downstream parts of a ship's journey. The figure shows that a very good agreement is found for all three simulations, across all vessel types and model sections, for both directions of travel. The second parameter can be analysed in two ways, i.e. the number of times a ship is being overtaken by any other ship during its journey, and the number of ships the ship overtakes during its journey.

Figure 9 compares the percentage of occurrence for both numbers for all three simulations with those derived from the measurements. The simulation that is expected to yield the best comparison actually performs the weakest, while the model with biggest uncertainty yields the best agreement. A possible explanation is the uncertainty that is connected to the APICS data and how the sometimes erroneous data is interpreted in the translation to the traffic series for the first simulation.

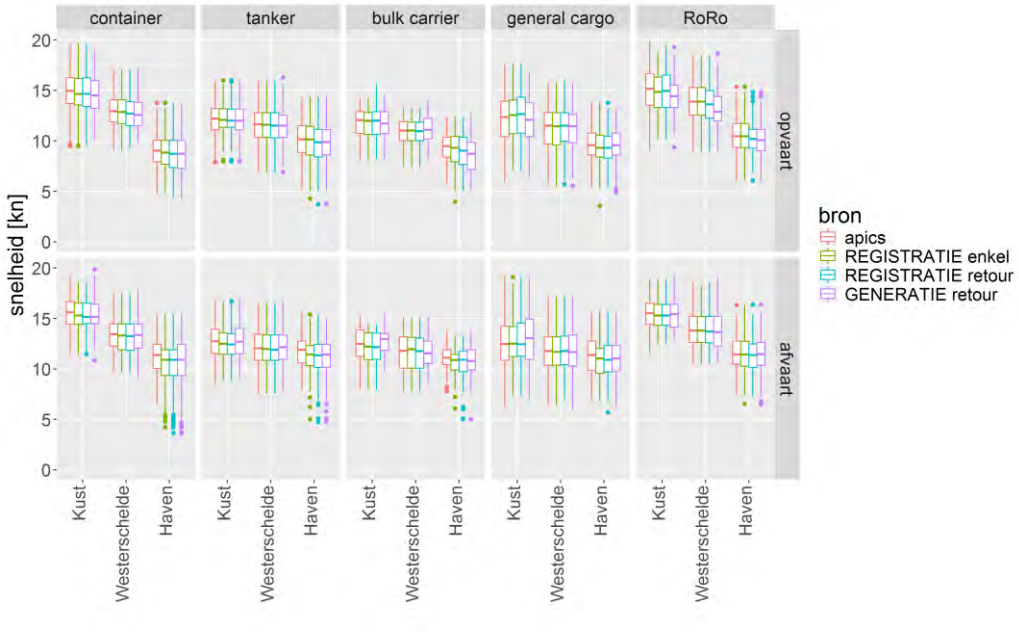

Figure 8: Comparison of registered ship velocities (APICS) with the velocity output of three simulations, for three sections of the river. Upper frame: portbound traffic, lower frame: seabound traffic.

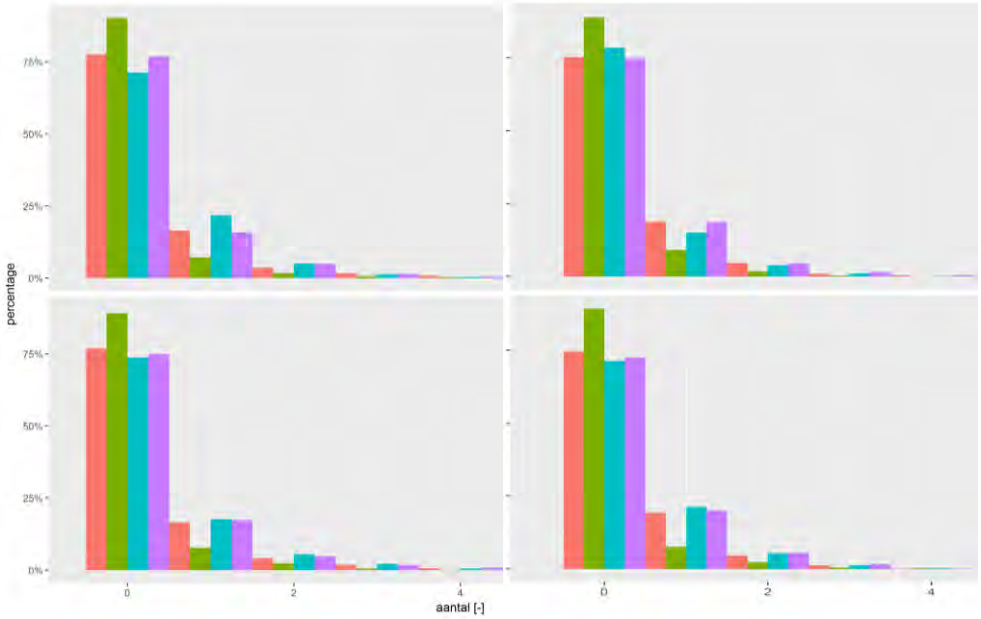

Figure 9: Number of times a ship is overtaken (left) overtakes another ship (right) in the APICS dataset and the three validation simulations. Upper frame: portbound traffic, lower frame: seabound traffic. Red: APICS data; Green: registry one way; Blue: registry return; Purple; generated traffic.

In such cases, it is possible that swapping this data uncertainty for a modelled 'general' value smoothens out any outliers or 'bad ships' that would contaminate the comparison, thereby improving the model agreement with the logged journey data. In any case, the very good agreement of the overtake parameters derived from the third simulation and the APICS data respectively, is a testimony of the apt functioning of the planning module and the traffic generator.

7. THE CAPACITY OF THE WESTERN SCHELDT

7.1 Theoretical capacity analysis

Simulations were carried out with an increased traffic flow to investigate whether an increase in traffic would saturate the Western Scheldt. The traffic generator was used to generate times series of ships for twice, three and four times the traffic flow, respectively. These times series are generated using the non-homogeneous Poisson process described in section 4. Figure 10 shows the variation of traffic (flow and density) summarized over a tidal cycle as a function of time. The variation is random. Both density and flow show a similar evolution, which indicates that capacity is not yet reached for these traffic multiplication factors.

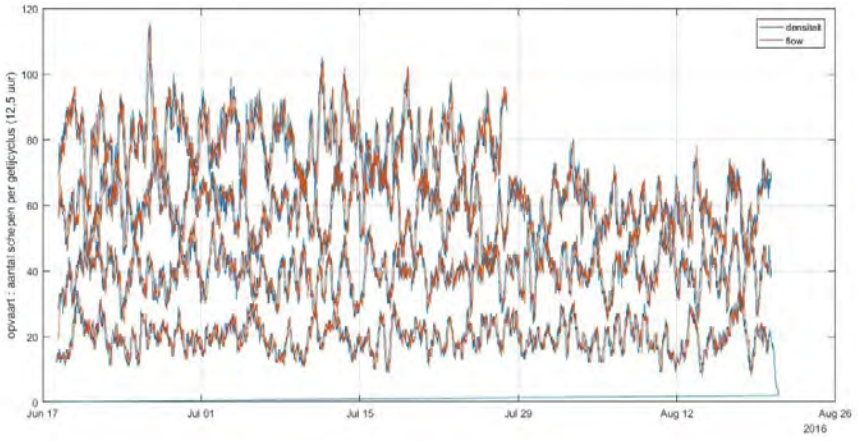

Figure 10: Traffic (flow = red curve, density = blue curve) expressed as number of ships over a 12.5 hour period of portbound traffic. Seabound traffic shows a similar view.

Plotting density as a function of flow in Figure 11 still shows a linear relation, which again implies that the capacity of the river system has not yet been reached for the increased traffic.

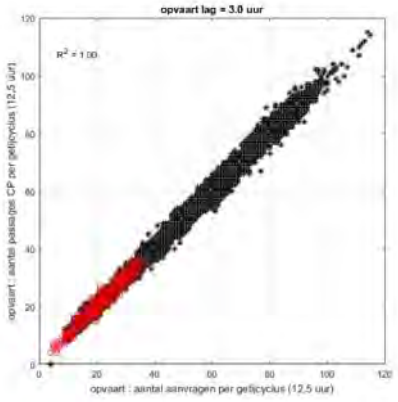

Figure 11: flow/density chart resp. passages at CP and requests for departure (time difference 3 hours). The figure can be considered as an example of the linearly increasing part of the curve in Figure 1. The red zone indicates the traffic of the prognosis.

7.2 Prognosis 2030

A prognosis for the expected traffic in 2030 was carried out in the frame of the ECA project, in which alternatives for additional container capacity for the Port of Antwerp are being investigate. This was translated by the Port of Antwerp to the total amount of ships that would sail on the Western Scheldt and towards the different port terminals in that year, distributed over the different ship categories.

The main question when simulating with future traffic is if the ability of the fairway to get all of the vessels at their destination without any notable delays and/or problems. In order to answer this question, Figure 12 and Figure 13 again compare ship velocities and overtake maneuvers, respectively, this time comparing the results for the future traffic with the reference case established at the end of the validation exercise (i.e. simulation 'generate retour').

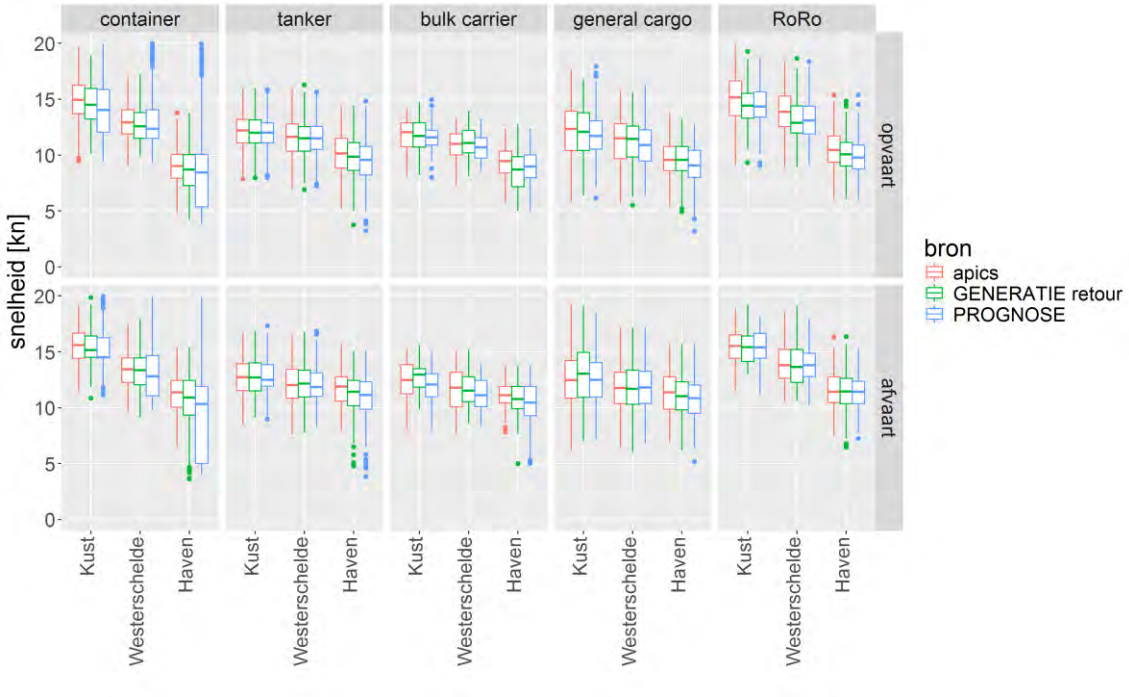

Figure 12: Comparison of registered ship velocities (APICS, red) with the velocity output of the reference case (green) and the prognosis simulation (blue), for three sections of the river. Upper frame: portbound traffic, lower frame: seabound traffic.

The figures show that the ship conduct in the prognosis simulation is analogous to that of the reference case.

There is an increase in the number of overtake maneuvers and overtaken ships, which indicates that there is still plenty of room left on the fairway to engage in ship maneuvers and capacity is far from reached. Indeed, as the fairway reaches its capacity, one would expect an increasing difficulty at conducting overtake maneuvers as:

1. the room between ships decreases and the overtaking distance - i.e. the distance a ship must sail next to other ships it is overtaking before it can sail in its 'proper lane' – increases and
2. the opposing traffic intensity increases, as do the amount of crossing maneuvers in both directions, which pose an extra threat to the ability to perform an overtake maneuver (cf. section 3). At full capacity, ships would be stuck in an endless 'traffic jam', sailing in one single, continuous file in each direction, adapting to the speed of the slowest ship.

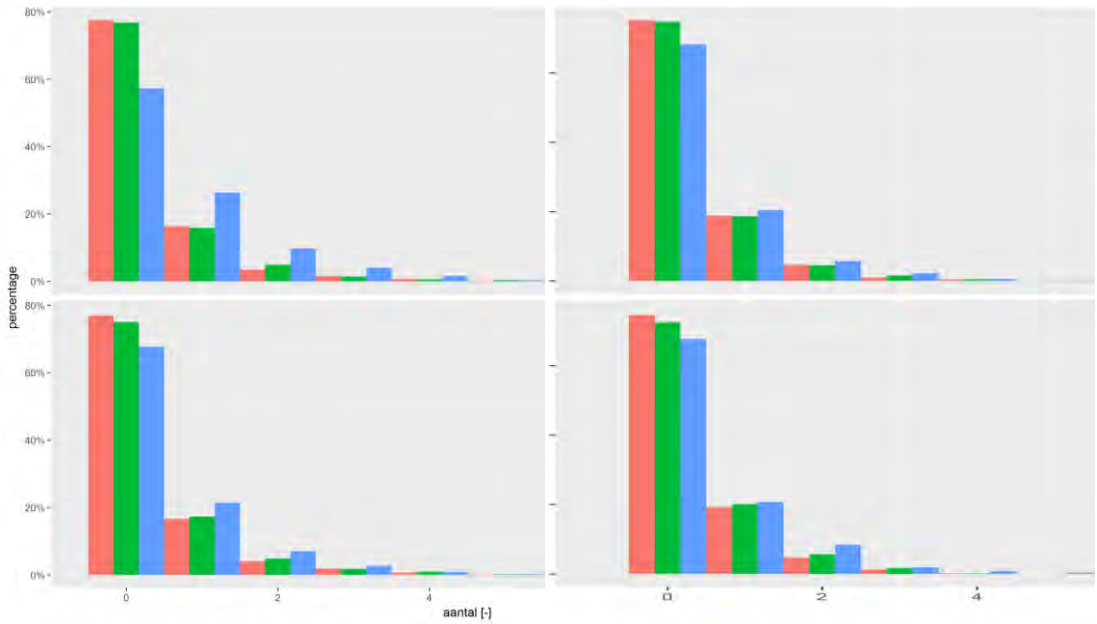

Figure 13: Number of times a ship is overtaken (left), a ship overtakes another ship (right) in the APICS dataset (red), the reference case (green) and the prognosis simulation (blue).. Upper frame: portbound traffic, lower frame: seabound traffic.

Overall the ship velocities are in good agreement across all river sections and ship categories, a significant decrease in average velocity is not noticeable, as would be expected in case of saturation. However, some ships appear to sail at higher speed, particularly in the port area, indicating that in order to respect the ATS compensation is required by increased sailing speed. Therefore, at this stage, it must be concluded that the model is not yet decisive. Therefore, modifications are required to effectively limit speed in the port area, and to check whether delays can be compensated earlier.

8. CONCLUSION

A traffic model for waterway networks was expanded to investigate the fairway capacity of the Western Scheldt. Main additions are a planning module that regulates when ships start and end their journey, and the inclusion of ship maneuvers that frequently occur.

Validation results indicate that the traffic generator, the planning module and the network module are all capable of adequately simulating the development of traffic in estuarine channels and port basins with complex connections to tidal terminals and dock and port basins connected with locks for the current situation.

Although preliminary results tend to indicate that the fairway has not yet reached capacity for the traffic predicted for 2030, the model needs additional modifications to allow for decisive conclusions in the port area itself.

9. REFERENCES

Adams R., Bayart P. & Doorme S. (2014). IMDC WATERWAYS, A design tool tailored to the need of integrated design of waterway infrastructure. 33rd PIANC World Congress, San Fransisco.

Verwilligen, J.; Vantorre M.; Eloot, K.; Mostaert F. (2008). Haven van Antwerpen, Op- en afvaartregeling voor 8000 en meer TEU containerschepen. WL Rapporten, 689_04. Waterbouwkundig Laboratorium & Universiteit Gent.

COFASTRANS (Container Vessel Fast Transhipment System)

G Rankine[1], I Netherstreet[2], D Perez Romero[3], J Palmer[4]

ABSTRACT

This paper picks up from earlier research (Beckett Rankine, 2015) and considers a new port layout that will enable faster loading and unloading of containers at the quayside, particularly for the new largest container vessels. The concept is novel and yet practical, using indented berths with innovative ship-to-shore overhead portal cranes. The efficiency of COFASTRANS is built from adaptation of the latest container handling techniques combined with large crane technology from the shipbuilding industry as well as vessel navigation in confined waters, such as seen at the Panama Canal.

Key Words: Container Handling, Mega Ships, Container Terminal, Ship to Shore, Indented Berth

1 INTRODUCTION

1.1 A Revolution of Disruptive Development

New and very much larger container vessels have recently been introduced on the world's main shipping routes to increase efficiency and to bring down costs. This requires faster unloading at ports, but even with new larger cranes the bigger ships cannot be unloaded any quicker because their greater width means having to move faster just to unload at the same speed as before. Ports have simply grown by evolution into much larger versions of the same concept and have now been left behind in the challenge to provide a more efficient, faster and more environmentally friendly link in the supply chain.

Figure 1: COFASTRANS Indented Berth Concept

COFASTRANS, seen in Figure 1, solves this problem by positioning the ship, which is the biggest and most valuable single element in the overall terminal delivery system, at the heart of the central working area, surrounded by port operations with direct access to the shoreside container stacks on both sides of the ship. This compares with the conventional arrangement where vessels are at the periphery and restricted to access over only one side. The indented berth layout opens the way to relieve the quayside congestion that has been building up in recent years, providing twice the area available for landing and loading containers to the ship. The innovative new portal crane (Konecranes 2018, Nevsimal 2018) makes this possible and, with 4 hooks per crane, places up to double the number of lifting spreaders over the ship, with the average trolley travel distance over the vessels halved. This will result in 35-45% reduction in average ship time in port, as well as improved land utilisation, often in environmentally sensitive areas.

[1] Gordon Rankine BSc ACGI CEng FICE MIStructE; Beckett Rankine, gordon@beckettrankine.com
[2] Ian Netherstreet BSc (Eng) Hons MICE; Beckett Rankine, 47 Gillingham Street, London, UK
[3] Dulce Perez Romero PhD; Beckett Rankine
[4] James Palmer ACGI CEng MICE; Beckett Rankine

2 WORLDWIDE CONTAINER SHIPPING

2.1 World Trade

Seaborne container trade has increased dramatically since introduction over 50 years ago and until recently the global supply chain has worked well in a mature stability with well-balanced vessel and port dimensions. Apart from the global downturn correction, world container growth has been consistently positive, typically tracking or beating world GDP and related trade growth, as seen in Figure 2.

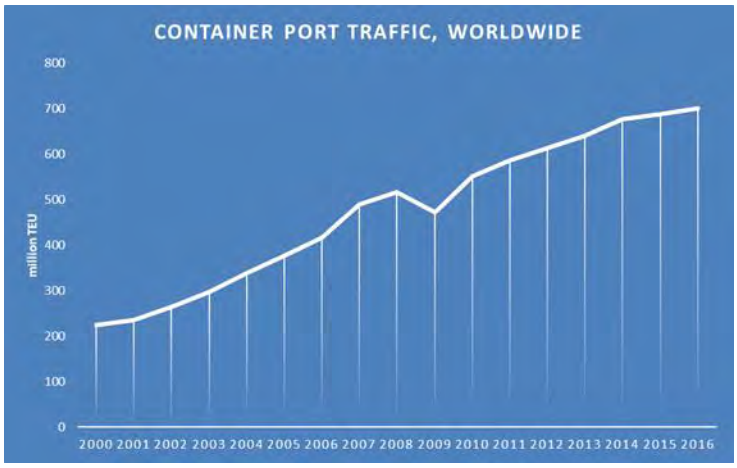

Figure 2: Container Port Traffic (UNCTAD, 2018)

This has meant that ports have consistently been required to invest in additional berthing and land areas and to employ increasingly sophisticated cargo handling equipment to meet demand.

A parallel pattern for ship owners has meant steadily increasing vessel size and the continual search for the fastest possible handling performance in order to keep vessel time in port to a minimum. These larger vessels demand longer berths and bigger ship-to-shore cranes. They have brought inefficiencies that have made some question the benefits of the mega carriers that were intended to improve things.

2.2 Container Supply Chain

The port's role is as a key link in the container supply chain, the ultimate test for which has to be the cost and time taken for the containers' full journey, extending well beyond the port gates. The overall pattern is complex, with regular shipping schedules required for "just-in-time" logistics, empty containers to be returned and a variable mix of 20ft / 40ft containers. Commercial considerations will drive the many options for vessel size and choice of transhipment through major port hubs or direct calls between smaller ports.

As various elements of the supply chain are improved, bottlenecks are created elsewhere, which must be overcome for the full benefits of these improvements to be realised. Recently the shippers have driven the trend for larger ships to make their operations more efficient, and the port operators have had to play catch up to keep their place at the table. But with quayside cargo handling rates not improving as much as shippers would have liked, the benefits to the shipping lines are limited, which in itself has not helped the terminal operators.

2.3 Container Vessels

In the early days of container shipping the vessels evolved from conventional cargo vessels that could sail the oceans and visit ports with few restrictions. Now they have developed into 400 metre long Ultra Large Container Vessels (ULCVs), with a Maersk fleet of 20No. 18,000TEU Triple E class vessels ordered in 2011, only to be followed by further increases to 19,380TEU capacity now being constructed. Other fleets now include vessels of over 20,000TEU eg OOCL Hong Kong with a capacity of 21,413TEU and similar principal dimensions. And even larger vessels can be expected, see Figure 3.

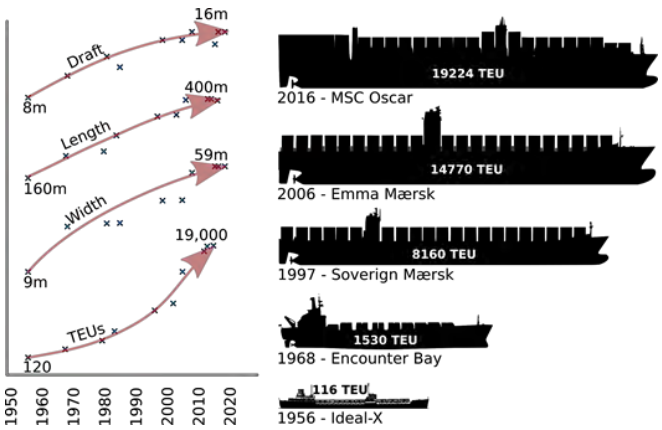

Figure 3: Chart of Vessels vs Year

Cargo handling equipment in ports can also be a restriction to the vessel size, especially on the beam. The largest vessels might be more efficient for the shipping lines, but to meet their profit targets the shipping lines need reduced time in port, which is not possible to achieve with conventional shoreside cranes. If the restriction on vessel beam imposed by conventional port cranes could be lifted, the next generation of vessels could be more efficient with possible benefits of reduced fuel consumption and shallower draughts.

2.4 Container Ports

Other than progressive development, there has been no disruptive innovation in ship-to-shore container handling since the start of containerisation in the 1960's, despite pressure from the large international shipping lines. Since the early days of containers, the recognised approach has been to construct long straight lines of berths. Development has been evolutionary within the framework of the same old layout with a longer line of berths resulting in the larger ports extending for more than 5km over a narrow coastal strip. Such distances can make operations difficult and, impressive as the new cranes are, the longer 60-72m cantilever booms over the ship inevitably need faster equipment just to be on par with the cargo handling speeds attained by the cranes on smaller vessels, never mind the increase in productivity that is sought. The pros and cons of this typical layout are outlined in Table 1.

Arrival of the new mega vessels has been problematic for the ports with a need to invest heavily just to make provision for handling these vessels and avoid loss of trade to competitors. But the sudden deluge of containers from a single ship creates more congestion with peaks and troughs in workload and equipment requirements that are difficult to handle with conventional arrangements.

Advantages	Disadvantages
Flexibility to berth various sizes	Operational inefficiencies
Maximise utilisation of cranes	Environmental and permitting viewpoint

Table 1: Conventional Berths

Looking at the largest 100 container ports (Figure 4) a general growth can be seen globally, albeit more significant in locations strategically important to the global supply train (Figure 5).

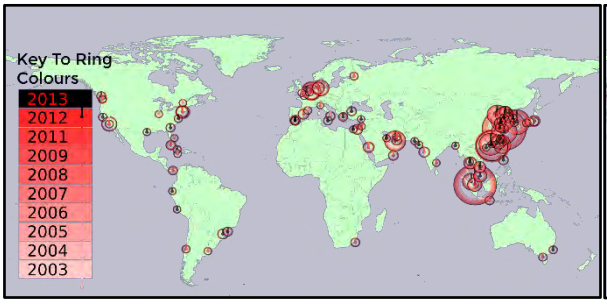

Figure 4: Largest Container Ports

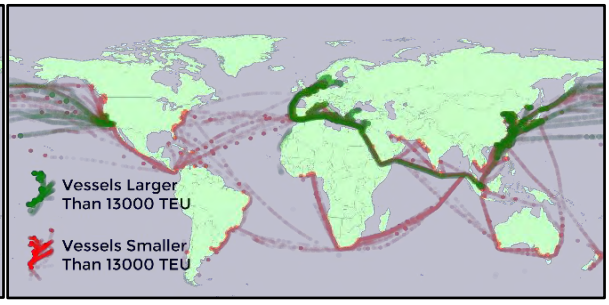

Figure 5: Global Trade Routes

3 ADVANCES IN CONTAINER HANDLING

3.1 Ship-to-Shore Cranes

Successive increases in vessel beam has meant that the ship to shore gantry (SSG) cranes, as seen in Figure 6 have correspondingly longer and higher booms (dimensions in metres). This has required progressive increases in the structures and weight of the cranes and also demands higher trolley speeds to maintain the overall throughput rates. With the present crane technology and berth arrangements, most ports find that 6 or 7 cranes are the maximum that can be operated efficiently on a single ship, with some ports able to deploy 8 or 9 cranes for some time over the largest vessels.

	1970	1995	2002	2013	2018
Outreach	37	54	67	72	72
Backreach	15	20	25	25	
Lift Height +	25	38	41	52	55
Lift Height -	10	14	17	17	

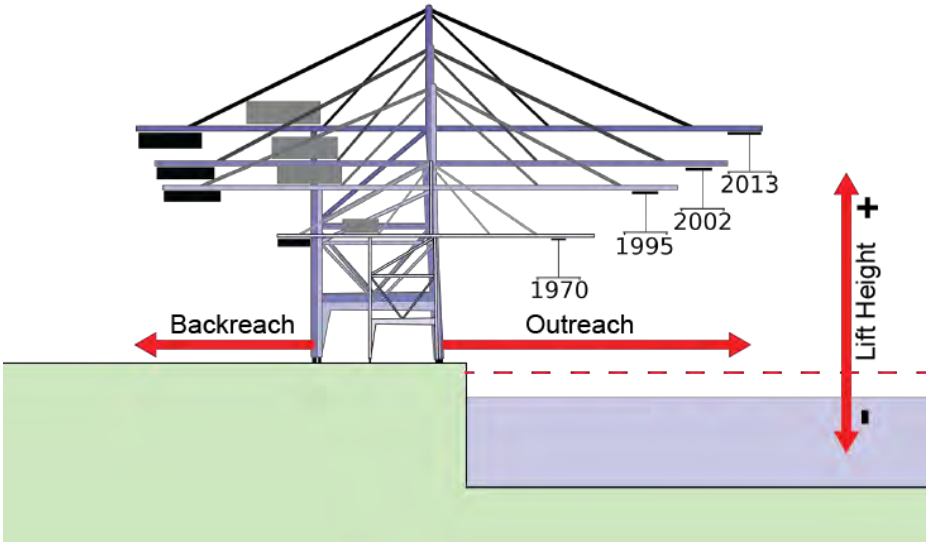

Figure 6: Evolution of Container Cranes

But the original SSG concept is inherently inefficient in two respects: firstly, reaching out to pick up a heavy object using a cantilever means that additional weight has to be placed on the other side to prevent the crane from toppling over, adding to the crane's wheel loads and consequently the need for stronger foundations (see Figure 7 below). Secondly, the further out the crane has to reach the longer it will take to get there, making it slower to handle the bigger ships at a time when the industry is looking to reduce ship time in port.

It has been possible to overcome these problems with larger foundations and greater operating speeds that are now at a practical limit. But as the cranes become ever larger we are facing up to diminishing returns that might not have been widely expected with the advent of the mega ships.

3.2 Quayside Construction

The gauge between crane rails has widened to be generally 30m for modern SSG cranes, the wheel loads have increased with bigger cranes and the dynamic variation in these loads has also increased with the bigger transient loads caused by twin and tandem container lifting.

As can be seen in Figure 7, crane outreach over the vessel (blue) has grown, but this has been linear or at a slightly reducing rate since 1950, following the trend of vessel beam described earlier. And yet leg load (red) is growing at an increasing rate, due to the increase in container loading (twin lifts etc) but

also compounded by the cantilever format of the conventional SSG cranes, and associated need for additional counterweights.

This increase in leg load is causing problems for port design engineers in providing adequate and yet efficient foundations for the crane rails, often with construction in poor ground conditions. This is also to be combined with the large retained height of the quayside associated with modern vessel draughts. A reduction in this crane leg load could offer savings on capital cost of civil works.

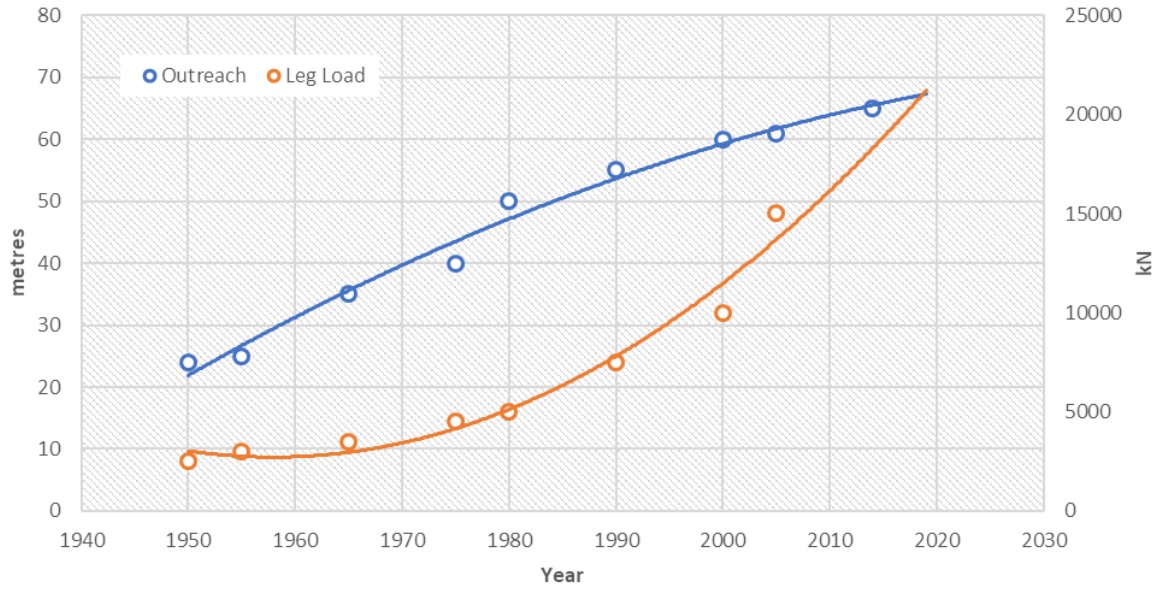

Figure 7: SSG Outreach and Leg Load (data source: de Gijt, 2010)

3.3 New Ideas

Some attempts have been made to change the status quo. A simple indented berth was operated successfully between 2006 and 2008 at the Ceres Paragon (latterly the Amsterdam Container Terminal (ACT)). But as conventional gantry cranes were used from both sides, the interference between cranes inevitably resulted in inefficient utilisation. Further, the berth was never able to demonstrate its full potential because it was accessible only through restricted-tidal locks and close to Rotterdam, which made it a less desirable destination.

Research around this concept continued (Rankine, 1998, 1999, 2000, 2001) exploring various indented berth layouts for the largest ships at that time. Associated work linked this to development of concepts for multi-storey container warehouse systems.

Presumably in response to Maersk's request that a step-change was needed in container handling for the new larger vessels, APM Terminals have spent much time preparing new ideas, including a new concept called Fastnet with narrower cranes intended to enable a greater number of individual cranes to work simultaneously on a vessel. But this was found to be over complicated and has not been adopted.

In 2013, The Maritime and Port Authority of Singapore set a challenge to create a new idea for container handling based broadly on their planned new container port for the 2020's. The winning team focused largely on creating a double height stacking yard on-shore using conventional cantilever ship-to-shore cranes fitted with double-hoist systems to serve both upper and lower levels. It will be interesting to see how this turns out.

Port layouts are still being developed by looking back over the successes of the last 50 years, but the next step cannot be made with normal port layouts and conventional ship-to-shore equipment that have reached full maturity. The basic geometry needs to be re-assessed to create greater efficiency with a view forward to the next 50 years.

4 COFASTRANS - INDENTED BERTHS

4.1 General Description

COFASTRANS is a system for loading and unloading large container ships in international container ports using an innovative portal crane and indented berth, instead of the existing cantilever cranes and long straight line berths. The objective is to substantially improve the efficiency of container transportation in terms of time, cost and environmental impact.

The ship is central to the working area with cargo handled over both sides (as seen in Figure 8), cutting in half any congestion at the quayside. The new portal cranes have been designed so that each crane can line up and address two rows of on-ship containers simultaneously, with each row being serviced by two trolleys. This can double the number of lifting hooks over the ship and reduces the outreach distance by half. Shipping companies have been calling for 250 berth moves per hour (up from about 150 at present) and no current system can get close (Davidson, 2015). COFASTRANS can exceed 250 and also uses less seafront land.

Figure 8: COFASTRANS puts the Vessel at the Heart of the Terminal

With a conventional layout an equivalent port expansion would involve taking a greater length of coastal strip, installing heavier and less efficient cranes and moving containers greater distances between vessel and storage. In contrast COFASTRANS offers port operators a more manageable Mega ship berth arrangement that is equivalent to handling two vessels of half the size using the conventional system. It also removes the in-port vessel width restriction for shipping lines as they seek to further expand their vessel sizes.

Both key elements to COFASTRANS have a tried and tested pedigree from use in other applications and are being used here in an innovative way. The crane has evolved from the latest technology of large shipyard cranes (Nevsimal 2009, 2013, 2017), and the indented berth has evolved from dock and lock entrances. COFASTRANS has been designed to be flexible and versatile so that it can be slotted into existing terminals as well as into plans for new ports. It is compatible and can be used in conjunction with all forms of onshore container handling equipment.

COFASTRANS will offer expansion opportunities for port operators and attract shipping lines to ports that introduce the system because of the significantly reduced vessel time in port.

4.2 New Bespoke Terminal Layouts

COFASTRANS is targeted at the largest international container ports where one or more new berths can augment the existing operation and transform the performance and turnaround time for the largest vessels. New greenfield locations also provide a significant opportunity.

Container ports across the world have very different natural layouts, constraints and requirements, so there are many ways and opportunities for COFASTRANS to be implemented. Each will be different in some way so as to match the operational requirements with the available land and sea conditions.

For this paper, generic information has been distilled and focused on to three arrangements to demonstrate a typical range of layouts that take into account terminal cargo profiles, together with storage and traffic constraints as well as navigational and berthing requirements for the berthing vessels. Clearly any of these layouts will have to be crafted and refined to match commercial and geographical requirements to create an individual bespoke solution that will provide the optimum benefit for any specific terminal, whether it be a single indented berth to enhance an existing heavily invested terminal or a multi indented berth transhipment hub or even an entirely new port. These various types of installation all have the potential to substantially improve efficiency of global container transportation in terms of time, cost and environmental impact on the world's main trading routes.

This concept is all about the introduction of a new layout with a novel crane to enable the change, rather than creating new ways of moving containers around on the ground. There are now many ways of handling containers on-shore and COFASTRANS will work with any of these. Any on-shore container handling equipment and systems that can be applied to a conventional terminal can also be applied to a COFASTRANS layout with correspondingly faster and more efficient results. But it is expected that more development and improvements will be made with increasing use of automation.

4.3 Novel Ship-to-Shore Portal Crane

The concept for the Ship to Shore Portal Crane (SSPC) envisages placing 2 spanning beams with 2 trolleys on each beam over the indented berth to provide 4 independent lifting points per crane (Nevsimal, 2017), as shown in Figure 9, each capable of undertaking a single, twin or tandem lift (i.e. 4 No. TEU or 2 No. 40ft containers side by side). The buffer to buffer length of the cranes will be less than the 53m distance that would allow a maximum of 5 SSPC units to be deployed over a 400m long vessel. However, it is considered more likely that greater efficiency could be achieved by deploying only 3 or 4 SSPC units. In the case of 4 cranes the result will be simultaneous operation of up to 16 spreaders over 8 holds of the vessel. This provides the ability to undertake up to 328 moves /hour on each indented berth assuming only a conservative average of 21 moves per spreader/hour.

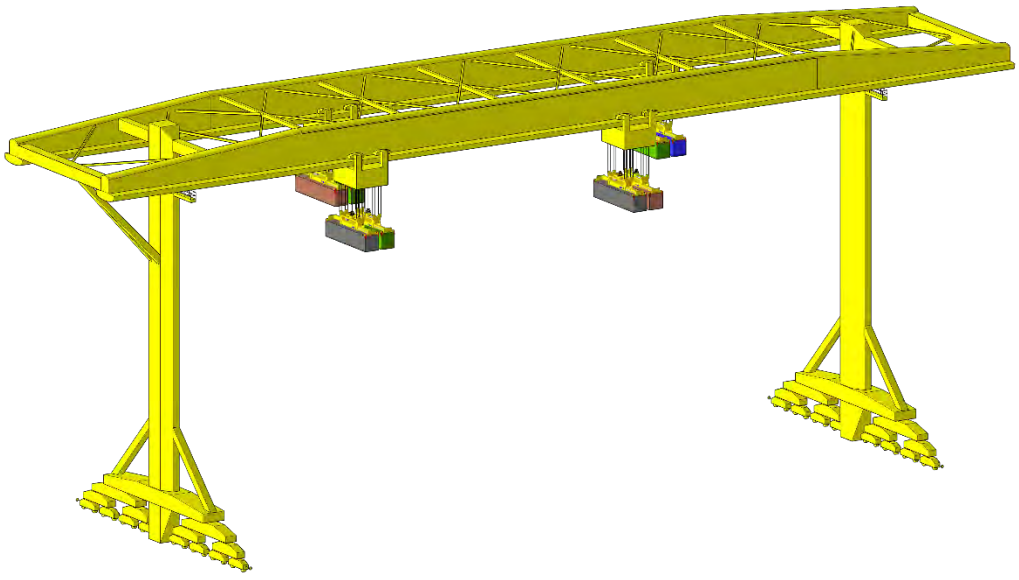

Figure 9: COFASTRANS Ship to Shore Portal Crane

An additional benefit of using a portal crane is that, due to absence of the moment from the eccentric load on the SSG crane, the loads on each runway are significantly reduced and almost equal. Furthermore, the heavily loaded crane rail beams on the jetty superstructure can be located well behind the quay cope line, allowing use of bearing piles only thereby reducing crane beam and runway construction costs.

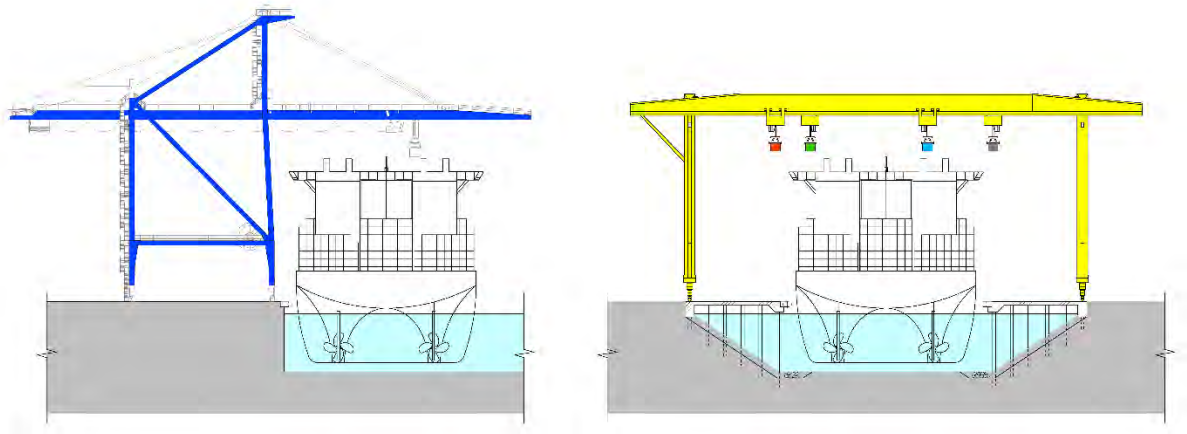

Figure 10: Comparison of SSG and SSPC

The general parameters of the innovative portal crane have been taken as:

- A span between crane rails of 129m, obviating the risk of vessel contact with the crane;
- Two lifting beams set about 30m apart so that each crane works upon 2 non-adjacent vessel holds at once;
- Each lifting beam has 2 trollies operating along it (Trollies will be fitted with proximity switches to ensure that they cannot collide and the hooks can lift eccentrically by a suitable amount to take account of variability of vessel hold spacing);
- With 4 cranes operating, 16 hooks can therefore be used to unload vessels in the indented berth, whereas in standard berths a maximum of 8 hooks can be deployed;
- The cantilevers on each side of the berth will be able to lift containers up to 25m beyond the rail;
- The soffit of the lifting beams needs to be set to clear the largest vessels with the minimum operational draught;
- Trollies will be stored over the quay during berthing;

Operational parameters using twin lift spreaders are taken as:

- Lifting and lowering - Loaded: 90m/min; Unloaded: 180m/min; acceleration: ±0.75m/sec^2;
- Trolley transit speed: 125m/min; acceleration: ±0.55m/sec^2;
- Gantry travel speed: 30m/min; acceleration ±0.15m/sec^2;
- The cranes will be located in advance of the vessel arrival so that unloading operations can commence as soon as the vessel is moored.

It is assumed that the cranes will complete the unloading and loading of each pair of holds before moving to the next adjacent holds and that double cycling is undertaken when possible. With 3 SSPC cranes deployed, the stern-most crane would initially be positioned over the rearmost hold which has been assigned the number 1 and number 3 hold, the crane will complete unloading and loading these then move to holds 2 and 4 and so on. The central crane will start over holds 8 and 10 and the foremost crane over holds 17 and 19. The cranes have sufficient room between them that they can move independently of the others. If dimensions of the funnel and bridge units are the same as the container holds, within the tolerance of the crane boom spacing, then 3 cranes can cover the entire ship each with 3 moves, alternatively 4 cranes can cover it with 2 moves each.

Currently the largest super-post Panamax crane (SPP-SSG) units weigh around 2,500t with an outreach of 72m. It is anticipated that the SSPC crane with lifting hooks spanning 129m would weigh about 20% more than one and cost considerably less than two of these SPP-SSG units.

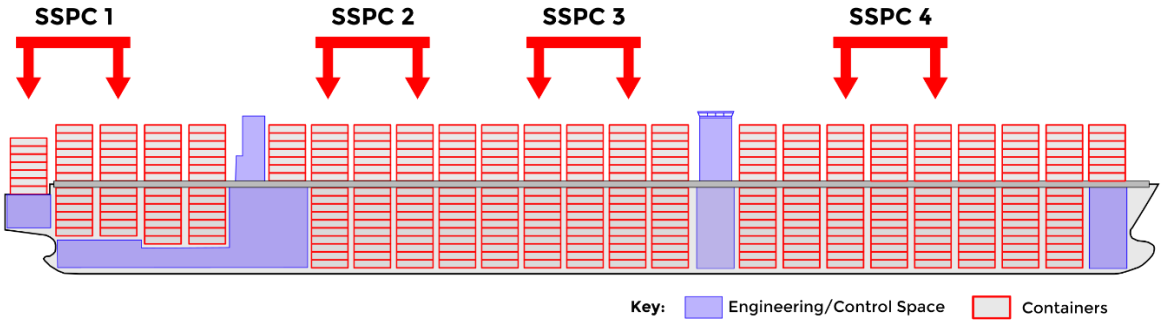

Figure 11: Typical ULVC showing possible SSPC locations

4.4 Intensive Use of Quayside Land

With the ship and indented berth at the heart of the operation, it is important that the berthside container stacks are set up to service the SSPC cranes as efficiently as possible. The concept is that in all cases an envelope is created around the ship that is totally dedicated to transferring containers as quickly as possible between the ship and shore, see Figure12. Clearly when the ship is in the berth, servicing the crane and ship is highest priority with redistribution of containers carried out when possible. When ship handling has been completed and the when the berth is empty the focus would shift to getting everything in place for the next ship.

The berth-side container stacks have to operate with a maximum intensity to service the indented berth. These will be "churning" all the time, moving containers so that their positioning is always being "nudged" and made better for the activities that will be coming up, in accordance with the terminal's operating system and ship loading plans. This would be done even when ship is in, but especially when it is not. This process already happens at modern terminals in existing Automated Stacking Crane (ASC) stacks, but contrasts with the traditional container handling concept of minimising movements within the terminal.

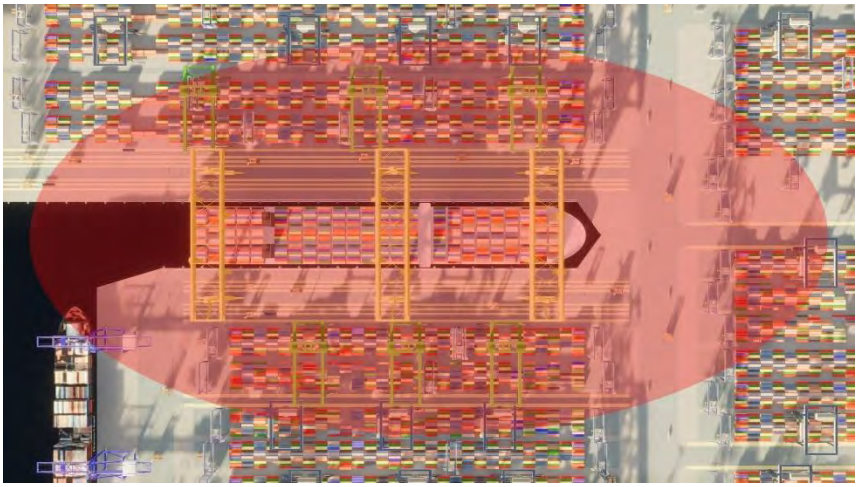

Figure 12: Quayside Zone around an Indented Berth

With COFASTRANS, the ship will always slot into the same position inside the indented berth so shore stack container positions can be pre-determined to suit the vessel length. It is not expected at this stage to transfer directly between vessel and stack because the vessel hold arrangements can differ and are typically more widely spaced than on shore, but means by which this can be achieved are under development. The transfer of containers to and away from the berth will be through ends of the berth-side stacks rather than directly from the ship, thus creating a combined factory style intensive operation encompassing the ship plus shoreside stacks.

It is envisaged that all stacks could be served by ASCs. The intention is that the export containers will be preplaced in the stacks closest to the SSPC crane which will be delivering them to their location on the vessel. The same stacks will also receive all of the import containers from that SSPC crane to reduce the travel distances of the Automated Lift Vehicles (ALVs).

To maximise intensity the berth-side stacks for the “parallel to berth” cases are located in pairs which are also serviced by Automated Rail Mounted Gantry (ARMG) to provide transfer directly to, or close to, the SSG cranes.

4.5 Traffic Circulation and Container Storage

The indented berth layouts have been designed for use with all types of terminal traffic. However there would be some significant differences in the operation for the various types of equipment, as there is at modern present-day terminals. Automation is preferred but manual terminal equipment could also be used. Automated Guided Vehicles (AGVs) or ALVs can be used to transfer containers on the internal roadways.

At this stage ALVs appear to be more efficient with the COFASTRANS concept, taking advantage of the disconnect between the SSPC crane and the pick up or delivery unit.

Traffic circulation at the berth will normally be one-way driving lanes serving the quayside cranes. For most cases a series of circulatory routes will be pre-defined with designated stacks serving each side of each of the cranes in order to minimise potential areas of conflict in road traffic. But there may also be the option to utilise the automated vehicles’ ability to reverse course in some cases.

Transfer of containers to other stacks or feeder vessels would be from the aprons remote from the berth where possible to avoid congestion, especially when this berth is occupied. Typically traffic on a COFASTRANS terminal will have shorter journeys because of the more compact layout compared with elongated conventional terminals, see Figure 13.

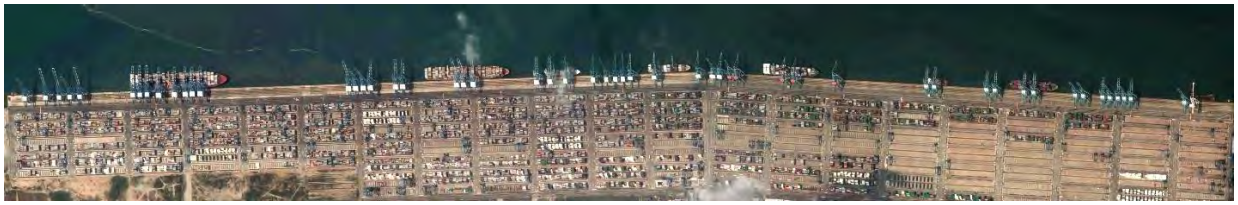

Long and narrow conventional terminal
Map data Google, DigitalGlobe

COFASTRANS compact equivalent

Figure 13 Land Use Comparison

4.6 Navigational & Vessel Services

For any indented berth terminal it will be necessary for the largest container vessels to safely and promptly berth in the constrained dock configuration. An initial assessment of requirements was based on information arising from the fendering and configuration of the Panama Canal lock entrances, modelling of the Ceres Paragon (ACT) indented berth and winch arrangements for bringing an aircraft carrier into a dry dock.

Rubber tyred wheel fenders would be located along the length of the dock and a combination of large winches at the head and entrance to the dock and mules on quayside rails will be used to draw the vessel in and assist its departure. To avoid large currents developing as the vessel moves in and out of the dock, the preferred form of quay construction is suspended deck over a revetment slope that will maximise the water area in the cross section. Alternate types of quay wall can be considered depending on the local geotechnical conditions but the width of the indented berth may need to be increased and/or scour protection measures introduced.

Experience from the Ceres Paragon indented berth demonstrated that tugs should be able to control the stern of the vessel within a reasonably sheltered waterway even without a lead-in jetty. However some form of lead-in is preferred to facilitate berthing and the layouts have shown that this can also be beneficial in providing additional near berth container stacking.

For all options:

- Vessels enter the indented berth “bow in” to minimise damage risk to propellers and rudders.
- Bunkering could be undertaken using a small barge moored at the stern of the vessel.
- Provisions can be delivered along a 4m wide 1-way service road immediately adjacent to the quay edge that can also be used as a route for direct delivery of containers to the quayside.

On arrival the incoming vessel will undertake a quarter point berthing with tug assistance against the outer end of the lead-in jetty. Bow lines will then be attached to a hauling system, based on Panama Canal experience as shown in Figure 14, with rails set along the top of the cope line on each side of the indented berth and tugs controlling the stern until the stern lines can be attached to adequately constrain the stern. It is anticipated that the lines will keep the vessel in the centre of the indented berth in a similar way to dry docking but roller fenders on each side will keep the vessel off the cope should conditions keep the vessel alongside. When the vessel is in position additional lines will be deployed to static bollards. The draw in and pull out operations are assumed to be completed within a total of 2 hours.

Because the cranes are already in place and do not need lowering into position, the unloading operation will commence without further delay. The positioning of the vessel during the offloading in the centre of the berth or against the fenders on one side of the dock will depend upon local preference or prevailing conditions.

When the vessel is ready to depart the static lines will be released and the inhaul operation reversed until the bow of the vessel is sufficiently clear of the indented berth entrance that the vessel can safely depart with tug assistance.

Figure 14: Panama Canal Hauling System

4.7 Vessel Improvements

Until now the beam of the vessel has been limited by the outreach of the ship to shore quayside cranes at the destination ports. This has placed a restriction on the vessel designers. The new system decouples the ship from the crane as additional width on an overhead crane is structurally far easier to achieve than on a cantilever, so the berth can be made wide enough even to allow for future larger ships. This gives freedom to naval architects to develop vessels with optimum length / beam / depth to maximise efficiency through the water, improve manoeuvrability or even to adopt wider, shallower profiles for routes with ports that find dredging too costly.

There is much to be done to coordinate the design of the next generation of mega container ships with the indented berth concept to secure even greater benefits for both shippers and port operators.

For example, the SSPC cranes proposed for the indented berth have double lifting beams which will unload alternate holds simultaneously. The efficiency of these cranes will be enhanced if the bridge and funnel structures have the same dimensions as the holds, i.e. if the hold separation is 14.8m then the bridge and funnel upstands should have the same dimension. Also, the position of these elements within the ship should be configured to allow minimum repositioning of the SSPCs during cargo handling. For a full cargo transfer with all holds to be accesed a good configuration would be 4 holds aft, 12 amidships and 8 hold forrard. As the crane height is determined by the highest level of the vessel, a reduction in the height of the bridge and funnel elements would be advantageous.

The position of containers loaded in the holds on arrival is a key driver in efficient handling. This will have to change with the new method of ship handling and compatibility will have to be sought with other terminals on the shipping route that might not yet be operating with indented berths.

5 COFASTRANS - PROOF OF CONCEPT

5.1 Indented Berth Layouts

A COFASTRANS installation might be a completely new all-indented multi-berth terminal or just the addition of a single new indented berth to augment and enhance the ship handling operations for the ULCVs adjacent to an existing terminal, with standard berths handling the smaller feeder vessels using standard SSG cranes. A module could be constructed on reclaimed or redeveloped land to include a single indented berth together with the high-density container storage stacks alongside. Whatever the layout, it is clear that efficient delivery of cargoes to both sides of the vessel has the potential to reduce turnaround times significantly, however this will require a complete re-appraisal of the navigation and landside operations within the terminal.

Many terminal layouts have been considered and reviewed; inevitably some of these have turned out to be more efficient than others. To demonstrate the concept, modular units of the indented berth, complete with the cranes, have been developed along with adjacent container stacking areas either parallel or perpendicular to the berth. Modules have then been assembled into 3 quite different scenarios to represent various contrasting types of terminal operations and these can easily be compared and contrasted with a view to further optimisation at a later stage. Preliminary throughput analysis of all these layouts has just focused on the operation of a single indented berth, because the interactions with the feeder berths and other indented berths would be terminal specific and will have to be assessed on a case by case basis.

It is also recognised that specific local circumstances will have to be used to guide the planning of layouts at particular terminals.

The general parameters have been taken as:

- Width inside indented berth between cope lines of 69m, giving 5m clearance on both sides to the present largest vessels with 59m beam and provide access to vessels with up to 66m width to be accommodated in future (this could be more if needed);
- Roller fenders installed along each side of the indented berth at 30m centres, projecting 500mm beyond cope line;
- Overall length of the indented berth is 490m including a triangular end over last 25m;
- Depending upon the exposure of the site, it is anticipated that, to maintain maximum utilisation, vessels will berth against a 200m long lead-in jetty,
- The portal crane rail gauge can be different but here is taken as 129m;
- It is anticipated that the crane beam support piles will be constructed as a combi or solid wall to retain the filling, with the 30m of suspended deck between the cope and the crane rails formed in order to permit escape of displaced water during the docking procedure;
- For all layouts a deck level of +5mCD has been assumed with high water at +3mCD and low water 0mCD.

It is assumed that vessels entering an indented berth will have been loaded efficiently to minimise the need for repositioning moves. In order to reach the boxes within a hold it is necessary to totally clear the boxes stored on the hatch cover and in an efficient operation all of the boxes on top of a particular hatch cover would be destined for import or transhipment at this terminal. When one hatch has been cleared and the hatch cover removed it is assumed that the columns of boxes will have been loaded so that particular columns hold all boxes for this destination. After one of these columns has been completely unloaded the first of the export boxes can be loaded, and at this stage the double cycling operation for this hold can commence. During double cycling period the unloading and loading will be balanced until the last “import” box is removed after which the single cycling operation will be adopted until the loading operation has been completed for that hold. As each crane is offloading 2 holds simultaneously then the 2 holds should have been unloaded and loaded in such a way that more or less the same number of moves is required for each.

One of the objectives of working the vessel with the SSPC is to completely work the 2 holds under the crane beams until all import containers, both above and below the hatches, are unloaded and the export containers loaded before moving on to the next designated holds.

5.2 Design Vessel

For the purpose of reviewing the effectiveness of the new crane and berth layout the following exemplar ULCV vessel similar to the Marie Maersk shown in Figure 15 has been used with the following assumed parameters:

- Max Capacity 18,270TEU;
- LOA 400 m; LPP. 385m; Beam 59 m;
- Max. Draught 16.5m; Lightest Operational Draught 10.5m; Height above keel 73m;
- Hatch covers are typically 14m x 12.8m.

Figure 15: ULCV

5.3 Conventional Crane Benchmark

On a conventional berth each SPP-SSG occupies a quay length of approximately 30m and, although they can be placed buffer to buffer, a nominal minimum gap of 15m is needed to permit independent adjustment of the crane over the centre of a bay. For a 400m long vessel, the fore-most and aft-most container stacks are spaced by approximately 320m, which means a maximum deployment of 8 SPP-SSG units. However, to allow flexibility it is normal practice for 6 cranes to be deployed on a vessel at major terminals. Each SSG can only put 1 hook over the vessel hold with typically 25, up to a maximum of 35, moves per hour, which, assuming a 6 crane operation might deliver as between 150 and 210 moves/hour of crane operation/berth. Assuming twin lift and an average of 1.6TEU/move, then between 240 and 336TEU/hr/berth may be possible. If we assume 100% exchange for a 19,000TEU vessel, unloading will take a minimum of 2.4 days and loading another 2.4 days. On many of the latest SPP-SSG cranes, tandem-twin lifting (4 TEU) is possible allowing TEU lifting rates to double and, in theory, the time for crane operations to halve. Double cycling, which involves loading and unloading in the same crane cycle, can also increase the handling rate and allowing the move rates to double during these periods.

5.4 Productivity Benchmark

Various handling rates are announced from time to time, for example the ECT Delta Terminal website on 28 October 2014 with 10,557 moves on a single ship with 150 moves per berth per hour of crane operation and on 5 October 2017 APL Tangier Med terminal used 8 Super-post-Panamax cranes on one vessel for 27 hours to perform 7,072 moves (262 moves/hour of crane operation). Inevitably in a competitive marketplace there is a lack of clarity and it is difficult to make direct comparison in performance without a robust benchmark.

JOC research in their 2014 white paper proposed using vessel log data recording the time of arrival and departure, which is referred to as “lines down” and “lines up” (JOC, 2014, 2017). The calculation of moves per hour between these two times is referred to as “unadjusted gross berth productivity” and includes any delays in commencement. Gross moves per hour for a single vessel call is defined as the total container moves (onload, offload and repositioning) divided by the number of hours for which the vessel is at berth. Productivity is defined as the average of the gross moves per hour for each call recorded during the reporting year. The best performing terminals in 2013 achieved an average of 152 gross moves/hour of berth occupancy for vessels larger than 8,000TEU.

In their 2017 paper JOC has sought to extend the port productivity to include berth productivity + waiting time + steam-in (harbour limits, all fast). It reports from 2016 data for the top 30 terminals the average was 1,300 moves in 25 hours which includes 3.6 hours average time waiting before berthing, 1.7 hours for steam-in time/all-fast and 1.0 hour before first container move. With regard to large vessels it records that the average was 2,430 moves which, assuming that these can be completed in the average 15.6 hours with 1 hour before 1st container move, may in 2016 have achieved an average of 146 gross moves/hour for the ULCV vessels excluding the steam in and waiting time.

It is, however, clear that the primary time constraint at the berth lies in the number of crane hooks that can be placed over the vessel and used effectively.

5.5 Layout A - Single Indented Berth

Figure 16: 3D View of Layout A

Here we are presenting the concept in its simplest form. Just one indented berth, as seen in Figure 16, probably installed at a port near to an existing container terminal, but it could be standalone by itself. On each side of the indented berth we have a layout that reflects the best and most modern container terminals, eg London Gateway or Kalifa Port with container stacks set perpendicular to the ship. This could have a high proportion of gate cargo, maybe with some transhipment to nearby terminals via truck transfers. The addition of a single indented berth could transform a terminal forming the first step in a longer-term masterplan development adding additional indented berths as demand increases.

The stacks on each side of the indented berth have a maximum storage capacity of 2,000 TEU per block with the 12 stacks giving a maximum storage of 24,000 TEU for each side. Additional blocks with similar dimensions are provided at the head of the indented berth giving additional storage capacity of 24,000 TEU and a total storage capacity of 72,000TEU for the berth on an overall land area of 72.5Ha.

Each stack has 10 wide by 40 long TEU ground slots (TGS) with the containers stacked 1 over 5 and managed by 2 ASCs working on a 30m rail gauge. Horizontal transport linking these stacks with the berth have been taken as 1 over 1 ALVs. These are 5m wide, so the apron areas on each stack are divided into 4 lanes, each 7m wide, with 4 TGS in each. It is noted that AGVs could also be used and, as these are narrower, 5 lanes could be provided on the aprons.

It is assumed that the arrangement of cargo on the vessel and in the stacks is managed to maximise efficiency of the SSPCs. The container stacks would normally be arranged prior to the arrival of the vessel with the designated export containers in the correct stack for its location on the vessel, and that there are sufficient empty bays to hold the import containers offloaded from the vessel. With 3 SSPCs at the berth, each would have access to 12 aprons and onshore storage capacity of 24,000 TEU/SSPC. In the case of 4 SSPCs, this would be 9 aprons and 18,000 TEU/SSPC.

Two different cargo handling cases have been considered In order to provide an indication of the performance of the Layout. Cargo 1 is an exceptionally large cargo transfer with over 21,000TEU and Cargo 2 is an average cargo transfer of about 4,500TEU (representing the average ULCV 2,430 moves from the JOC 2017 report). Both models assumed twin-lift spreader operation with an allowance of 2% for single TEU lift and SSPC average single cycle time of 140secs and double cycle time of 210secs. A summary is shown in Table 2.

	Cargo 1		*Cargo 2*	
Import	10,459 TEU		2,269 TEU	
Export	10,897 TEU		2,293 TEU	
Double Cycle	62%	62%	0%	0%
Number of SSPCs	3	4	3	4
Crane Operating Time	33 hrs	26 hrs	9.29 hrs	7.42 hrs
Berth Operating Time	35 hrs	27 hrs	11.29 hrs	9.42 hrs
Moves per Crane Operating Hour	327	415	262	328
Moves per Berth Occupancy Hour	299	385	215	258
ALVs required	24	30	24	30

Table 2: Indented Berth Estimated Performance Summary

5.6 Layout B - Indented Berth Pair

This layout, shown in Figure 17 with two indented berths and adjacent conventional berths for feeder vessels, is more complex and looks at maximising the interaction between the ship and the berth side container stacks which are aligned parallel to the berth with aprons at either end. A minimum separation between the indented berths provides adequate space for the required import, transhipment and export stacks.

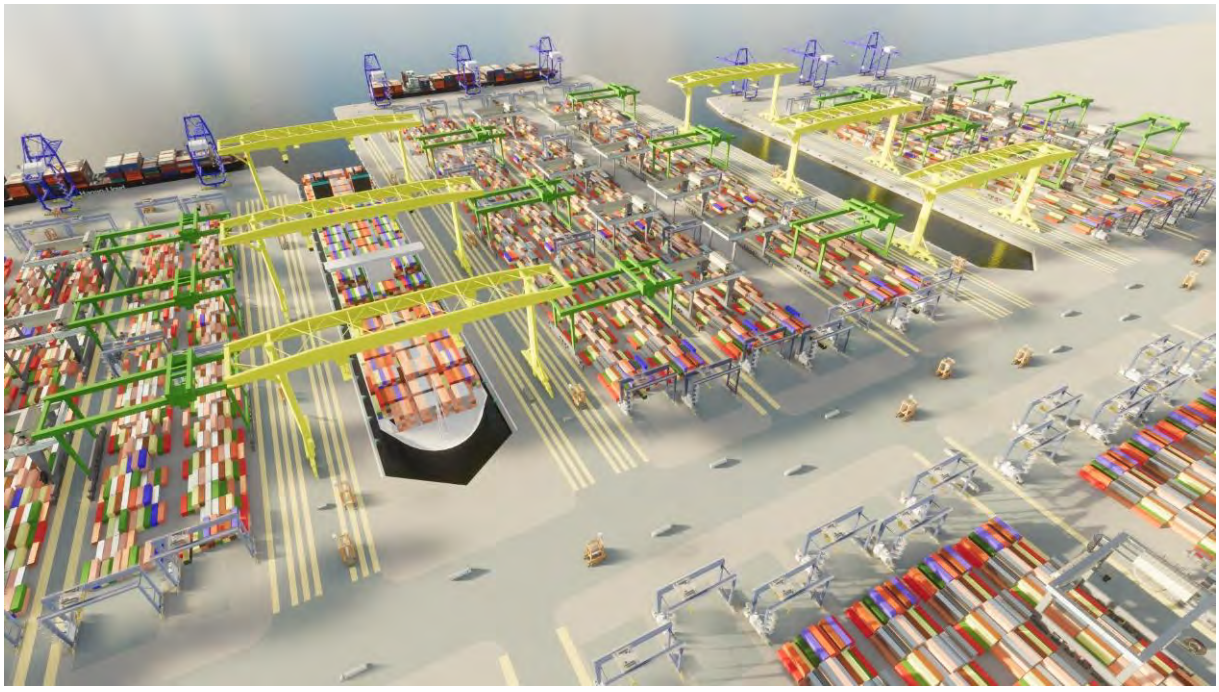

Figure 17: Layout B

The lead in jetty from Layout A has become an extension to one side of the indented berths and feeder vessel berths are provided for post-panamax vessels (7,000TEU with up to 42.5m beam) between the indented berths and for smaller vessels on the other side. All vessels longer than 350m LOA will be accommodated in the indented berths.

In this option the SSPCs spanning the indented berth still have a 129m gauge but, unlike the Layout A, the cantilevers on either side have a lift outreach of 16.6m rather than 25m. This is designed to permit the stacks on either side of the berth to be brought closer to the berth and will provide 3 runway lanes under the cantilevers, giving 6 runway lanes on each side of the berth.

In this case cantilever Rail Mounted Gantry cranes (RMGs) are used over the ASC stacks, working in combination to focus service to the STS cranes. To keep congestion to a minimum up to three different modes of transfer can be enabled. Firstly, the horizontal terminal transport would pick up / deliver from under the cantilever at the stack sides to enable the shortest journeys to the crane pick up zone. Secondly, service can be provided from the ends of the container stacks and the main driving lanes under the cranes. And thirdly in some cases there could be the option of direct transfer provided from RMG to STS crane, thus avoiding the need for some of the horizontal transport units.

This layout would suit a major transhipment terminal with existing terminals close by.

In this example (see Figure 18), the pairs of berthside container stacks served by the ARMG units have a maximum capacity of 5,600 TEU on one side (stacks B8 & B9) and 8,600 TEU on the other (stacks B6 & B7). (This based upon a 1 over 5 arrangement, but consideration could be given to further improvement with a 1 over 6 arrangement on these blocks). As the seaward section of B6 and B7 is primarily for containers on the feeder berth, it is assumed that about 60% of the containers for the indented berth will pass through stacks B6-B9. This means that during the unloading operation import containers will be required to be removed from these stacks and export containers brought in. It will therefore be necessary to provide additional ASCs in these stacks and additional ALVs to move import and export containers between stack B6 to B9 aprons and stack A7 to A12 aprons during the period while the vessel is occupying the indented berth.

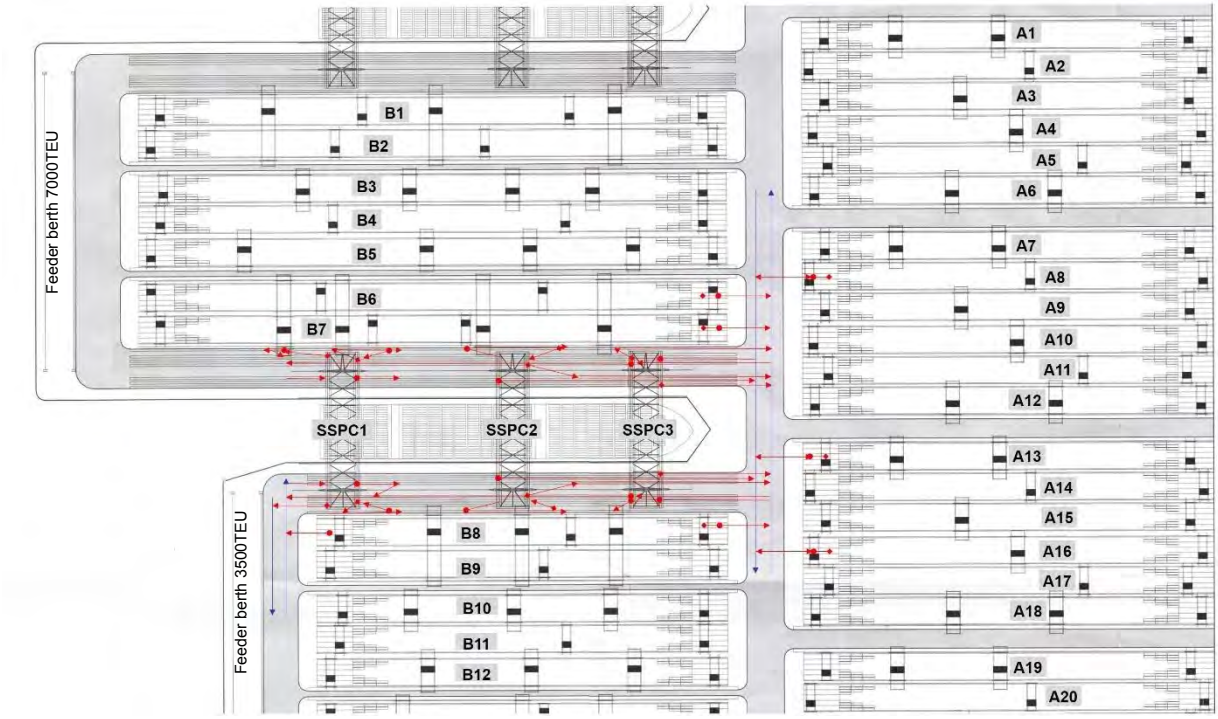

Figure 18: Plan with Indicative Traffic Moves

In order to accommodate the throughput from 3 SSPC cranes this example shows 4 ARMG units over stacks B6 and B7, receiving and delivering containers to/from cranes SSPC 1 and SSPC 2. Only 3 ARMG units will be required over the stacks B8 and B9 to service cranes SSPC1 and SSPC2, because the aprons at the feeder berth end close to SSPC1 can also be used. The SSPC3 crane at the shore end will be serviced from stacks A6 to A18 as for Layout A.

It is envisaged that during single cycle loading or unloading, one ALV will operate between each ARMG and the landing point in the outermost runway lanes of the SSPC1 and SSPC2 units. During double cycling two ALV units could operate a phased circular route, one clockwise and the other counter clockwise, with the 2nd ALV depositing the import containers under the ARMG after the 1st ALV has picked up the export containers from that machine. The 2nd ALV will then move to the 2nd ARMG to collect the next export containers just before the 1st ALV arrives with the import containers collected

from the SSPC unit landing point. To separate the routes, the outermost lane will be designated for landing points for export and imports from one ALV and the second lane for the other ALV. A similar circular route is envisaged between the B8 apron and the SSPC1 crane, but may require a 3rd ALV during double cycling. It is assumed that the ARMG cycle times will be close to the shortest cycle times for the SSPC units.

With ship handling performance as Layout A it is estimated that 28 ALVs will be required for 3 SSPCs and 32 ALVs for 4 SSPC.

5.7 Layout C – Multiple Indented Berths

For new very large ports the indented berth pair module can be expanded to provide a highly intensive operation with ship access to both sides of a central core. This would provide a high performance solution for some of the world's largest container ports of over (say) 20m TEU pa with berths lined up on both sides of a central storage area to facilitate fast transfer between many berths. A central spine road or other form of transfer system would be used to link with the off berth central storage areas.

The layout shown in Figure 19 considers a multi-indented berth terminal with high proportion of transhipment cargo.

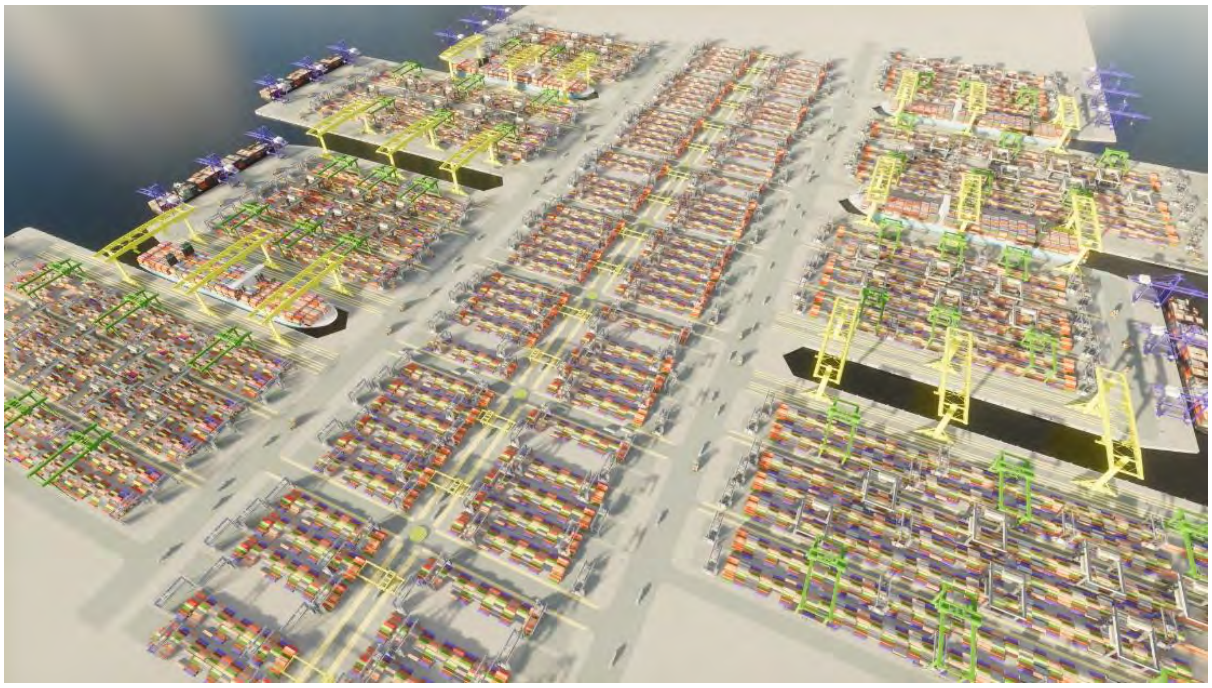

Figure 19: 3D View of Layout C

This is likely to be a transhipment hub, but there could be some local import and export with connections to the gate complex central from the main spine road. A modular layout of indented and feeder berths as shown in Layout B is mirrored on each side of this spine roadway. Operation of the berths would be as Layout B, although a stack arrangement similar to Layout A could also be possible.

One feature of this terminal example is that import and export boxes would be taken off or placed upon trucks using an ARMG spanning the central roadway by means of a rotating spreader to help reduce potential congestion. The ARMG will operated along groups of 6 stacks with ASC units from these delivering or removing boxes from the aprons under the cantilevers of the ARMG, then moving away before the ARMG is positioned. Trucks will be loaded/unloaded in runways on either side of the roadway inside the portal legs. Roundabouts will be provided at the cross roads between each group of block stacks to permit the unloaded vehicles to turn. When not required to unload or load vehicles the ARMGs will be used to transfer transhipment containers across the roadway to be adjacent to their allotted berth.

6 COFASTRANS - CONCLUSIONS

6.1 Benefits

Advantages of implementing a COFASTRANS terminal have been outlined above. The resulting benefits will vary from place to place, depending on a multitude of technical, operational and political factors at the designated port location. Here is a summary of the main points:

- Faster turnaround of big ships in port means that fewer ships are needed in the world fleet, resulting in cost and environmental savings.
- A more even traffic distribution can be created during cargo handling with access to both sides of the vessel at the berth, enabling shorter distances to the on-shore container stacks. This results in shorter journeys and fewer horizontal container movers on shore.
- An improved and more compact terminal shape can be created using a mix of indented berths interspersed with conventional berths for smaller vessels. This leads to a more efficient use of coastal land with more cargo throughput achieved in a smaller area.
- Improved safety, especially at the ship / crane interface with the crane leg set back from the quay edge, thus eliminating the risk of ship / crane contact.
- Eliminates the “beam bottleneck”, with options for developing even wider vessels.
- The berthed vessel would be better protected and likely to be less susceptible to motions from wind and hydrodynamic activity such as swell.
- Quayside construction is more efficient with only one crane rail within the structure and smaller loads per spreader.
- Cranes can operate at slower speeds with resulting improved maintenance profile and fatigue life.

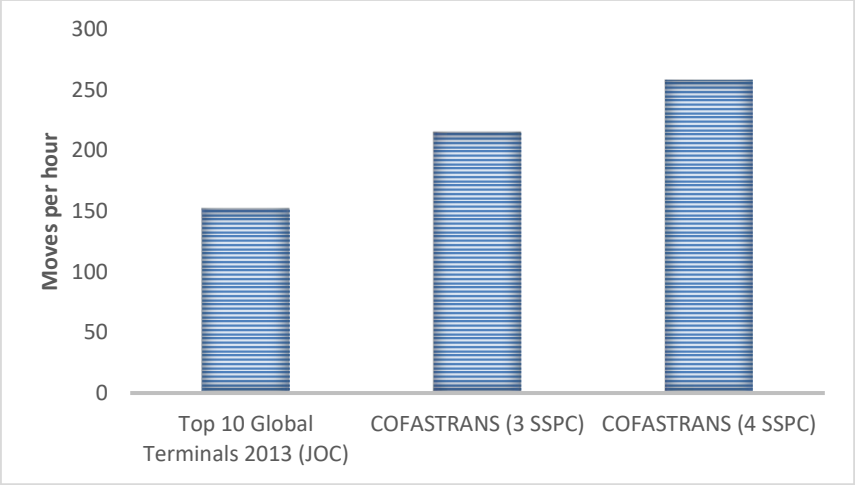

Figure 20: Port Productivity (Refer Section 5.4)

6.2 Challenges

While the benefits are clear, it is recognised that implementation of a COFASTRANS terminal is a major disruptive step. It is not easy to introduce change in a well established industry. The challenges that will be faced will be different across the world, here are some general points:

- This is a significant change in philosophy and will need foresight and confidence to take it to development.
- There is a large initial investment to create the first berth (which can be minimised by selecting the right location).
- Cargo loadplans for vessels will have to be worked out to be compatible with traditional terminal requirements as well.
- Owners of existing terminals that have recently invested heavily and suppliers of conventional equipment will have vested interest in maintaining the status quo.

- Navigation into indented berths may be new for a container vessel crew and will have to be optimised.
- A future proof width to the indented berth will have to be selected before construction.
- The available number of cranes on the berth will be fixed rather than the flexibility of transferring conventional cranes along a straight line berth.

6.3 Opportunities

Implementation of the COFASTRANS system can open up many different opportunities to port operators, shipping lines and wider users of the global container supply chain. Here are some aspects that could be explored further to provide further benefits at various locations:

- An all indented layout could be developed with vessels slotted into known positions.
- By aligning vessels precisely more automated methods for cargo handling can be developed.
- The system would be even more efficient when ships have been built to suit the indented berths.
- The system is a potential game changer in hub / direct call debate because of more efficient and faster loading and unloading of the largest ships.
- This will benefit the increasing number of ports that are in places where growth has become restricted either because of environmental sensitivity of the coastal strip or constraining urban development surrounding the port.
- The system is well suited to further development of double cycling operations.
- Ports with shallow draught restrictions could benefit from wider shallower vessels rather than over dredging.

6.4 Summary

While the concept is novel, it is practical and builds on previous work with adaptations from the latest container handling techniques combined with large crane technology from the shipbuilding industry. There will be challenges to overcome during implementation and making changes to the well-developed container handling industry. But the potential benefits are large, albeit complex to quantify because every port has different geography, historic facilities and customer needs. The COFASTRANS container handling solution addresses the challenge laid down a couple of years ago by the shipping lines on their unexpected introduction of the much larger vessels. A “step-change” was called for with an increase to 250 container moves per crane operation hour at each berth (up from about 150 / 160 at present). While various ideas have been proposed none have so far come close to achieving this aspiration. However COFASTRANS can exceed 300 berth moves per crane operation hour and, by using a more efficient layout, it can occupy a smaller amount of port land.

With more Mega container vessels coming into operation the time is now right for an in-depth discussion on the fundamentals of port layouts for these vessels, as shippers consider placing more orders and port operators seek to gain an advantage over their neighbouring competitors. The COFASTRANS terminal has now been enabled by the introduction of a new patented crane design that will substantially increase efficiency and performance.

Website online at: www.COFASTRANS.com

7 REFERENCES

Beckett Rankine. 2015. COFASTRANS Indented Berths Feasibility Study. Horizon 2020 SME Ph 1.

Davidson N. 2017. Time to Get Real on Container Terminal Berth Productivity? Linkedin.

JOC Port Productivity. 2014. Berth Productivity - The Trends, Outlook and Market Forces, Impacting Ship Turnaround Times.

JOC.com, IHS Markit. 2017. Port Productivity: Finding new efficiencies through collaboration.

Konecranes. 2018. Robotisation and Automated Terminals – COFASTRANS. Container Terminal Automation Conference, London.

Nevsimal-Weidenhoffer V. 2009. Portique Geant: PCT patent no. WO2009125127 A1.

Nevsimal-Weidenhoffer V, Tsouvalis N, Papazoglou V I. 2013. Goliath Gantry Cranes Their Steel Structure: A Neglected Element (including SP2000/SP2000 A New Concept of 2nd Generation Heavy Gantry Cranes for Shipyards). (http://users.ntua.gr/tsouv/Goliath_Gantry_Cranes/).

Nevsimal-Weidenhoffer V. Goliath Gantry Cranes - Extension of operational life of the structure (http://users.ntua.gr/tsouv/Goliath_Gantry_Cranes_Life_Extension/)

Nevsimal-Weidenhoffer V. 2017. New multi-trolley STS crane concept. PCT patent no. WO 2017071736 A1.

Nevsimal-Weidenhoffer V, Oja H. 2018. Next-Gen STS Cranes - A Model for The Future. www.porttechnology.org, Edition 77.

Rankine G A. 1998. Container Ship Docking. Ports and Terminals Group Conference London.

Rankine G A. 1999. Innovative Terminal Design – Developing Docking Systems. TOC ’99 Genoa.

Rankine G A. 1999 Keynote Paper: Developing a Container Vessel Docking System. MPA Seminar on Port Design & Operation Technology, Singapore.

Rankine G A. 2000. Harbour Layout. PIANC Harbours Meeting London.

Rankine G A. 2001. Next Generation Berth and Yard Layout. TOC Asia Hong Kong.

BERTH SCOUR PROTECTION FOR SINGLE & TWIN PROPELLERS

by

Martin Hawkswood[1], Josh Groom[2] and George Hawkswood[3]

1. ABSTRACT

Quay structures can be reduced by design using thinner scour protection. The performance of thinner protections as 'Sealed' or 'Open' to flow entry is described.

Established design methods for insitu concrete mattress and rock protections under single propeller action are reviewed. These methods are extended to twin propeller action based upon scale model testing undertaken. Comparison is made to current guidance by PIANC (2015) and PIANC (1997).

Vessels with twin propellers are outlined along with design implications for berths.

2. INTRODUCTION

2.1 Berthing Structures

Common types of berthing structures are shown in Figures 1 to 3. The progressive increase in vessel size has created a need for deeper berthing structures subjected to greater propeller actions.

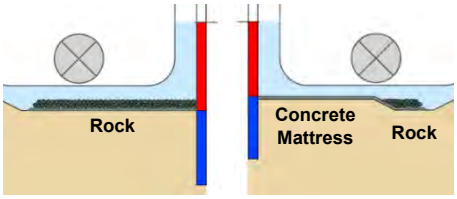

Figure 1. Piled Walls

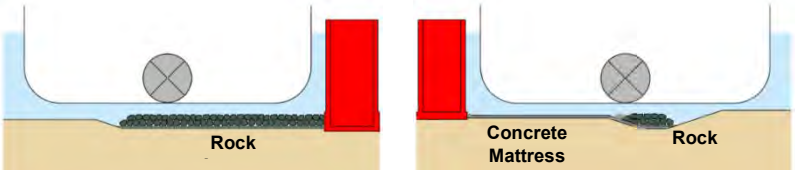

Figure 2. Caisson or Block Walls

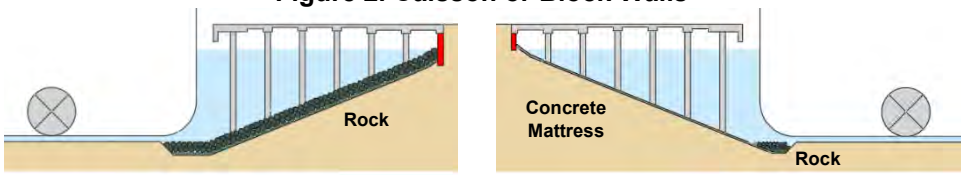

Figure 3. Open Piled Quays

Historically, rock protection has been the most common to berths but larger rock size is now often needed and the rock construction depth can significantly increase the size of piled walls and gravity walls (Figures 1 and 2), HAWKSWOOD, LAFEBER & HAWKSWOOD (2014). Significant savings can be made to these structures using thinner yet reliable mattress construction which is becoming increasingly understood. The use of insitu concrete mattress with rock falling edge aprons is often a beneficial combination. It is also effective for berth deepening projects to existing quay walls.

Open piled quays (Figure 3) can be constructed by the Land Infill method with insitu concrete mattress installed under completed piled platforms, HAWKSWOOD & KING 2016. This gives the prospect of savings in time and cost compared to construction involving marine plant.

[1] Director & Principal Engineer, Proserve Ltd, UK, office@proserveltd.co.uk
[2] Project Engineer, Proserve Ltd, UK, office@proserveltd.co.uk
[3] Maritime Civil Engineer, Mott MacDonald, UK, george.hawkswood@mottmac.com

2.2 Vessels with Twin Propeller

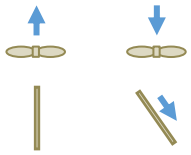

Figure 4. Plan of Crabbing Action

Twin propellers are common to ferries, cruise vessels, inland vessels plus many other types of vessel. Some recent large container vessels (Maersk Triple E) also have twin propellers to give better fuel efficiency, redundancy and manoeuvrability. Scale model testing using twin propellers has allowed greater understanding and improved guidance to be developed. Vessels with twin propellers often perform a 'crabbing' movement at berth with one propeller ahead and one astern with rudder deployment to move the stern sideways. Relatively high engine power can be used and high levels of scour can occur particularly where berths are near to turning areas.

2.3 Protection Types

The performance of mattress protection types largely depends upon whether it is 'Sealed' to flow entry as Figure 5 or with 'Open' joints and edges where higher trapped flow pressures can occur as indicated in Figure 6, HAWKSWOOD, FLIERMAN et al (2016). This aspect significantly affects performance, the protection thickness needed and design methods to be used. The constructability of various mattress types as a 'Sealed' protection are described in Sections 5 and 6, along with grouted rock described in Section 7.

Figure 5. 'Sealed' Protection

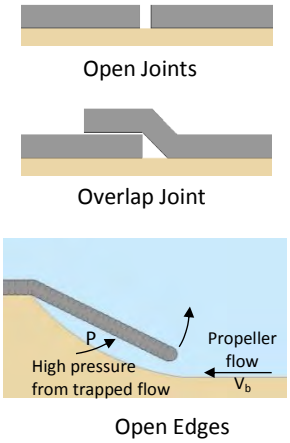

Figure 6. 'Open' Protection

2.4 Insitu Concrete Mattress

Insitu concrete mattress can be reliably installed as a 'Sealed' protection with suitable quality control, which is described in Section 5. Insitu concrete mattress forms a generic and consistent layer of plain concrete for which performance can be reliably predicted and design methods formed. Design methods by HAWKSWOOD, FLIERMAN et al (2016) for insitu concrete mattress under single propellers are presented in a simplified format in Section 5. Design examples for the combination of insitu concrete mattress and rock under both single and twin propellers are shown in Section 10.

2.5 Prefabricated Mattress

Prefabricated mattress types such as concrete block mattresses, asphalt mattresses and gabion mattresses are generally not a generic and consistent layer of material and vary by type, material, joints, manufacture etc. Reliable joints are more difficult to achieve when lowering heavy mattress in marine conditions onto harbour beds. A design method for flexible mattresses as an 'Open' protection by RAES et al (1996) is summarised in Section 6 along with references to some recent testing.

2.6 Rock Protection

The original design method by FÜEHRER & RÖMISCH (1977) was generally supported by previous scale model testing of rock protection by HAWKSWOOD, FLIERMAN et al (2016). This design method for single propellers will be reviewed in Section 8. An improved design method for twin propellers is also proposed in Section 8 following testing of rock subject to twin propeller action presented in Section 9.

2.7 Readership

The paper may assist with design and construction of berth scour protection, aid further testing, and development of design guidance. The paper may be of use to Port Authorities, Design Engineers, Contractors, Operators plus Research and Guidance Authorities.

2.8 Index

3. NOMENCLATURE

V_o	Max. propeller jet velocity	V_b	Bed velocity	L	Jet length
(c)	Propeller type, open/ducted	H_p	Height of propeller axis from bed	S	Propeller axis spacing
f	Ratio of engine power at berth	D_{min}	Design protection thickness	SF	Safety factor
P	Engine power	u	Surface undulation	C_L	Stability Coefficient (Raes *et al,* 1996)
ρ	Density	w	Width between undulations		
D_p	Propeller diameter	I_Q	Surface undulation factor	D_{S50}	Rock size (sphere), 50%
n	No. of propeller revolutions/s	C_S	Stability coefficient for suction	B_S	Stone stability coefficient
K_T	Propeller thrust coefficient	g	Acceleration due to gravity	P_Y	Offset factor for stone size
C	Propeller tip clearance	Δ	Buoyant relative density	Y	Offset distance
R	Propeller radius	C_F	Stability coefficient for flow		

4. PROPELLER ACTION

4.1 Propeller Jet Velocity

Jet flow constricts behind open propellers where the maximum jet flow occurs. In berths the maximum jet velocity normally occurs when the vessel is stationary or slow moving, typically during unberthing and can be calculated from the established formula (1): -

Maximum propeller jet velocity $$V_o = (c)\left(\frac{f\ P}{\rho\ D_p^{\ 2}}\right)^{1/3} \quad (1)$$

Where:		
	Coefficient for open propellers	(c) = 1.48
	Coefficient for ducted propellers (with Kort Nozzles)	(c) = 1.17
	Propeller diameter (m)	D_p
	Engine power (kW)	P
	Ratio of engine power at berth	f
	Water density, Sea water 1.03 t/m^3	ρ

This equation is commonly used with guidance for the ratio of engine power at berth taken from PIANC Report 180 (2015) and PIANC WG22 (1997). Alternatively, where the maximum propeller revolutions and propeller thrust coefficient K_T are known, the established formula (2) usually provides more accuracy: -

$$V_o = 1.6\ n\ D_p\ \sqrt{K_T} \quad (2)$$

Where:		
	N° of revs. per second (rps)	n
	Propeller thrust coefficient	K_T

A design berthing event is usually the occurrence of low clearance and a design vessel action, as shown in the probabilistic approach outlined in HAWKSWOOD, FLIERMAN et al (2016).

Ship simulation is increasingly used to model vessel movements in berths and harbours. This can help determine the engine power or propeller revolutions for design conditions in particular harbours.

4.2 Bed Velocity

The maximum bed velocity V_b is dependent upon the maximum propeller jet velocity V_o, propeller type, the propeller clearance ratio C/R and whether a central rudder is present behind the propeller, as is most common. A central rudder splits the rotational flow into two jets and creates higher bed velocity as indicated in Figures 7 and 8 from CFD modelling by Marin, HAWKSWOOD, LAFEBER & HAWKSWOOD (2014).

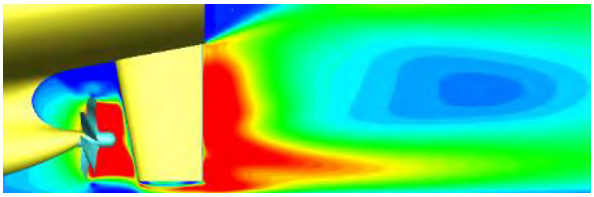

Figure 7. Velocity – *With Straight Rudder*

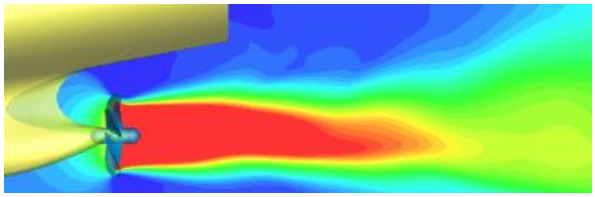

Figure 8. Velocity - *No Rudder*

For single propellers, bed velocities can be taken from Figure 9 based upon graphs from the original work by FÜHRER & RÖMISCH (1977) and PIANC BULLETIN 109 (2002). This method adequately takes into account the significant effect of a central rudder HAWKSWOOD, FLIERMAN et al (2016).

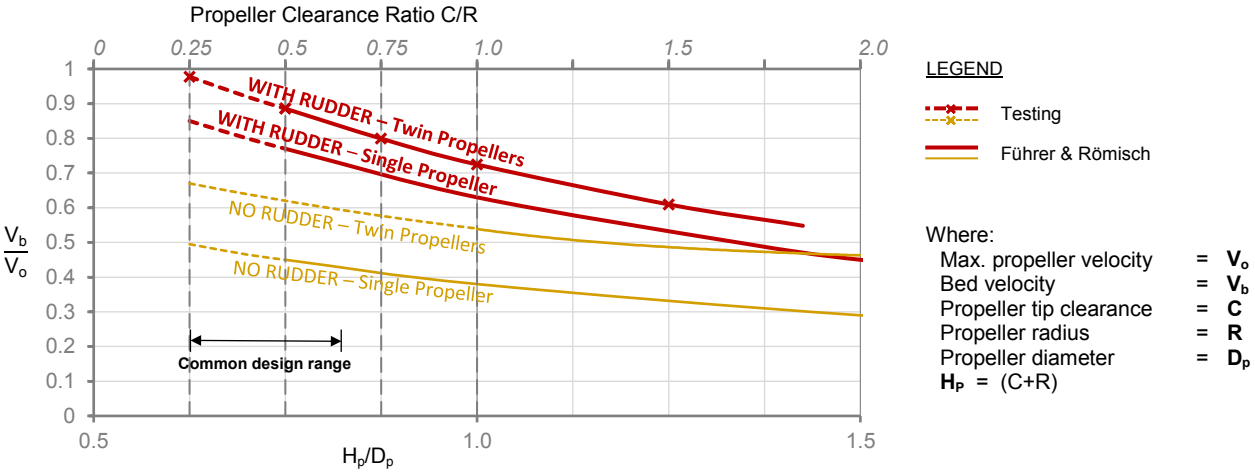

Figure 9. Bed Velocity, V_b Graph

Twin propeller jets combine and this creates higher bed velocities than for a single propeller. Figure 9 also shows recommended bed velocity established from testing, as Section 8.2. It also incorporates guidance from Führer & Römisch given in PIANC Report 180 (2015) Equation 8-34 for twin propellers with no central rudders and C/R > 1. This is supported by recent testing, MUJAL-COLLILES et al (2017). Bed velocities determined by Figure 9 are the basis of design methods for insitu concrete mattress and rock scour protection in the following sections.

The bed velocity for ducted propellers (with Kort nozzles) can be estimated from PIANC Report 180 (2015). Established guidance is not known to be readily available for ducted propellers with central rudders. It is suggested that Azimuthal thrusters (pushers) can be taken as open or ducted propellers as the case may be, without a rudder. Azipods (pullers) can conservatively be taken as open propellers with a central rudder as suggested by HAWKSWOOD, LAFEBER & HAWKSWOOD (2014) until testing guidance becomes available.

4.3 Hydrodynamic Bed Loads

Examples of hydrodynamic loads upon a bed are shown in Figures 10 and 11 from scale model testing conducted at Marin, HAWKSWOOD, LAFABRE & HAWKSWOOD (2014). A large area of bed suction occurs in front of propellers and impermeable protections need to be designed for this effect.

Behind the propeller, hydrodynamic loads upon the bed are higher but more variable. Areas of standing suction and pressure combine with fluctuating waves of suction and pressure in the propeller jet.

For a single propeller with a rudder, the flow is split by the rudder and has relatively low turbulence initially which then increases as the jet velocity decays.

For a single propeller with no rudder, the velocities reaching the bed are much lower but with higher turbulence and rotation.

The hydrodynamic distribution upon the bed is not symmetrical and is dependent upon the direction of rotation of the propeller. For twin propellers, inward and outward propeller rotation combines these different effects.

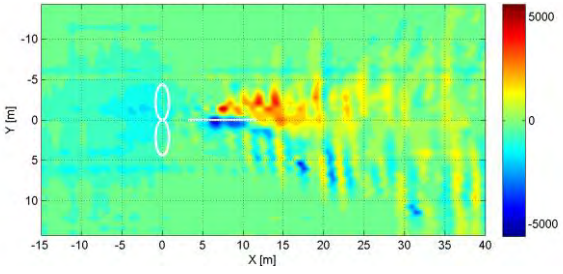

Figure 10. With Rudder

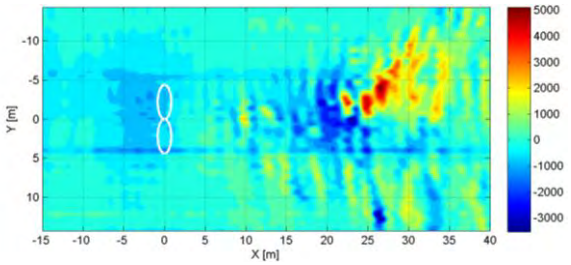

Figure 11. Without Rudder

5. INSITU CONCRETE MATTRESS

5.1 Introduction

Insitu concrete mattress aprons resist vessel actions to harbour beds and slopes. A rock falling edge apron is often used in erodible strata to provide a 'Sealed' edge detail as Figure 12. Constant Thickness Mattress types (CT) as Figure 13 are normally used to beds and permanently submerged slopes. Porous mattress types are needed to wave zones, HAWKSWOOD & ASSINDER (2013).

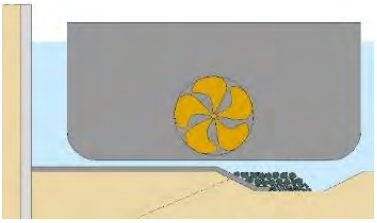

Figure 12. Typical Section

Insitu concrete mattress aprons are formed by divers rolling out mattress fabric underwater (Figure 14) which is zipped together and pump filled with highly fluid small aggregate concrete. The fluid concrete is protected from wash out by the mattress fabric. The system typically comprises two layers of woven fabric interconnected with thickness ties as shown in Figure 13. The fabric mattress is essentially a temporary works system. Joints between mattress panels are formed using zipped or sewn 'ball and socket' concrete shear joints, Figure 13. CT mattresses are typically pump filled with a sand: cement micro concrete mix of 35 N/mm² strength. This produces an apron of interlocked plain concrete slabs underwater. Seals to walls are achieved by using a concrete bolster detail as Figure 15. For sheet piled and combi walls, any inpans are infilled with tremie concrete.

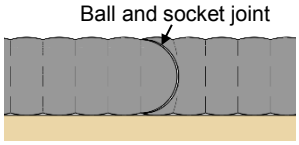

Figure 13. Constant Thickness Mattress (CT)

Figure 14. Lowering mattress to be rolled out by divers

Concrete mattress is generally installed without the need for marine plant by divers working from the quay. Installation is not practical in currents above 0.5 m/s. Concrete mattress has a high durability and abrasion resistance created from the 'free' water bleed of the fluid mix through the fabric resulting in a low water: cement ratio at the surface. Mattress panel widths are typically some 3m to 5m due to the weaving process. A 200mm minimum thickness is recommended to berth beds to cater for controlled maintenance dredging. For protection in more critical locations such as at gravity wall foundation levels as shown in Figure 2, thickness is often increased to 300mm for increased robustness.

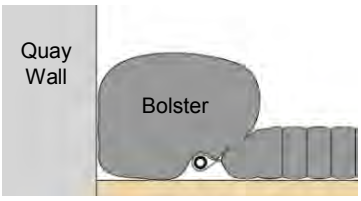

Figure 15. Wall Bolster Seal

Residual ground water movement may occur under quay structures, piling or slopes created by tidal movement etc. Weep holes can be provided to provide low porosity to cater for these effects. For soils, a geotextile should be provided to the bottom of the weep holes to retain fines, with the weep-hole size and spacing designed to suit. Most berths are dredged into natural ground strata where bed soils will have been previously over consolidated and are therefore not generally prone to settlement. In these cases, no precautions for mattress flexibility have been required, with mattress panels extending the width of the apron. In filled ground, or other cases where settlement or heave is an issue, the mattress panel size can be reduced to increase flexibility HAWKSWOOD, LAFEBER & HAWKSWOOD (2014).

5.2 Marine Quality Control System

Work in the marine environment benefits from good skills, experience and procedures. Insitu concrete mattress can be reliably installed as a 'Sealed' protection using a proven marine quality control system, overseen by professional engineers with experience in the system. This should be specified and typically includes: -

- assessment of working conditions
- risk analysis
- concrete mix development
- mattress layouts, fabrication drawings
- temporary works design
- method statement
- installation training, demonstration trials
- bed preparation control
- quality control record system
- supervision (possible check diving)

This specialist engineering is normally provided by manufacturers who should have professional engineering capability and proven performance, which should be specified.

This insitu concrete mattress system is described in PIANC Report 180 (2015) along with the need for a suitable marine quality control. Insitu concrete mattress, reliably installed, can be used for high

velocities. It has been used as berth protection to HSS vessels resisting inclined jet action upon the bed up to some 12 m/s, HAWKSWOOD, EVANS & HAWKSWOOD (2013).

5.3 Design Introduction

Insitu concrete mattress under propellers should be designed for:

- propeller suction
- propeller flow

Design methods for both propeller suction and propeller flow are taken from HAWKSWOOD, LAFEBER & HAWKSWOOD (2014) and relate to 'Sealed' protection with the following parameters: -

- sealed joints and edges (protected from underscour)
- concrete panels 3 to 5m wide between interlocked joints
- concrete strength 35 N/mm^2 (MPa)

Design for propeller suction is based upon work by Wellicome originally provided in HAWKSWOOD & ASSINDER (2013) as referred to in PIANC Report 180 (2015). At lower clearance ratios C/R, suction is usually the design condition for vessel actions. Where protection is offset from propeller locations, it should be designed for rudder deflected flow which is usually greater than bow thruster effects for larger seagoing vessels. Concrete mattress should be designed and constructed with suitable safety factors and robustness.

5.4 Surface Undulation Ratio

The spacing of mattress thickness ties *w* controls the surface undulation u as shown in Figures 16 and 17. The surface undulation ratio is given by u/w. Higher surface undulation increases hydrodynamic loading and reduces load distribution ability due to stress concentrations, HAWKSWOOD, LAFEBER & HAWKSWOOD (2014). Figure 18 shows an example of low surface undulation ratio with spacing of thickness ties at 100 mm centres.

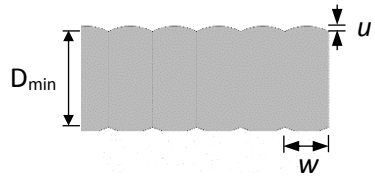

Figure 16. Low Surface Undulation

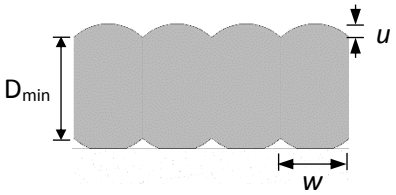

Figure 17. High Surface Undulation

Figure 18. Low Surface Undulation

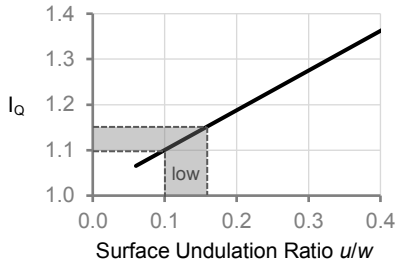

Figure 19. Surface Undulation Factor I_Q

The surface undulation factor I_Q for design is taken from Figure 19 and is related to the undulation ratio *u/w*. Mattress with low surface undulation ratio of 0.1 to 0.16 as Figure 16 are preferred and should be specified as they are subject to lower suction loads and distribute loading better. Mattress types with higher undulation ratios as Figure 17 are less effective and need a greater thickness.

Insitu concrete mattress is specified by:-

- Design thickness D_{min}
- Tie spacing w and I_Q value

Both of these should be verified during initial trial sample filling on site.

5.4 Design for Propeller Suction – Single Propellers

Insitu concrete mattress has good load distribution properties and is designed for the large area of bed suction which occurs to the intake side of a propeller as outlined in Figure 20 and shown in Figures 10 and 11.

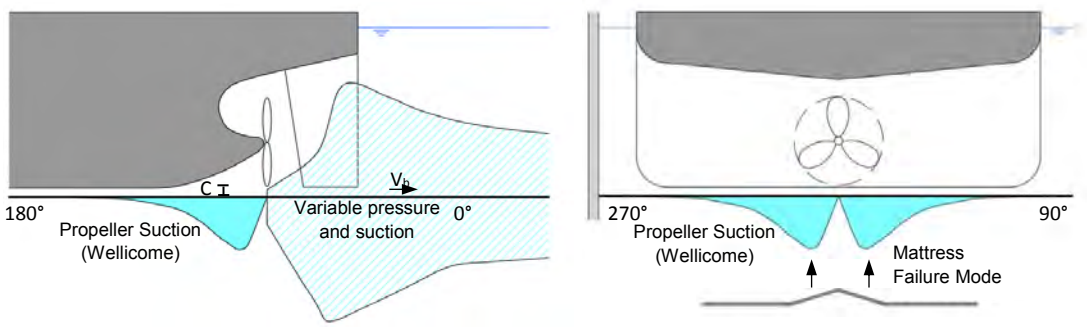

Figure 20. Propeller Suction

The dead-weight design method by HAWKSWOOD, LAFEBER & HAWKSWOOD (2014) is used for 'Sealed' protection, based upon the propeller exit velocity V_o, and is presented in a simplified format below: -

Simplified dead-weight design method

$$D_{min} = C_S \frac{V_o^2}{2\,g\,\Delta} \times \frac{I_Q}{1.15} \qquad (3)$$

Where: Stability coefficient for insitu concrete mattress propeller suction C_s
Mattress surface undulation factor (Figure 19.) I_Q

The stability coefficient for propeller suction C_S is taken from Figure 21. Propeller suction upon the bed reduces as the bed clearance ratio increases.

This method applies to open propellers with or without a rudder. For ducted propellers (with Kort nozzles), the original design method in HAWKSWOOD, LAFEBER & HAWKSWOOD (2014) should be followed.

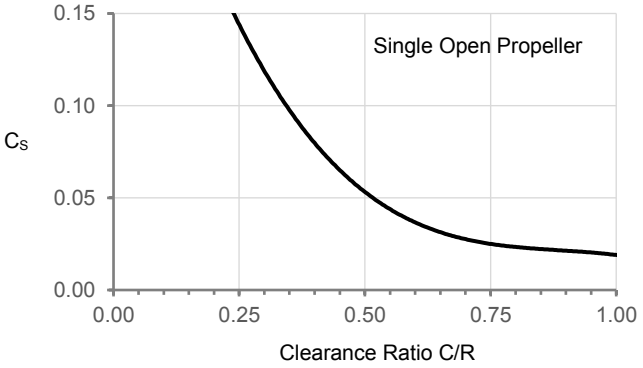

Figure 21. Propeller Suction Coefficient Cs

5.5 Design for Flow – Single Propellers

The design method for 'Sealed' insitu concrete mattress under propeller flow as Figure 22 is based upon the maximum bed velocity V_b as below:-

$$D_{min} = C_F \frac{V_b^2}{2\,g\,\Delta} \times \frac{I_Q}{1.15} \qquad (4)$$

Where: Stability coefficient for insitu concrete mattress under propeller flow C_F
Mattress surface undulation factor (Figure 19.) I_Q

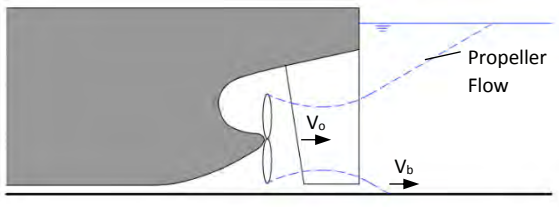

Figure 22. Propeller Flow

Design Condition	C_F
With rudder, Level beds	0.12
With rudder, Slopes + variable bottom	0.16
No rudder, Level beds	0.19
No rudder, Slopes + variable bottom	0.23

Table 1. Mattress Flow Coefficient C_F

The coefficient for propeller flow C_F can be taken from Table 1. This is based upon performance examples by PILARCZYK (2000), HAWKSWOOD & KING (2016) plus recent testing shown in Section 5.9. A variable bottom is assumed when bed undulations/ construction tolerances exceed 600mm. Where bed forms cause large areas of accelerated flow and suction, uplift can be estimated using Bernoulli's equation and mattress thickness designed accordingly.

5.6 Rudder Deflected Flow

Where protection is offset from the propeller, as with open piled quays (Figure 23), the protection should be designed for flow from deflected rudders, PIANC WG22 (1997).

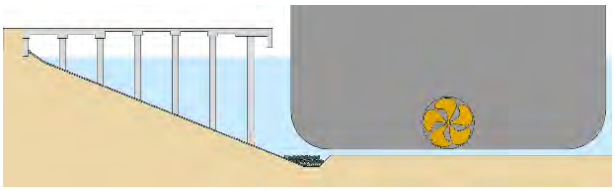

Figure 23. Open Piled Quay

Standard rudder types to container and seagoing vessels typically rotate to 35° with oil tankers often to 45°. Greater rotation is obtained from 2 stage (Becker) type rudders. Flow deflection is taken as 0.9 x the rudder rotation as shown in Figure 24, HAMILL et al (2009).

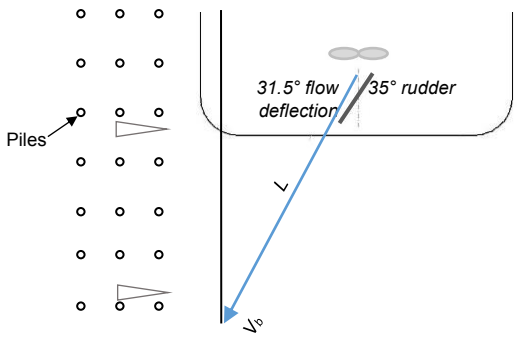

Figure 24. Rudder Deflected Flow

The propeller jet velocity is slowed by maximum rudder rotation by an approximate factor of 0.85, BAW (2010). To estimate bed velocity V_b at offset locations, this factor can be used along with the established propeller jet decay formula, from PIANC Report 180 (2015) Eq (1) for single propellers as shown in (5): -

$$\text{Bed velocity at offset locations} \qquad V_b = 0.85 \times V_o \times \frac{2.6\, D_p}{L} \qquad (5)$$

Where: Jet length (to offset location) L (For $L > 2.6\, D_p$)

To design insitu concrete mattress around piles, the increased velocity due to blockage of the piles should be used in (4) and the thickness further increased by ratio of the blockage velocity to approach velocity, HAWKSWOOD & ASSINDER (2013). Concrete mattress should be installed on stable slopes as it does not increase slope stability. Further guidance on construction is given in HAWKSWOOD & KING (2016).

5.7 Design for Propeller Suction – Twin Propellers

The suction distribution for twin propellers can be taken by combining the suction distributions for single propellers as shown in Figure 25. Analysis for various clearance ratios C/R and propeller shaft separations enables the stability coefficient Cs for insitu concrete mattress and twin propeller suction to be taken from Figure 26. This allows mattress thickness to be calculated from (4). This method is confirmed by recent testing. Section 5.9.

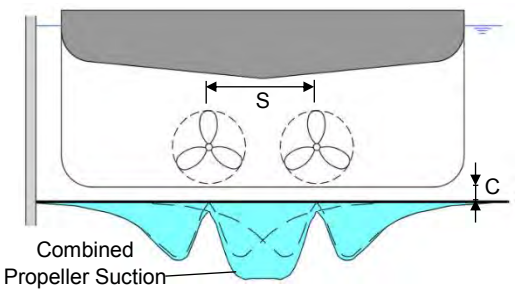

Figure 25. Suction Distribution - Twin Propellers

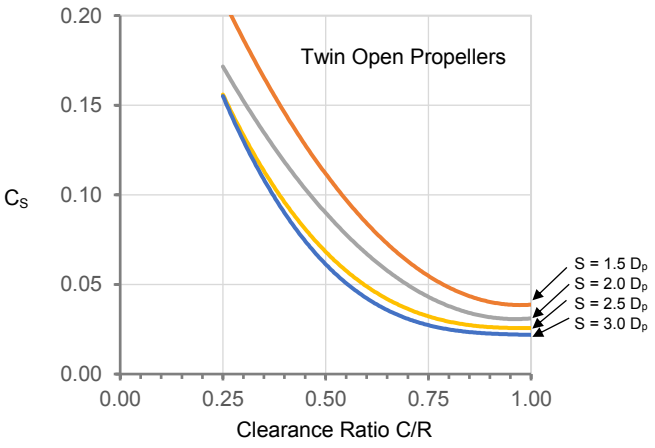

Figure 26. Suction Coefficient Cs - Twin Propeller

5.8 Design for Propeller Flow – Twin Propellers

For insitu concrete mattress under twin propellers, the maximum bed velocity V_b can be taken from Figure 9 and stability coefficients for flow C_F as Table 1 for single propellers. The design mattress thickness can then be obtained from (4). This basis has been confirmed by recent testing presented in Section 5.9. If bed tolerances are greater than 0.6m, coefficients for variable bottom should be taken.

5.9 Scale Model Testing of Insitu Concrete Mattress – Twin Propellers

The test mattress had a strength and Young's Modulus replicated approximately to scale with interlocking joints. Scale model testing of insitu concrete mattress was undertaken as described in HAWKSWOOD, FLIERMAN et al (2016) for previous testing under single propeller action. Previous testing under single propeller action did not create failure but established a safety factor SF > 2.8 for propeller suction and a SF > 2.1 for propeller flow when compared to the design methods proposed. The simplified deadweight design method (3) for propeller suction has a nominal safety factor of 1.5 included but this excludes flexural capacity of the concrete apron and other stabilizing effects.

Figure 27. Test Arrangement

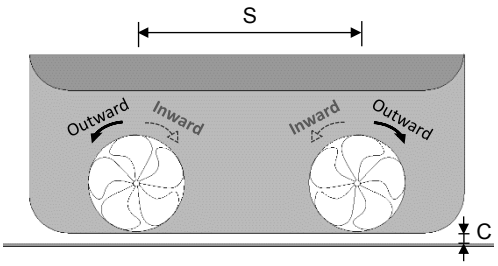

Figure 28. Test Arrangement, Rear View

The test arrangement for twin propellers is shown in Figures 27 and 28. For propeller suction, safety factors of greater than 2.8 and 5.3 were obtained without failure being reached as shown in Figure 29 for the worst case propeller separation S=1.5 D_P. The comparison is based upon the design method given in Section 5.8. Both inward and outward propeller rotations were tested, although this is not considered to be a significant influence.

For propeller flow, safety factors SF greater than, 5.0 and 6.4 were obtained for the various conditions shown in Figure 30. The tests included the conditions with and without a rudder. The test conditions were for a worst case propeller separation S=1.5 D_P and comparison based upon the method given in Section 5.8.

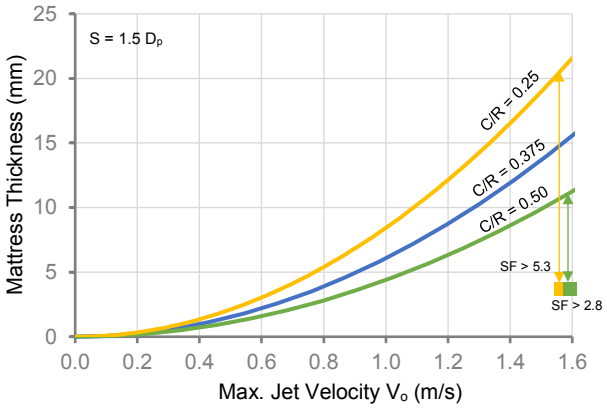

Figure 29. Suction – Twin Propeller

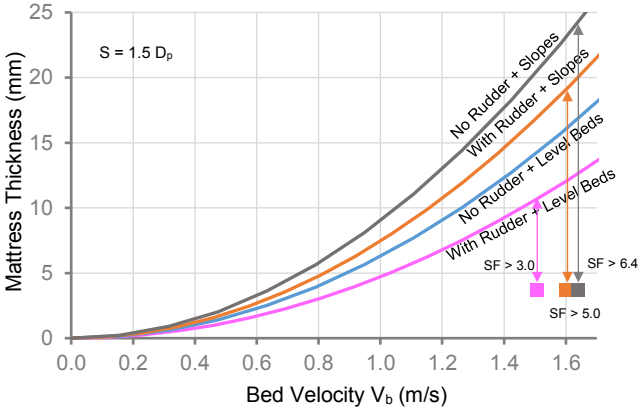

Figure 30. Flow – Twin Propeller

The testing indicates the design methods for both suction and flow have safety factors well above 2 for 'Sealed' protection.

6. PREFABRICATED MATTRESS

Precast concrete block and asphalt mattresses can be prefabricated with good quality control and offer the prospect of rapid installation, however installation often requires heavy marine plant and lowering presents an entrapment risk to divers during placement. Also, joints with reliable performance are more difficult to form working on the seabed. Prefabricated mattress performance is normally dependent upon the following: -

- Joints and edges
- Material
- Reinforcement / Ties
- Manufacturers mattress arrangement

RAES, ELSKENS, RÖMISCH & SAS (1996) provided a formula (6) for the stability of thin flexible bottom protections determined by experiment for overlapping or open joints and underscoured edges:-

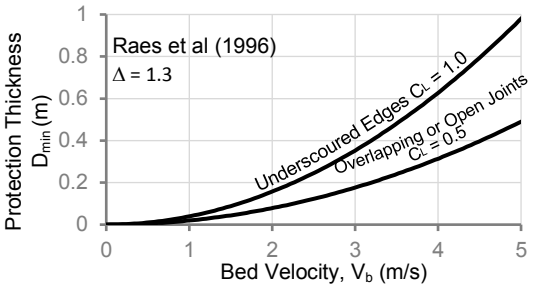

Figure 31. Open Mattress Stability

$$\textit{Thickness, } D_{min} = \frac{C_L V_b^{\,2}}{2\,\Delta\, g} \times I_Q \qquad (6)$$

Where C_L = 0.5 for overlapped or open joints and C_L = 1.0 for underscoured edges. The resulting thickness design curves are shown in Figure 31. This method can be compared to Bernoulli's equation applied to trapped flow pressure. Previous scale model testing of an example concrete block mattress by HAWKSWOOD, FLIERMAN et al (2016) indicated a safety factor SF of the order of 1.5 for both joints and edges, Figures 32 and 33.

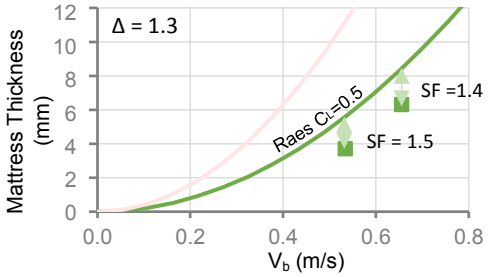

Figure 32. Testing of Block Matt – *Joints* Single Propeller

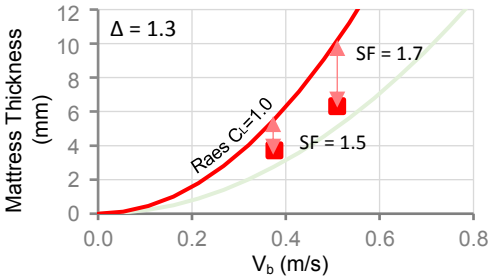

Figure 33. Testing of Block Matt – *Edges* Single Propeller

It has been common past practice for prefabricated mattress to have unprotected edges and failure by rolling up of edges has been reported. For propeller flow and scour depths now commonly occurring, suitable edge protection details are needed. Recent testing at Deltares by VAN VELZEN, DE JONG et al (2016) replicated likely bed tolerances and reported lower performance than estimated by Pilarczyk's formula, (PIANC Report 180 (2015). Pilarczyk's formula does not adequately take into account 'Sealed' and 'Open' conditions and the parameters were estimated and not validated for propeller flow, PILARCZYK (2011).

Design methods could be developed for particular types and manufacture of prefabricated mattress from scale model tests taking into account the worst condition of joints and edges likely to be achieved in projects, supported by case history performance.

7. GROUTED ROCK

Typically a rock layer is placed over a geotextile which is then pump in-filled typically with grout or tremie concrete. However, it is difficult to use on sloping areas and toe trench slopes to form important embedded edge details. Grouted rock is common in northern Europe where specialist skills in its reliable use are more available. There are some construction and environmental aspects to overcome for reliable berth protection, HAWKSWOOD, LAFEBER & HAWKSWOOD (2014).

For propeller action, if the protection is reliably constructed as a 'Sealed' protection, then the thickness design method for insitu concrete mattress can be used taking into account appropriate surface roughness and allowance for construction thickness tolerances.

8. ROCK DESIGN

8.1. Introduction

Rock protection generally comprises two layers of rip rap or armour stone upon a bedding/filter stone layer and often a geotextile filter membrane (Figure 34). The design, specification and construction of the rock protection can follow authoritative guidance by FÜHRER & RÖMISCH (1997), PIANC Report 180 (2015) and PIANC WG22 (1997) as outlined in earlier sections. The Rock Manual (2007) and PIANC WG22 (1997) give useful construction guidance. Rock protection has many good qualities, being porous and flexible; it performs well as falling edge aprons and is relatively easy to repair unless the bedding layer is lost. Rock protection often needs to be grouted at walls and structures to prevent wash out from flow down or along walls. (Figure 34). Rip rap stone with a wider grading than armour is generally preferred for lower flows as it can be mass placed by excavator bucket etc. rather than individual placement of armour stone PIANC WG22, (1997). Rock protection can be installed in modest currents. The rock construction depth can have a significant effect on structures, increasing the effective span height to piled walls, Figure 1, and increasing the depth of gravity walls, Figure 2.

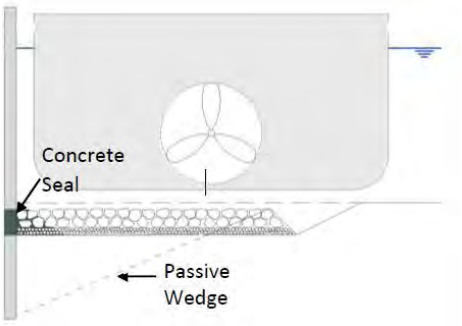

Figure 34. Rock Protection

Design of rock for no movement is particularly important where rock movement would cause grounding or loss of berthing clearance.

8.2. Level Bed Protection under Single Propellers

Design methods for rock stability have generally been based upon the 'threshold of motion' for no movement or scour. The most common design method emanates from the original testing work of FÜHRER & RÖMISCH (1977) who produced curves for bed velocity V_b as partly reproduced in Figure 9. They also provided a formula for rock protection size with no movement BAW (2005) as (7) below: -

Rock size, with no movement

$$D_{s50} = B_s \frac{V_b^2}{g\,\Delta} \qquad (7)$$

Following recent testing, the following stability coefficients B_S are proposed: -

With Rudder	$B_S = 0.64$	FÜHRER & RÖMISCH (1977), BAW (2005)
No Rudder	$B_S = 1.55$	HAWKSWOOD, FLIERMAN et al (2016)

The above method and stability coefficients were generally well supported by recent testing by HAWKSWOOD, FLIERMAN et al (2016). The stability coefficient for no rudder of $B_S = 1.23$ by FÜHRER & RÖMISCH (1977) was found to be too low.

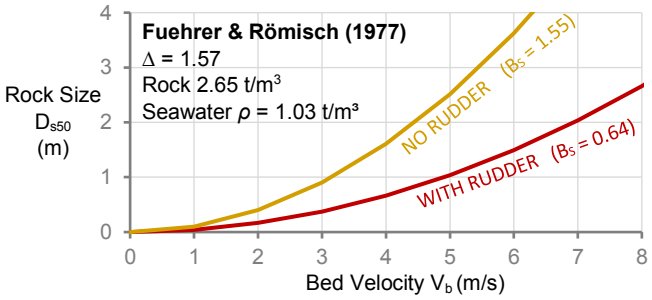

Figure 35. Stone Size for Vessel Actions

The relationships of rock size D_{s50} to bed velocity V_b are shown in Figure 35 for the general case with a central rudder behind the propeller, and with no rudder. The higher stability coefficient B_S for no rudder is created by the increased rotation and turbulence within the critical area of the flow acting upon the bed

The recent testing also showed that propeller tip clearance C can be taken from the centre of the top layer of rocks as Figure 36, HAWKSWOOD, FLIERMAN et al (2016). This takes into account the increasing stability effect for larger rock sizes which has been demonstrated in testing. This effect can make a useful saving to larger rock sizes.

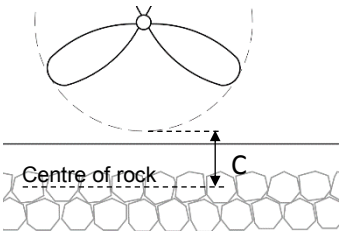

Figure 36. Propeller Tip Clearance, C

The method following Führer & Römisch's original work is termed the German method in PIANC Report 180 (2015) but with D_{85} used for stone size and a more conservative formula used for calculation of bed velocity. The design method termed the Dutch method has been found to underestimate bed velocity and rock sizes, particularly the effect of rudders, HAWKSWOOD, FLIERMAN et al (2016).

8.3. Rudder Deflected Flow

Where rock protection is offset from the propeller, such as open piled quays as Figure 37, the stone size should be designed for rudder deflected flow PIANC WG22 (1997). This is usually greater than bow thruster flow for seagoing vessels. A design method for rock size can be used by HAWKSWOOD, FLIERMAN et al (2016) for a single propeller with a level bed, and a standard rudder rotation of 35°, as shown in Figure 38 and the relationship given in (8) below:-

$$\text{Offset rock size } D_{s50} = \text{Rock size directly under the propeller } D_{s50} \times P_Y \quad (8)$$

Where: Offset factor P_Y
Offset distance Y
Offset ratio Y/D_P

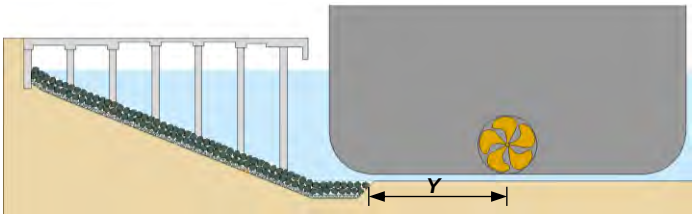

Figure 37. Open Piled Quay, Section

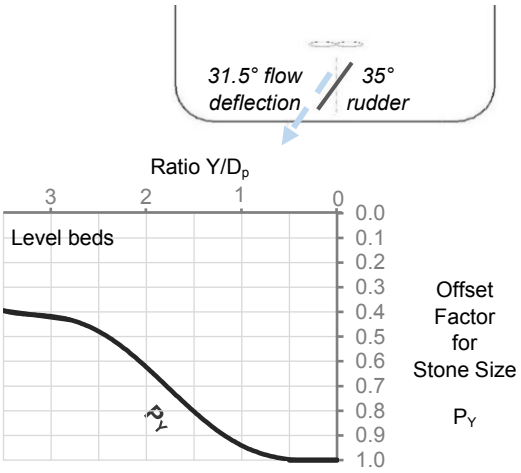

Figure 38. Offset Factor for Stone Size, P_Y, for Rudder Deflected Flow

This method was determined by testing and takes into account the increase in turbulence as the jet velocity decays. The flow deflection angle is taken as 0.9 x the rudder rotation, HAMILL et al (2009). This method can be applied to the crabbing action of a single deflected jet for twin propeller vessels, Figure 4.

This method should only be used for rudder rotation angles of 35° or below. For rudder rotation angles above 35°, the rock size needed can be interpolated from Figure 38 by using an equivalent jet length.

8.4. Slopes and Piles

The increase in rock size needed for slopes can be obtained using a slope factor by Pilarczyk, PIANC Report 180 (2015). The increased flow and turbulence around piles can cause rock stability failure. A pile effect factor estimated by Van Doorn, interpreted from PIANC Report 180 (2015) can be used.

Slope protection under piled quays is also described in HAWKSWOOD & KING (2016).

8.5. Rock Falling Edge Aprons

For propeller flow, the quantity of armour rock needed in a falling edge apron should give at least 1 layer of armour on a 3:1 slope down to the required scour protection level, HAWKSWOOD, FLIERMAN et al (2016). A fully deployed apron is likely to function only in the short term due to the risk of potential suffusion between the layer of dispersed armour and bedding stones. Where longer performance is required, some additional 50% of rock is suggested as Figure 39, shown as Deployed. This also provides for greater robustness as edge scour depths are often difficult to estimate along with the use of future vessels.

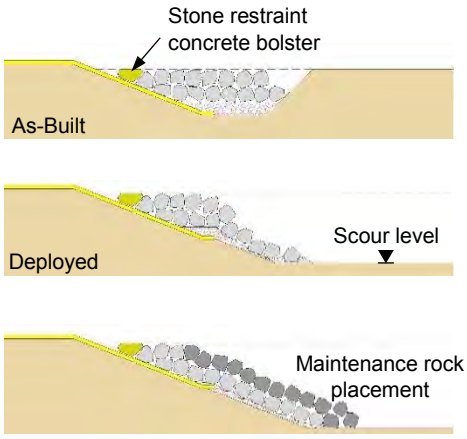

Figure 39. Falling Edge Apron Maintenance

Rock falling aprons provide an effective way to manage this risk. They are particularly useful when used in conjunction with insitu concrete or mattress protection types where 'Sealed' edges are required. Falling edge aprons can achieve a relatively high protective depth (VAN VELZEN et al 2014) and importantly can be monitored and maintained. In harbours, it is common to monitor performance of berth beds on an annual basis.

Rock aprons start to deploy when the edge scour exceeds the trench embedment depth as shown in Figure 39. Before aprons fully deploy and possibly fail, additional rock can be placed to any local scour areas.

The rock size is designed as for level beds with the support of testing, HAWKSWOOD, FLIERMAN et al (2016). A stone restraint concrete bolster is cast insitu to restrain edge rocks from movement, as shown in Figure 39. A rock falling edge apron design example is sown in Section 10.4.

8.6. Rock Design for Twin Propellers

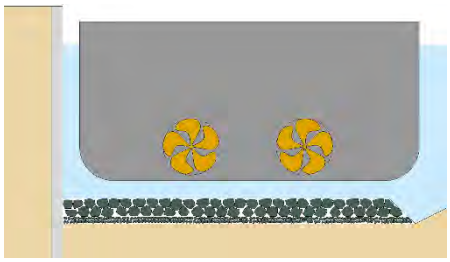

Figure 40. Rock Protection for Twin Propellers

Rock design for twin propeller action to level beds, as Figure 40, can be based upon the estimated bed velocity provided in Figure 9 for twin propellers, and used in (7) with the same rock stability coefficients B_S proposed for single propellers.

This method is supported by the stability testing shown in Section 9.

9. ROCK STABILITY TESTING FOR TWIN PROPELLERS

9.1 Test Arrangements

Scale model testing of rock was undertaken using two 150 mm diameter open propellers, as Figures 41, 42 and 43. The propeller rotation to initiate movement of various rock sizes was determined. To replicate actions in berths, the following effects were tested: -

- with rudders and without rudders
- varying propeller clearance C
- varying propeller separation S
- inward and outward propeller rotation (Figure 43)

Figure 41. Test Arrangement

The testing was carried out with a range of model rock sizes with W_{85}/W_{15} ratios from 1.8 to 2.6. This testing was an extension of a previous testing programme for single propellers with similar arrangements, HAWKSWOOD, FLIERMAN et al (2016). It has allowed the effect of twin propellers to be demonstrated and appropriate design guidance suggested. The testing covered a common range of low clearance ratios and a pair of handed twin propellers were used with 5 blades. The propellers were produced by MARIN with a K_T value of 0.587 which is now common.

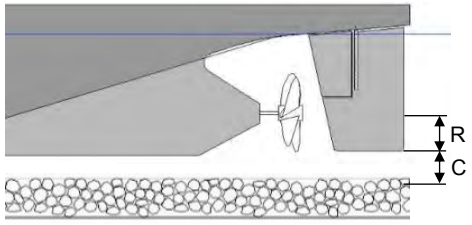

Figure 42. Test Arrangement, Elevation

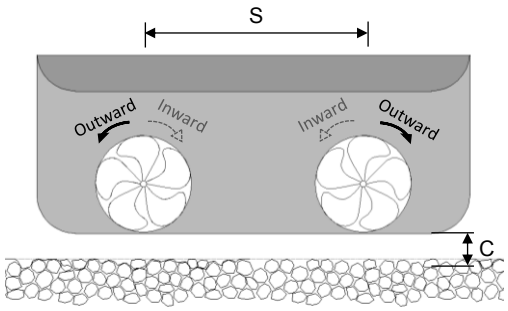

Figure 43. Test Arrangement, Section

9.2 Test Results and Findings

The bed velocities assumed in testing are based upon Figure 9. The test results for twin propellers with rudders are shown in Section 9.3. For twin propellers with no rudders, results are shown in Section 9.4. Both Figures 44 and 48 show that rock movement is predominately within the zones of single propeller jet flow rather than in zones where the jets are considered to merge, BAW (2010). This suggests the stability coefficients B_S for single propellers can also be used for twin propellers.

Rock stability testing results with a rudder are shown in Figures 45 to 47 for varying propeller separation S. These tests support the use of bed velocity as Figure 9, stability coefficient B_S = 0.64 and also taking the propeller clearance C from the centre of the top layer of rocks, Figure 36, as is suggested for single propellers, HAWKSWOOD, FLIERMAN et al (2016). Increase in the propeller separations made little difference, as the lower jets were still observed to combine.

Test results for rock stability without a rudder are shown in Figures 49 to 51 for varying propeller separation S. The results support the use of bed velocity as Figure 9, stability coefficient B_S = 1.55 and propeller clearance C to centre of top rocks, Figure 36. The increased rotation and turbulence in this action caused a wide spread of results with outward rotation being the worst case for larger stone sizes. Increase in propeller separation S made only a slight increase in stability, Figure 51, as the jet were still observed to combine upon the bed.

PIANC Report 180 (2015) advises bed velocities for twin propellers should be based upon those for single propellers x $\sqrt{2}$. For twin propellers with rudders this overestimates the rock size by a factor of some 1.5. For twin propellers with no rudders, the rock size is similar.

Rock movement in the tests was usually smaller stones below the D_{s50} size. Rock with lower W_{85} / W_{15} ratios were slightly more stable and indicate ratios below 2.0 are preferable for design.

Testing was conducted for ‘crabbing’ with one propeller ahead with rudder deployment and the other propeller astern as Figure 4. No change in rock stability was found, but the size of the scour zone appeared to be increased and this may contribute to significant scour often observed to turning areas next to berths by vessels crabbing, often with high power. This appears to be more common with ferry vessels.

Further comparison to rock performance in harbours would be useful along with testing to cover other propulsion types such as ducted propellers (Kurt nozzles), podded propulsors and azimuthal thrusters.

9.3. Rock Stability for Twin Propellers with Central Rudders

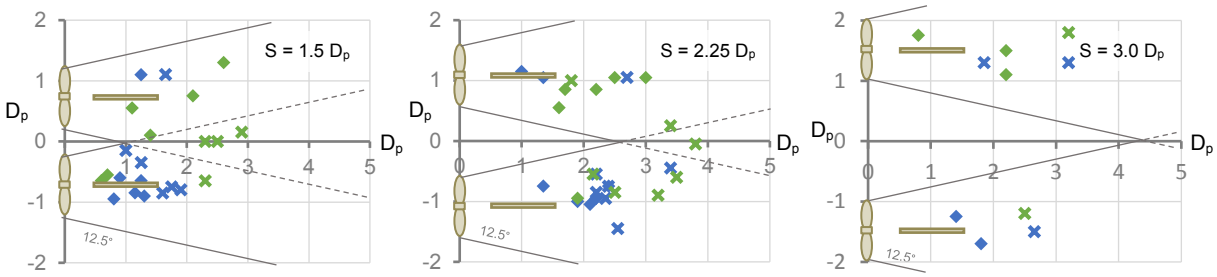

Figure 44. Plan of Rock Movement – With Rudder

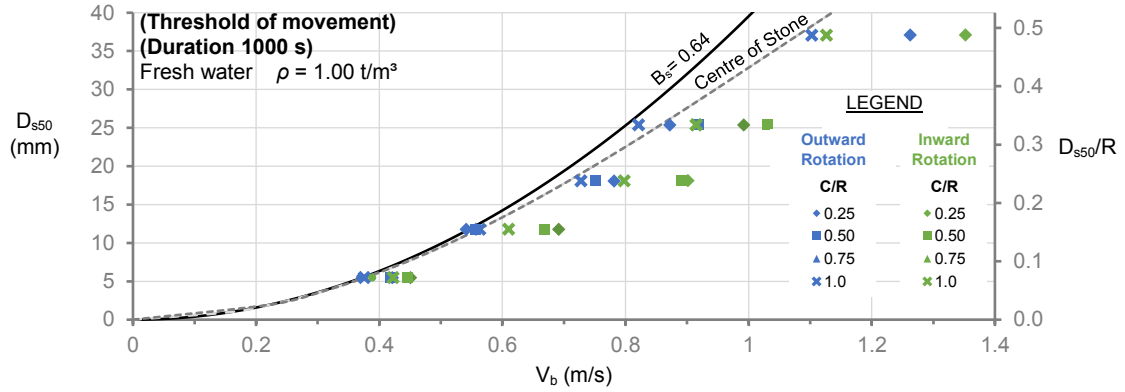

Figure 45. Rock Stability Testing – S = 1.5 D_p

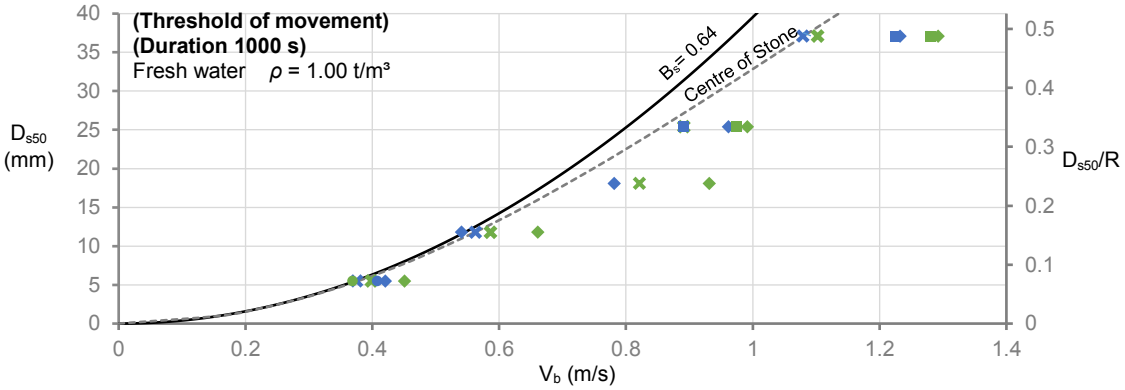

Figure 46. Rock Stability Testing – S = 2.25 D_p

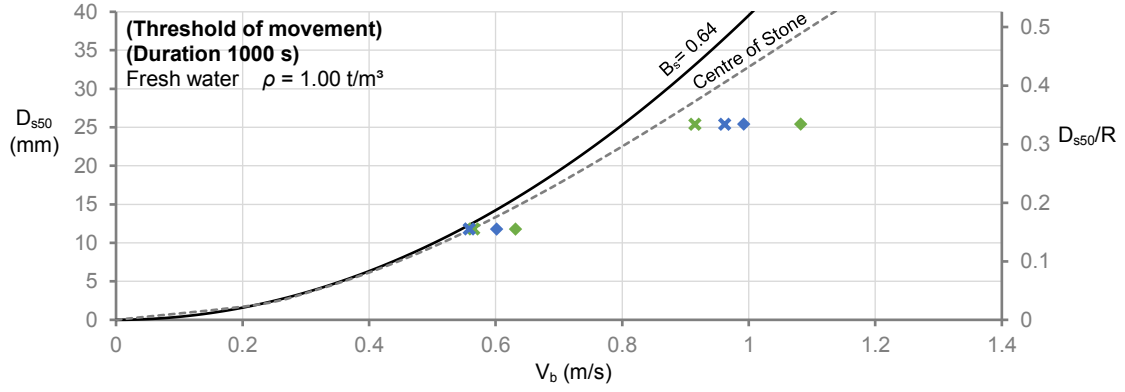

Figure 47. Rock Stability Testing – S = 3.0 D_p

9.4. Rock Stability for Twin Propellers with No Rudders

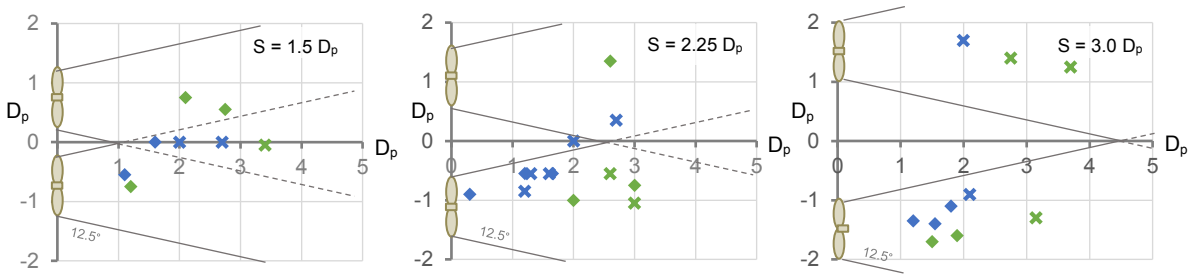

Figure 48. Plan of Rock Movement – Without Rudder

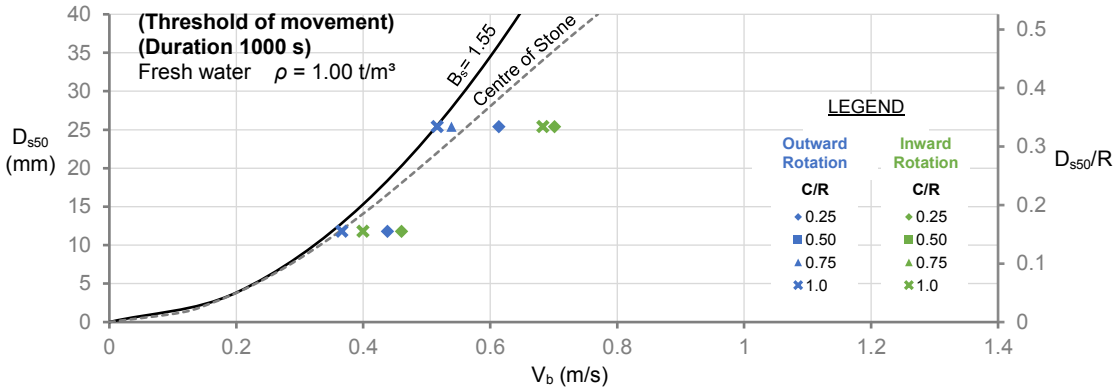

Figure 49. Rock Stability Testing – S = 1.5 D_p

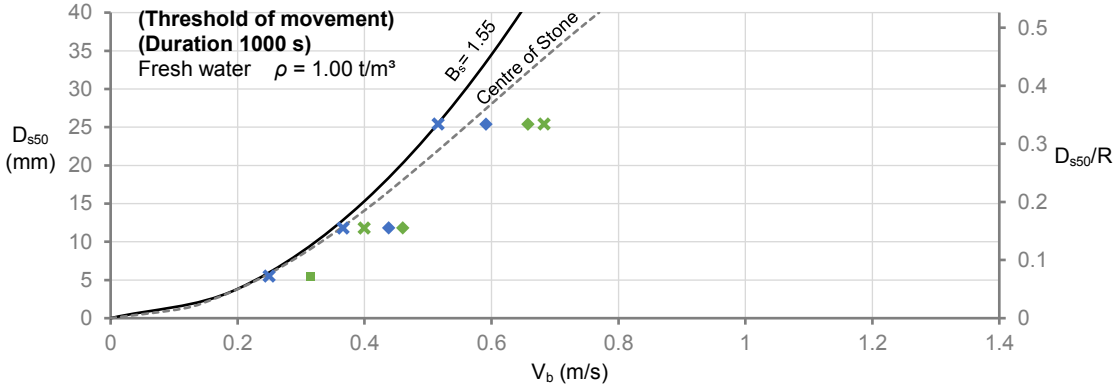

Figure 50. Rock Stability Testing – S = 2.25 D_p

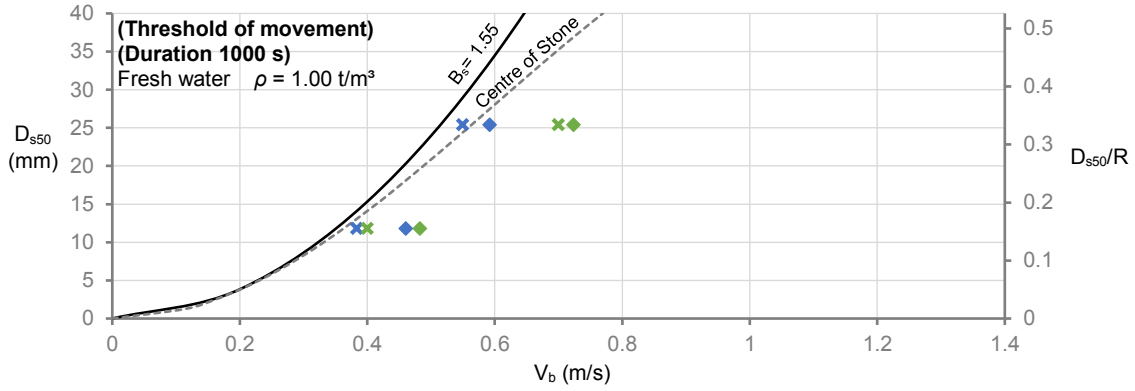

Figure 51. Rock Stability Testing – S = 3.0 D_p

10. DESIGN EXAMPLE

10.1. Single Propeller Vessel

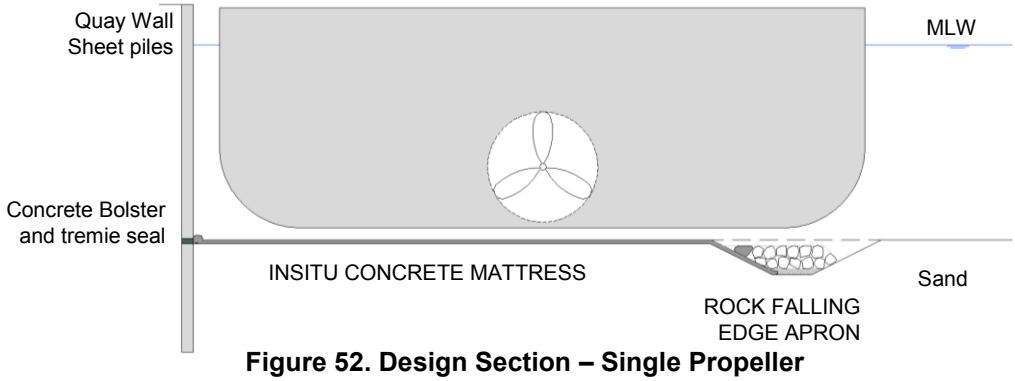

Figure 52. Design Section – Single Propeller

Design Parameters: Container Vessel

Propeller type	Single open propeller	
Propeller diameter (m)	D_p= 9.6 m	(R = 4.8 m)
Engine power (kW)	P = 80,080 kW	
Rudder type and max. deflection	Standard rudder, 35º deploy range	
Ratio of Engine power at berth	f = 0.1	PIANC Report 180 (2015)
Propeller Tip Clearance to Bed	C = 1.3 m	at MLW

Max. jet velocity: $V_0 = 1.48 \sqrt[3]{\frac{0.1 \times 80{,}080}{1.03 \times 9.6^2}} = 6.5$ m/s PIANC Report 180 (1)

Use 250 mm Thick Insitu Concrete Mattress (CT250) Tie spacing w = 100 mm, I_Q = 1.15 *(Fig. 19)*

Prop. tip clearance ratio to matt: $\frac{C}{R} = \frac{1.3}{4.8} = 0.27$ $\left[\frac{H_P}{D_P}=0.64\right]$

Design for Suction: C_S=0.13 *(Fig. 21)*

$$D_{min} = C_S \frac{V_o^2}{2\,g\,\Delta} x \frac{I_Q}{1.15} = 0.13 \frac{6.5^2}{2\,g\,1.3} x \frac{1.15}{1.15} = 0.22 \text{ m} < 0.25 \text{ m OK} \quad (3)$$

Design for Flow: C_F = 0.12 *(Table 1)*

Bed velocity reduction factor: $\frac{V_b}{V_0} = 0.85$ *(Fig. 9)*

Bed velocity onto mattress: V_b = 0.85 x 6.5 m/s = 5.5 m/s

$$D_{min} = C_F \frac{V_b^2}{2\,g\,\Delta} x \frac{I_Q}{1.15} = 0.12 \frac{5.5^2}{2\,g\,1.3} x \frac{1.15}{1.15} = 0.14 \text{ m} < 0.25 \text{ m OK} \quad (4)$$

Use Rock Falling Edge Apron 2 layers 1.5-3 t rock ($D_{s,50}$ = 1.18 m), with 0.5 m thick bedding stone layer

The top of rock is 0.5 m below maintenance dredging level (PIANC WG 22, 1997).

Prop. tip clearance ratio to centre of top rock: $\frac{C}{R} = \frac{1.3 + 0.5 + (1.18 \times 0.5)}{4.8} = 0.5$ $\left[\frac{H_P}{D_P} = 0.75\right]$

Bed velocity reduction factor: $\frac{V_b}{V_0} = 0.77$ *(Fig. 9)*

Velocity onto rock: V_b = 0.77 x 6.5 m/s = 5.0 m/s

Rock Stability Factor: B_S = 0.64 Single propeller with rudder

Rock size: (Δ = 1.57) $D_{s,50} = B_S \frac{V_b^2}{g\,\Delta} = 0.64 \frac{5.0^2}{g\,1.57} = 1.04$ m < 1.18 m provided OK (7)

10.2. Twin Propeller Vessel

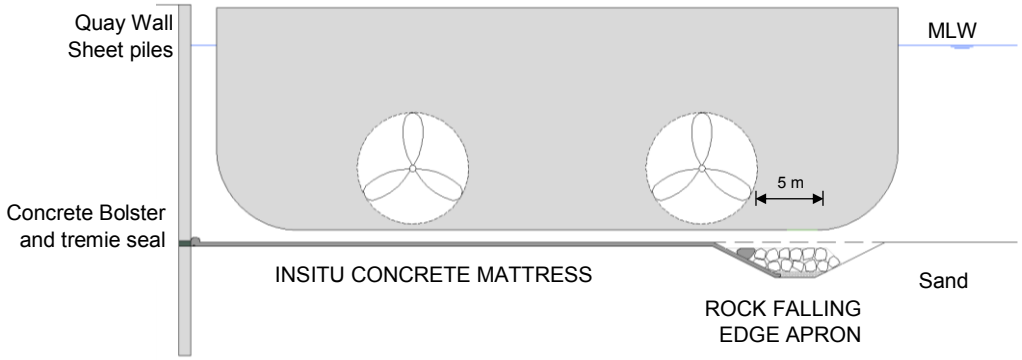

Figure 53. Design Section – Twin Propellers

Design Parameters: Container Vessel

Propeller type	Twin open propellers	
Propeller diameter (m)	D_p= 9.6 m	(R = 4.8 m)
Propeller axis separation (m)	S = 25 m	(25 m / 9.6 m = 2.6 D_p)
Engine power (kW)	P = 59,360 kW	
Rudder type and max. deflection	Standard rudders, 35º deploy range	
Ratio of Engine power at berth	f = 0.1	PIANC Report 180 (2015)
Propeller Tip Clearance to Bed	C = 1.3 m	at MLW

Max. jet velocity: $V_0 = 1.48 \sqrt[3]{\frac{0.1 \times 59{,}360}{1.03 \times 9.6^2}}$ = 5.9 m/s PIANC Report 180 (1)

Use 250 mm Thick Insitu Concrete Mattress (CT250) Tie spacing w = 100 mm, I_Q = 1.15 *(Fig. 19)*

Prop. tip clearance ratio to matt: $\frac{C}{R} = \frac{1.3}{4.8} = 0.27$ $\left[\frac{H_P}{D_P} = 0.64\right]$

Design for Suction: C_S=0.15 *(Fig. 26)*

$$D_{min} = C_S \frac{V_o^2}{2\,g\,\Delta} x \frac{I_Q}{1.15} = 0.15 \frac{5.9^2}{2\,g\,1.3} x \frac{1.15}{1.15} = 0.2 \text{ m} \quad < 0.25 \text{ m OK} \qquad (3)$$

Design for Flow: C_F = 0.12 *(Table 1)*

Bed velocity reduction factor: $\frac{V_b}{V_0} = 0.97$ *(Fig. 9)*

Bed velocity onto mattress: V_b = 0.97 x 5.9 m/s = 5.7 m/s

$$D_{min} = C_F \frac{V_b^2}{2\,g\,\Delta} x \frac{I_Q}{1.15} = 0.12 \frac{5.7^2}{2\,g\,1.3} x \frac{1.15}{1.15} = 0.15 \text{ m} \quad < 0.25 \text{ m OK} \qquad (4)$$

Use Rock Falling Edge Apron – 2 layers 1.5–3 t rock, ($D_{s,50}$ = 1.18 m) with 0.5 m thick bedding stone layer
The top of rock is 0.5 m below maintenance dredging level (PIANC WG 22, 1997).

Prop. tip clearance ratio to centre of top rock: $\frac{C}{R} = \frac{1.3 + 0.5 + (1.18 \times 0.5)}{4.8} = 0.5$ $\left[\frac{H_P}{D_P} = 0.75\right]$

Bed velocity reduction factor: $\frac{V_b}{V_0} = 0.89$ *(Fig. 9)*

Velocity onto rock: V_b = 0.89 x 5.9 m/s = 5.2 m/s

Rock Stability Factor: B_S = 0.64 Twin props with rudders

Rock size: (Δ = 1.57) $D_{s,50} = B_S \frac{V_b^2}{g\,\Delta} = 0.64 \frac{5.2^2}{g\,1.57}$ = 1.12 m < 1.18 m provided OK (7)

10.3. Insitu Concrete Mattress Parameters

– Use a proven Marine Quality Control System for 'Sealed' protection construction	Section 5.2
– Use CT mattress with tie spacing w = 100 mm (surface undulation ratio < 0.16)	Section 5.4
– Use Ball and Socket Joints between mattress panels	Figure 5
– Panel width 4.4 m typically	Section 5.3
– Concrete strength 35 N/mm^2 (MPa) C28/35	Section 5.3
– 250mm thickness > 200mm minimum thickness recommended for maintenance dredging and robustness	Section 5.1
– Use Concrete bolster seal to wall with tremie concrete infill to inpans, 0.3 m thick	Figure 52
– Use 1 row of 90 mm Ø weep holes @ 4.5 m centres along wall for nominal tidal water movement under wall in fine/medium sand	Section 5.1

10.4. Use 4.5m Wide Rock Falling Edge Apron

The extent of Scour Protection is to be 5 m beyond outer propeller. PIANC Report 180 (2015), p114.
Provide Stone Restraint Bolster to secure edge rocks upon mattress.

From scour assessment experience, twin propeller vessels are the worst case, design rock falling edge apron for 5 m scour depth.

Top of rock depressed 0.5 m below maintenance dredge level M.D.L. to avoid damage, PIANC WG22 (1997).

Rock apron construction thickness take
(2 × 1.18 m × 0.8) + 0.5 m bedding layer = 2.4 m

Provide rock apron average length L = 4.4 m

The deployed apron depth is calculated for a single layer of rock protection on a 3:1 slope, 25% allowance as short term protection

Passive embedment 2.4 m + 0.5 m = 2.9 m
Active deployment $2 \times \frac{4.5\text{ m}}{1.25\text{ m}} \times \frac{1}{3.16} = \frac{\sim 2.3\text{ m}}{5.2\text{ m}}$ < 5 m OK

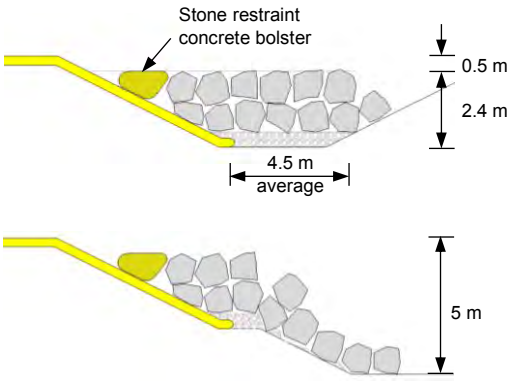

Figure 54. Falling Edge Apron Deployment

Rock edge to be monitored by annual bathymetric surveys. Any areas approaching ultimate deployment are to be inspected by diver and if required maintained locally with additional rock, HAWKSWOOD, FLIERMAN et al (2016).

11. CONCLUSIONS

Significant savings can often be made to piled and gravity quay wall structures using thinner scour protection than traditional rock construction, Figures 1 and 2.

The stability of thinner scour protections depends upon whether they are 'Open' or 'Sealed' to flow entry. A 'Sealed' protection has better performance and is normally more economic. Insitu concrete mattress protection is often used in conjunction with rock falling edge aprons and can be reliably installed as a 'Sealed' protection using a proven marine quality control system. Simplified design methods are now available for single propeller action, which have now been extended to twin propeller action following the research testing which has been presented. The formation of reliably 'Sealed' joints and edges using prefabricated mattress lowered onto harbour beds is more difficult to achieve. Prefabricated mattress designed as an 'Open' protection can be conservatively used.

The previous testing programme for rock protection generally supported use of the original method by FÜHRER & RÖMISCH (1997) for single propeller action, but with a stability coefficient B_S = 1.55 for the no rudder condition and propeller clearance taken to the centre of the top rocks (Figure 37). Further testing for twin propeller action has allowed an extension of the method to cover twin propeller action. Compared to PIANC Report 180 (2015), this shows significant savings in rock size to be made for twin propellers with rudders by a factor of some 1.5.

The number of large container vessels, cruise ships and ferries with twin propellers is growing and designers should take this into account. Vessels with twin propellers may need an increase in scour protection size and an increase in protection width to protect under both propellers. The testing has shown that bed velocities for twin propellers with rudders are lower than estimated by PIANC Report 180 (2015) and this results in savings in rock size by a factor of some 1.5.

12. ACKNOWLEDGMENTS

This paper presents the views of the authors, not necessarily their employers, clients or organisations. The test rig was developed by P. Holloway, R. De Haan and D Macalay with twin propeller testing undertaken by J. Groom. Every effort has been made to ensure that the statements made and the opinions expressed in this paper provide a safe and accurate guide; however, no liability or responsibility of any kind can be accepted in this respect by the publishers or the authors. Any subsequent amendments will be listed at www.proserveltd.co.uk

13. REFERENCES

BAW (2005), Principals for the Design of Bank and Bottom Protection for Inland waterways, Bulletin 85, Karlsruhe - Germany

CIRIA; CUR; CETMEF (2007), The Rock Manual. The use of rock in hydraulic engineering (2nd edition), CIRIA - London.

EAU (2004) Recommendations of the Committee for Waterfront Structures: Harbours and Waterways, Germany

FÜHRER M., RÖMISCH (1977), Effects of Modern Ship Traffic on Inland and Ocean Waterways , 24th International Navigation Congress, PIANC, Leningrad - Russia, pg. 236-244.

FÜHRER, M., RÖMISCH, K and ENGELKE, G (1981), Criteria for Dimensioning the Bottom and Slope Protections and for Applying the New Methods of Protecting Navigation Canals, PIANC 25th Congress, Permanent International Association of Navigation Congress, Brussels, Belgium.
HAWKSWOOD, M.G., ASSINDER, P., (2013) Concrete mattress used for berth scour protection, GhIGS GeoAfrica 2013, Accra - Ghana

HAWKSWOOD, M.G., EVANS, G., HAWKSWOOD, G.M., (2013) Berth Protection for Fast Ferry Jets, Coasts, Marine Structures and Breakwaters 2013, ICE, Edinburgh – UK

HAWKSWOOD, M.G. LAFEBER, F.H., HAWKSWOOD, G.M., (2014) Berth Scour Protection for Modern Vessels, PIANC World Congress, San Francisco - USA.

HAWKSWOOD, M.G., KING, M. (2016), Slope Protection Under Piled Quays, ASCE COPRI Ports 2016, New Orleans - U.S.A.

HAWKSWOOD, M.G., FLIERMAN, M., DE HAAN, R., KING, M.G., & GROOM, J.A., (2016) Propeller Action and Berth Scour Protection, PIANC-COPEDEC IX, Rio de Janeiro, Brasil.

MUJAL-COLILLES, A., GIRONELLA, X., CRESPO, A.J.C., SANCHEZ-ARCILLA, A., (2017) Study of the Bed Velocity Induced by Twin Propellers, ASCE Journal of Waterway, Port, Coastal, and Ocean Engineering 143.5

PIANC Report 180, (2015) Guidelines for Protecting Berthing Structures from Scour Caused by Ships.

PIANC Bulletin 109, (2002).,Input Data of Propeller Inducted Velocities for Dimensioning of Bed Protection Near Quay Walls, RÖMISCH, K. & HERING, W.

PIANC Report of Working Group 22, Bulletin no 96 (1997), Guidelines for design of armoured slopes under open piled quay walls.

PILARCZYK, K.W. (2000), Correspondence 02/08/2011

RAES, L., ELSKENS, F., RÖMISCH K.W. AND SAS, M. (1996) The Effect of Ship Propellers on Bottom Velocities and on Scour Near Berths and Protection Methods Using Thin Flexible Revetments, Proceedings 11th International Harbour Congress, Antwerp - Belgium, pp. 433-443.

VAN VELZEN, G., DE JONG, M.P.C., QUATAERT, J.P., VERHEIJ, H.J., (2016) The Stability of Block Mattress in a Propeller Induced Jet, 8th International ICSE, Oxford, UK.

NEW TECHNOLOGIES WITH CONCRETE BLOCKS FOR TSUNAMI PROTECTION AND LONG-PERIOD WAVE ABSORPTION

by

Shin-ichi Kubota[1], Jun Mitsui[2], Masashi Tanaka[3] and Akira Matsumoto[2]

ABSTRACT

In Recent years, tsunami and long-period waves have caused problems in Japan. Numerous breakwaters were seriously damaged by the 2011 Off the Pacific Coast of Tohoku Earthquake Tsunami. Many ports suffered disturbance in cargo handling due to ship motion caused by long-period waves. This paper presents our new methods using concrete blocks for tsunami protection and long-period wave absorption as countermeasures to such problems. A simple and highly accurate stability estimation method for concrete blocks covering the rubble mound of a breakwater against tsunami overflow is proposed. In this method, the overflow depth is used to represent the external force. This enables an easier and more robust estimation of the required mass of the concrete blocks over that of the conventional method based on flow velocity. A submerged mound type long-period wave absorbing structure is proposed. It becomes clear that submerged structures display a higher wave absorbing performance compared with those of conventional structures.

1. INTRODUCTION

In recent years, among the various types of coastal structures, concrete blocks have gained wider use as one of the important components due to their effectiveness against wind wave attacks. The design method for wind waves is well established and concrete blocks work best. On the other hand, tsunami and long-period waves also cause problems in Japan. For many decades, tsunami protection for facilities has been studied. However, the 2011 Off the Pacific Coast of Tohoku Earthquake Tsunami which was beyond the scope of assumption damaged numerous breakwaters and new problems have emerged. Meanwhile, many ports suffer from disturbances in cargo handling due to ship motion caused by long-period waves. In this paper, we introduce some new methods using concrete blocks for tsunami protection and long-period wave absorption as countermeasures to such problems.

In the 2011 Off the Pacific Coast of Tohoku Earthquake Tsunami, one of the causes of failure of breakwaters subjected to tsunami attack was a scouring of the rubble foundation and subsoil on the harbor-side of the breakwater. This was previously inconceivable as a type of failure (Ministry of Land, Infrastructure, Transport and Tourism, 2013). One possible countermeasure is placement of widened protection using additional rubble stones behind the breakwater to prevent sliding of the caisson. Placing concrete blocks on the widened protection would also be required to prevent the scouring around the rubble mound (Fig. 1). The Isbash formula (Coastal Engineering Research Center, 1977) has been applied previously as the method to estimate the required mass of concrete blocks against tsunami. The required mass calculated by this formula is proportional to the sixth power of the flow velocity near the armor unit. This causes the practical problem that the required mass is too sensitive to variations in the estimated flow velocity. In this context, the establishment of a more practical method to determine the mass of concrete blocks is one urgent issue towards the achievement of resilient breakwaters against tsunamis. Hydraulic model experiments in a wide range of conditions were conducted to extract key factors for concrete block stability by using a wave flume equipped with tsunami generator. Based on the experimental study, a new stability estimation method for concrete blocks placed on widened protection against tsunami overflow is proposed. The stability of the concrete blocks is estimated using an overflow depth of tsunami instead of flow velocity.

---

[1] FUDO TETRA CORPORATION, Technical Research Institute, shinichi.kubota@fudotetra.co.jp
[2] FUDO TETRA CORPORATION, Technical Research Institute
[3] FUDO TETRA CORPORATION, Civil Engineering Division

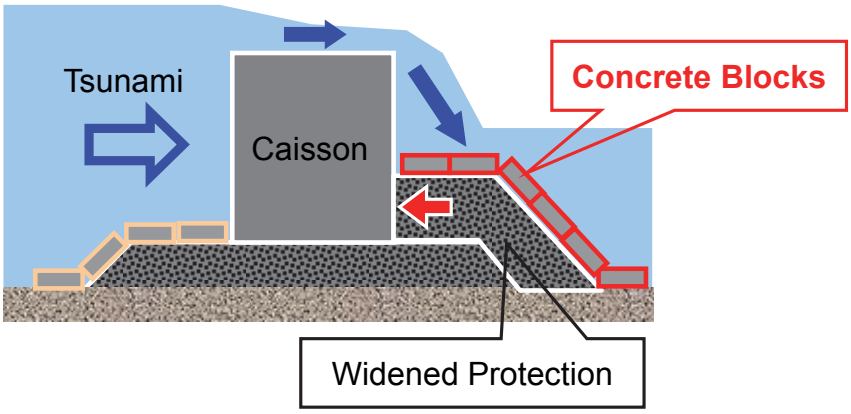

Figure 1: Countermeasure against Tsunami of Breakwaters

On the other hands, it has been reported that long-period waves with period of 30 to 200 s cause serious problems in cargo handling in many Japanese ports. The problems in cargo handling are mainly related to large motions on moored vessels which are caused by resonance with long-period waves in a harbor. As a countermeasure, wave absorbing mounds installed on the harbor side of breakwaters have been proposed and constructed. The crown heights of the rubble mounds are almost equal to those of the caissons. However, because of the poor wave absorbing performance of such conventional structures, the required mound width at the still water level for long-period waves becomes more than 30 m. It is important to reduce the size of the structure to apply to specific site condition. In this study, a submerged mound type long-period wave absorbing structure with high performance is proposed (Fig. 2). The basic concept of this proposed structure is to level the crest elevation to the water surface to establish high efficiency in energy dissipation on the surface of the crown of the concrete blocks. A series of hydraulic model experiments were carried out to evaluate the wave absorbing performance. The wave absorbing mechanism was investigated using hydraulic model experiments and numerical analyses.

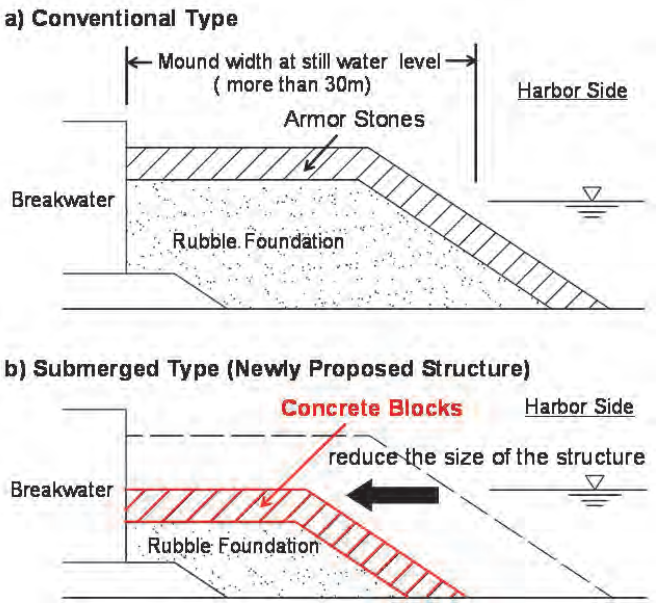

Figure 2: Long-period Wave Absorbing Structure

2. NEW TECHNOLOGY FOR TSUNAMI PROTECTION USING CONCRETE BLOCKS

2.1 Wave Flume Equipped with Tsunami Generator

A tsunami generating facility which consists of a circulating pump and a vacuum chamber has been installed in our wave flume (Fig.3). This tsunami generator can create various types of tsunami, such as steady flow which continuously overflow breakwaters and bores having steep wave fronts. A piston-type wavemaker is also available. It is possible to use this in combination with the circulating pump and the vacuum chamber. Hence, it will make possible to conduct wide-ranging studies of tsunami measures.

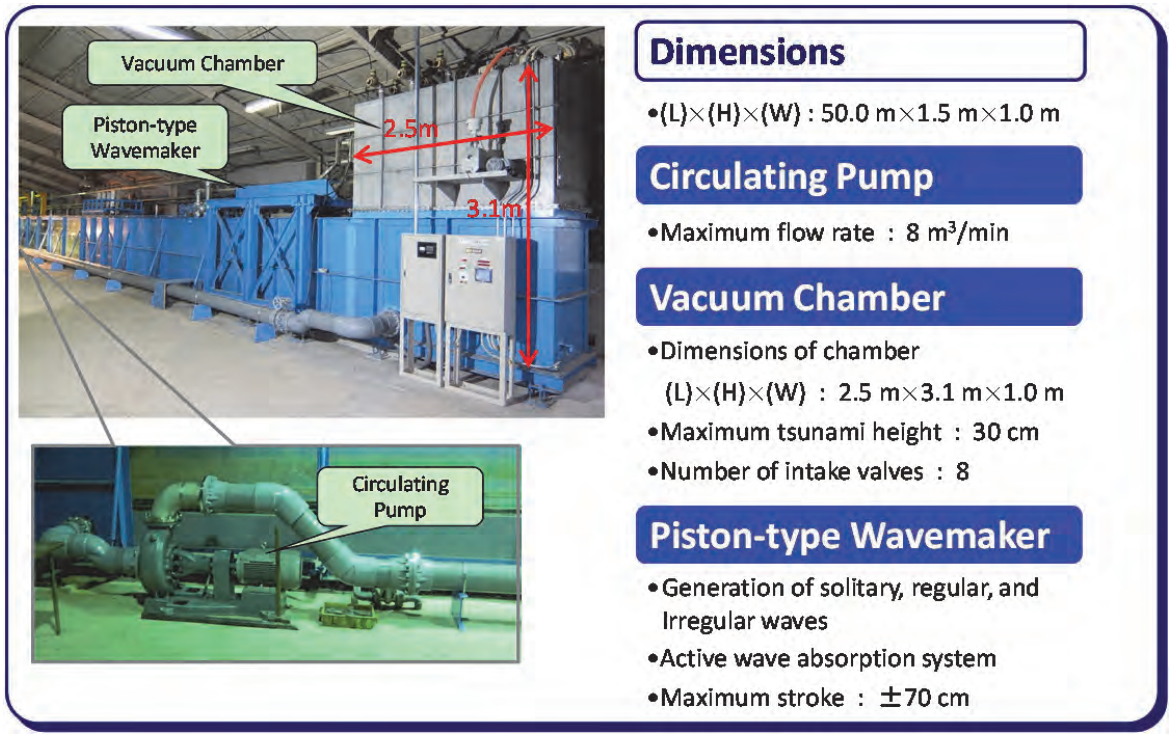

Figure 3: Overview of Tsunami Generator

2.2 Experimental Setup

Experiments were carried out in a 50 m long, 1.0 m wide, and 1.5 m deep wave flume equipped with the tsunami generator shown in Fig. 3. Fig. 4 shows test setup in the flume. A horizontal mortar seabed was partitioned into two sections along the length, and a breakwater model was installed in one 50 cm wide waterway. A submersible pump and discharge port were located on the harbor-side and sea-side of the breakwater model respectively to generate a steady overflow. A water level difference was generated between the inside and outside of the breakwater by operating the pump. The height of the sea-side water level could be changed by varying the height of the overflow weir installed on the sea-side of the breakwater model. The height of the overflow weir could be varied in a range of 0 to 50 cm. A vent hole with diameter of about 25 mm was provided in the partition wall close behind the caisson to maintain the space between the caisson and overflow nappe in ambient atmospheric pressure conditions.

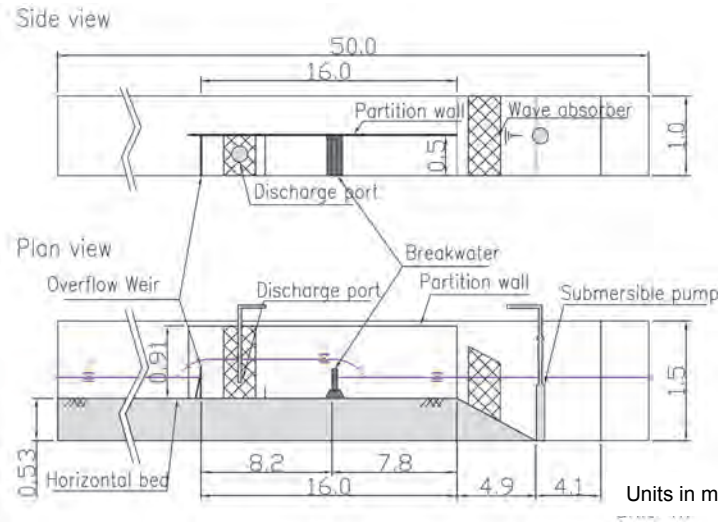

Figure 4: Test Setup in the Flume

A schematic layout of the breakwater model is shown in Fig. 5. The model scale is 1/50. Experiments were carried out by changing the shape of the harbor-side rubble mound, the harbor-side water level, and the shape and mass of the concrete blocks. Two kinds of flat-type blocks and a wave-dissipating block were used in the experiments as shown in Fig. 6. The flat-type block with five holes is a recently developed block named “Permex” produced by refining the “X-block” which has been used conventionally. The large holes in the block have been found to contribute to high stability against wave action due to the reduction of the uplift force (Hamaguchi et al. 2007, Kubota et al. 2008). The caisson model was made of wood and was fixed with a weight so that it would not be moved by tsunami action since this study was focused on the stability of concrete blocks.

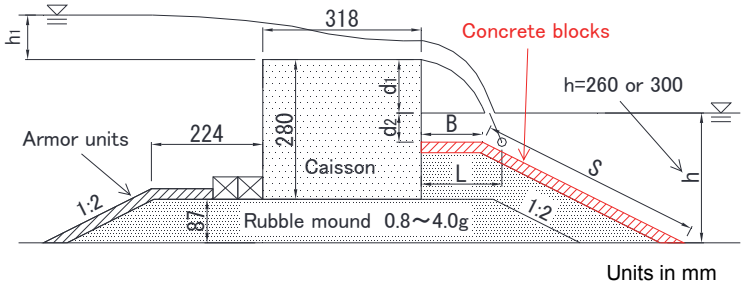

Figure 5: Schematic Layout of the Tested Breakwater

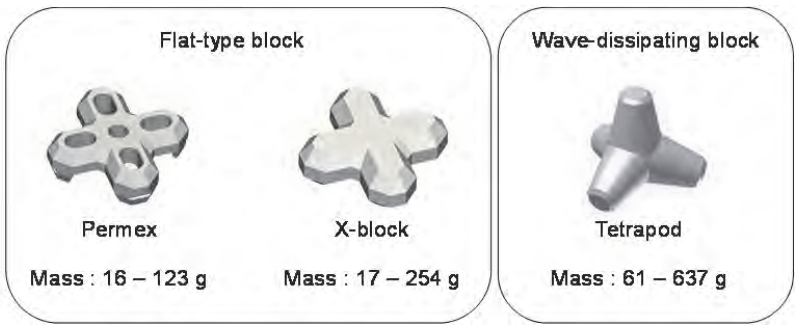

Figure 6: Concrete Blocks Used in the Experiment

The duration time of the steady overflow of tsunami was set to 127 s (15 min in the prototype scale) to simulate the actual event observed in Hachinohe port during the Tohoku tsunami on March, 11th in 2011. As it took about 60 s until the water level achieved a steady state from the start of operating the pump, the total operation time of the pump was set to 187 s. The stability limits of the armor units were examined by increasing the overflow depth in increments of 1 cm. The overflow depth was defined as the difference between the sea-side water level (measured at 2 m on the offshore side from the front of the caisson) and the crest height of the caisson. The harbor-side water level was measured at 2 m on the onshore side from the rear wall of the caisson. The section was not rebuilt after tsunami attack with each overflow depth. The number of the moved concrete blocks was counted as an accumulated number. The damage to concrete blocks were defined using the relative damage N_0, which is the actual number of displaced blocks related to the width of one nominal diameter D_n (Van der Meer 1988). The nominal diameter D_n is the cube root of the volume of the armor unit. In this study, N_0=0.3 was applied as the criterion of damage.

2.3 Feature of the Damage by Tsunami Overflow

Fig. 7 shows snapshots of the tsunami overflow in the experiment. As soon as the concrete blocks at the slope section were washed away, the scouring of the rubble mound progressed rapidly and reached to the sea bottom within about 1 minute (7 minutes in the prototype scale). Though widened protection using additional stones exhibits a function to delay scouring, the damage expands rapidly if the armor units are washed away and the rubble mound is exposed. This is one of the features of damage by tsunami overflow.

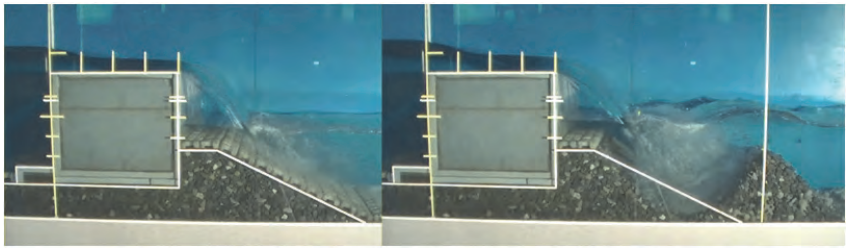

Figure 7: Snapshots of Tsunami Overflow

2.4 Influence of Impingement Position of Overflow Jet

The impingement position of the overflow jet will change with various factors such as the shape of the harbor-side mound and the overflow depth. The influence of the impingement position on block stability was examined by changing the crown width of the harbor-side mound. Fig. 8(a) shows an example of the stability test results. In this condition, the overflow jet impinged on the slope section when the number of armor units on the crown section was one or two, whereas it impinged on the crown section in the case of more than four units on the crown section. The cases in which the jet impinged on the slope section showed higher stability than the cases of impingement on the crown section. This shows that impingement position largely affects the block stability. Because the effect of the impingement position depended on the structural conditions such as the shape of the concrete block and the presence or absence of widened protection, it is necessary to incorporate properly this effect into the estimation of the block stability.

2.5 Influence of Harbor-side Water Level

When a tsunami overflows the caisson, the discharged water from the rear end of the caisson accelerates during the freefall above the water surface, and decelerates under the water surface due to diffusion. Therefore, the stability of concrete blocks should decrease as the crown height of the caisson above the harbor-side water level increases. Also, it should increase as the submerged depth above the concrete blocks increases. Fig. 8(b) shows a comparison of the stability test results with two different harbor-side water levels. On the whole, the results of deep-water cases showed higher stability than those of shallow-water cases.

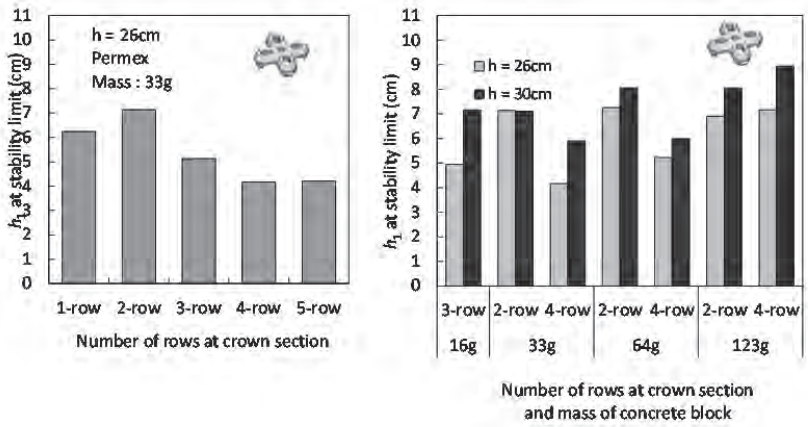

(a) Influence of Impingement Position **(b) Influence of Harbor-side Water Level**

Figure 8: Influence of Impingement Position and Harbor-side Water Level on the Overflow Depth h_1 at Stability Limit

2.6 Failure Modes of Concrete Blocks

Two failure modes for flat-type blocks were observed in the experiments. One was an overturning mode in which the concrete blocks near the impingement position overturned. The other was a sliding mode in which all the blocks on the slope section slid together. Fig. 9 shows the relationship between the nominal diameter of the concrete block D_n and the overflow depth h_1 on the occurrence of damage. In the cases of overturning mode, the overflow depth at the occurrence of damage was almost proportional to the nominal diameter D_n. On the other hand, in the cases of sliding mode, it had only a small dependence on D_n. These results suggest that enlargement of the block size causes an increase in the acting force as much as the increase in the resistance force with regard to the sliding mode. For the wave-dissipating blocks, almost every failure pattern was that of blocks near the impingement position being displaced individually.

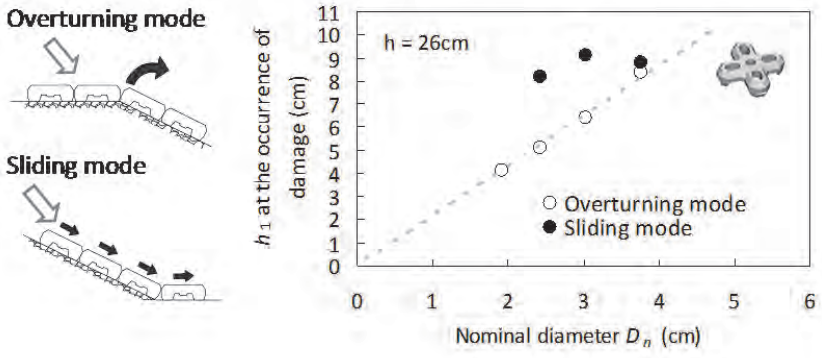

Figure 9: Relationship between the Nominal Diameter D_n and the Overflow Depth h_1 at the Occurrence of Damage by Each Failure Mode

2.7 Performance of the Wave-dissipating Concrete Blocks

A characteristic of the wave-dissipating blocks installed in two layers is that scouring becomes hard to progress rapidly even when many blocks are displaced. The reasons are considered to be the following:

(1) it takes a longer time before the rubble stones are exposed since they are covered with the two layers, (2) displaced blocks piled up behind the impingement position prevent the progress of the scouring by staying interlocked without being washed away. Avoiding the rapid progress of scouring is important from the viewpoint of resilience of a breakwater in the prevention of large scattering of the caisson (Arikawa et al. 2013). The widened protection mound covered with wave-dissipating blocks may provide such resilience.

2.8 Stability Estimation Method

Two empirical formulae for the stability estimation were derived based on the experimental results mentioned above. The overflow depth was used in the formulae to represent the external force. The overflow depth of the stability limit corresponding to each failure mode was obtained by the two formulae. The final stability limit was determined by the severer one. The formulae for the overturning mode and sliding mode are expressed as follows:

$$\text{Overturning mode :} \quad \frac{h_1}{(S_r-1)D_n} = N_{S1} = f\left(\frac{B}{L}, \frac{d_2}{d_1}\right) \tag{1}$$

$$\text{Sliding mode :} \quad \frac{h_1}{(S_r-1)S} = N_{S2} = f\left(\frac{d_2}{d_1}\right) \quad \text{for} \quad \frac{B}{L} \le 1.1 \tag{2}$$

where, h_1 is the overflow depth, S_r is the specific gravity of concrete with respect to seawater, S is the slope length of the harbor-side rubble mound, N_{S1} and N_{S2} are the stability numbers, B is the crown width of the harbor-side mound, L is the impingement position of the overflow jet, d_1 is the crown height of the caisson above the harbor-side water level, and d_2 is the submerged depth above the armor units (regarding the definition of symbols, see Fig. 5). Stability numbers N_{S1} and N_{S2} are functions of B/L and d_2/d_1, which are the parameters representing the influence of the impingement position and the harbor-side water level respectively. The stability is determined only by Eq. (1) if B/L is larger than 1.1 since failure by sliding mode does not occur when the overflow jet impinges on the crown section. Similarly, the stability of wave-dissipating blocks is also determined only by Eq. (1).

For the overturning mode, the overflow depth h_1 represents the acting force on armor units, whereas the nominal diameter of concrete blocks D_n represents the resistance force as shown in Eq. (1). For the sliding mode, on the other hand, the slope length S is used to represent the resistance force as shown in Eq. (2). This is because the resistance force should be represented by the total length of the blocks on the slope as the whole blocks on the slope section slide together in the sliding mode. As a result, the overflow depth of the stability limit in the sliding mode is not dependent on the block size as can be seen from Eq. (2). This corresponds with the experimental results described above (see Fig. 9).

2.9 Calculation Method of the Impingement Position

It is necessary to calculate the impingement position L to apply the estimation method. It can be calculated approximately using the overflow depth h_1 as shown below. The definition of each symbol is shown in Fig. 10.

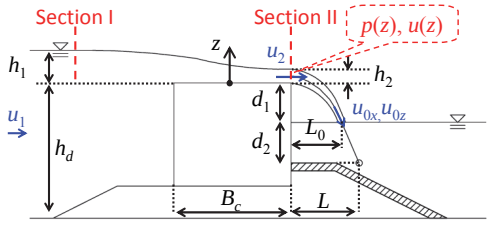

Figure 10: Definition of the symbols used in the calculation of the impingement position

The overflow discharge per unit width q is calculated by using the Hom-ma formula (Hom-ma 1940b):

$$q = 0.35h_1\sqrt{2gh_1} \tag{3}$$

where g is the acceleration due to gravity. The application condition in this formula is $h_1/B_c < 1/2$. The effect of the approaching velocity u_1 can be disregarded if $h_1/h_d < 0.5$ (Hom-ma 1940a). The water depth above the caisson at the rear end of the caisson h_2 and the cross sectional averaged flow velocity u_2 are calculated according to Hom-ma (1940a) as shown below.

Applying the Bernoulli's theorem to Sections I and II yields the following relation:

$$h_1 = z + \frac{p_{(z)}}{\rho g} + \frac{u_{(z)}^2}{2g} \tag{4}$$

where, z is the height measured from the top of the caisson, and $p_{(z)}$, $u_{(z)}$ are the pressure and the flow velocity at Section II, respectively. The overflow discharge q is obtained by integrating the flow velocity $u_{(z)}$ as follows:

$$q = \int_0^{h_2} \sqrt{2g\left(h_1 - z - \frac{p_{(z)}}{\rho g}\right)}dz \tag{5}$$

If the pressure distribution $p_{(z)}$ is obtained, h_2 can be calculated using Eq. (3) and Eq. (5). The pressure distributions were assumed as the following triangle distributions:

$$\begin{aligned} p_{(z)} &= \rho g\left(h_2 - z\right) \quad \text{for} \quad h_2/2 \le z \le h_2 \\ p_{(z)} &= \rho g z \quad \text{for} \quad 0 \le z \le h_2/2 \end{aligned} \tag{6}$$

Using Eq. (3), Eq. (5), and Eq. (6), one obtains Eq. (7):

$$0.35h_1\sqrt{2gh_1} = \sqrt{2g}\left\{-\frac{1}{3}\left[\sqrt{\left(h_1 - h_2\right)^3} - \sqrt{h_1^3}\right] + \sqrt{h_1 - h_2}\,\frac{h_2}{2}\right\} \tag{7}$$

The relationship between h_1 and h_2 are solved numerically with Newton's method as follows:

$$h_2 = 0.42h_1 \tag{8}$$

In this study, the following relationship was used considering its suitability to the experimental results:

$$h_2 = 0.45h_1 \tag{9}$$

The center of trajectory of the overflow water was then obtained under the following assumptions. The overflow water discharges horizontally from the rear end of the caisson at the flow velocity $u_2 = q/h_2$. The trajectory of the overflow nappe above the water surface is a parabola. The trajectory of the water below the water surface is a straight line.

The landing position of the overtflow water on the harbor-side water surface, L_0, and the flow velocity u_{0x}, u_{0z} are calculated as follows:

$$L_0 = u_2\sqrt{\frac{2\left(d_1 + h_2/2\right)}{g}} \tag{10}$$

$$u_{0x} = u_2, \quad u_{0z} = \sqrt{2g\left(d_1 + h_2/2\right)} \tag{11}$$

The impingement position L was thus obtained as follows:

$$L = L_0 + \frac{u_{0x}}{u_{0z}} d_2 \tag{12}$$

The stability numbers N_{S1} and N_{S2} are determined by applying the impingement position L calculated in this manner.

2.10 Determination of Stability Numbers

Fig. 11(a) shows the influence of the impingement position by plotting the stability number N_{S1} against B/L. The conditions of water depth are almost at the same level (d_2/d_1 = 0.47 to 0.66). The damage data with sliding mode is excluded in the figure to reveal the stability limit of overturning mode. The stability limit is expressed in a single line as a function of B/L regardless of the mass of the block. Also, the difference in the stability due to the impingement position appears clearly. Fig. 11(b) shows the influence of the harbor-side water depth by plotting the N_{S1} against d_2/d_1. The data on the conditions of B/L > 1.0 is used. The stability tends to increase as d_2/d_1 increases.

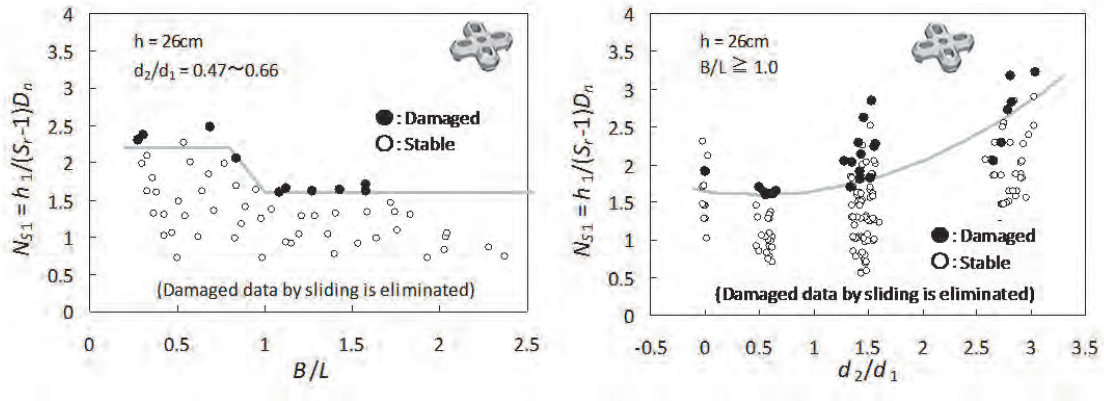

(a) Influence of B/L on N_{S1} **(b) Influence of d_2/d_1 on N_{S1}**

Figure 11: Influence of B/L and d_2/d_1 on N_{S1}

Fig. 12 shows the stability numbers N_{S1} and N_{S2} for flat-type blocks determined through all the test results. Different lines are used according to the B/L in Fig. 12(a). When B/L is between 0.8 and 1.0, the value is obtained by linear interpolation. The stability of the Permex is higher than that of the X-block for both failure modes. The stability number for the wave-dissipating block is shown in Fig. 13. In the case of the wave-dissipating block, the influence of the impingement position was different from the case of the flat-type blocks. Namely, the cases in which the jet impinged on the crown section showed higher stability than the cases of impingement on the slope section. This result was reflected in Fig. 13.

Fig. 14 shows a comparison of the estimated overflow depth of stability limit with the damaged overflow depth in the experiments. The estimated results are on the safe side as a whole, and they show good agreement for both failure modes.

The estimation method mentioned above is referred in the design guideline of breakwaters against tsunami (Ministry of Land, Infrastructure, Transport and Tourism, 2013) and is used for actual design.

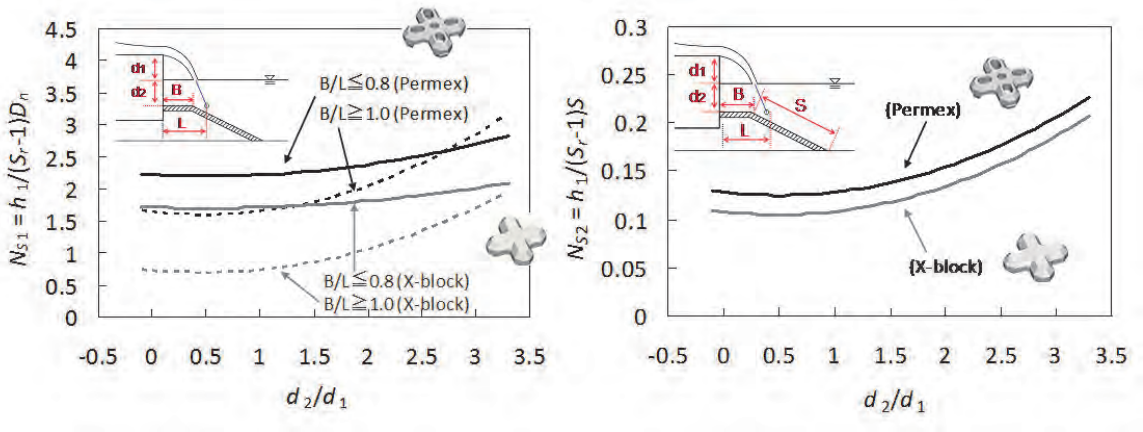

Figure 12: Stability Numbers for Flat-type Concrete Blocks

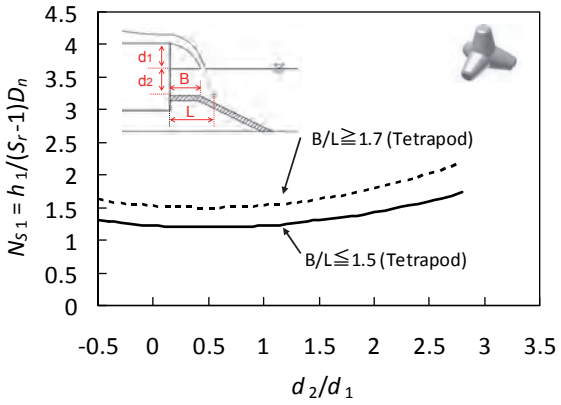

Figure 13: Stability Numbers for Wave-dissipating Concrete Blocks

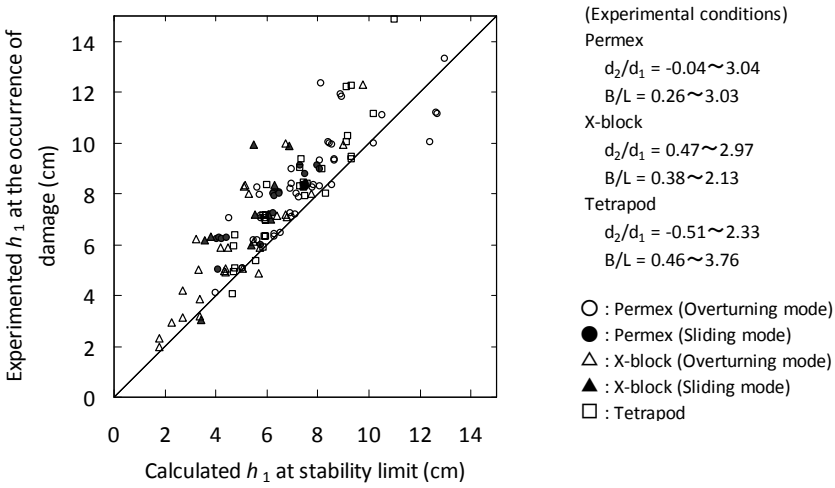

Figure 14: Calculated and Experimented Overflow Depth h_1 of the Stability Limit

3. NEW TECHNOLOGY FOR LONG-PERIOD WAVE ABSORPTION USING CONCRETE BLOCKS

3.1 Experimental Setup

The fundamental properties in the wave absorbing performance of the conventional and newly developed submerged type long-wave absorbing structures were examined by hydraulic model experiments. A series of experiments was conducted using a 50 m-long, 1.0 m-wide and 1.3 m-deep wave flume equipped with a piston type wave generator. Fig. 15 shows the test setup in the flume. The long-period wave absorbing structure model was situated on a horizontal bottom modeling a uniform depth in the harbor. The wave reflection coefficient K_R was estimated based on Goda and Suzuki (1976) using instantaneous records of water surface elevation obtained by two wave gauges located at the center of the horizontal bottom keeping the gauge spacing one-fourth of a wavelength. Since monochromatic waves corresponding to the resonance frequency of the harbor are an important factor, regular waves with periods of 4.24 to 16.97 s and heights of 0.5 to 3.0 cm were used. The model scale was set to 1/50 based on the Froude number.

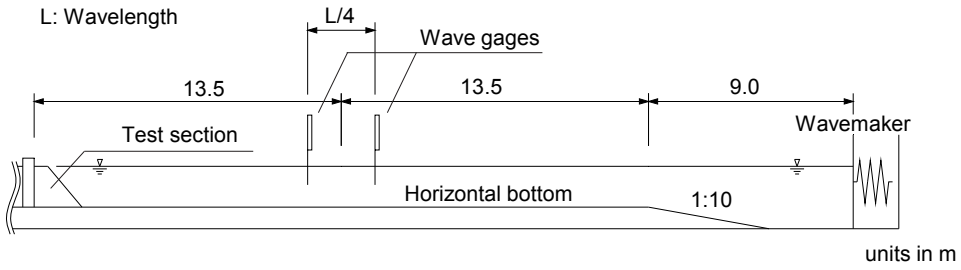

Figure 15: Test Setup in the Flume

In the initial stage, fundamental properties in wave absorbing performance of conventional and submerged type were investigated. After this, the characteristics of the submerged type were analyzed in detail. The test sections in the initial stage are shown in Fig. 16. The crown heights above the water level for the conventional type were set to 10.0 cm. On the other hand, the crest elevation of the submerged type coincided with the water level.

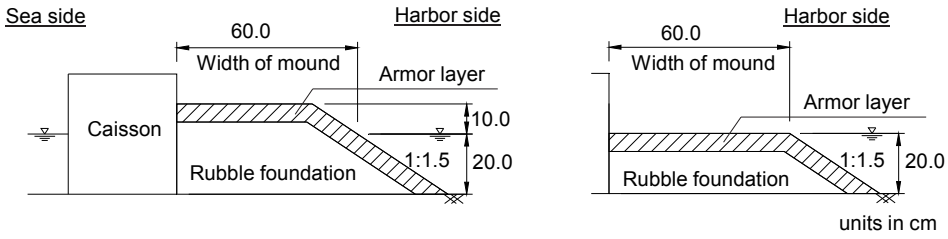

(a) Conventional Type **(b) Submerged Type**

Figure 16: Test Sections for Wave Absorbing Properties

The experimental conditions are shown in Table 1. The rubble foundation consisted of 0.4 to 1.6 g stones. In the initial stage, the water depth was 20.0 cm. The width was set to 60.0 cm. Armor stones were used because the conventional type structures had been installed with armor stones on site. In the second stage, the water depth was 14.0 to 32.0 cm. The widths were set to 30.0 cm or 60.0 cm. Tetrapod and X-block were used as examples of concrete blocks. Fig. 17 shows the geometry of the blocks.

Table 1: Test Conditions for Wave Absorbing Properties

	Model		Prototype	
Scale	1/50		1	
Wave period	4.24 – 16.97s		30 – 120s	
Wave height	0.5 – 3.0cm		0.25 – 1.50m	
Crown height above the water level	Conventional: 10cm Submerged: 0cm		Conventional: 5m Submerged: 0m	
Rubble foundation	0.4 – 1.6g		50 – 200kg	
Mound slope	1:1.5		1:1.5	
Water depth	Initial stage	Second stage	Initial stage	Second stage
	20cm	14, 20, 26 and 32cm	10m	7, 10, 13 and 16m
Width of mound	60cm	30 and 60cm	30m	15 and 30m
Armor material	8.0g armor stones (two-layer)	14.5g, 60.5g, 121.0g, 235.1g Tetrapods (two-layer) 16.2g X-Blocks	1t armor stones (two-layer)	2t, 8t, 15t, 29t Tetrapods (two-layer) 2t X-Blocks

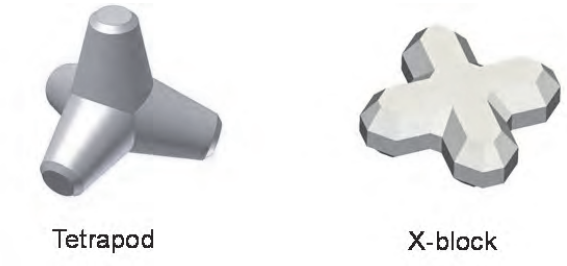

Figure 17: Concrete Blocks Used in the Experiment

3.2 Influence of Crown Height

Hereafter a prototype scale notation is used unless a particular explanation is given. Fig. 18 compares the reflection coefficients of the conventional and submerged type shown in Fig. 16. Both structures are covered with armor stones and of width at the still water level of 30 m. The reflection coefficient of the submerged type is smaller than that of conventional type independent of the wave period. As is often pointed out in the literature, for example Madsen (1983), the energy dissipation of a permeable breakwater takes place not only inside the porous structure but also on the surface of the structure due to friction. Since the submerged type has a larger amount of surface area compared to that of the conventional type, it is thought that the surface area of submerged type leads to effective energy dissipation due to the friction there. In the rest of this paper, the submerged type is mainly focused on.

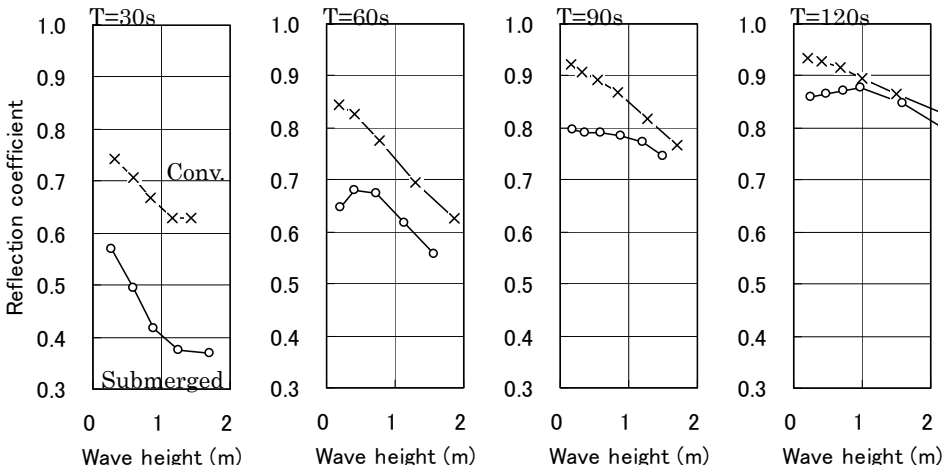

Figure 18: Reflection Coefficients of Conventional Type and Submerged Type

3.3 Influence of Armor Material

Fig. 19 shows the relationship between the wave period and the reflection coefficients of the submerged type with various armor materials, i.e., armor stones, Tetrapod and X-block. When the wave period is below 80 s, the K_R with Tetrapod covering is the smallest among all the structures, while that with the armor stone covering is the smallest against wave periods above 80 s. The K_R with Tetrapod covering seems to converge to 0.9 within the range of this study. The change in K_R with X-block covering with variation in the wave period is almost the same as that with armor stone covering. Although the details are not shown, a non-significance in the dependency of the size of the Tetrapod on K_R was observed. Because the Tetrapod covered mound can realize low wave reflection in a wide range of wave periods, the use of Tetrapod is effective for this structure.

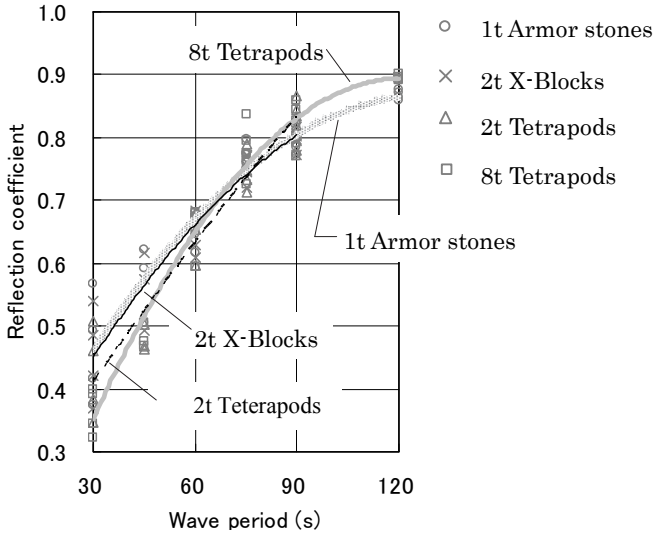

Figure 19: Relationship between Wave Period and K_R

3.4 Influence of Water Level Change

In the previous subsection, the usefulness of submerged mound type structure was clearly confirmed. The high wave absorbing performance for idealized conditions, i.e., the crest elevation coincided with the water level was well verified. However, in an actual site condition, the structure would be exposed to water level variation. Accordingly, in the following, the influence of water level change is discussed. In the coasts around Japan, the difference between flood and ebb tide is less than 2.5 m with a few exceptions. Therefore in our experiments, a tidal variation of ± 1.5 m was provided by changing the water depth from 8.5 to 11.5 m against the fixed mound geometries as shown in Fig. 16. In our experiments, 1 t armor stones or 8 t tetrapod was used for the conventional and submerged type as armor material. Fig. 20 shows the relationship between the water depth h and the wave reflection coefficient K_R under the condition where the wave height is 0.5 m. It is known that a long-period wave with wave height below 0.5 m caused decrease in the efficiency of cargo handling as shown in Hiraishi et al. (1996). The reflection coefficients of the conventional type increase with increase in water depth. On the other hand, those of the submerged type show a V-shaped distribution with a minimum value at the water depth of 10m, the idealized condition mentioned above. Although K_R increases when the water level varies from its idealized position, the K_R of the submerged type indicates smaller values than those of the conventional type within the tidal range of ± 1.0 m. This confirms the robustness of the submerged type with Tetrapod covering.

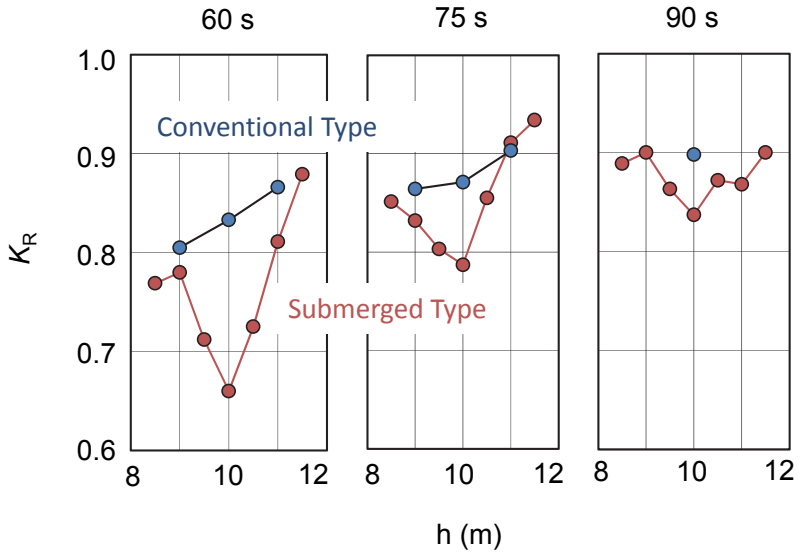

Figure 20: Relationship between Water depth and K_R

3.5 Wave Absorbing Mechanism

In the previous section, the usefulness of the submerged type was clearly confirmed. In this section, the wave absorbing mechanism is discussed through numerical analysis and hydraulic model experiments. A multiphase flow solver using the VOF method within the OpenFOAM CFD model (OpenFOAM foundation, 2011) was applied to the analysis. The hydraulic flow resistance R in the porous medium was expressed by a Dupuit-Forchheimer low (Forchheimer, 1901) as follows:

$$R = -\left(\alpha U + \beta |U| U\right) \tag{13}$$

where, U is the velocity vector, α is the laminar resistance coefficient and β is the turbulent resistance coefficient. These coefficients are expressed in the empirical formulae by Engelund (1953) as follows:

$$\alpha = \alpha_0 \frac{(1-\gamma)^3}{\gamma^2} \frac{\nu}{d^2} \quad , \quad \beta = \beta_0 \frac{1-\gamma}{\gamma^3} \frac{1}{d} \tag{14}$$

where, v is the kinematic viscosity of water, d is a nominal diameter of the stone, γ is the porosity, and α_0 and β_0 are the material constants. Although it is omitted here, the α_0 and β_0 were examined in advance in this study.

Fig. 21 shows the wave flume setup for computation. Long-period waves were made by oscillatory flow on a horizontal bottom of the wave flume. The wave energy dissipating unit was arranged in the opposite side of the mound structure model. The other computational conditions were the same as the experimental ones. Fig. 22 compares the wave reflection coefficient K_R of the mounds obtained by numerical analysis and by the experiments. Both mounds are covered with the armour stones. The computation reproduces the experimental value well. The validity of this analysis method was confirmed.

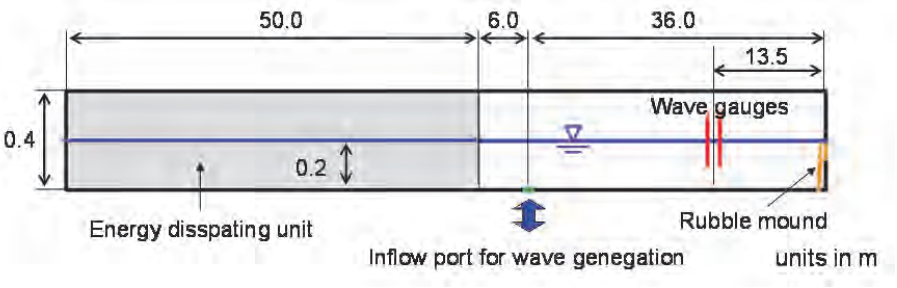

Figure 21: Wave Flume Setup for Computation

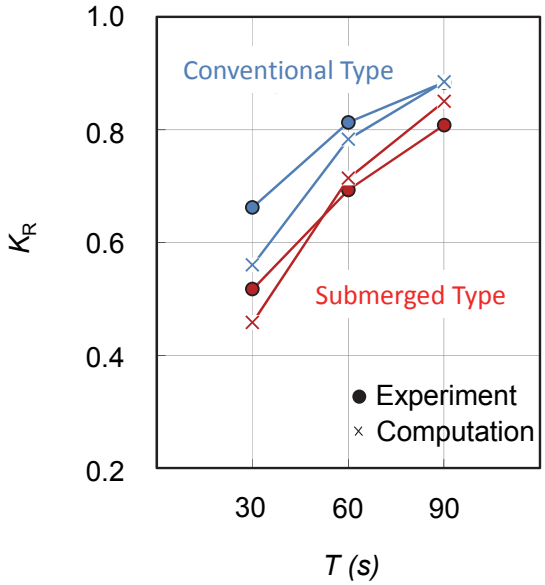

Figure 22: Comparison of Computation with Experiment

Energy breakdown was verified in the process of wave reflection on both mounds, for the purpose of looking into the wave absorbing factor. The incident wave energy flux is expressed as follows:

$$E_I C_G = \frac{1}{8}\rho g H_I^2 C_G \tag{15}$$

where, E_I is the incident wave energy, C_G is the group velocity, ρ is the density of the water and H_I is the incident wave height at the center of the two wave gauges. This energy flux $E_I C_G$ is balanced to the total energy flux of the energy dissipating flux E_D and the reflected wave energy flux E_R calculated as K_R^2. Furthermore, the E_D can be parted a dissipated energy ratio E_{Res} by the fluid resistance generated in passing through the porous structure and a remaining dissipated energy ratio E_{Etc} due to others like sea bottom and surfaces or gaps of caissons. The E_{Res} can be calculated from the value of 1 cycle average of the absorbed energy due to the mound units per unit time. Equation (15) shows the absorbed energy per unit time P:

$$P = \int_S \rho R \cdot U dS \tag{16}$$

Fig. 23 shows the wave energy balance in each type with armour stones shown in Fig. 16. The rate of the total energy flux is expressed as 1.0 by dividing by the incident wave energy flux $E_I C_G$. As shown in this figure, the same tendencies with experimental results were obtained. The value of E_R increases with increase in wave period. The value of E_R of the submerged type is smaller than that of the conventional type independent of wave period. As for the energy dissipating flux E_D, E_{Etc} is almost constant regardless of the calculation condition. This result suggests that the energy dissipation due to the mound by fluid resistance is predominant for a long-period wave absorption.

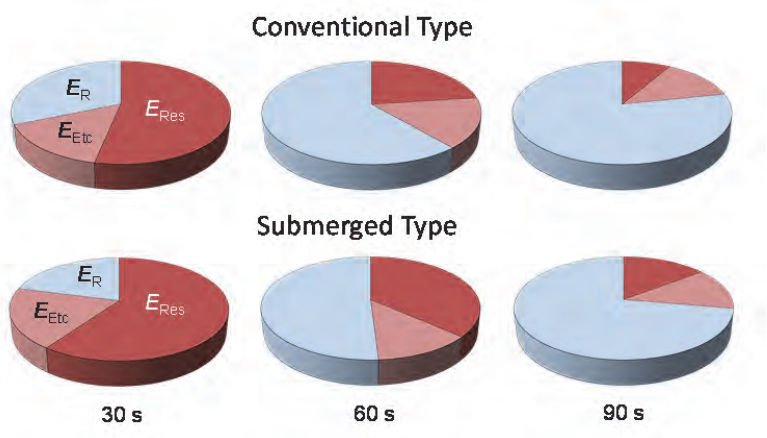

Figure 23: Wave Energy Balance in Conventional Type and Submerged Type

Since the submerged type has a larger amount of surface area in the vicinity of the water surface compared to that of the conventional type, it is expected that the surface area of the submerged type leads to effective energy dissipation. Accordingly, K_R of the mounds with impermeable rubble foundation was examined to investigate the effect of the material in armor layer for the energy dissipation. Total energy dissipating flux of the impermeable foundation $E_{D\text{-}imp}$ and E_D of the submerged type are expressed as follows:

$$E_{D-imp} \approx E_{Res-imp} = E_{C-imp} + E_{S-imp} \tag{17}$$

$$E_D \approx E_{Res} = E_C + E_S + E_F \tag{18}$$

where, E_C is the energy dissipation at the crown of the armor layer by the fluid resistance, E_S is that at the slope of the armor layer and E_F is that in the rubble foundation as show in Fig. 24. The figure shows the rate of change r_{imp} of the $E_{D\text{-}imp}$ to that of the E_D, with Tetrapod armor, calculated as $1\text{-}K^2_R$ by the experiment respectively. Although, the r_{imp} of the conventional type decreased in 27 to 40 %, the r_{imp} of the submerged type increased in 3 to 19 % in range of the wave period of 60 to 90 s. It is thought that the energy dissipation of the submerged type mainly occurred at the armor layer since the $E_{D\text{-}imp}$ was larger than E_D without any effect of the E_F. That is, it can be thought that the cause of the effective energy dissipation of the submerged type is related to a significant increase in the flow velocity inside the armor layer due to the flow contraction onto the crest.

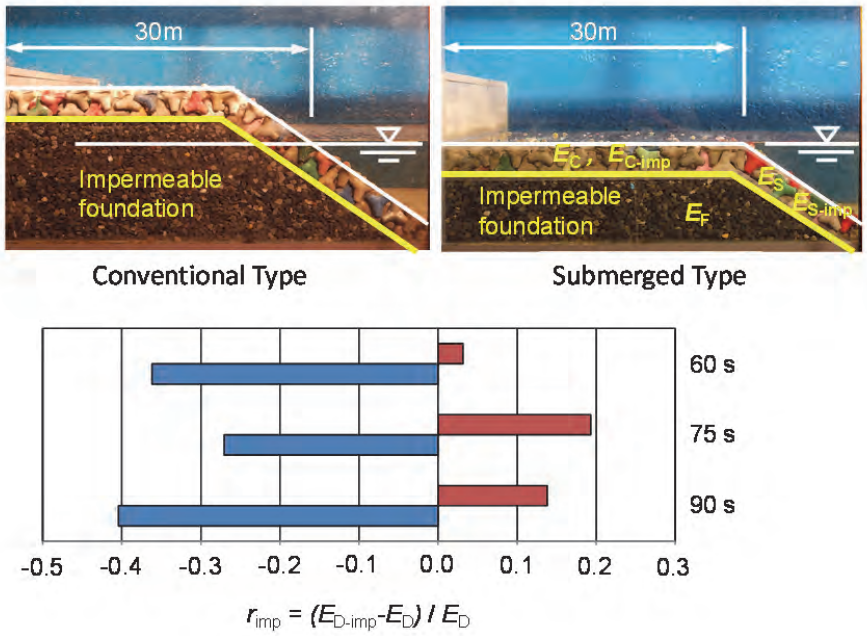

Figure 24: Rate of Change of Wave Energy Dissipation

3.6 Structure Width Estimation Method

Fig. 25 shows the relationship between the equivalent mound width normalized by the wavelength B^*/L and the reflection coefficient K_R of the submerged type with 8t Tetrapod armor layer for various combinations of water depths and widths of the mound. A definition of B^* is found in the figure. Because water particle motion of long-period waves is still present even near the sea bottom, the use of B*, which includes the influence of water depth, is more appropriate when compared to the simple crown width B which is used for the current design of conventional type. It can be seen that K_R can be estimated by using B*/L independently of the water depth and width of the mound.

By using this diagram, the required widths of structure were obtained under specified reflection coefficients, water depths, wave periods and slopes of the structure. For example, a 16.8 m width was calculated for the submerged type with tetrapods while a 32.8 m width was obtained for the conventional structure with armor stones if the required reflection coefficient was 0.85, the water depth was 10 m, the wave period was 60 s and the slope of structure was 1:1.5. Table 2 summarizes the details of the derivation.

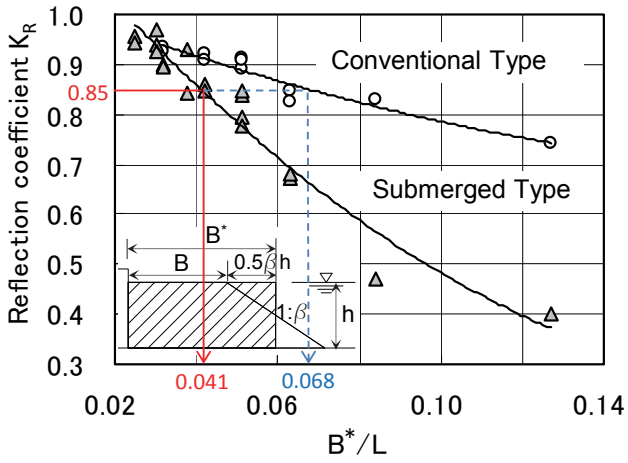

Figure 25: Design Diagram of Required Mound Width

Table 2: Comparison of Structural Width between Conventional Type and Submerged Type

K_R	Slope	h (m)	T (s)	L (m)	B^*/L		B^* (m)		B (m)	
					Submerged	Conv.	Submerged	Conv.	Submerged	Conv.
0.85	1:1.5	10.0	60.0	593	0.041	0.068	24.3	40.3	16.8	32.8

3.7 Experience of Construction

In Kashima Port located northeast of Tokyo, the submerged type structure with concrete blocks was constructed for a countermeasure against long-period waves. Kashima Port, an artificially excavated industrial port, was constructed on a sand beach of total length of about 70 km (Kashima-Nada) which faces the Pacific Ocean. Fig. 26 shows the location. Breakwaters have been extended in order to reduce the energy of the long-period waves from the sea. A submerged type structure has been installed behind the breakwater.

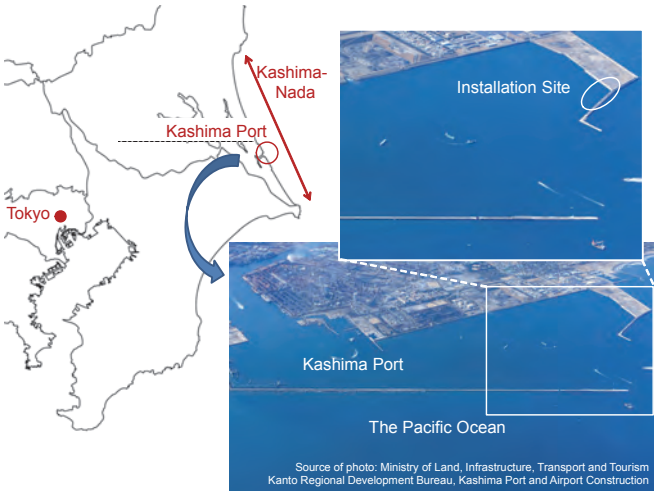

Figure 26: Installation Site of Submerged Type Structure (Kashima Port)

4. Conclusions

A practical design method with concrete blocks to cover a widened protection at the rear of a caisson breakwater against tsunami overflow has been proposed. The features of this method are summarized as follows:

- The overflow depth is used to represent the external force. This enables the estimation of the required mass of the concrete blocks to be done more robustly and easily than in the conventional method based on flow velocity.
- Two formulae are used corresponding to the two failure modes, overturning and sliding.
- This method takes into account the influence of the impingement position of an overflow jet and the influence of the harbor-side water depth. These factors are important for block stability.
- The stability numbers N_{S1} and N_{S2} for each armor unit were determined through experiments conducted in a wide range of conditions. The estimated results by this method agreed well with the experimental ones.

As a countermeasure to problems in cargo handling, a submerged type long-period wave absorbing structure has been developed. The features of this newly proposed structure are summarized as follows:

- The submerged type is more effective than the conventional type on dissipating long-period waves. As a result, the cost and space of the wave absorbing structure can be improved.
- The predominant factor for the energy dissipation of the long-period waves was the dissipated energy flux due to the armor units by the fluid resistance. It is also thought that the cause of the effective dissipation of the submerged type is related to a significant increase in the flow velocity inside the armor layer due to flow contraction on to the crest.
- It is possible to design an appropriate width of submerged type in general breakwater conditions by using the proposed design diagram.

References

Arikawa, T., M. Sato, K. Shimosako, T. Tomita, G. Yeom, and T. Niwa. (2013). Failure mechanism and resiliency of breakwaters under tsunami, Technical Note of the Port and Airport Research Institute, No. 1269 (in Japanese).

Coastal Engineering Research Center. (1977). Shore Protection Manual, U.S. Army Corps of Engineers, U.S. Government Printing Office, Vol. II, 7_213-7_216.

Engelund, F. (1953). On the laminar and turbulent flows of ground water through homogeneous sand, Transactions of the Danish Academy of Technical Sciences, Vol. 3, No. 4.

Forchheimer P. (1901). Wasserbewegung durch Boden, Zeit. Ver. Deut. Ing., Vol 45, pp 1781-1788.

Goda, Y. and Suzuki, Y. (1976). Estimation of incident and reflected waves in random wave experiments. Proc. 15th International Conference on Coastal Engineering, Honolulu, Vol.1, pp.828-845.

Hamaguchi, M., S. Kubota, A. Matsumoto, M. Hanzawa, M. Yamamoto, H. Moritaka, and K. Shimosako. (2007). Hydraulic stability of new flat type armor block with very large openings for use in composite breakwater rubble mound protection, Proceedings of Coastal Structures 2007, ASCE, 116-127.

Hiraishi, T., Tadokoro, A. and Fujisaku, H. (1996). Characteristics of Long Period Wave Observed in Port, Report of the Port and Harbour Research Institute, Vol.35, No.3, pp.3-36. (in Japanese)

Hom-ma, M. (1940a). Discharge coefficient on overflow weir (part-1), JSCE Magazine, Civil Engineering, Vol. 26, No. 6, 635-645 (in Japanese).

Hom-ma, M. (1940b). Discharge coefficient on overflow weir (part-2), JSCE Magazine, Civil Engineering, Vol. 26, No. 9, 849-862 (in Japanese).

Kubota, S., M. Hamaguchi, A. Matsumoto, M. Hanzawa, and M. Yamamoto. (2008). Wave force and stability of new flat type concrete block with large openings for submerged breakwaters, Proceedings of 31st International Conference on Coastal Engineering, ASCE, 3423-3435.

Madsen, P. A. (1983) Wave Reflection from a Vertical Permeable Wave Absorber. Coastal Engineering, Vol.7, pp.381-396.

Ministry of Land, Infrastructure, Transport and Tourism, Port and Harbor Bureau. (2013). Design guideline of breakwaters against tsunami (in Japanese).

OpenFOAM foundation Ltd. (2011). OpenFOAM User Guide version 2.0.1, http://www.openfoam.org

Van der Meer, J.W. (1988). Stability of cubes, tetrapods and accropode, Proceedings of Conf. Breakwaters ’88, 71-80.

FULL-SCALE MEASUREMENTS TO ASSESS SQUAT AND VERTICAL MOTIONS IN EXPOSED SHALLOW WATER

by

Jeroen Verwilligen[1], Marc Mansuy[2], Marc Vantorre[3] and Katrien Eloot[4]

ABSTRACT

The paper presents the results of full scale measurements performed on seven cape-size bulk carriers sailing inbound to the port of Flushing/Vlissingen (the Netherlands). The voyages of this type of vessels correspond to small under keel clearances (to a minimal value of 16%) and exposed wave conditions (with a wave height up to 2.6 m). The main interest in this paper concerns the vertical motions experienced by the vessels and the identification and assessment of the major factors influencing these motions. As the vertical ship motions for bulk carriers operating in coastal waters are mainly related to seakeeping and squat, the unsteady and steady ship motions were analysed separately.

The observations will be applied to validate a prediction tool for vertical ship motions, which is implemented by the Common Nautical Authority (Flanders / the Netherlands) to assess probabilistically the accessibility of deep-drafted vessels to the harbours along the river Scheldt.

1 INTRODUCTION

The shipping traffic to the Belgian and Dutch ports located at the Western Scheldt estuary and the river Scheldt follows an access channel of which the depth is restricted. As a result, deep-drafted vessels cannot always sail 24 hours a day on the river Scheldt. The period in which these vessels may proceed inbound or outbound is called the tidal window. The Common Nautical Authority (CNA) calculates these tidal windows and gives permission for the vessels to proceed.

In order to optimize the accessibility for deep-drafted vessels, the CNA is in the process of adopting a probabilistic access policy to determine the tidal windows. In a probabilistic approach a prediction tool for vertical ship motions is the basis for defining minimal under keel clearances. Some of the major phenomena influencing the vertical ship motions concern squat and seakeeping effects.

For the port of Flushing/Vlissingen (NL), part of the North Sea Port, the design vessel is a cape size bulk carrier with a draft of 16.5 m. As these vessels all have similar dimensions and hull shape, they are expected to have a very similar motion behaviour. As a consequence these vessels were an

[1] Flanders Hydraulics Research, Expert Nautical Research, Belgium, jeroen.verwilligen@mow.vlaanderen.be

[2] Ghent University, Maritime Technology Division, Nautical Researcher, Belgium, marc.mansuy@ugent.be

[3] Ghent University, Maritime Technology Division, Professor, Belgium, marc.vantorre@ugent.be

[4] Flanders Hydraulics Research, Senior Expert Nautical Research, Belgium, katrien.eloot@mow.vlaanderen.be

interesting test case for comparing ship motion predictions to actual measurements on board of the vessels.

For a total number of seven inbound bulk carriers, the ship motions were measured by the Dutch Pilotage. Then Flanders Hydraulics Research (FHR) together with Ghent University (UGent) related the position data with environmental data such as tide, current, bottom, waves and other shipping traffic. The analysis on both ship behaviour and environmental circumstances revealed the impact of operational, meteorological and environmental parameters on both squat and seakeeping.

2 TIDAL WINDOWS

Access channels to harbours are often subject to tide, so that arrival and departure of ships may be limited to a certain window. This tidal window is mainly determined by under keel clearances resulting from variations of the water level and is therefore of particular importance for deep-drafted vessels. Furthermore also other parameters such as air draft clearance, lateral and longitudinal current components, wind conditions or penetration of the keel into soft mud layers may be limiting factors for the tidal window (Eloot et al., 2009).

2.1 Keel clearance and vertical motions

During the transit of the ship through the access channel, a comparison between the vertical dimensions of the vessel and of the waterway should result into acceptable margins (Vantorre et al. 2013). Below the waterline, a suitable vertical distance should be maintained between the ship's keel and the channel bottom. This distance also referred to as the under keel clearance (UKC) should accommodate the following functions:

- avoid contact between keel and bottom;
- guarantee the ship's controllability and manoeuvrability.

The under keel clearance depends on a number of factors that may be related to the ship, the water level, hydro-meteorological conditions and the bottom:

- Ship related factors:
  - the **static ship's draft (**aft and fore) in still water conditions;
  - hydrostatic impact of water **density** on the ship's draft;
  - the vertical motion of the ship due to **squat**, which depends mainly on the ship's speed through the water, the ship's geometry, the water depth and the blockage;
  - **wave** induced vertical ship motions (heave, pitch, roll);
  - **wind** induced heel;
  - heel due to centrifugal forces in **bends**.
- Water level related factors:
  - **tidal** effects (astronomical);
  - meteorological effects (wind, discharge of fresh water).
- Bottom related factors:
  - dredging maintenance **depth**;
  - dredging execution tolerance;
  - sedimentation;
  - accuracy of bathymetric survey data;
  - nautical bottom.

Under keel clearance (UKC) related channel access criteria can be formulated in a deterministic or a probabilistic way, or in a combination of both.

2.2 Deterministic approach

Deterministic criteria mostly prescribe a minimum value for the gross under keel clearance (i.e. the difference between the bottom depth and the static draft), expressed either in metre or as a percentage of the ship's draft. This value depends on the channel, taking account of the local wave climate and the ships' speed range. In the channels giving access to the ports located along the river Scheldt, the following values are currently applied (Fig. 1):

- 15.0% of draft for *Scheur West* and *Scheur East*;
- 12.5% for the Dutch part of the *Western Scheldt*;
- 10.0% for the Dutch part of the *Western Scheldt* and for vessels with destination Flushing/Vlissingen ;
- 10.0% of draft for the Scheldt river on Belgian territory;
- 1.0 m for the Sea Canal from Terneuzen to Ghent (operated by vessels with draft up to 12.5 m).

Figure 1: .Access channels and harbours in the Scheldt estuary: 1: Scheur West, 2: Pas van het Zand, 3: Scheur East, 4: Wielingen, 5: Western Scheldt, 6: Lower Sea Scheldt. A: Antwerp/Antwerpen (B), G: Ghent/Gent (B), O: Ostend /Oostende (B), T: Terneuzen (NL), V: Flushing/Vlissingen (NL), Z: Zeebrugge (B), Wa: Wandelaar (B).

2.3 Probabilistic approach

Probabilistic approach policies are based on an acceptable probability of bottom-ship contact during the passage of one single ship. Such an acceptable probability of bottom touch is related to the consequences of such a contact – as after all it is the risk (probability * consequence) which has to be kept under control – and an accepted return period for such an undesired event, so that the intensity of the shipping traffic making use of the channel is also important. However, a probability of bottom touch criterion needs to be accompanied by an additional condition to guarantee the manoeuvrability and controllability of the vessel, as these properties deteriorate significantly with decreasing under keel clearance. Such a criterion can be formulated in terms of either a minimum gross under keel clearance or a minimum manoeuvrability margin, the latter being defined as the time-averaged clearance under the ship, incorporating the effects of water depth, draft, squat and (wind and bends induced) heel, but excluding the oscillatory effects caused by wave action. The manoeuvrability margin criterion will overrule the probability of bottom touch criterion in areas protected from wave impact and in case of favourable weather conditions. PIANC (2014) suggests a minimum manoeuvrability margin of 5% of draft or 0.6 m, whichever is greater.

2.4 Probabilistic Policy Scheldt Harbours

Taking into account the expected beneficial effects on accessibility (Vantorre et al., 2014), the CNA is implementing a probabilistic method for providing tidal windows to the harbours along the river Scheldt. In order to assure the probabilistic calculations to be sufficiently safe, a validation project was initiated in which ship measurements in the Scheldt Estuary were compared to predictions of vertical ship motions. For the following reasons, at first, the validation project was restricted to inbound cape-size bulk carriers sailing to the port of Flushing/Vlissingen:

- very similar ship dimensions (length, beam, draft) and hull shape, allows to assess the influence of different operational and environmental conditions;
- small differences in water density along the trajectory, so that vertical motions due to density changes could be ignored;
- FHR possesses an exact scale model (292 m x 45 m x 16,5 m at scale 1/75) of the ships tested at full scale. Furthermore a wide range of towing tank results were available at UKC 10%; 20%, 35% and 100%. This opened the possibility to compare squat measurements at scale and in nature;
- open deck structure of bulk carrier was very suitable for installing the measurement equipment;
- the Dutch Pilotage developed a ship positioning system allowing to position the vessel in 6 degrees of freedom;
- the bulk carriers to Flushing/Vlissingen have a very restrictive current window, to ensure that the vessels arrive at the port 45 minutes after high tide, when current speeds are negligible. As a consequence the tidal conditions in all measurements are similar;
- as full ship types (such as a bulk carrier) squat by the bow, the influence of propulsion on the maximum ship squat is negligible.

Within this project the Dutch Pilotage provided positioning data, while FHR and UGent processed these data to ship motions in 6 degrees of freedom. Further processing allowed to assess both squat and seakeeping effects and to relate the results to the determining parameters.

3 SHIP MEASUREMENTS

For seven cape size bulk carriers the inbound trajectory from the anchorage area ‘Wandelaar’ to the Kaloothaven in the port of Flushing/Vlissingen was studied.

3.1 Trajectory

The trajectory covers the fairways Scheur West and Scheur Oost on Belgian territory, and the fairways Wielingen and the Western Scheldt on Dutch territory (see Fig. 1, Fig 2 and Fig. 3). This tidal environment is subject to consecutive zones with shallow and very shallow conditions and strong wave conditions. Due to operational limitations, shipping traffic is allowed up to a significant wave height of 3.0 m.

Figure 2: Measured trajectory for 4 bulk carriers sailing inbound to the port of Flushing/Vlissingen (NL)

Figure 3: Trajectory of Asian Blossom on July 27th 2015 to Flushing/Vlissingen (Kaloothaven)

3.2 Ship particulars

The dimensions of the seven bulk carriers measured, were very similar, as can be seen from Table 1. Except for the vessel Panormos, all vessels had an even keel draft of approximately 16.5 m. The vessel Panormos had a smaller draft and was trimmed by the stern.

Also the length between perpendiculars for the vessel Cape Canary deviates from the other vessels measured. The reason for the larger L_{PP} for Cape Canary was the bow shape of the vessel. Cape Canary was the only vessel that was not designed with a bulbous bow.

Vessel	Asian Blossom	Cape Canary	Wisdom of the Sea	Lancelot	Bulk Mexico	Cape Harmony	Panormos
Date	27/07/'15	29/07/'15	24/09/'15	8/10/'15	19/11/'15	29/06/'16	1/10/'16
L_{OA} (m)	292	292	292	291.8	292	292	292
L_{PP} (m)	283.8	288	283	282.2	278	282	282
B (m)	45	45	45	45	45	45	45
T_F (m) at 1025 kg/m³	16.43	16.5	16.4	16.44	16.5	16.5	15.55
T_A (m) at 1025 kg/m³	16.43	16.5	16.4	16.47	16.5	16.5	16.25
GM (m)	5.59	4.86	5.76	5.36	-	6	5.38

Table 1: Ship particulars of vessels measured

3.3 Ship motions

When analysing vertical ship motions the terminology as presented in Table 2 is applied throughout this document. A distinction is made between steady motions (low frequency) mainly related to ship squat and unsteady motions (high frequency) mainly related to seakeeping.

Table 2: Ship motions terminology

Motion	Steady	Unsteady
Heave	Steady heave	Unsteady heave
Roll	Heel	Unsteady roll
Pitch	Trim	Unsteady pitch

3.4 Measurement equipment

For manoeuvring marginal vessels the Dutch and Flemish pilotages apply an accurate positioning system called Full SNMS[5] (van Buuren, 2005). The Full SNMS positioning system is based on positions provided by two RTK-GPS antennas (called POS and HDG1) mounted on each bridge wing respectively (see Fig. 4). This setup allows to measure horizontal ship motions (surge, sway and yaw) relevant for manoeuvring purposes. Furthermore, based on the altitude of the GPS antennas the height of the vessel (referred to a vertical reference level) and the roll of the vessel can be assessed.

In order to perform a full six degrees of freedom measurement an additional pitch measurement had to be integrated in the Full SNMS setup. In 2013 the Dutch Pilotage made an investment to upgrade the positioning system with a third RTK-antenna (HDG2) mounted at the ship bow. By combining altitude measurement from the HDG2 antenna, with the altitude measurements of the other antennas the pitch motion could be obtained. The Full SNMS positioning system upgraded with a third antenna is referred to as the Full-Plus SNMS positioning system. In optimal conditions the Full-Plus SNMS positioning system has a measuring frequency of 5 Hz.

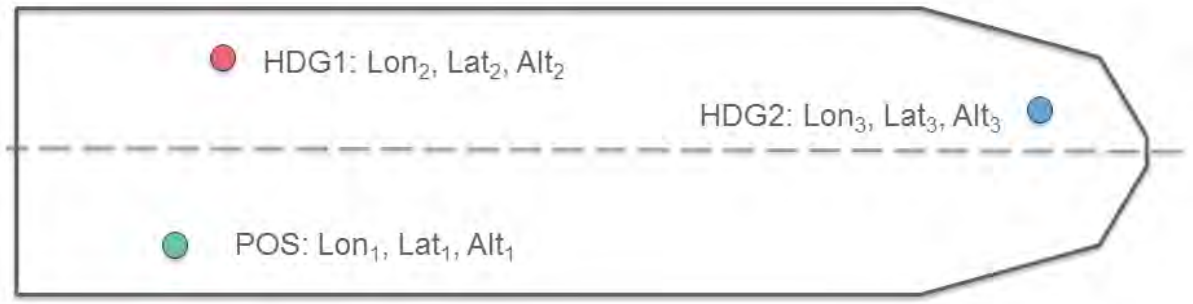

Figure 4: Positions and naming of GPS antennas

3.5 Vertical motions with respect to waterline

The Full-Plus SNMS positioning system provides ship motions with respect to an earth bound coordinate system. When assessing the hydrodynamics involved in vertical ship motions these ship motions should be referred to the static waterline (see Fig. 5).

At first the altitude measurements with respect to the GRS80 ellipsoid were converted to a geodetic reference level (NAP). Then for a static measurement (at negligible ship speed) the vertical antenna positions were compared to the water level in order to know the vertical distance between the antennas and the static waterline (ΔZ_{Static}). Finally, for a sailing vessel the vertical distance between the antennas and the instantaneous and local mean waterline ($Z_{Tide} - Z_{Antenna}$) were subtracted from the static vertical distance (ΔZ_{Static}) in order to assess the sinkage of the vessel at the position of the antenna.

[5] SNMS: Schelde Navigator Marginale Schepen; Scheldt Navigator Marginal Vessels

In a tidal environment the accuracy of the measurement of the vertical ship motions with respect to the waterline (sinkage) depends on:

1. the accuracy of the altitude measurement on the antennas (0.03 m);
2. the accuracy of the conversion method to a geodetic reference level;
3. the horizontal distance of the antennas with respect to the outer contour of the vessel (limited impact as the antennas were installed on the bridge wings and at the bow);
4. the accuracy by which the water level along the trajectory could be reproduced (0.05 m).

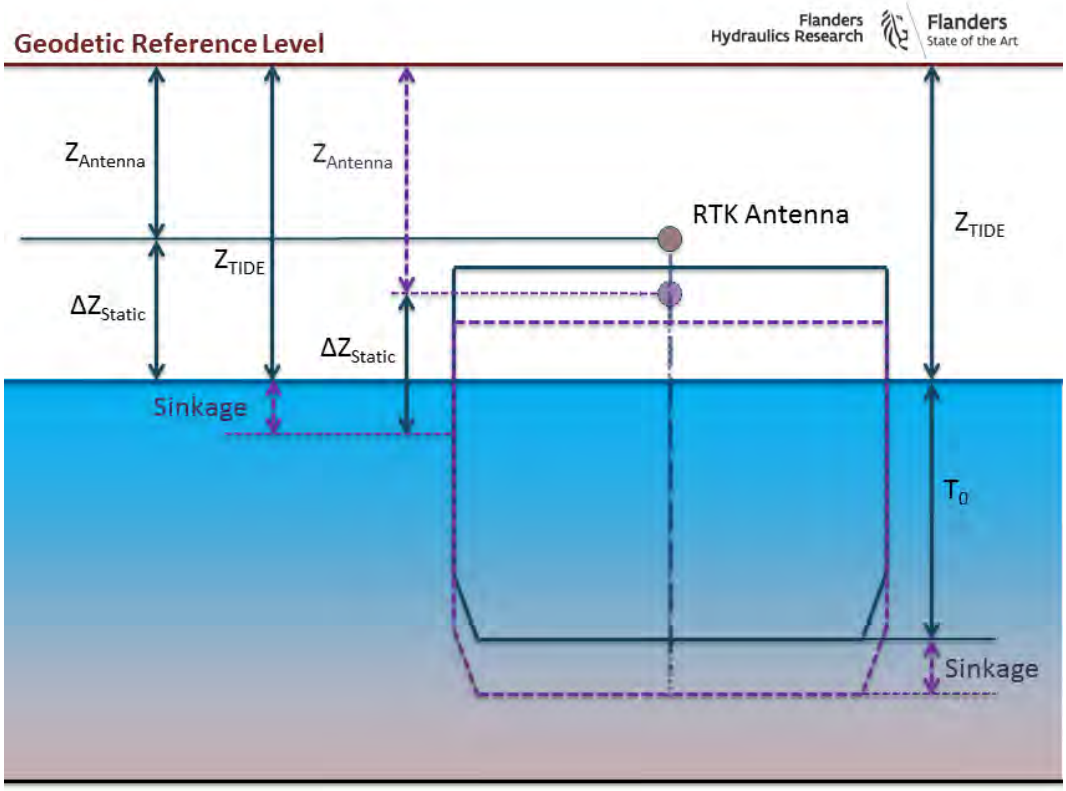

Figure 5: Calculating vertical motion with respect to waterline (sinkage). Full line: static condition; dashed line: sailing condition.

3.6 Steady and unsteady motions

Depending on the cause of the vertical ship motion, steady and unsteady motions can be distinguished. The following parameters are varying rather slowly and are associated to steady motions:

- ship speed influencing squat;
- under keel clearance and blockage influencing squat;
- tide;
- density;
- overtaking manoeuvres;
- bends;
- wind.

On the other hand unsteady motions can be the result of the following phenomena:

- ship response to waves (seakeeping);
- ship meetings (encounters);
- rudder deviations;
- wind gusts.

In order to separate the vertical ship motions in a steady part and an unsteady part, the following procedure was followed:

- The steady motions were calculated as the running average over a period of approximately 60 s taken on the full vertical motion signal. The period of the running average was defined as four times the dominant period obtained from a Fourier analysis for each degree of freedom separately (the dominant period was typically 15 s to 20 s).
- The unsteady motions were calculated by subtracting the steady motions from the full vertical motion signal.

4 ENVIRONMENTAL DATA

The main environmental parameters influencing the vertical motions of cape-size bulk carriers concern:

- water depth and blockage;
- current velocities;
- waves;
- wind;
- shipping traffic.

In the following sections the processing of environmental data is presented in order to assess the influence of the above mentioned parameters.

4.1 Tide and current

In section 3.5 it was already mentioned that reproducing accurately the water level along the trajectory is of utmost importance for the calculation of the ship's vertical motions. Furthermore tide information is required to retrieve water depth information from a bottom survey.

In a first step the tide along the trajectory was derived from hindcast simulations performed with the numerical model ZUNOv4 (Dutch ministry of infrastructure and water management, Rijkswaterstaat). This model provides full area coverage and an update period of 30 minutes for both tidal levels and current vectors. By performing a geographical triangulated interpolation and a time interpolation the ZUNOv4 grid files could be projected on the shipping trajectory. However, when comparing the hindcast data with available tide stations in the environment (see Fig. 7), it was noticed that tide from the hindcast data differed up to 0.15 m to the tide measured in the stations. As a result a supplementary correction factor (both depending on place and time) was applied on the tide data retrieved from the ZUNOv4 grids. In Fig. 6 the tidal information from the hindcast model and measured in the tide stations is compared. Also the tide along the shipping trajectory is presented with and without correction factor applied.

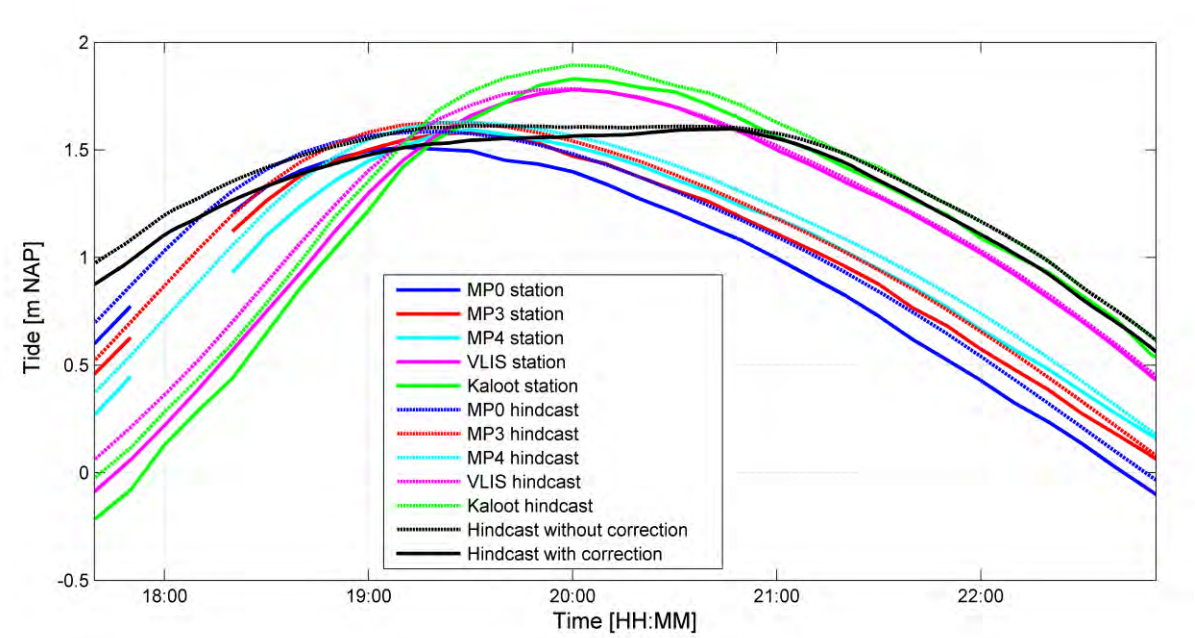

Figure 6: Reproducing tide along the trajectory of Cape Harmony (black), with (full line) and without (dashed line) correction factors

Figure 7: Tide measurement stations available along the trajectory

4.2 Bathymetry

In order to assess the water depth, under keel clearance and blockage along the trajectory, the bathymetry was retrieved from the most recent survey data available at the time of the ship measurements. The survey information from the Scheldt ECS database (Flemish Hydrography and Rijkswaterstaat) was used as an input. The survey data were projected on an automatically generated triangular grid with high resolution (10 m) at the shipping trajectory and courser resolution (50 m) on the edge of the fairway (see Fig. 8).

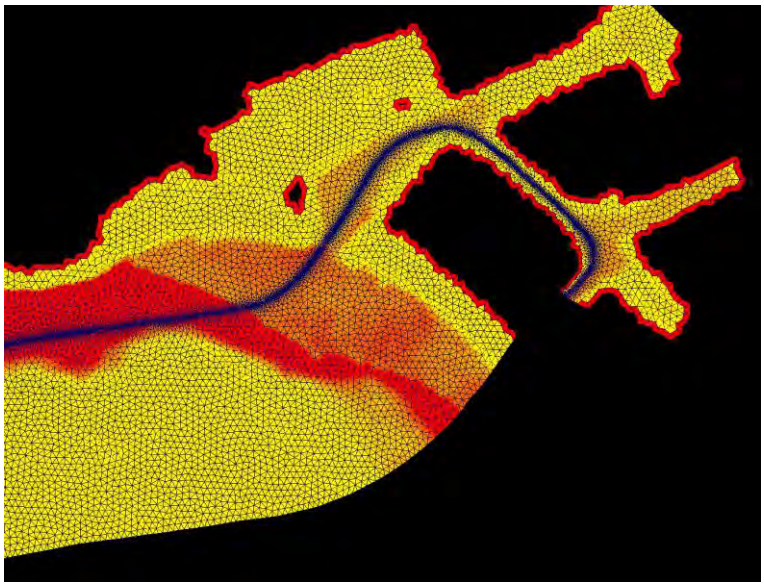

Figure 8: Scheldt ECS Survey data projected on an automatically generated grid (trajectory Asian Blossom)

4.3 Waves

At the time of the measurements, coastal wave spectra data were available at the positions presented in Fig. 9. Within the project the following parameters were derived from the directional (green) wave spectra:

- significant wave height [m];
- dominant wave direction [Deg];
- swell height (≤0.1Hz) [m];
- swell direction [Deg].

Figure 9: Wave rider buoys in the studied environment. Green buoys providing directional wave spectra

4.4 Wind

Wind conditions during the measurement were based on wind information from the measuring stations Westhinder and Wandelaar (see Fig. 9). As no impact of wind on ship motions could be observed, wind will not be discussed further in the paper.

4.5 Shipping traffic

Encounters with other shipping traffic may have a large effect on the squat of a vessel (Eloot et al., 2011). As a consequence when studying vertical ship motions, the impact of other shipping traffic should be taken into account. The presence of other shipping traffic was deduced from AIS-information provided by the Scheldt Radar Chain (SRC). A processing tool was developed in order to filter the AIS data of the vessels that operated in the proximity of a reference vessel (see Fig. 10) and subsequently provides a table with ship meetings. For the meetings performed during the seven ship measurements to Flushing/Vlissingen, no significant impact on vertical ship motions could be observed.

Figure 10: Presentation of the vessel Asian Blossom with filtered AIS-vessels

5 RESULTS

The graphs presenting the results can be provided with two horizontal axes (for an example see Fig. 11). The bottom axis shows the UTC-time of the trajectory (for date: see Table 1), while the top axis shows the running distance (s) along a reference trajectory. The geographical parameter, running distance, allows to compare different measurements. The origin of the running distance was defined at the breakwaters of the port of Flushing/Vlissingen (see Fig. 3) with positive values inside the harbour and negative values outside. In Table 3 the running distances corresponding to different fairways are presented.

Fairway	Country	Running distance	
		From	To
		[km]	[km]
Scheur West	BE	-60.0	-37.4
Scheur East	BE	-37.4	-26.0
Wielingen	NL	-26.0	-8.1
Western Scheldt	NL	-8.1	0.0
Port of Flushing/Vlissingen	NL	0.0	3.5
Kaloothaven	NL	2.5	3.5

Table 3: Running distances corresponding to fairways

5.1 Vertical motions

In Fig. 11 the vertical motions processed for the vessel Asian Blossom are visualised. In this figure the steady and unsteady part of the heave, pitch and roll motion at midship position are presented.

The following conclusion can be drawn from Fig. 11 .

- The filtering method for steady and unsteady motions (see section 3.6) gives satisfactory results.
- The unsteady motions are symmetrical (the mean value of the unsteady motions is negligible).
- Significant unsteady motions can be observed when the vessel was operating in the fairways Scheur, Wielingen and the downstream part of the Western Scheldt. The unsteady motions are rapidly decreasing when the vessel entered the Western Scheldt.
- The unsteady motions decrease significantly when entering the port (running distance = 0 km)
- The unsteady motions are related to sea conditions. The influence of waves on ship motions is studied in section 5.3.
- Significant steady motions were observed for heave and pitch. These motions correspond to the squat of the vessel. In section 5.2 squat will be discussed in detail.
- The steady roll angle is negligible. This indicates the small influence of wind on the vertical ship motions (the wind condition was WSW 7).

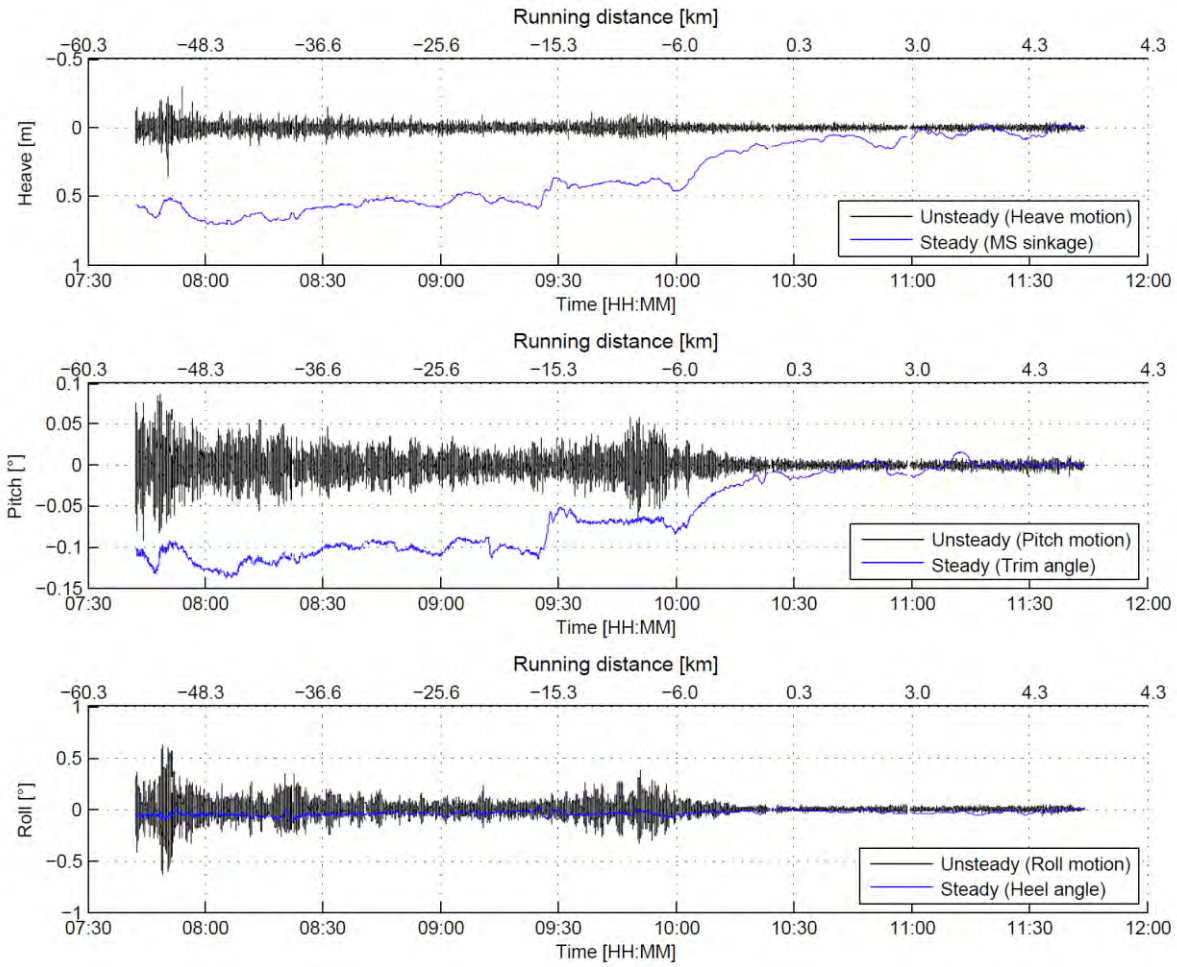

Figure 11: Vertical motions at midship position for Asian Blossom sailing to Flushing/Vlissingen

5.2 Squat (steady motions)

According to PIANC (2014) squat is defined as follows:

> *Squat is a steady downward displacement consisting of a translation and rotation due to the flow of water past the moving hull. This water motion induces a relative velocity between the ship and the surrounding water that causes a water level depression in which the ship sinks. Shallow water and channel banks significantly increase these effects. The velocity field produces a hydrodynamic pressure change along the ship that is similar to the Bernoulli effect since kinetic and potential energy must be in balance (Newman, 1977). This phenomenon produces a downward vertical force (causing sinkage, positive downward displacement) and a moment about the transverse axis (causing trim) that can result in different values at the bow and stern. Thus, squat is composed of this overall decrease in UKC due to sinkage and change in trim.*

From the measurements, squat was defined as the vertical motions corresponding to steady heave and steady pitch or trim (see Fig. 11). For ship types with a full hull form in even keel conditions, maximum squat always occurs at the bow, so that in this paper only bow squat will be discussed.

The major parameters influencing the ship squat are:

- ship particulars;
- ship speed through water;
- under keel clearance and blockage.

As the measurements were performed on very similar vessels with (except for the vessel Panormos) very similar loading conditions, it may be expected that the squat behaviour of the tested vessels is also similar.

In Fig. 12 the results of bow squat, ship speed[6] and gross under keel clearance are presented. It can be observed that the largest squat motions appeared on the vessel Asian Blossom when operating in the fairway Scheur West. For this vessel both the influence of ship speed and UKC is clearly demonstrated.

The vessel Asian Blossom applied in the fairway Scheur West a speed of approximately 12 kn (s = -55 to -42 km) leading to a bow squat varying between 0.75 m and 1.05 m. The evolution of squat in this area is clearly related to the evolution of the water depth. The most shallow parts of the fairway (UKC 24% at s = -54 km and s= -46 km) corresponded to the largest squat values (app. 1.0 m), while a very deep part of the fairway (s = -52 km) resulted in a squat value that was limited to 0.75 m.

When operating in the fairways Scheur East and Wielingen the variations in ship speed immediately result in important changes in ship squat. The most striking example is the speed drop of the vessel Asian Blossom in the fairway Wielingen (at s = -15 km). A ship speed decreasing from 10.5 kn to 8.2 kn resulted in a decrease of squat from 0.85 m to 0.54 m at more or less constant UKC.

Also for the other vessels the relation between ship squat, speed through water and UKC can be observed from Fig. 12.

As a result of the different loading condition, the squat behaviour of the vessel Panormos deviates from the other vessels (Härting, 2009). However, when comparing the squat behaviour of the other six vessels it can be noticed that at similar conditions the squat of Cape Canary and Cape Harmony was smaller than for the other vessels. This was for example the case at s = -50 km. At that position the ship speed of Cape Harmony was identical to the ship speed of Wisdom of the Sea (9.5 kn), while the bow squat of Cape Harmony was 0.18 m smaller. At the same position it was observed that the bow squat of Cape Canary was very close to the squat of Wisdom of the Sea (0.58 m), while the speed of Cape Canary was 1.0 kn larger than the speed of the Wisdom of the Sea. For the vessel Cape Canary the smaller values of bow squat could be associated to the different bow shape of the vessel. From the L_{PP} (see Table 1) and from photographs of the vessel in ballasted conditions it could be observed that Cape Canary was the only vessel without a bulbous bow. As a bulbous bow alters the pressure distribution at the ship bow, an increase of bow squat is likely. This effect is confirmed by the observations on the vessel Cape Canary. On the other hand for the vessel Cape Harmony, no different bow shape could be observed. The smaller bow squat experienced on the vessel Cape Harmony could not be explained.

[6] If not specified otherwise, ship speed refers to ship speed through water.

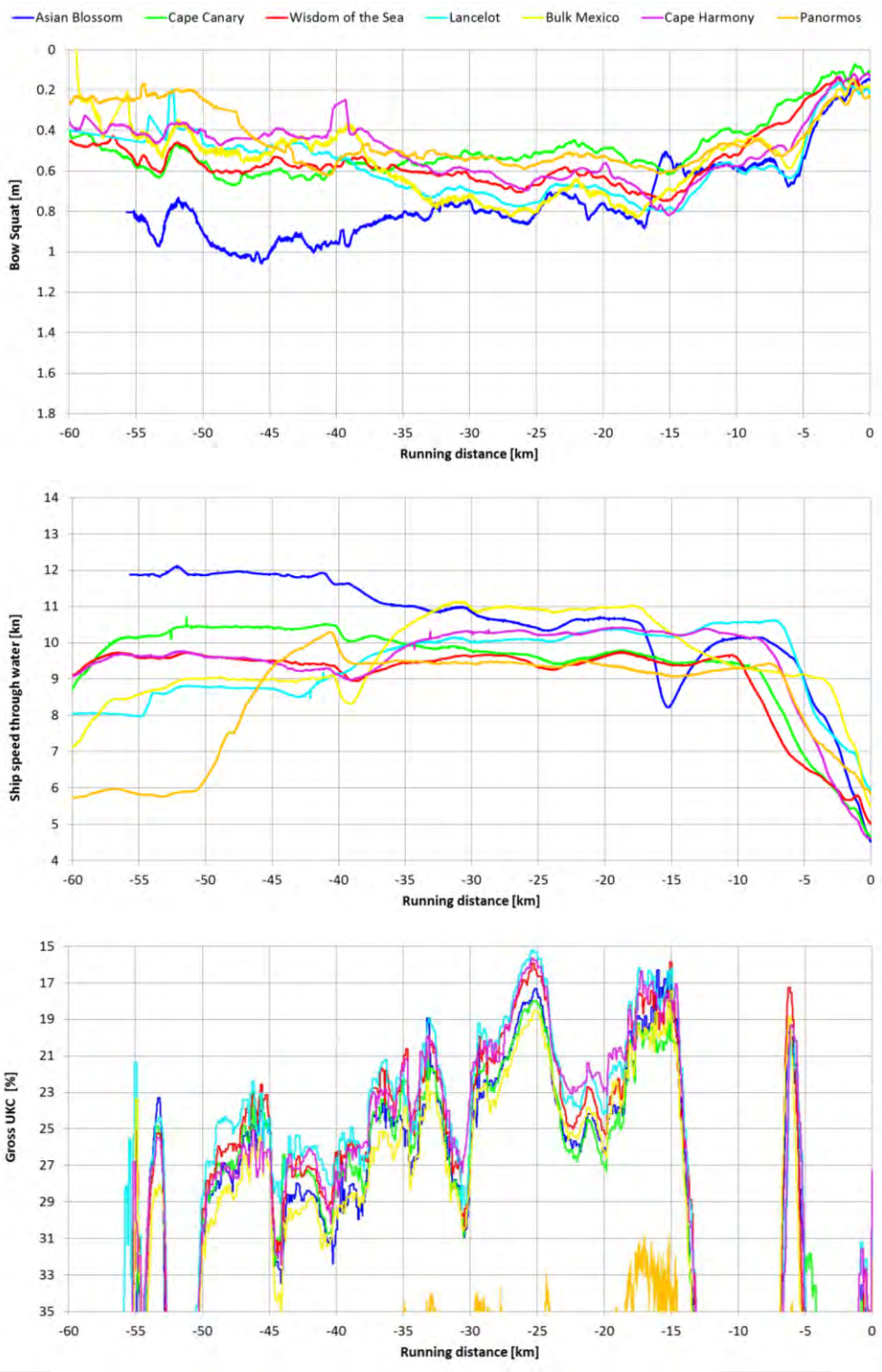

Figure 12: Squat (top), Ship speed (centre) and UKC (bottom) for seven full-scale measurements

5.3 Seakeeping (unsteady motions)

The unsteady heave, pitch and roll motions are mainly resulting from the wave climate present in the fairway. In order to compare the unsteady vertical motions for different ship measurements, the envelope of the unsteady motions at the bow (see Fig. 13) was calculated for a ship position at the FP at port side and at starboard side. The maximum unsteady motion was obtained by taking the maximum from the port and starboard envelope and is presented in Fig. 14 for the seven measurements performed.

Fig. 14 reveals the large deviation in unsteady ship motions, leading to a sinkage of almost 1.0 m for the vessel Bulk Mexico and much smaller values for the other vessels. For the vessels Cape Canary, Wisdom of the Sea, Cape Harmony and Panormos the unsteady vertical motions are limited to a maximum value of 0.25 m.

Now a comparison is made between the unsteady ship motions and the wave parameters deduced from directional wave spectra (see section 4.3). When observing the significant wave heights (see Table 4) it can be noticed that the largest wave heights were present during the passage of Asian Blossom. Despite the much smaller unsteady motions experienced on the vessels Cape Canary, Wisdom of the Sea and Cape Harmony, the significant wave height for those vessels was larger than for the vessel Bulk Mexico. It can be concluded that the significant wave height does not show any relation with the unsteady motions of a cape-size bulk carrier. The swell (see Table 5) on the other hand reveals to be a more appropriate parameter for assessing seakeeping of cape-size bulk carriers. The largest swell values were present for the vessel Bulk Mexico. The swell for Bulk Mexico (0.27 m) was approximately 2.25 times the swell for Asian Blossom (0.12 m), while the unsteady vertical motion for Bulk Mexico (0.95 m) was 2.20 times the value for Asian Blossom (0.43 m). Also for the other measurements a strong dependency of seakeeping and swell can be observed.

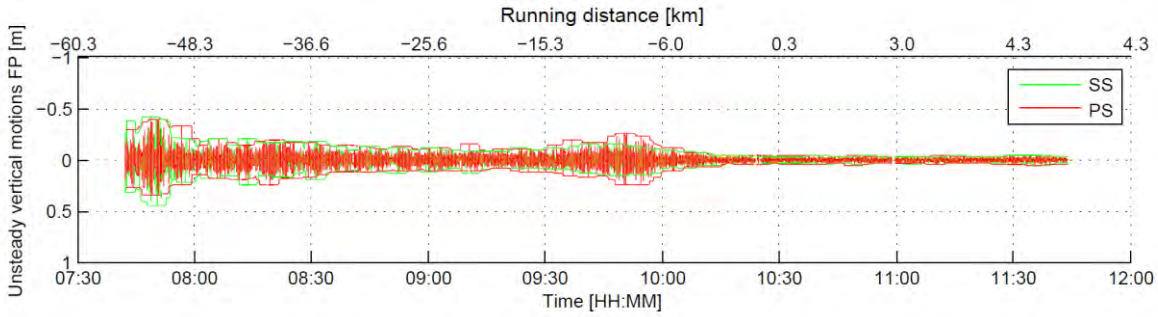

Figure 13: Envelope of unsteady vertical motions at bow of Asian Blossom

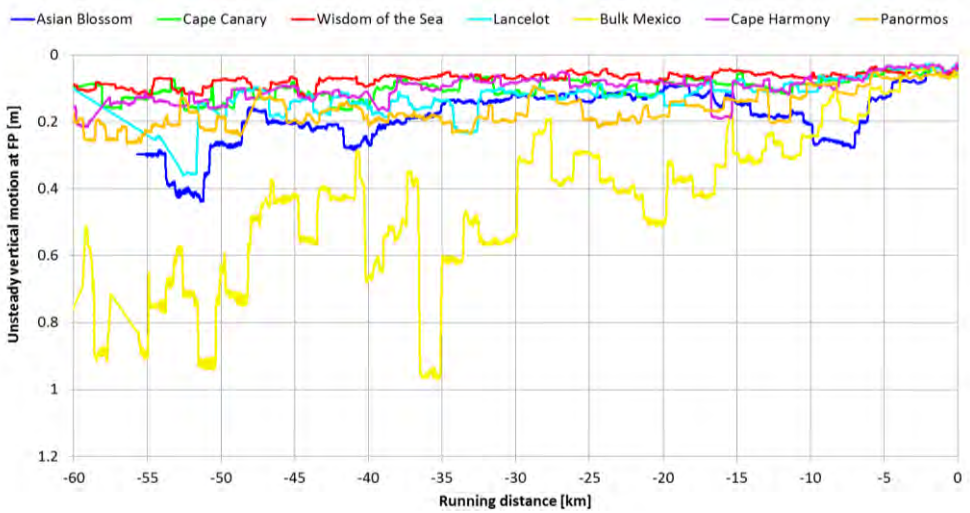

Figure 14: Unsteady vertical motion at bow (envelope) for seven full-scale measurements

	Significant Wave Height [m]						
	Asian Blossom	Cape Canary	Wisdom of the Sea	Lancelot	Bulk Mexico	Cape Harmony	Panor-mos
Kwintebank	2.26	1.36	1.29	0.86	1.18	1.36	0.86
Westhinder	2.59	1.40	1.61	0.98	1.34	1.96	1.22
Bol van Heist	1.87	1.16	0.99	0.75	0.90	no data	0.76

Table 4: Significant wave height during seven measurements

	Swell [m]						
	Asian Blossom	Cape Canary	Wisdom of the Sea	Lancelot	Bulk Mexico	Cape Harmony	Panor-mos
Kwintebank	0.11	0.07	0.06	0.06	0.27	0.07	0.07
Westhinder	0.15	0.08	0.08	0.07	0.28	0.12	0.10
Bol van Heist	0.10	0.07	0.04	0.07	0.26	no data	0.09

Table 5: Swell during seven measurements

6 CONCLUSIONS

By combining ship measurements with accurately reproduced water levels, the vertical ship motions could be processed for seven cape-size bulk carriers operating in a tidal environment subject to exposed and shallow water conditions.

The vertical ship motions were split in steady motions related to squat and unsteady motions related to seakeeping. Furthermore the environmental conditions such as tide, current, waves, bottom, wind and other shipping traffic were processed in order to analyse all significant parameters influencing the vertical ship motions.

The squat measurements did clearly reveal the effects of ship speed and under keel clearance. Furthermore, despite the very similar ship particulars for six vessels, different squat behaviour was noticed for two of them. This indicated that the bow shape may have an important effect on the (bow) squat of the vessel.

The unsteady motions corresponding to seakeeping show large variety for the seven measurements. In four measurements the vertical motions resulting from waves are limited to 0.25 m, while in one measurement unsteady vertical motions up to 1.00 m were reached. Seakeeping of cape-size bulk carriers is related strongly to the swell conditions, while no relation with the significant wave height could be observed.

The vertical motion measurements will be applied to validate a prediction tool for vertical ship motions, which is implemented by the Common Nautical Authority (Flanders / the Netherlands) to assess probabilistically the accessibility of deep-drafted vessels to the harbours along the river Scheldt.

7 ONGOING AND FUTURE WORK

The processing method and the results presented in this report, provide valuable validation data for prediction tools for vertical ship motions. The following items for future work are in progress:

- Comparison of full-scale squat measurements to towing tank results (FHR/UGent);
- Developing a squat formula for cape-size bulk carriers by combining full-scale and towing tank data (FHR/UGent);
- Comparison of full-scale steady and unsteady motion measurements to results of squat and seakeeping software (CNA);
- Measurement campaign on container vessels to the port of Antwerp (upstream the river Scheldt, see Fig. 1) which will take account of supplementary effects such as bending, wind, ship meetings, rudder and propeller application and density effect (Flemish Pilotage/FHR/UGent).

8 ACKOWLEDGEMENT

The work presented in this paper is the result of a fruitful collaboration between several partners involved. The authors want to acknowledge in particular the Common Nautical Authority and the Dutch Pilotage Scheldemonden. For reproducing the environmental conditions a lot of data from different sources and databases were provided by: the Flemish Hydrography, Dutch ministry of infrastructure and water management (Rijkswaterstaat) and the Scheldt Radar Chain. This research could not be executed without the financial support of the Common Nautical Authority in which the Flemish Shipping Assistance Division (BE) and the Dutch ministry of infrastructure and water management, Rijkswaterstaat (NL) are represented.

REFERENCES

Eloot, K.; Vantorre, M.; Richter, J.; Verwilligen, J. (2009). Development of decision supporting tools for determining tidal windows for deep-drafted vessels, in: Weintrit, A. (2009). Marine navigation and safety of sea transportation. pp. 227-234.

Eloot, K.; Vantorre, M.; Verwilligen, J.; Prins, H.; Hasselaar, T.W.F.; Mesuere, M. (2011). Squat during ship-to-ship interactions in shallow water, in: Pettersen, B. et al. (Ed.) 2nd International Conference on Ship Manoeuvring in Shallow and Confined Water: Ship to Ship Interaction, May 18 - 20, 2011, Trondheim, Norway. pp. 117-126

Härting, A.; Laupichler, A.; Reinking, J. (2009). Considerations on the squat of unevenly trimmed ships, Ocean engineering 36 (2009) 193-201

Newman, J.N. (1977). Marine hydrodynamics. MIT Press: Massachusetts. ISBN 0-262-14026-8

PIANC (2014). Report 121-2014 Harbour approach channels design guidelines, 121–2014. PIANC. ISBN 9782872232109. 1-317 pp.

Puertos del Estado (1999). Recommendations for Maritime Works (Spain) ROM 3.1-99: Designing Maritime Configuration of Ports, Approach Channels and Floatation Areas, Spain: CEDEX.

Vantorre, M.; Candries, M., Verwilligen J. (2013). Optimization of tidal windows for deep-drafted vessels by means of ProToel. IWNTM13: International Workshop on Nautical Traffic Models 2013, Delft, The Netherlands, 5-7 July, 2013.

Vantorre, M., Candries, M., Verwilligen, J., (2014) Optimisation of tidal windows for deep-drafted vessels by means of probabilistic approach policy for access channels with depth limitations, PIANC world congress 2014, San Francisco, USA, pp. 1-18

van Buuren, W. (2005). Beschrijving van de NMS type ADX. November 2005. Versie 0.1 (Nederlands Loodswezen, Ed.)

The proposal of countermeasures against level 2 earthquakes and tsunamis to -7.5m pier of Futami port in Chichijima islands of Ogasawara

by
Masafumi SAITO[1], Satoshi TOKUYAMA[2], Terutaka HOSHIJIMA[2], Kenji NARIYOSHI[2] and Yoshiaki HIGUCHI[2]

ABSTRACT

This paper describes an improved design for level 2 earthquake ground motion and level 2 tsunamis in the -7.5 m pier of Futami Port of Chichijima island of the Ogasawara Islands, about 1,000 km south-southeast of Tokyo.

1. Introduction

The coast of Japan is an area subject to frequent earthquakes and tsunamis. Since the Great East Japan Earthquake and the resulting tsunami in 2011, countermeasures against earthquakes and tsunamis have been implemented rapidly and extensively in Japan for facilities such as breakwaters and quay walls of commercial and fishing ports. Countermeasures are also being considered for port facilities on remote islands. Japan's Ogasawara Islands, a world heritage site, is located about 1,000 km for Japan's main island, south-southeast of Tokyo, and consists of 30 large and small islands. Among these lies inhabited Chichijima island (population approximately 2,000), and Futami port serves as the only logistics mode and provides transportation for the flow of people, including tourists. A regular service is provided by a cargo and passenger ship, Ogasawara Maru (11,035 tons, 150 meters long), from Tokyo port on a round trip a week basis. In addition, since Futami Port is the only port on Chichijima, it is also required to fulfill the function of an emergency transportation facility in the event of a disaster such as an earthquake or tsunami. The main mooring facility, - 7.5 m quay is expected to withstand level 2 earthquakes and the resulting tsunamis.
In this paper, the result of seismic performance surveys and tsunami wave performance surveys on the quay of the pier structure are presented, and countermeasures to satisfy the required performance are discussed. For the seismic performance, dynamic analysis was conducted on the level 2 earthquake by the effective stress analysis FLIP program. On the other hand, for anti-tsunami performance, a tsunami simulation based on nonlinear long wave theory for level 2 tsunami was conducted and stability for the tsunami level was checked. Based on these results, a structure was proposed that can withstand level 2 earthquake motions and tsunami, and is superior in economic efficiency and constructability. Note that the level 2 earthquake ground motion is the earthquake ground motion having the greatest strength from the past to the present and the future at the designated design point. The level 2 tsunami indicates a tsunami occurring about once in 1000 years. Level 2 earthquake motions and tsunamis are applied as external forces to particularly important facilities in the port among port facilities.

Figure 1. Location of Ogasawara islands and map of Chichijima island


Photo 1. Bird's-eye view of Futami port

[1] ORIENTAL CONSULTANTS Co., Ltd. saioh-ms@oriconsul.com
[2] ORIENTAL CONSULTANTS Co., Ltd.

2. Earthquake and tsunami in the Ogasawara Islands

2.1 Countermeasures against tsunami and earthquakes in Japanese harbors

Since the East Japan Pacific Offshore Earthquake Tsunami that occurred in 2011, the Nankai Trough massive earthquake was set up as the largest class earthquake hypothesized in Japan and various disaster prevention measures have been taken against earthquakes and tsunamis.
For port facilities, concepts of level 1 earthquake and level 2 earthquake, level 1 tsunami and level 2 tsunami were introduced.
The level 1 earthquakes are highly likely to occur during the design and service period, based on the relationship between the reproduction period of the earthquake motion and the design service period of the facility at the site where the facility is installed, the approximate reproduction period is 75 years. The level 2 earthquake is the earthquake motion having the largest scale of the assumed earthquake ground motion at the site where the facility is installed.
Level 1 tsunami is a tsunami with a high possibility of occurring during the service period of the facility, and its occurrence frequency is from once in several decades to once in one hundred and fifty years. The protection target against the level 1 tsunami is that the necessary port functions can be used immediately after the disaster. The level 2 tsunami is the largest assumed tsunami at the site where the facility is installed, and its occurrence frequency is once every several hundreds to one thousand years. The protection target is the early restoration of the port function.
In the case of ordinary facilities, measures are taken for level 1 earthquake ground motion and level 1 tsunami, and for more important facilities, level 2 earthquake ground motions, level 2 tsunami measures are taken. Normally, for earthquakes and tsunamis exceeding level 1, it is fundamental to protect human life including implementing evacuation measures. When damage to facilities has a significant impact on economic activity, when damage is seriously affecting human life, and when facilities are important for disaster prevention measures will have to be taken against level 2 external forces.

2.2 Previous tsunami and earthquake in Chichijima islands

It is said that the Ogasawara Islands were discovered by the Japanese in 1593, and that people settled in the Ogasawara Islands around 1820. Since 1826, a number of earthquakes and tsunamis have been recorded in the Ogasawara archipelago.
Yoshinobu TSUJI (2006) [1)]has reported the record of the earthquake tsunamis that hit the Ogasawara archipelago. A list of tsunami and earthquake records is shown in Table 1. No serious damage is reported, but the data show that many tsunamis hit the region and that tsunamis countermeasures are necessary.

Table 1. List of tsunamis which hit the Chichijima Ogasawara islands

The date the tsunami occurred	The place the tsunami occurred	Details	The magnitude of the earthquake	The tsunami height along the Ogasawara coast
1826	Sea near the Ogasawara Islands	This tsunami hit Chichijima after a massive earthquake occurred in Chichijima.	?	6 m
1854	Eastern Sea of Japan	The epicenter off Tokaido was the Pacific side of Japan.	8.4	3 m-5 m
1872	Sea near the Ogasawara Islands	Damaged by flooding. According to local people, the tsunami hit 6 or 7 times	?	3 m

1896	Off Sanriku	22,000 people were killed by the tsunami in the Tohoku Sanriku region of Japan.	7.6	4 m
1923	Kanto southern part	At Futami Port, a tsunami with a height of 90 cm and a period of 30 minutes attacked several times.	7.9	3 m
1933	Off Sanriku	The tsunami arrived 90 minutes after the earthquake occurred, 145 minutes later the maximum tsunami came.	8.1	3 m
1944	East-west coast	Tsunami caused by the Tonankai earthquake.	7.9	3 m
1946	Off the Kii Peninsula Shikoku	Nankai Earthquake Flood under floor at Chichijima	8.1	3 m
1960	Chile South America	Tsunami caused by the Chile earthquake	9.2	4 m

2.3 Necessity of countermeasures against tsunami and earthquakes at ports of the Ogasawara Islands

The Tokyo Metropolitan Port Administration, which manages Futami Port, aims to prevent Chichijima from being isolated even when a level 2 earthquake or a level 2 tsunami occurs, and for this it was aimed to strong then the -7.5 m quay. This is because Chichijima Island is a remote island that is 1,000 km away from Tokyo and has no airport, so the -7.5m quay is the only facility to be utilized for the supply of living necessities, rescuing victims and the evacuation of islanders at the time of a disaster.

3. Study of Level 2 tsunami countermeasure based on tsunami simulation

3.1 Tsunami analysis method in this study

In general, when checking the stability of a structure against a tsunami, the maximum water level at the front of the structure is calculated based on the tsunami simulation and the tsunami wave force is estimated by a reliable tsunami wave force formula.
In the technical standards of port facilities in Japan (2007)(translated in 2009[2)]), for the breakwaters of the gravity structure, Tanimoto's formula is recommended. And for gravity quay and steel sheet pile structure, a method for calculating the tsunami wave force using the water level difference is defined, but there is no clear mention for the pier structure.
Therefore, in this study, in the first stage, a two-dimensional planar tsunami simulation based on nonlinear long wave theory was carried out and the time series of the tsunami level on the front of the target structure was calculated.
In the second stage, the tsunami wave force acting on the pier was directly calculated from the numerical simulation by numerical wave trough tank using the time series of the tsunami level as the input condition.

3.2 Analysis and results based on tsunami simulation

3.2.1 Conditions of tsunami simulation

Numerical simulations of tsunami inundation were conducted using the non-linear shallow water wave theory. Basic equations are as below, and the numerical scheme is the Leap-Frog method.

$$\frac{\partial \eta}{\partial t}+\frac{\partial M}{\partial x}+\frac{\partial N}{\partial y}=0 \tag{1}$$

$$\frac{\partial M}{\partial t}+\frac{\partial}{\partial x}\left(\frac{M^2}{D}\right)+\frac{\partial}{\partial y}\left(\frac{MN}{D}\right)+gD\frac{\partial \eta}{\partial x} - K_h\left(\frac{\partial^2 M}{\partial x^2}+\frac{\partial^2 M}{\partial y^2}\right)+\gamma_b^2\frac{M\sqrt{M^2+N^2}}{D^2}=0 \tag{2}$$

$$\frac{\partial N}{\partial t}+\frac{\partial}{\partial x}\left(\frac{MN}{D}\right)+\frac{\partial}{\partial y}\left(\frac{N^2}{D}\right)+gD\frac{\partial \eta}{\partial y} - K_h\left(\frac{\partial^2 N}{\partial x^2}+\frac{\partial^2 N}{\partial y^2}\right)+\gamma_b^2\frac{N\sqrt{M^2+N^2}}{D^2}=0 \tag{3}$$

where,

t:time

x,y; coordinates

¯; water surface elevation

M,N; flux in x-direction and y-direction

h; still water depth

D; total depth $(D=h+\eta)$

g; acceleration of gravity

K_h; horizontal diffusion coefficient

K_b;friction(=gn^2/D^3,n: friction coefficient of Manig)

Calculation method, setting conditions such as calculation range, natural conditions such as wave source and tide level are as shown in the following table 2.

The wave force of the level 2 tsunami acting on the pier was calculated and the stability check of the entire structure was carried out for the tsunami wave force acting on the whole structure of the pier.

The Japanese Cabinet Office published a report on the “Nankai Trough's Great Seismic Model Review Committee (Second Report)" (2012). The report includes an examination of a total of 11 tsunami fault models of the Nankai Trough massive earthquake: 5 "basic examination cases" and 6 "other derivation study cases". Each municipality on the coast of Japan will conduct a tsunami simulation using these tsunami fault models and implement damage estimation. The Tokyo Metropolitan Port and Harbor Bureau, which manages Futami Port, conducted a comparative study of 5 of the 11 cases and adopted Case 5. Case5 fault model is shown in Figure 2. In this case the large slip region and the super large slip region were set off the coast of Shikoku island and Kyushu island.

Table 2. List of Conditions of numerical simulations

Item	The contents	The values
Basic equation	non-linear shallow water wave theory	
The earthquake	Nankai Trough huge earthquake	
Bathymetry (mesh size) (see Figure 3)	Area 1, Area 2,Area 3, Area 4, Area 5, Area 6, Area 7	2,430m,810m,270m,90m,30m 10m, 5m
Calculation time step		0.10s
Calculation run time		12h
Tide level	H.W.L. L.W.L.	D.L.+1.10m D.L.±0.00m

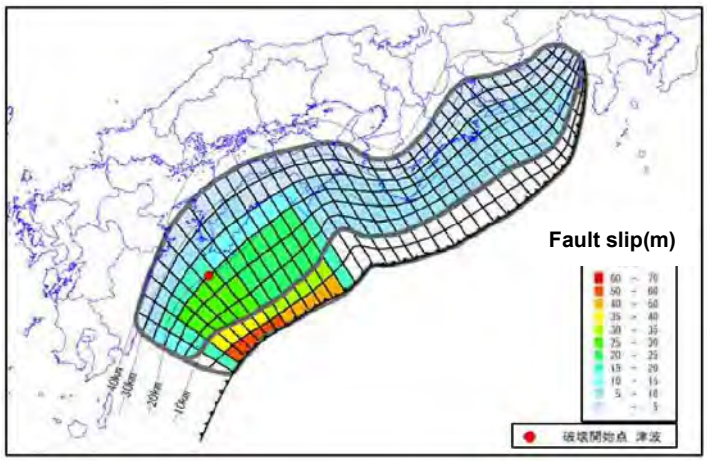

Figure 2. Case5 fault model

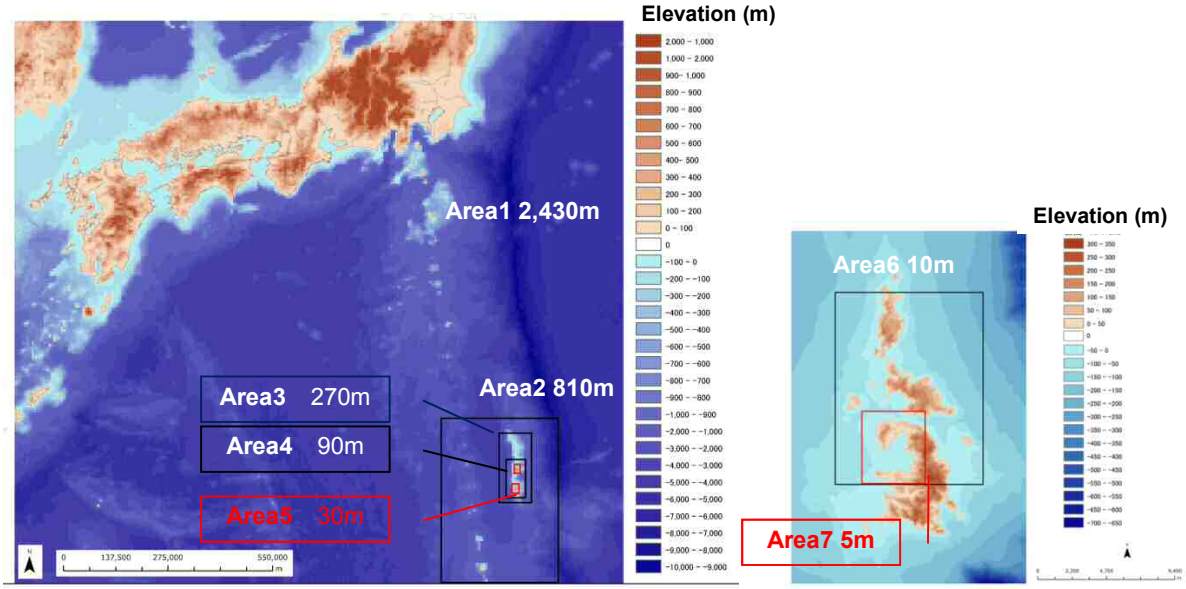

Figure 3. Calculation area（left:2,430m-30m, right:10m-5m）

3.2.2 Result of tsunami simulation

The result of the tsunami simulation, a distribution map of the maximum tsunami height around Chichijima, and a distribution map of the maximum inundation depth around Futami Port, are shown in the following Figure 4. A water level variation of time scale of point "★" is shown in Figure 5. According to the maximum water level distribution chart, it can be seen that the tsunami converges and increases in Futami Bay located on the western side of Chichijima, similarly in the southern bay in the west side and in the northern bay on the east side. The maximum inundation depth is around 5 m in the vicinity of Futami Port and it can be seen that inundation spreads to the mountain side mainly in Futami Port. According to the time series fluctuation of the tsunami water level, the first wave of the tsunami has reached Futami Port in about 1.5 hours after the occurrence of the tsunami, and it is found that the maximum water level is about 6 m at the third wave. Furthermore, although the tsunami of about 2 to 3 m repeatedly reached until 6 hours after the occurrence of the tsunami, the tsunami rapidly declined after 6 hours.

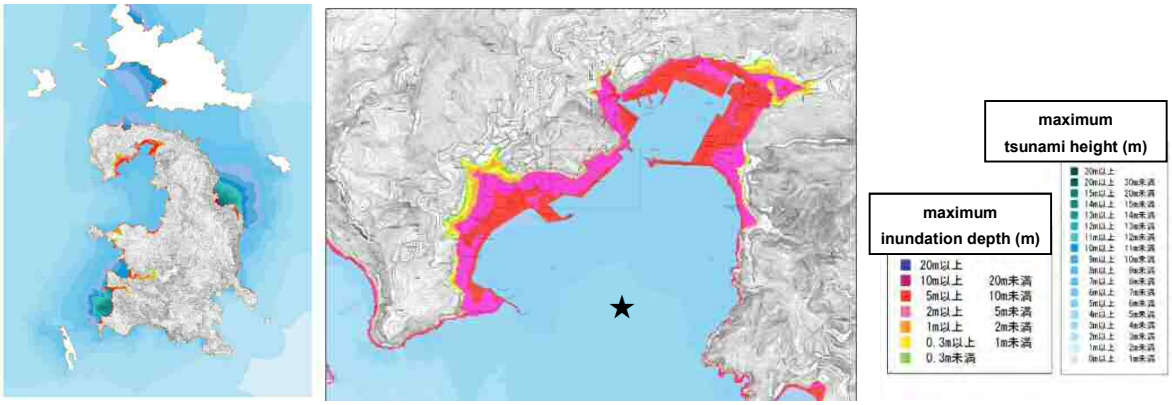

Figure 4. Maximum tsunami height distribution map and maximum inundation depth distribution map

(Left: Maximum tsunami height around Chichijima, Right: Maximum inundation depth map around Futami Port)

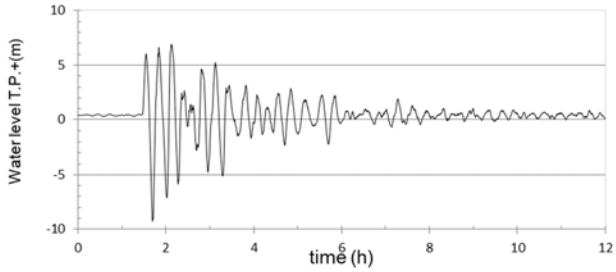

Figure 5.Time series water level variation of tsunami (at point ★ shown in Figure 4)

3.3 Analysis and results based on numerical wave water tank

3.3.1 Conditions of numerical wave water tank

Currently, there is no established method to check the stability of the pier against the wave power of the tsunami. Also, the existing tsunami wave pressure equation cannot be applied.

Therefore, be using numerical wave water tank method for the numerical calculation, the tsunami wave force acting on the pier was directly estimated. Numerical wave water tank (CADMAS - SURF) is a numerical simulation model developed by Coastal Development Institute of Technology in 2001. The simulation model numerically solves the Navier-Stokes equation, which is a fundamental equation of a fluid, and the VOF（Volume of Fluid）method is used for the free surface processing method. This model can quickly and easily carry out numerical simulation of complicated phenomena accompanied by wave, flow, and ground interactions, and it is possible to directly calculate the tsunami wave force, with time series variation of the tsunami water level as an input condition. The seabed topography in the numerical wave motion tank was set taking into account the direction of the tsunami from the front of the -7.5 m quay wall shown in Figure 6. The range of the modeled seabed topography was set from the front of the -7.5 m quay wall to a depth of 25 m, and horizontally 100 m from the front of the -7.5 m quay wall. The water depth change with respect to the horizontal distance from the front of the quay wall is shown in the following figure below.

The lattice spacing of numerical wave water tank was set as $\triangle z = 0.20$ m for the vertical direction and as $\triangle x = 4.00 - 0.2$ m for the horizontal direction as the basis. These spacing was obtained considering 1/10 of wave height vertically and 1/100 of wave length horizontally. The ratio of lattice spacing for vertical direction vs horizontal direction lies among 1/10 and 1/5. For decay zones numerical wave

water tank, lattice spacing was expanded to reduce the calculation time.
The input waveform was set so as to reproduce the water level on the front of the quay in the tsunami simulation.
With reference to the water level time series at the front of the quay wall obtained from the tsunami simulation, two ways of water level adjustment for the flow velocity matrix (i.e. the water level variation distribution matrix and the long wave approximation matrix) were tried. As a result, matrix data using the input waveform as a long wave approximate waveform was used.
The outline of the analysis model for pier structures is as follows.

Model 1: An analysis model to express a steel pipe pile as an upright wall was set up in order to calculate an external force acting as a push wave on a steel pipe pile of a jetty.

Model 2: An analysis model with just the upper part was set up in order to calculate the external force acting as lifting pressure on the upper part of the pier. The main calculation conditions are as shown in Table 3.

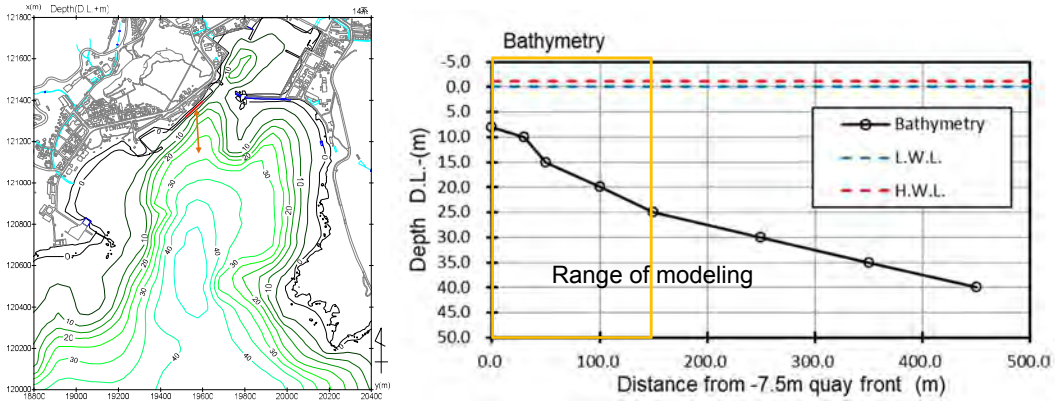

Figure 6. -7.5 m quay offshore topography (left: plane view, right: cross-sectional view)

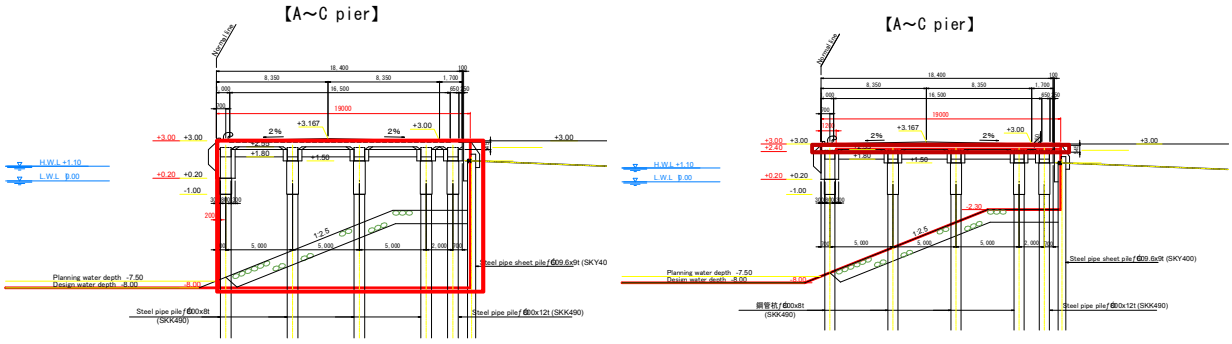

Model 1 Model 2

Figure 7. Image diagrams of pier structure modeling

Table 3. List of conditions of numerical wave moving tank simulations

Item	Conditions
Input waveform	Waveform adjusted to long wave approximation from the tsunami simulation waveform. The maximum water level and the period are adjusted to 8 m and of about 16 minutes respectively
Calculation time	Period 16 minutes: 1000 s
Time step of calculation	Automatic, initial value 0.001 s, minimum value 1×10^{-8} s
Physical property value	Density 1030kg/m^3, Kinematic viscosity coefficient 1×10^{-6}m^2/s Gravitational acceleration 9.8m/s^2
Difference scheme	VP-DONOR 0.2

3.3.2 Result of calculation

As examples of numerical calculation results by numerical wave water tank (CADMAS - SURF), snapshots of waveform and velocity vector are shown in Figure 8. These figures show the state of overflow of the tsunami at about 450 s at which the water level is at its maximum.
Numerical calculations were performed with numerical wave water tank (CADMAS - SURF), and the wave power of each Model 1 and Model 2 were calculated. Results of the numerical calculation are obtained in result is the wave force per unit area, and the wave force acting to the steel pipe pile is calculated considering the actual diameter.
The horizontal wave force is the force acting in the direction of the pier from the offshore side and is about 65 kN/m^2. The vertical wave force is the force applied from the lower part of the pier to the upper work direction, and the force is 34 kN/m^2 the vertical downward negative pressure. The load distribution map is shown in Figure 9.

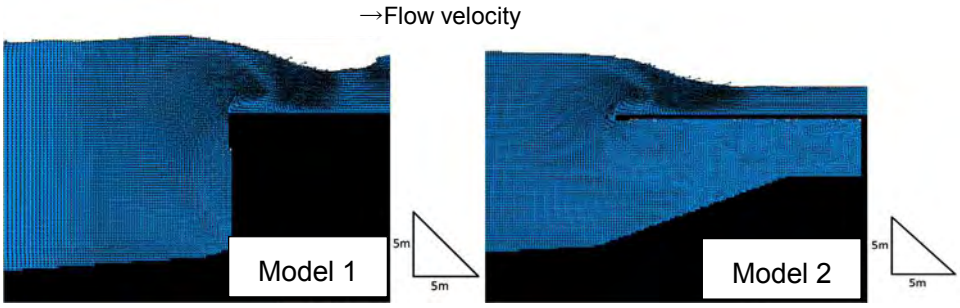

Figure 8. Water level and flow velocity just before the peak of the tsunami at the position of just in front the quay wall (tide: H.W.L.)

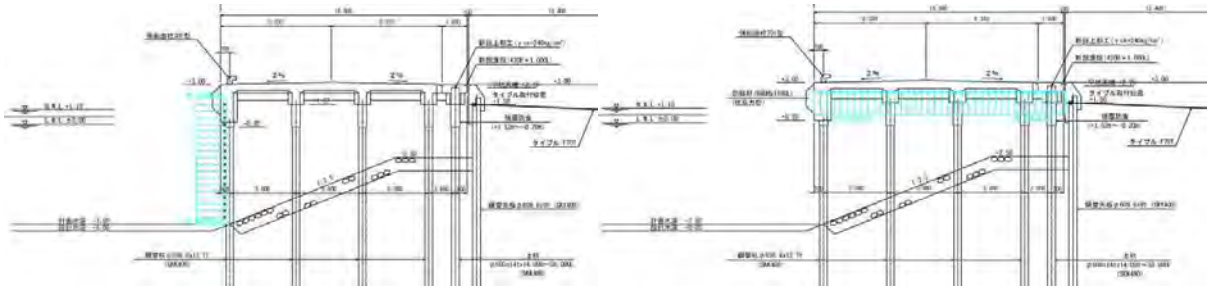

Figure 9. Horizontal direction wave force(left), and vertical wave force wave force(lift pressure) (right)

3.4 Stability check of the entire -7.5m pier against the tsunami

At present, there is no established method for checking the stability of the pier against the wave power of tsunamis. Also, the existing tsunami wave pressure equation cannot be applied here. Therefore, the two-dimensional frame calculation was carried out from the tsunami wave force calculated by the numerical wave water tank described in section 3.3 and the stability check of the pier in case the level 2 tsunami would arrive carried out. The results as shown in Table 4 reveal that the pier will keep stable for the level 2 tsunami.

Table 4. List of Level 2 tsunami check result

The state of action of the load	Direction of facility inspection	Element	Items to be checked	Verification result
The accidental state of the level 2 tsunami push wave	Pier cross section direction	Steel pipe pile 1	Stress (compression)	0.67≦1.000 OK
			Displacement	21.027(mm) OK
			Supporting force (indented)	R=353.925≦ Ra=2905.953（kN） OK
			Pile head moment Md/Mu	0.345≦1.000 OK
The accidental state of the level 2 tsunami lift pressure	Pier cross section direction	Steel pipe pile 3	Stress (tension)	0.053≦1.000 OK
			Displacement	0.442(mm) OK
			Supporting force (withdrawal)	R=146.226≦ Ra=1132.253（kN） OK
			Pile head moment Md/Mu	0.001≦1.000 OK
		Superstructure	Stress (bending)	8.458≦65.126 OK

4. Analysis of level 2 earthquake by dynamic analysis and examination of countermeasure works

4.1 The estimation of earthquake induced liquefaction

The soil structure of the ground where the -7.5m quay wall is installed consists of an embankment soil layer, a clayey soil layer, a gravel soil layer, a sandy soil layer, and a bedrock layer, i.e. the support layer from the surface.

The list of ground constants is shown in Table 5.

To check the response to the earthquake, first the study of liquefaction was conducted.

According to the liquefaction judgment flow shown in “The liquefaction countermeasure handbook”, the judgment is to be conducted in 3 stages: a method based on particle size in the first stage, a method using the equivalent N value and the equivalent acceleration in the second stage, and a method using the result of the repeated triaxial test in the third stage. As a result, most of the targets were judged to liquify (See Figure 10) .

According to the aforementioned determination method, the As layer clearly liquefied.

When the As layer liquefies, it was judged that the pore water pressure raised in the As layer will be propagated to the upper Ac layer, resulting in liquefaction of the Ac layer.

However, since the Ac layer contains as much as 25% clay, the Ac layer can be expected not to liquefy by itself.

As a result, it was decided that liquefaction countermeasures be executed only for the As layer.

Table 5. List of ground constants

Symbol	Soil classification	N value	Underwater weight $\bar{}$ (kN/m^3)	Wet weight $\bar{}$(kN/m^3)	Adhesive force C(kN/m^2)
E	Embankment soil layer	12	10	18	0
Ac	Viscous soil layer	3	7.2	17.2	-0.69(Z)+8.59
Ag	Gravel soil layer	20	9.8	19.5	0
As	Sandy soil layer	14	8.6	18.2	0
Tb	Bedrock layer	50	10	20	0

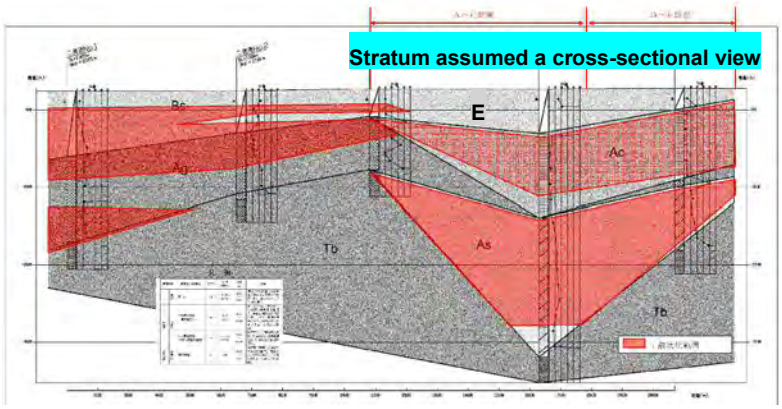

Figure 10. Result of liquefaction layer determination

4.2 Analysis and results by FLIP

4.2.1 Outline of analysis method

Response of the -7.5 m quay against level 2 earthquake motion and an examination of the countermeasures against Level 2 earthquake motion were carried out based on dynamic analysis by FLIP.

Here, FLIP stands for Finite element analysis program of Liquefacqtion Process. The FLIP programs include the constitutive model called cocktail glass model, three-dimensional effective stress analysis with various structural elements, and two-dimensional large deformation/finite strain effective stress analysis. And the program is applicable to the analysis of clayey materials.

4.2.2 Result of the analysis for the current facility

In order to clarify the situation of seismic performance of the current facility, analysis by FLIP was carried out.

The results of the FLIP analysis of are shown in Table 6 and Table 7. The residual displacement amounts in the normal and horizontal direction are less than the minimum allowable value 1,000 mm for both the jetty and the seawall behind the jetty (Table 6). However, regarding the stress of the steel pipe pile, it was revealed that the maximum moment generated reached the total plastic moment and did not satisfy the earthquake resistance performance.

The model diagram, distribution diagrams of residual displacement amounts, excess pore water pressure, and shear strain are shown in Figure 12, which compares with the case with countermeasures.

Table 6. List of residual deformation amount in the horizontal direction

Item checked	Location of check	Residual deformation amount in the normal horizontal direction (mm)	Tolerance of deformation amount (mm)	Judgment result
Pier	crown height	-687.0	1000	OK
	Installation ground on the seabed	-669.8	-	-
sea wall	crown height	-528.4	1000	OK
	Installation ground on the seabed	-672.1	-	-

Table 7. List of result of analysis of stress of steel pipe pile

Elements pile row	Elements	Maximum moment(kN・m)	Total plastic moment(kN・m)	Moment ratio Mp/Md	Judgment result
a	Maximum value	291.2	291.2	1.000	NG
b	Maximum value	290.9	290.9	1.000	NG
c	Maximum value	291.4	291.4	1.000	NG
d	Maximum value	292.9	292.9	1.000	NG
e	Maximum value	481.1	481.1	1.000	NG
Comprehensive evaluation		NG			

4.3 A Study on Countermeasures against Level 2 Ground Motion

4.3.1 Extraction of countermeasure method

The results of the analyses on 4.1 and 4.2 show the necessity of countermeasures for liquefaction. The following items are prerequisite when conducting a study on liquefaction measures at this facility.

KTerms of use: This quay is the only quay on the island for logistics to and from mainland Japan, and the construction works must be carried out while using the facilities. Also, on the front of the -7.5 m quay, the vessel is often moored 3-4 days per week.

KGeographical condition: Since the island is located more than 1,000 km from the mainland of Japan, it takes time and expenses to carry construction materials and machines to the island.

KSoil condition: Basically, a silt layer is deposited in the upper layer and a sand layer is deposited in the lower layer. The composition of the soil layer differs greatly from place to place in the sectional direction of the quay.

KCondition behind the facility: Behind the soil protection steel piles, tie material is installed at a pitch of 2 m in the normal direction of the quay.

Based on the prerequisites described above, the liquefaction countermeasure methods to be studied must result in only small ground deformation, must not affect the existing structure, and must not affect ships' berthing or navigation. 4 candidate methods were proposed and compared. The followings are cited as countermeasure construction methods: method 1: cement based soil improvement method, method 2: chemical liquid injection system ground improvement method, method 3: reinforcement method using a structure, and method 4: drain construction method, are cited as a countermeasure construction method.

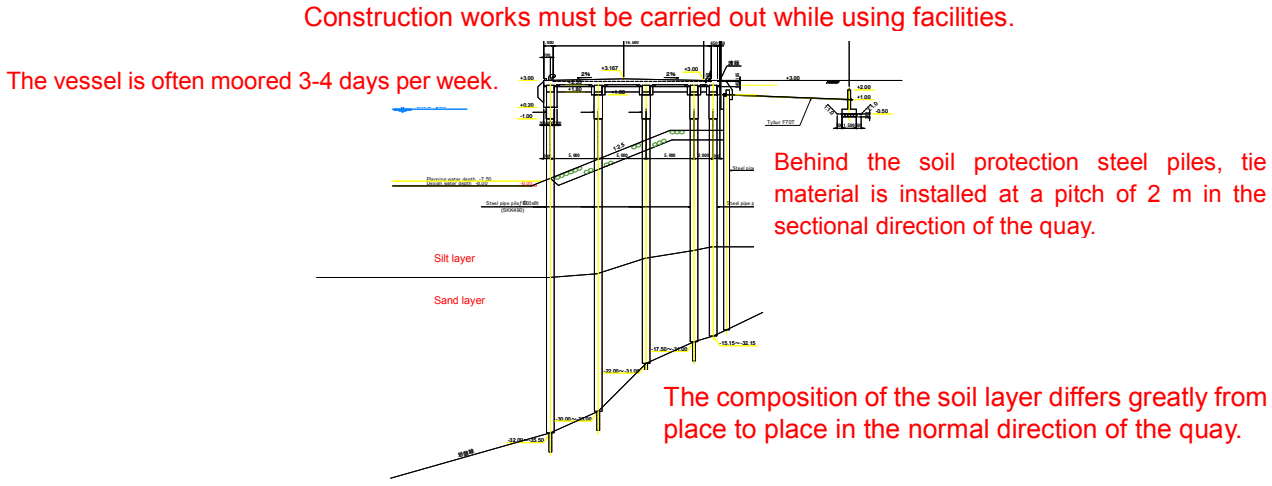

Figure 11. Image sketch of constraints on construction

Table 8. Comparative chart of structural form

Method 1: Cement based soil improvement method	**Method 2: Chemical liquid injection system ground improvement method (Permeation solidification treatment)**
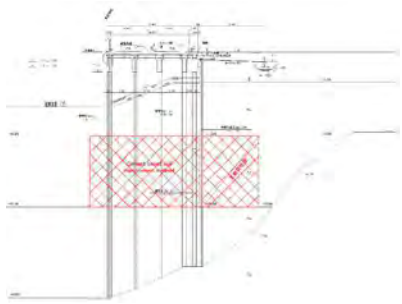	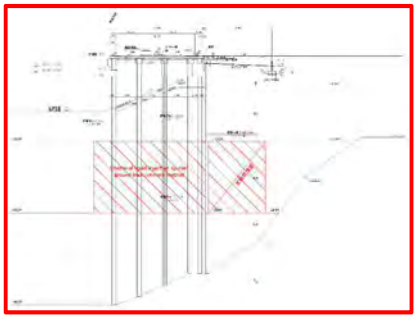
Outline of construction method: The ground behind the steel sheet piles is prevented from liquefaction by using the cement-based soil implement system. The stress acting on the soil retaining pile and steel pipe piles is thus reduced and stabilized.	**Outline of construction method:** The ground behind the steel sheet piles is prevented from liquefaction by using a liquid chemical system to solidify and improve the soil, the stress acting on the sheet piles and the steel pipe piles is reduced and stabilized. The method cannot be applied to ground with a high content of fine grains. The application range is fine particle content up to 40% fine particle content.
Evaluation: This method directly prevents liquefaction of the ground, which is a factor of deformation, so that earthquake resistance can be reliably secured. However, due to the occurrence of sludge in the construction work, it is necessary to carry out the primary mud treatment at the site, and further final treatment in the mainland Japan is necessary. Because of the cost for treatment of sludge, this method was judged unadaptable.	**Evaluation:** This method directly prevents liquefaction of the ground, which is a factor of deformation, so that earthquake resistance can be reliably secured. It is possible to execute construction works at night, and the construction works can be executed without affecting service even when constructing on the quay. Furthermore, this method only injects a chemical solution, and no sludge is generated.
Method 3: Reinforcement method using structure	**Method 4: Drain construction method**
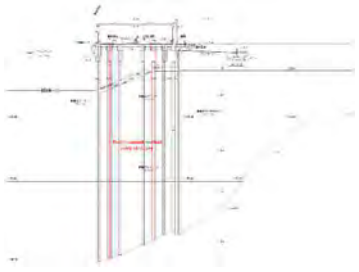	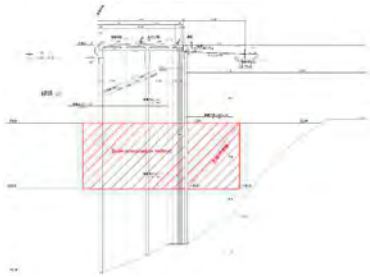
Outline of construction method: In this method, by placing piles on the ground behind the sheet piles, it is expected to suppress the deformation of the ground and reduce the stress on the sheet piles and the steel pipe piles.	**Outline of construction method:** This method prevents liquefaction by installing drain piles in the ground behind the sheet pile, and reduces the stress on the sheet pile and the steel pipe pile.
Evaluation: It is necessary to excavate the ground behind the sheet piles. Therefore, it is not possible to use the cargo handling yard during the construction period. Also, in order to prevent plastic failure of the steel pipe piles, it is necessary to make the steel pipe piles of the back ground more than ϒ 900. Therefore, construction becomes expensive.	**Evaluation:** Judging from the grain size distribution of the liquefaction area, this method was judged unadaptable.

4.3.2 Study of countermeasures by FLIP

From the comparative study described in the previous section, the penetration solidification treatment method was selected as a countermeasure construction method. A model for the selected penetration solidification method was made and the analyses of the level 2 earthquake motion by FLIP were coducted. The model diagram and the check result are shown in Figure 12. The residual displacement amount was within the allowable range. The stress degree of the steel pipe piles was also within the allowable range.

Figure 12. Result of dynamic analysis by FLIP

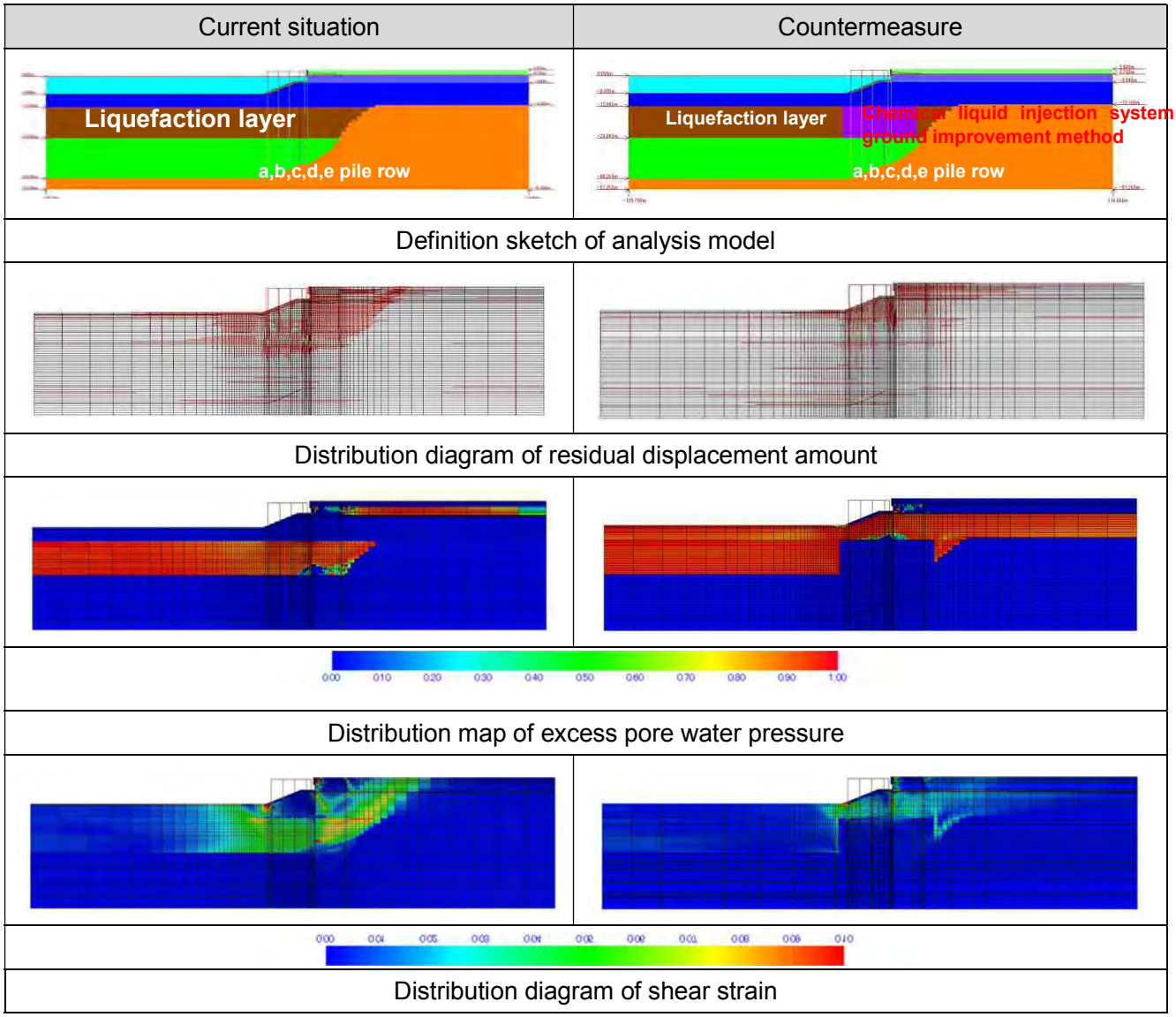

Table 8. Result of inspection of residual displacement amount against level 2 earthquake motion

Element	Position	Current situation	Countermeasure	Tolerance of deformation amount(mm)	Judgment
		Residual deformation amount in the horizontal direction(mm)			
Pier	crown height	-687.0	-172.1	1000	OK
	Installation ground on the seabed	-669.8	-130.7	-	-
Sea wall	crown height	-528.4	-201.2	1000	OK
	Installation ground on the seabed	-672.1	-174.2	-	-

Table 9. List of Result of inspection of stress of steel pipe pile

Current situation					Countermeasure			
Pile row	Maximum moment (kN・m)	Total plastic moment (kN・m)	Moment ratio Mp/Md	Judgment	Maximum moment (kN・m)	Total plastic moment (kN・m)	Moment ratio Mp/Md	Judgment
a	291.2	291.2	1.000	NG	201.0	294.5	0.682	OK
b	290.9	290.9	1.000	NG	-186.0	294.3	0.631	OK
c	291.4	291.4	1.000	NG	-393.0	393.0	1.000	NG
d	292.9	292.9	1.000	NG	-357.3	394.1	0.906	OK
e	481.1	481.1	1.000	NG	-495.0	529.1	0.935	OK
	Comprehensive evaluation NG				Comprehensive evaluation OK			

4.4 Chemical liquid injection system ground improvement method (Permeation solidification treatment)

The application range of the penetration solidification treatment method is ground having a fine particle content of 40% or less. In the present study, the soil layers to which the penetration solidification treatment method can be applied mainly in the As layer are the B layer, the Ag layer, and the As layer.
The range of construction on the land side and the sea side of the permeation solidification treatment method was determined based on analysis by FLIP. The improvement strength was 70kN/m^2. The improvement rate was set to 100%.

4.4.1 Study on construction method

Improvement work on the quake resistant quays of Futami Port will be under construction in about 10 years. An example of a one-year construction plan is shown below. The engineering type will be Machine Transfer → Drilling Work → Sleep Injection Process → Infiltration Solidification Process Injection → Check Boring → Machine Removal.
Machine loading, marine transport from Tokyo Port to Futami Port is about one thousand kilometers one way.
In the drilling work, 10 holes are drilled in 1 m ^{2} of the reinforced concrete member of the apron part and 100 mm in diameter. At that time, careful attention should be paid to the position of the reinforcing bar of the reinforced concrete member.
The quality of ground improvement is ensured by check boring.

5. Conclusions

The conclusions in this study are as follows.
1) The level 2 tsunami to be designed for is the tsunami of the Nankai Trough massive earthquake. Based on the tsunami simulation for the level 2 tsunami by the tsunami fault model of the Nankai Trough massive earthquake, the maximum water level and the minimum water level at Chichijima Futami Port were calculated. From the results of the water level and the minimum water level, the stability of the accidental condition against the level 2 tsunami was examined, and it was revealed that it possesses sufficient strength.
2) In addition, anti-tsunami resistance performance of the elements of the piers was examined by the two-dimensional numerical wave motion channel, and it became clear that the structure has sufficient resistance.
3) For the accidental state of the level 2 earthquake, dynamic analysis by FLIP was carried out, and the structure which ensures the stability (an allowable displacement in the horizontal direction of within 1 m) was examined. Based on the results, a ground improvement as follows was proposed as an earthquake-resistant reinforcement construction method; a ground improvement plan by the injection solidification method (medicinal fluid penetration solidification processing method) which suppresses liquefaction of the ground by stiffening the ground at the lower part of the facility with a permeable chemical liquid, reducing the stress to the steel material.
4) At present, detailed examination of the countermeasure construction method focusing on the construction plan is being carried out based on the ground improvement plan utilizing the injection solidification method (chemical infiltration solidification processing method).

References:

1) Yoshinobu TSUJI (2006): History of the tsunamis of the Bonin Islands, earthquake research Institute, the University of Tokyo
2) The Overseas Coastal Area Development Institute of Japan (2009): Technical standards and commentaries for port and harbour facilities in Japan.
3) The Coastal Development Institute of Technology (1997): The liquefaction countermeasure handbook (in Japanese)

AN INTEGRATED ANALYSIS FOR THE PASSING SHIP PROBLEM ON SANTOS PORT CONSIDERING REAL-TIME SIMULATIONS AND MOORED SHIP DYNAMICS

by

R. A. Watai[1], F. Ruggeri[1], E. A. Tannuri[2] and K. Nishimoto[2]

ABSTRACT

An integrated analysis methodology for the passing ship problem considering real-time simulations and moored ship dynamics is presented. The methodology is introduced as an alternative to the traditional method, which defines a criterion based only on safe distances and maximum velocities, neglecting crucial navigation aspects of the ship. In this sense, the proposed methodology extends the standard one by including results of pilot guided real-time simulations into the analysis process. An application of the method analyzing the effects caused by the passage of a 366 m long container ship next to small capsize vessels moored at different berths of the Port of Santos, Brazil, is presented. Results are discussed by means of moored ship motions and mooring loads, including also possible improvements on the mooring arrangements applied nowadays in the port.

1. INTRODUCTION

The search of the shipping line companies to achieve economies of scale has given rise to sharply growths of container ship sizes in the last years, increasing the port challenges to improve its capabilities. Besides the necessity of physical interventions on the access channel depth and turning basins, redefinition of tug bollard pull requirements, among others, the port new facilities must also be prepared to provide safe mooring conditions to the moored ships that will be subjected to strong hydrodynamic interaction effects induced by the passing of the new large vessels. This interaction effect, for instance, can result in the rupture of the mooring lines, emergency unberthing as well as damages to the loading and offloading pieces of equipment, being the main cause of some accidents occurred in the past, such as, the ones involving the ships New York and Titanic, when leaving Southampton, in April 1912, and ships Buffalo and Jupiter in September 1990.

(Remery, 1974), one of the first authors to study the passing ship problem, has conducted an experimental campaign for measuring the forces on captive and moored tanker vessels under the passage of another tanker ship, investigating the influence of passing ship size, distance to the moored ship, loading conditions, speed, as well as the effects of mooring system stiffness. (Flory, 2002) has applied Remery's experimental data to propose a set of equations to calculate peak forces and moments produced by the passing tanker ships, in which corrections to other under keel clearance (UKC) were also proposed based on data given in (Muga & Feng, 1975). Other examples of extensive model test programs and empirical formulas for the loads involved in the passing ship problem are presented in (Vantorre, Verzhbitskaya, & Laforce, 2002) and (Kriebel, 2005).

With the increasing of computational capacity, numerical models capable of simulating the time-dependent fluid flow and pressure field of the passing ship problem are being often more applied. Over the last years, 3D panel methods based on the potential flow theory have been the most often applied technique to model the passing ship problem. (Korsmeyer, Lee, & Newman, 1993) are one of the first to apply a double-body potential model to the analysis of ship interactions, in which, at moderate Froude number, the interaction loads were calculated by neglecting free surface effects and shed vorticity. (Pinkster J. , 2004) has investigated the passing ship problem including free surface effects by developing a method based on the mixed application of the double-body model and linear wave diffraction computations, from where he has verified significant free surface effects in a situation where the ship is moored in a confined dock positioned next to a canal where the passing ship sails and very low contributions of the free surface effects for passing ships sailing next to vessels moored at open waters or along vertical quay walls. Again, the results were generated at moderate Froude number.

More recently, several investigations focusing on the passing ship problem were performed in the context of the Joint Industry Project ROPES ("Research on Passing Ship Effects on Ships"), which culminated in the development of the user-friendly software tool ROPES (see (Pinkster J. A., 2014)). For such development, full-scale field measurements (Wictor & van den Boom, 2014) and scaled model tests (see (Talstra & Bliek, 2014) and (van der Hout & de Jong, 2014)) have been carried out

[1] **Argonáutica Engineering & Research, watai@argonautica.com.br**
[2] **University of São Paulo, Numerical Offshore Tank, Brazil**

for validation purposes, what enabled one to determined the limitations and versatility of the ROPES software under many different geometries (e.g. straight channel and complex harbour configurations) and current conditions (e.g. following and counter currents). Moreover, (Talstra & Bliek, 2014) have also proposed a correction factor which compensates the ROPES underprediction in high-Froude number range (> 0.3), which was mainly attributed to the fact the free-surface effects are not included in the double-body model.

The present paper presents a methodology to support the definition of operational limits to passing ships based on the use of a in-house potential flow solver for the calculation of the hydrodynamic interaction forces, a dynamic simulator to evaluate the passing ship impacts on the moored ship motions and mooring system loads, and also real-time simulations campaigns that provides maneuverings paths of the passing ship along port navigation channels. Differently from the common approach of defining operational limits based exclusively on safe minimum distances and maximum allowable speeds extracted by parallel passing ship analysis, in this approach pilot oriented ship trajectories and velocities are incorporated into the analysis. This is indeed an important aspect to be included in the definition of operational limits because in many circumstances it is not possible to restrict the ship forward speed to the maximum velocity established by the passing ship analysis, either for keeping the ship rudder efficiency or by the simple fact that even the ship dead slow speed is higher than the safe limit value.

The proposed methodology starts with the definition of the berths most susceptible to the passing ship problem, as well as the selection of typical ships. Approximate ship maneuvering trajectories with different distances to the berths are then prescribed and used for the calculations of the interaction forces time histories, mooring loads and ship motions, these being compared to operational limits criteria, providing a first estimate of safe speed and distance to moored ships. At this stage, inbound and outbound real-time maneuvering simulations are conducted by local pilots with the aid of colored areas (defined by passing speed and distance to moored ships) printed in the electronic nautical chart highlighting the main risk zones. Further ahead, the hydrodynamic interactions forces and mooring system loads are recalculated with the updated ship trajectories, which were resulted from the pilot's instructions during the real-time simulations. Finally, recommendations are provided in terms of the new ship maneuvering and improvements (if applicable) on the mooring system arrangements.

In order to illustrate the procedure, the methodology is applied to analyze the maneuvering feasibility of a 366 m long contained ship in the curve and narrow channel of the Port of Santos, Brazil. With such purpose, it is considered the use of a dynamic simulator of moored ships berthed alongside quay walls (MeDuSa®), the real-time simulator of the Numerical Offshore Tank of the University of São Paulo (Tannuri, et al., 2014) and a derivative version of the program TDRPM (Time Domain Rankine Panel Method), a 3D-BEM originally developed for solving seakeeping problems of floating systems (see (Watai, 2015) and (Watai, Ruggeri, Sampaio, & Simos, 2015)), which was adapted to applications on the passing ship problem as previously presented in (Watai, Ruggeri, Tannuri, & Weiss, 2013) and (Ruggeri, Watai, & Tannuri, 2016). The description of the numerical models applied is presented next.

2. NUMERICAL MODELS

2.1. Mooring Design System (MeDuSa®) Tool

In MeDuSa®, the ship motions are formulated in time domain under the retardation function approach for the hydrodynamic reaction forces, as proposed in (Cummins, 1962). This is a usual approach when considering arbitrary time varying excitation forces, not restricting, therefore, the formulation to steady state oscillatory motions with frequency independent hydrodynamic coefficients. As already discussed in (Oortmerssen, 1976), the assumption of constant hydrodynamic coefficients cannot be justified, especially in shallow water and near quay walls where these coefficients appear to be very sensitive to changes in frequency.

$$\big(\boldsymbol{M} + \boldsymbol{A}(\omega_\infty)\big)\ddot{\boldsymbol{x}}(t) + \int_0^\infty \boldsymbol{R}(\tau)\dot{\boldsymbol{x}}(t-\tau)d\tau + \boldsymbol{K}\boldsymbol{x}(t) = \boldsymbol{f_{ext}}(t) + \boldsymbol{f_{ext}^{visc}}(t) \quad (1)$$

In (1), M denotes body mass/inertia matrix, $\boldsymbol{A}(\omega_\infty)$ the added mass/inertia matrix at infinite frequency, $\boldsymbol{R}(\tau)$ is the retardation functions matrix, $\boldsymbol{x}$ the ship motions vector for the six degrees of freedom (surge, sway, heave, roll, pitch and yaw), $\boldsymbol{K}$ is the linear hydrostatic restoring coefficient matrix, $\boldsymbol{f_{ext}}(t)$ is external forces and moments vector, which are composed by forces due to current, wind, passing ships and mooring systems, and $\boldsymbol{f_{ext}^{visc}}(t)$ is external damping forces and moments of viscous origin.

The hydrodynamic coefficients $\boldsymbol{A}(\omega_\infty)$ and $\boldsymbol{R}(\tau)$ are calculated externally by solving the so-called radiation problem in frequency domain using a higher order BEM code based on the linearized free

surface Green's function. The damping forces $\boldsymbol{f_{ext}^{visc}}(t)$ are considered by splitting it in linear ($\boldsymbol{B^{lin}}$) and quadratic terms ($\boldsymbol{B^{quad}}$), as presented in (2).

$$\boldsymbol{f_{ext}^{visc}}(t) = -\boldsymbol{B^{lin}}\boldsymbol{x}(t) - \boldsymbol{x^{T}}(t)\boldsymbol{B^{quad}}\boldsymbol{x}(t) \tag{2}$$

These coefficients stand for the viscous linear roll damping, as well as fluid reactive forces on the moored ship in surge, sway and yaw mode, defined following (OCIMF, 2008) convention:

$$\boldsymbol{B_{11}^{quad}} = \frac{1}{2}\rho C_{C,1} L_{pp} T \quad \boldsymbol{B_{22}^{quad}} = \frac{1}{2}\rho C_{C,2} L_{pp} T \quad \boldsymbol{B_{66}^{quad}} = \frac{1}{2}\rho C_{C,6} L_{pp}^2 T \tag{3}$$

where T and L_{pp} are the ship draft and length between perpendiculars, respectively, and $C_{C,j}$ are the current drag coefficients for the j degree of freedom (here, only surge, sway and yaw motions are considered).

The mooring lines and fenders are represented by nonlinear spring elements and characterized by their respective undeformed lengths l_i and d_i, nonlinear load-elongation curves f_i^l, nonlinear reaction deflection curves f_i^f, initial coordinates of the ship chocks $\left(x_{i,0}^c, y_{i,0}^c, z_{i,0}^c\right)$ and the positions of the bollards $\left(x_i^b, y_i^b, z_i^b\right)$ and fenders along the quay $\left(x_i^f, y_i^f, z_i^f\right)$. The simulation starts with the center of gravity of the moored ship at the origin of the fixed coordinate system and with the i_{th} line set with an user defined amount of pretension $L_{i,0}$ that results in initials line lengths $l_{i,0}$ and elongations $\delta l_{i,0} = l_{i,0} - l_i$. Figure 1 shows a schematic representation of the coordinate system and the main mooring system elements considered by MeDuSa®.

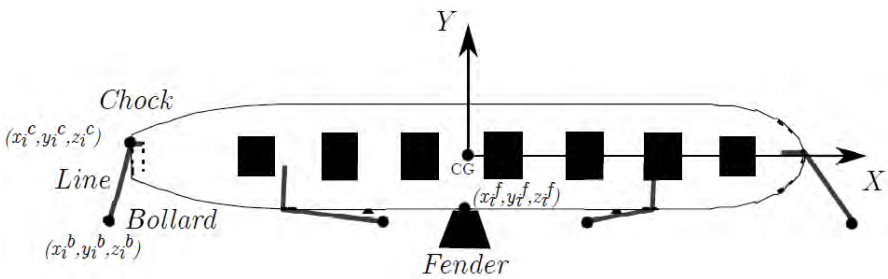

Figure 1: Definition of coordinate system and mooring system elements

Assuming small rotative motions, the instantaneous coordinates of the ship chocks can be written in terms of the six degrees of freedom ship rigid modes ($\boldsymbol{x_1}, \boldsymbol{x_2}, \ldots, \boldsymbol{x_6}$), as presented in (4).

$$\begin{aligned} x_i^c(t) &= x_{i,0}^c + \boldsymbol{x}_1(t) - \boldsymbol{x}_6(t) y_{i,0}^c + \boldsymbol{x}_5(t) z_{i,0}^c \\ y_i^c(t) &= y_{i,0}^c + \boldsymbol{x}_6(t) x_{i,0}^c + \boldsymbol{x}_2(t) - \boldsymbol{x}_4(t) z_{i,0}^c \\ z_i^c(t) &= z_{i,0}^c - \boldsymbol{x}_5(t) x_{i,0}^c + \boldsymbol{x}_5(t) y_{i,0}^c + \boldsymbol{x}_3(t) \end{aligned} \tag{4}$$

The mooring line loads $L_i(t)$ are determined through the nonlinear load-elongation curves $f_i^l(\varepsilon_i^l(t))$, i.e.

$$\begin{aligned} L_i(t) = f_i^l(\varepsilon_i^l(t)) \quad &\text{if } \Delta l_i(t) > 0 \quad \text{(tensioned)} \\ L_i(t) = 0 \quad &\text{if } \Delta l_i(t) \leq 0 \quad \text{(slack)} \end{aligned} \tag{5}$$

where $\Delta l_i(t)$ and $\varepsilon_i^l(t)$ are the instantaneous line deformation and elongation, respectively, which are defined in terms of the instantaneous line length $l_{i,f}(t)$, as follows:

$$\begin{aligned} l_{i,f}(t) &= \sqrt{(x_i^c(t) - x_i^b)^2 + (y_i^c(t) - y_i^b)^2 + (z_i^c(t) - z_i^b)^2} \\ \Delta l_i(t) &= l_{i,f}(t) - l_{i,0} + \delta l_{i,0} = l_{i,f}(t) - l_i \\ \varepsilon_i^l(t) &= \Delta l_i(t) / l_i \end{aligned} \tag{6}$$

The resulting forces and moment about the ship center of gravity induced by the N_l mooring line are calculated following (7).

$$\boldsymbol{f}^{\boldsymbol{l}}_{\boldsymbol{ext,1}}(t) = \sum_{i=1}^{N_l} L_i(t)\left(x_i^b - x_i^c(t)\right)/l_{i,f}(t)$$

$$\boldsymbol{f}^{\boldsymbol{l}}_{\boldsymbol{ext,2}}(t) = \sum_{i=1}^{N_l} L_i(t)\left(y_i^b - y_i^c(t)\right)/l_{i,f}(t)$$

$$\boldsymbol{f}^{\boldsymbol{l}}_{\boldsymbol{ext,3}}(t) = \sum_{i=1}^{N_l} L_i(t)\left(z_i^b - z_i^c(t)\right)/l_{i,f}(t) \tag{7}$$

$$\boldsymbol{f}^{\boldsymbol{l}}_{\boldsymbol{ext,4}}(t) = \sum_{i=1}^{N_l} -\boldsymbol{f}^{\boldsymbol{l}}_{\boldsymbol{ext,2}}(t)\left(z_i^c(t) - \boldsymbol{x_3}(t)\right) + \boldsymbol{f}^{\boldsymbol{l}}_{\boldsymbol{ext,3}}(t)\left(y_i^c(t) - \boldsymbol{x_2}(t)\right)$$

$$\boldsymbol{f}^{\boldsymbol{l}}_{\boldsymbol{ext,5}}(t) = \sum_{i=1}^{N_l} \boldsymbol{f}^{\boldsymbol{l}}_{\boldsymbol{ext,1}}(t)\left(z_i^c(t) - \boldsymbol{x_3}(t)\right) - \boldsymbol{f}^{\boldsymbol{l}}_{\boldsymbol{ext,3}}(t)\left(x_i^c(t) - \boldsymbol{x_1}(t)\right)$$

$$\boldsymbol{f}^{\boldsymbol{l}}_{\boldsymbol{ext,6}}(t) = \sum_{i=1}^{N_l} -\boldsymbol{f}^{\boldsymbol{l}}_{\boldsymbol{ext,1}}(t)\left(y_i^c(t) - \boldsymbol{x_2}(t)\right) + \boldsymbol{f}^{\boldsymbol{l}}_{\boldsymbol{ext,2}}(t)\left(x_i^c(t) - \boldsymbol{x_1}(t)\right)$$

The fenders loads are split in reaction $D_i^r(t)$ and friction forces $D_i^f(t)$, in which the former is calculated through the nonlinear deformation-reaction curves $f_i^f(-d_i(t))$, described in (8), and acts on the ship only in the transversal direction Y, whereas the friction force is calculated through Coulomb's expression (9) and acts on the body exclusively in the longitudinal direction X. In these equations, μ is the fender friction coefficient and the fender deformation $d_i(t)$ is found by (10).

$$\begin{aligned} D_i^r(t) &= f_i^f(-d_i(t)) \quad \text{if } d_i(t) < 0 \quad \text{(compressed)} \\ D_i^r(t) &= 0 \quad \text{if } d_i(t) \geq 0 \quad \text{(not in contact)} \end{aligned} \tag{8}$$

$$\begin{aligned} D_i^f(t) &= -\mathrm{sgn}(\dot{\boldsymbol{x}}_{\boldsymbol{1}})\mu D_i^r(t) \quad \text{if } d_i(t) < 0 \quad \text{(compressed)} \\ D_i^f(t) &= 0 \quad \text{if } d_i(t) \geq 0 \quad \text{(not in contact)} \end{aligned} \tag{9}$$

$$d_i(t) = \boldsymbol{x_2}(t) + \left(x_i^f - \boldsymbol{x_1}(t)\right)\boldsymbol{x_6}(t) - \left(z_i^f - \boldsymbol{x_3}(t)\right)\boldsymbol{x_4}(t) \tag{10}$$

Finally, resulting forces and moments about the ship center of gravity of the N_f fenders are determined by expressions in (11).

$$\boldsymbol{f}^{\boldsymbol{f}}_{\boldsymbol{ext,1}}(t) = \sum_{i=1}^{N_f} D_i^f(t) \quad \boldsymbol{f}^{\boldsymbol{f}}_{\boldsymbol{ext,2}}(t) = \sum_{i=1}^{N_f} D_i^r(t) \quad \boldsymbol{f}^{\boldsymbol{f}}_{\boldsymbol{ext,3}}(t) = 0$$

$$\boldsymbol{f}^{\boldsymbol{f}}_{\boldsymbol{ext,4}}(t) = \sum_{i=1}^{N_f} -\boldsymbol{f}^{\boldsymbol{f}}_{\boldsymbol{ext,2}}(t)\left(z_i^f - \boldsymbol{x_3}(t)\right) \quad \boldsymbol{f}^{\boldsymbol{f}}_{\boldsymbol{ext,5}}(t) = 0 \tag{11}$$

$$\boldsymbol{f}^{\boldsymbol{f}}_{\boldsymbol{ext,6}}(t) = \sum_{i=1}^{N_f} \boldsymbol{f}^{\boldsymbol{f}}_{\boldsymbol{ext,2}}(t)\left(x_i^f - \boldsymbol{x_1}(t)\right)$$

The external forces $\boldsymbol{f}^{\boldsymbol{l}}_{\boldsymbol{ext}}(t)$ and $\boldsymbol{f}^{\boldsymbol{f}}_{\boldsymbol{ext}}(t)$ are then combined to the others on the right hand-side of (1), which is solved numerically by a Runge Kutta 4th order method. As output of the computations, MeDuSa® provides the time histories of ship motions, mooring lines and fender loads.

2.2. Hydrodynamic Interaction Forces

The external force and moments induced by the passing ship on the moored vessel are calculated by a 3D panel method upon the considerations of potential flow theory, in which the velocity field is defined by the gradient of the velocity potential $\Phi(\boldsymbol{X})$, where $\boldsymbol{X}$ is a vector in the earth-fixed reference frame (X, Y, Z) that is defined such that X and Y axes lie on the plane of the free surface and Z axis points upwards and out of the fluid volume. In addition, for each independent body, right-hand oriented body-fixed reference frames $\boldsymbol{x} = (x, y, z)$, centered at the center of gravity of the bodies, are used to describe the body geometries and resultant forces and moments, in which x and y axes point to ship's bow and port side, respectively.

The double-body formulation here applied assumes the passing ship sailing at moderate Froude number and neglects the free surface effects and shed vorticity. The governing equations for determining $\Phi(\boldsymbol{X})$ are defined by Laplace's equation:

$$\nabla^2\Phi = 0 \text{ in fluid domain} \tag{12}$$

under the following boundary conditions (BC):

$$\nabla\Phi \cdot \boldsymbol{n}_{fs} = 0 \text{ on } S_{fs} \text{ (Free Surface rigid-lid BC)} \tag{13}$$

$$\nabla\Phi \cdot \boldsymbol{n}_{m} = 0 \text{ on } S_{m} \text{ (Moored vessel no-flux BC)} \tag{14}$$

$$\nabla\Phi \cdot \boldsymbol{n}_{\boldsymbol{p}} = U(t) \cdot \boldsymbol{n}_{\boldsymbol{p}} \text{ on } S_{p}(t) \text{ (Passing Ship no-flux BC)} \tag{15}$$

$$\nabla\Phi \cdot \boldsymbol{n}_{\boldsymbol{fix}} = 0 \text{ on } S_{fix} \text{ (Bottom and port structures no-flux BC)} \tag{16}$$

$$\nabla\Phi \to 0 \text{ at } \sqrt{X^2 + Y^2 + Z^2} \to \infty \text{ (Far field evanescent condition)} \tag{17}$$

where $\boldsymbol{n}$ and S are the normal unit vector with positive direction into the fluid and the wetted surfaces of the bodies and other port structure surfaces. Besides that, the subscripts fs, m, p and fix refer to the free surface, moored ship, passing ship and all fixed surfaces (bottom, quay wall, banks etc.), respectively.

A similar numerical scheme presented in (Hess & Smith, 1967) has been applied to solve the boundary value problem by introducing a distribution of Rankine's sources with density σ on all wetted surfaces:

$$\Phi(\boldsymbol{P}) = \iint_{\partial\Omega} \sigma(\boldsymbol{Q}) G(\boldsymbol{P}, \boldsymbol{Q}) d\partial\Omega(\boldsymbol{Q}) \tag{18}$$

where $\boldsymbol{P}(x_P, y_P, z_P)$ and $\boldsymbol{Q}(x_Q, y_Q, z_Q)$ are the respective field and the source points on all wetted surfaces S, and $G(\boldsymbol{P}, \boldsymbol{Q})$ is the Green's function constructed to satisfy the free surface rigid-lid, bottom (at $Z = -h$) and fair field boundary conditions:

$$G(\boldsymbol{P}, \boldsymbol{Q}) = \sum_{i=-\infty}^{\infty} \left(\frac{1}{r_i} + \frac{1}{r_i'} \right) \tag{19}$$

where:

$$r_i = \sqrt{\left(x_P - x_Q\right)^2 + \left(y_P - y_Q\right)^2 + \left(z_P + z_Q + 2ih\right)^2} \tag{20}$$

$$r_i' = \sqrt{\left(x_P - x_Q\right)^2 + \left(y_P - y_Q\right)^2 + \left(z_P - z_Q + 2ih\right)^2} \tag{21}$$

The boundary conditions on wetted surfaces are then imposed by the following integral equation:

$$2\pi\sigma(\boldsymbol{P}) = \iint_{\partial\Omega} \sigma(\boldsymbol{Q}) \frac{\partial G(\boldsymbol{P}, \boldsymbol{Q})}{\partial n(\boldsymbol{P})} \mathrm{d}\partial\Omega(\boldsymbol{Q}) = f(\boldsymbol{P}) \tag{22}$$

in which the right-hand side term $f(\boldsymbol{P})$ reads $f(\boldsymbol{P}) = \boldsymbol{U}(\boldsymbol{P}) \cdot \boldsymbol{n}(\boldsymbol{P})$ for the boundary condition of the passing ship and $f(\boldsymbol{P}) = 0$ for the other surfaces.

Once (22) is solved for an specific position of the sailing ship, the components of the force and moment acting on the moored ship are calculated by integrating the pressure from Bernoulli's equation over the body surface, as expressed in (23) and (24), where A_j is the area of the j-panel.

$$\boldsymbol{F} = -\rho \sum_{j=1}^{N} \left(\frac{\partial \Phi_j}{\partial t} + \frac{1}{2} \nabla\Phi_j \Phi_j \right) \boldsymbol{n}_j A_j \tag{23}$$

$$\boldsymbol{M} = -\rho \sum_{j=1}^{N} \left(\frac{\partial \Phi_j}{\partial t} + \frac{1}{2} \nabla\Phi_j \Phi_j \right) (\boldsymbol{r_j} \times \boldsymbol{n}_j) A_j \tag{24}$$

2.3. Real-Time Maneuvering Simulator

The real-time simulator of the Numerical Offshore Tank of the University of São Paulo (TPN-USP) was applied for conducting the maneuvering simulations with the container ship of length 366m. This simulator was officially opened in 2012 and is a result of several research projects that have been conducted during more than ten years in close cooperation with Petrobras, research institutes and universities. It consists on a Full Mission Maneuvering Simulator with 270° field view comprised by a 12m diameter screen, 30 image projectors, 10 panels for commands and instruments, and 4 overhead screens, immersing the pilots and ship masters into very realistic scenarios. The description of the numerical model adopted is presented in (Tannuri, et al., 2014). The Figure 2 shows the pilot in the simulator bridge during the 366m long container ship simulation.

Figure 2: Pilot in the real-time simulator bridge

3. APPLICATION TO THE PORT OF SANTOS

3.1. Selection of critical berths and ships

As a first step of the methodology, twelve berths have been selected by the local port authority (CODESP) and pilots as the most critical berths of the port in terms of the passing ship problem. The locations of the berths along the channel are presented in Figure 3. For the sake of conciseness and to focus on the understanding of the analysis methodology, only the berth 21, which presented the largest number of fail cases in the real-time simulations, will be considered. The berth 21 is equipped with T-Head bollards of capacity 100 tf and π-type fenders (MV1000L1500) of maximum energy absorption and reaction of 71.4 tfm and 155.4 tf, respectively. The water depth considered in the analysis was 16 m.

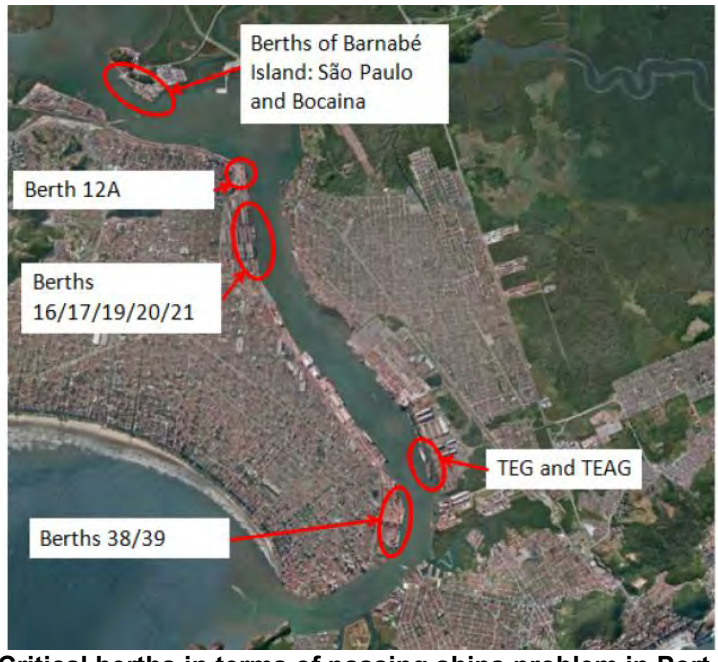

Figure 3: Critical berths in terms of passing ships problem in Port of Santos

The moored vessel selected to be analyzed is a Small Capesize ship of 125,000 tons of deadweight, 275m long, 43 m width, 22.4 m height and draft 14.2 m. This ship is normally equipped with 12 polyblend lines of diameter 72 mm and Minimum Breaking Load (MBL) of 84 tf. The lines Load x Elongation and fenders nonlinear Reaction x Deflection curves are presented in Figure 4.

Typical mooring arrangement applied in the Port of Santos has been applied, being composed of 12 mooring lines spread in 4 stern lines, 2 stern springs, 2 bow springs and 4 head lines. In an equilibrium position, the ship side hull touches 10 fenders. The mooring arrangement is shown in Figure 5.

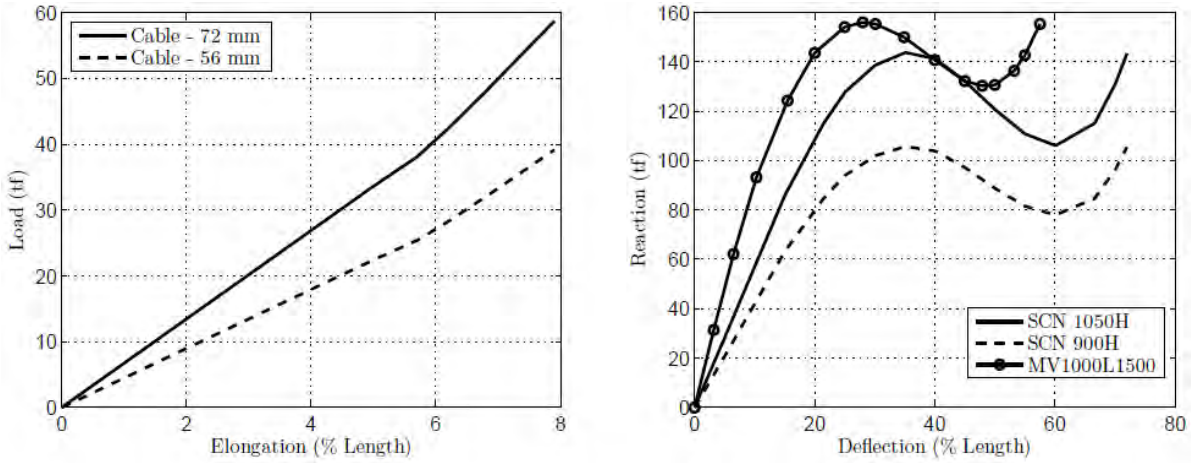

Figure 4: Line Load x Elongation (left) and Fender Reaction x Deflection curves (right). Sources: (OCIMF, 2008) and (Trelleborg, 2017)

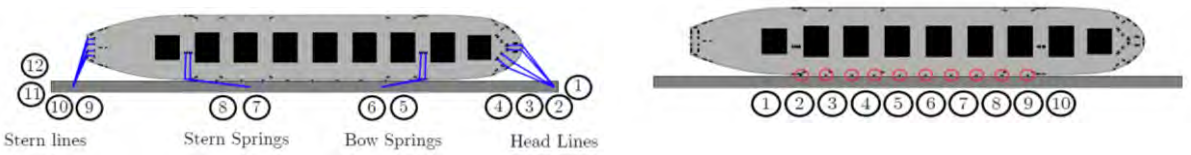

Figure 5: Mooring arrangement of small capsize at berth 21. Mooring lines (left) and fenders (right)

3.2. Preliminary Hydrodynamic Interaction Loads and Mooring Calculations

As aforementioned, the passing effects are analyzed considering the maneuvering of a 366 m long container ship, whose main dimensions and gear features are presented in Table 1.

Table 1: Main characteristics of the sailing ship

Cargo capacity	13,8	[TEU]
Deadweight	124,479	[ton]
Ship Length (LOA)	366	[m]
Ship Beam	51.2	[m]
Ship Draft	14.2	[m]
Ship Height	29.9	[m]
Dead slow ahead	7.9	[m]
Slow ahead	10.8	[kts]
Half ahead	13.2	[kts]
Full speed	16	[kts]
Full sea speed	23.9	[kts]

The second step of the methodology is then dedicated to obtain first estimates of the passing ship safe speed and distance to the moored ship by analyzing the mooring loads and ship motions induced by the ship advancing on the prescribed trajectories illustrated in Figure 6, which correspond to minimum distances of 60m (on the right margin), 150m (on the center) and 230m (on the left margin) to the moored ship. For each prescribed trajectory, different sailing velocities in the range between 5kts and 10kts are also assumed.

The checking of failure cases is performed comparing the moored ship motions, line loads and fender compression forces with the safe working values recommended in (PIANC, 1995) and (OCIMF, 2008), here summarized in Table 2.

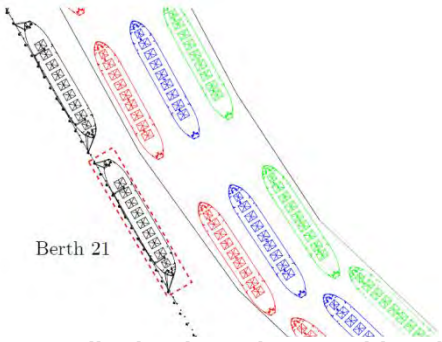

Figure 6: Ship maneuvering prescribed trajectories considered for the passing ship loads estimate at berth 21.

Table 2: Safe working values considered in the analysis

	Criteria	
Surge [m]	5.0	Peak-peak value
Sway [m]	2.5	Zero-peak value
Yaw [°]	3.0	Peak-peak value
Cables [tf]	42	50% of the line MBL
Fenders [tf]	105	100% of the fender maximum reaction

Figure 7 presents examples of moored ship hydrodynamic loads and motions induced by the container ship sailing at 7 kts under the different trajectories, whereas Figure 8 presents the loads on the mooring lines and fenders. Although, in this case, the small capesize motions did not exceed the criteria in any of the tested cases, there were some mooring lines and fenders that had their limits overtaken when the container ship passed by under the closest trajectory simulated.

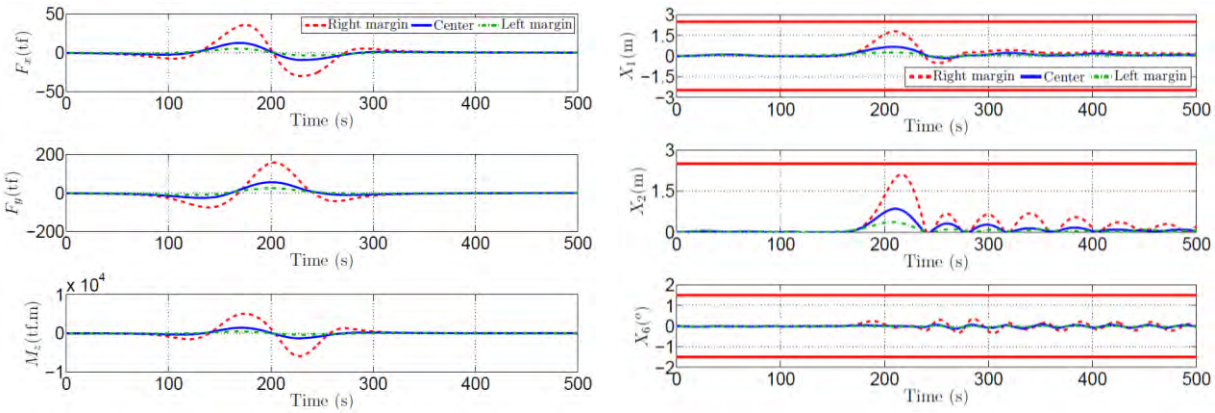

Figure 7: Moored ship hydrodynamic loads (left) and motions (right) time series induced by the container ship sailing at 7 kts. Solid horizontal lines indicate tolerated margins

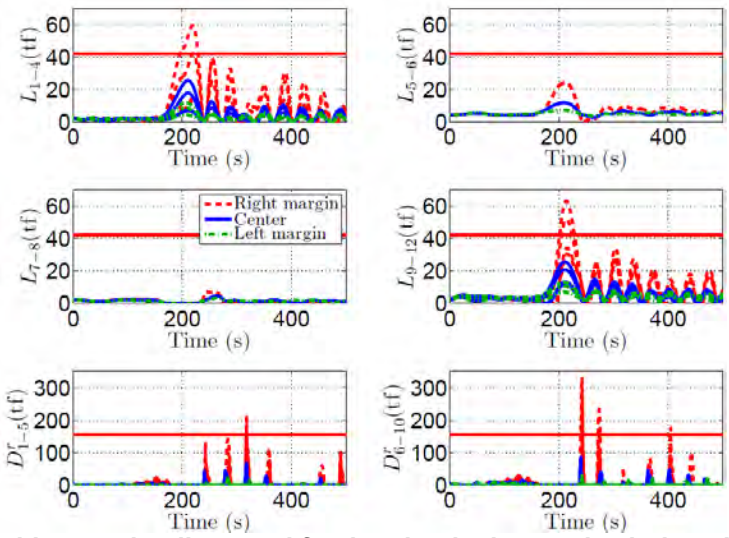

Figure 8: Moored ship mooring lines and fenders loads time series induced by the container ship sailing at 7 kts. Solid horizontal lines indicate tolerated margins

The results were made available as a guide for the pilots during the real-time simulations through operational maps which were also printed in the local nautical chart, as shown in Figure 9. The colored area in the nautical chart represents the conditions of passing distance and associated velocity, which the pilots should avoid crossing during the maneuvering in order to keep the mooring loads and motions of the moored vessel below the acceptable limits.

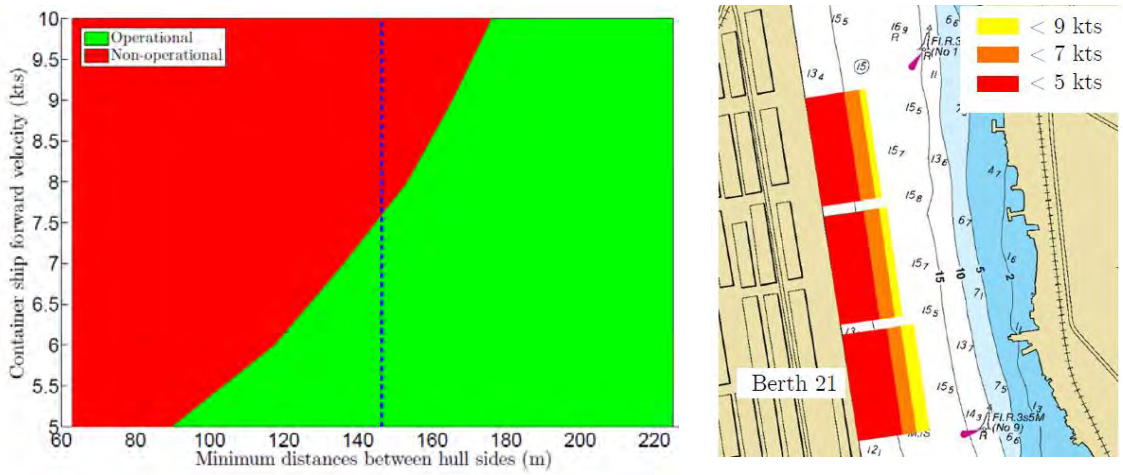

Figure 9: Operational limits is terms of passing distance and forward velocity for berth 21

3.3. Real Time Maneuvering Simulations

The proposed methodology now follows to the conduction of real-time simulations commanded by local and experienced pilots of the Port of Santos. This is a very important step of the present work, since it becomes possible to evaluate whether the ship can be indeed controlled and kept distant enough to the moored ships with relatively low speed. In total, 10 maneuvering simulations were carried out, comprising combinations of draft, outbound/inbound maneuvers, flood/ebb tides, wind and wave conditions, the latter acting only on the approach channel which is exposed to waves. Since the work methodology is here represented by the analysis of berth 21, the ship maneuvers that did not pass by this berth have been disregarded. Table 3 presents the simulation matrix with the main characteristics of each test, whereas Figure 10 presents some illustrative screenshots of the real-time simulation for Case 6, at different instants.

Table 3: Matrix of real-time maneuvering simulations

Case	Maneuvering	Current	Wind
1	Inbond	0.5 kts (ebb)	17 kts (E)
2	Outbound	0.5 kts (flood)	17 kts (E)
3	Inbond	0.8 kts (flood)	17 kts (E)
4	Outbound	0.8 kts (ebb)	17 kts (NW)
5	Inbond	0.8 kts (ebb)	17 kts (SW)
6	Inbond	0.8 kts (flood)	17 kts (NW)

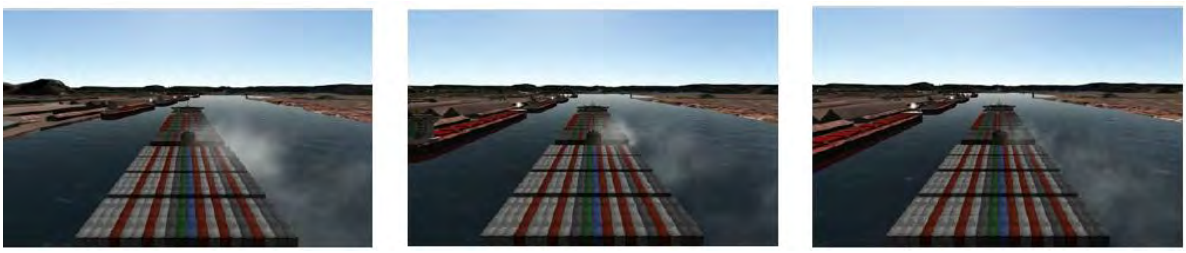

Figure 10: Screenshots of the real-time simulation at different instants during the passage of the container ship by the small capsize at berth 21, on the left

Figure 11 illustrates the forward velocity of the container ship when passing by berth 21. The two most critical cases are 4 and 6 in which neither the velocity nor the minimum recommended distance from berth 21 could be respected. As illustrated in Figure 11, the container ship has crossed the colored areas with forward velocities above 10 knots, exposing the small capesize mooring system to severe hydrodynamic interaction forces as will be presented ahead.

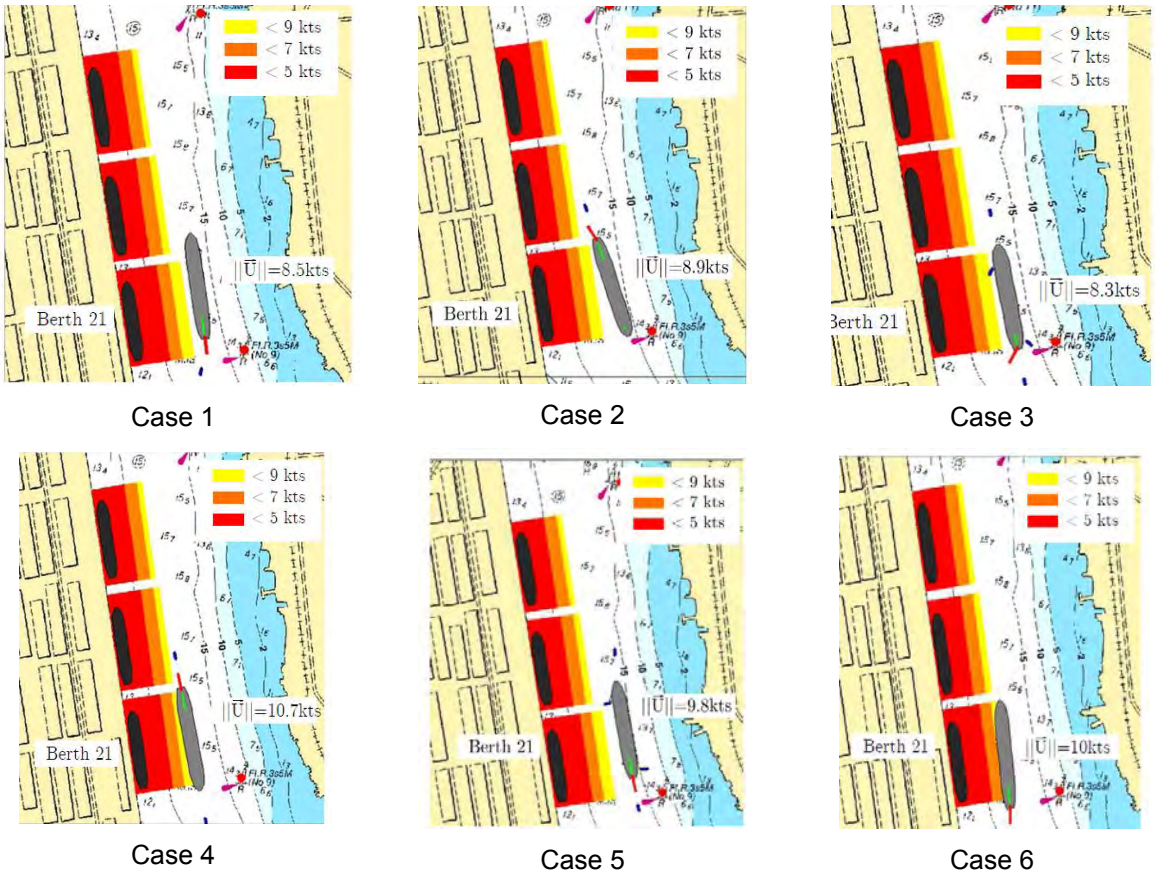

Figure 11: Container ship velocity when passing by berth for the 6 different cases

3.4. Reassessment of Ship Motions and Mooring Loads

In this stage of the methodology, the container ship trajectories and velocities obtained in the real-time simulations are used as input to calculate the ship motions and mooring loads by following the procedures aforementioned. For these simulations, the lines were set with low pre-tensions values of 2.2 tf (or 2.6\% of MBL) in order to increase the conservatism of the analyses.

The obtained time histories of motions, mooring line loads and fender compression forces for the two most critical cases 4 and 6 are presented in Figure 12 and Figure 13, respectively. In addition, in case any of the criteria is exceeded, the correspondent mooring element is highlighted on the ship illustration located on the top right corner of each figure. As may be observed, the small passing distance associated to over speed pointed out in Figure 11 was responsible to strong interaction forces which led the moored ship to present large horizontal offsets and, consequently, high mooring loads. These results illustrate that the simulations based on simplified ship trajectories can be used as a first estimate of the operational limits for the passing ship problem in a specific berth, since they were confirmed when applying the ship paths obtained in the real-time simulations. On the other hand, it is clear that they are not sufficient for a full comprehension of the problem, since they do not guarantee that the ship can be maneuvered under the limits established which could only be evaluated by conducting real-time simulations commanded by experienced local pilots.

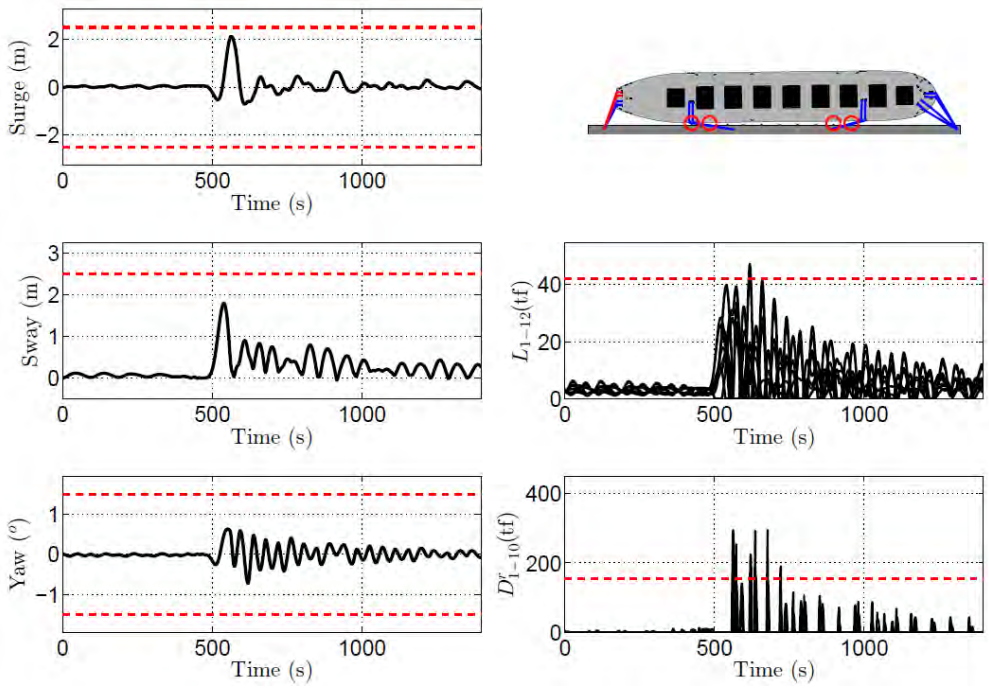

Figure 12: Case 4: Time histories of ship motions, mooring line loads and fender compression forces. Horizontal traced lines indicate tolerated margins

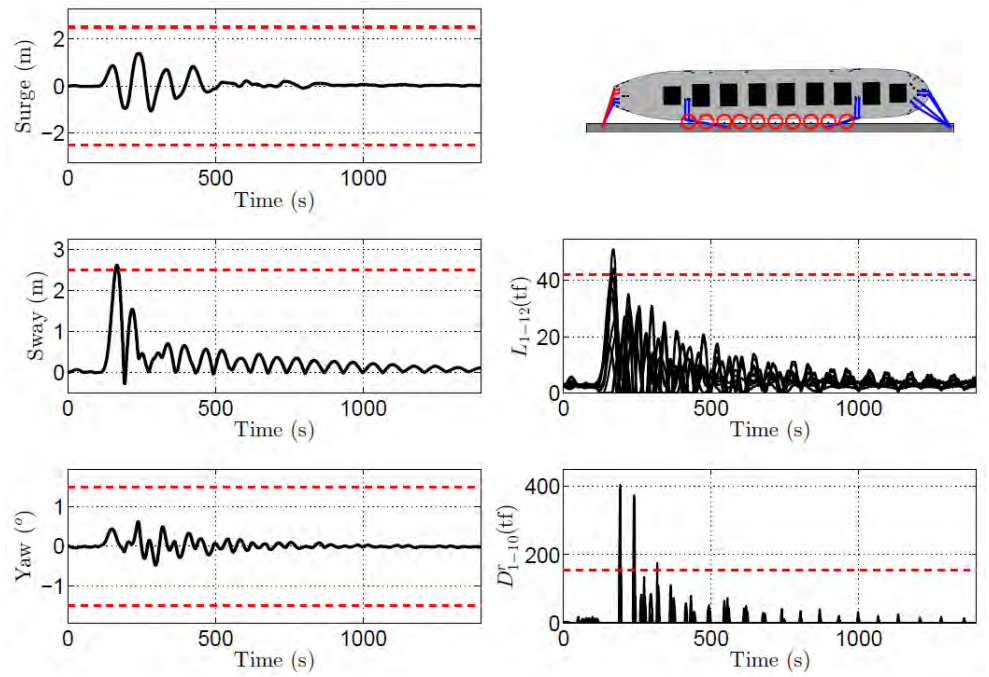

Figure 13: Case 6: Time histories of ship motions, mooring line loads and fender compression forces. Horizontal traced lines indicate tolerated margins

3.5. Improvements on the Mooring System

Two possibilities of improvements on the mooring system have been considered as an attempt to improve the mooring system performance observed in the cases 4 and 6. In the first, the two cases were tested assuming the same mooring arrangement, but increasing the lines pre-tensions to 6.6 tf (reasonable value to be applied in reality). The results are presented in Figure 14 and Figure 15 showing that the ship motions, lines loads and fenders compression forces become smaller by increasing the lines pre-tensions. In case 4, for example, this change was enough to reduce line loads to acceptable values. Nevertheless, it was not sufficient to reduce the sway amplitude and avoid the strong impacts between the ship and the fenders, which caused loads over 200tf in case 4 and 400tf in case 6.

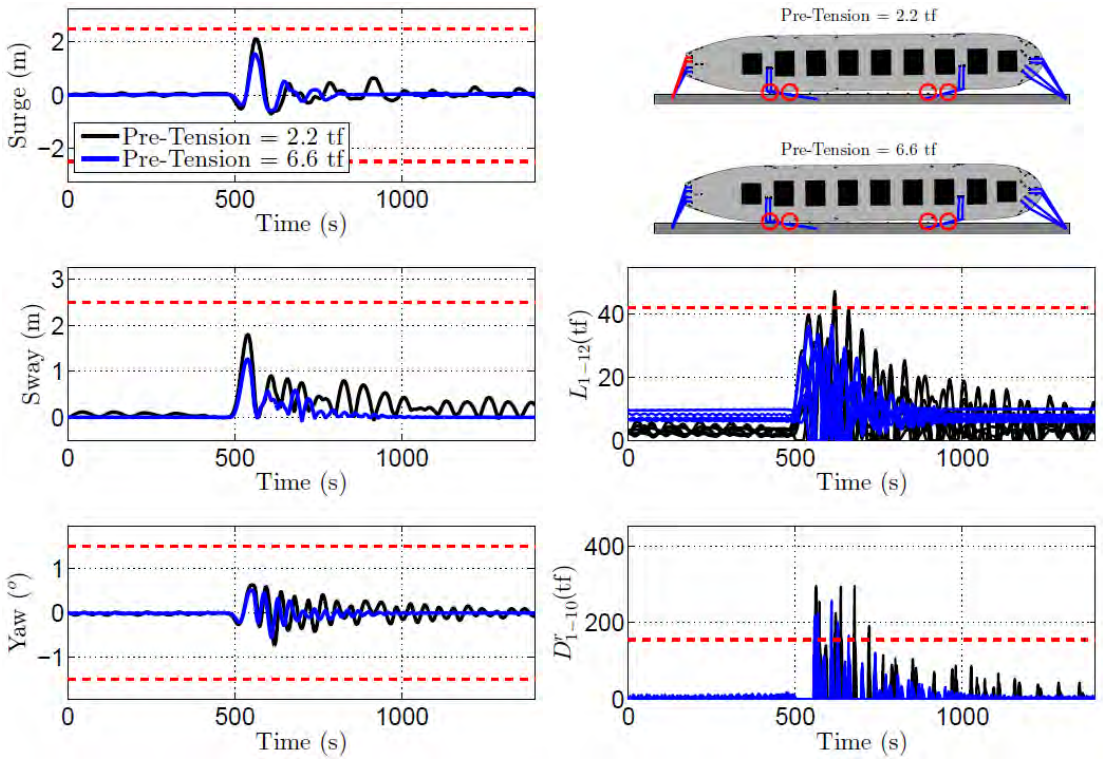

Figure 14: Case 4: Time histories of ship motions, mooring line loads and fender compression forces for two values of pre-tension. Horizontal traced lines indicate tolerated margins

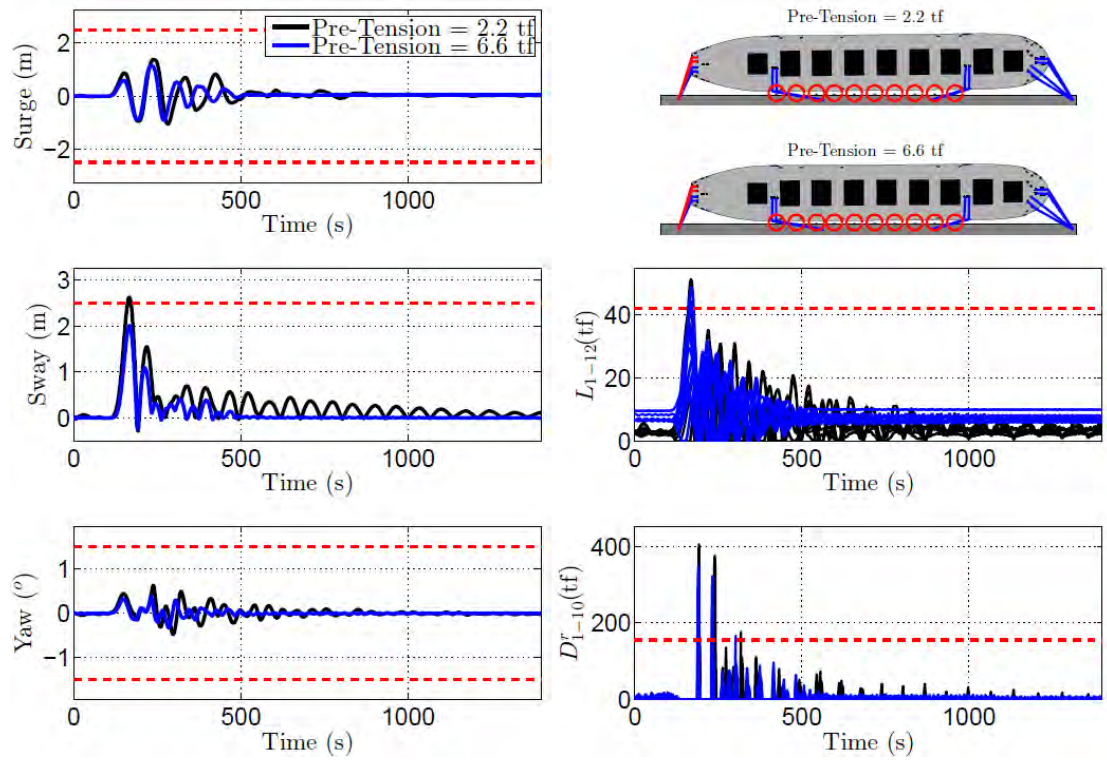

Figure 15: Case 6: Time histories of ship motions, mooring line loads and fender compression forces for two values of pre-tension. Horizontal traced lines indicate tolerated margins

The second test was performed by changing 2 stern lines and 2 head lines for stern and bow breast lines, as illustrated in Figure 16, increasing, therefore, the transversal and rotational stiffness of the mooring system. The results obtained are presented in Figure 17 and Figure 18 where reductions of the maximum sway and yaw motion amplitudes as well as the maximum mooring loads are observed. In case 6, however, practically all the fenders still exceeded the limit value, indicating that in this case a modification on the mooring system only would not be enough to avoid a problem, in which a change of the fenders to ones of more capacity would be indicated.

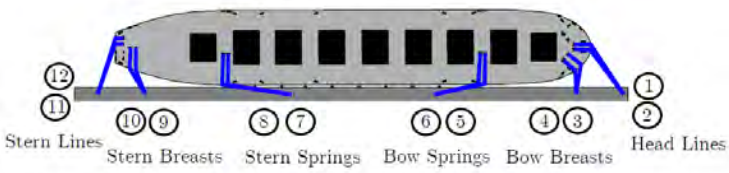

Figure 16: Alternative mooring arrangement of the small capsize at berth 21

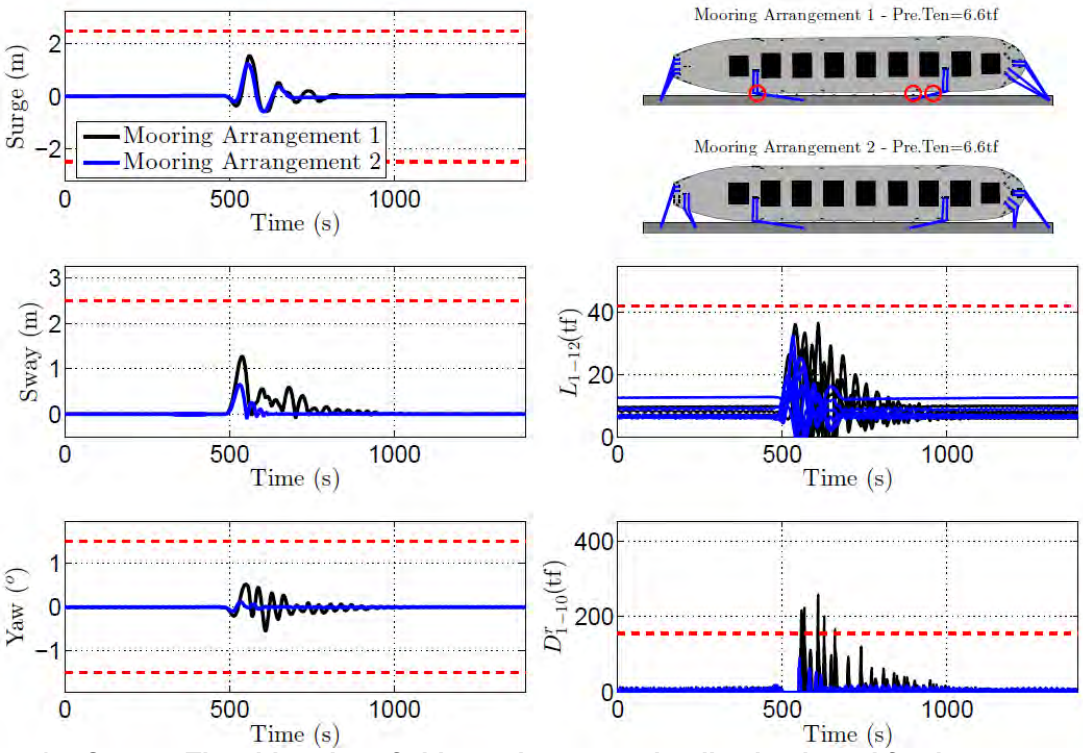

Figure 17: Case 4: Time histories of ship motions, mooring line loads and fender compression forces for two values of pre-tension. Horizontal traced lines indicate tolerated margins

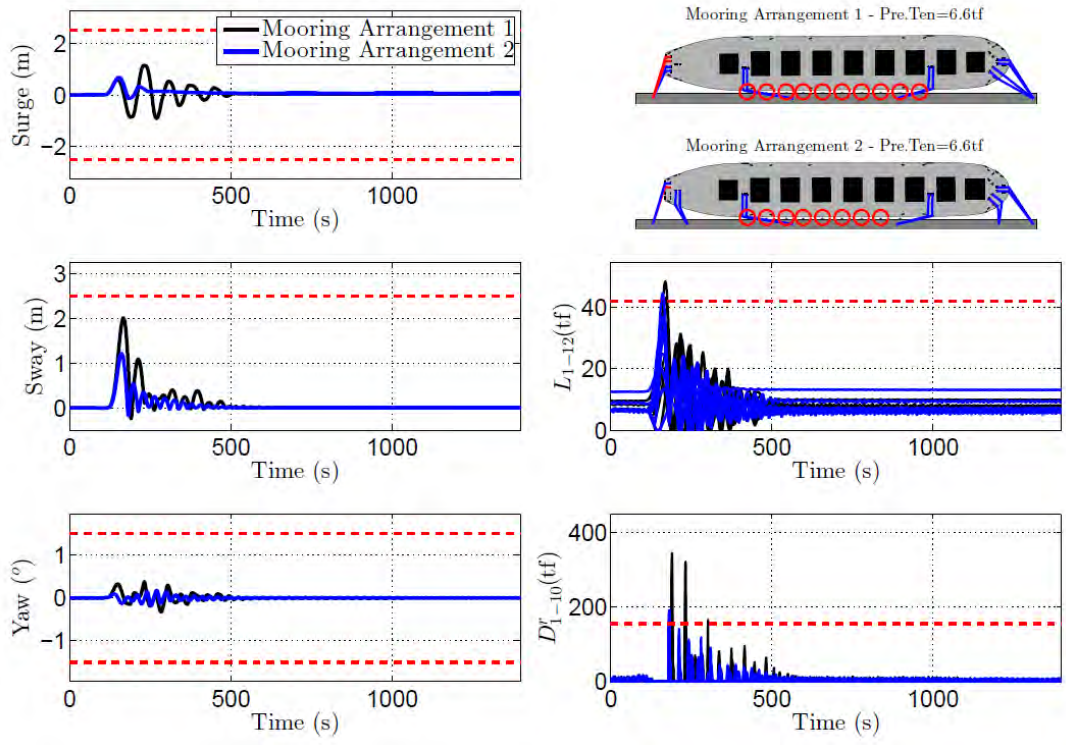

Figure 18: Case 6: Time histories of ship motions, mooring line loads and fender compression forces for two values of pre-tension. Horizontal traced lines indicate tolerated margins

4. CONCLUSIONS

An analysis methodology integrating a potential flow model, a dynamic simulator for moored ships and a real-time simulator was here presented for the assessment of the passing ship hydrodynamic problem.

From the results, it can be concluded that the standard approach of defining operational limits based on simplified ship trajectories can indeed be used as first estimate of the passing ship effect in a berth of interest, but requires special attention to the fact that they do not guarantee whether the ship can be maneuvered under the limits established. Therefore, it is indicated the conduction of real-time simulations commanded by experienced local pilots for a better understanding of the navigation scenario.

Besides the ship maneuvering aspect, the results have shown that significant improvements are obtained by setting the mooring lines with appropriate pre-tension values and also by choosing a mooring arrangement with higher transversal and rotational (in Z axis) stiffness, introducing, for instance, breast lines to the system. These measures tend to increase the mooring system safety, especially in situations where the pilot has to increase the ship speed so as to raise the rudder efficiency, what inevitably exposes the moored ships to higher passing ship forces.

5. ACKNOWLEDGMENTS

The authors gratefully acknowledge CODESP (Port Authority of Santos), represented by the company's president Jose Alex Botêlho de Oliva, for sponsoring this study. The authors also thank the Santos Pilots for their valuable advices and practical experience. Third author thanks the National Council for Scientific and Technological Development (CNPq process 308645/2013-8) for the research grant.

6. REFERENCES

Cummins, W. (1962). The impulsive response function and ship motions. *Technical Report, Department of Navy David Taylor Model Basin.*

Flory, J. (2002). The effects of passing ships on moored ships. *Prevention First 2002 Symposium, California State Lands Commission.*

Hess, J., & Smith, A. (1967). Calculation of potential flow about arbitrary bodies. *Progress in Aerospace Sciences.*

King, G. (1977). Unsteady hydrodynamic interactions between ships. *Journal of Ship Research.*

Korsmeyer, F. T., Lee, C.-H., & Newman, J. N. (1993). Computation of ship interaction forces in restricted waters. *Journal of Ship Research.*

Kriebel, D. (2005). Mooring Loads due to Parallel Passing Ships (Technical Report TR-6056-OCN). *Tech. rep., Naval Facilities Engineering Service Center.*

Krishnankutty, P., & Varyani, K. (2004). Force on the Mooring Lines of a Ship due to the Hydrodynamic Interaction Effects of a Passing Ship. *International Shipbuilding Progress.*

Muga, B., & Feng, S. (1975). Passing ship effects - from theory and experiment. *Offshore Technology Conference.*

OCIMF. (2008). *Mooring Equipment Guidelines (MEG3), 3rd Edition.*

Oortmerssen, G. (1976). The Motions of a Moored Ship in Waves. *Publication No 510 of the Netherlands Ship Model Basin, Wageningen, The Netherlands.*

PIANC. (1995). *Criteria for Movements of Moored Ships in Harbours.* Rapport du Groupe de Travail n.27, Brussels (Belgium).

Pinkster, J. (2004). The influence of a free surface on passing ship effects. *International Shipbuilding Progress.*

Pinkster, J. A. (2009). Suction, Seiche and Wash Effects of Passing Ships in Ports. *SNAME Annual Meeting and Expo and Ship Production Symposium, Providence, Rhode Island, USA.*

Pinkster, J. A. (2014). A Fast, User-Friendly, 3-D Potential Flow Program for the Prediction of Passing Vessel Forces. *PIANC World Congress San Francisco, USA.*

Remery, G. (1974). Mooring forces induced by passing ships. *Offshore Technology Conference.*

Ruggeri, F., Watai, R., & Tannuri, E. (2016). Passing ships interactions in the oil terminal of São Sebastião (Brazil): An applied study to define the operation limits. *4th International Conference on Ship Manoeuvring in Shallow and Confined Water with Special Focus on Ship Bottom Interaction, May 23-25, Hamburg, Germany.*

Talstra, H., & Bliek, A. J. (2014). Loads on Moored Ships due to Passing Ships in a Straight Harbour Channel. *PIANC World Congress San Francisco, USA.*

Tannuri, E., Rateiro, F., Fucatu, C., Ferreira, M., Masetti, I., & Nishimoto, K. (2014). Modular mathematical model for a low-speed maneuvering simulator. *Proceedings of the ASME 2014 33rd International Conference on Offshore Mechanics and Artic Engineering OMAE2014.*

Trelleborg. (2017). Trelleborg Marine Systems, Fender Systems Product Brochure.

van der Hout, A., & de Jong, M. (2014). Passing Ship Effects in Complex Geometries and Currents. *PIANC World Congress San Francisco, USA.*

Vantorre, M., Verzhbitskaya, E., & Laforce, E. (2002). Model test based formulation of ship-ship-interaction forces. *Ship Technology Research.*

Wang, S. (1975). Dynamic Effects of Ship Passage on Moored Vessels. *ASCE Ports Proceedings, California, USA.*

Watai, R. (2015). A Time Domain Boundary Elements Method for the Seakeeping Analysis of Offshore Systems. *PhD Thesis, University of São Paulo.*

Watai, R., Ruggeri, F., Sampaio, C., & Simos, A. (2015). Development of a time domain boundary elements method for numerical analysis of floaring bodies responses in waves. *Journal of the Brazilian Society of Mechanical Sciences and Engineering.*

Watai, R., Ruggeri, F., Tannuri, E., & Weiss, J. (2013). Evaluation of empirical and numerical methods on the prediction of hydrodynamic loads involved in the passing ship problem. *3rd International Conference on Ship Manoeuvring in Shallow and Confined Water, June 3-5, Ghent, Belgium.*

Wictor, E., & van den Boom, H. (2014). Full Scale Measurements of Passing Ship Effects. *PIANC World Congress San Francisco, USA.*

EVALUATION OF PROPOSED JETTIES FOR PORT OF SANTOS NAVIGATION CHANNEL DEPTH MAINTENANCE

by

Thiago Bezerra Corrêa[1,2], João Henrique Oliveira Costa [1], Tiago Zenker Gireli[1] and Patricia Dalsoglio Garcia[1]

ABSTRACT

In order to become a hub port in South America, Port of Santos intends to deepen and widen its Navigation Channel to support New Panamax vessels. Some authors proposed jetties geometries and evaluated the variation of currents velocities along Navigation Channel of Port of Santos. Five jetty options, previously proposed by other authors, were simulated with 2DH model and compared with a baseline scenario (without jetties). Flood and ebb current maps of each scenario with jetty were compared to flood and ebb current maps of baseline scenario, respectively. In addition, the siltation rate along Navigation Channel of Port of Santos was considered in this evaluation. Among the five jetties options (J1 and J3 with one jetty, J2 and J5 with two spaced jetties and J4 with two jetties with narrow channel), J4 has the best performance. For all options no significant current velocity variations were observed in the inner part of the estuary, so the jetties would only soften siltation in Stretch 1 (outer part of Navigation Channel). Moreover, the option J4, if implemented, would block the longshore induced current in Bay of Santos. Moreover, it is likely that the construction of jetties would increase the time required to renew water in bay of Santos, which would be a concern considering that Bay of Santos has a submarine outfall.

Keywords: Port of Santos, Jetties, Dredging, New Panamax, Coastal Engineering

INTRODUCTION

Background

The Panama Canal expansion has been an important pressure for Port of Santos improvements. Panama Canal Authority (ACP) announced the Panama Canal expansion project in 2006, and the works started in the following year (ACP, 2016a). The main purposes are the widening and deepening of existing channels, and the construction of Post Panamax dimension locks on the Pacific and Atlantic sides, also known as Third Set of Locks (URS, 2007). The expanded locks were inaugurated in 25th June 2016 (ACP, 2016b), and the new locks dimension established new vessel reference for Panama Canal, also known as “New Panamax” (Table 1).

Vessel Reference	Draught (m)	Beam (m)	Length Overall (m)
Panamax	13.2	32.2	290.0
New Panamax	15.2	49.0	366.0

Table 1: Vessel size references for Panama Canal. Source: PIANC (2014).

Therefore, São Paulo State Docks Company (CODESP) released in 2006 a Zoning Directive Plan (PDZ) aiming the expansion of Port of Santos and operation efficiency (CODESP, 2006). The plan foresaw the construction of new terminals, the deepening dredging of the Access Channel, Navigation Channel and berths, improvements in port and nearby infrastructure, and the perspective of Port of Santos assuming a role of Hub Port in South America due to its vast hinterland (Figure 1 – Map of Port of Santos hinterland).

In response to external pressures and port bottlenecks, Brazilian Federal Government published the law N 11.610/2007 (BRASIL, 2007). This law instituted the National Dredging Program (PND 1), which aimed the deepening dredging of Brazilian ports, allowing several ports to receive larger vessels with deeper drafts (BRASIL, 2007). PND 1 summed an investment of R$1.6 bi, and dredged about 73 million m³ of sediments from 16 ports (BRASIL, 2015).

[1] School of Civil Engineering, Architecture and Urban Design, University of Campinas – UNICAMP, Brazil
[2] Ramboll, Brazil – email: thiago.correa011@gmail.com

Figure 1: Port of Santos hinterland. Source: Adapted from IPEA (2009).

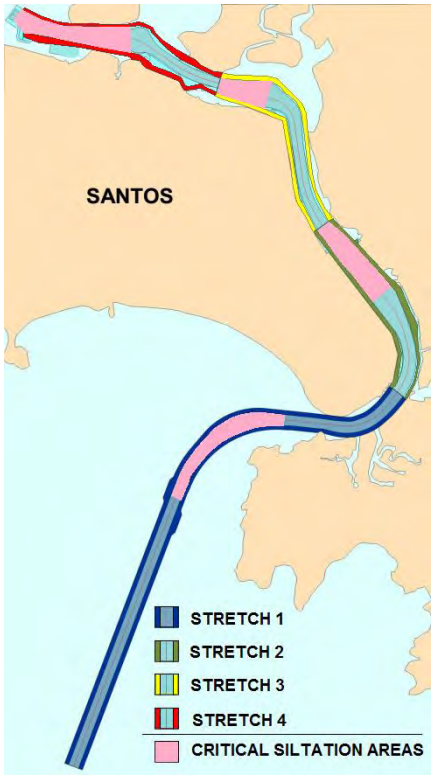

Figure 2: Port of Santos navigation channel dredging stretches 1 (blue), 2 (green), 3 (yellow) and 4 (red), with siltation critical areas (magenta) (based on Carvalho, 2016).

Thus, CODESP took advantage of PND 1 investments to manage its deepening dredging. INPH (2007) projected three phases for the deepening and widening dredging (see Table 2 with Port of Santos channel dimensions for each phase and Figure 2 with a map showing the different dredging stretches). Despite Phase 1 is fully accomplished, Port of Santos is one step behind from Panama Canal, because it does not support the traffic of large draft vessels, such as New Panamax.

Stretch	Extent	Depth (m)			
		Before Deepening Dredging	Phase 1	Phase 2	Phase 3
1- Access Channel until "Entreposto de Pesca"	9.5	14.0	15.0	16.0	17.0
2- From "Entreposto de Pesca" to "Torre Grande"	4.5	13.0	15.0	16.0	17.0
3/4- From "Torre Grande" to "Alemoa"	8.5	12.0	15.0	15.0	16.0
Minimum Channel width (m)		150.0	220.0	220.0	250.0*

*Except from Ponta da Praia to Ferry-Boat (220.0 m).

Table 2: Port of Santos projected channel dimensions for each phase (INPH, 2007).

Current Scenario

Currently, Port of Santos navigation channel is 15 m deep and 220 m wide, with two navigation lanes (Phase 1 – Table 2), and CODESP depth target is 17 m deep and 250 m wide (Phase 3 – Table 2). This deepening dredging would allow the traffic of New Panamax vessels in Port of Santos. Gireli & Vendrame (2012) estimated the Access Channel (contained in stretch 1) siltation evolution using

monthly siltation records from May 1997 to March 2003. According to their estimates, the Phase 3 deepening depth would significantly increase siltation rate along navigation channel, requiring larger maintenance dredging volume (GIRELI & VENDRAME, 2012). Carvalho (2016) estimated the monthly siltation along Port of Santos navigation channel by comparing bathymetries from October 2010 to November 2013 (Table 3). The navigation channel has four critical siltation areas (Figure 2); according to Carvalho (2016), these areas are responsible for 19%, 12%, 6%, and 14% of total siltation in stretches 1, 2, 3, and 4, respectively.

Stretch	1	2	3	4
Siltation rate (m³/month)	248,597	103,871	80,566	108,629
Percentage of total siltation (%)	45.90%	19.18%	14.87%	20.05%
Mean vertical accretion (cm/month)	8.7	5.9	7.3	9.9

Table 3: Port of Santos navigation channel mean monthly siltation rate from October 2010 to November 2013 (Carvalho, 2016).

Moreover, the Federal Public Ministry (MPF) claims that Port of Santos deepening dredging has aggravated the progressive erosion of *Ponta da Praia*, an adjacent beach to the Port, due to wave heightening and longshore current acceleration (MPF, 2015). Indeed, the Environmental Impact Assessment (EIA) of Port of Santos deepening dredging (FRF, 2008) has a gap, since the beaches were not included in the Direct Impact Area (DIA). Thus, CODESP signed a Term of Conduct Adjustment (TAC) recognizing the impact on the beach erosion, and committing themselves to design and afford a structure, which cannot be rigid and must be submerse, that mitigates *Ponta da Praia* beach erosion.

Therefore, this study evaluates jetties previously proposed for depth maintenance of Port of Santos navigation channel (REIS, 1978; ALFREDINI et al., 2013), based on the variation of currents velocities along the navigation channel and the siltation on each stretch.

METHODOLOGY

Port of Santos has been facing challenges with depth maintenance of navigation channel for a long time. In order to minimize siltation along the navigation channel and decrease the volume of dredged sediments, Reis (1978) proposed several geometries of jetties for Port of Santos (Figure 3), and tested them with small-scale physical model.

This physical model had a movable-bed filled with cellulose acetate, horizontal scale of 1:600 and vertical scale of 1:100, and its domain comprised only part of the Bay of Santos. The bathymetry of the physical model was based on nautical chart no. 1701 DHN (Directory of Hydrology and Navigation) and bathymetric data collected by INPH in 1974, when the navigation channel was dredged up to -14 m deep. Reis (1978) proposed six options of jetties, but two were discarded, the four remaining options have distinct geometry and length (J1, J2, J3, and J4), as shown in Figure 3 and described in Table 4. Later, Alfredini et al. (2013) proposed another geometry of two curved jetties (J5 as described in Table 4 and shown in Figure 3) for depth maintenance of Port of Santos navigation channel.

Jetty Options	No. of jetties	Type (right/left)	Extension (r/l)	Depth of head (r/l)
(J1)	Single jetty	Straight	2,900 m	-9 m
(J2)	Two jetties	Straight/ Straight	2,900 m/ 700 m	-9 m/ -9 m
(J3)	Single jetty	Curved	2,910 m	-9 m
(J4)	Two jetties	Curved/ Straight	4,350 m/ 1,590 m	-11 m/ -11 m
(J5)	Two jetties	Curved/ Curved	4,360 m/ 2,150 m	-12 m/ -12 m

Table 4: Description of each jetty option (Source: Reis, 1978 and Alfredini et al., 2013).

The evaluation consisted of comparing velocity maps of each jetty option (J1, J2, J3, J4 and J5) during ebb and flood (in the instant of maximum velocity at Santos estuary inlet) for a Spring tide with the Baseline Scenario (BS), as described in Figure 4.

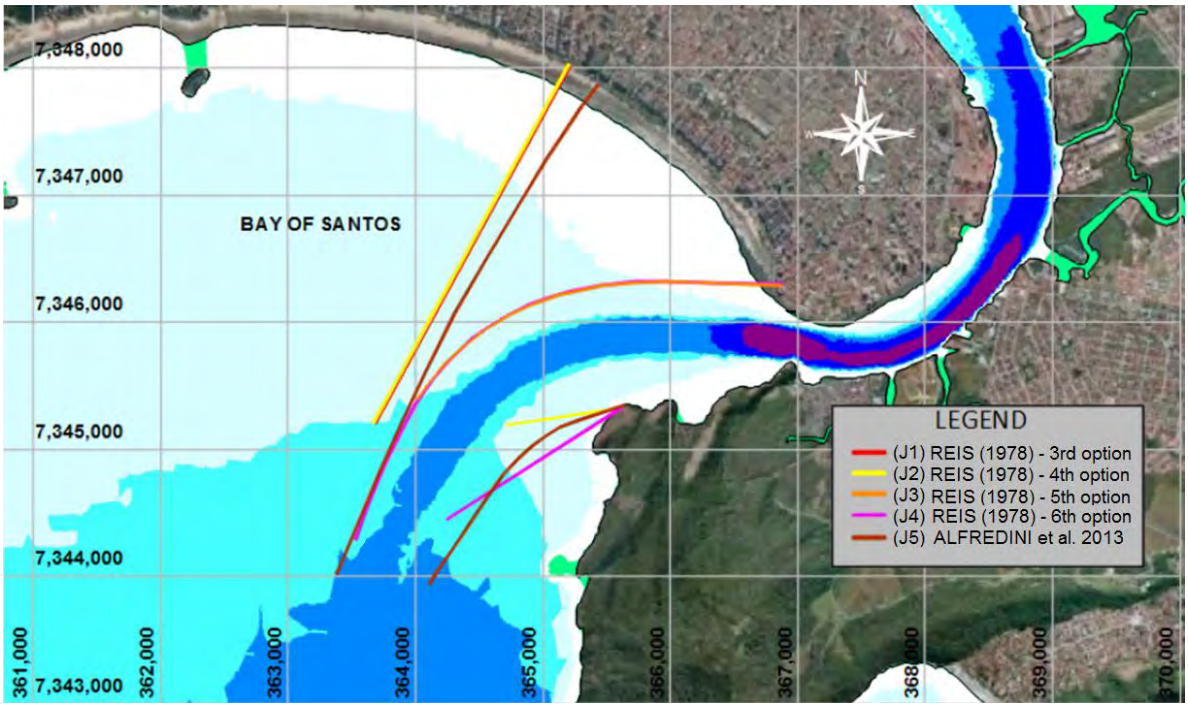

Figure 3: Proposals of jetties for Port of Santos marine Sandbar transposition (Source: Adapted from Gireli et al. 2017).

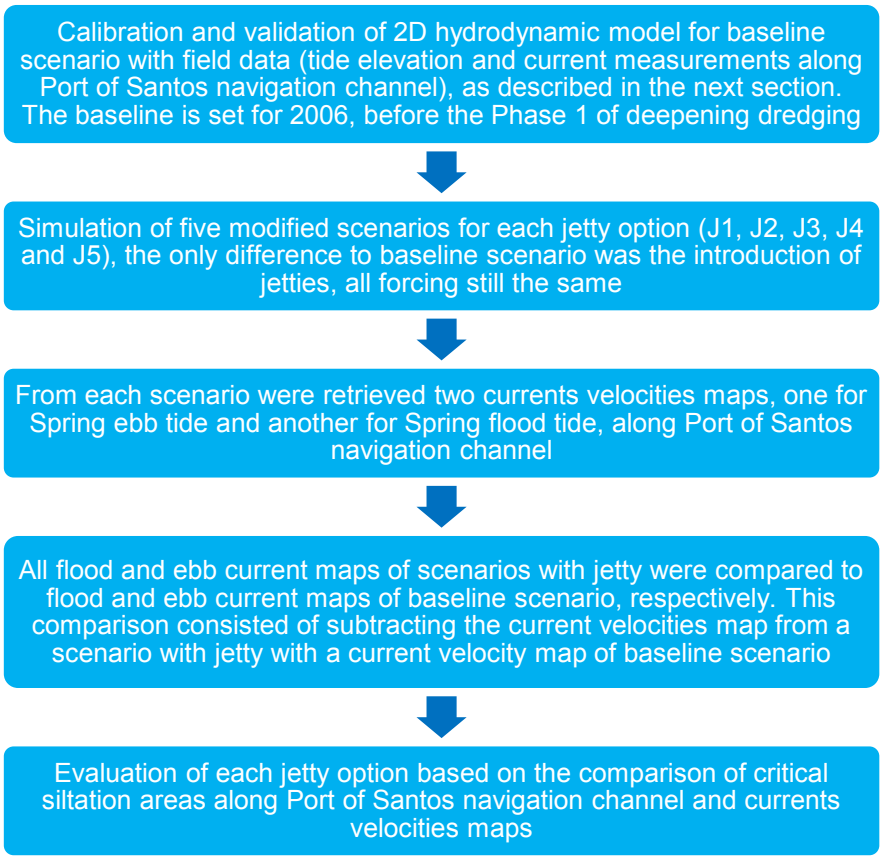

Figure 4: Evaluation process of each jetty option, considering current velocities maps for Spring ebb tide and Spring flood tide.

HYDRODYNAMIC NUMERICAL MODEL SET UP

The current study applies a 2DH model with flexible mesh (Mike 21 Flow Model FM). This hydrodynamic module solves two-dimensional shallow water equations (the depth-integrated incompressible Reynolds averaged Navier-Stokes equations), the spatial discretization of equations is performed using a cell-centered finite volume method, and in the horizontal plane an unstructured grid is adopted comprising triangles or quadrilateral elements (DHI, 2015).

Data set

Due to data availability, the baseline of this study is set for 2006, before the deepening dredging. The Port of Santos Access and Navigation Channel are retrieved from bathymetric data of the baseline year (INPH, 2007). Parts of the estuary are from older surveys (MARMIL, 2015; GARCIA et al., 2002) or are interpolated values (SOUZA, 2017), and the nearshore area and some parts of the estuary are retrieved from nautical charts and DHN bathymetric data, which the scatter data is composed of data from 1969 to 2004 (MARMIL, 2015; GARCIA et al., 2002). Figure 5 shows the bathymetry from 2006 interpolated with older surveys using Mike Mesh Generator.

The major model forcing is tidal elevation, Santos estuary has tides with diurnal inequalities and tidal range up to 1.5 meter (HARARI & CAMARGO, 2003), so the sea boundary consists of nine nodes and eight segments (Figure 5). The tidal forcing for each node were computed using the nine most energetic tidal constituents in Santos region (Q1, O1, P1, K1, N2, M2, S2, K2 and M3). Each node has amplitude adjustment and phase lag, based on a shelf model with observations during 46 years in the Port of Santos, from 1944 to 1989, for these nine constituents (HARARI & CAMARGO, 1994). The hydrodynamic model has nine points of river discharge along the estuary (Figure 5), considering long-term river discharges retrieved from Roversi et al. (2016).

The elements of the mesh are triangular, with angles smaller than 30° (degrees), and each polygon has a local maximum area element. The model consisted of an unstructured mesh with 31,897 nodes and 57,039 elements.

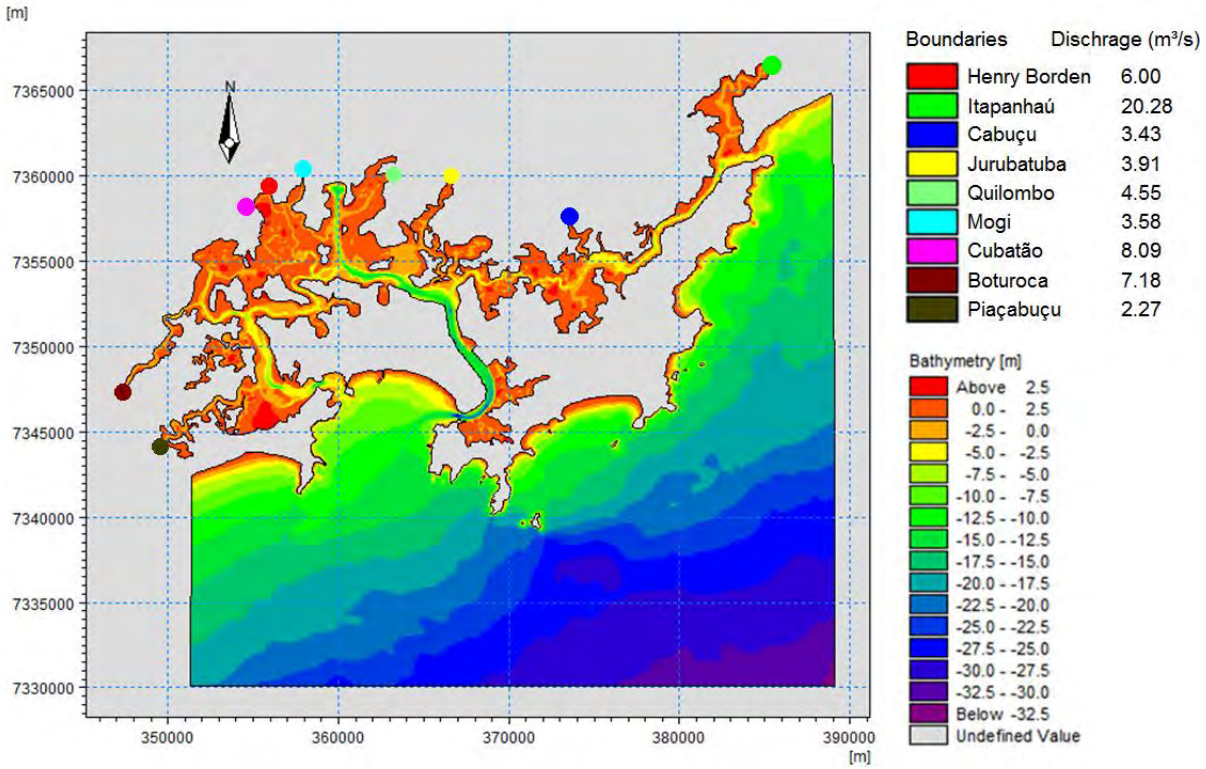

Figure 5: Model of Santos Estuary System and nearshore region 2006 bathymetry interpolated using Mike Mesh Generator and long-term river discharges (m³/s).

Model calibration and validation

The model period of simulation covers 13 days, from 4th to 17th March of 2006. The calibration consisted on adjusting the bed roughness to minimize the errors in five tide gauge stations (Figure 6), and validation consisted of comparing current measurements in eight sections (INPH, 2007) along the estuary (Figure 7) with current velocities retrieved from model simulation.

Calibration showed good agreement with field data. The comparisons between harmonic analysis and simulated results are shown in Figure 8 and the Root Mean Square Error (RMSE) (equation 1) is acceptable. Due to lack of data, the period of validation covers only 8 days, from March 9th to 17th of 2006, and the model had no adjustment in the validation process. Figure 9 shows comparison between flow measurement and simulation. The validation results show good or acceptable agreement with measured values from flow stations along Santos Estuary. Skill score (equation 2) for S07 and S09 flow stations may be lower because the bathymetry has coarser scatter data in this area.

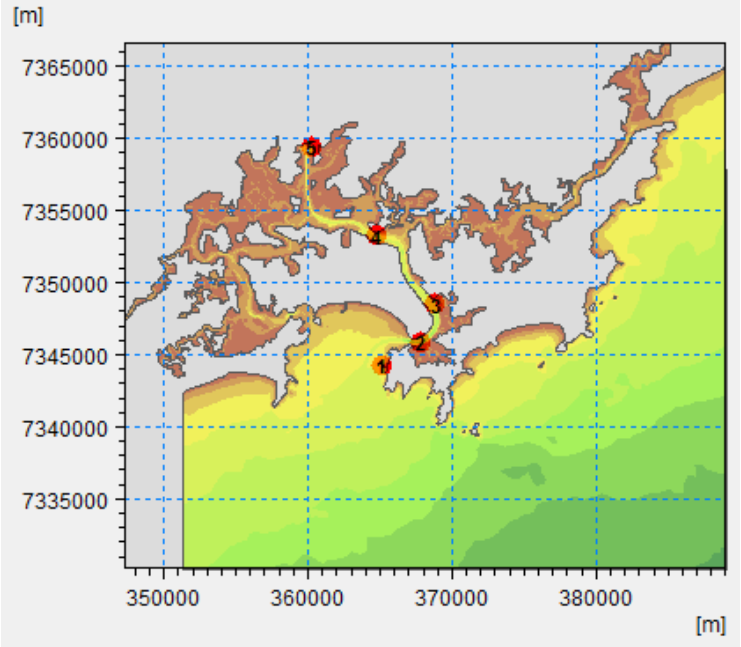

Figure 6: Tide gauge stations along Santos estuary used to calibrate the hydrodynamic model. 1-Ilha das Palmas, 2-Praticagem, 3-Conceiçãozinha, 4-Ilha Barnabé and 5-Cosipa.

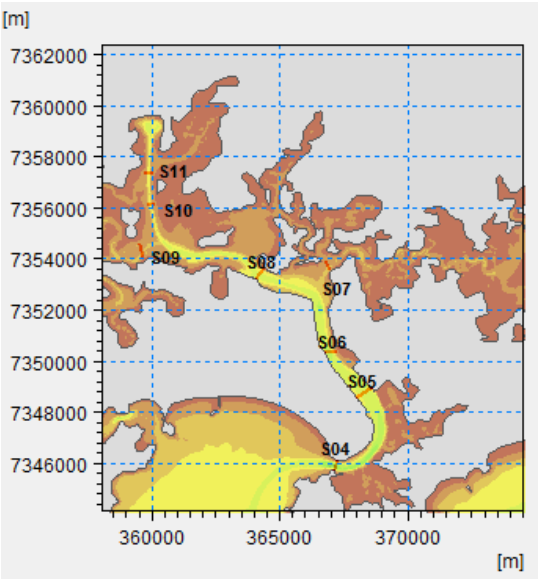

Figure 7: Eight flow stations (S04, S05, S06, S07, S08, S09, S10, S11) along Santos estuary used to validate the hydrodynamic model for currents.

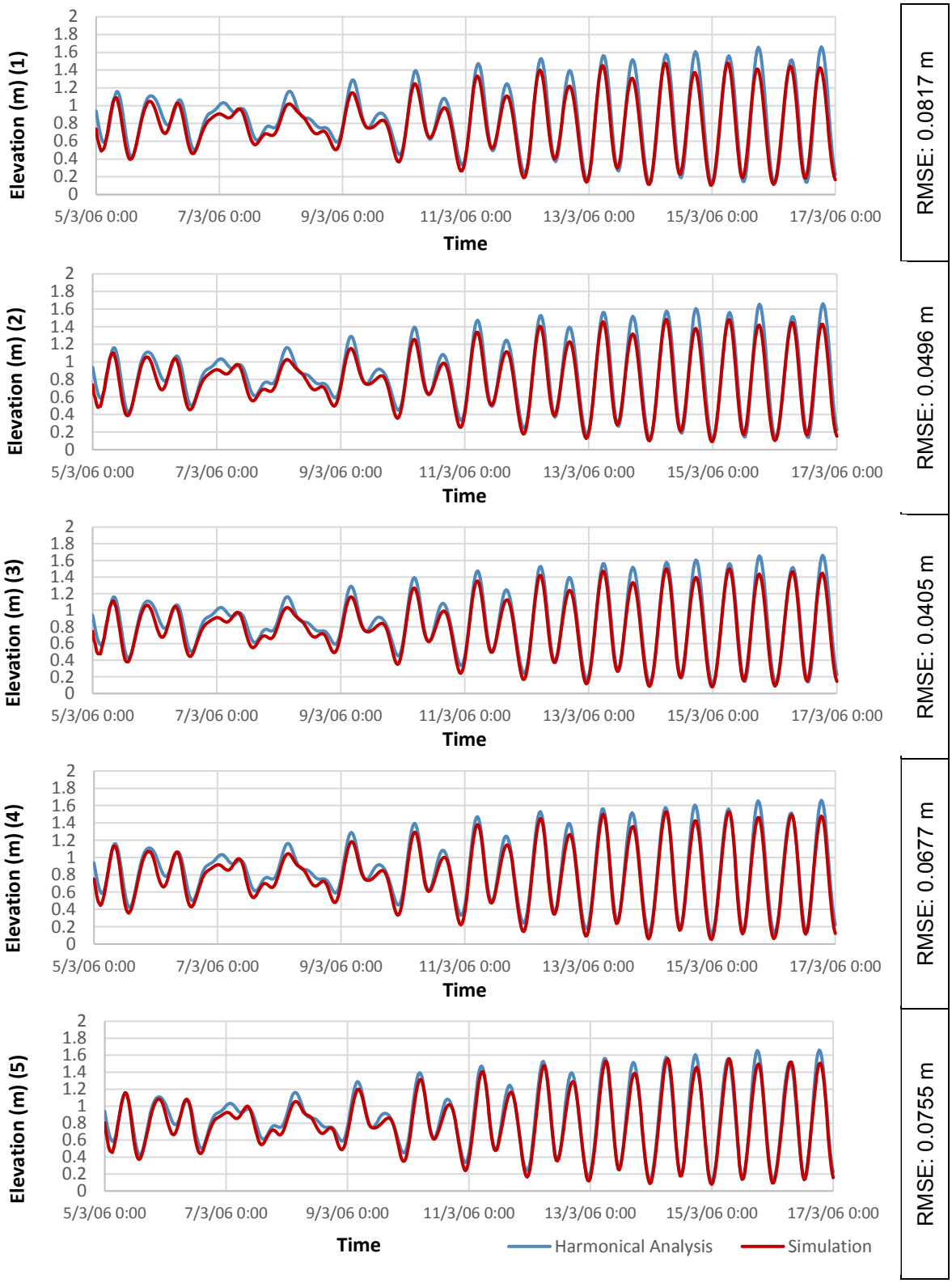

Figure 8: Time series comparative between harmonic analysis (blue) and simulation (red) for tide gauge station (1) Ilha das Palmas, (2) Praticagem, (3) Conceiçãozinha, (4) Ilha Barnabé e (5) Cosipa.

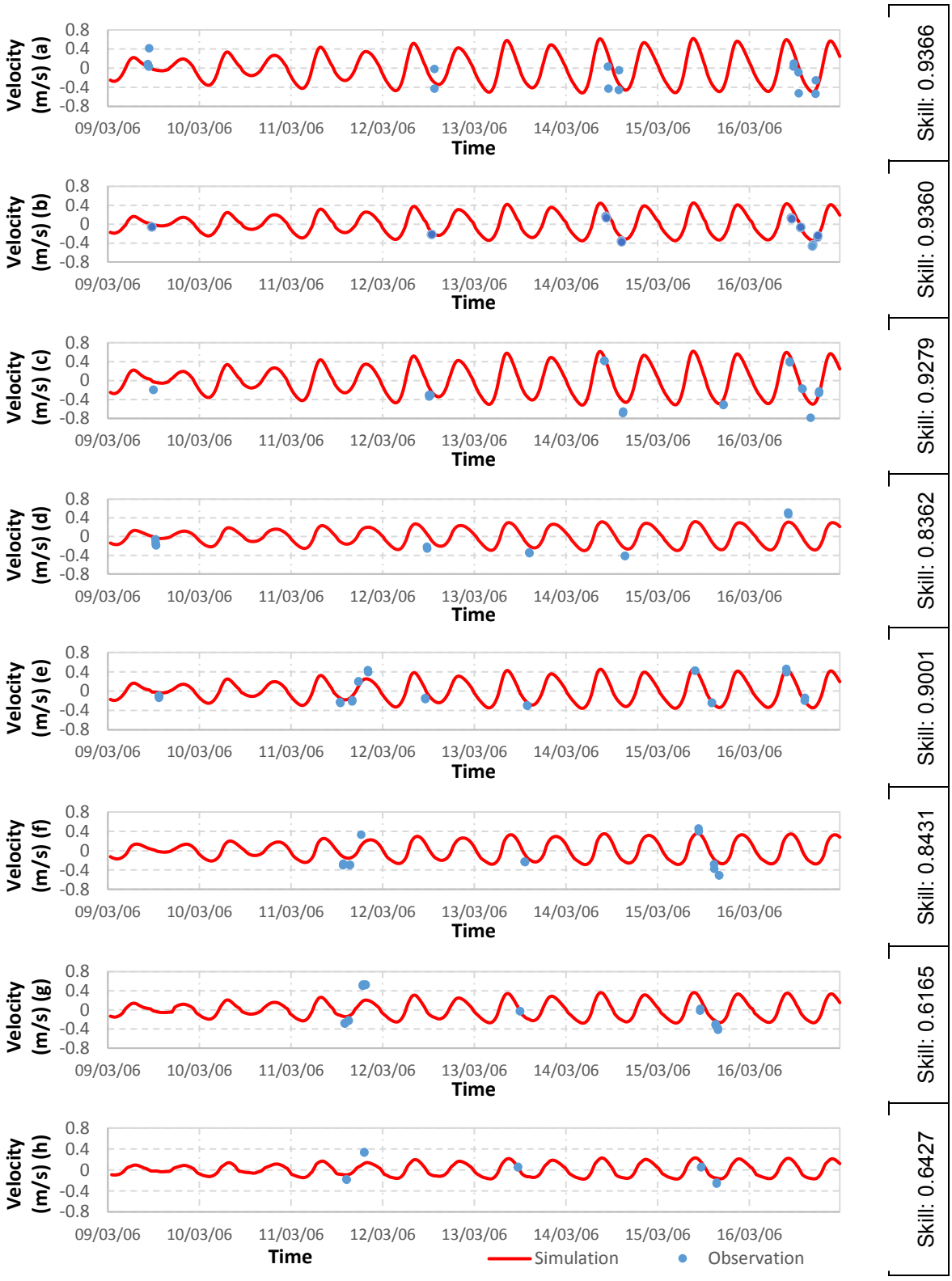

Figure 9: Model validation for flow stations S04 (a), S05 (b), S06 (c), S07 (d), S08 (e), S09 (f), S10 (g), S11 (h). Comparative between flow measurement (blue) and simulation (red). Skill score for current measurements in each section (0 – poor agreement and 1 – good agreement)

$$RMSE = \sqrt{\frac{\sum_{t=1}^{n}(S_t - O_t)^2}{n}} \quad (1)$$

where: t is the time step, n is the amount of data acquired or the sample size, S are the simulated values, and O are the observed values. RMSE is easy to understand because it has the same metric as S and O (Willmott, 1981)

$$SKILL = 1 - \frac{\sum_{t=1}^{n}(S_t - O_t)^2}{\sum_{t=1}^{n}(|S_t - \overline{S_t}| + |O_t - \overline{O_t}|)^2} \quad (2)$$

where: t is the time step, n is the amount of data acquired or the sample size, S are simulated values, O are observed values and O is the average of observed values (Willmott, 1981).

RESULTS

Baseline Scenario

During the flood, in the outer part of Stretch 1, the currents reach up to 20 cm/s in the straight part of the navigation channel and between 30 cm/s and 55 cm/s in the curvy part of the navigation channel. In the inner navigation channel, the currents reach up to 70 cm/s in the end of Stretch 1, varies between 30 cm/s and 6 cm/s in the Stretch 2, varies between 30 cm/s and 50 cm/s in the Stretch 3, and reach up to 45 cm/s in the Stretch 4 (Figure 10). During the ebb, in the outer part of Stretch 1, the currents reach up to 25 cm/s in the straight part of the navigation channel and between 40 cm/s and 60 cm/s in the curvy part of the navigation channel. In the inner navigation channel, the currents reach up to 90 cm/s in the end of Stretch 1, varies between 40 cm/s and 75 cm/s in the Stretch 2, varies between 30 cm/s and 70 cm/s in the Stretch 3, and reach up to 60 cm/s in the Stretch 4 (Figure 10).

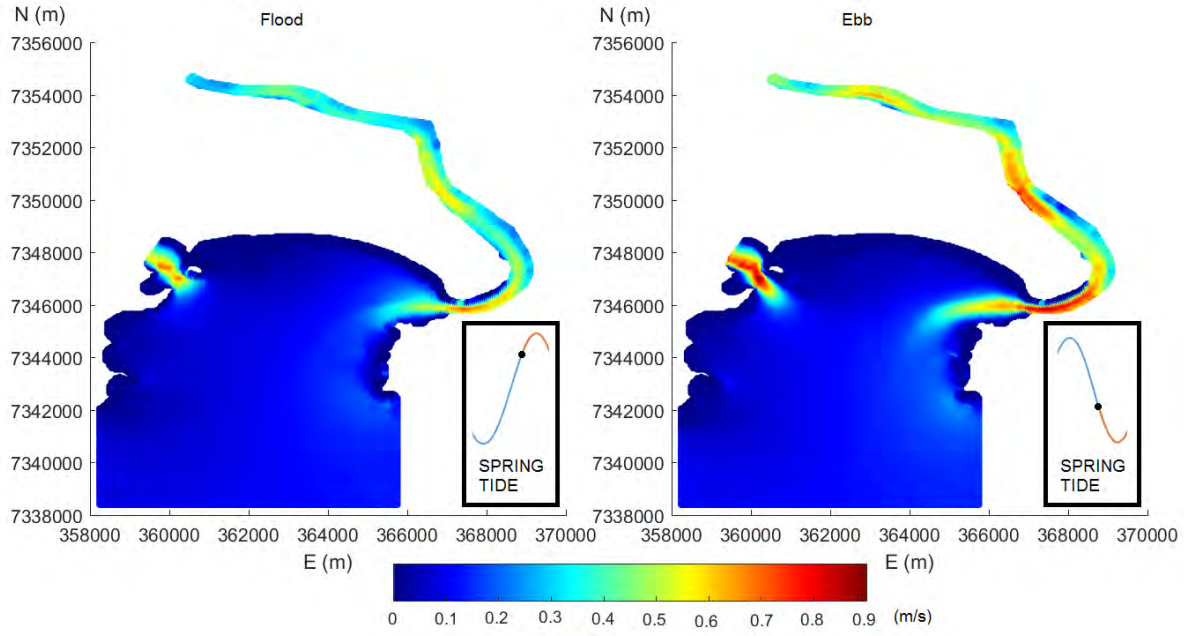

Figure 10: Currents velocities maps of Baseline Scenario (BS), without jetty, for Spring tide (flood) at 14/3/06 4:00 (left) and Spring tide (ebb) at 15/3/06 9:38 (right).

J1

Comparing the current velocity maps of option J1 (Figure 11) with BS (Figure 10), is possible to notice that near the jetty head, in the straight part of navigation channel near the curvy part, the option J1 increases the current velocity up to 15 cm/s during flood and ebb (Figure 12). Furthermore, no significant current velocity variations were observed in the inner part of the estuary.

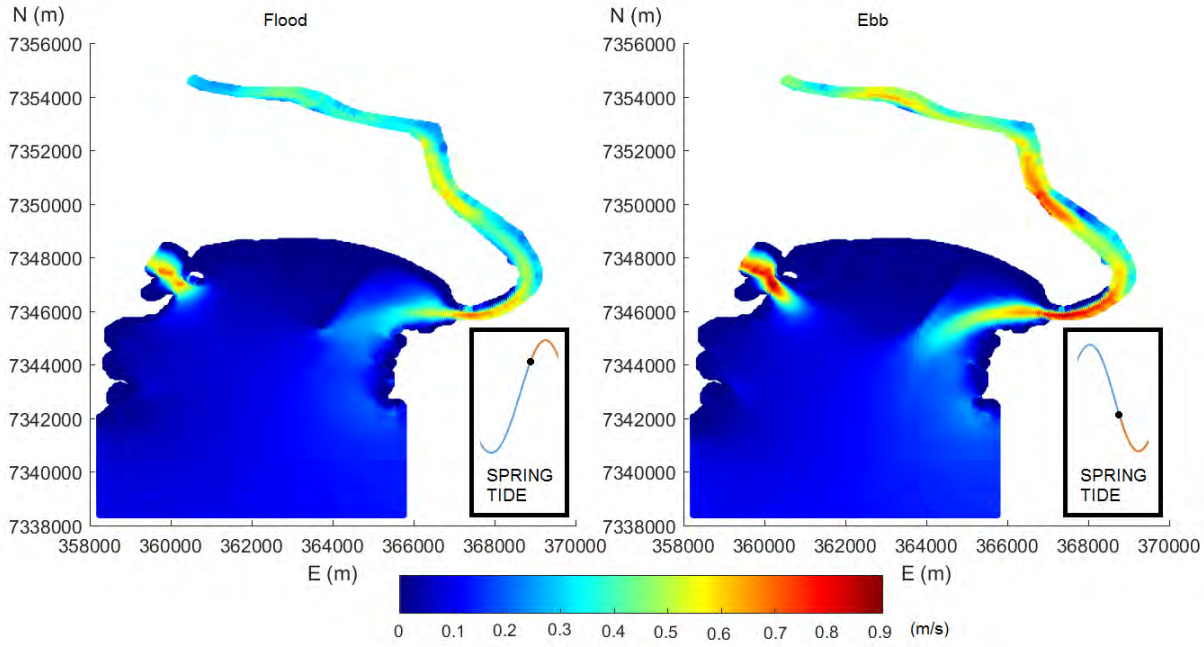

Figure 11: Currents velocities (m/s) maps of Jetty option no. 1 (J1), with one jetty, for Spring tide (flood) at 14/3/06 4:04 (left) and Spring tide (ebb) at 15/3/06 9:38 (right).

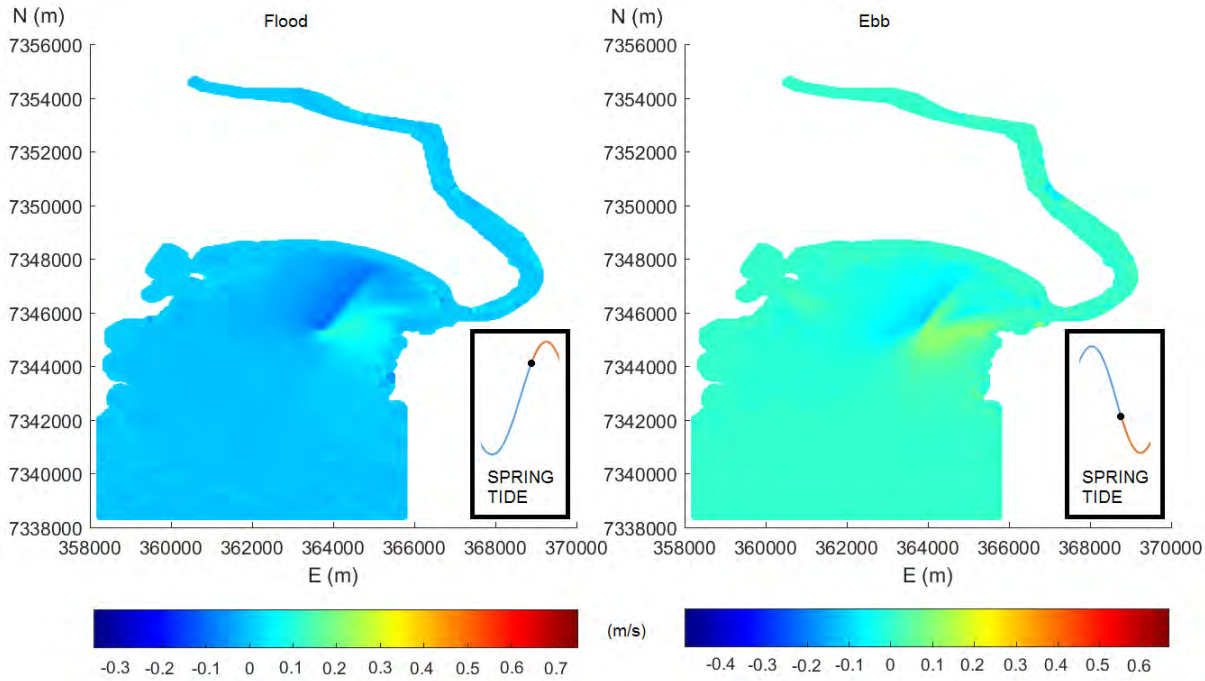

Figure 12: Maps with absolute difference of currents velocities (m/s) between Jetty option no. 1 (J1), with one jetty, and BS for Spring tide - flood (left) - and Spring tide - ebb (right).

J2

Comparing the current velocity maps of option J2 (Figure 13) with BS (Figure 10), is possible to notice that between the jetties walls, in the straight part of navigation channel near the curvy part, the the current velocity increases by more than 10 cm/s during flood, and increases up to 15 cm/s during ebb (Figure 14). Near the jetties head, the current velocity increases up to 40 cm/s during flood and ebb (Figure 14). Furthermore, no significant current velocity variations were observed near the estuary mouth and in the inner part of the estuary.

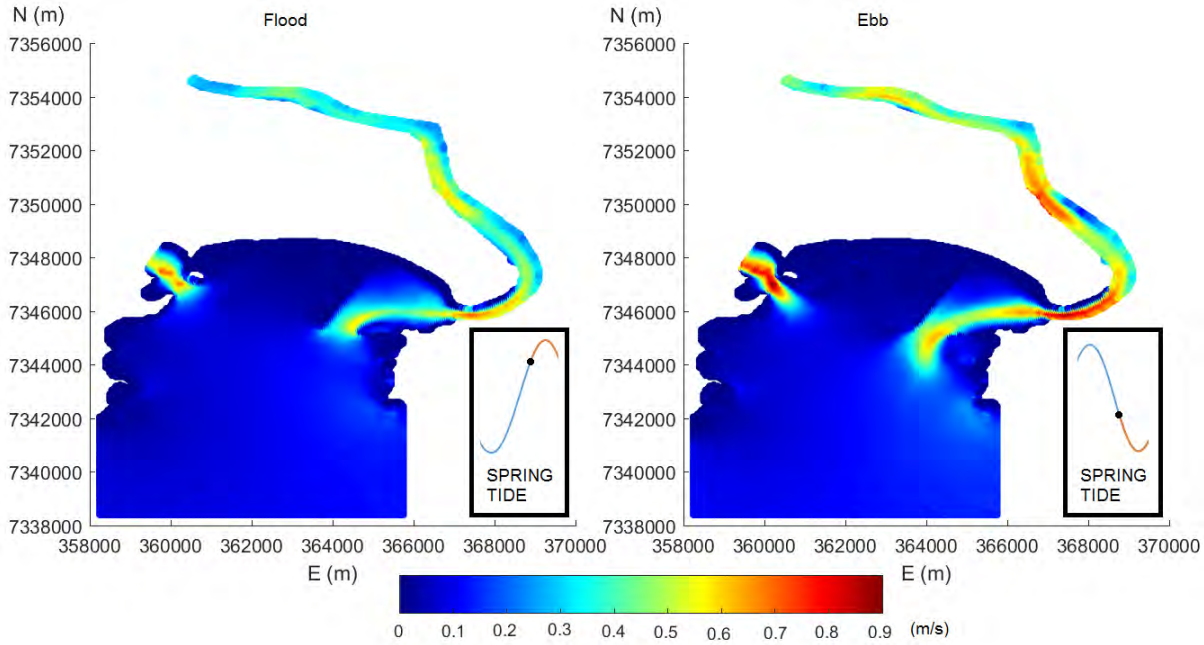

Figure 13: Currents velocities (m/s) maps of Jetty option no. 2 (J2), with two jetties, for Spring tide (flood) at 14/3/06 4:18 (left) and Spring tide (ebb) at 15/3/06 9:38 (right).

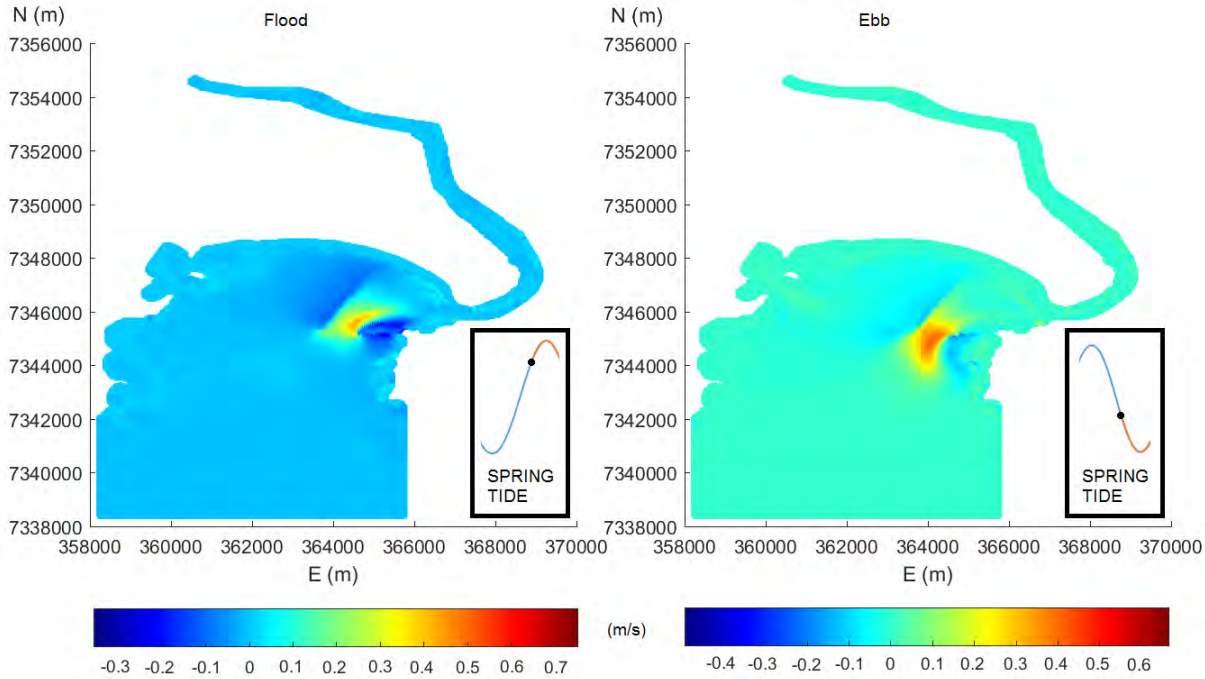

Figure 14: Maps with absolute difference of currents velocities (m/s) between Jetty option no. 2 (J2), with two jetties, and BS for Spring tide - flood (left) - and Spring tide - ebb (right).

J3

Comparing the current velocity maps of option J3 (Figure 15) with BS (Figure 10), is possible to notice that near the jetty structure, the current velocity increases up to 10 cm/s during flood and up to 15 cm/s during ebb (Figure 16). Furthermore, no significant current velocity variations were observed in the inner part of the estuary.

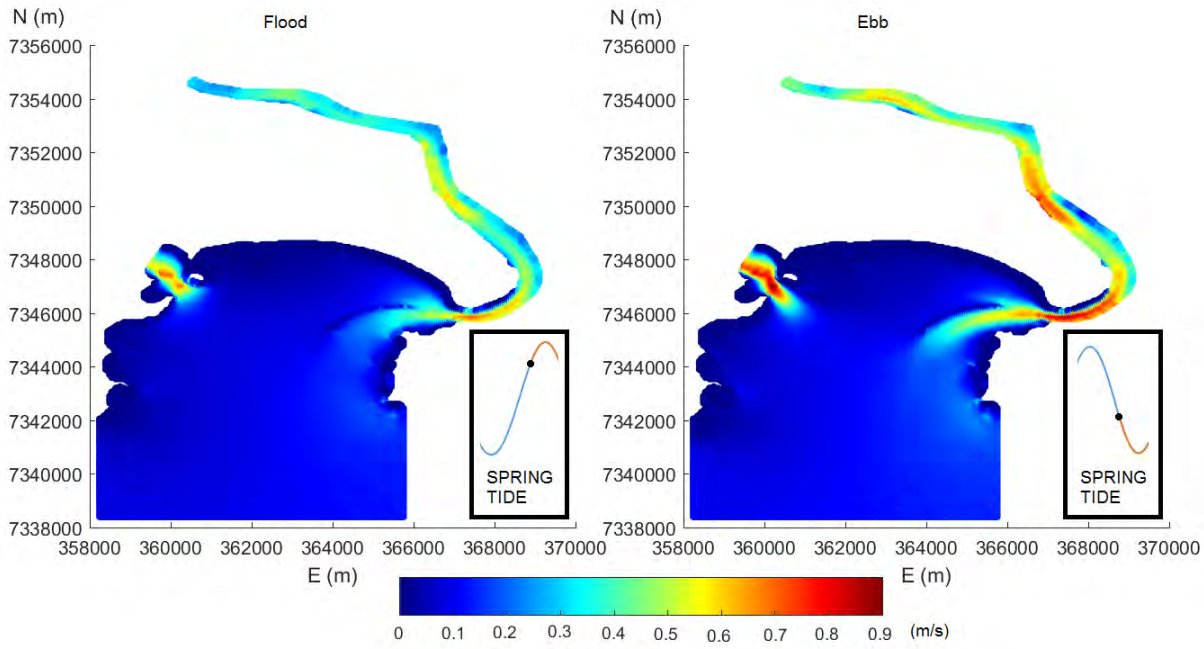

Figure 15: Currents velocities (m/s) maps of Jetty option no. 3 (J3), with one jetty, for Spring tide (flood) at 14/3/06 4:06 (left) and Spring tide (ebb) at 15/3/06 9:40 (right).

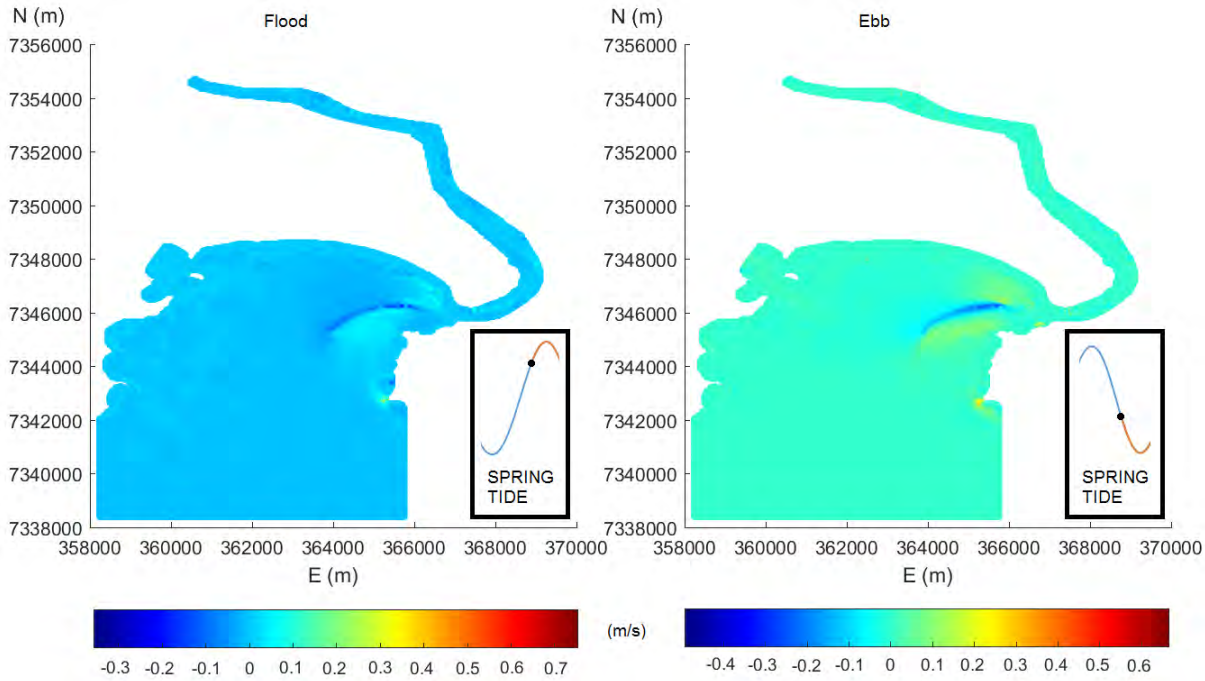

Figure 16: Maps with absolute difference of currents velocities (m/s) between Jetty option no. 3 (J3), with one jetty, and BS for Spring tide - flood (left) - and Spring tide - ebb (right).

J4

Comparing the current velocity maps of option J4 (Figure 17) with BS (Figure 10), is possible to notice that between the jetties walls, the current velocity increases by more than 30 cm/s during flood and ebb (Figure 18). Near the jetties head, the current velocity increases up to 60 cm/s during flood and increases up to 65 cm/s during ebb (Figure 18). Furthermore, no significant current velocity variations were observed in the inner part of the estuary.

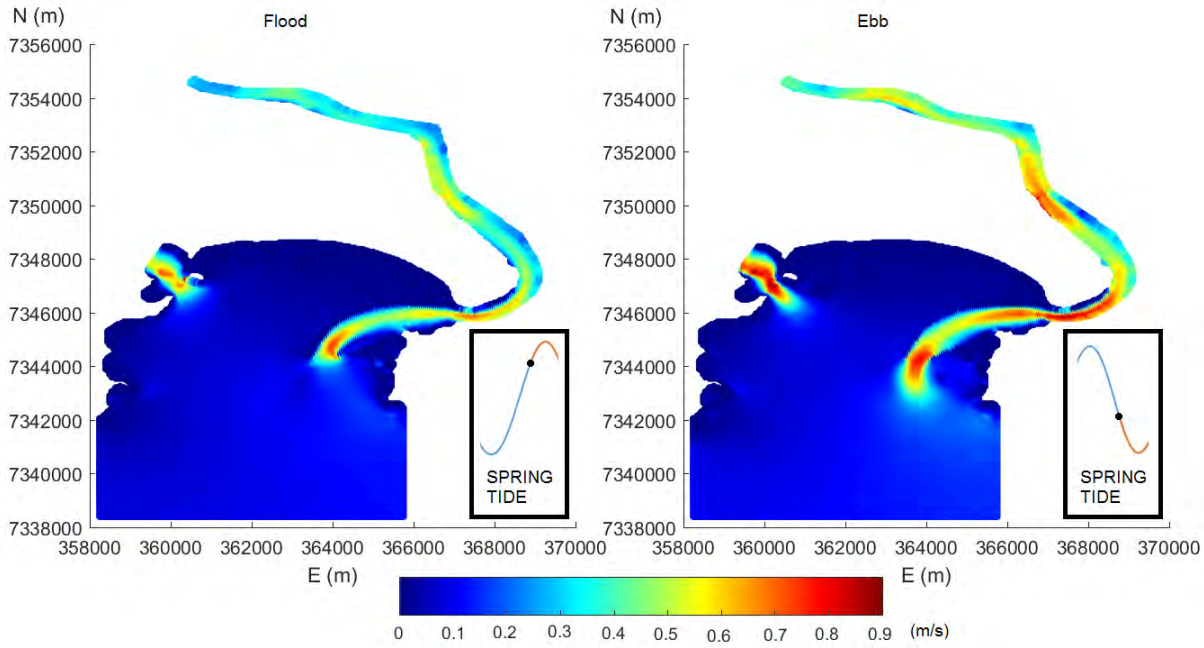

Figure 17: Currents velocities (m/s) maps of Jetty option no. 4 (J4), with two jetties, for Spring tide (flood) 14/3/06 4:20 (left) and Spring tide (ebb) at 15/3/06 9:32 (right).

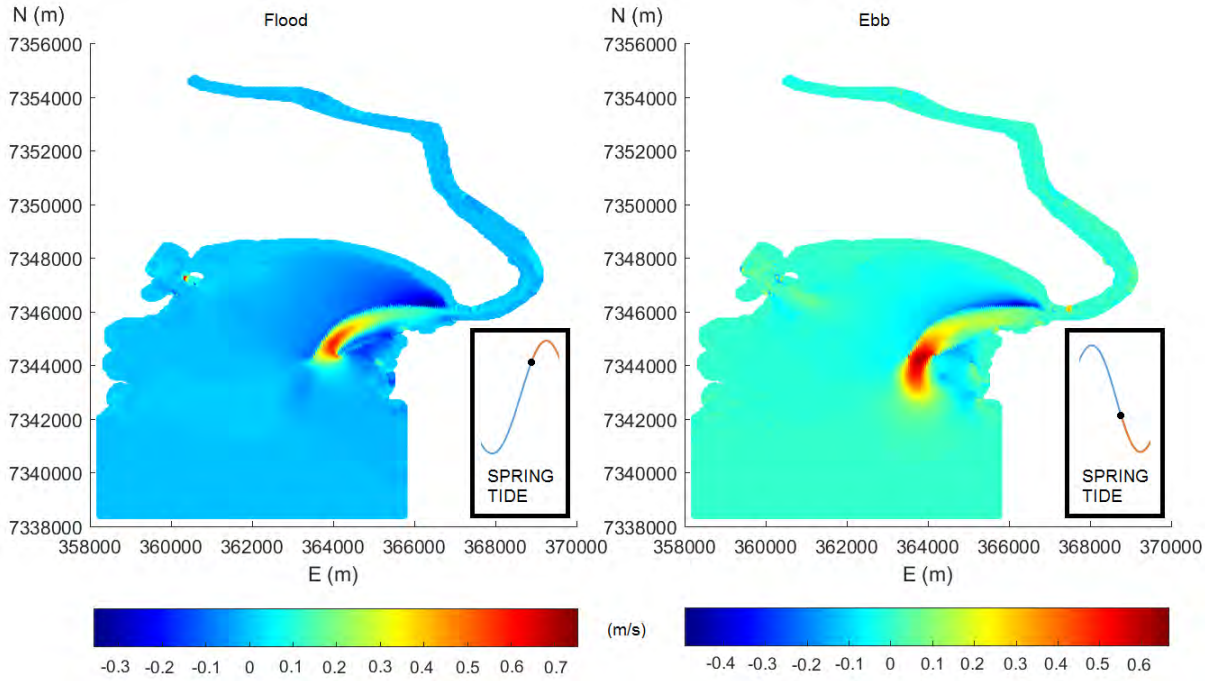

Figure 18: Maps with absolute difference of currents velocities (m/s) between Jetty option no. 4 (J4), with two jetties, and BS for Spring tide - flood (left) - and Spring tide - ebb (right).

J5

Comparing the current velocity maps of option J5 (Figure 19) with BS (Figure 10), is possible to notice that between the jetties walls, in the straight part of navigation channel near the curvy part, the the current velocity increases by more than 15 cm/s during flood and ebb (Figure 20). Near the jetties head, the current velocity increases up to 40 cm/s during flood and increases up to 50 cm/s during ebb (Figure 20). Furthermore, no significant current velocity variations were observed near the estuary mouth and in the inner part of the estuary.

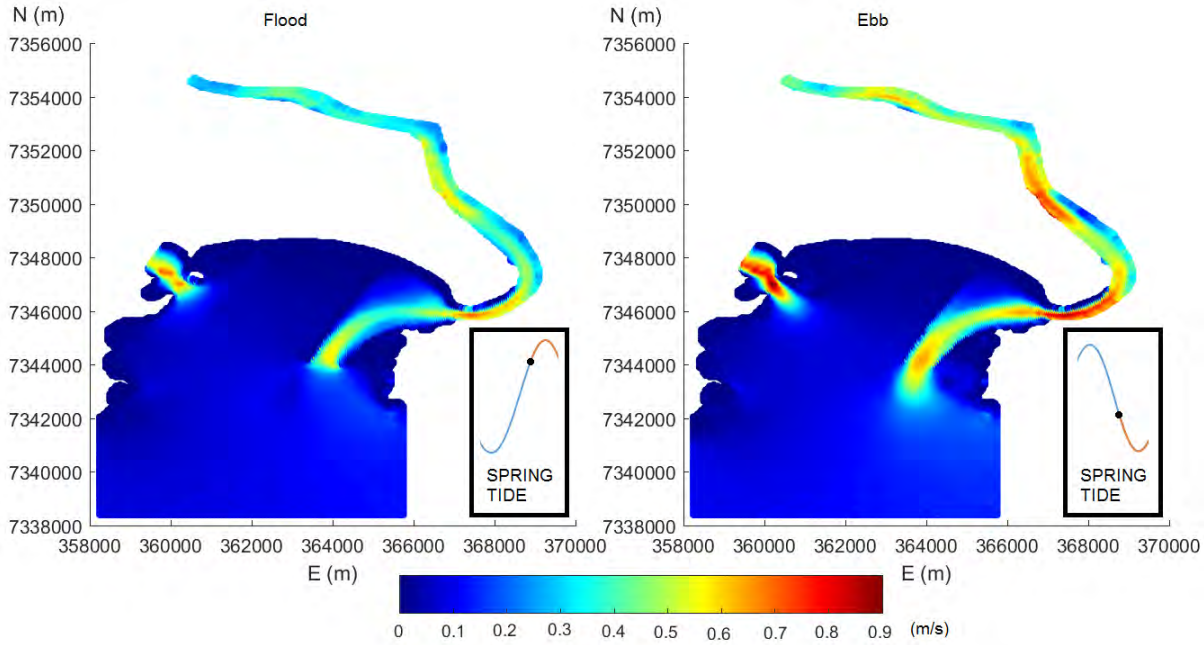

Figure 19: Currents velocities (m/s) maps of Jetty option no. 5 (J5), with two jetties, for Spring tide (flood) at at 14/3/06 4:18 (left) and Spring tide (ebb) at 15/3/06 9:40 (right).

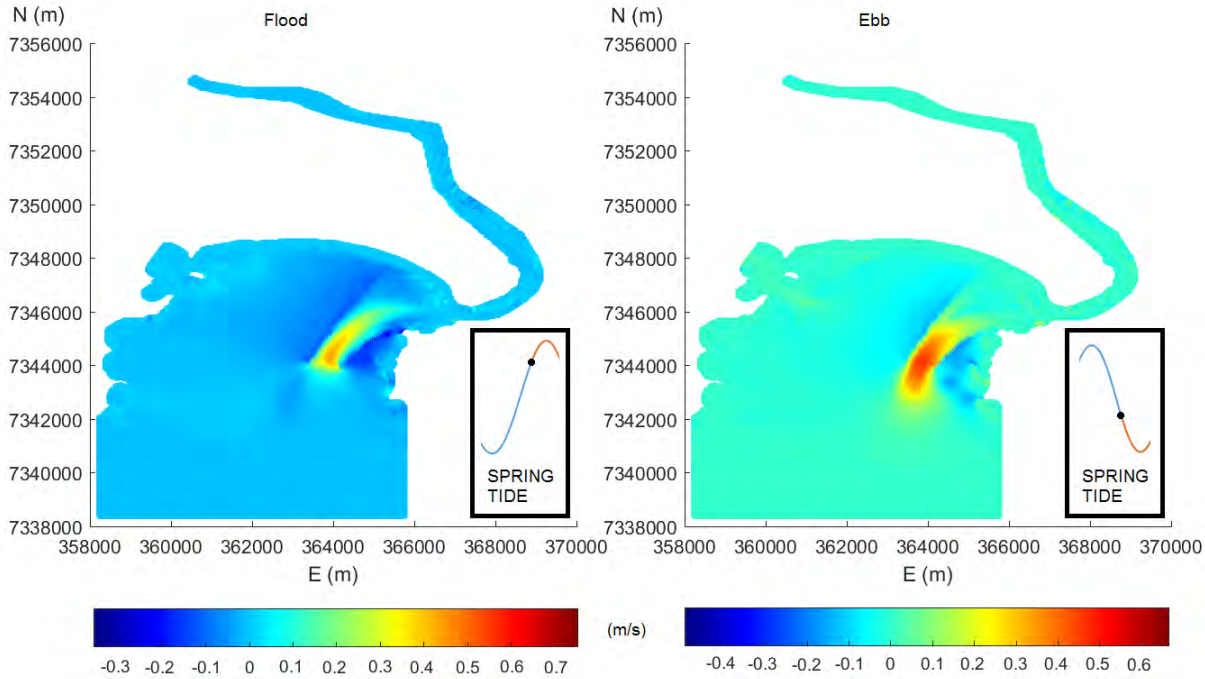

Figure 20: Maps with absolute difference of currents velocities (m/s) between Jetty option no. 5 (J5), with two jetties, and BS for Spring tide - flood (left) - and Spring tide - ebb (right).

DISCUSSIONS

Considering the critical siltation areas of Navigation Channel of Port of Santos defined by Carvalho (2016) (Figure 2) and the currents velocities variation of all five jetty options (Figures 12, 14, 16, 18 and 20), only Stretch 1 critical area would have its siltation softened. For all options, no significant current velocity variations were observed in the inner part of the estuary.

Among all options, J4 (two jetties with narrow channel) provides the highest velocity increment in Stretch 1, and its currents velocities increment area coincides with the siltation critical area in Stretch 1. Indeed, this observation is in accordance with Gireli et al. (2017) results. They have proposed jetties with similar geometry to J4, and the areas of current velocity increment are similar as well. Options J1 and J3 (with only one jetty in the right margin of Santos estuary) do not increase velocity significantly, while options J2 and J5 (two spaced jetties) provide considerable velocity increment in Stretch 1, but only in the straight area of Stretch 1.

Nevertheless, J4 reduces the currents velocities along Bay of Santos beaches, especially during flood. Magini et al. (2007) studied the circulation of currents in Bay of Santos before the deepening dredging (Phase 1). As shown in Figure 21, the Navigation Channel of Port of Santos induces currents alongshore and seawards (Magini et al., 2007). Therefore, the construction of J1, J2, J4 and J5 would block the longshore induced current in Bay of Santos, so the coastline morphology shall be studied too.

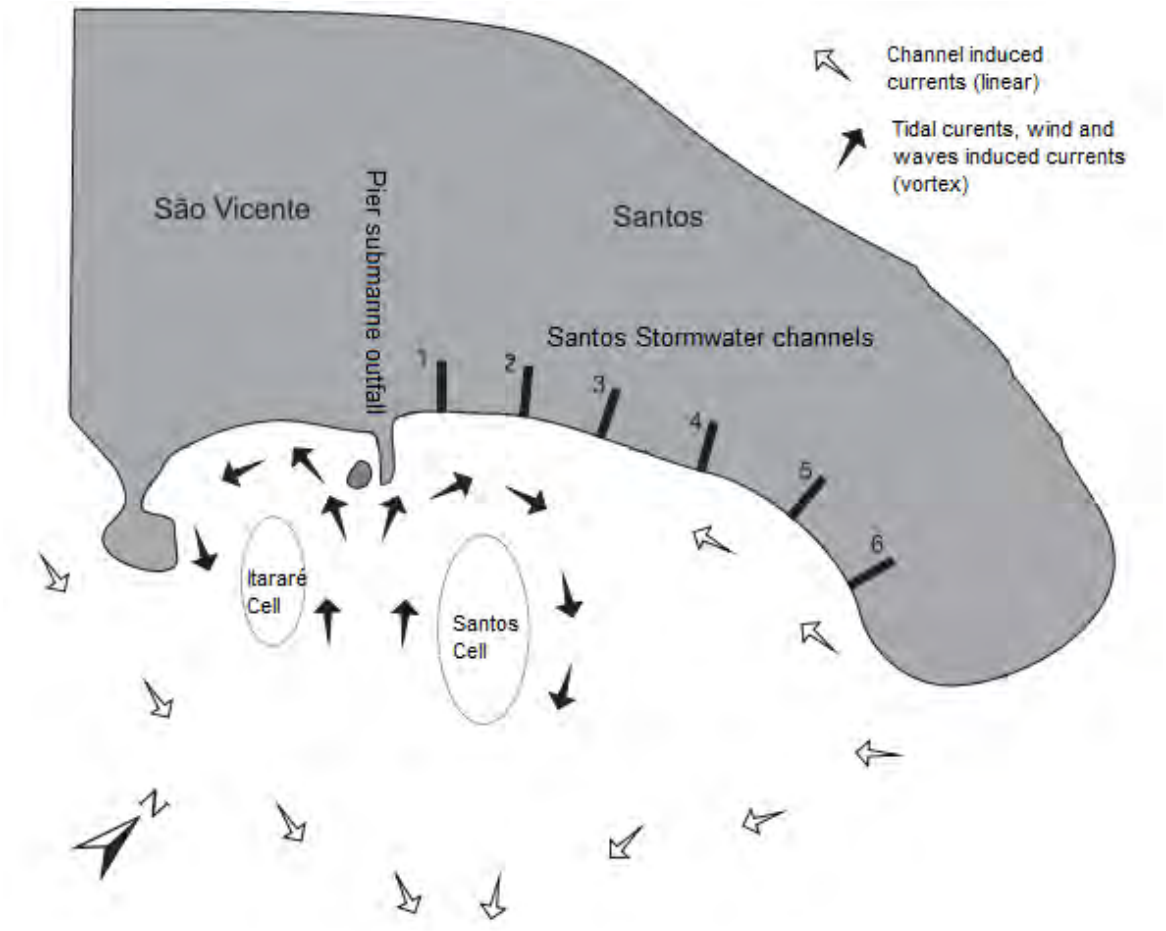

Figure 21: Currents pattern in Bay of Santos (Source: Adapted from Magini et al., 2007).

Moreover, this reduction in tide currents velocities in Bay of Santos combined with the blocking of the longshore current induced by Navigation Channel would reduce water renewal in the bay. According to Roversi et al. (2016), before the deepening dredging (Phase 1) the Bay of Santos used to take approximately 15 days to renew 95% of water. It is likely that the construction of jetties would increase the time required to renew water in bay of Santos.

Reis (1978), who simulated J1, J2, J3 and J4 in movable bed model, warned about the difficulty to discharge pollution in Bay of Santos with the construction of any of simulated options (J1, J2 and J3), and recommended an environment study on the combined impact of the submarine outfall (Figure 22) and the jetties. Therefore, another concern is the submarine outfall, which is 4 km long and discharges approximately 3 m³/s of sewage effluent in the bay of Santos (Gregorio, 2009). Further studies must be conducted to assess the combined impact of submarine outfall and jetties in the Bay of Santos pollution.

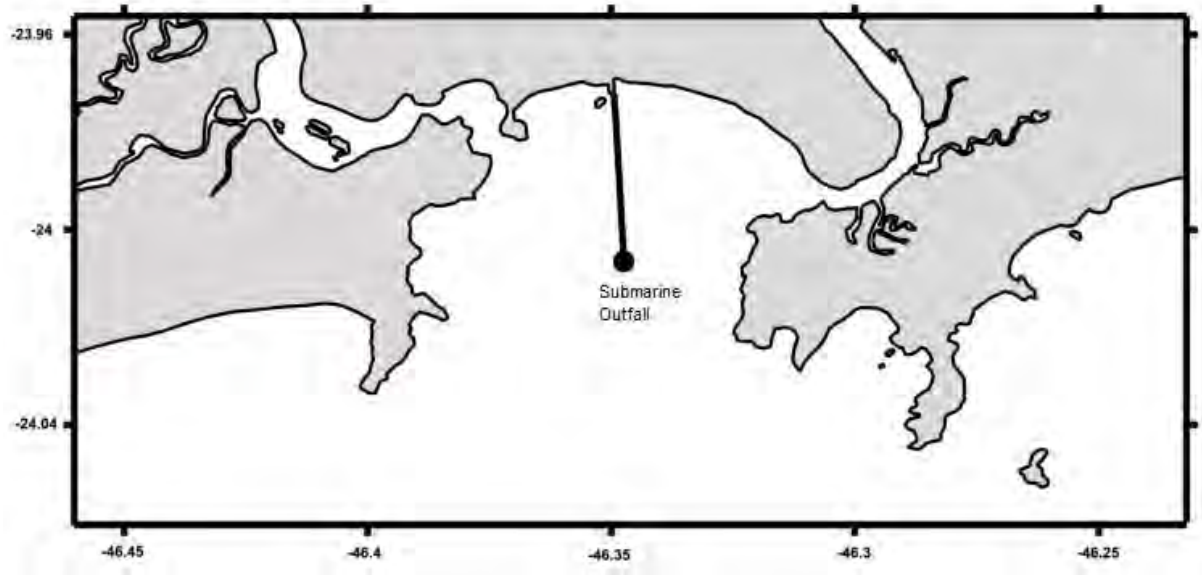

Figure 22: Location of Santos' Submarine Outfall (Source: Adapted from Gregorio, 2009).

None of previous studies that proposed jetties for Santos (Reis, 1978; Alfredini et al., 2013; Gireli et al. 2017) assessed the impact of these structures in coastline morphology, sediment transport, currents circulation, wave height, refraction and diffraction, water renewal, or water quality. The objective of these studies was strictly the evaluation of currents velocity variation. Moreover, the lack of updated bathymetric data in Bay of Santos, and the unequal distribution of tide gauges and flow measurement stations in the region give insufficient field data to validate Bay of Santos area results in hydrodynamic models.

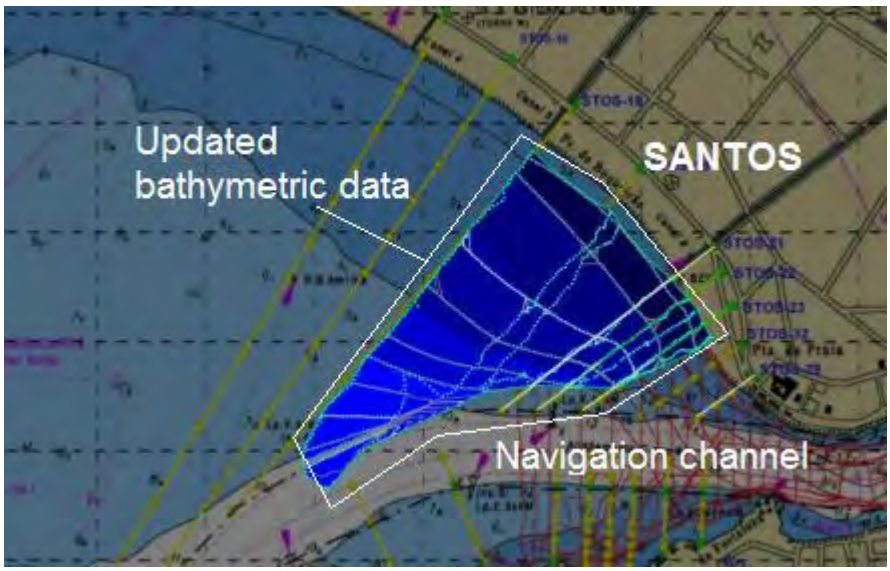

Figure 23: Updated bathymetry polygon near *Ponta da Praia* beach (Source: Adapted from Venancio, 2018).

According to Garcia et al. (2002), Bay of Santos last bathymetry dates back from 1982, since then only Port of Santos Navigation channel has been updated. Simulations with minor bathymetric updates near the northeastern beach *Ponta da Praia* (Figure 23), which currently is under an erosion process, have identified soft induced vortex currents between the beach and the curvy area of Stretch 1 (Venancio, 2018). This result is in accordance with FUNDESPA (2014), which measured residual longshore sediment budget in Bay of Santos. Moreover, all the permanent tide gauges are located along Navigation Channel of Port of Santos (Figure 6).

CONCLUSIONS

In order to become a hub port in South America, Port of Santos intends to deepen and widen its Navigation Channel to support New Panamax vessels. Some authors proposed jetties geometries and evaluated the variation of currents velocities along Navigation Channel of Port of Santos.

Hydrodynamic model results show that options with one jetty (J1 and J3) do not increase the velocity significantly, and options with two spaced jetties (J2 and J5) provide considerable velocity increment in the straight part of Stretch 1, which is only part of a critical siltation area. Only options with two jetties with narrow channel (J4) provide velocity increment in the critical siltation area of Stretch 1. However, considering that Stretches 2, 3, and 4 mean monthly siltation volume is 293,066 cubic meters (54.10% of total volume, as shown in Table 3) and that the jetties would only soften siltation in Stretch 1, even with the construction of J4 the monthly dredged volume along Navigation Channel would still huge. Thus, the construction of jetties alone would not allow Port of Santos to become a hub Port.

Hence, the chosen option must seek balance between low impact in Santos Bay beaches, water renewal, sediment transport, wave regime, and depth maintenance in Navigation Channel of Port of Santos. The option J4, if implemented, would block the longshore induced current in Bay of Santos, which is an important tide current for sediment dynamics in Bay of Santos. Moreover, it is likely that the construction of jetties would increase the time required to renew water in bay of Santos.

Field data in Bay of Santos are outdated, and tide gauges and flow stations are concentrated in Port of Santos Navigation Channel. Thus, before the implementation of any jetty option is highly recommended a comprehensive field data collection that includes currents measurements and tide gauge stations in different location of Bay of Santos, updates in Bay of Santos bathymetric data, and measurements of sediment budget. Moreover, a suitable Environmental Impact Assessment must include all beaches in the Direct Impact Area, because the construction of jetties changes wave refraction and diffraction, which impacts coastline morphology. Also, a sediment transport model should be used to evaluate new siltation trends along the Navigation Channel of Port of Santos, and alongshore.

ACKNOWLEDGEMENTS

The authors thank DHI for providing a time-limited license for thesis of the Mike 21 FM software and the National Council for Scientific and Technological Development (CNPq) for providing João H. O. Costa a one-year Junior Scientific Initiation scholarship.

This applied research work is a private initiative of the authors and is not related to any present or past commercial services contracts of the firm Ramboll, or of the institution UNICAMP. Opinions in this paper are those of the authors alone and do not reflect the views of Ramboll or UNICAMP.

REFERENCES

ACP - Autoridad del Canal de Panamá (2016a). Expansion Program. Panama Canal.

ACP - Autoridad del Canal de Panamá (2016b). First-Ever LNG Vessel Transits the Expanded Panama Canal, Ushering in New Era for the Segment and Global LNG Trade. Press Releases. Available at: https://micanaldepanama.com/expansion/2016/07/first-ever-lng-vessel-transits-the-expanded-panama-canal-ushering-in-new-era-for-the-segment-and-global-lng-trade/ (Access: February, 9th of 2017).

Alfredini, P., Arasaki, E., Pezzoli, A., & Fournier, C. P. (2013). Impact of Climate Change on the Santos Harbor, Sao Paulo State (Brazil). *TransNav*, *7*(4), 609-617.

BRASIL (2007). Programa Nacional de Dragagem 1 - PND 1. Available at: http://www.portosdobrasil.gov.br/assuntos-1/pnd/arquivos/programa-nacional-de-dragagem-pnd1-pac-1.pdf (Access: February, 7th of 2017).

BRASIL (2015). Programa Nacional de Dragagem - PND. Available at: http://www.portosdobrasil.gov.br/assuntos-1/pnd (Access: February, 7th of 2017).

Carvalho, V. de O. (2016). Estimativa da Taxa de Assoreamento do Canal de Navegação do Porto de Santos. Projeto de Graduação apresentado ao Curso de Engenharia Ambiental da COPPE, Universidade Federal do Rio de Janeiro.

CODESP - Companhia de Docas do Estado de São Paulo (2006). Plano de Desenvolvimento e Zoneamento do Porto de Santos. PDZPS.

DHI. (2015). MIKE 21 & MIKE 3 Flow Model FM - Hydrodynamic and Transport Module, Scientific Documentation. Copenhagen, Denmark. Danish Hydraulic Institute.

FRF - Fundação Ricardo Franco (2008). Capítulo 8: Diagnóstico Ambiental. EIA - Dragagem de Aprofundamento do Canal de Navegação e Bacias de Evolução do Porto Organizado de Santos/SP, Rio de Janeiro.

FUNDESPA (2014). *Plano Básico Ambiental da Dragagem de Aprofundamento do Porto de Santos*. Santos: CODESP/FUNDESPA, 2014. Relatório do Monitoramento dos Sedimentos da Superfície de Fundo e Caracterização do Transporte Sedimentar Residual no Setor Nordeste da Baía de Santos. Amostragem 2013.

Garcia, P. D., Araújo, R. N., Silva, G. D. C., Baptistelli, S. C. and Alfredini, P. (2002), "Preparo de bases batimétricas, de agitação e circulação para o litoral do estado de São Paulo". Boletim Técnico da Escola Politécnica da USP. BT/PMI, Escola Politécnica da USP, 105 (1), 1–56.

Gireli, T. Z., & Vendrame, R. F. (2012). Aprofundamento do Porto de Santos: uma análise crítica. Revista Brasileira de Recursos Hídricos, 17(3), 49-59.

Gireli, T. Z., Souza, C. M. M. A. D., Nobre, L. B., & Garcia, P. D. (2017). The efficiency of curved jetties in Bay of Santos–SP: numerical modeling. *RBRH*, *22*. http://dx.doi.org/10.1590/2318-0331.011716092.

Gregorio, H. P. (2009). Modelagem numérica da dispersão da pluma do emissário submarino de Santos (Doctoral dissertation, USP - University of São Paulo).

Harari, J. & Camargo, R. (1994), "Simulação da propagação das nove principais componentes de maré na plataforma sudeste brasileira através do modelo numérico hidrodinâmico". Bolm. Inst. Oceanogr., 42(1), 35-54.

Harari, J., & Camargo, R. (2003). Numerical simulation of the tidal propagation in the coastal region of Santos (Brazil, 24 S 46 W). *Continental Shelf Research*, *23*(16), 1597-1613.

INPH (2007). Relatório INPH nº 018 / 2007 - Projeto Geométrico da Infra-Estrutura Aquaviária ao Porto de Santos - SP. Anexo XI, Rio de Janeiro.

IPEA (2009). Texto para Discussão 1408: Portos brasileiros 2009: Ranking, área de influência, porte e valor agregado médio dos produtos movimentados. Rio de Janeiro. Available at: http://www.ipea.gov.br/portal/images/stories/PDFs/TDs/td_1408.pdf.

Magini, C., Harari, J., & Abessa, D. M. D. S. (2007). Circulação recente de sedimentos costeiros nas praias de Santos durante eventos de tempestades: Dados para a gestão de impactos físicos costeiros. *Geociências*, 349-355.

MARMIL - *Centro de Hidrografia da Marinha*. Marinha do Brasil (2015). Available at: http://www.mar.mil.br/dhn/chm/box-cartas-raster/raster_disponiveis.html (Access: September, 30th of 2015)

MPF – Ministério Público Federal (2015). Inquérito Civil Público n° 1.34.012.000536/2011-13 - Santos, 25 de julho de 2015.

MPF – Ministério Público Federal (2017). Termo de Acordo para Homologação Judicial nos Autos da Ação Civil Pública Nº 0004665-36.2015.403.6104 da 3ª Vara Federal em Santos – Santos, 15 de dezembro de 2017.

PIANC (2014). Harbour approach channels design guidelines. PIANC Report no. 121 – Maritime Navigation Commission.

Reis, L.B.F. (1978) Estudo de modelo reduzido de fundo móvel do Porto de Santos. Rio de Janeiro: INPH. Apresentado no primeiro ciclo de palestras de Engenharia costeira.

Roversi, F., Rosman, P. C. C., & Harari, J. (2016). Análise da renovação das águas do Sistema Estuarino de Santos usando modelagem computacional. *Ambiente & Água - An Interdisciplinary Journal of Applied Science*, *11*(3).

SOUZA, M. M. A. (2017). Comparação de modelos numéricos bidimensional e tridimensional para a avaliação de mudanças ambientais, aplicado à região costeira de Santos. PhD Thesis — School of Civil Engineering, Architecture and Urban Design – UNICAMP (University of Campinas).

URS Holdings, Inc. (2007). Chapter 3: Project Description. Environmental Impact Study – Panama Canal Expansion - Third Set of Locks Project.

Venancio, K. K. (2018). Evolução hidromorfodinâmica da região da Ponta da Praia em Santos (SP) no período entre 2009 e 2017 (Masters dissertation, UNICAMP - University of Campinas).

Willmott, C. J. (1981). On the validation of models. *Physical geography*, *2*(2), 184-194.

THE DEVELOPMENT OF REDRAFT® SYSTEM IN BRAZILIAN PORTS FOR SAFE UNDERKEEL CLEARANCE COMPUTATION

by

Felipe Ruggeri[1], Rafael Watai[1], Guilherme Rosetti[1], Eduardo Tannuri[2], Kazuo Nishimoto[2]

[1]*Argonautica Engineering & Research, Brazil*

[2]*University of São Paulo, Brazil*

ABSTRACT

The increase of ship dimensions in the latest years combined to the requirements regarding the reduction of environmental impact during the maintenance dredging and economic constrains in the Brazilian ports require technological solutions in order to optimize the safe accessibility of large vessels. Most of these ports operate under a static draft rule regardless the environmental condition acting during the maneuver, which is theoretically a conservative approach. The bay close or restriction is usually performed based on experience, which may fail in the absence of objective parameters to define the adequate underkeel clerance, providing some unsafe situations mainly in the presence of misaligned wind and swell waves and/or negative meteorological tides. The development of computational resources, monitoring systems and communication technology in the last years provided the basis for integration of these tools into an automatic draft computation system, called as ReDRAFT, which integrates the environmental conditions collected in real-time to the hydrodynamic model of the port and ship dynamic model customized for each specific maneuver (ship properties, loading condition, inbound/outbond) in order to define the safe underkeel clearance for the maneuver. Moreover, the draft windows may be predicted based on the forecast models, which is also a powerful tool for planning. The numerical models allow more accurate predictions of the estuary environmental conditions, mainly waves, current and tide, which combined to the vessel numerical model can provide the ship motions in 6DoF. The ship motions on these large vessels are reduced for short period waves, thus allowing the increase the vessel draft. On the other hand, the vessel motions are significant for long waves, requiring the reduction of the vessel draft in order to mitigate the risk of bottom touch. The system is already operational in Santos and Rio de Janeiro ports, two of the most important ones in South America, for vessels considered as critical according to the nowadays port traffic. The PIANC Report n° 121 – 2014 factors are considered in the computation of the maximum safety draft. The ship related factors considered are the squat, dynamic heels due to turning and wind, wave response and net ukc. In order to simplify the utilization and avoid mistakes in the input data, a large database of vessels was created and summarized in a user-friendly interface, where the characteristics of each specific vessel is defined based on the IMO number, BZ code or vessel name. If a new vessel is operating in the port, the vessel is included in the software database using Lloyd's register information available in a standard "xml" format. The vessel hydrostatic/hydrodynamic characteristics are then interpolated using the software database if the dimensions are in the ranges of LOA, beam, depth and draft. The database contains the maximum wave motions of several points at the ship bottom considering a collection of wave periods, incidence direction, ship speed (encounter frequency correction), underkeel clearance, LOA, beam, depth, draft and ship type (tanker, bulk carrier or containership). The computations are performed in frequency domain using a higher order panel method based on spectral theory and a probabilistic approach. Since the ship geometry (stations) regarding each individual vessel is not available, some standard "design ships" are assumed and scaled to meet the desired LOA, beam, depth and draft, providing a NURBS (Non-uniform Rational Basis Spline) surface. The squat is computed based on literature regressions according to the Cb, ship speed (corrected to take into account the current effect) and channel geometry based on the database of hydrostatic properties, the pilots expertise regarding required ship speed to keep an adequate maneuverability and the channel bathymetry. The heel due to turning is computed according to the lateral wind, the metacentric height provided in the database and the wind measurements. The heel due to turning is computed using the ship speed and the turning radius computed from the channel alignment. The maneuvering margin (MM) is defined based on the pilots experience to guarantee the safety according to the environmental conditions, ship dimensions and available tugs. The system is already operational in Santos Port since 2015 and in Rio de Janeiro port since October 2016 for validation in order to provide reliability to the system.

INTRODUCTION AND MOTIVATION

The main Brazilian ports receive some of the largest vessels built in the last years to obtain gain of scale and reduce transportation costs related to export of oil, iron ore and other goods. The oil exploration has grown appreciably in the last years due to the discover of large oil reservoirs in the pre-salt layer in Santos Basin, requiring VLCCs (Very Large Crude Oil Carrier) to operate more often. A large project of iron ore exploration in the northeast region of Brazil and the increase of iron ore price motivates the increase of ULOC (Ultra Large Ore Carriers) maneuvers. The 366m containership class shall be operating in Brazilian ports in a near future, providing about 40,000 ton of additional displacement compared to the 333m class. These facts are also verified in (ANTAQ, 2015) (Brazilian Agency for waterway transportation) statistics, which show an average growth of 12.4% per year of cargo transportation since 2011 and a prediction of 150% growth in 2030 compared to 2012.
Beyond the large costs involved in the modification of the ports to receive these large vessels in a safety/efficient way, there is a large pressure from society for environmental sustainability in the new green world, see for instance, the several IMO regulations regarding ship efficiency, emissions and pollution. Each added tonnage during a vessel maneuver means an increase of ship efficiency by the increase of transport work, which is nowadays measured by EEOI (Energy Efficiency Operational Indicator) index defined by IMO (IMO - International Maritime Organization, 2009). A rule of thumb regarding the added transportation capacity considering an additional 10cm of operational draught can be seen in Figure 1.

$$EEOI = \frac{CO_2\ emissions}{Transported\ cargo\ \times distance} \qquad (1)$$

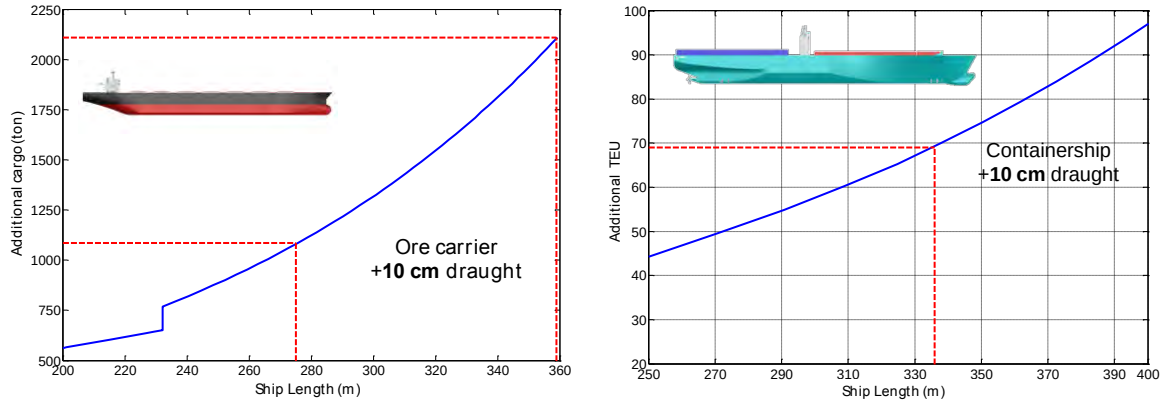

Figure 1 - Rule of thumb of added transportation capacity for 10 cm of added ship draught for ore carriers and containerships.

Moreover, navigation safety is a major concern during the maneuver of these large vessels, since the consequences are huge, requiring technological solutions to support these decisions.

The ReDRAFT® was developed to evaluate the maximum safety draught for navigation based on a scientific approach, combining almost real-time data measurements with the numerical model of the port and a digital model of each specific vessel, providing a customized draught rule for each maneuver. The system can also provide short and long-term forecasts of the maneuver window/maximum safety draught, the first one applied during the day-to-day ship planning and the second one for the maintenance dredging support decision. This digital twin of the port is one of the steps for the maritime 4.0 industry and it can be applied for several other applications, for instance, design of new terminals, evaluation of new vessels, queue studies, risk assessment, dredging optimization, environmental impact, oriented user database etc.

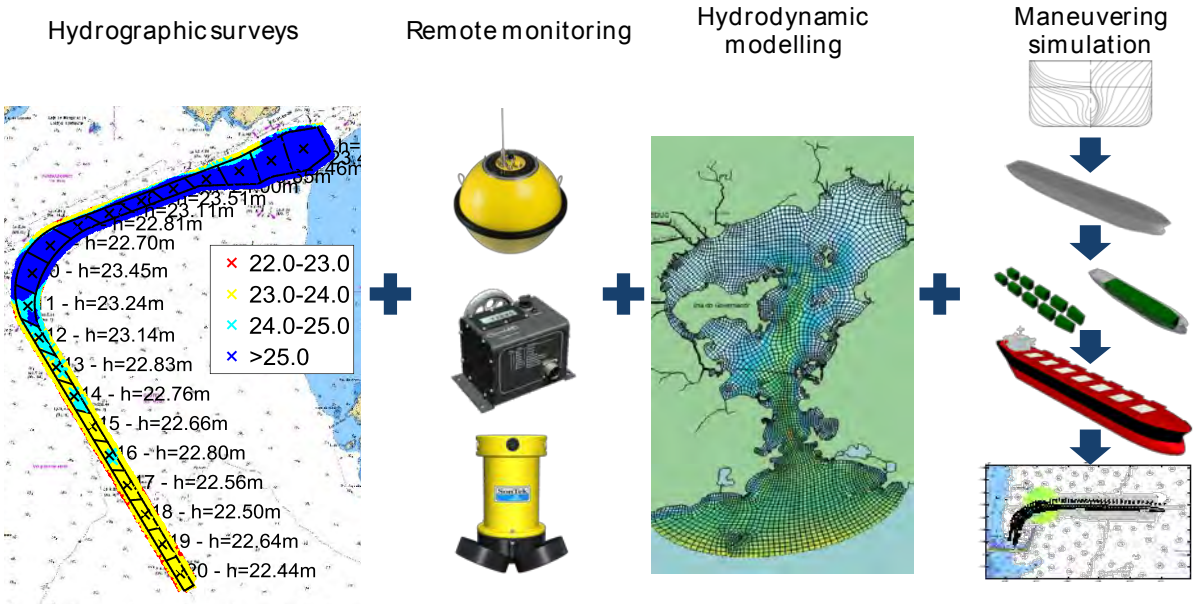

Figure 2 – ReDRAFT® Maritime Digital Twin

The definition of maximum safety draught is a challenge task due to the several variables involved, which may change in time and space according to the port specific conditions and the navigating ship. The traditional approach to this problem is to assume the environmental conditions as constant during the entire maneuver and take the channel depth as constant based on the lowest value, claimed as the channel depth. In some conditions the ship speed is also considered as constant during the entire maneuver to simplify the calculations, providing a single squat, wave motion, wind heeling etc, which is combined to a net underkeel clearance according to the bottom hardness.

Based on the predominant environmental conditions and pre-established operational limit in the design stage (directly related to the port downtime/efficiency assessment), a single safety margin for draught is usually defined in the Brazilian ports, regardless the day-to-day acting environmental condition during maneuver or ship type, as illustrated in Figure 3. This margin may lead to potential unsafe maneuvers if the environmental condition is beyond these pre-established values, requiring empirical expertise to avoid these risks, in some cases supported by using monitoring systems (wave buoys, adcp, tide gauges etc). However, in several complex conditions, e.g. multidirectional sea state condition and meteorological tides, the evaluation of ship interaction may be a challenge task.

On the other hand, in several conditions the draught may be increased without compromising the safety, improving cargo transportation efficiency, reducing the transportation cost and carbon footprint.

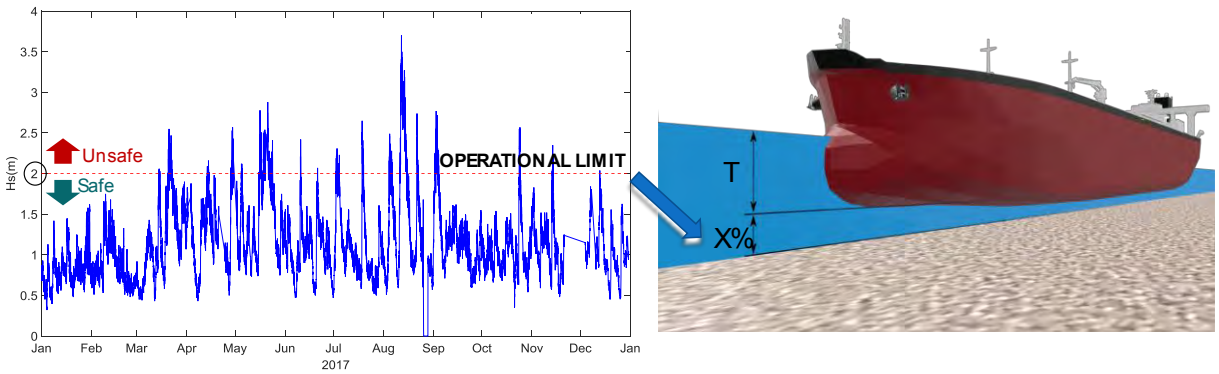

Figure 3 - Example of measured environmental condition and operational limit defined for the establishment of draft margin.

However, in several cases there are large variations in the channel depth, wave attenuation, current velocity, ship speed etc during the maneuvering, requiring an automatic tool to take in account all these aspects.

Moreover, several parts of the channel closer to the natural depth (routes to deep water) have softer bottoms compared to the regions closer to the berth, since the natural sand and muddy layers have not been modified yet, providing a spatially variable net underkeel clearance requirement.

A simplified comparison regarding wave energy propagation coefficients for 10 points in the access channel of an export port can be seen in Figure 4 considering the south and southwest incidence directions for 10s peak period spectrum. It can be verified the large attenuation of southwest condition compared to the south one, as the reduction of wave energy comparing point 1 (closer to the berth) to point 10 (in the outer region). These propagation coefficients shall change according to wave spectrum, wave frequency and offshore significant wave height, changing the vessel motions, therefore the required underkeel clearance for a safe navigation. The water level, channel depth, current, vessel speed and wind at each section of the channel will also change and influence in a different way at each section of the channel.

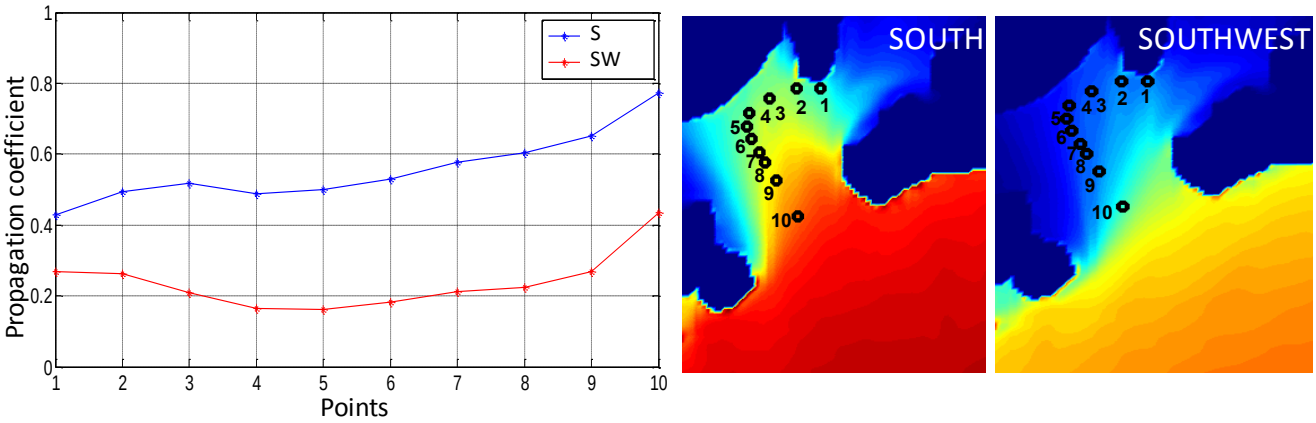

Figure 4 - Example of wave propagation coefficients for south and southwest incidence considering 10 points in the access channel of an export port for sea spectrum with peak period 10s.

The hydrographic surveys applied in the computations shall be in accordance with special class requirements defined in NORMAM 25, Brazilian navy standards, which is similar to S44 (International Hydrographic Organization, 2008) requirements from IHO (International Hydrographic Organization). The depths can be updated based on siltation maps computed using the validated hydrodynamic/wave propagation model to provide the bottom evolution, which is directly applied into the underkeel clearance assessment. An example of siltation map for an export port can be seen in Figure 5. The larger siltation is located closer to the coast (berth), while a smaller value is expected in the beginning of the access channel. The sinkage due to wave and squat are smaller closer to the berth since the ship speed is also smaller, as the wave incidence compared to the outer section. Based on that it can be expected different required depths in the channel, as different effects of siltation into the maneuver. The port digital model runs to provide the bottom evolution during the year, taking into account the winter and summer wave incidence, since harsh waves may modify accelerate the siltation/erosion appreciably of different parts of the channel.

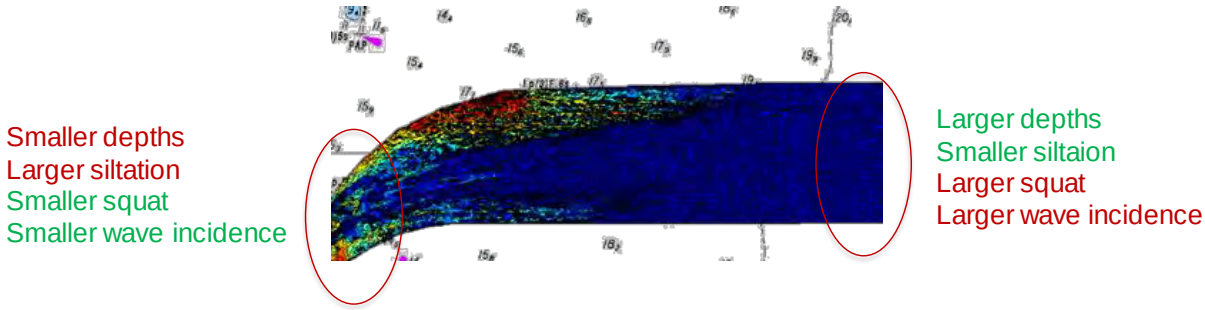

Figure 5 - Example of siltation map for an export port (blue color represents smaller siltation and red color a larger one).

SHIP MODELLING

The ship properties are defined based on large database of similar vessels, therefore for each one there is a specific digital model, containing the hydrostatic properties, hull geometry, panel meshes, loading conditions etc.

In some cases, the shipowner still has the lines plan of the ship, allowing an even more accurate digital model. If the lines plan is not available, the appropriate benchmark hull may be scaled and changed by Lackenby transform (Lackenby, 1950) to achieve the desired hydrostatic properties. Some examples of benchmark containership may be seen in Figure 6.

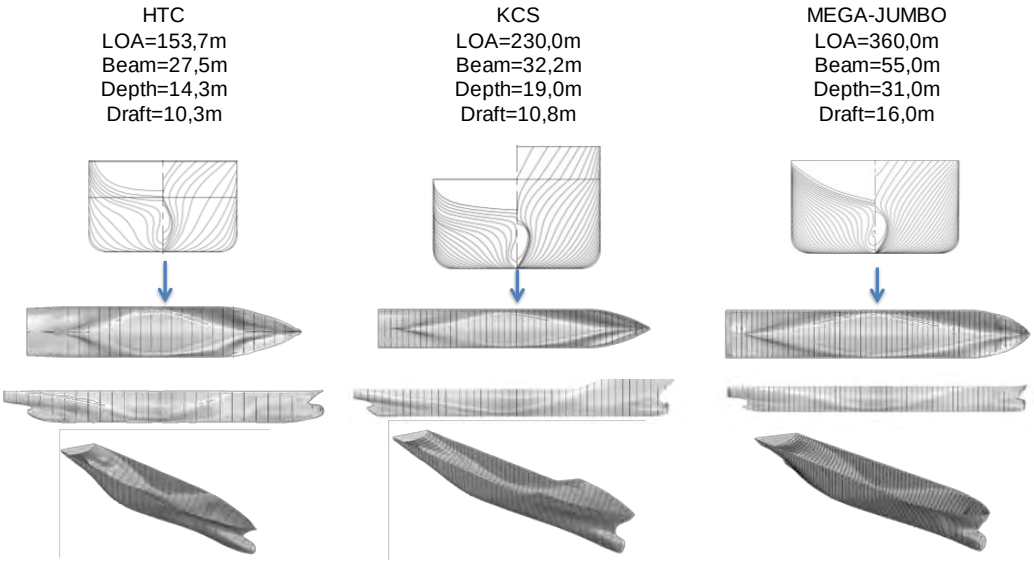

Figure 6 - Examples of benchmark containerships.

The ship geometry is generated using NURBS (Non-uniform Basis Spline), one of the standards formats applied in CAD industry, which is applied in the hydrostatic properties, wave response and squat assessment, as described next. The NURBS surface is described considering several patches, each one described based on *(2)*, where p is the degree of the spline, $N_{i,p}$ is the basis function, $\vec{C}_{ij}$ are the control points, w_{ij} are the control points weights and u, v is the unitary surface domain. This approach allows a simple, efficiency and robust way to store the hull surface. Moreover, the surface is continuous, therefore the normal vector and Jacobian are also continuous, which will be important in the seakeeping computations due to a continuous potential function, as discussed later. More details may be found in (Ruggeri, et al., 2018) and (Ruggeri, 2016).

$$\begin{Bmatrix} x(u,v) \\ y(u,v) \\ z(u,v) \end{Bmatrix} = S(u,v) = \frac{\sum_{i=1}^{N_u}\sum_{j=1}^{N_v} w_{ij}\vec{C}_{ij}N_{i,p}(u)N_{j,p}(v)}{\sum_{i=1}^{N_u}\sum_{j=1}^{N_v} w_{ij}N_{i,p}(u)N_{j,p}(v)}, 0 \le u \le 1, \qquad 0 \le v \le 1 \tag{2}$$

The ship digital model also considers the cargo and ballast tanks to obtain the cargo distribution and free surface effect more accurately, as illustrated in Figure 7. The loading condition is evaluated based on the general arrangement, capacity plan and trim& stability booklet.

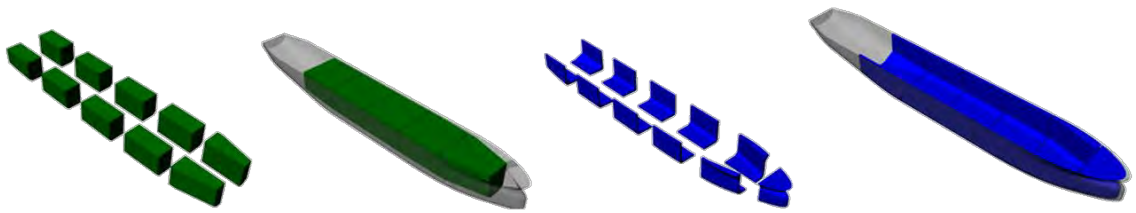

Figure 7 - Example of digital model of a crude oil carrier considering the cargo (left) and ballast (right) tanks highlighted applied for moment of inertia and vertical center of gravity calculation.

The vertical center of gravity is evaluated based on (3), where $\mathrm{VCG_{light}}$ is the vertical center of gravity of the lightship, $\mathrm{W_{light}}$ is the lightship weight, $\mathrm{VCG_{i,cargo}}$/$\mathrm{VCG_{i,ballast}}$ are the center of gravity of the several cargo/ballast tanks (or containers) and $\mathrm{W_{i,cargo}}$/ $\mathrm{W_{i,ballast}}$ are the weight of each specific item. The center of gravity may also be provided by ship master based on the planned load, if the data is provided.

$$VCG = \frac{\left(VCG_{light}W_{light} + \sum_{i=1}^{N_c} VCG_{i,cargo}W_{i,cargo} + \sum_{i=1}^{N_b} VCG_{i,ballast}W_{i,ballast}\right)}{W_{light} + \sum_{i=1}^{N_c} W_{i,cargo} + \sum_{i=1}^{N_b} W_{i,ballast}} \quad (3)$$

The moment of inertia in x direction (surge) is evaluated using Steiner's theorem given in (4), where $\mathrm{I_{xx,LS}}$, $\mathrm{I_{xxi,cargo}}$ and $\mathrm{I_{xxi,ballast}}$ are the moments of inertia regarding the lightship, cargo and ballast tanks computed considering the principal axes, $\mathrm{W_{i,cargo}}$/$\mathrm{W_{i,ballast}}$ are the cargo/ballast weights, $(\mathrm{x_{Gi,cargo}}, \mathrm{y_{Gi,cargo}}, \mathrm{z_{Gi,cargo}})$/ $(\mathrm{x_{Gi,ballast}}, \mathrm{y_{Gi,ballast}}, \mathrm{z_{Gi,ballast}})$ are the cargo/ballast centers of gravity and $(\mathrm{x}_{CG}, y_{CG}, VCG)$ the ship center of gravity coordinates considering a coordinate system located in the baseline amidship.

$$I_{xx} = I_{xx,LS} + \sum_{i=1}^{N_c} \left\{ I_{xxi,cargo} + W_{i,cargo}\left[\left(y_{Gi,cargo} - y_{CG}\right)^2 + \left(z_{Gi,cargo} - VCG\right)^2\right]\right\} + \sum_{i=1}^{N_b} I_{xxi,ballast} + W_{i,ballast}\left[\left(y_{Gi,ballast} - y_{CG}\right)^2 + \left(z_{Gi,ballast} - VCG\right)^2\right] \quad (4)$$

Since the computation of the lightship moment of inertia taken into account each structural stiffener and the variation of plate thickness along the entire ship would be very difficult due to the huge number of details, see for instance Figure 8, an equivalent thickness is defined ($t_{eq} = W_{light}/S_{total}$) taking into account the ship plating without these elements.

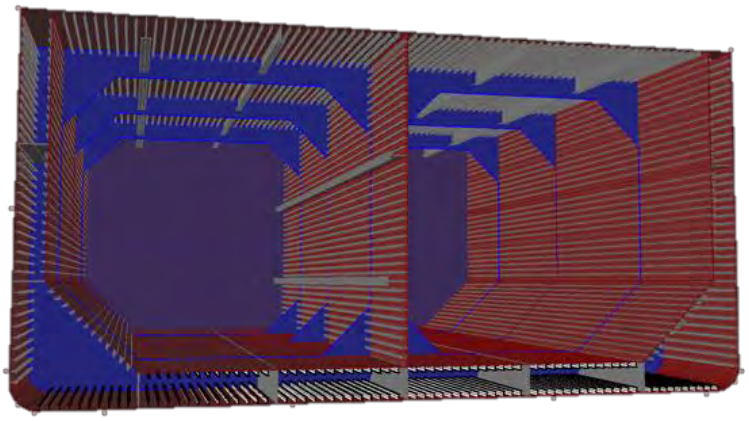

Figure 8 - Example of structural section considering the all stiffener elements of a real tanker.

The lightship moment of inertia in x direction is then computed using (5), considering only the plates. The moments of inertia in other directions are computed analogously.

$$I_{xx,LS} = t_{eq} \iint_{S_{total}} \left[\left(z - VCG_{light}\right)^2 + y^2\right] dS \quad (5)$$

The 6x6 hydrostatic restoration matrix is computed using Gauss theorem in the submerged hull surface considering the appropriate vector field combined to center of gravity position, as demonstrated in

(WAMIT Inc, 2015), (Ruggeri, 2012) and (Ruggeri, 2016). The linear free surface effect corrections are also taken into account for loaded tanks within 5% to 95% of the nominal capacity.

If the detailed loading condition is not available, some variations of cargo loading are performed to obtain the mean draft, trim and list following the stability requirements from IMO (IMO - International Maritime Organization, 2008) and maximum allowed bending moment and shear stress. These combinations are usually limited for bulk carriers and tankers but quite more complex for containerships due to the several possibilities of cargo allocation and container weight, see for instance in Figure 9.

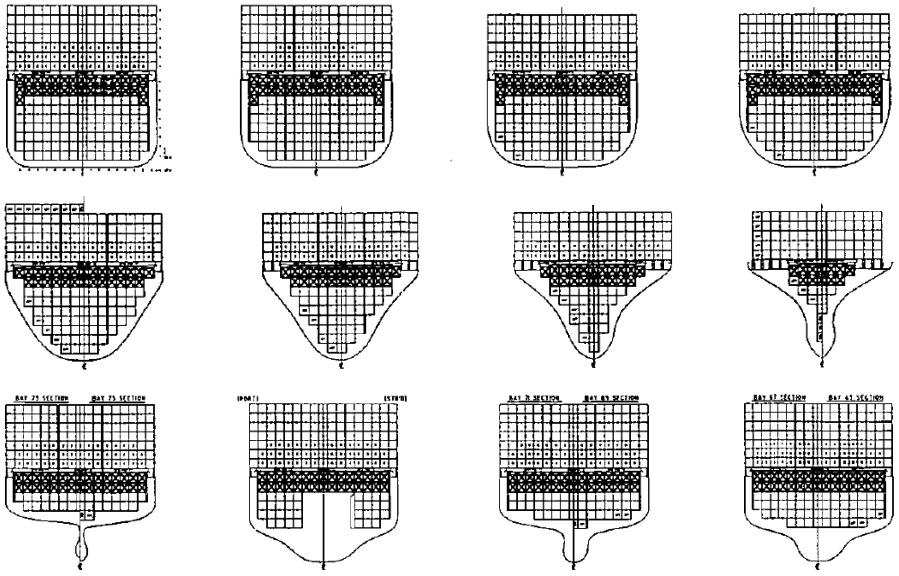

Figure 9 - Example of 366m containtership section.

The metacentric height and moments of inertia are compared to reference values, for example (Journée, et al., 2011), (Schneekluth, et al., 1998), (Yilmaz, et al., 2001) and (PIANC, 2014), to verify the coherence of the data. The flat bottom, propeller, rudder and bulb are discretized considering several points based on the 3D model of each specific ship. There are significant differences between a bluff ship (e.g. large bulk /crude oil carrier) and slender one (e.g. container ship, LNG carriers etc.) due to the different hull lines and block coefficient, as illustrated in Figure 10.

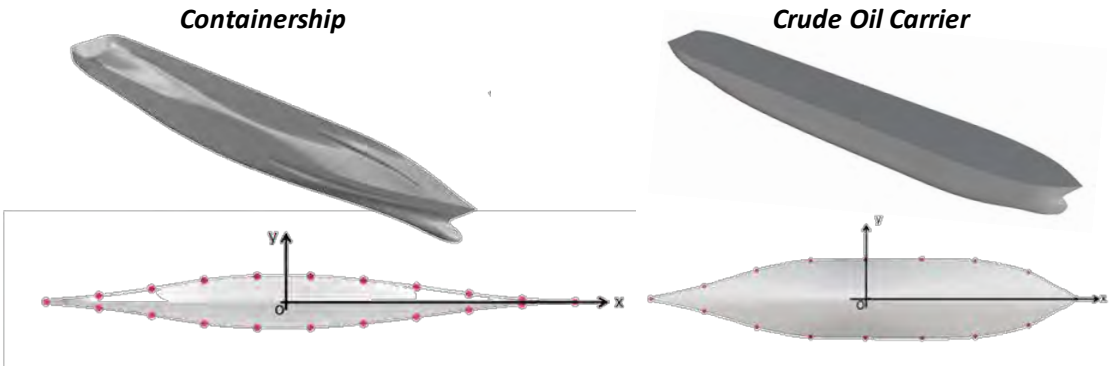

Figure 10 - Critical points in the flat bottom of a containership (left) and a crude oil tanker (right).

A pre-defined database is built for the several ship types based on fleet study and regressions, see for instance, (Kristensen, 2012) and (Kristensen, 2013). In the operational tool this data is automatically obtained from class societies database according to IMO number. It shall be noticed that following this approach the ship is no longer only a simple combination of LOA, Beam and DWT, which is usually considered in the simplified safety margin computation. Instead the ship now has a complete detailed digital model applied during the computations.

SHIP SPEED

The ship speed during the several sections of the channel can be suggested during the maneuver to reduce the risk of bottom touch. However, there are limits related to the maneuverability margin (MM) that cannot be exceed, which are evaluated in a real-time simulation campaign. One of the main references is the TPN Simulator, developed by University of São Paulo, Petrobras and Transpetro with the technical collaboration of the Brazilian Pilots Association (CONAPRA) (Tannuri, et al., 2014).

If the ship already operates in the port with a constrained draught under static rules a first guess of the ship velocities in the several sections can be obtained based on track records of past maneuvers, as the drift angles, which may be combined to current speed, water level, wind etc to obtain a better comprehension of these limits. The pilots' expertise provides additional insights regarding the key aspects of the maneuver and points of additional attention during the studies.

An example of ship speed distribution along the channel section can be seen in Figure 11, where each dot is an observed maneuver, with section 1 closer to the seaside and section 99 closer to the turning basin/berth basin. Based on these records, the speed statistical distribution for each section can be created, as the probability of exceedance.

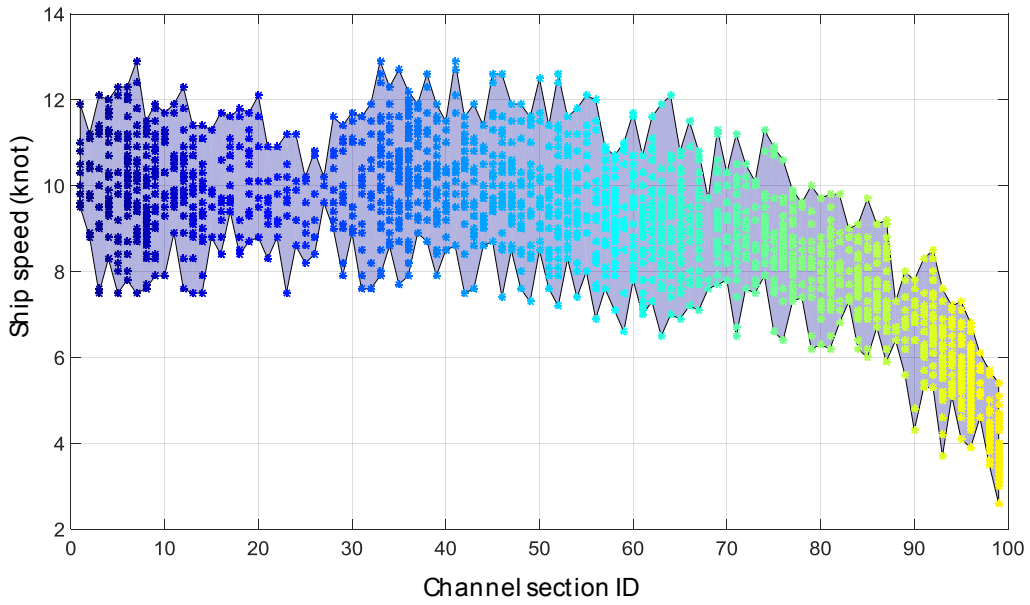

Figure 11 – Example of ship speed records along the channel sections considering several observed maneuvers.

SQUAT

The squat may be computed following several different techniques, from simplified regression formulas to customized model tests and state-of-art higher order panel mesh using the "real" bathymetric surveys combined to the tide level and current values. An example of panel mesh applied for squat computation considering a real bathymetric survey can be seen in Figure 12. It shall be noticed that even this method has some limitations inherent to potential flow theory.

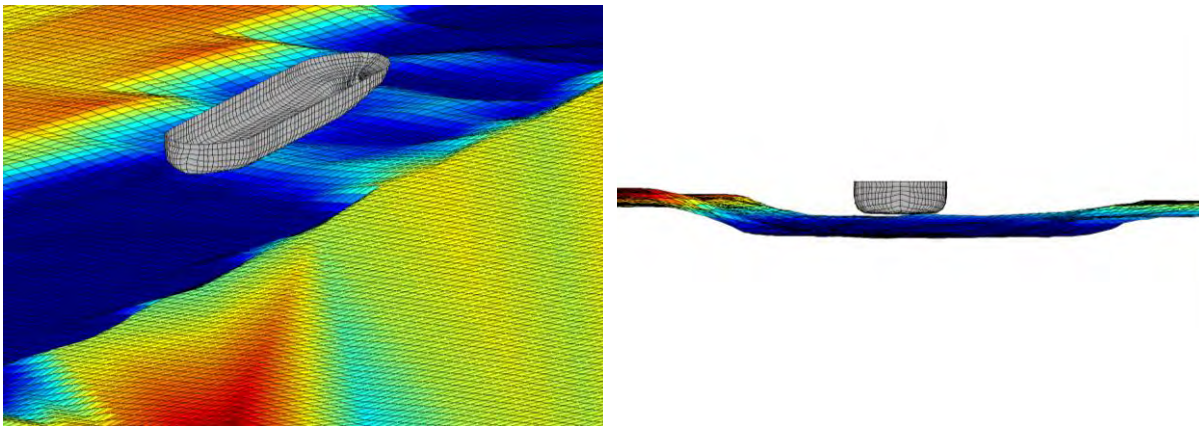

Figure 12 - Example of panel mesh considering a specific ship and the bathymetric survey.

In the 10 last years the CFD (Computational Fluid Dynamics) techniques based on FVM (Finite Volume Meshes) and FEM (Finite Elements Method) have evolved appreciably in terms of computational efficiency and mesh generation capability to represent the real seabed in the computations. However, the time required does not allow the application for an operational tool and the convergence process still not robust enough without an expert supervision.

The regression formula proposed by Huuska (Huuska, 1976) still the most accepted approach, which is applied section by section according to the ship speed (discussed earlier) considering the current effect (relative velocity) and the blockage correction K_{Si}, which defines the unrestricted, restricted and channel conditions. The squat value can be computed according to (6), where C_S is an adjustment coefficient based on block coefficient, L_{pp} is the length between perpendiculars and F_{nhi} is the Froude number based on the mean water depth and tide level. The same channel may have different configurations according to the blockage effects, see for instance Figure 13 considering several sections of the same channel.

$$\Delta z_{squat,i} = C_S \frac{\nabla}{L_{pp}^2} \frac{F_{nhi}^2}{\sqrt{1 - F_{nhi}^2}} K_{Si} \tag{6}$$

$$C_S = \begin{cases} 1.7, if\ C_B < 0.70 \\ 2.0, if\ 0.70 < C_B < 0.80 \\ 2.4, if\ C_B > 0.80 \end{cases} \tag{7}$$

$$F_{nhi} = \frac{V_{shipi} + V_{corr}\, cos(\theta_{curr} - \theta_{ship})}{\sqrt{g(h_{Mi} + m_i)}} \tag{8}$$

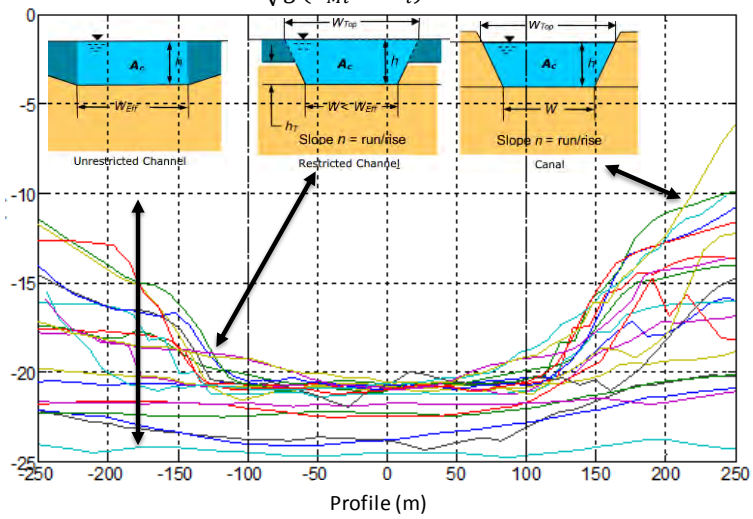

Figure 13 – Example of several section profile in the same access channel (each line is a specific section).

WIND HEELING

The sinkage due to wind heeling is computed based on *(9)*, where θ_{Wi} is the heeling angle at section i and x_p is the x-coordinate of each point p located at the ship bottom, as described previously. The wind heeling angle is obtained based on ship stability *(10)*, where M_{Wi} is the wind heeling moment, ρ_W is the salt water density and GM_T is the transversal metacentric height. The metacentric height is also obtained based on the ship modelling procedure described earlier.

$$\Delta z_{wind,pi} = x_p sin(\theta_{Wi}) \quad (9)$$

$$sin(\theta_{Wi}) = \frac{M_{wi}}{\rho_W g \nabla G M_T} \quad (10)$$

The wind heeling moment is computed applying *(11)* following (PIANC, 2014), where ρ_{air} is the air density, A_L is the projected lateral windage area, $V_{WR}i$ is the relative wind velocity in section I and C_{Wy} the transversal wind force coefficient, computed by *(12)*, where C_{Ynk} are coefficients obtained from tables provided in (Yamano, et al., 1197), A_F is the frontal area, B is the beam and x_L is the distance between the forward perpendicular and the center of projected area, computed using the general arrangement draw, see for instance Figure 14.

$$M_{Wi} = \frac{1}{2}\rho_{air} C_{wy} A_L V_{WRi}^2 \left(KG - \frac{T}{2}\right) \quad (11)$$

$$C_{wy} = \sum_{n=1}^{3}\left[\left(C_{Yn0} + C_{Yn1}\frac{A_{V,L}}{L_{pp}^2} + C_{Yn2}\frac{x_L}{L_{pp}} + C_{Yn3}\frac{L_{pp}}{B} + C_{Yn4}\frac{A_L}{A_F}\right) sin(n\theta_{WRi})\right] \quad (12)$$

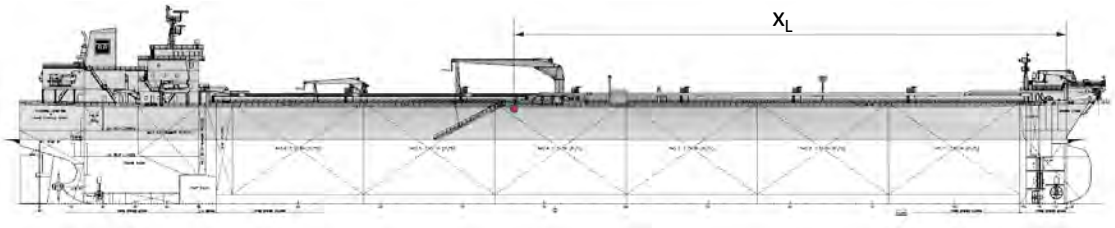

Figure 14 - Example of general arrangement used for x_L computation.

It should be noticed that several other references are available in the literature, see for instance (Isherwood, 1972), (Blendermann, 1994) and (Lindeen, 2008) for container ships coefficients. The application of CFD may be performed, as wind tunnel tests, to obtained the wind coefficients, mainly for new vessels without data available. The advantage of CFD simulations is the possibility to compute in both model and full scale taken into account the scale effects accurately.

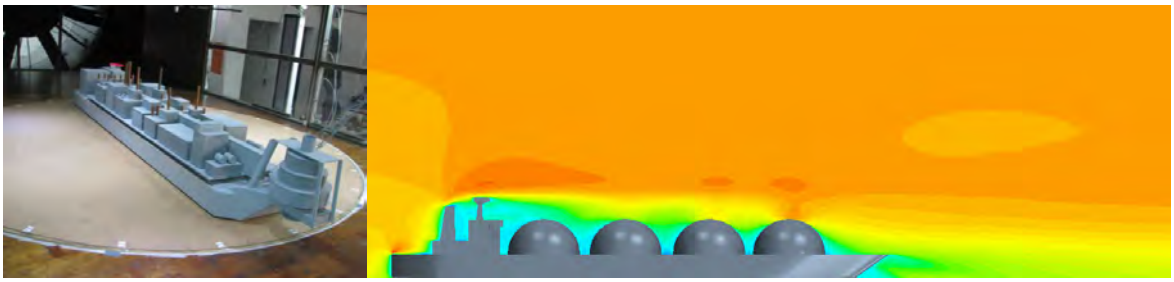

Figure 15 - Example wind tunnel test (left) for a FLNG and CFD simulation (right) considering the velocity field around a LNG Carrier.

The wind areas stored are in the ship modelling are defined in the design draft condition, therefore these values shall be corrected for other drafts based on *(13)*, where T_{des} is the design draft.

$$A_F(T) = A_F(T_{des}) + (T_{des} - T)B,\ A_L(T) = A_L(T_{des}) + (T_{des} - T)L_{pp} \quad (13)$$

The sinkage due to wind action in the longitudinal direction is required since the longitudinal metacentric height is in the order 100 times the transversal metacentric height. Moreover the frontal wind area is usually appreciably smaller than the transversal one.

DYNAMIC HEELING

The dynamic heeling angle is computed using *(14)* according to (PIANC, 2014), where V_{SRi} is the relative ship speed taken into account current effects in section i, l_R is the heeling lever *(15)* and R_C is the turning radius, computed from the nautical chart at each section. The additional sinkage due to the dynamic heeling is then computed applying *(16)*. The turning radius is defined as the minimum value at each section and for straight ones the value tends to infinity therefore the heeling angle tends to zero. An example of the outer curve in the access channel of Santos port is shown in Figure 16.

$$\phi_{Ci} = \frac{l_R V_{SRi}^2}{g R_C GM} \tag{14}$$

$$l_R = VCG - \frac{T}{2} \tag{15}$$

$$\Delta z_{dyn,pi} = x_p \, sin(\phi_{Ci}) \tag{16}$$

Figure 16 - Example of outer curve in the access channel of Santos port.

WAVE RESPONSE ASSESSMENT

The wave response is evaluated in frequency domain based on the ship RAO (Response Amplitude Operators) of each specific ship during the maneuver. The potential flow theory is applied (Newman, 1977), (Faltinsen, 1990), (Bertram, 2000), (Mei, et al., 2005) using a higher order panel method based on the NURBS surface presented earlier for the geometric description and B-spline description regarding the potential function, therefore velocity field and other quantities. The double-flow linearization is applied for low ship speeds/depth Froude numbers ($F_{nh} < 0.3$). An example of panel mesh can be seen in Figure 17 considering the b-spline potential subdivision and the normal vectors in the center of the higher order panels.

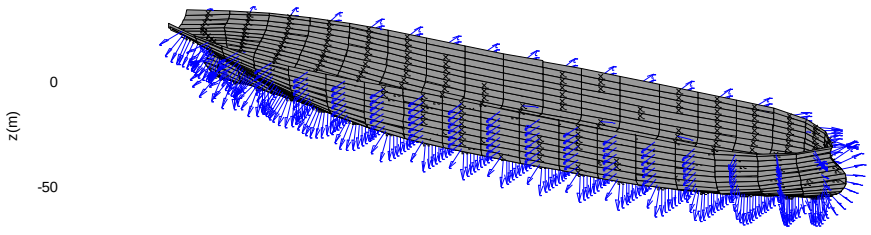

Figure 17 - Example of panel mesh and normal vectors for a tanker.

The basis flow is solved using the Green function considering the Rankine source mirror technique to guarantee the no-flux condition in the bottom and mean free surface, illustrated in Figure 18. Since the no-flux condition is considered in the bottom and mean free surface, an infinite number of images shall be applied. The mean hydrodynamic depth is applied as reference depth applying the algorithms proposed by (Newman, 1992), (Breit, 1991) for the series evaluation since the convergence is low for reduced underkeel clearances.

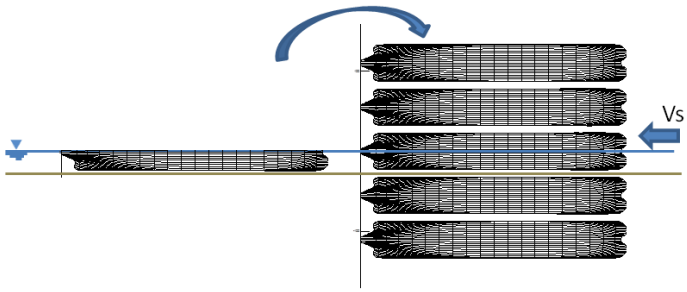

Figure 18 - Source mirror technique for basis flow computation.

The widely known transient Green function (Wehausen, et al., 1960) is applied for the wave-body interaction during the first order radiation and diffraction potential computations, as shown in (17). The evaluation of the Green function is performed using the auto-function expansion proposed by (John, 1949) combined to the algorithms presented in (Li, 2001), (Newman, 1985), (Liu, et al., 2015) and (Guha, et al., 2016) according to the ratio R/h ($R = \sqrt{(x_i - x_j)^2 + (y_i - y_j)^2}$ and h the mean water depth).

$$G_{ij} = \frac{1}{r_{ij}} + \frac{1}{r_{ij}'} + 2PV \int_0^\infty \frac{(\mu + K)\, exp(-\mu h)\, exp(-\mu h)\, cosh\left(\mu(z_j + h)\right) cosh\left(\mu(z_i + h)\right)}{\mu\, sinh(\mu h) - K cosh(\mu h)} J_0(\mu R) d\mu \qquad (17)$$

$$+ \frac{i2\pi(k + K)\, exp(-kh)\, sinh(kh)\, cosh\left(k(z_j + h)\right) cosh\left(k(z_i + H)\right)}{Kh - sinh^2(kh)} J_0(kR)$$

The solution of the so-called radiation and diffraction problems together with the basis flow potential solution provides the added mass, wave damping and excitation forces acting in the ship for each specific regular wave. The RAOs are obtained applying *(18)*, where $\omega_e = \omega - kV_s \cos\theta$ is the encounter frequency (ω is the wave frequency, V_s is the vessel speed, k the wave number and θ the wave direction, [M] is the generalized physical mass matrix, [A] are the added mass matrix, [C] is the external damping, [B] the potential damping, [K] the hydrostatic stiffness matrix, $\{F^{(1)}\}$ is the generalized excitation force vector and $\{X\}$ is the RAO in 6 degrees of freedom.

$$\{-\omega_e^2([M] + [A]) + i\omega_e([C] + [B]) + [K]\}\{X\} = \{F^{(1)}\} \qquad (18)$$

The validation of the RAOs are performed in model scale in wave basins or towing tanks following the International Towing Tank Conference (ITTC) guidelines, some examples are the active absorption wave basin of the Numerical Offshore Tank and IPT towing tank in Brazil. A comparison between numerical and experimental RAOs obtained for several wave frequency and wave directions, without forward speed, can be seen in Figure 19 for a large tanker considering the heave degree of freedom. The points in the figure are the experimental measurements including an error bar while the continuous lines are the numerical computations. The wave incidence orientation is 0º for following seas, 90º for beam seas starboard and 180º for head seas.

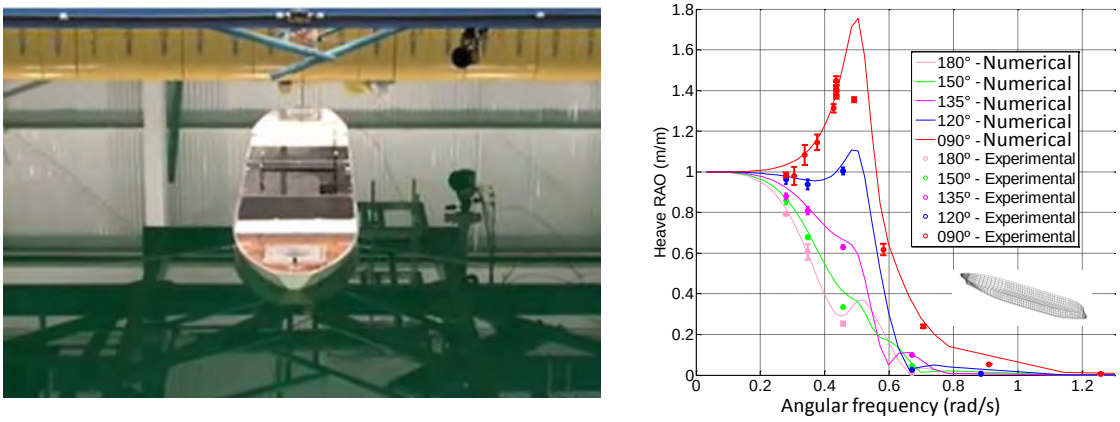

Figure 19 - Example of RAO comparison considering wave basin test and numerical computation for a large tanker.

Since in the potential theory the viscous damping effects are neglected an external damping shall be included, mainly in the roll degree of freedom to provide more realistic results. Several studies have been performed in the last 40 years to provide a consistent approach to compute this effect, see for instance (Ikeda, et al., 1976), (Ikeda, et al., 1977), (Ikeda, et al., 1977), (Ikeda, et al., 1978), (Himeno, 1981) and (Ikeda, 1982). The roll damping prediction in harsh environmental conditions and irregular sea states still a challenge, which is even more complex in shallow waters due to the small gap between the ship and seabed, that affects the vortex shedding pattern. An illustration of vorticity for several roll amplitudes of a crude oil carrier in deep water can be seen in Figure 20, where it can be verified the difference in vorticity pattern. In the absence of measured data or Ikeda's prediction method a conservative 5% critical damping may be considered.

5º 7º 10º

Figure 20 - Example of the vorticity field in the roll motion of a crude oil carrier under regular waves for several roll angles.

The heave, roll and pitch motions are combined to provide the vertical motion of each point presented earlier using (19), where (x_p, y_p) are the coordinates of each point and $X_k(\omega, \theta, V_s)$ (k=3,4,5) are the complex RAOs.

$$RAO_{zp}(\omega, \theta, V_s) = X_3(\omega, \theta, V_s) + X_4(\omega, \theta, V_s)(y_p - y_{CG}) - X_5(\omega, \theta, V_s)(x_p - x_{CG}) \quad (19)$$

The ship responses are evaluated based on the spectral moments computed for each sea-state in the several sections of the access channel according to (20), where $S_{\zeta i}(\omega_e, \theta)$ is the directional sea spectrum at section i.

$$m_{npi}(V_s) = \int_0^{\infty} \int_0^{2\pi} \omega_e^n(\omega, \theta, V_s) \left| RAO_{zp}(\omega, \theta, V_s) \right|^2 S_{\zeta i}(\omega, \theta, V_s) d\theta d\omega \quad (20)$$

The directional sea spectrum measured using the wave buoy is transferred using up to 27 bins or using the Fourier coefficients of energy distribution in terms of direction for each wave frequency. Due to the inherent multidirectional sea state conditions generated offshore, several ports in Brazil are exposed to multidirectional sea state conditions, mainly the ones outside bays. The sea spectrum changes in shallow water due to the bottom friction, refraction and other effects, acting differently according to the frequency and direction.

An example of this phenomenon is illustrated in Figure 21 for an exposed port in Brazil, where it can be verified that in the outer section of the access channel there are two different main sea components from east and south, while in the middle section the energy from south has been almost dissipated.

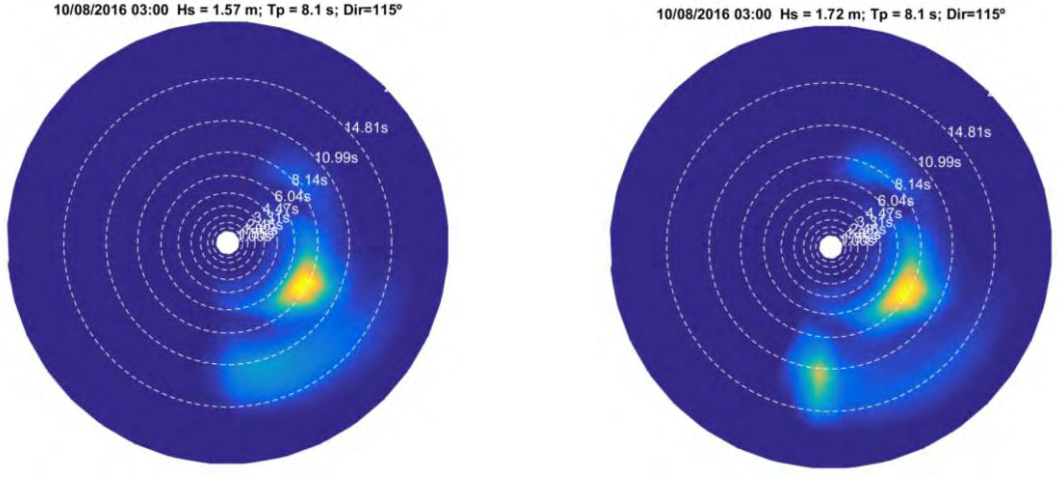

Middle section Outer section

Figure 21 - Example of sea spectrum in the outer section and middle section of an access channel.

The complex nature of the Brazilian coast does not allow a simple parametric sea spectrum based only on significant wave height, peak period, wave direction and spread factor to describe the wave energy distribution properly in several locations. In several cases the parametric sea spectrum approach may identify a higher peak period due to wind influence or some wave components, neglecting wave energy in low wave frequencies (high periods).

An example of comparison regarding significant wave height and peak period for a port located in the northeast region of Brazil, considering the measured data (with a single peak period output) and numerical results regarding the two main partitions of the directional sea spectrum obtained using a watershed technique can be seen in Figure 22. It can be verified that according to the energy distribution (significant wave height) the wave buoys output alternates between the first and second partitions peak period identification, although there are no appreciably modifications in the sea state. In fact, when the second partition is not present anymore the wave buoy measurement and numerical simulation identify the same peak period with a good accuracy. The analysis of one year of wave data provides that about 85% of the records contain more than one partition.

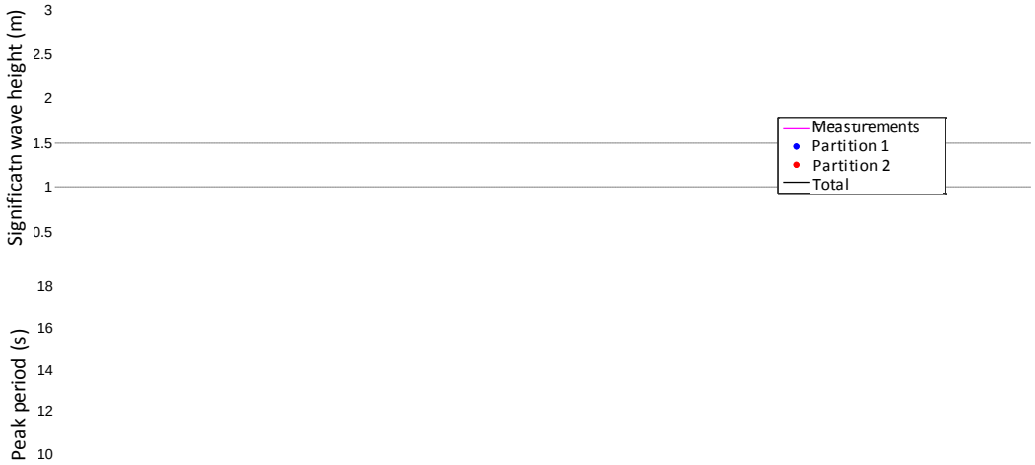

Figure 22 – Example of significant wave height and peak period measured with a wave buoy with a single peak period output and the numerical simulations for a port located in the northeast region of Brazil.

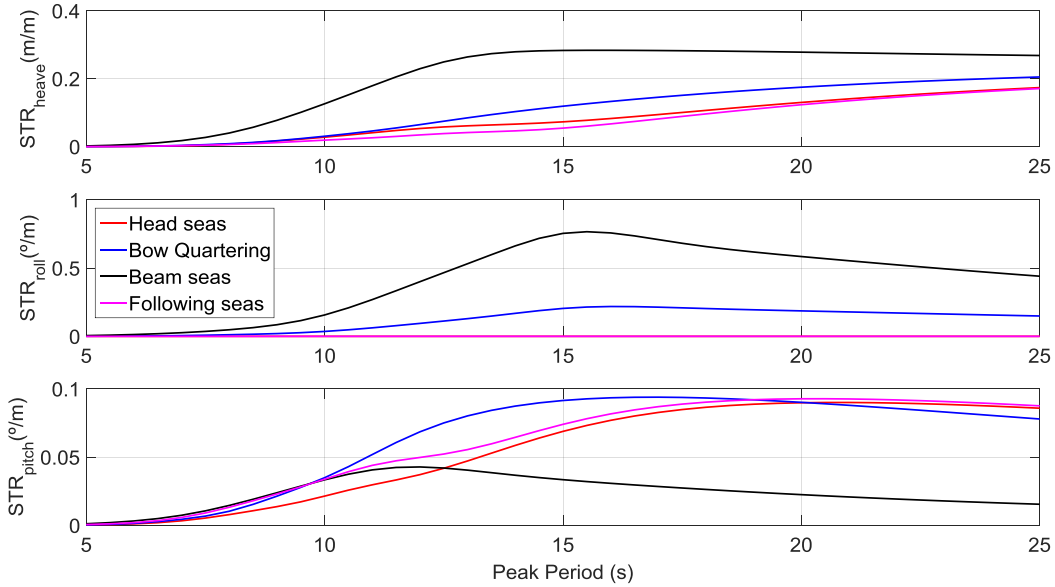

Figure 23 - Example of numerical computation of Short-term responses (STR) for several peak periods of a Very Large Ore Carrier at 8 knots under several wave incidences for standard Jonswap sea spectrums.

However, since large vessels are susceptible only to wave energy in higher periods, a simplified sea spectrum description would provide unsafe vessel motion predictions when identifying the lower peak period, motivating the use of the full directional sea spectrum in the vessel motions prediction. The short term responses regarding heave, roll and pitch motions for several peak periods and wave incidences computed numerically for a very large ore carrier at 8 knots of forward speed can be seen in Figure 23, where the variation of vessel responses according to peak period may be verified, as the influence of wave direction.

The measured data is extrapolated to the other sections of the channel based on the numerical propagation model after the appropriate calibration and validation procedure. The application of ANN (Artificial Neural Network) technique for energy adjustment in the sea spectrum is applied to improve the wave condition extrapolation and forecast more accurately.

The sea spectrum is transformed from the fixed reference to the ship one based on the encounter frequency spectrum as proposed in (Lewis, 1988). Some modification shall be performed to include the shallow water effect, as shown in *(21)*, with the dispersion relation for shallow water given in (22). The derivative of wave number according to wave frequency is evaluated using the implicit differentiation method.

Since the computations are performed considering the directional sea spectrum, for each wave frequency and wave direction a different encounter frequency is obtained, which shall be considered very carefully from the computational point of view, mainly under following sea condition, where there is not an unique solution between the wave frequency and encounter frequency.

$$S_\zeta(\omega,\theta,V_s) = \frac{S_\zeta^*(\omega,\theta)}{\left|1-\frac{dk}{d\omega}V_s\cos\theta\right|} \quad (21)$$

$$\frac{\omega^2}{g} = k\tanh(kh) \quad (22)$$

The maximum motion of each point located in the ship bottom is computed using (23) assuming the vessel motions as a Gaussian process, thus the amplitude of the motion as a Rayleigh distributions (Ochi, 1998). The bandwidth factor $\epsilon = \sqrt{1-\frac{m_{2pi}^2}{m_{0pi}m_{4pi}}}$, t is the exposed time and the period between ascendant zeros is $T_{zp} = 2\pi\sqrt{\frac{m_{0pi}}{m_{2pi}}}$.

$$\Delta z_{wave,pi} = 2\sqrt{m_{0pi}}\sqrt{\frac{1}{2}ln\left(\frac{2\sqrt{1-\epsilon^2}}{1+\sqrt{1-\epsilon^2}}\frac{t}{T_{zpi}}\right)} \quad (23)$$

The maximum vertical motion is combined to the probability of bottom touch to obtain the maximum safety draft for the maneuver.

INTEGRATION OF THE VARIABLES

In the forecast model the wave, current, wind and tide level predictions at each section of the channel are applied into the prediction of the underkeel clearance or maximum safety draft for the maneuver. If the tide window shall be predicted for a pre-established draft the computation is simpler because the ship model is invariable. On the hand, for the maximum safety draft prediction, the ship modelling shall change according to different possible loading conditions.

Regardless the analysis performed there is always an error between the predicted environmental condition and the “real” condition acting during the maneuver since there are several complex phenomena to be modelled. Although the best efforts are made during the calibration process and a good precision may be achieved, the accuracy of some extreme meteorological tides or harsh wave conditions may be a problem. Moreover, there is a lag between the measured data received and the “actual” environmental condition during the maneuver. In order to handle this fact, some allowances

curves are created based on the data applied during the validation phase of the hydrodynamic/wave propagation model in order to evaluate the probability that the environmental conditions is different of the predicted one.

An example of the difference between the numerical prediction of significant wave height and the measured one can be seen in Figure 24. This probability curve is discretized in several different ranges and for each one the probability of bottom touch is evaluated. The same procedure is performed for ship velocity and water level prediction, the former based on ship velocity records presented earlier for the several sections of the channel.

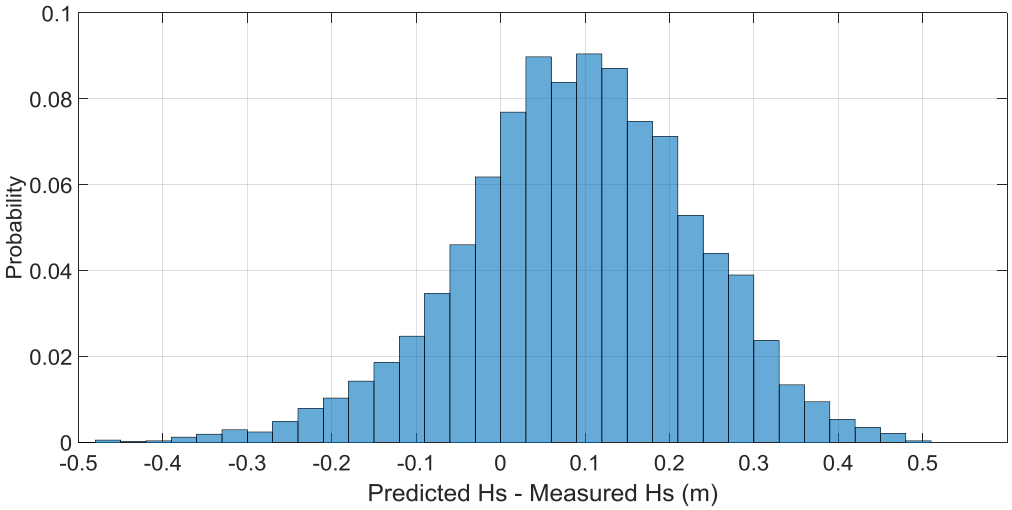

Figure 24 - Example of error probability distribution of the difference between the predicted significant wave height and the measured one.

The net ukc is defined according to (PIANC, 1985), as what is left after the summation of the several effects presented earlier, and it is computed based on (24).

$$net\ ukc_{i,p} = h_i + \Delta h_i - \Delta z_{wind,pi} - \Delta z_{dyn,pi} - \Delta z_{wave,pi} \qquad (24)$$

Since several quantities are changing during the maneuver the probability of bottom touch is computed using ***(25)***, which is the complement probability of the no bottom touch probability in any section of the channel, where Δt_i is the time of navigation in section i and $P\left(net\ ukc_{i,p} \leq 0\right)$ is the probability of bottom touch of the point p in section i of the channel, which is equal to the probability that the wave response to exceed the net ukc under a specific water level, ship speed and wave condition times the probability of cooccurrence of this condition. The continuous version of this expression can be found several references, for instance (Krogstad, 1985) and (Ochi, 1998), and it is applied since it is more convenient from the computational point of view.

$$P\left(net\ ukc_p \leq 0\right) = \left\{1 - \prod_{i=1}^{n}\left[1 - P\left(net\ ukc_{i,p} \leq 0\right)\right]^{\frac{\Delta t_i}{T_{zi,p}}}\right\} \qquad (25)$$

The acceptance criteria for a soft bottom seabed is defined as: the net underkeel clearance shall be at least 0.5m for the average predicted environmental condition; the maximum bottom probability must be less than 10^{-2}; the average probability of bottom touch must be less than 10^{-4}; the maneuverability margin (without wave motions) shall be satisfied in all sections.

In the real time mode the “GO” or “DO NOT GO” decision is performed based on the environmental condition parameters. If these parameters are in the range of the allowance curves presented earlier the decision is “GO”. If they are not, the maneuver is postponed to guarantee the safety until the parameters is the pre-established ranges.

Nowadays the cloud computing provides a large computational capacity and the data transfer of the monitoring system is very robust, as the internet access in several platforms. The measured metocean data (from wave buoys, tide gauge, anemometer and adcp) are downloaded from a specific ftp and the

maneuvering information are provided by the pilot's datacenter using a standard "xml" format. The computations are performed in the cloud and the outputs format and platform may be customized according to the user preferences, as illustrated in Figure 25. Since different users may require different data, a single database is managed in the cloud to provide each user with the required information. The underkeel clearance computation, best predicted window and metocean data is available for all users with different levels of complexity (e.g: directional sea spectrum data, two partition sea spectrum or single partition information).

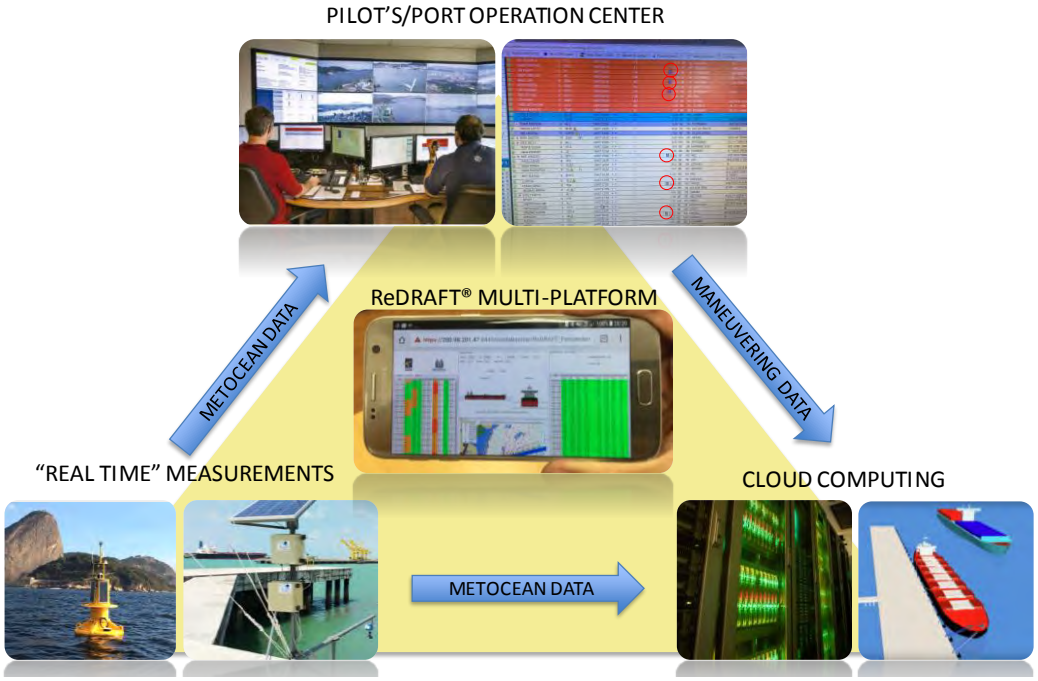

Figure 25 – ReDRAFT® integration of metocean data and maneuver list.

RESULTS AND CONCLUSIONS

The system has been operational since 2015 in Santos Port, the largest one in Latin America with 62 berths and it receives vessels with draft up to 14.2m under favorable environmental conditions. A total of approximately 5000 ships are maneuvered in the port annually. The port is located in São Paulo state and is responsible for almost 30% of the international trades in goods, being, therefore, very important for the country economics. The system was developed in partnership with the Numerical Offshore Tank (TPN) of University of São Paulo and Santos Pilots Association in order to provide more safety and efficiency to the port due to the increase of maneuvers with larger vessels, specially the 336m container ship class. Besides the port is located inside a bay with a huge siltation rate, which may achieve up to 10 cm/month in some parts of the access channel if no maintenance dredging is performed.

The results of 515 critical maneuvers monitored during the years of 2016/2017 are presented in Figure 26, where the blue bars represent cases where the dynamic draft is larger than the static one, providing more efficiency in terms of waiting time. On the other hand, the red bars represent cases where the static rule is not enough to provide navigation safety and a reduction in ship draft is proposed. It can be verified that the ReDRAFT® system can increase both efficiency and safety of the port, which could be also verified based on the downtime of the port due to draft restrictions, which was reduced in almost 50% comparing the years of 2015 and 2016. The results are even better because during this period the number of maneuvers with larger vessels increased almost 20%.

The system awarded the ANTAQ prize together with Santos Pilots C3OT due to the contribution to navigation safety and efficiency of the port.

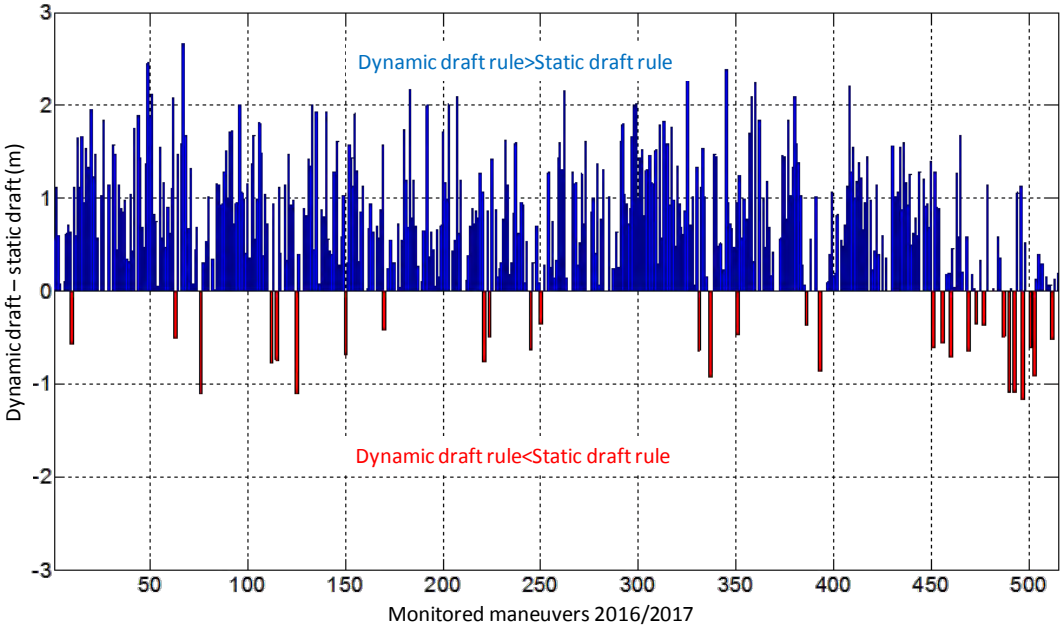

Figure 26 - Comparison of dynamic draft computed by ReDRAFT® and the static draft for critical maneuvers in Santos port.

The system has been extended to Rio de Janeiro Port for containerships, where a validation campaign is being performed together with Rio de Janeiro pilots and containers terminals. The results for 312 observed critical maneuvers can be seen in Figure 27 considering different ship speeds. It can be verified that in some cases a reduction in the draft would be suggested to provide more safety for navigation. However, in most of the cases an increase in ship draft would provide more efficiency without comprising safety.

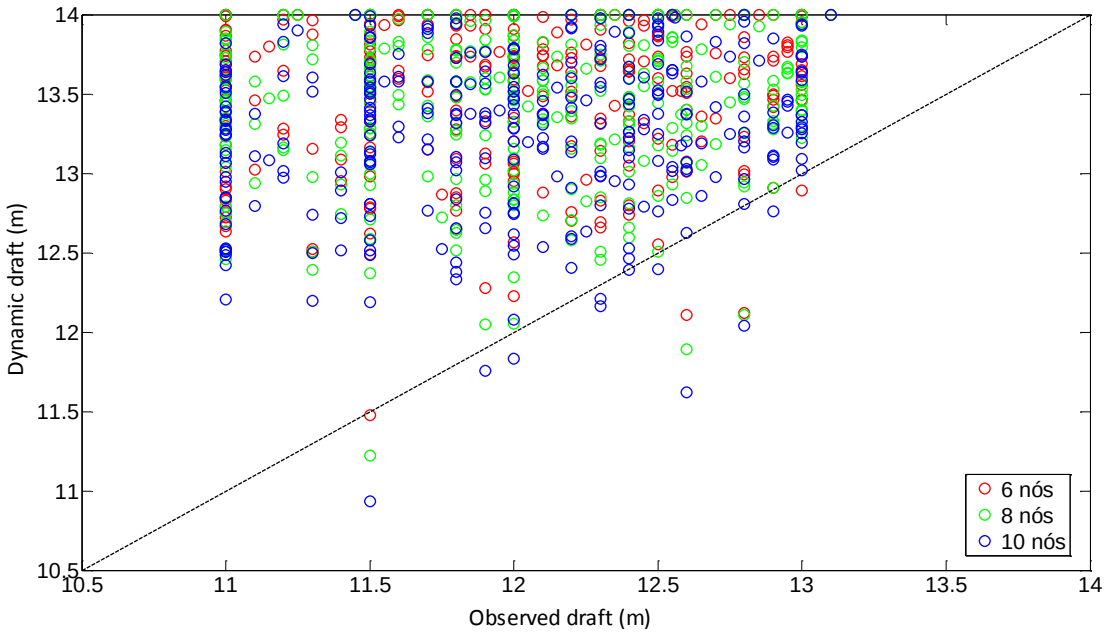

Figure 27 – Comparison of dynamic draft computed by ReDRAFT® and the observed draft for container ship maneuvers in Rio de Janeiro port.

ACKNOWLEDGMENTS

The authors thank the Santos and Rio de Janeiro Pilots for their valuable advices and practical experience during the development. Third and fourth authors thank the National Council for Scientific and Technological Development (CNPq) for the research grant.

REFERENCES

ANTAQ Setor Portuário Nacional. Audiência: Comissão de serviços de infraestrutura. [Relatório]. - Brasilia : [s.n.], 2015.

Bertram Volker Practical Ships Hydrodynamics [Livro]. - 2000.

Blendermann W. Parameter Identification of wind loads on ships [Periódico] // Journal of Wind Engineering and Industrial Aerodynamics. - 1994. - Vol. 51. - pp. 339-351.

Breit S. R. The potential of a Rankine source between parallel planes and in a rectangular channel [Periódico] // Journal of Engineering Mathematics. - 1991. - Vol. 25. - pp. 151-163.

Faltinsen Odd Sea Loads on Ships and Offshore Structures [Livro]. - Cambridge : Cambridge University Press, 1990.

Guha Amitava e Falzarano Jeffrey The effect of small foward speed on prediction of wave loads in restricted water depth [Artigo] // Ocean Systems Engineering. - 2016. - pp. 305-324.

Himeno Y. Prediction of Ship Roll - State of the Art [Relatório]. - Michigan : Dept. of Naval Architecture & Marine Engineering, 1981.

Huuska O. Report Vol 9 - On the Evaluation of Underkeel Clearances in Finnish Waterways [Relatório]. - Helsinki University of Technology. : [s.n.], 1976.

Ikeda Y. [et al.] On Roll Damping Force of Ship. Effects of Hull Surface Pressure Created by Bilge Keels [Periódico] // Journal of the Kansai Society of Naval Architects. - 1977. - Vol. 165. - pp. 31-40.

Ikeda Y. Prediction Method of Roll Damping [Relatório]. - [s.l.] : University of Osaka, 1982.

Ikeda Y., Himeno Y. e Tanaka K. Components of Roll Damping of Ship at Forward Speed [Periódico] // Journal of the Society of Naval Architects. - 1978. - Vol. 143. - pp. 121-133.

Ikeda Y., Himeno Y. e Tanaka K. On Eddy Making Component of Roll Damping Force on Naked Hull [Periódico] // Journal of the Society of Naval Architects. - 1977. - Vol. 142. - pp. 59-69.

Ikeda Y., Himeno Y. e Tanaka N. On Roll Damping Force of Ship. Effects of Frction of Hull and Normal Force of Bilge Keels [Periódico] // Journal of the Kansai Society of Naval Architects. - 1976. - Vol. 161. - pp. 41-49.

IMO - International Maritime Organization GUIDELINES FOR VOLUNTARY USE OF THE SHIP ENERGY EFFICIENCY (EEOI) - MEPC.1/Circ.684 [Relatório]. - London : [s.n.], 2009.

IMO - International Maritime Organization RESOLUTION MSC.267(85) [Relatório]. - 2008.

International Hydrographic Organization IHO Standards for Hydrographic Surveys. - [s.l.] : International Hydrographic Bureau, 2008.

Isherwood R. M. Wind resistance of merchant ships [Periódico] // Transactions of the Royal Institution of Naval Architects. - 1972. - Vol. 114. - pp. 327-338.

John F On the motion of floating bodies I [Periódico] // Pure Applied Mathematics. - 1949. - pp. 13-57.

Journée J. M. J. e Massie W. W. Offshore Hydromechanics [Relatório]. - [s.l.] : Delft University, 2011.

Kristensen H. O. Determination of Regression Formulas for Main Dimensions of Tankers and Bulk Carriers based on IHS Fairplay data [Relatório]. - University of Southern Denmark : [s.n.], 2012.

Kristensen H. O. Statistical Analysis and Determination of Regression Formulas for Main Dimensions of Container Ships based on IHS Fairplay Data [Relatório]. - University of Southern Denmark : [s.n.], 2013.

Krogstad Harald E Height and period distributions of extreme waves [Artigo] // Applied Ocean Research. - 1985. - pp. 158-165.

Lackenby H. On the systematic geometrical variation of ship forms. [Periódico] // Trans. of INA. - 1950. - Vol. 92. - pp. 289-316.

Lewis E. V. Principles of Naval Architecture - Volume III - Motions in Waves and Controllability [Livro]. - 1988.

Li Lin Numerical Seakeeping Predictions of Shallow Water Effect on Two Ship Interactions in Waves. - Halifax : Doctor of Philosophy - Dalhousie University, 2001.

Lindeen C. Wind Resistance Generated by Containers on Reefer Vessels [Livro]. - Stockholm : Master thesis, 2008.

Liu Yingyi, Iwashita Hidetsugu e Hu Changhong A calculation method for finite depth free-surface green function [Artigo] // International Journal of Naval Architecture and Ocean Engineering. - 2015. - pp. 375-389.

Mei Chiang C., Stiassnie M. e Yue Dick K.-P. Theory and applications of ocean surface waves. Part 1: Linear Aspects [Livro]. - [s.l.] : World Scientific, 2005.

Newman J. N. Algorithms for the free surface Green function [Artigo] // Journal of Engineering Mathematics. - 1985. - pp. 57-67.

Newman John Nicholas Marine Hydrodynamics [Livro]. - [s.l.] : MIT Press, 1977.

Newman John Nicholas The Green function for potential flow in a rectangular channel [Periódico] // Journal of Engineering Mathematics. - 1992. - Vol. 26. - pp. 51-59.

Ochi Michel K. Ocean Waves: the stochastic approach [Relatório]. - [s.l.] : Cambridge University Press, 1998.

PIANC Report n. 121 - Harbour Approach Channels Design Guidelines [Relatório]. - [s.l.] : The World Association for Waterborne Transport Infrastructure, 2014.

PIANC Report nº121 - Harbour Approach Channels Design Guidelines [Relatório]. - Bruxelles : [s.n.], 2014.

PIANC Underkeel clearance for Large Ships in Maritime Fairways with hard bottom (Bulletin Nº51). - Bruxelas : [s.n.], 1985.

Ruggeri F. [et al.] On the development of a higher order time-domain Rankine panel method for linear and weakly non-linear seakeeping computations [Periódico] // Journal of the Brazilian Society of Mechanical Sciences and Engineering. - 2018. - Vol. 40. - p. 70.

Ruggeri F. A Higher Order Time Domain Panel Method for Linear and Weakly Non Linear Seakeeping Problems.. - São Paulo : [s.n.], 2016.

Ruggeri F. A Time Domain Rankine Panel Method for 2D Seakeeping Analysis. - São Paulo : [s.n.], 2012.

Schneekluth H. e Bertram V. Ship Design for Efficiency & Economy [Livro]. - 1998.

Tannuri E. A. [et al.] Modular Mathematical Model for a Low-Speed Maneuvering Simulator [Artigo] // Proceedings of the ASME 2014 33rd International Conference on Ocean, Offshore and Arctic Engineering. - 8-13 de June de 2014.

WAMIT Inc WAMIT USER MANUAL 7.2 [Relatório]. - 2015.

Wehausen John V e Laitone Edmund V Surface Waves in Fluid Dynamics III [Seção do Livro]. - 1960.

Yamano T. e Saito Y. An Estimation Method of Wind Force Acting on Ship's Hull [Artigo] // Journal of Kansai Society of Naval Architects. - 1197.

Yilmaz H. e Guner M. An Approximate Method for Cross Curves of Cargo Vessels [Livro]. - 2001.

CONTAINER TERMINAL PLANNING TOWARDS OPTIMIZING SUPPLY CHAINS LOGISTICS

ENG. KLIMANN, INGRID MARIA[1]

Abstract

Supply chains need competitive and efficient container port terminals that are up to the challenge of the dynamic cargo flows passing through them. Consequently, port terminal planning and its associated engineering strategies are the tools that let them achieving high operational competitiveness and leadership for any possible complex situation on land and on water side.

Furthermore, it is important to stress that each container terminal presents restrictions due to the geography where it is located. These site conditions can either influence the available operational areas or the connections to the hinterland resulting in potential inefficiencies for the supply chains that they support.

Thereafter, the following analysis focuses on solutions developed by container terminals located on the riverbanks of the City of Buenos Aires and its neighbouring Dock Sud, both located upstream of the River Plate estuary in Argentina.

This paper elaborates on how port terminal planning is implemented in a practical way, and under complex scenarios, to develop efficient operational management strategies towards designing all logistic processes and cargo flows from the containerships to the delivery out of the terminal and on the other way around. To summarise, it can be concluded that appropriate port terminal planning allows the integration of various value-added services to enable a container terminal to be developed as a multimodal operations platform serving and optimising supply chains logistics that cross it.

1. THE CONNECTION BETWEEN THE TERMINAL AND THE SUPPLY CHAINS LOGISTICS

Everyday thousands of merchandising cross a port terminal through the supply chains that they belong to. Nowadays, the competition is between the supply chains and not the products like it used to be. So if a company wants to be competitive and remain in the world markets it is necessary to have dynamics flows in this supply chains.

Although the ports are one node in this process it is important to give a full support to the chain and guarantee efficiencies avoiding scraps. The ports play a major role being the interface between the waterside and the hinterland transport.

To make this possible, it is required to have a productive business model in the terminal. The main activity that aloud this, is the planning engineering strategies in the yard.

Therefore, having an efficient design of the planning strategies permit that this flows of containers movements stay in the yard the shortest time and goes to the vessel, trucks or train as soon as possible. With this, it is obtained a dynamic model that impact on the speed of the supply chains.

The port terminal should emphasise to develop as a multimodal operations platform giving in this way support to the supply chains. Thus the terminal helps optimizing part of the supply chains logistics.

Working in this develop allow the terminal to add-value to the products and this gives to the region the possibility to develop their economies in short, medium and long-term. This integration is useful not only for the market but also for the society too. Gives the possibility to develop in long-term better life conditions to its.

[1] Exolgan Container Terminal, Planning Operations Department, ingridklimann@hotmail.com

2. MAKING A CONTAINER TERMINAL A CASE OF SUCCESS

Ports terminal main mission is to be as efficient as possible and having high levels of production. What this means is to have the best combination of the production factors, being efficient with the machines, workers, customers, suppliers and environment. Hence, the terminal have to agree with individual demands of each stakeholder. Are part of this, the shareholders, workers, customers, suppliers, residents, government and unions. This topics made the terminal to work in develop planning strategies to optimize times and spaces; is part of the business to operate the vessel in a productive way and fulfil the indicators between the terminal and the shipping company. The strategies must go with production quay and yard indicators. Having and adequate layout design allow a good optimization of the space and aid to order the containers distribution in the yard.

To focus on operational excellence it is necessary to know the production capacity of each process involve. This means to balance the system capacity and avoid bottlenecks. Bigger ships generates a demand concentration, and the planning design engineering strategies should remove peaks and transform in an equal demand. The system is made by the customer demand, the gates, yard and berth capacity, the human and the equipment resources, all together for a certain service level.

Besides, hundreds of customers go through the terminal every day to pick up the import container and the empty ones to consolidate products, and leave the full containers for the exportation process.

Making all this process possible and in an efficiently way reach the terminal to have a competitive business model and put it at the vanguard. With these engineering solutions takes the region to better market economies.

3. KNOWING THE SCENARIO RESTRICTIONS WHERE THE STRATEGIES ARE APPLIED

Since 1700 different areas bordering Buenos Aires City where used as a port. The later develop of the city was always concentrated here, all the connections to other parts of the country where made by train or wagon from here. Port terminal final design was made by Eng. Luis A. Huergo on the riverbanks of Buenos Aires City and afterwards it was created the terminal in the neighbouring Dock Sud. It is important to mention the first restriction that appears here, the original quay design by Huergo is used nowadays. This consist in a finger piers design that were useful for the cargo vessel, but now for the containers ones brings restrictions to administrate the cranes and the services[2]. Dock Sud port terminal doesn't have this restriction, because it was conceive in a period were the containers vessels exists and it was design with side continuous berths. Although, in returns, a quay of a chemical industry operates in front of it restricting the breath of the vessels that the terminal can attended.

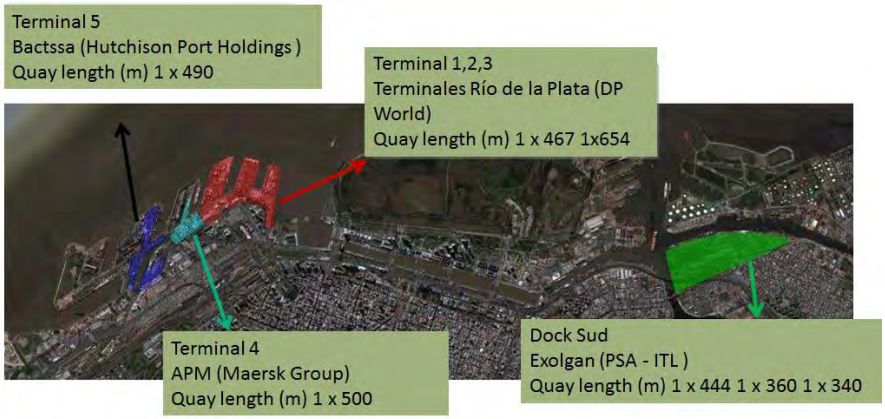

Figure 1: Buenos Aires and Dock Sud Port Terminals plan

[2] Nowadays the Government Port Administrations had present the new construction design plan with side continuous berths.

Actually, different industries that used the port are located in a radius of 80 km, the bigger part (80%) of the origin-destination of the products belongs for this distance. That's made ports terminal that in certain time slots the truck congestion increase. This situation put the terminals in a complicated place, because they can't develop in another place and have to give a high service to all the parts. Here is concentrated the industry and the logistics centres that serves all the country.

Current restrictions that makes planning engineering a big solution

- Depth restrictions: Currently the River Plate presents an available draft of 34 feet (using tidal windows) and where navigational channels must be permanently dredged. This aspect limit the quantity (Q) that a vessel can transport and it wouldn't be possible to take to the market more than the maximus number that the vessel can support with this depth.
- Breadth of the channel: the Access Chanel to Buenos Aires Port is 100 m of breadth. The operative dimension that Buenos Aires Port terminals are design for is a New Panama Vessel, with a capacity of 12,500 TEU and 366 x 49 x 15, 2 meters -*these vessels enter the port but not complete, as indicated in the previous paragraph*-.
  Bottom of the channel: two of the biggest ships that arrive to the port can´t navigate in one way or another the channel. Prefecture[3] only allows for security and safety one type of this vessel at a time. This made that if the terminal has to attend more than one service one ship will wait in the common area until the other cross the channel. Just from the 27, 5 km from La Plata to Buenos Aires two New Panama Vessel can transit at the same time.
  Another problem is that the passengers vessels use the same channel to navigate, and they have exclusiveness of channel, so this increase the cost of ship waiting to be attended.
- Customs times: approximately the 40% of the exportations must be scan and control because of Customs´ Office regulation, while in many parts of the world, like Chile, USA, the percentage is the 5%. This made to attend the freight with all the resources preventing to roll it to another vessel and increase the cost of the product for the customer. In addition, all the documents that must be present to evacuate the containers impact in the flows of the terminal because if the trucks congestion.
- The existence of 2 common areas to take trailer: this made more expensive the vessel cost, so the final impact will be in supply chain. The first part begin when the vessel arrives to Recalada Pilot Station, here a coast-pilot takes control up to La Plata where another coast-pilot finish the navigation. It takes 8 hours from Recalada to La Plata waiting area and 3 more navigation hours from La Plata to Buenos Aires Port.

Figure 2: Map of the sections to take trailer and TEUs capacity of the terminals in the zone

[3] In Argentina, Prefecture is the militarized police force that governs navigation, both in rivers and seas.

- Empty administration: in the total TEUs movements of Buenos Aires Port the 50% belongs to importations and the other 50% to exportations, but the 40% are products and the other 10% empty containers. So this makes the terminal to prepare a place in the yard for the evacuation, taking space for the full ones.
- Distance of the waiting area: when the ships arrives the waiting area is situated at 26 NM (48 km). The impact of this is that when a terminal couldn't attend more vessels, the finalization of one generate operational bumps. When it finish and leave the terminal, this has to wait up to the other ship begins navigation.
- Union force: the topic affect because in Buenos Aires Port live together more than five different forces. This made that any decision that has to be done must reach an agreement with each representative.
- Hinterland: Buenos Aires Port connexions have several problems to be cross. Even though the biggest part of the cargo distance is near the port, the saturation of the roadways, the lack of railways and the trucks condition made a considerable increase of speed in the supply chain. Therefore, the Port Terminal should take part on this to aid the supply chains.[4]
- Weather conditions: in the last times, a new meteorological phenomenon has appeared. The historical changes of atmospheric pressure that produce winds has increased because of the Climate Change, so now they get unpredictable: the fronts changes quickly and strong winds appear suddenly. This generates a dangerous operation with all the parts of the terminal. The equipment stops the work and the vessel could cut the mooring line. In this cases, the containers take down levels in the stowage to prevent risks.
- Goods production: It´s important to note that Argentina mainly exports products suitable for 20-foot containers (bulk cargo of high density), while it imports manufactured products in 40-foot containers, which generates an imbalance between the demanded and offered containers.
- Trains connections: Although in the past there were railway branches that served the port, for decades they had get deteriorated and are used eventually. The government is carrying out works to replace the railway in the port. As consequence, not even have been developed the twin container train system.

4. FUNDAMENTAL PLANNING PILLARS TO GET THE HIGHEST BUSINESS PRODUCTIVITY

Consequently, the different strategies that are used to let an efficiency and productive model will be develop. It should be point out, that the key to have successful strategies is the plan´s flexibility design. This suggests the need to consider continuous changes and to reply in a dynamic way, with this the model will guarantee an impact on the supply chain speed. If a change of plans happen a quickly solution appear.

Make planning process possible it´s need the support of a software; for this work it was used Navis (N4), but there are other ones that can be used too.

The first thing that will be design in the yard is the layout, the strategy should consider some parameters like: yard blocks to segregate importations, exportations, throughputs and transhipments containers, reefers power points, over dimension and IMDG containers, trucks garage and not in use machines. Then the information processing will allow to know exportations quantities per ports destinations by vessel services, getting this obtains an order in the yard.

EMPTIES CONTAINERS STRATEGIES

From the moment that an empty container is returned begins the supply chains organization. It´s important to administrate the trucks flow that will be in the hinterland. To make this possible it´s necessary the design of a web organiser to let customers choose a time slot to return the container. With this tool the terminal design the truck flow per hour. Besides, in the system can be added the line and the container type that will be given back. Empty container web administration, allow to the planning area take decision about the available space in the yard, for example to know how many space you will need to put reefers, 20' foot or 40' foot containers units. Buenos Aires Port have a relationship for 20'

[4] The new truck roadway construction had begun, this way is parallel to the port and the main purpose is to remove trucks from the city.

and 40' containers of 1:4. Meaning that per 1 x 20´ container its reception 4 x 40´ containers. As a result, the yard design should include more space for this type of container, this information is get from the analysing of the vessel discharge and the lack to fill exportations of add-value goods.
Once the trucks get in to the verification area, a qualify inspector classifies the container type, this mean to kwon if it´s or not: a reinforced, a food grade, standard, damage or special one. In the moment is charged in the system and process between the software and the gate decides the yard place to go. A part of this containers will go the empty exportation area near the vessel charges and the other segregate by type to deliver to customers. Having containers type in order allow a quick answer wen a trucks goes to the terminal and pick up empty containers.
Another important part in the process is the administration of reefers containers, these type have to be check and ready for the moment that they are pick up. A failed container could imply dead freight costs or loosing customer time when these are consolidate and doesn't work. In all these cases the impact is directly in the supply chains.
Sometimes the container terminal is the bridge between the customers and the shipping company, this means that the terminal should administrate the stocks and give a warehouse system. Thus, all the improvements given from the port terminal to the process will impact directly in the customers and as a consequence directly in the supply chains speeds.

EXPORT CONTAINER STRATEGIES

As mention above, the first strategy that will be design is where and how many containers should be found. It´s important to segregate by service and then by destination port. Having this planning design helps to optimize the vessel charge and to make as dynamic as possible.
The vessel planning doesn't depends on the port terminal, it comes design from the maritime company, some consideration can be change, but these defines that the terminal have to take this information and change into efficient business process. An important aspect is that the vessel charge by destination port. Depending on the volume of each port, the design shouldn't be close, if these is open to other yards blocks, at the charge moment it will let have a productive flow, optimizing the process. The resources gets a better use and have less no-operative time.
Small volume ports can share stowages, because their impact in the process is less than big ports, and space limitations is a very common aspect. However, the flexibility need, makes sometimes to put a container in a wrong stowage avoiding trucks contestation, what it consider here it make a later housekeeping.
When the customers begins the container exportation process first it important for the port terminal to have a coordination system, where they can choose a slot-time to enter to the terminal. This aids the terminal to balance flows with the client demand, affording to have an efficient combination of the productive factors, it will not receive more clients than the process can supply. The benefices here are not only for the terminal but also for the customers, the truck will not have delays, so it will attended more process for them, for example taking more containers per day optimizing the trip and of course the uses fuel.
Another two important parts that needs planning strategies are the VGM process and the scanner one. By international regulations all the charge have to be weight, the information should be process and sheltered giving traceability to the process. The item mention above defines the place to put the balance (it´s recommended near the gate-in) doesn't intercede with the other port flows. Other part, is the scanner, customs indicates what containers shall done the process. Here the impact is very high because in Argentina around the 40% of the charge must be scan, in other countries of the region like Chile or Brazil the percentage is around the 5%, this gives as result the place to located the scanner to prevent damage the efficiencies of other process. All this information obtain for the mention process is shield by the software and in case of need avoid doing two times the same process, in other words increases efficiency and let the container loading in the service hire preventing the possibility of losing the vessel.
The last part but not least, is in what yard blocks the terminal will receive the exportations containers. The best strategies, indicate that should be in the blocks near the gates-in, because the flow will be more dynamic with the trucks and will not interrupt with the vessel discharge process. Part of the yard

blocks flexibility is for example to use it for empty export containers in case that are not allow the empty yard blocks.
Therefore, using this engineering strategies will give as result efficiencies in the model.

IMPORT CONTAINER STRATEGIES

Once the discharged is processed -*this items depends on the maritime agency and gives the information to the port terminal*- begins the strategies used for this parts. It should be taken as considerations the discharge of over dimension and IMDG container, the terminal will have the information of quantities of 20´ and 40´ containers, to size the yard allocations need. Importations containers should use yard blocks near the quay, to reduce the truck time from the discharge up to the time to the stowage. Here happens a combinations of yard blocks, the strategy will use a combination of the terminal sites thus avoiding congestions, and other yard blocks wouldn't be used because they will destiny to the import delivery customers. The combination given have to support both process at the same time, the discharge and the delivery of full containers. Having clashing process generates inefficiencies that affect not only the terminals productivity but also the vessel one. And this is one of the factor that's differentiates a terminal from another giving a successful business model.
A strategy used here is to respect the combination discharge plan with the vessel service and the yards blocks, this gives a better combination for the limit dates that the containers should be deliver and the operation of the vessel. Depending the operation in the terminal a daily quantity it´s define for the delivery process, having this parts in time-slots provides an optimum resources combination.
Over dimension containers should be discharge in yard blocks far away from the principal process yard blocks, because the charge of its need special equipment, more time and appropriate trucks accompanied by a delivery in a minor time-slot.

5. FINAL CONSIDERATIONS FOR AN EFFICIENT PORT TERMINAL

All these individual strategies gives as result efficiencies on the different process. But definitely all the improvements given to the system impact directly in all the logistics of it, thus the supply chains get highly benefited, reducing death-times and getting dynamics flows helping without doubt to have competitive supply chains. The terminal is a main node for it, so given support, having operational excellence gives not only the business model but also in all the process that go thought it.

World fleet by principal vessel type, 1980–2017:

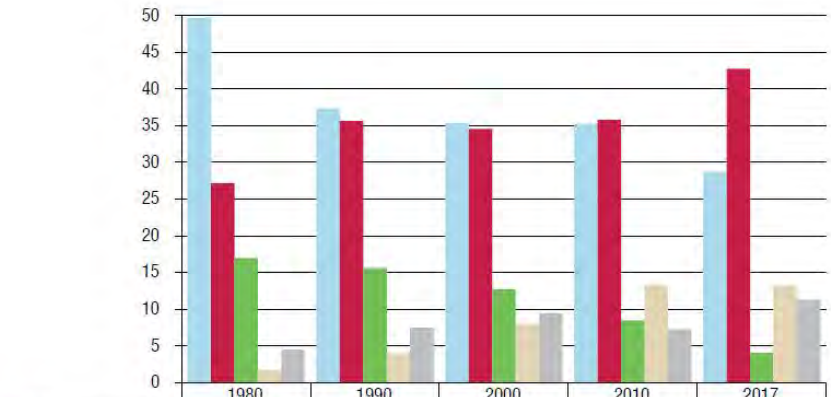

	1980	1990	2000	2010	2017
Oil tankers	49.7	37.4	35.4	35.3	28.7
Dry bulk carriers	27.2	35.6	34.6	35.8	42.8
General cargo ships	17.0	15.6	12.7	8.5	4.0
Container ships	1.6	3.9	8.0	13.3	13.2
Other	4.5	7.5	9.4	7.2	11.3

Figure 4: UNCTAD secretariat calculations, based on data from Clarksons Research and the Review of Maritime Transport

Density map of container ship movements:

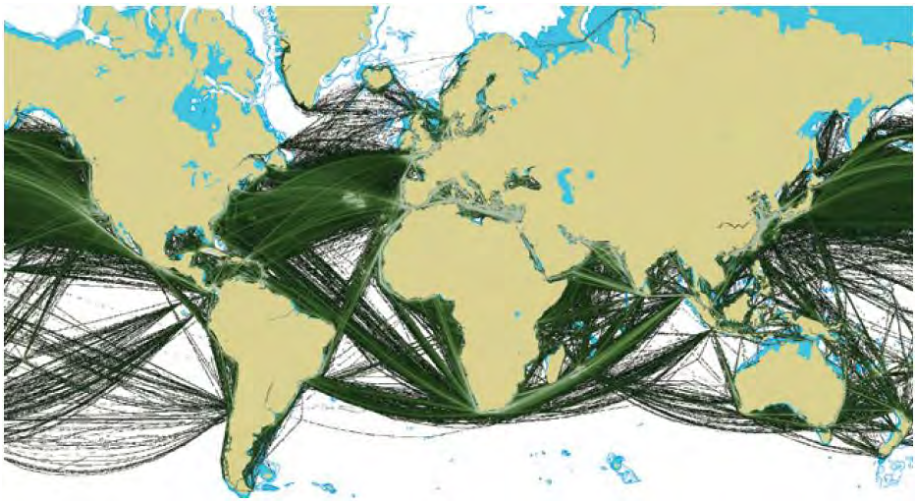

Figure 5: Prepared for UNCTAD by Marine Traffic. Data depict container ship movements in 2016

What is shown in the pictures before is the increasing container vessel trend, this is very important because when the port terminal can´t give a quick answer to infrastructure situations having design planning strategies gives the opportunity to optimise all the resources, including the utilization of the yard.
Each year, more goods use containers to be transport, so more supplies chains cross the ports terminals, giving the responsibility to made dynamic process avoiding death-times and inefficiencies.

KEY ASPECTS TO CONSIDER

A. Demand get concentrate in bigger ships, increasing stress port terminal situation, to prevent process clashing it´s necessary to flat the demand. For avoid variability process it should be work in:

- Having vessel berth windows.
- Having a coordination system with appointment hour for empty, import and export containers.
- Having expected connections with the parts of the logistics chains.

B. It should be calculated the capacities of each process to balance the working charge.

C. The tack time and the cycle of it should be well-known for the port terminal.

D. Simulations tools could be used to get better process and efficiencies.

E. Develop clear performance indicators to know the weak links and the bottlenecks of each process.

F. Have dynamic information flows with the stockholders.

G. Having decisions at the last moment.

H. Work with a resources pool to optimize them.

References:

[1] UNCTAD (2017). Review of Maritime Transport, New York and Geneva. ISBN 978-92-1-112922-9.

[2] Sánchez, Ricardo and others (2018). Latin America Infrastructures Inversions. CEPAL. ISSN: 1680-9025.

[3] Maritime and Port Yearbook 39° Edition (2017). Buenos Aires Port.

Expansion of Port Infrastructures

By Jens Kirkegaard[1], Kjeld Dahl Sørensen[2], Christian Vrist[3], Peter Ydesen[4]

1. INTRODUCTION

Ports on the Danish North Sea coast were built over the last 150 years to serve as basis for fishery and transport of goods between Denmark and UK and Norway. These ports were all constructed on sandy shores in a dynamic morphological setting. During the recent past the ports have been challenged by new demands for increased activity in other areas than the traditional fishery and related industries. The exploitation of oil and gas resources in the North Sea and development of offshore wind farms require good and safe port infrastructures. Also the increase in handling other commodities and international trade has added to the demand for expansion of the port infrastructures.

The present paper presents the challenges related to expansion of these ports, which were originally planned and constructed for less demanding purposes.

2. COASTAL CHARACTERISTICS OF THE DANISH WEST COAST

This section serves as basis for the descriptions of port infrastructures on the Danish West Coast.

The West Coast of the Danish peninsula Jutland faces the North Sea. The landscape was modelled during the glacial periods when ice covered north Europe. When the ice cover receeded, sand and clay were deposited, and created the low hilly landscape so characteristic for Denmark. Variations of the sea level after the latest glacial period in combination with isostatic rebound formed a number of islands, which today are seen as cliffs at several locations along the coast. Between these, the land increase formed a shallow coastline with bays. Subject to wind, waves and current the coast gradually turned into a mixed littoral cliff and dune coast. Larger bays and lagoons were cut off by naturally formed spits and sandy barriers.

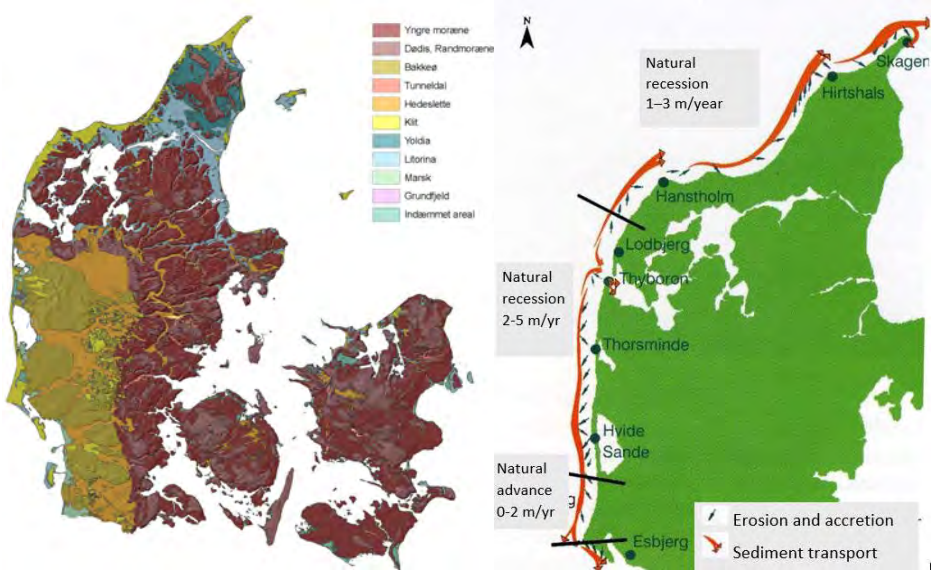

Figure 1: Geological map of Jutland (left) and map of littoral transport along the coast (right)

[1] Senior Consultant, DHI, Agern Alle 5, DK-2970 Horsholm, Denmark, Email: jkj@dhigroup.com
[2] Head of Technical Dep., Port of Esbjerg, Hulvejen 1, DK-6700 Esbjerg, Denmark, Email: kds@portesbjerg.dk
[3] Technical Manager, Port of Thyborøn, Tankskibsvej 4, DK-7680 Thyborøn, Denmark , Email: cvr@thyboronport.dk
[4] Technical Manager, Port of Hirtshals, Norgeskajen 11, DK- 9850 Hirtshals, Denmark, Email: p.ydesen@hirtshalshavn.dk

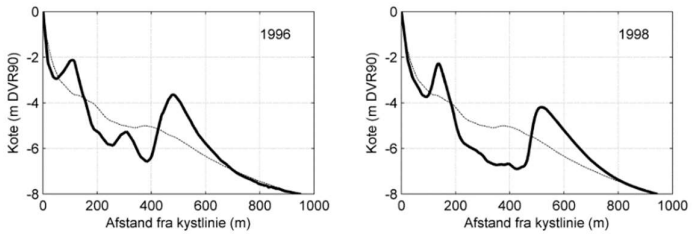

Figure 2: Typical barred profile of the central part of the coast

Over large stretches, the coast is almost linear and due to the strong wave action from the North Sea and resulting littoral transport, there are typically at least two bars along the coast. The 8 m depth contour is typically 900 -1000 m from the shoreline.

The geological map of Denmark, Figure 1, illustrates these features. The coast is in fact suspended between a number of hard points, typically cliffs composed of either hard clay or limestone. Some of the shallow stretches between the cliffs are severely exposed to the dominant west and northwest storms. In one particular location an inlet gives access to a natural waterway, the Limfjord, crossing the northern part of the peninsula.

The southern part of the Danish coast is part of the Wadden Sea, which also covers the coastal zone of Germany and The Netherlands. Here the morphology is governed by high astronomical tides – up to 1.9 m range - and storm surges, whereas the tides at the northern spit of Jutland is only about 0.4 m.

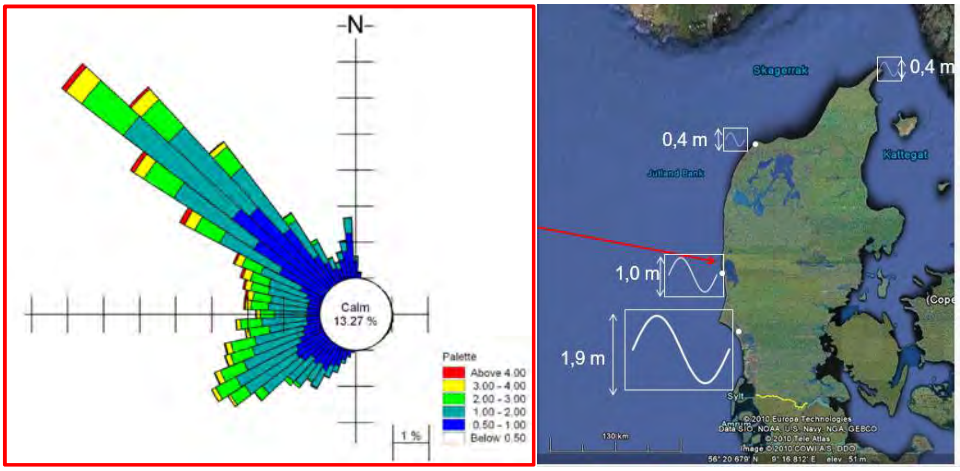

Figure 3: Waves and tides on the Danish West Coast

Winter storms are typically generated by low pressure centers moving over southern Scandinavia and often peaking with waves from northwest as shown by the wave rose above.

3. CHALLENGES FOR PORT DEVELOPMENT ON EXPOSED SANDY COASTS

Planning and construction of ports on exposed sandy coasts must consider the littoral processes, DHI (2017). This is the case for harbours on the open coast as well as for ports in tidal inlets. In most cases the ports and navigation areas need to be protected by breakwaters and sufficient water depths in the port and in the approach area have to be secured by dredging. Dredged channels are subject to sedimentation, thus maintenance dredging will be a continuous effort, FRISCH (1991), MANGOR et al (2010).
Construction of breakwaters impact nearby coastlines. As long as breakwaters are within the littoral zone there is a risk that the port will be buried in sand shortly after its construction. This means that a port needs to have a significant size to be economically viable.

Figure 4: Beach landing of fishing boats at the village of Klitmøller (Cold Hawaii)

It was not – in the first place – a natural consideration for the Danes to build ports on the West Coast. Small fishing communities used to pull their vessels on the beach as seen in Figure 4. Today fishing has ceased in most of these communities. The major part of the population was living on the islands and along the east coast of Jutland. These neighborhoods have good naturally protected sites for ports and harbours to support domestic transport of goods, which to a large extent was by sea. Thus port construction on the West Coast was only considered from late in the19th century as a result of the changed border to Germany after the war in 1864, development of the society and demand for increased international transport of goods, SØRENSEN et al (1996). On the West Coast these challenges were considered and in this paper we will describe how three of the ports were established and developed and how they cope with today's demand for efficient transport infrastructure.

4. OVERVIEW OF DANISH WEST COAST PORTS

The ports on the Danish West Coast can be divided in three types according to the characteristics of the coastal sites – not counting the beach landing places:

- Headland ports, located on the open coast and protected by breakwaters, Hirtshals and Hanstholm.
- Inlet ports at natural inlets or stabilized breaches of lagoon barriers, Thyborøn, Thorsminde and Hvide Sande.
- Tidal region ports, Esbjerg.

Turnover in 2016

Port	Cargo (1000t)	Fish (1000t)
Hirtshals	1718	53
Hanstholm	213	158
Thyborøn	1617	223
Thorsminde	~	1
Hvide Sande	173	43
Esbjerg	4549	~

Figure 5: Ports on the Danish West Coast and their turnover in 2016

The ports of Thorsminde and Hvide Sande are mainly fishing ports whereas the others have a major activity as logistic centres.

All these ports were in 2000-01 transferred from state ownership to independent entities linked to local municipal control. As part of the transfer agreements, the state guarantees minimum depths of approach channels and is responsible for regular maintenance dredging to keep sufficient navigational depth.

Three of the ports are described in details in the following sections as examples of Danish Port expansion over the last century.

5. PORT OF HIRTSHALS

Figure 6: Hirtshals port viewed from the entrance

5.1 The history of Port of Hirtshals

Hirtshals Harbor is built as a fishing port on the shoulder of Jutland, following the thoughts of engineer Jørgen Fibiger's point theory. The harbor is thus built where the coast is strong and not erodible. The original water depth at the entrance was 7 m.

Figure 7: Port of Hirtshals on the northwestern corner of Denmark

Already in 1936, seven years after commissioning in 1929, the first ferry route between Hirtshals and Norway opened, as a number of people saw the possibilities in the port's unique geographic location.

The logical reason for construction of the port when it was planned and built has since evolved into the port's commercial foundation.

From the establishment of the port based on fishing, the port has been through continuous development, and by 2017 transport activities accounted for 70% of the revenue.

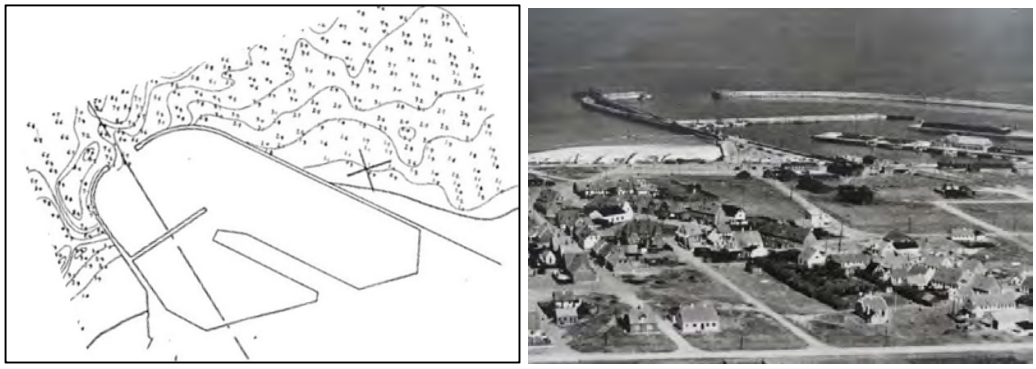

Figure 8: Port of Hirtshals by 1930 – same scale as in Fig. 9

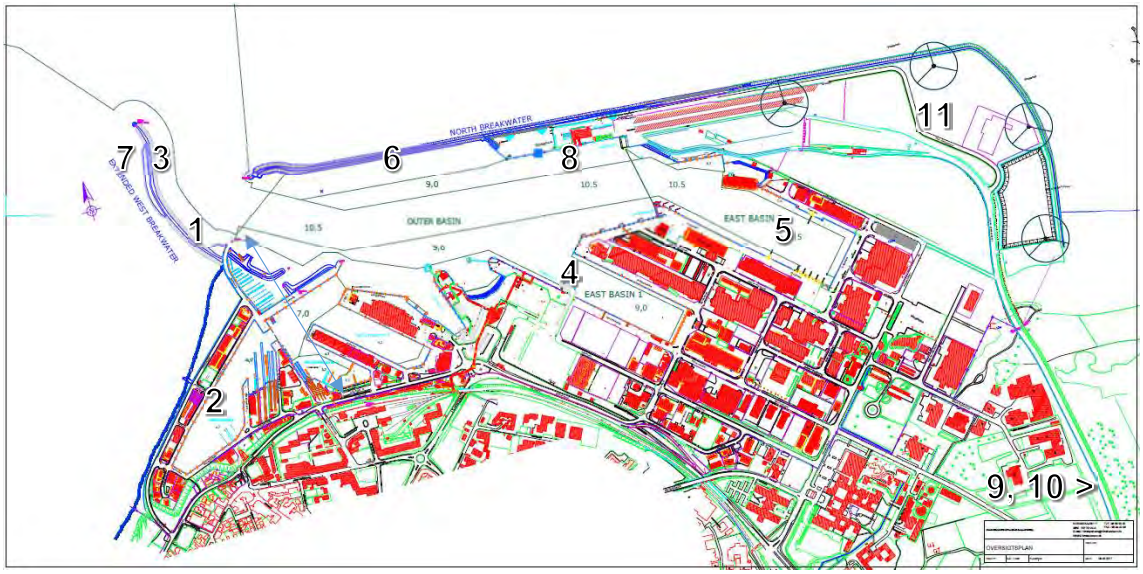

Figure 9: Port of Hirtshals by 2017

Since its inauguration in 1929, the port has been stepwise expanded to keep track of developments. The subsequent developments were typically in response to actual needs of the port. The sedimentation problem in the entrance has been a continuous struggle, BRUUN (1966). To keep the 7 m depth an outer main breakwater extension of 245 m was made and later a further extension to 430 m. Severe storms often result in sudden reductions of the depth, which requires immediate dredging efforts. The relocation of the north breakwater in 1995 was the first strategic move since the building of the port, aiming at a future development towards east.

The following significant construction work has been completed, see Figure 9:

1. The first part of the main breakwater was built in 1937.
2. The first port expansion to the west with a fishery basin in 1959.
3. Extension of the outer breakwater by 185 m in 1974 with the aim to reduce sedimentation in the port entrance.
4. Second expansion was built in 1973 - East Basin 1.
5. Third expansion was built in 1976 - East Basin 2.

6. The north breakwater was relocated in 1995.
7. The outer breakwater has been relocated in 2002-2003 to provide more navigational space.
8. The container berth was built in 2003.
9. New highway connection was built in 2015.
10. Combi-terminal built in 2015.
11. Land expansion established in 2015 - 2017.

Figure 10: The ferry berths in the center of the port area and new combined ferry and container berth along the north breakwater

5.2 Changes of the port use in recent decades

Port of Hirtshals has experienced a continuous development, which means that the activities at the port have increasingly changed the character of fishing towards logistics and transport. Consequently, the port is used by larger ships than originally provided for. The shipping companies that control the regular traffic in the port also adjust to the currently available possibilities, thus approaching the port with as large ships as possible.

Figure 11: Traditional and modern fishing vessels in Port of Hirtshals

With the development that Port of Hirtshals has undergone, there has been a similar investment in infrastructure, while at the same time the perspectives have shifted from the primary port view to a broader perspective focusing on the overall transport system - a multimodal approach that combines all modes of transport.

The port entrance sector was rebuilt in 2002 - 2003 in order to improve the navigational safety.

In 2003 the first new quay (Container wharf) was constructed for about 10 years. The building of the quay opened for container traffic and the traffic has later been shifted to RORO traffic that logically exploits the port's location.

In 2005, the E39 motorway was opened, thus connecting the port to the European motorway network, which strengthened the port's position as a European focal point.

Hirtshals Transport Center was built in the harbor's hinterland in 2011. The transport center operates with the port in relation to road transport services and thus forms a central part of the overall logistics setup in Hirtshals.

The Danish state invested in a combined terminal including railway service in 2015, thus all modalities were connected in Hirtshals and the port position as the intermodal logistics center was finally cemented.

5.3 Challenges and solutions

The challenges relating to ongoing development of the port activities has been the basis for decisions taken about fixed capital investments.

The sedimentation problem traditionally resulting from the port's location on the west coast of Jutland has been solved with traditional maintenance dredging of about 400,000 m^3/year in order to keep a water depth of 10.3 m. So far no initiative has been taken to investigate other methods that can reduce sedimentation significantly. Dredging strategies including proactive dredging on the west side have been tested to counteract sudden water depth reductions during storms.

As a consequence,of the growth of Port of Hirtshals it is necessary to expand the existing port area with emphasis on space for vehicles. Correspondingly, about 10,000 m^2 of fishing industry has been demolished.

Figure 12: All ferry berths in operation

The continued pressure on the need for land and an efficient infrastructure has resulted in an extension of the port with additional land area by 2017.

5.4. The future

Port of Hirtshals and the town of Hirtshals are central to a forward-looking modernization of logistics in Scandinavia, based on efficiency, minimizing climate impact and social impact in Norway by transfer of cargo transport from road to sea. The Port is thus, due to its location, important to the future infrastructure networks in Scandinavia.

The changes that will shape and change logistics in Scandinavia also mean that Port of Hirtshals changes the thinking from "maritime port" to "intermodal logistics center in the heart of Scandinavia". It is a more out-going consideration, and a considerably more complex thinking. To intensify this focus the

Port of Hirtshals has entered collaboration with a number of scandinavian ports, a.o. Kristiansand and Gothenburg, with Zeebrugge in Belgium and with Greenland.

Figure 13: 2017 land reclamation for new marshalling area

The future will lead to construction of local distribution centers and focus on multimodal transport solutions for the industries and logistics companies that will utilize Hirtshals' location in their future developments.

The future will also require improvements of the port access area, so the navigational safety is further improved and the port is accessible for larger vessels under tougher weather conditions. This in order to safeguard the port for future development. This improvement will also be planned with a view to further reduce the sedimentation as much as possible.

Figure 14: Ferry from Norway enters the port

Over the past few years, Port of Hirtshals has increasingly focused on renewable energy and limiting resource consumption. The port has installed solar cells for the production of electricity for the service yard and corresponding measures will be taken in the future.

Within a shorter time horizon the port will initiate actions to obtain an ISO certification in the environmental field in order to optimize resource utilization while implementing an efficiency consideration.

6. PORT OF THYBORØN

Figure 15: Port of Thyborøn

6.1 The history of Port of Thyborøn

Thyborøn Channel was created by a violent breakthrough of the isthmus in 1862, where the North Sea and the Limfjord were connected. Extension of the channel and construction of a port at Thyborøn was decided by the Civil Planning Act in 1914, thus creating the foundation for establishing the port in Thyborøn.

Figure 16: The isthmus at Thyborøn before and after the breakthrough in 1862.

Port of Thyborøn celebrated its 100 years anniversary in 2014. The harbour was founded with a wooden pier and a small wooden breakwater. The basis for the decision was a work carried out by the Third District of the State Coastal Authority. The harbour grew strongly from the start and through the 30's and 40's based on fishing. The development of the harbour remained quiet during the last years of World War II and the following years, as there was doubt about the possibility of keeping the inlet (Thyborøn Canal) open. From the latter half of the 50s and up to 2001, the port had a stable and forward-looking development and is today the third largest fishing port in Denmark

6.2 Changes of port use in recent decades

2001 became a landmark year for Port of Thyborøn. This year, the port went from being a state port to becoming an independent municipal port. Since then, the development has been very fast. The port has grown in turnover, area, water depth and quay structures. Around DKK 400 million has been invested in the port since 2001, and today it is both a fishing and commercial port.

Port of Thyborøn is in a development where other goods than fishing related are becoming more and more important. The harbor is situated with an east-facing entrance to the North Sea, which means that there is good navigational access in all weather conditions.

Port of Thyborøn has several business areas. Fishing still remains a cornerstone. In addition, maritime service companies, sand and gravel and other goods as well as support of offshore activities are important business areas. The port is still expanding with new reclamations and quays, which today allow for a physical separation of the port by business area.

Figure 17: Expansion of Port of Thyborøn towards south 2017.

6.3 Challenges and solutions

The biggest challenge of the port at present is the water depth for access. The guaranteed water depth through the Thyborøn Canal is 8 meters. The Danish state guarantees this depth to the port and 4.5 meters of water depth in the remaining part of the Limfjord until the port of Aalborg. The evolution of the ship tonnage means that the port must increase the water depth to between 9 and 10 meters within a few years.

The inlet is characterized by very dynamic bed conditions. Large sand banks move depending on water level variations and wave directions. In the winter of 2008 waves suddenly reached the port with unusual height as seen in Figure 18. This incident was investigated by DHI using the MIKE21 software tools.

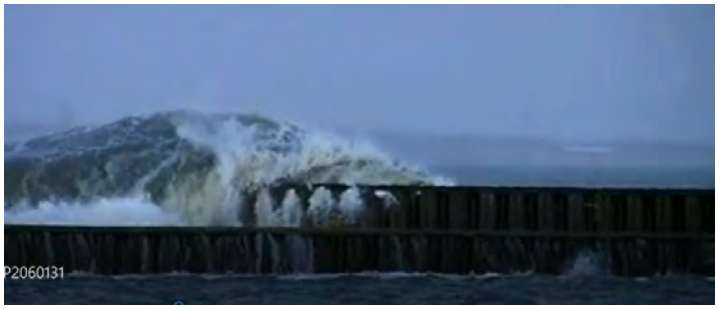

Figure 18: Overtopping of Thyborøn breakwater during northwesterly storm on 06.02.2008.

The investigation demonstrated that a sand bank had developed on the south side of the inlet as shown in Figure 19. This bank caused refraction of the northwesterly waves, which then focused on the port entrance and the outer breakwater as seen Figure 20.

Figure 19: Sand bank development off Thyborøn between 2004 and 2008.

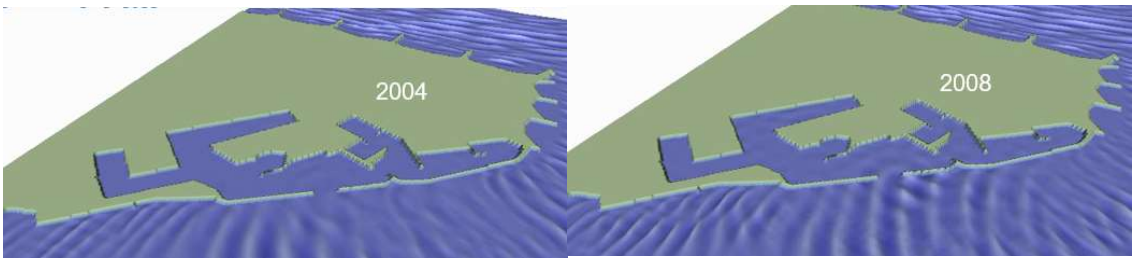

Figure 20: Wave propagation in Thyborøn canal before and after sand bank development.

It is presently expected that the Port of Thyborøn itself will be responsible for the maintenance through the canal to the port entrance. This will provide the basis for deepening to 10 meters of water so that it can be used by larger ships. The limitation of the water depth is a hindrance for both the fishing fleet and the merchant fleet and an increase will be required for the port to maintain its development. By transferring the responsibility of dredging the access, the port will have the opportunity to control the development and is not dependent on the state's desire or priority of maintenance, but can, on the other hand, take action on the problem when it arises. It will be a benefit for the harbour's customers.

This development is of major importance to the whole municipality and region. According to the latest survey, Port of Thyborøn generates 2200 jobs and the revenue from the port of 1.8 billion DKK. Therefore, the whole region takes great interest in the development of the harbor in these years.

6.4 Predicted and planned changes in the future

The Danish ports are still undergoing transformation of both developments in freight routes, ship tonnage development and structural developments throughout the fisheries sector.

Port of Thyborøn continuously works to influence policy makers that set the framework conditions for the sector both nationally and internationally. This effort is through active participation in debates and by inviting politicians to visit the harbour.

In addition, there is a focus on developing both the infrastructure and business processes to meet the customer's needs, driving the development. In the coming years, investments will be in new breakwaters and quays. The port actively engage in quality issues and environmental conditions, for example for unloading protein fish for fish protein industries in Thyborøn and in energy optimisations and digitalisation of many administrative procedures.

The motto in Thyborøn is "we will find out". Customers never get a no, and service companies and other stakeholders around the port cooperate with Port of Thyborøn to solve the wishes and problems to their mutual benefit.

Figure 21: New wind turbines in Thyborøn canal 2017.

7. PORT OF ESBJERG

Figure 22: Port of Esbjerg in 2017. The arrow points at the original triangular dock basin constructed in 1873

7.1 The history of Port of Esbjerg

In 1868 the Danish parliament decided to construct a port at Esbjerg on the west coast of Denmark and at the same time establish a railroad connection between Copenhagen and Esbjerg to meet the demand from the raising agricultural and livestock export to United Kingdom.

The location was selected because of a good natural shelter by the isle of Fanoe, a 4 m deep tidal channel to the sea and the possibility to use high water caused of a tidal range 1.5 m twice a day. At that time there was only a minor village in the neighborhood and a poor road connection.

The local fishermen have until then landed directly on the beaches on the open coast. Shortly after the port was finished in 1874 the fishermen saw the much better opportunities with a harbour and asked for suitable facilities.

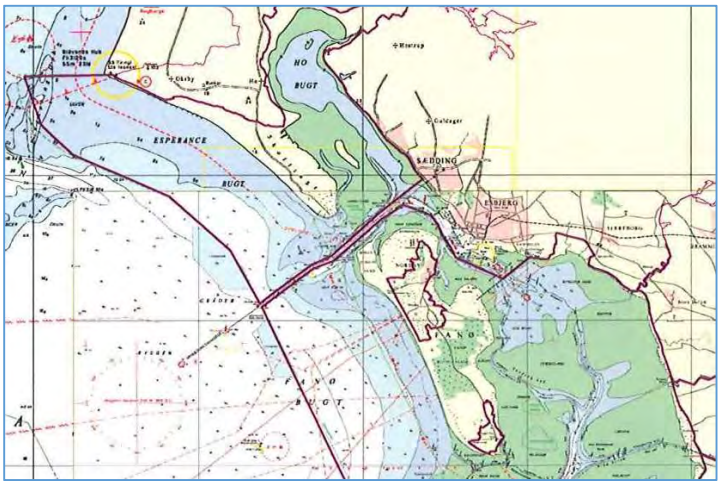

Figure 23: Location of Port of Esbjerg with access channel.
The purple line indicates the NATURA 2000 area of the northern part of Wadden Sea

Since then the port has expanded and has been transformed to suite the demands for general cargo, RO/RO goods, increasing size of fishery vessels (until 2010) and factories, oil and gas activities, export of wind energy components, servicing oil and installations rigs etc.

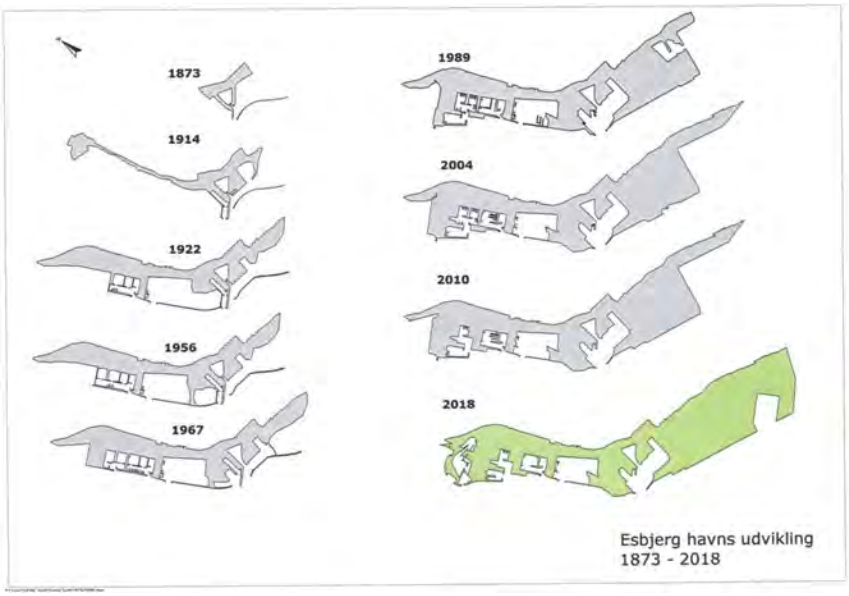

Figure 24: The development of Port of Esbjerg from the initial dock basin in 1873 until today

In 2000 the ownership of the port was transferred from the Danish State to the local Municipality and gave rise to a closer interaction between the city and the port. Anyhow the IMO restrictions (ISPS) in 2004 cut off the easy access to some port areas.

Step-by-step the water depth in the fairway has been increased for accommodation of larger vessels and today a 10 Nm long channel with 10.3 m water depth at Mean Low Water Spring (MLWS) and 200-500 m width leads to 13 km quay side, the harbour area size 4.5 million m^2 and good connection to highway and railroad. The largest vessels arriving in the port today are bulk carriers and RORO vessels with L_{oa} up to 235 m and/or draft 9.5 m and oil rigs and installation vessels with width up to 100 m.
Maintenance dredging is essential and around 1 million m^3 sediment (medium to fine sand from the channel and silt from the basins) must be dredged in the channel and the basins (50/50 distribution) each year to keep the sea chart depths.

The major port activities today are related to RORO import/export of general cargo and servicing offshore oil-, gas- and wind energy installations in the North Sea.

7.2 Changes of port use in recent decades

In 1980 about 700 vessels and the largest fish flour and oil factory in the world was situated in Esbjerg. During the latest 15 years the fishery has stopped in Esbjerg and the fishing fleet and industries have moved to other ports for a number of reasons such as fish quotas, distance to fishing grounds and restructuring of the industries.

Figure 25: Part of the fishing port in 1980

The five former fishing port basins are now used for servicing rigs, shipyard activities, service and crew vessels and as a marina. One basin has been filled to get more berths.

The need for new berths with high carrying capacity and large hinterland areas for the wind turbine industry and RORO handling has increased dramatically. The harbor is extended to the east, the navigation channel is extended, a new turning basin has been established, 1.2 million m^2 hinterland and 3 km new quays have been constructed during the last 10 years.

7.3 Advantages of the location today

The naturally sheltered entrance is still a great advantage, and reduces the need for breakwaters when the port expands.

The connection to the highway system was updated 6 years ago with financial aid from the Trans-European Transport Network (TEN-T) as a Motorway of the Sea project (MoS). The project should and have strengthened and developed a Benelux-Scandinavia short sea connection. As part of the project, the RORO connection between Esbjerg and Zeebrugge was improved by installing a floating RORO ramp and extending the port access road.

Figure 26: Road and railroad connections to Port of Esbjerg

The railroad was electrified from the railway station and a new railway terminal has been located on the port area.

The location of Port of Esbjerg is geographically attractive:

- For servicing the oil- and gas fields in the North Sea
- For export of wind mill components.
- As base for pre-installation and shipping-out of elements for offshore wind parks in the North Sea.

Figure 27: Loading of towers for offshore wind turbines at the new east basin.

During all the years of its existence the port has played a major role for the people of Esbjerg and even today the citizens show a general acceptance, when plans for changes and expansions are in public hearing. More than 10,000 people are employed directly in companies in the port areas. Education can take place on universities and a number of higher education facilities in the city.

7.4 Challenges/ Environmental Concerns:

The expansion possibilities for the Port of Esbjerg are limited, while the port is surrounded by environmentally sensitive areas such as NATURA 2000, a National Park in the Wadden Sea which is

designated as an UNESCO heritage site since 2014, see Figure 23. These environmental restrictions must be taken care of when planning for expansion or change in the activities on land and at sea.

Activities all around the clock sometimes disturb citizens living close to the port. The port captain assigns berths for incoming vessels. Based on expectations and experience specific attention is paid to the impact on neighbourhoods. Since the Port of Esbjerg has avoided residential construction at the port areas, the proximity of the town has not limited the expansion possibilities significantly.

It is difficult to make transport of freight on railroad economically attractive. For environmental reasons the Danish State has decided to improve conditions for transport by rail. However, the size of the country and the flexibility of trucking by road makes railway transport less competitive. This situation may change in the future by introduction of new charges and fees for trucking.

7.5 Ongoing construction works and planning for future demands

Two new ramps for RORO vessels up to 235 m loa and for handling of very long and heavy wind mill components have just been taken in use in the East harbour.

Plans are being implemented for cold ironing (SPS electricity) and more use of renewable energy.

The preparations for a new 1 million m^2 port area and 1 km quay in the east are ongoing. A comprehensive program with hydraulic survey, monitoring and investigations for environmental impact has started and the first phase of the environmental impact assessment is in progress.

In the present planning period (2015-25) it is not intended to deepen the approach channel.

To the North the municipality has taken over a project with marina, a cultural museum and more facilities for the citizens, partly to compensate for the ISPS restrictions in the commercial harbour.

Figure 28: The new marina complex north of the port.

The power plant is using coal today but will change to wood pellets within the coming 7 years. The same quays can be used for unloading, but other cranes and covered silos will be needed.

We try to incorporate much flexibility in our construction, so they can be adapted for future needs.
As an example, the East harbour developed in steps:

- Step 1: Wind mill activities. Strong quays covered with compacted crushed stones.
- Step 2: RORO with hard surface, and possibly
- Step 3: LOLO with mobile or gantry cranes.

To our experience an ongoing revision of a public masterplan is essential, so customers, the local community, etc. are made aware of possibilities and intentions.

To our experience an Environmental Impact Assessment shall be based on a project close in design to the final layout. This process takes time, but a well-prepared plan will usually shorten the time for realization of the project.

The design criteria/parameters increase (e.g. the capacity of the cranes working at the quayside have increased from 80 t in 2004 to 1,000 t today and axel loads on reach stackers from 80 to 160 t), so close contact to users and potential customers is essential during the planning period and detailed design is made “just in time”.

8. CHALLENGES FOR THE FUTURE PORT INFRASTRUCTURES

The ports described above face a number of development challenges due to societal changes and changes in the sectors they are to serve in the future.

- Fishing is concentrated on fewer and larger vessels, which need efficient handling in the ports.
- Increased offshore energy related activities (oil and gas, wind power and other renewables).
- International trade increases with demand for larger ferries and container operations.
- Expanding cruise industry.
- Separation of different port activities.
- Improvements of transport corridors to the hinterland.

The key issue for the ports is to create more space for the operations. This includes i.a. expanding port areas, dredging and reclamation, new and deeper quays and improved navigational access. All of these developments shall respect actual environmental legislation.

References

Bruun, P., (1966). Tidal Inlets and Littoral Drift, University Book Company, Oslo

Frisch, P. Hofmann, (1991). Coastal inlets on the Danish West Coast. PIANC Bulletin 1991, N° 72, pp 52-57

Mangor, Karsten, Brøker, I., Deigaard, R., Grunnet, N., (2010). Bypass Harbours at Littoral Transport Coasts, Paper No.313, PIANC MMX Congress Liverpool 2010.

DHI (2017)., Shoreline Management Guidelines, 4th edition. E-book published by DHI https://www.dhigroup.com/upload/campaigns/shoreline/assets/ShorelineManagementGuidelines_Feb2017-TOC.pdf

Sørensen, T., Fredsøe, J. and Roed Jacobsen, P., (1996). History of coastal engineering in Denmark. *History and heritage of coastal engineering, ASCE*

Optimizing Pier Structures using Dynamic Mooring Forces Modelling

by

Oliver Stoschek[1], *Stefan Leschka*[2], *Christian Hein*[3] and Anja Brüning[4]

1. INTRODUCTION

Existing mooring facilities in Ports were usually planned several years or even decades ago and were focusing on small ships, when compared to ship sizes seen today. Ship sizes have increased considerably in the last and recent years. We are now facing ship length >400m. Thus, formerly planned mooring facilities were often not designed for these kind of Post New Panamax ship sizes. The existing international guidelines (PIANC, OCIMF) and local guidelines (e.g. EAU in Germany) do not particularly account for the latest ship sizes. Applying them can lead to considerably overestimated mooring facilities.

To assess the real capabilities of existing or new planned mooring facilities on piers and in harbors, dynamic mooring simulation should be performed. Such methods will in general lead to more realistic loads. As a first step, they help determining the priority for updating the infrastructure. Such analyses can further be used to expand the lifetime of existing mooring facilities.

DHI developed a new software to calculate dynamic mooring forces (MIKE 21 Mooring Analysis (MA), DHI, 2017). Compared to other dynamic mooring analyses software, two-dimensional flow fields (incl. infra gravity seiching waves) can be incorporated. Their consideration can be of evidence in ports. The software and its predecessors were already applied in several port studies worldwide. Three examples from the German North Sea coast, namely in Bremerhaven, Wilhelmshaven and Hamburg, will be presented here. Their location is indicated in Figure 1.

In Bremerhaven, special ship forms and passing ships requested a dynamic mooring force assessment. In Wilhelmshaven, wind, passing ships and currents are determining the mooring forces. In Hamburg mainly wind forces on Post New Panamax Plus ships demand for detailed mooring force assessment. By using dynamic mooring analyses methods in these examples, the safety of the investigated berths could be re-evaluated. In this paper, the dynamic mooring analysis method is briefly described, followed by a description of the aforementioned examples.

[1] DHI WASY GmbH, Branch Office Bremen, Knochenhauerstr. 20-25, 28195 Bremen, ost@dhigroup.com
[2] DHI WASY GmbH, Branch Office Bremen, Knochenhauerstr. 20-25, 28195 Bremen, sle@dhigroup.com
[3] Bremenports GmbH & Co. KG, Am Strom 2, 27568 Bremerhaven, christian.hein@bremenports.de
[4] Sellhorn Ingenieurgesellchaft mbH, Teilfeld 5, 20459 Hamburg, anja.bruening@sellhorn-hamburg.de

Figure 1: Location Overview

2. DYNAMIC MOORING ANALYSIS

The hydrodynamic interaction between the fluid and the floating body is assumed to be well described by linear potential flow theory. This approach is valid as long as the parameter $\frac{kA}{tanh(kh)} \ll 1$, in which A is the wave amplitude, k is the wave number and h is the water depth. It is further assumed, that the body motion remains small (ensured by the mooring system) and estimates for the neglected hydrodynamic effects can be included via empirical coefficients.

Under these assumptions, the equation of motion can be solved in the time domain and reads

$$\sum_{k=1}^{6}\left(M_{jk}+a_{jk}\right)\ddot{x}_k(t)+\int_0^t K_{jk}(t-\tau)\dot{x}_k(\tau)d\tau+C_{jk}x_k(t)=F_{jD}(t)+F_{jnl}(t) \qquad (1)$$

The first term at the left-hand side describes the inertia forces, the second term the hydrostatic forces and the third term the hydrodynamic forces to first order in the body motion and the wave steepness (Bingham, 2000). They are referred to as impulse-response functions (IRF's). The matrices M_{jk}, C_{jk} and K_{jk} are 6 x 6 matrices of the floating body system. M_{jk} and C_{jk} are the inertia restoring matrix and the hydrostatic restoring matrix, respectively. a_{jk} are impulsive (added mass) contributions, originating from the t = 0 limit of the radiation problem. The forces due to radiated waves generated by the body's motions are expressed as a convolution of the radiation IRF's, K_{jk}.

The right-hand side summarizes all non-linear external forces, such as those from the mooring system and viscous and frictional damping (Froude-Krylov force), $F_{jnl}(t)$, and the wave exciting forces due to scattering of the incident waves $F_{jD}(t)$.

The position and angular rotation of the body in six rigid-body degrees of freedom (DOF) $x_j(t)$ are expressed in Cartesian coordinates, where $x_1 = x$ is aligned with the longitudinal ship axis pointing forward. The translations are indicated as x_1 = surge, x_2 = sway and x_3 = heave. The rotational motions are x_4 = roll angle, x_5 = pitch angle and x_6 = yaw angle. The over-dot indicates differentiation with respect to time t (Bingham, 2000).

The second term in equation (1) makes deriving of the matrices $K_{jk}(t)$, $a_{jk}(t)$ inefficient in the time domain due to the convolution with time t. Therefore, these hydrodynamic calculations are performed in the frequency domain. The hydrodynamic coefficients in the frequency domain, the frequency response functions (FRF's)

$$\sum_{k=1}^{6}\{-\omega^2[M_{jk} + A_{jk}(\omega)] + i\omega B_{jk}(\omega) + C_{jk}\}\tilde{x}_k(\omega) = \tilde{F}_{jD}(\omega),\ j = 1,2,\dots,6 \qquad (2)$$

$\tilde{F}_{jD}(\omega)$ are the exciting forces as a function of the wave frequency ω, $\tilde{x}_k(\omega)$ is the unit vector for the six degrees of freedom (DOF). A complete radiation analysis of the structure is performed by computing the added mass coefficient matrix $A_{jk}(\omega)$ as real part and the damping coefficient matrix $B_{jk}(\omega)$ as the imaginary part of the radiation potential $\varphi_j(\omega)$ at evenly spaced frequencies over the entire significant domain of frequencies (including $\omega = 0, \infty$).

The radiation potential is derived using the Boundary Element Method. The wave exciting forces are expressed by means of the radiation potentials from Boussinesq wave fields via the Haskind relation. All transformations from the frequency domain to the time domain are done by performing Fast Fourier Transformation. 2nd order wave drift forces are calculated using Newman's approximation (Newman, 1977). For further details, please refer to Babarit & Delhommeau (2015) and DHI (2018).

MIKE 21 MA accounts for

- Two-dimensional fields of waves, currents and wind and its combinations or, if not available,
- Time series, which can be derived from spectral information.
- The elastic behavior of mooring lines and fenders are considered via working curves, available from the software installation or from manufacturers
- The real ship hull and it's frequency response (Eigenfrequency) is used.

This allows for detailed investigation of realistic causes and their effects. Figure 2 presents a typical situation, in which MIKE 21 MA is applied.

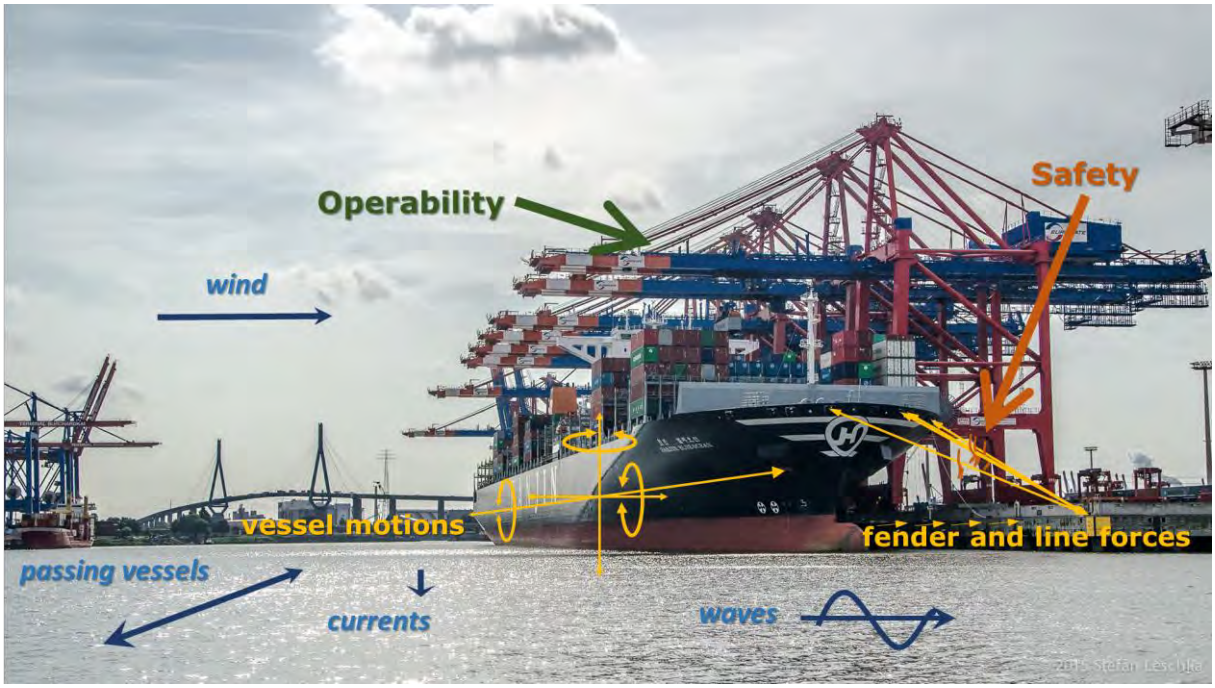

Figure 2: Typical application of MIKE 21 MA.

3. OFFSHORE TERMINAL BREMERHAVEN

To manifest its leading position as one of the main ports for the offshore wind industry in North Germany, Bremerhaven started the development of the former “Fischereihafen”. To support this industrial developing area with best infrastructural connection, a new offshore terminal (OTB) located in the “Blexer Bogen” - a bend of the Weser River right before the estuary mouths into the Wadden Sea - is planned for shipment of offshore components. The location is presented in Figure 3 and Figure 4.

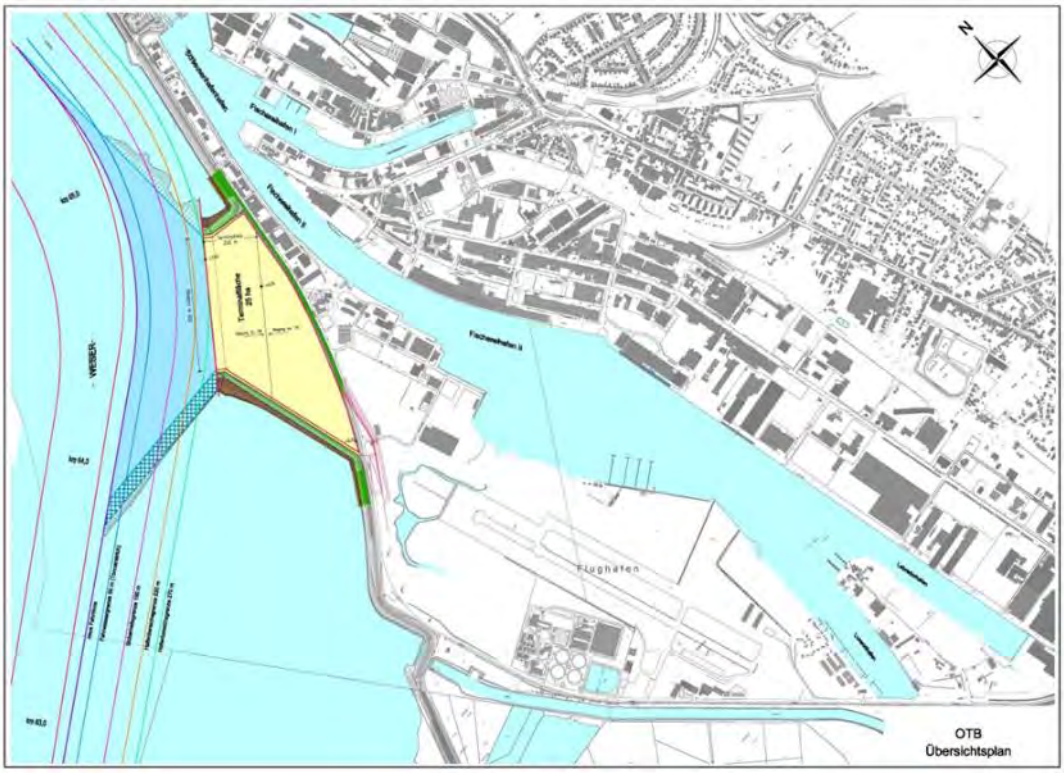

Figure 3: Location of the planned OTB at the "Blexer Bogen"

Figure 4: Areal overview of the planned OTB at the "Blexer Bogen"

At the "Blexer Bogen", large Bulkers are passing this planned terminal in close distance. Therefore, interplay of ship traffic and mooring forces of ships with special size and forms will occur. The main objective of this study was to prove that the drawdown generated by passing vessels does not endanger the applied mooring systems.

DHI's mooring assessment tool in combination with the hydrodynamic module was used to analyze the mooring forces for special offshore installation vessels. The methodology is depicted in Figure 5.

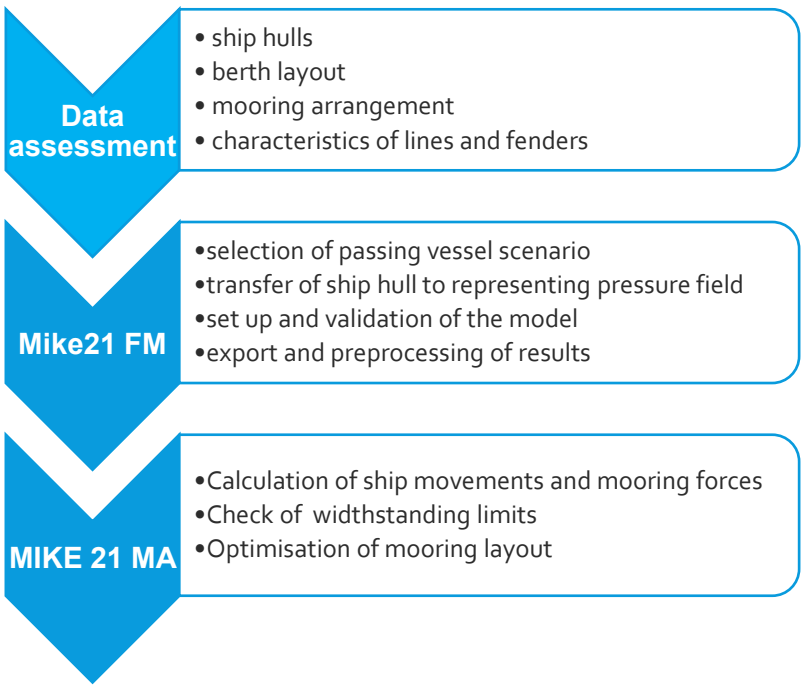

Figure 5: Study methodology

A significant effort was made to achieve and process the data (e.g. ship hulls, berth layout, characteristics of mooring lines). The second and very important aspect was to set up and validate the MIKE 21 Flexible Mesh (FM) Hydrodynamic Model (HD) based on a selection of passing ship scenarios. In the process of assessing the drawdown induced ship motions and mooring forces, the initial mooring arrangement was improved by iteration.

Since most of the empirical formulae include neither the effects of bathymetric changes nor the effect of a river bend or varying distances to the shore, DHI's approach of using a moving pressure field within a MIKE 21 FM HD was applied to reproduce the underlying physics within the numerical model. The model approach uses a flexible mesh (FM) based on unstructured triangular or quadrangular elements and applies a finite volume numerical solution technique. For further information it is referred to DHI (2017).

The characteristics of different passing vessel, its pathway and maximum speed were transferred into the model domain. The resulting drawdown waves were compared to in situ measurements to proof the reliability of the model results.

The moving ship was represented by a moving pressure field that represents the submerged vessel hull. The left part of Figure 6 shows a close up of the mesh, revealing several resolutions, in the vicinity of the OTB. The right part of the figure presents a snapshot of the drawdown wave.

For the identification of the most dangerous ship passage affecting moored vessels at the berth, nautical simulations have been revised regarding the effective vessel speed over ground (SOG), trough water (STW) and their pathway with regards to the passing distance to the quay. The highest vessel speed (SOG or STW) derived from the nautical simulations were used as a conservative approach within the MIKE 21 FM HD model. As a second step, these first order ship (drawdown) waves and its corresponding current speeds in the vicinity of the terminal area were coupled to the mooring analysis software.

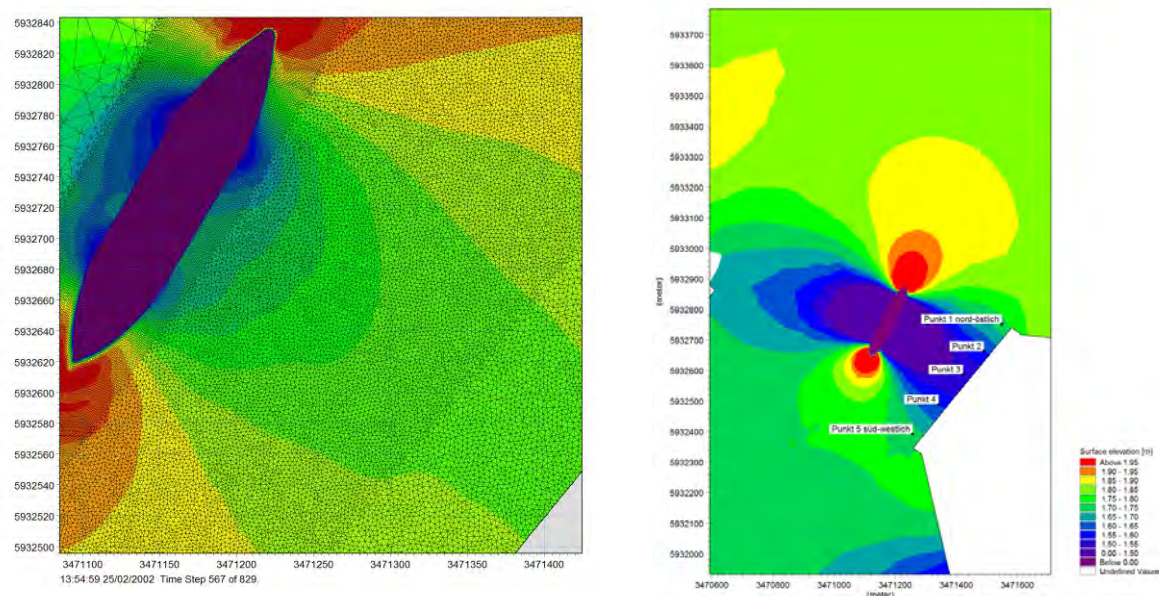

Figure 6: Passing ship hull included in the mesh and the calculated drawdown in front of the OTB

Different cargo ships and Jack up barges were investigated. As one example, the P2-Class cargo ship was investigated with two mooring arrangements, which are shown in Figure 7. Since the initial number of eight synthetic mooring lines was judged insufficient, an additional optimized mooring set up with two more spring and two more breast lines was examined. As the number of mooring winches of this ship was limited, too, it was assumed that an onshore system, such as shore tension devices, could be installed to assure the pretension.

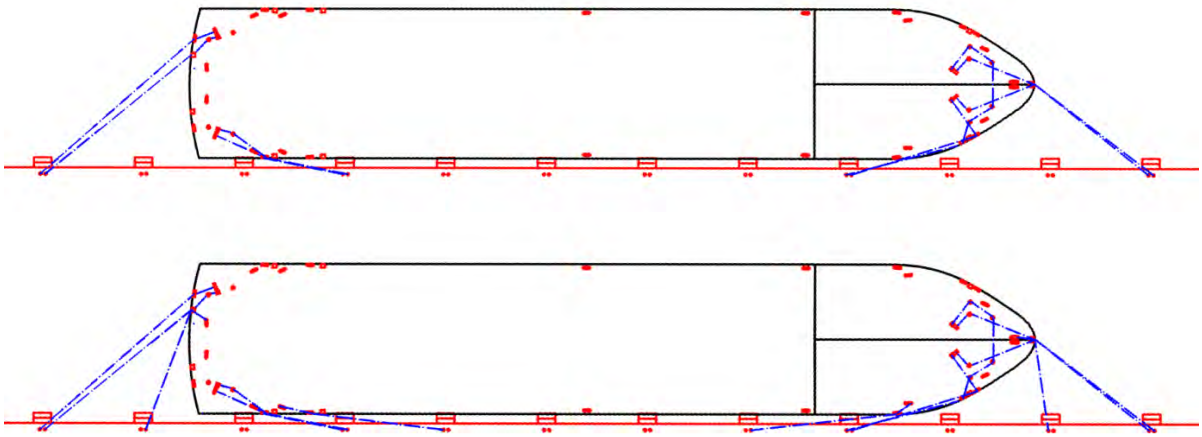

Figure 7: Mooring arrangements of the cargo ship P2-800. Upper panel: Initial mooring arrangement, Lower panel: Optimized set up with additional mooring lines.

Exemplarily, the highest mooring forces and the rate of line usage obtained in this study are summarized in Table 1. The results show that for some cases additional mooring lines were required to withstand the external load induced by the drawdown waves of passing vessels. The maximum absolute ship motions occurring within the simulations are summarized in Table 2.

Ship type	MBL [kN]	Reduced MBL [kN]	Max. Force [kN]	Initial set up
Cargo ship P2-class (8 Lines)	480	240	291	**121 %**
Cargo ship P2-class (8 + 4 lines with shore tension)	480	240	203	84 %
Pontoon (ballasted)	990	495	144	29 %
Pontoon (loaded)	990	495	280	56 %
Jack-Up ship 1 (initial set up 6 lines)	511	230	263	**114 %**
Jack-Up ship 1 (6 lines + 2x spring lines)	511	230	180	78 %
Jack-Up ship 2 (initial set up 12 lines)	850	425	277	65 %

Table 1 : Max mooring forces per line occurring during dynamic load assessment. Exceedance of MBL are indicated red.

Ship type	Surge [m]	Sway [m]	Heave [m]	Roll [°]	Pitch [°]	Yaw [°]
Cargo ship P2-class (8 Lines)	4.49	0.06	0.40	1.62	0.19	0.16
Cargo ship P2-class (8 + 4 lines with st)	2.72	0.05	0.40	0.60	0.19	0.14
Pontoon (ballasted)	0.19	0.03	0.39	0.11	0.18	0.08
Pontoon (loaded)	0.94	0.17	0.41	0.34	0.20	0.51
Jack-Up ship 1 (initial set up 6 lines)	2.40	0.12	0.40	0.21	0.21	0.40
Jack-Up ship 1 (6 lines + 2x spring lines)	1.58	0.12	0.40	0.13	0.19	0.32
Jack-Up ship 2 (initial set up 12 lines)	0.94	0.17	0.39	0.22	0.20	0.14

Table 2 : Max motions absolute values assessed from ship motion simulations. Exceedance of motion limits are indicated red.

As a reference for safe operations, the max. allowable ship motions during loading and unloading conditions after PIANC (1995) were applied. The guideline is based on experience and investigations and provided a good guidance for different vessel types.

In general, the simulation results are significantly lower than the recommended thresholds. Still, the surge motion is critical in some cases. For example, the P2-Class Cargo ship with optimized mooring layout and shore tension devices is not able to reduce the motion into an acceptable range and the threshold for surge of 2 m is exceeded by 36%. However, it must be stated that this situation would rarely occur, and operations can be stopped during the passage of such vessel. The exceedance of surge motions for both Jack up vessels is assumed to be not critical since loading operations will

most probably take place in a jacked position. Detailed project information can be found at Brüning et al (2014).

4. BULK TERMINAL NIEDERSACHSENBRÜCKE, WILHELMSHAVEN

The Jade-Weser Port of Wilhelmshaven provides a deep access channel and is focusing on large container, general cargo and bulk carriers. The so-called “Niedersachsenbrücke” is the main pier for coal import for northern parts of Germany. The terminal is a pile founded pier located about 1100m offshore of the mainland. Two coal-fired power plants are directly picking up the coal from this pier. It was originally planned in the late 60’s of the last century, having a berth on the landside for feeder bulk carriers and another berth on the seaside for Post Panamax bulkers of more than 300m length. The terminal can also be used for transferring cargo directly between two simultaneously moored ships.

After the construction of the Jade-Weser Port north of the Niedersachsenbrücke, modifications to the existing bulk terminal were necessary. Consequently, currents and current-induced loads were changing. Re-assessments of the mooring forces (CES, 2002) took static design loads (wind, current) into account. As part of a more recent assessment of expected operational conditions by WK Consult, it turned out that the static forces on both sides of the Pier can take values close to the maximum allowed static load of the pier. A simplified static analysis showed critical loads in some parts of the structure. No information was available for simultaneously moored ships and for the condition of vessels passing the pier. Other dynamic loads, e.g. due to waves, were not considered. This was seen critical, particularly in the light of future requirements, where two large Bulk Carriers are to be hosted simultaneously at the pier.

To get a comprehensive and more realistic overview of mooring forces, dynamic mooring force calculations, which combined wind and currents (from measurements) and passing ships (from a hydrodynamic simulation) were carried out by DHI. The analyses were performed in cooperation with Manzenrieder und Partner, who performed water level and current measurements, and Nautisches Büro Bremen, who performed AIS data analyses to derive a representative passing vessel situation.

The ships, mooring lines and fenders are characterized in Table 3. An exemplary mooring configuration is presented in Figure 8.

Berth	**Outer**	**Inner**
Vessel type	**Bulk carrier**	**Bulk carrier**
DWT	250,000	40.000
LOA	323.5 m	220 m
LPP	310 m	210 m
Beam	52 m	28 m
Draft	18.5 m	11.5 m
Loading condition	75 %	100 %
Freeboard	9.5 m	4.5 m
Transversal windage area	1600 m²	1200 m²
Longitudinal windage area	6500 m²	4000 m²
Mooring lines	**HTTP**	**HTTP**
Line number	16	12
Diameter	72	60
Min. breaking load	84 t	60 t

Berth	Outer	Inner
Vessel type	**Bulk carrier**	**Bulk carrier**
Fenders	**Super Cone SCN 1100**	**Cylindrical fender 2000x1200**
Max. reaction force	2348 kN	2000 kN
Max. deflection	1.65 m	1.2 m
Longitudinal windage area	6500 m²	4000 m²

Table 3: Ship parameters (Voss, 2008; Albrecht 2011; CES, 2011; Salzgitter Colsult, 1989)

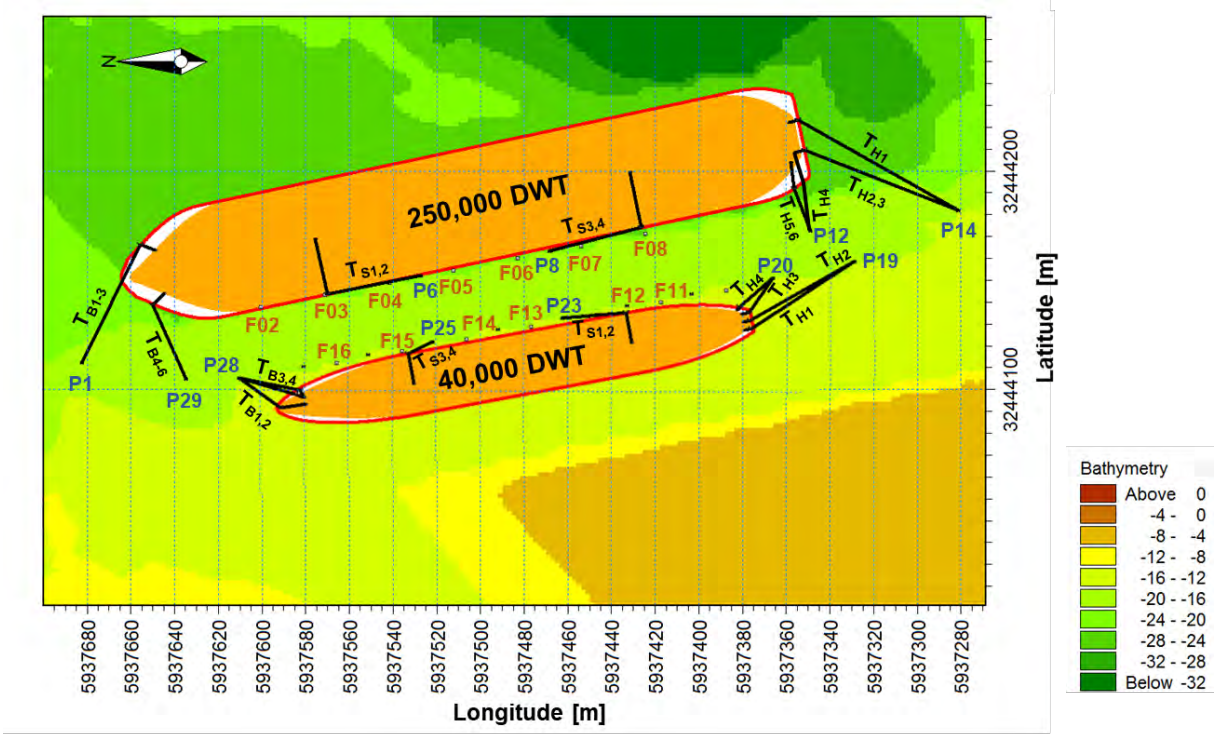

Figure 8: Exemplary mooring configuration at the Niedersachsenbrücke in Wilhelmshaven (coordinates in ETRS 1989 UTM 32N), "F" = fenders, "P" = bollards, "T" = mooring lines (based on Albrecht, 2011).

A test matrix comprising of 22 scenarios was set up. The scenarios addressed combinations of loads due to wind, current, wave and passing vessels. AIS data revealed a minimum passing distances of 200 m (inbound), which was combined with a bulker of 166.7 m length, 25 m width and 14 m draft, which was moving through water with 8 knots (Meyer, 2017). The study methodology follows the one shown in Figure 4.

The most critical environmental condition was characterized with wind speeds of 32.4 m/s from west, waves of 1.6 m significant height and a peak period of 4.5 s from east-northeast and ebb current of 0.9 m/s. The wind induced wave was combined with a long period wave of 0.5 m significant height and a peak period of 12 s from north, which was derived from scatter analyses of wave data, extracted from DHI's Northern Europe Hindcast (1979-2016), available from https://waterdata.dhigroup.com/octopus/home.

The following conclusions were formulated:

- The highest loads in the spring lines occur when tidal currents are directed towards the stern of the ship.

- Loads due to waves are small due to the small period of wind-induced waves and the orientation of the berth, resulting in a small approaching angle of long waves.

- The highest bollard loads occur due to wind from westerly direction on the outer berth (similar to previous studies)

- Expected loads due to passing vessels are small.

It could be confirmed that the construction of the bulk terminal Niedersachsenbrücke provides safe mooring conditions for the investigated design ships also under the condition of changed current fields and dynamic conditions due to waves and passing vessels. No modification to the pier construction was necessary.

5. ULCV BERTH FINKENWERDER PFÄHLE, PORT OF HAMBURG

The Hamburg Port Authority (HPA) is planning to enforce mooring facilities along the Elbe at the port entrance to mainly host Ultra Large Container Vessels (ULCVs) in case that a suitable berth inside the port cannot be approached. The existing facilities are detached from the river bank and located near the fairway in Finkenwerder. They were designed for Panamax size ships. The following considerations were taken into account:

- It is planned to use the mooring facility for Bulk Carriers up to 250m length and for the next generation ULCV (up to 450m).
- The existing facilities should be reused.
- Mainly wind induced loads are to be taken into account. Wind forces on ULCVs were evaluated for different load conditions in model tests in a wind test facility.
- Different mooring configurations are to be investigated for the ULCVs.
- Assessment of fender forces for land going wind events for the existing dolphins.
- Upgrade of the berth with additional dolphins

Using standard guidelines (e.g. the German EAU), would lead to the requirement of large pile groups to host the mooring facilities. Since the berths are mainly used by ULCV's, wind and currents play an important role. HPA decided to use the dynamic mooring software from DHI to assess the operational limits of the existing mooring facilities in order to prevent any damage to the infrastructure. Additionally, dedicated piles were set to cover some critical situations identified by the dynamic mooring simulations.

5.1 Baseline situation

The length of the mooring facility "Großschiffsliegeplatz Finkenwerder" is limiting the mooring capabilities. Only 2 dolphins at each berth are located outside the ship length which can host bow and stern mooring lines. With the existing hooks, up to 4 lines can be hosted at each dolphin. Only 4 lines at the bow and at the stern and 2 spring lines can be used, as shown in Figure 9, but the general mooring configuration of ULCV's includes 6 lines at bow and stern.

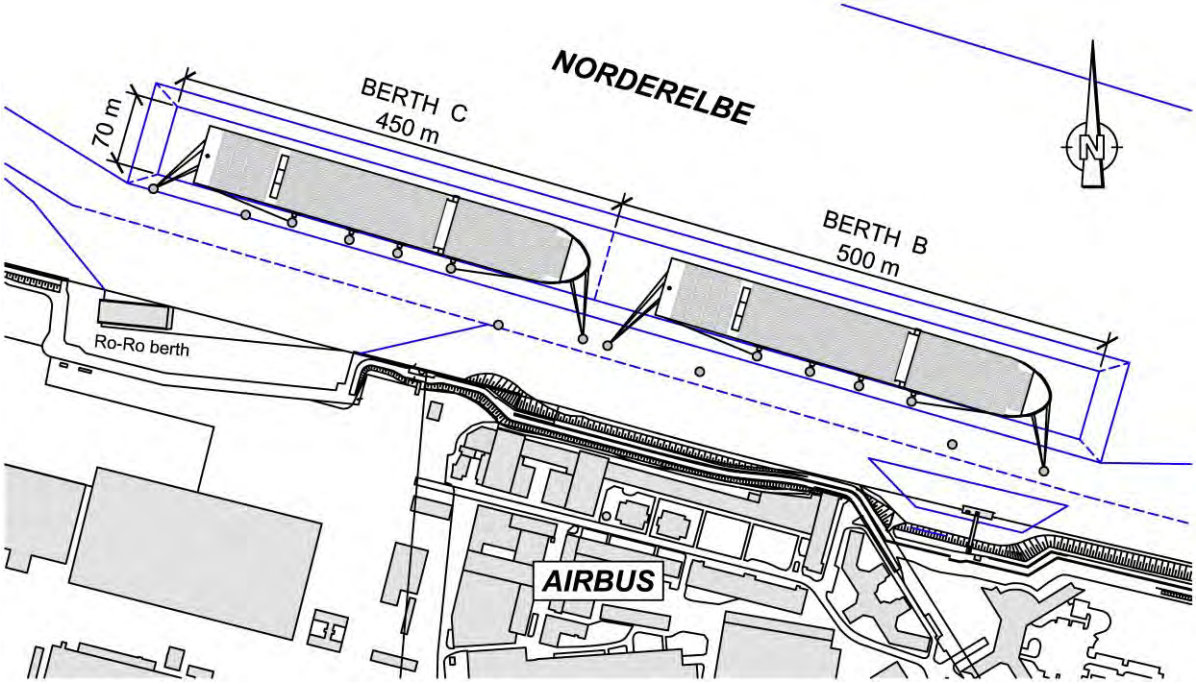

Figure 9: Existing mooring facilities in Finkenwerder, Hamburg

5.2 Bounding conditions

As a first step, the bounding conditions for the expansion of the mooring facilities were defined. There are geometrical limitations due to the Ro-Ro berth of Airbus, located onshore. The height and diameter of the planned dolphins must be similar to existing ones.

Four reference vessels were identified for the assessment of the mooring forces. The reference vessel data base includes the past development of vessels, feeder ships (8,000 TEU, 335 m length), actual classes (15,000 TEU and 19,000 TEU) and future classes of container vessels up to 24,000 TEU (450 m length).

Natural wind speeds were taken from measurements provided by the Deutschen Wetterdienst (DWD). It contains a statistical analysis of the 2% exceedance probability (50 year return period) 10 m above ground. The wind sector discretization was 30°.

A height-averaged wind speeds were defined at the center point of the reference ships. It was assumed that all reference ships have a height of approximately 64 m. The variation in the vessel height found in Hamburg was < 3% and considered too small for consideration. The relevant wind speed used in the calculations is summarized in Table 4. A local influence (shelter) of the Airbus buildings on the wind can be noted during southwesterly wind events (120°N to 270°N).

Richtung		30°	60°	90°	120°	150°	180°	210°	240°	270°	300°	330°	360°	0°-360°
LP B [1]	$V_{w,2\%}$ [m/s]	22,1	25,6	27,9	15,1	11,6	13,9	22,1	23,2	32,5	33,7	17,4	15,1	34,9
LP C [2]	$V_{w,2\%}$ [m/s]	22,1	25,6	27,9	20,9	16,3	18,6	27,9	32,5	33,7	33,7	17,4	15,1	34,9

1) LP B = Liegeplatz B; 2) LP C = Liegeplatz C

Table 4: Local height averaged windspeed (m/s) for a 50 year return period divided by sectors of 30°. Height of the reference vessel 64 m.

Table 5 shows the minimum requirements for lines and winches. The values base on a questionnaire of the Hamburg Pilots and experiences of the Oberhafenamt, the body responsible for policing the harbor.

Bezeichnung	Bulker	Handy New Panamax	New Panamax	Post New Panamax	Post New Panamax Plus [2]
Schiffstyp	Bulker	Container	Container	Container	Container
Baujahr (ab)	-	2000	2008	2006	ZUKUNFT
DWT/ TEU	230.000 T	8.000-12.000	12.001-14.500	14.501-21.500	21.501 +
Material der Leinen[1]	PP/PE oder PA	PP/PE oder PA	PP/PE oder PA	PP/PE oder PA	PP/PE oder PA
min. Leinenanzahl (ausgelegt)	12 (4,2 vertäut)	8 (3,1 vertäut)	12 (4,2 vertäut)	16 (6,2 vertäut)	22[3] (8,3 vertäut)
Minimum Breaking Load MBL	siehe New Panamax	90 t	110 t	130 t	150 t
zul. Regelbeanspruchung PA =45% / PP/PE =50%	siehe New Panamax	40,5 t/ 45 t	49,5 t/ 55 t	58,5 t/ 65 t	67,5 t/ 75 t
SWL Winden (≈ min MBL)	siehe New Panamax	90 t	110 t	130 t	150 t
Designlast Bremse (≈ 80% MBL)	siehe New Panamax	72 t	88 t	104 t	120 t

1) PP/PE = Polypropylene/ Polyester; PA = Polyamid (Nylon)
2) Werte basieren auf Grundlage von [4] und Abschätzungen
3) Annahme auf Basis einer Lastabschätzung

Table 5: Minimum conditions for mooring ropes and winches for the selected reference vessels

Selected design parameters for the mooring analysis

It is assumed that 16 nylon lines are used by default (6-2 mooring). The minimum breaking load (MBL) of the lines is 150 t. The safe working load (SWL) of the winches is equal to the MBL of the line used.

As allowed line tension, 45 % of the MBL is considered (67.5 t) for a single line and 135 t for a double line.

Due to the defined design condition (storm) it is considered that these limits cannot be maintained. As during storm events, the given rule states that winches shall operate “on breaks” instead automatically, a modification of the safety thresholds is recommended.

For the result evaluation, in subsequent analyses a limit of 80 % of the minimum breaking load (MBL) for all lines was assumed. This is to ensure at least 20 % elongation reserve during “break” operation of the winches. As an exception, the limit for the 19,000 TEU ship was selected equal to the design load of the winch break of 120 t x 80 % = 96 t (192 t for double winches). This limit is in accordance with the design load of the slip hooks, which is stated to be 1,000 kN (~100 t) per hook. It is also noted, that the design load of 96 t means a usage of 64 % of the MBL (150 t). Thus, the load reserve in the lines is 36 %.

5.3 Recommendations

The analyses lead to the following recommendations for operating the berths B and C of the ultra large vessel terminal Finkenwerder:

1. During wind speeds of 6 Bft or higher, highly increased ship motions are to be expected. This information is to be transferred to the captains.
2. Additional mooring lines can be used. This is to be understood as temporal solution and requires special caretaking, because the lines need to be taught and growed slack manually using the winch head. Otherwise, changing tides lead to slack or too tight lines.
3. If the number of lines on the ship is not sufficient or the lines are too small, or resulting ship motions lead to uncertainties, then for southern and southwesterly winds of 8 Bft and higher, the captains shall demand for tug boat assistance, so that the lines do not exceed 80 % of the MBL.

5.4 Summary of results

Baseline situation

The results of the mooring analyses show that the existing berth Finkenwerder Pfähle does not suffice for hosting recent ship generations with lengths of 400 m. 6 to 8 bow and stern lines cannot be moored on with the existing dolphins due to geometrical reasons. At least two dolphins are missing.

The analyses of line and dolphin forces show that the existing situation, where the airbus hangars lead to wind shading for berth B, a 4-2 mooring configuration of a 19,000 TEU ship is sufficient to host the vessel during a design storm event. Horizontal design loads of 3,000 kN on the dolphin heads were not exceeded. In case of seaward wind of 6 Bft and higher, the ship can lose the contact with the fenders.

A 4-2 mooring configuration for 19,000 TEU ships is not sufficient under design wind conditions **without** airbus hangar shading. The loads exceed 45 % of MBL and, partly, MBL. Furthermore, horizontal loads at the dolphin heads are doubled (approximately 6,000 kN). The horizontal ship motions (surge, sway and yaw) lead unacceptable values (surge of approximately 8 m).

Extension for 400 m ships

In order to ensure mooring with a 8-2 configuration (or a 6-2 mooring at berth B) during storms, the preferred options (VB5-1 and VC10 OST/ VC10-1 WEST) for both berths show the demand for two to three additional dolphins for re-assessment case of the 19,000 TEU ship without wind shading from the Airbus hangars. All dolphins shall be designed for loads of approximately 3,500 kN. This is shown in Figure 10.

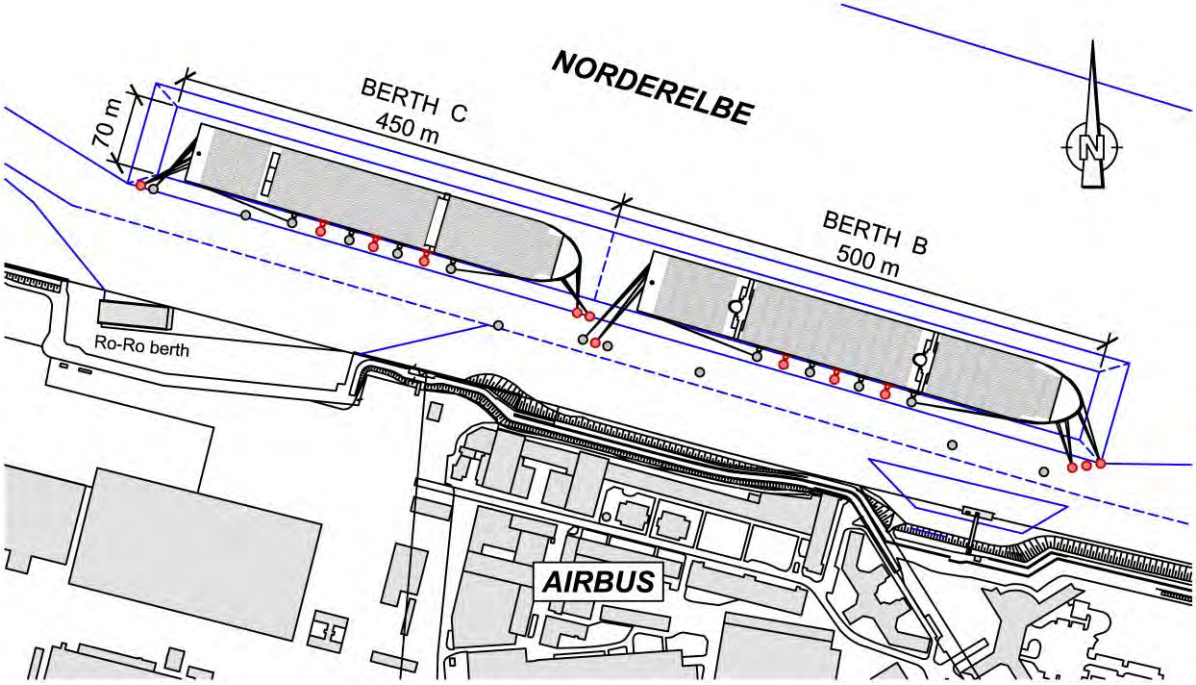

Figure 10: Extended mooring facilities in Finkenwerder, Hamburg

The loads from the spring lines do not exceed the design loads of the existing dolphins. The fenders on these dolphins are able to take the wind loads from ships of up to 400 m length of 2,800 kN. This is due to the load reserves in additional dolphins, which leads to load redistributions. Additional bollards furthermore improve the berthing situation for container carriers with smaller fender contact areas.

The estimated loads confirmed that smaller ships (bulkers, handy new Panamax) are not relevant for the design as they comprise of smaller windage areas and carry less lines. They can be moored with less lines (e.g. 4-2 mooring) also during storm events. It should be ensured that the lines used are appropriate for the here derived mooring forces.

Future ship generations – Confirmation of initial estimated by dynamic mooring analyses

Future ship generations (Post New Panamax Plus, e.g. design ship “Tomorrow”) come with windage areas of more than 20,000 m³. This will lead to roughly 30 % higher loads in the dolphins. It is assumed that such ships are moored using an 8-3 configuration.

The re-assessments of mooring forces for 24,000 TEU ships (VB5) confirmed the estimated values stated above. The design loads for the first dolphin in berth B were exceeded for ships of LOA > 400 m. This demands for constructing another bollard. Furthermore, increased line numbers (e.g. 12-4 moorings) shall be considered. Therefore, another dolphin in berth B should be constructed.

Increasing line numbers as a consequence of increasing ship sizes will, as shown in table 7, comes along with increasing MBL of the lines used. As shown in the dynamic mooring analyses results, the existing slip hooks will reach its design loads.

A general renewal based on static load assumptions could be avoided.

6. CONCLUSIONS

This summarizes three applications of dynamic mooring analyses with the purpose to reassess safety and efficiency of pier structures. The mathematical background is briefly described and the most important assumptions are outlined. The example of dynamic mooring analyses for the Offshore Terminal Bremerhaven showed the ability of the applied methods to assess impacts from passing vessels in constrained waters. In Wilhelmshaven, an existing pier structure was re-analyzed under changing conditions and, additionally, dynamic wave loads. Compared to static methods, the more detailed dynamic method verified the safety of the existing structures also for dynamic conditions. Recommendations for increased safety were derived. In Hamburg, the method was applied to the largest container vessel classes. The analysis revealed necessary amendments to the existing berth. Furthermore, recommendations on the operations were given.

In all applications, dynamic mooring analyses lead to an improved understanding of the processes allowing for less conservative designs. Thereby, the applied method can lead to improved safety and reduced construction costs for pier structures.

7. REFERENCES

Albrecht, H. (2011): “Niedersachsenbrücke in WHV. Neue Slipgeschirre P30 und P31 auf der Umschlagbrücke. Nachweise der Vertäusysteme”

Babarit, A., Delhommeau, G. (2015): “Theoretical and numerical aspects of the open source BEM solver NEMOH” LHEEA CNRS UMR 6598, Ecole Centrale de Nantes, France.

Bingham, H.B. (2000): “A hybrid Boussinesq-panel method for predicting the motion of a moored ship”, Coastal Engineering, 40., 21-38.

Brüning, A., Stoschek, O., Spinnreker, D., Kraus, U. (2014): „Assessing mooring forces at an offshore wind terminal, Bremerhaven, Germany”, PIANC World Congress, San Francisco, USA.

CES (2002): “Gutachterliche Stellungnahme zu Vertäusystemen für Massengutfrachter der 190.000 dwt-Klasse“, in co-operation with tewis AG.

DHI (2017): „MIKE 21 Flow Model & MIKE 21 Flood Screening Tool-Hydrodynamic Module, Scientific Documentation”, Hørsholm, Denmark.

DHI (2018): “MIKE 21 Maritime – Frequency Response Calculator and Mooring Analysis, Scientific Documentation”, Hørsholm, Denmark, (in review).

EAU (2012): “Empfehlungen des Arbeitsausschusses Ufereinfassungen: Hafen und Wasserstraßen“, 11th Edition, Ernst & Sohn.

Meyer, M. (2017): “Nautische Einschätzung Nr. 12102417“, Nautisches Büro Bremen, March 2017.

Newman, J.N. (1977): “Marine Hydrodynamics” MIT Press, Cambridge, MA, USA.

PIANC (1995): „Criteria for Movements of Moored Ships in Harbours, A Practical Guide” Report of Working Group no. 24, Supplement to Bulletin no. 88, 1995.

Salzgitter Consult (1989): “Studie über den Ausbau der Niedersachsenbrücke in Wilhelmshaven zur Abfertigung von vollabgeladenen Massengutfrachtern bis 250.000 dtw Tragfähigkeit“, November 1989.

Voss, L. (2008): „Statische Berechnung. Verbundwand Niedersachsenbrücke Teil 1: Grundlagen und Schnittgrößenermittlung für die Spundwand.“

OPERATIONAL ANALYSIS OF CRUISE SHIPS AGAINST LONG WAVES: THE EXPERIENCE AT VALPARAISO

by

Benjamín Hernández[1], Ricardo Figueroa[2] and Fernando González Chana[3]

ABSTRACT

The cruise industry has been undergoing considerable expansion in South America, particularly in Chile. To meet demand, Port of Valparaíso is planning to accommodate the cruise vessels at a dedicated terminal to promote the cruise industry and to provide passengers a world-class cruise experience. The existing passenger terminal is co-located with cargo terminals, and a dedicated cruise ship terminal is needed to reduce overlap between cargo and passenger operations. Valparaíso is a busy harbor, and several ongoing cargo terminal expansion projects are underway. A site has been selected for the dedicated cruise terminal that would provide separation from the cargo terminal, but place the moored cruise ships outside of the port's breakwater protection. In this paper, a methodology is presented for selecting the cruise terminal location, developing the swell wave climate at the site, and developing terminal solutions to minimize cruise ship movement and obtain a cost-effective solution.

To characterize the wave climate at the proposed terminal, a 36-year wave hindcast was used, based on re-analysis of Pacific Ocean winds. The spectral hindcast was propagated using a methodology that allows estimating the spectra at the nearshore project site considering the contribution of each component present in the spectra in deep water. This is important in bays like Valparaíso, since it considers the energy coming from all directions where it is possible for the waves to enter the bay. Wave simulations were developed using the Mike21 SW-FM (Spectral Waves-Flexible Mesh) numerical model, which is able to solve wave transformation processes such as refraction and shoaling, the energy balance of the inputs (induced by winds or conditions of distant swells), and attenuations (background friction and wave breaking).

The results of the wave modeling analysis showed that the terminal is exposed to long northwesterly swell waves, which are unfortunately present predominantly during Chile's summer cruise season. The peak wave period exceeds 16 seconds during these events. Consequently, a moored ship's response to the waves and the potential downtime due to ship motion behavior were modeled.

The aNyMOOR.TERMSIM model was used to determine the behavior of the ships under swell conditions. The model predicted the motions of the vessel as well as loads in mooring lines and fenders. The movements of the ship were studied through 6 degrees of freedom, which are defined with respect to the ship. Through orientation of the berth and optimization of mooring arrangements, the cruise ship could be moored safely at the location. However, excessive motion at the berth may affect passenger safety and comfort.

To evaluate the potential downtime due to motion, we reviewed the literature in regard to guidelines and recommendations for acceptable motion of cruise ships. References available includes PIANC (1995), Spanish ROM, and Nordforsk (1987). The recommended ranges varied greatly between the references. For the purposes of the evaluation, we adopted a median criterion for lateral movements and the Nordforsk guidelines for acceptable acceleration. In conducting the analysis, we identified a need for further investigation and developing guidelines and recommendations regarding the accommodation and the behavior of moored cruise vessels in locations where long period waves are present.

1 INTRODUCTION TO THE GLOBAL CRUISE INDUSTRY

Looking over the short-, medium- and long-terms, most lines and experts continue to feel the global cruise industry's best days are ahead. The broader industry fundamentals responsible for its dramatic rise over the past two decades are expected to remain in place: Introduction of new vessels and products, guest retention, an elevated level of guest satisfaction and value for money, adaptable business model, mobile assets, globalization of product offerings, and limited competition. These

[1] Moffatt & Nichol, Santiago, Chile, bhernandez@moffattnichol.com
[2] Moffatt & Nichol, Santiago, Chile, rfigueroa@moffattnichol.com
[3] Moffatt & Nichol, Santiago, Chile, fgchana@moffattnichol.com

fundamental trends will continue to propel the industry forward in terms of passenger and financial expansion.

Looking ahead, total cruise passenger levels are projected to increase worldwide over the next 15 years. The anticipated projection calls for cruise passenger levels to grow from 24.0 million in 2016 to between 36.0 and 44.0 million by 2030, with the medium projection scenario suggesting 38.0 million passengers by the end of this projection horizon. The leading cruise conglomerates—Carnival, RCCL, NCL, and MSC Cruises—are all poised to continue to expand, with Disney, Viking and other lines also looking to add supply and consumer momentum based on their unique brand positioning. Expansion of worldwide cruise and passenger activities will place continued demand for new and larger ports and destinations, as well as cruising regions.

These macro trends point to positive prospects for Valparaíso over the long term.

2 VALPARAISO'S CASE STUDY

Located along central Chile's Pacific Coast, Valparaíso is a vital center of maritime commerce and leisure. The city and its port are also important to the cruise industry, playing a strategic role in the delivery of several itinerary offerings in South America. As a homeport—tethered to the airlift and hotels available from nearby Santiago—the city and port of Valparaíso provide the logistical gateway to cruises transiting the wilds of Patagonia, the Strait of Magellan, Cape Horn, and visiting Chilean and Argentinean ports along the way. As a transit port, Valparaíso opens its doors to a varied number attractions and excursions, from exploring the UNESCO designated Historic Seaport Quarter to Chilean wine country and other inland offerings. Figure 1 shows the strategic location of the Bay of Valparaíso.

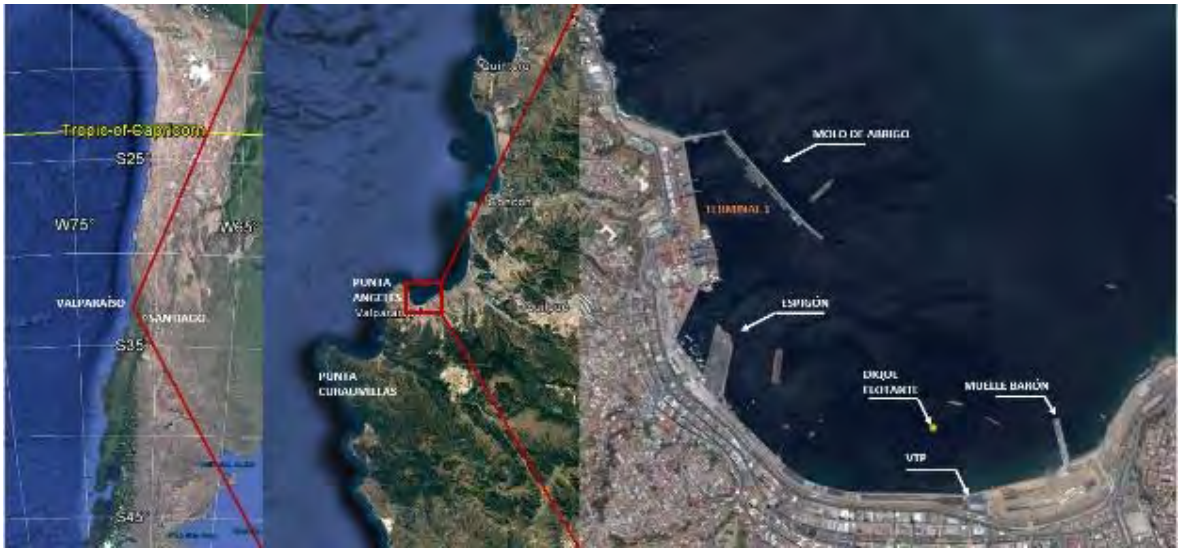

Figure 1: Location of Bay of Valparaíso

Currently, homeporting and visiting cruise ships berth at the Port of Valparaíso's cargo wharfs. While the current arrangement meets the basic operational needs of these vessels, it is less than ideal from a guest experience perspective. Reliance on extensive ground transportation and other logistical support from Valparaíso's remote cruise terminal—Valparaíso Terminal de Pasajeros (VTP)—adds cost and time to the overall homeport and port-of-call operations. Container vessels are also given priority at the cargo wharfs, creating berthing conflicts for cruise vessels and potentially placing vessels at anchor and/or creating other logistical difficulties.

In addition to the limitations of the existing cruise ship operation, there is nowhere within the footprint of the existing port facility for the cruise industry to grow to deliver a guest experience commensurate with the attractiveness of the region, while supporting larger vessels and more frequent vessel calls.

To address these challenges, the Empresa Portuaria Valparaíso (EPV) initiated a study to evaluate the potential for the port to develop a dedicated cruise pier within the harbor.

3 NEW JETTY LOCATION

An alternatives analysis was developed for different locations in the Bay of Valparaíso, which were evaluated and compared using a multicriteria analysis. The selected alternative is a jetty located in front of the passenger terminal, with a single berthing position and an optional second berthing position in the opposite face of the structure.

The selection of the alternative considered the following aspects:

- Legal
- Environmental conditions
- Existing and projected infrastructure
- Logistic/operation of the new jetty with the existing passenger's terminal
- Capex and Opex

The selected option was the simplest and most cost effective; however, the seabed depth presented a design challenge. The solution included dredging works to allow ships to come in closer to the coast and to avoid high depths for pile driving. Figure 2 presents the proposed jetty location, whereas Figure 3 shows the proposed layout.

Figure 2: New Jetty Location

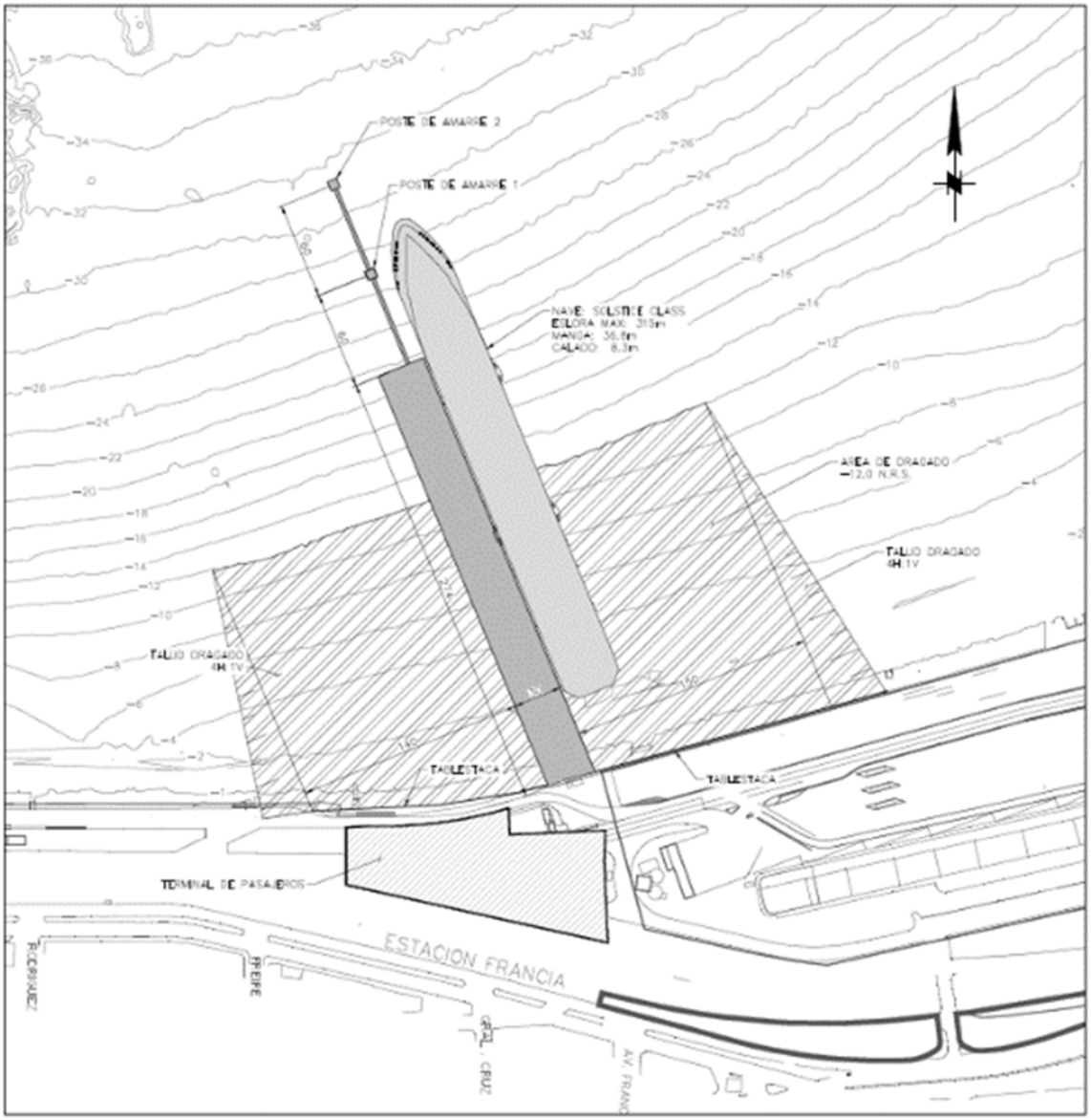

Figure 3: New Jetty Layout

4 RELEVANT ENVIRONMENTAL CONDITIONS

For purposes of the feasibility and concept study, mainly wave and wind conditions were studied to evaluate operational downtime, and water levels were analyzed to develop the concept design. However, additional phenomena, such as currents within the bay, should be considered during future design phases (basic and detailed design).

4.1 Waves and Winds at the Project Site

The Bay of Valparaíso historically has the main port terminal of Chile, because of the natural protection it offers against strong Pacific swells coming from the south, which are present on the Chilean coasts throughout the year. In addition, wave energy from the north increases agitation inside the bay. These waves are typically longer than the swells coming from the south. Also, the vulnerability of the bay to waves coming from the northwest quadrant, can be observed during extreme events, when the worst conditions are caused by local storms that approach the bay from the north-northwest.

A 36-year spectral hindcast was performed, propagating to the site within the bay. An appropriate methodology to transform waves in deep water to the coast consists of the simulation of unitary waves

from deep waters that cover the spectra domain in frequency and direction. The results of these simulations provide enough information to determine the energy variations within the numerical domain and the directional distribution of the spectral components when propagating towards the coast. Then, these coefficients of agitation and redistribution of energy allow the transformation of the spectra from deep water to the locations near the coast at the project site.

For the Bay of Valparaiso, 130 combinations of periods from 4 to 22 seconds and directions from 180 to 360 degrees were defined, which correspond to the ranges of wave conditions in deep water. These cases were propagated with unitary wave heights, to directly obtain the transformation coefficients in each element of the numerical domain. The estimation of the spectra in the project site allows for the calculation of the bulk parameters commonly used for wave characterization, such as spectral wave height, peak period, and peak direction.

It should be noted that the estimation of the spectra in the project site, from the contribution of each spectrum bin in deep water, is important in bays like Valparaíso, since the estimate considers the energy coming from all directions that waves enter the bay. The morphology of Valparaíso presents a natural shelter provided by Punta de Angeles and Punta Curaumilla. Both headlands generate a significant transformation/decrease of the wave energy that comes from the south, which are commonly the most energetic systems within each sea state in deep water. However, swells from the northwest quadrant, which are not typically the most energetic offshore system in the spectrum, when propagated within the bay—although they do not undergo important transformation processes—can sometimes contribute to the increase of conditions of agitation inside the bay. A typical offshore spectrum in front of Valparaíso and a schematic transformation of each system into the Bay of Valparaíso are shown in Figure 4. As it can be seen, the transformation process play an important role in the final wave bulks parameters, which will ultimately be used for assessing the dynamic behavior of the vessels berthed at the project site. The wave analysis should be carefully examined and the study consider any wave system present in the wave spectrum.

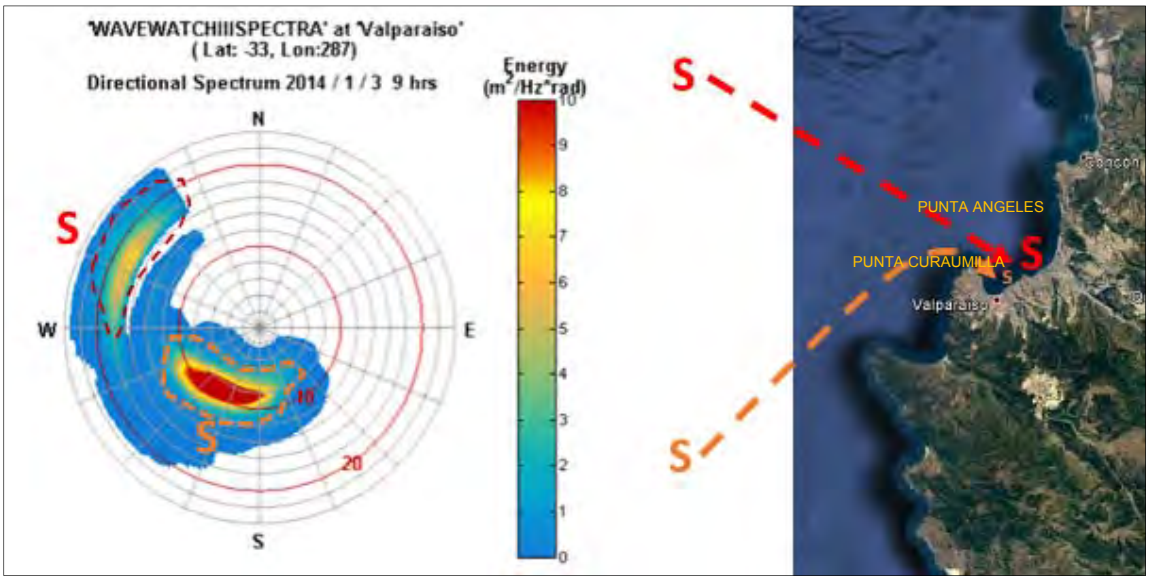

Figure 4: Offshore Representative Spectrum and Schematic Transformation of Each System into the Bay of Valparaíso

A Mike21 SW-FM (Spectral Waves-Flexible Mesh) numerical model was used to simulate the propagation of waves to the shore. Mike21 SW can solve the most relevant transformation processes, such as refraction and shoaling, the energy balance of the contributions induced by winds or swells conditions, and decreases from bottom friction, breaking, etc. In addition, Mike 21 SW-FM presents approximations to consider diffraction and reflection phenomena.

Validation of the wave analysis was carried out, comparing the propagated hindcast against wave field measurements located near the project site. Wave measurement campaigns on site involved approximately two months of measurements at the Yolanda 1 site and seven months at the Baron 2 site. Figure 5 shows the location of both measurement nodes and presents a comparison between the wave

height and period measured at Yolanda 1 and Baron 2 (red dots), and the model results (line and black dots). Quantile-quantile graphs for each of the variables considered are also presented.

Regarding the comparisons in both nodes, it was observed that the results of the simulation manage to capture in form and magnitude the measured events for wave heights and peak periods. It should be noted that the time series located in Baron 2 includes the extreme event of August 2015, a storm that corresponds to the largest event presented in the 36 years of statistics.

Considering the correlation between the simulated and measured data in both locations, it was concluded that the models and methodology used in the present study can characterize waves in an appropriate way in this sector of the bay.

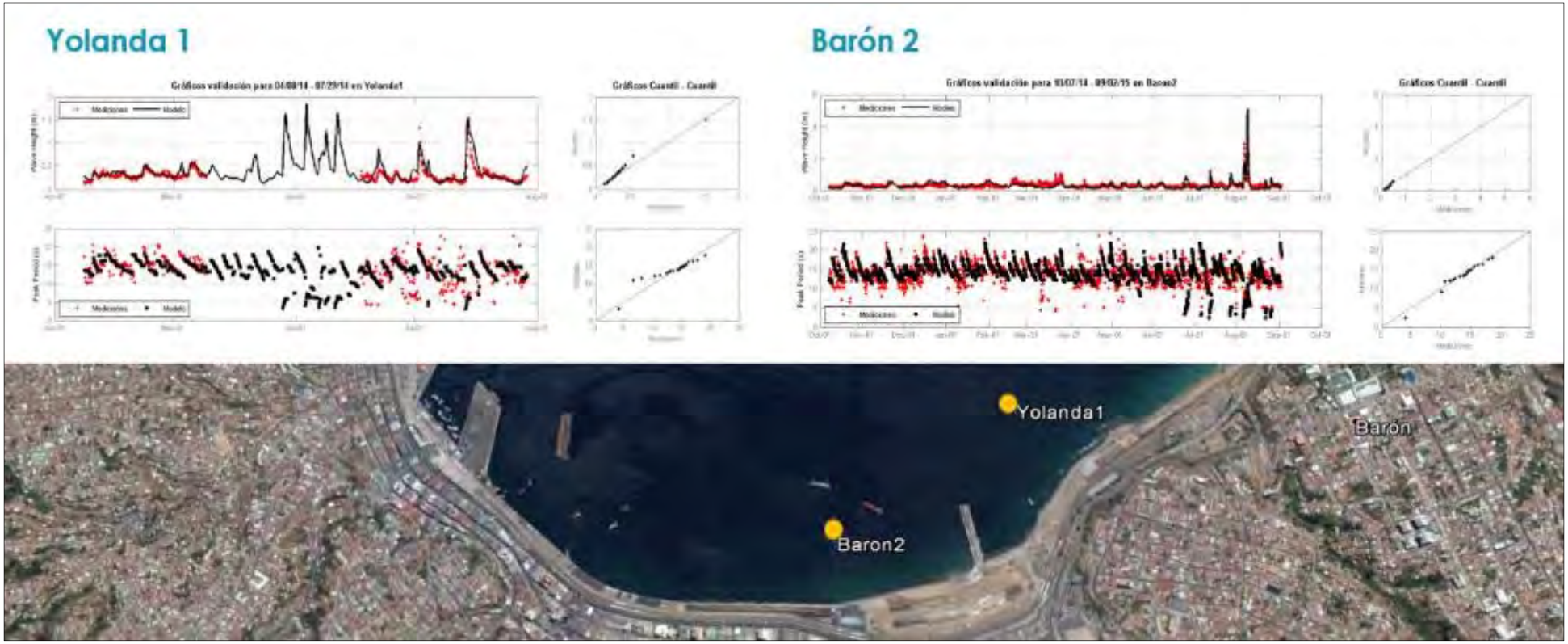

Figure 5: Wave Bulk Parameter Comparisons at Locations Yolanda 1 and Barón 2

For wind conditions, one year of statistics close to the project site was provided.

Both environmental factors, wind and waves, are shown in Figure 6. From these, the berth site of the proposed terminal was oriented considering that waves are driving the moored vessel behavior when berthed.

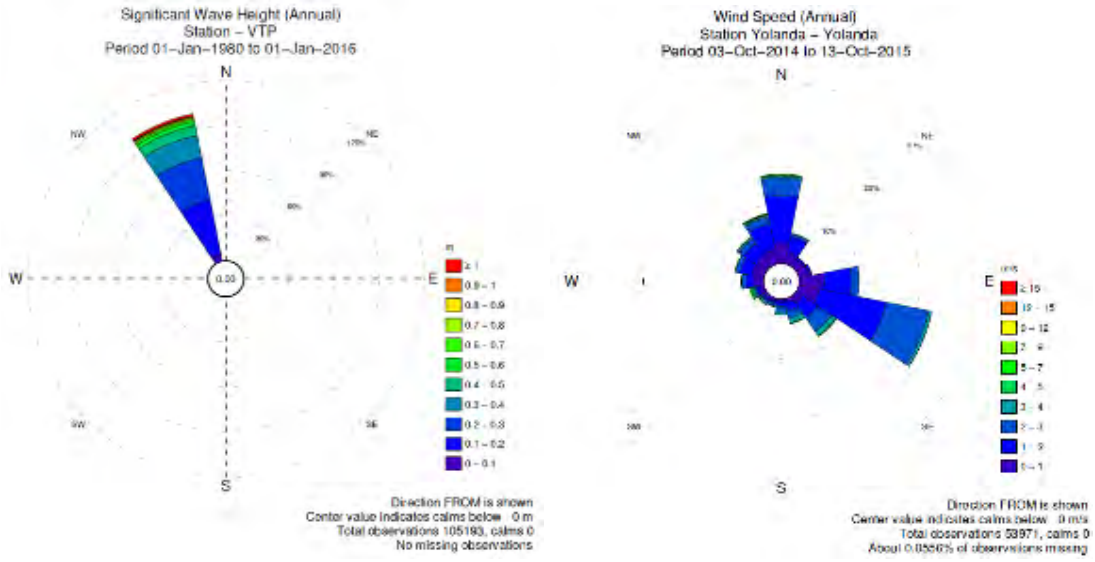

Figure 6: Waves and Winds at the Project Site

5 DETERMINATION OF THE EXPOSED SITE AVAILABILITY

Berth availability was a key element in the design because of the site exposure and the correlation between the cruise season and summer time when the energy from northwest quadrant tends to be more important than during the rest of the year. Short operational windows of 12 or 24 hours, and the rigidity of cruise schedules, implied that the likely availability of the berth site should be high enough to meet cruise line expectations.

Figure 7 shows the flowchart of the process adopted to estimate the availability and downtime due to environmental conditions. The environmental conditions (waves and winds) and vessel specifics were considered to establish the response of the berthed vessel due to the environmental influences. Vessel specifics included ropes, ship geometrics, terminal configuration, mooring arrangements, fenders, and bollards. Then, for a specific action, the vessel response output plus the given criteria can be compared to determine the following:

- Peak mooring line loads
- Peak fender loads
- Peak bollard loads
- Peak motions

If the results of one of the factors listed above is exceeded, then safe operating conditions may not be assumed. Thus, downtime must be considered under those particular conditions, with the corresponding decrease in berth availability.

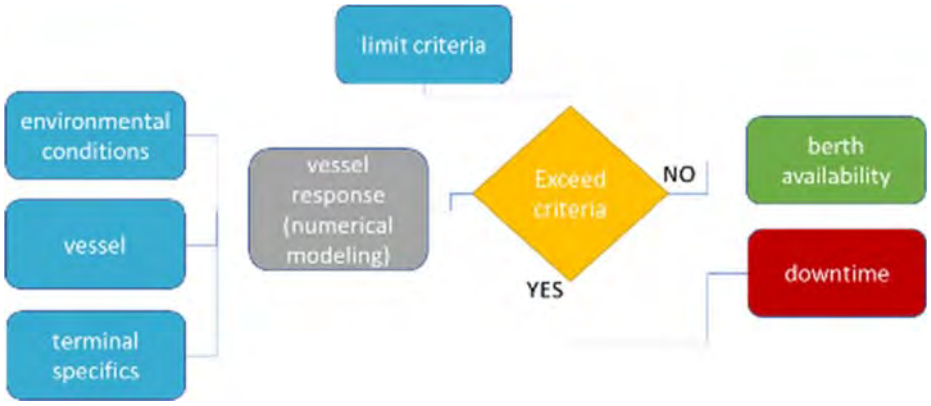

Figure 7: Availability/Downtime Estimation Flowchart

To determine the dynamic response of a ship berthed at the proposed project site, the model aNyMOOR.Termsim developed by Marin (Maritime Research Institute Netherlands) was used. The results of aNyMOOR provide a timeseries of ship movements, forces developed by the mooring lines, and reaction forces in the fenders and bollards at the proposed terminal.

The market study identified the characteristics of the cruise ships that could potentially call the new terminal. Vessels specifics are presented in the Table 1.

	Celebrity Cruises' Solstice-Class	**Holland America's Rotterdam Class**
Class:	Solstice-Class	Rotterdam-Class
Gross Tonnage:	122,000 GT	61,500 GT
LOA:	317 m	238 m
Beam:	36.8 m	32 m
Draft:	8.23 m	8.10 m
Capacity (Passengers):	2,850	1,400

Table 1: Design Vessel Characteristics

It is clear from the flow chart shown in Figure 7 that the berth availability is controlled by the thresholds selected as limiting criteria, and, consequently, choosing the appropriate set of values becomes crucial. The main challenge was selecting criteria that, while being conservative given the early stage of design, would not penalize the technical feasibility of the project.

5.1 Downtime Scenarios

To estimate the percentage of time during which the ship exceeds the movements and maximum forces allowed for its safe operation (downtime), the process shown in Figure 7 was applied, considering the following environmental conditions:

- Thirty-six years of wave hindcast, which consist of sea states every three hours from 1980 to 2015.
- One year of winds with records for every hour, corresponding to 2010.

Three scenarios were performed based on the available statistics, as follows:

(1) year 2010, using wave and wind statistic, both varying throughout the year;

(2) year 2010, waves varying along the year with most frequent wind conditions; and,

(3) 34 years of waves with most frequent wind condition.

These scenarios present multiple combination of wind statistics, since cruise ships are characterized by having a significant superstructure, and wind can have a significant impact on the vessel behavior when moored.

To estimate the response of the ship to the demands jointly generated by winds and waves together, 1,728 simulations were performed covering all possible combinations for each vessel. The ranges are presented in Table 2.

Parameter	Range	Number of cases
Wave height (m)	0.25, 0.50, 1.0, 1.5	4
Peak period (s)	7, 10, 13, 16, 19, 24	6
Peak direction (deg)	326,3 337.5, 348.8	3
Wind velocity (m/s)	1, 6, 11	3
Wind direction (deg)	22.5, 67.5, 112.5, 157.5, 202.5, 247.5, 292.5, 337.5	8
	Total Number of Simulations	**1728**

Table 2: Bulk Parameter Ranges for Waves and Wind

5.2 Limit Conditions for Safety Operation When Vessel is Moored

As mentioned, mooring limits are critical for estimating downtime. The following references were used to define the critical operating limits based on ship motions at berth and forces exerted on the mooring lines:OCIMF ¨Guidelines for safe working loads of mooring lines for line loads¨

- PIANC 1995¨Criteria for movements of moored ships in harbours¨
- Spanish Recomendación de obras marítimas ROM 2.0-11
- Nordforsk 1987 “Assessment of a ship performance in a seaway”

The maximum acceptable movements for safe operating conditions for ships at dock are presented in Table 3. It should be noted that reference material regarding the maximum movement of cruise ships is scarce. The ROM presents values for this type of vessel (Criteria A); however, there is no comment about the conditions under which these limits apply, and, comparatively, these movements are considerably more restrictive than for other types of ship/cargo. Therefore, a second criterion (Criteria B) for movement limits was established, which consists of the following:

- Criterion associated with passenger boarding/disembarking: A maximum motion at the vessel passenger door equal to 1 meter was employed to estimate an embarkation/debarkation threshold.
- Criteria associated with the comfort of passengers who remain on board while the vessel is docked: The maximum acceleration limits recommended by Nordforsk 1987 were used. These correspond to values under which people do not suffer from dizziness or experience loss of balance. The limits were applied to the maximum acceleration experienced on the upper deck of the cruise ship.

Reference	Lateral Acceleration (m/s^2)	Vertical Acceleration (m/s^2)	Surge (m)	Sway (m)	Heave (m)	Yaw (deg)	Pitch (deg)	Roll (deg)
Criteria A ROM 2011	-	-	0.8	0.8	0.5	0.2	0.2	0.2
Criteria B Nordforsk 1987 / From pilots and captains	0.2	0.3	1	1	1			2
PIANC 1995 Ferry	-	-	0.6	0.6	0.6	1	1	2
PIANC 1995 DWT>8000	-	-	0.3	0.3	0.3	1	1	1

Table 3: Criteria for Maximum Acceptable Ship Movement while Docked

With respect to the limits for the lines, maximum limits equal to 50% of the Minimum Breaking Load (MLB) of each line were adopted as a function of the corresponding vessel based on the OCIMF guideline.

5.3 Downtime Results Discussion

The results of the 1,728 simulations were used to estimate the vessel motions, forces on mooring lines, and maximum reactions to fenders. These variables were compared with the established limit criteria, identifying time periods when cruise ships would not operate safely due to one of the criteria being exceeded. The downtime estimation and its causes (excessive motions, mooring line tensions, or forces on fenders) were determined for the three scenarios defined in section 5.2.

With regards to operating limits, the analysis considered the limits established by the Spanish ROM, movements and the associated with the passenger doors, and accelerations. The analysis of the vessels response showed that events associated with long period swells produce that some parameters exceed the limits adopted for the ships operation, especially horizontal displacements (surge and heave) and the rotation around the ships longitudinal axis (roll). These waves principally occur during summer months, coinciding with the cruise ship season. In addition, the highest downtime and most adverse results were associated to the smallest design vessel.

A summary of the most relevant variables associated to the scenario that considered wave and wind during 2010 is presented in Figure 8, according to the following:

- (A) Wind speed and direction
- (B) Waves height and peak period
- (C) Peak to peak surge
- (D) Peak to peak roll for both design vessels

The subplots B and C in Figure 8 shows the thresholds for both criteria (A and B) for the motions that are driving the downtime estimation. There it can be seen that the threshold exceedance was associated with the high period, or events with wave heights greater than 0.5 m and peak periods above 15 seconds for both design vessels. In addition, winter waves also presented some events when these criteria were exceeded, which was associated with high sea waves and strong local winds.

By adopting the ROM criteria, the roll motion was found to be the critical parameter and drive the downtime estimation.

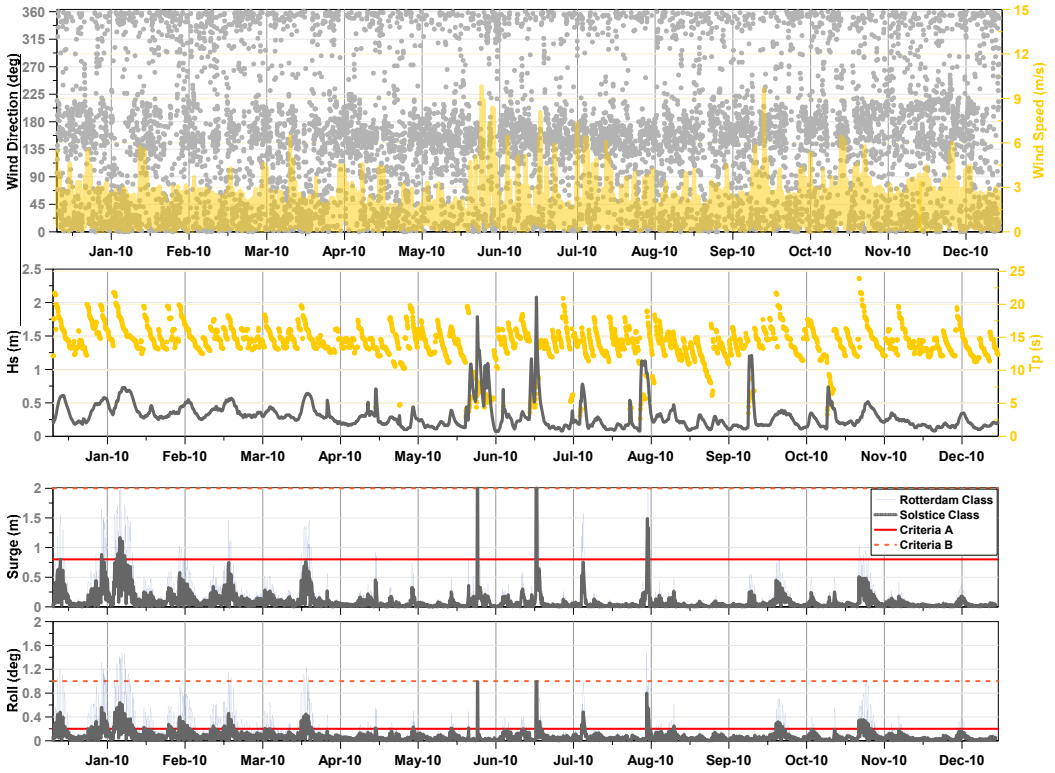

Figure 8: (A) Winds, (B) Waves, (C) Peak-Peak Surge, (D) Peak-Peak Roll. - for 2010 and operating thresholds under Criteria A and B

In contrast, the Nordforsk criteria developed for the operation of the ship at sea (seakeeping), where roll values of up to 2 degrees are allowed for cruises. The sensitivity between criteria is important for roll, where adopting a small threshold implies assuming a significant amount of downtime in contrast to the rest of the recommendations for similar ships. It must be kept in mind that the priority for this type of operation corresponds to avoiding mooring lines breakage due to ship movement.

For this particular case, differences on downtime estimations for both limit criteria analyzed, can reach 11% for the Solstice Class and 26% for the Rotterdam Class in Scenario 1 during the cruise season, while for the entire year the differences are 7% and 19% for the Solstice and Rotterdam Class respectively.

The results of Scenario 2 indicated that the wind and its variability are important, which makes sense when considering the characteristics of these ships with large superstructures. When variable wind speed was considered in the model, the downtime increased independently of the limit criteria adopted. Using an average constant wind value does not correspond to a conservative scenario for the estimation of downtime.

From the results of Scenario 3, it was evident that there are particularly severe years, which, in this particular case coincide with very intense El Niño/ENSO events, and some months experienced significantly higher downtimes than typically seen during regular years.

6 CONCLUSIONS OF THE VALPARAISO STUDY

The downtime analysis of the new jetty was conducted considering the following criteria:

- Allowable maximum vessel motion. The existing literature does not come to an agreement on reasonable thresholds for exposed cruise ship terminals, rather, a wide range of values can be adopted depending on the guideline/recommendation followed. The Spanish ROM establishes highly restrictive criteria for cruise ships without making any distinction on the type of terminal considered, specifically for rotational degrees of freedom, which 0.2 degrees (peak-to-peak) is recommended not to be exceeded. Given the ROM conservative recommendations, the Nordkforsk criteria was used instead to define the maximum allowable accelerations at the upper deck of the vessel while at berth and a maximum motion of one meter (peak-to-peak) at the passengers door.
- Tensions in mooring lines. A limit of 50% of the MBL was established for each line with a safety factor of two.
- Loads on fenders shall not exceed the rated reaction.
- Meteorological and oceanographic conditions. The analysis was conducted considering only one year of wind data from a publicly available source near the location of the new jetty. It was therefore recommended to develop a detailed wind study with site measurements that can reduce the uncertainty on the analysis and the impact over the downtime estimation.

Regarding the results, differences on downtime estimations for both limit criteria analyzed, can reach 11% for the Solstice Class and 26% for the Rotterdam Class in Scenario 1 during the cruise season While for the entire year the differences are 7% and 19% for the Solstice and Rotterdam Class respectively.

The existing literature for reasonable allowable downtime levels is scarce. Some authors proposed however a maximum annual average downtime of 2% for Nordic countries. On the other hand, Thoresen (2003) suggested two general recommendations without mentioning a specific type of cargo:

- Annual downtime (including stoppages caused by ship movements, maintenances, no availability of tugs, etc.) less or equal to 5%.
- Monthly downtime must not exceed 15%.

Thoresen highlights that these limits are specific to each project and must be evaluated case by case.

The Spanish ROM mentions that for liner service terminals (passengers, containers, ferries) 200 hours per year and 20 hours per month of downtime can be acceptable. These values can be increased twice when the utilization of the terminal is equal or less than 20%.

To decrease the probability that the cruise ship operation may be affected by site conditions, the following is recommended:

1. While the forecast systems allow for the advance warning of meteorological and oceanographic conditions, it is further recommended to develop a wind and wave forecast system in order to verify the operational windows for the cruise ship calls.
2. It is also recommended that the terminal implements a ship condition monitoring system, and establishes a protocol for recording vessel motions at the site, including extreme movements, breakage of mooring lines and damage on fenders.
3. To develop an action plan for those events the forecast and monitoring systems identify may affect the terminal operation
4. To implement state-of-the-art devices that reduce the ship movements at locations exposed to long swells. It is recommended to study the suitableness of these devices on the proposed site and the potential downtime reduction. Due to the characteristics of the exposed site, it is recommended that the terminal operators maintain a pre-tension system and change of the old mooring lines.

7 FINAL DISCUSSION

To evaluate the potential downtime due to motion, we reviewed the literature in regard to guidelines and recommendations for acceptable motion of cruise ships. References available includes PIANC (1995), Spanish ROM, and Nordforsk (1987).

In conducting the analysis, we identified a need for further investigation and developing guidelines and recommendations regarding the accommodation and the behavior of moored cruise vessels in locations where long period waves are present. Not only the recommended ranges varied greatly between the references, but the literature also suggested a wide range of decision parameters and variables.

It is therefore suggested further investigating, unifying criteria and developing new updated guidelines considering the specific requirements of the cruise ship industry, and defining, specifically, the following parameters:

- Maximum allowable vessel motion and rotation during berthing, unberthing and passenger disembarking
- Maximum wave height and period in relation to the design vessel dimensions
- Maximum wind speed in relation to the design vessel dimensions

8 REFERENCES

Carl A Thoresen (2003). Port designer's handbook, Recommendations and guidelines.

DHI (2014a). MIKE 21 Spectral Wave Module, Scientific Documentation. DHI Water Environment and Health, 2014. Horsholm, Denmark.

Nordforsk. (1987). Assessment of Ship Performance in a Seaway: The Nordic Co-operative Project: "Seakeeping Performance of Ships", Nordforsk.

Marin (2014) Rijken, Wiebe van der, aNyMOOR.TERMSIM Documentation, The Netherlands.

Marin (2017), Diffraction database of a cruise vessel, Technical note, Report No. 30344-1-PO. The Netherlands

Moffatt & Nichol (2017). Análisis de Mercado e informe de ingeniería, Estudio de factibilidad de nuevo muelle para naves crucero en puerto Valparaíso – estudio de mercado, Chile.

OCIMF (1997). Mooring Equipment Guidelines, Oil Companies International Marine Forum. 2nd Edition.

PIANC (1995), Report No.24, Criteria for movements of moored ships in harbors, PIANC, Brussels.

PIANC (2002), Report No.33, Guidelines for design of fender systems, PIANC, Brussels.

ROM (2011). Recomendaciones para Obras Marítimas - Serie 2, Obras Portuarias Interiores. Recomendaciones para el proyecto y ejecución en Obras de Atraque y Amarre. Capítulo IV Definición de los estados y situaciones de proyecto. Version 0.2-11, Spain.

Sandra D. Rice, William N. Seelig, (2010) ASCE, Cruise Vessel Wind Coefficients for Mooring Analysis, Washington, DC

TSUNAMI HAZARD ASSESSMENT FOR PERMANENTLY MOORED FSRU MARINE TERMINAL IN CHILE

by
Eric Smith[1], P. Lynett[2] and C. Rodriguez[3]

1 ABSTRACT

Evaluation of tsunami effects on moored vessels is not typically considered in marine terminal design due to the low probability of a vessel calling at a terminal simultaneously with a design-level tsunami event. A methodology is needed for permanently moored floating LNG storage and regasification units (FSRUs) in tsunami hazard areas like Chile. The authors present an innovative method for developing a design tsunami hazard assessment for permanently moored vessels consistent with other considered hazards (e.g. seismic) which may be used for terminal design.

2 INTRODUCTION

Chile has a long history of great subduction zone earthquakes and the local tsunamis produced by them. Since the 1500's, there have been 14 documented earthquakes with Mw greater than 8.0, including the 1960 Mw 9.5 Valdivia earthquake, the largest recorded earthquake in recent human history. The Andes LNG project is planned to store and regassify liquefied natural gas (LNG) onboard a Floating Storage and Regasification Unit (FSRU) vessel and deliver gas via pipeline to an onshore power plant. Evaluation of tsunamis for moored vessels is not typically considered for terminal design due to the low probability of a vessel calling at a terminal simultaneously with a design-level tsunami event. However, in the case of a FSRU, the vessel is on site continuously for 20 years or more, greatly increasing the probability of the moored vessel occupying the berth during a tsunami event. A methodology is needed for permanently moored floating LNG storage and regasification units (FSRUs) in tsunami hazard areas like Chile.

In the immediate vicinity of the project site, the earthquake of 1922 generated the largest recent tsunami, with a likely amplitude of 3m near the proposed terminal. In this paper, we present a tsunami hazard assessment approach to account for the great tsunamis generated by these local earthquakes, and the potential effects of this hazard on the Andes LNG floating vessels and marine terminal. A two-part approach was employed: First we analyze the propagation and variation of earthquake-generated tsunamis to the project site and evaluate the statistical probability of tsunami impacts; second we evaluate the impact of the tsunami currents and water levels on a moored LNG carrier.

3 PROJECT DESCRIPTION

Figure 1 shows the proposed marine facilities general layout and the single berth sea island jetty layout at the project site in Chascos Bay on the Chilean coast, approximately 650 km north of Santiago. The terminal will consist of a permanently moored FSRU secured by a conventional mooring system of mooring and breasting dolphins at a single berth sea island jetty, supplying gas to a subsea pipeline. The LNGCs will deliver LNG to the FSRU and will berth on a transient basis. The mooring analysis of the terminal assessed two discrete mooring arrangements: Mooring Arrangement A, where the LNGC deploys mooring lines directly to the FSRU; and Mooring Arrangement B, where two additional mooring dolphins (independent of the FSRU mooring system) provide additional breasting lines that connect the LNGC directly to the additional dolphins. Pneumatic fenders will be located between the LNGC and FSRU vessels and will be connected to the FSRU.

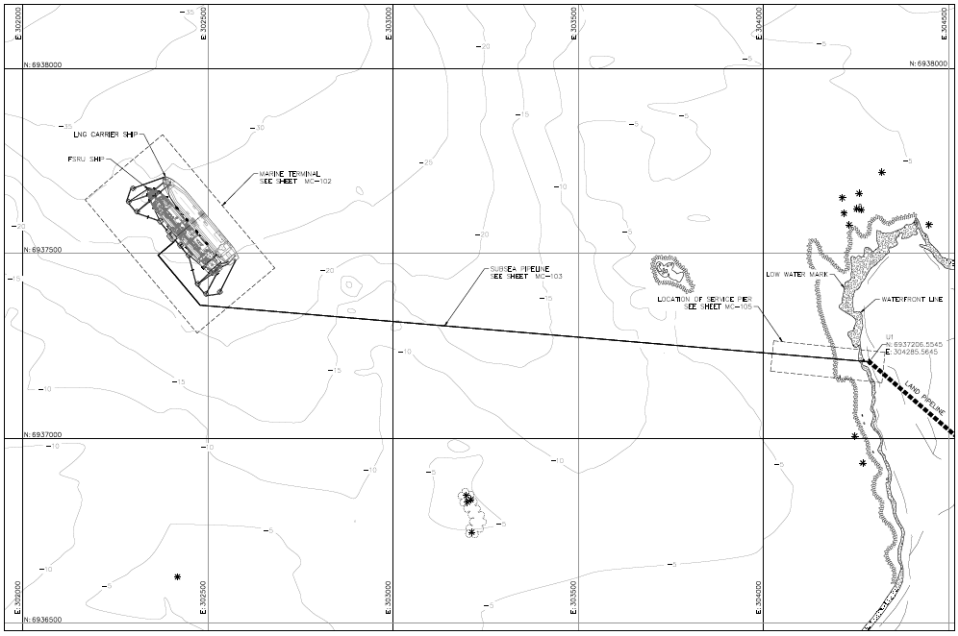

Figure 1 Project Site

4 TSUNAMI MODELING

For the work presented here, two different model suites are used. Each tsunami event is simulated with both modeling approaches. The purpose of using two different modeling suites is to confirm confidence in the models' accuracy with respect to the complex wave components and directions that exist along the Chilean coast during a tsunami. Furthermore, each simulation can be considered as a separate realization of a potential tsunami, adding to the statistical database of tsunami currents for use in the mooring analyses.

4.1 Simulation with Coupled COMCOT+COULWAVE

For the large-scale, regional propagation, the nonlinear shallow water model COMCOT is employed. Following Son et al. (2011), in the nearshore area where site-specific predictions are desired, COMCOT is coupled with the Boussinesq-type model, pCOULWAVE. pCOULWAVE then provides a detailed simulation of tsunami elevations and currents, with a resolution of approximately 10 m. Details about the models are provided below.

COMCOT is a well-established model for tsunami studies, and accurately predicts tsunami propagation. COMCOT solves the nonlinear shallow water wave equations in conservative form with the added effect of bottom friction. Bottom friction is formulated with a Mannings "n" coefficient. The numerical scheme employed by COMCOT is the explicit leap-frog difference method. Nonlinear terms in the model are approximated with upwind finite differences and linear terms by two-point centered finite differences. This numerical scheme is stable and robust but is a low-order accurate method, meaning that it is susceptible to numerical dispersion and dissipation errors. Physically, this implies that nearshore currents, where jets and eddies are important, may not be predicted properly with this model; such features may be overly damped due to numerical dissipation.

To generate the tsunami from an undersea earthquake, COMCOT uses the fault model of Okada (1985). The main assumptions of this model are a rectangular fault plane within an elastic deformation. The fault model predicts the deformation of the seafloor, which corresponds directly to the initial deformation of the ocean water free surface. Once the earthquake has been described with the above parameter set, COMCOT is able to propagate the initial disturbance across oceans.

pCOULWAVE solves the Boussinesq-type equations in conservative form, including turbulent viscosity and the associated horizontal and vertical vorticity terms (Lynett 2006, 2007; Lynett et al., 2010). Bottom friction in this study is also expressed with a Mannings "n" coefficient. The numerical method uses a fourth-order monotone upstream-centered schemes for conservation laws–total variation diminishing (MUSCL-TVD) to solve the leading order (shallow water) terms, while for the dispersive terms, a cell averaged finite volume method is implemented. For the time integration, a third order Adams– Bashforth predictor and the fourth-order Adams–Moulton corrector scheme has been used to keep numerical truncation errors small.

4.2 Simulation with MOST

Earthquake-generated tsunamis, with their long wavelengths, are ideally matched with Non-linear Shallow Water (NSW) for transoceanic propagation. Models such as those by Titov and Synolakis (1995) and Liu et al. (1995) have been shown to be reasonably accurate throughout the evolution of a tsunami and are in widespread use today. At present, the Method of Splitting Tsunami (MOST) hydrodynamic model is implemented. MOST was introduced by Titov and Synolakis (1995 and 1998). This model has been extensively validated and used for tsunami hazard assessments in the United States and is currently maintained and in operational use at National Oceanic and Atmospheric Administration / Pacific Marine Environmental Laboratory (NOAA/PMEL). Variants of the MOST model have been in constant use for tsunami hazard assessments in California since the mid 1990s. MOST solves the NSW equations using a wave-characteristic solver approach (Titov and Synolakis, 1998). The numerical scheme uses a second-order differencing approach for both linear and nonlinear terms, and bottom friction is included using the same Manning's roughness formulation used by COMCOT. To generate the tsunami from an undersea earthquake, MOST uses the fault model of Okada (1985), again just as with COMCOT.

4.3 Tsunami Model set up

The bathymetry/topography for the simulations is taken from different sources for the two different models. For the regional simulations performed by COMCOT, the bathymetry and topography are taken from the GEBCO database, using 2 arc-minute global bathymetry and topography. An image of the bathymetry map used for these simulations is shown in Figure 2. The pCOULWAVE domain is a much smaller area, centered on the site location. The data used to generate this bathymetry grid was provided in the form of depth contour lines, and these were interpolated to create a numerical grid with constant grid length of 10 meters.

The wave enters the pCOULWAVE domain through the offshore boundaries. The information about this incoming wave is provided by the COMCOT simulation. This coupling is one-way, in that pCOULWAVE receives boundary information from COMCOT, but not vice-versa. This is a common and efficient coupling technique when dealing with model domains that vary widely in grid resolutions.

Dissipation is included in the pCOULWAVE simulation through bottom friction and wave breaking. Bottom friction is modeled via a Mannings friction formulation, using a bottom roughness value of 0.025 $m^{1/3}$, which is a value commonly used for long waves in shallow waters, and conservatively represents a relatively smooth seafloor. Wave breaking is approximated through the equations developed for and included in the pCOULWAVE model, which have been shown to be accurate for a wide range of field cases.

The pCOULWAVE simulations are executed using a horizontal resolution of 10 m on a grid of 1,500 by 1,000 grid points in the x (east-west) and y (north-south) directions respectively. Each simulation is run for 400 minutes of physical time. Thus, the simulation domain is composed of 1.5 million grid points, and the duration is covered by 475,000 time steps (400 minutes of simulation time, using a time step of 0.05 seconds). Boussinesq-type simulations tend to be computationally demanding, and the simulations presented here are run on a large cluster to make use of parallel processing, each requiring about 40 hours of wall clock time on 120 processor cores.

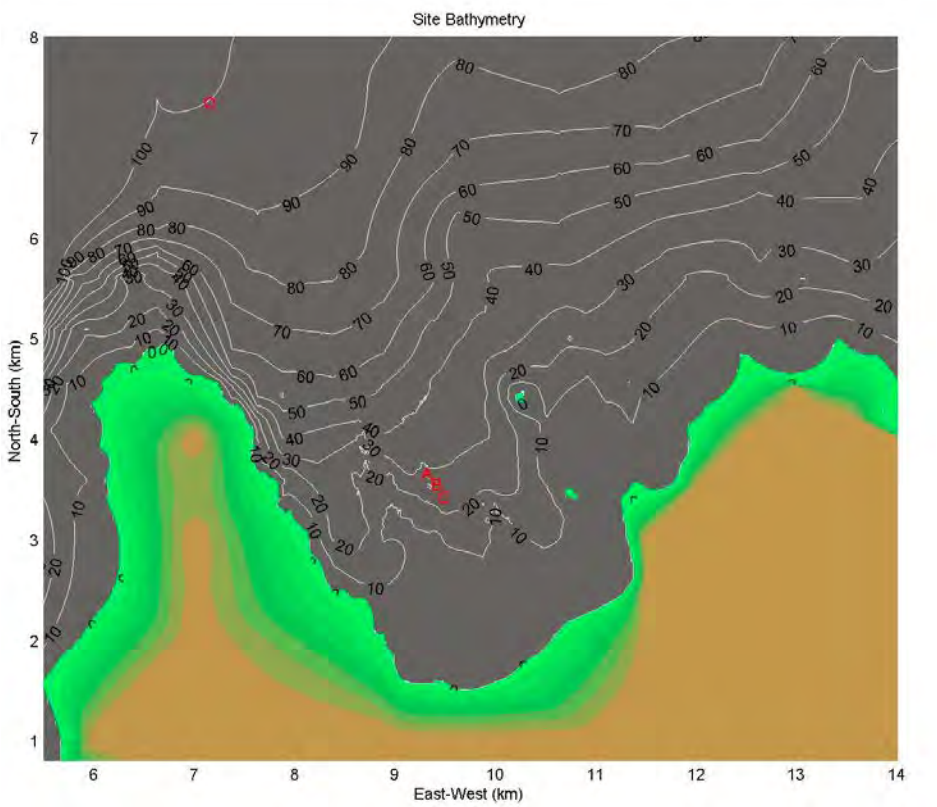

Figure 2 Bathymetry and Topography of the Study Area

For the MOST simulations, the tsunami waves were propagated across the SE Pacific Ocean though the same bathymetric grid used by COMCOT. In the finite-difference scheme employed in MOST, the changes in the tsunami as it travels into shallower water are accounted for by using three nested grids of increasing spatial resolution. The coarsest grid which covers the largest area has 12 arc-sec resolution, whereas the intermediate and finest grid have 3 arc-sec and 1/3 arc-sec (~10m) spatial resolution respectively. The coarse and intermediate grids were obtained by interpolating the 2014 GEBCO 30 arc-sec global relief dataset. The high resolution DEM for this study is identical to that used by pCOULWAVE and described above. Bottom friction is modeled using the same Manning's "n" coefficient as used in the COMCOT+pCOULWAVE approach

4.4 Design Scenarios

To provide a range of potential tsunami impacts at the design site, five different earthquake scenarios are examined with properties given in Table 1. These earthquake properties are provided by the seismic report (Comte and Ortega, 2015). These earthquake scenarios are chosen for study as they represent that largest known earthquakes in the local area.

Year	M_w	Fault Length [km]	Fault Width [km]	Rupture Area [km^2]	Average Slip [m]
1922	8.5	400	100	40,000	4.8
1730	8.7	450	80	36,000	10.60
1943	8.0	220	80	17,600	1.93
2015a	8.3	220	80	17,600	5.44
2015b	8.3	250	70	17,500	5.48

Table 1: Earthquake Properties of Tsunami Scenarios

In this section, the COMCOT+pCOULWAVE model is used. While simulation results will be discussed in detail in this section, first, a summary table showing the primary results from each earthquake scenario is provided. This data is given in Table 2 and Table 3 below, which shows the arrival time of the initial sea level change due to the tsunami, and the ranges in the maximum water level, minimum water level, and maximum speed at the design site. It is clear that the 1922 event, which is controlled by an earthquake in the immediate vicinity of the design site, controls all aspects of the tsunami hazard.

Source	Arrival Time Post-Earthquake of first 5 cm sea level change (minutes)	Arrival Time Post-Earthquake of the first tsunami crest (minutes) and its elevation (m)	Range of Predicted Maximum and Minimum Water Levels along Berth (meter w.r.t. MSL)
1922	4	14 min / +2.9 m	2.8 to 2.9 -3.2 to -3.4
1730	41	51 min / +0.6 m	1.2 to 1.3 -1.1 to -1.3
1943	36	43 min / +0.1 m	0.16 to 0.18 -0.15 to -0.16
2015a	36	45 min / +0.3 m	0.40 to 0.48 -0.41 to -0.42
2015b	35	45 min / +0.3 m	0.43 to 0.49 -0.50 to -0.51

Table 2: Summary of Tsunami Elevation from Scenario Simulations

Source	Current Associated with the First Tsunami Crest (m/s)	Range of Predicted Maximum Tsunami Current along Berth (m/s)
1922	1.2	2.0 to 2.6
1730	0.19	1.1 to 1.4
1943	0.03	0.35 to 0.40
2015a	0.10	0.58 to 0.65
2015b	0.10	0.41 to 0.56

Table 3: Summary of Tsunami Currents from Scenario Simulations

4.5 Tsunami Stochastic Approach

To provide tsunami hazard information for the FEED level design, a "stochastic scenario" approach is used that allows for the approximate expression of tsunami recurrence periods. From the five scenario simulations discussed above, it is clear that the 1922 earthquake source leads to the greatest tsunami impacts at the site; therefore, it corresponds to the design earthquake for tsunami hazard. With information provided in the scientific literature (Comte and Ortega, 2015), it is expected that a 1922-like earthquake (i.e., Mw 8.5 with rupture immediately offshore of the site) occurs once every 100-250 years. However, while the earthquake has this recurrence period, we cannot immediately assign this return period to the tsunami effects simulated by this source. The earthquake recurrence period is a function of its magnitude only, and other parameters, such as focal depth and internal rupture angles, while controlling the initial tsunami properties, play no role in this return period. Therefore, to quantify a tsunami recurrence period, we must understand the range of potential tsunami impacts that might be caused by different configurations of a Mw 8.5 earthquake offshore of the site.

The following set of tsunami simulations, each with a slightly different source condition, is performed:

1. A "baseline" earthquake, with best-estimated earthquake parameters (epicenter location, focal depth=15km, strike=0 degrees, dip=20 degrees, and rake=90 degrees) for a local Mw 8.5 earthquake, as provided by the seismic report (Comte and Ortega, 2015).
2. Shift epicenter to south by 25% of rupture length from "baseline" earthquake
3. Shift epicenter to north by 25% of rupture length from "baseline" earthquake
4. Shift epicenter to south by 50% of rupture length from "baseline" earthquake
5. Shift epicenter to north by 50% of rupture length from "baseline" earthquake

6. Shift epicenter to east by 25% of rupture width from “baseline” earthquake
7. Shift epicenter to west by 25% of rupture width from “baseline” earthquake
8. Use focal depth of 10 km with “baseline” earthquake
9. Use focal depth of 20 km with “baseline” earthquake
10. Use focal depth of 25 km with “baseline” earthquake
11. Change strike angle to 12 degrees from “baseline” earthquake
12. Change strike angle to 6 degrees from “baseline” earthquake
13. Change Dip angle to 17 degrees from “baseline” earthquake
14. Change Dip angle to 23 degrees from “baseline” earthquake
15. Change Rake angle to 102 degrees from “baseline” earthquake
16. Change Rake angle to 78 degrees from “baseline” earthquake

As noted previously, the parameters changed in this list represent quantities that can affect the tsunami significantly, but play no direct role in the quantification of earthquake magnitude. The range of these values are taken from recent large earthquakes in the region. While there are no available distributions for these values, which would be needed for a robust probabilistic analysis, it is reasonable to assume the distributions, within the values tested, resemble white noise distributions. Thus, each of the simulations tested has an equal chance of occurring; i.e., each of these scenarios has an equal chance of being the next Mw 8.5 earthquake to occur in this area.

All 16 scenarios were simulated by both modeling suites (i.e., the COMCOT/COULWAVE suite and the MOST suite), therefore, 32 different simulations are included in this analysis. For each of the simulations, the speed versus direction polar plots are generated for the berth location. Using the polar plots for each of the 32 simulations, probability of exceedance curves for maximum simulated speed as a function of direction can be generated. To perform this analysis, current heading was divided into 2-degree bins, and an exceedance curve developed for each bin. As there are 32 simulations, each exceedance curve is composed of 32 points. With this information, it becomes possible to express the relative likelihood of a specified current-direction pair, in terms of useful recurrence periods. For example, if the design earthquake for tsunami hazard is assumed to have a return period of 250 years, and a speed of 2 m/s (at a specific heading) is only exceeded in half of the tsunami simulations, then this information can be combined to state that a speed of 2 m/s (again, at this specific heading) will only be exceeded, on average, every 500 years. Similarly, a speed that is only exceeded in one out of every 10 simulations, or equivalently a 10% exceedance probability, would have a recurrence period of 2,500 years.

Figure 3 provides the maximum speed as a function of direction for three different exceedance levels. What is immediately clear is that, with decreasing exceedance level, or increasingly rare currents, the polar speed distribution becomes wider in the broadside direction. The physical reason for this “fattening” of the broadside current distribution is that eddies are present in this area. While these eddies exist in all of the simulations, then tend to occur in a chaotic fashion across the realizations, yielding a random but widely spread direction. Such a process is a primary motivating factor for this type of statistical analysis, where a single deterministic simulation might not provide a complete description of the potential variability of this complex velocity field.

The mooring analysis of the vessel targets a specific tsunami recurrence period or periods. To this end, it is necessary to assign each simulation a best-match exceedance value. This is performed by determining which simulation produces a maximum speed envelope that best matches the envelope for a specific exceedance level. Figures 4 and 5 provide these best-match scenarios for exceedance values of 10% and 50%, respectively. The best match is shown on the left, and the second best match on the right; black lines show the simulation time series, and the red lines the exceedance envelope.

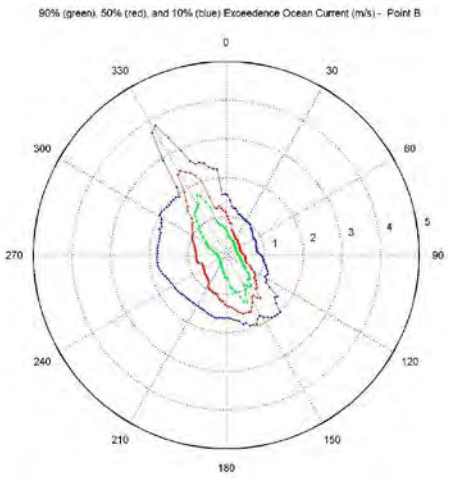

Figure 3: Maximum Tsunami Speed as a Function of Direction for Three Different Exceedance Levels

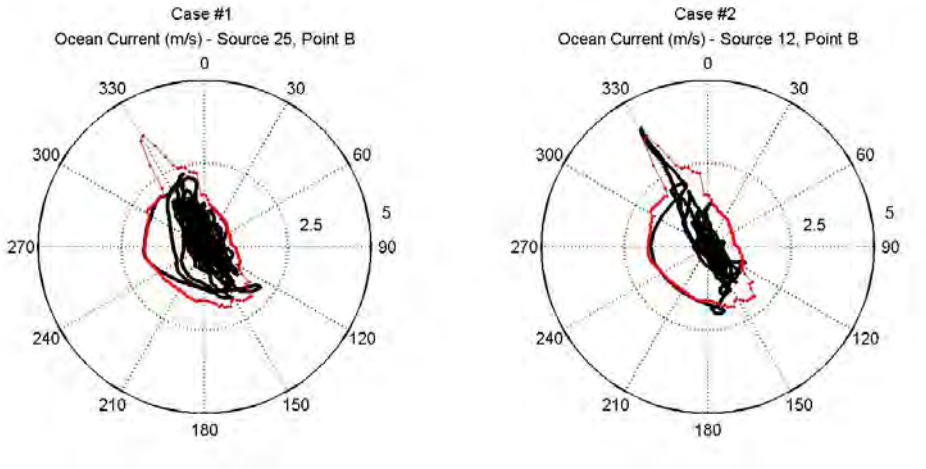

Figure 4: Best-Match Scenarios 10% Speed Exceedance Envelope from the Entire 6-Hour Simulation

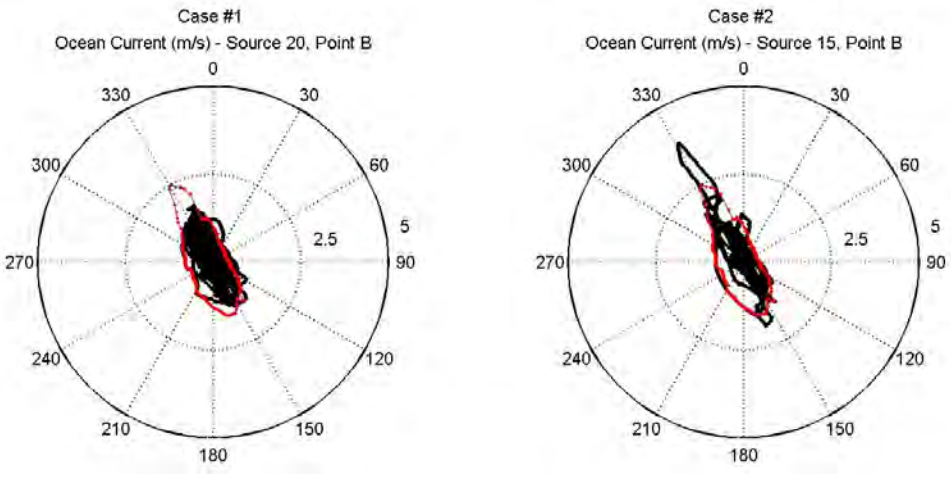

Figure 5: Best-Match Scenarios 50% Speed Exceedance Envelope from the Entire 6-Hour Simulation

4.6 Duration of Tsunami Events

In addition to the design exceedance level, the design duration is an important parameter. For this project, we determine exceedance envelopes based on simulation data from the first 60 minutes of the event, the first 90 minutes of the event, and the entire 6 hours of the simulation. From inspection of these envelopes, it is evident that the maximum currents along the 330-150 degree axis are insensitive to the design duration. The reason for this is that these currents are associated with the first waves of the event, occurring within the first hour. However, it is also evident that as the design duration increases, the off-main-axis currents grow significantly. This is due to the existence of eddies, which can create currents in any direction. Eddies take time to be generated and evolve, and thus are not a strong forcing during the early times of the event.

From comparison of the current predictions between the MOST and COMCOT+pCOULWAVE results, it is evident that the two approaches yield different behaviors for eddies. The current vs direction distributions for the MOST results tend to show relatively large on-axis (330-150 degree axis) currents and relatively small off-axis currents. The COMCOT+pCOULWAVE results, on the other hand, yield the opposite trends, with relatively low on-axis and relatively high off-axis currents. The reason for this difference lies in the physics of the two approaches, or more specifically the turbulence closure found in pCOULWAVE compared to that in MOST. The pCOULWAVE model includes various turbulent and rotational corrections, designed specifically to handle complex coastal currents created by tsunamis (i.e. Son et al., 2011). The manifestation of these physics results in dispersion of the current field in all directions through the generation and evolution of eddies. While the MOST model does predict the creation of eddies, the behavior of these features is different between the two models. As there is little data to demonstrate which model is a better predictor of currents for this particularly site, allowing realizations from both models to have equal weighting permits both relatively large on-axis and relatively large off-axis currents to be included in the analysis.

5 TSUNAMI MOORING ANALYSIS

The performance of the moored vessels was assessed by running a series of dynamic mooring analyses of the tsunami events. The design basis for the terminal specifies that the FSRU shall be capable of departing berth in an emergency. However, in order to investigate the effects on mooring infrastructure in case of having a moored vessel, the dynamic mooring simulations are conducted for two scenarios: the FSRU at the berth by itself; and the FSRU and LNG carrier in ship-to-ship (STS) transfer operations. Performance results of both the LNGC and FSRU mooring are predicated on departing berth within 60 minutes and 90 minutes, respectively, of the earthquake-generated tsunami event.

We selected tsunami events for the mooring analyses based on the combined return period of the earthquake event and the current exceedance threshold acceptable for the design of the berth. The FSRU-only mooring arrangement is simulated for the first 90 minutes of the 10% exceedance tsunami (return period of 1000-2500 years). The STS mooring arrangement is simulated for the first 60 minutes of the 50% exceedance tsunami (return period of 200-500 years).

5.1 Mooring Arrangements

The FSRU mooring arrangement, presented in Figure 6, consists of 22 mooring lines with 22 m polypropylene tails. There are sixteen (16) breasting lines and six (6) spring lines. All lines were modeled as Samson Amsteel Blue mooring lines, a high modulus polyethylene (HMPE) rope. For the FSRU Mooring Arrangement, the vessel was modeled at loaded draft condition, as the induced tsunami current loads associated with the loaded draft condition are assumed to be greater than those associated with the ballast draft condition. This is due to the greater submerged area of the loaded draft condition, relative to the ballast draft condition.

The primary mooring arrangement analyzed for the STS consistent of a LNGC is moored exclusively to the FSRU, presented in Figure 7. The analysis included separate analyses of the LNGC in ballast and loaded draft conditions. For analysis cases where the LNGC was modeled in ballast, the FSRU was modeled as loaded, and vice-versa. The STS Mooring Arrangement has twenty-two (22) mooring lines dedicated to the

FSRU (identical to the FSRU only mooring arrangement) and sixteen (16) ship-to-ship lines. Of these STS lines, ten (10) are breasting lines and (4) are spring lines. Four (4) fenders were modeled between the vessels. These fenders are fixed to the FSRU, and are spaced equivalently along quarter-points of the hull's broad, flat side area. The numbering scheme associated with Mooring Arrangement A is presented in Figure 7.

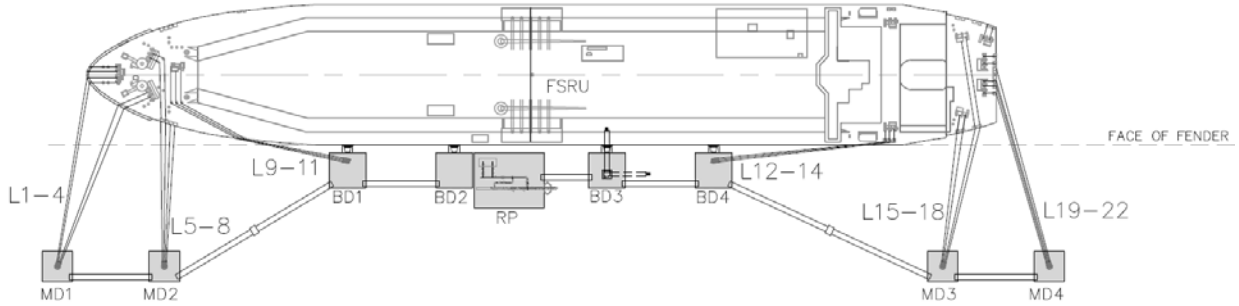

Figure 6: FSRU Only Mooring Arrangement

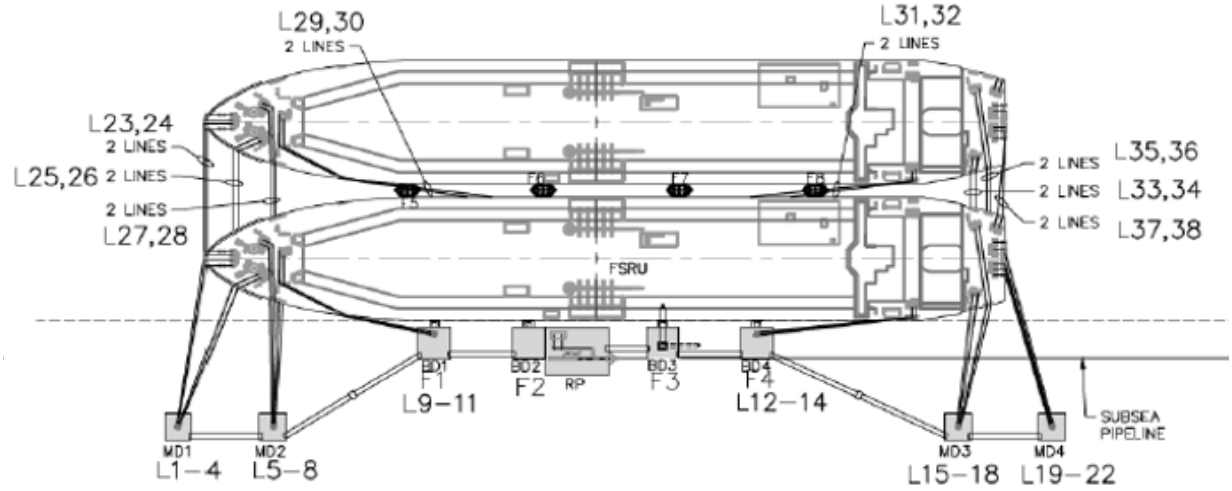

Figure 7: Mooring Arrangement for STS transfer

5.2 Analysis Software

The AQWA suite of software was used to model the dynamic response of the FSRU and LNGC mooring. AQWA comprises a suite of programs that performs three dimensional diffraction/ radiation analysis and calculates first order and second order (non-linear drift) forces on fixed or floating bodies. The submerged body surface is described by a finite element mesh. The software can resolve multiple floating bodies simultaneously as well as fixed structures. The model computes the hydrostatic and frequency response of the moored structures as well as hydrodynamic interactions between the floating structures and calculates the added mass and damping matrices for the floating bodies.

5.3 Modeling Assumptions

5.3.1 Mooring Line and Fender Stiffness Modeling

The load-deflection response of a mooring line and tail combination or a fender can be described by a polynomial function. Fifth order stiffness polynomials were input into the dynamic models to define the responses of mooring lines and fenders within the system. Similarly, fender stiffness polynomials describe the response of the fenders within the model, and are based on force/deflection data provided by the fender manufacturer.

For each vessel, a mesh panel model was created; this panel model provides the definition of the vessel's hull for the AQWA radiation/diffraction and time-domain analyses. Figure 8 presents the side-by-side model of hull meshes.

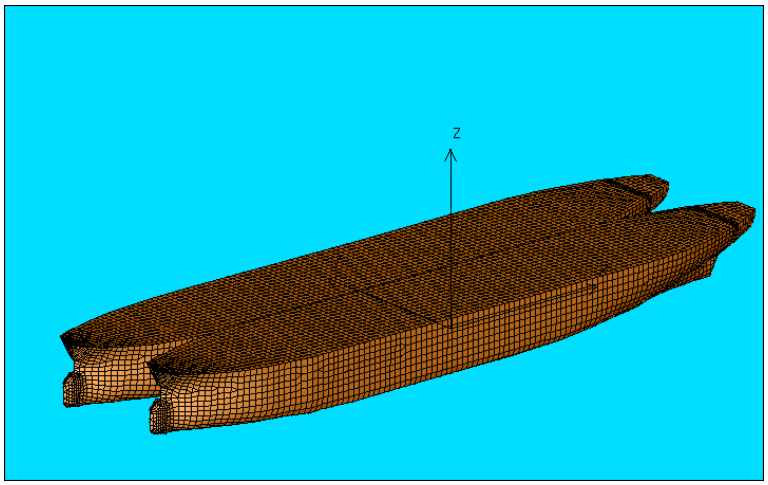

Figure 8: Panel Mesh AQWA Model of STS Transfer

5.3.2 Water Elevation Changes

AQWA modeling framework does not allow for changes of the baseline water level (except for waves) during a time-domain simulation. In order to account impact of changes of water level during the tsunami event, additional line stresses due to fluctuations of the water surface elevation were calculated and added to the mooring response. Each time-step in the tsunami time series applied to the model has a corresponding water surface elevation. As the elevation increases, mooring lines experience greater extension and, therefore, greater tensions. The additional forces from these effects were determined by assessing the additional extension of each line at every time-step and determining the corresponding increases in tension from the developed mooring line stiffness curves. These increases in tension were added to the tensions due to the tsunami current loads for each time-step during post processing of the AQWA simulation results.

5.3.3 Dynamic Response in Heave

Due to the long periodicity of the tsunami event (characteristic wave period on the order of 900 seconds), it is assumed that there is a negligible dynamic response in heave for both the FSRU and STS analysis cases, and that the vessels' response is quasi-static.

5.3.4 Modeling Tsunami Data in the AQWA Time Domain

The wind and current forces calculated within the AQWA time domain are derived from vessel-specific wind force and current force coefficients in conjunction with the current speeds defined within the time-history. The force coefficients are defined in units of force per velocity-squared (for either wind or current velocities).

Conventionally, AQWA only accommodates wind-speed time-histories, and does not have an input option for current-speed time-histories. This limitation was circumvented by defining the tsunami current time-history data as a wind time-history within AQWA; accordingly, the current force coefficients were duplicated and input in the wind force coefficient data category, replacing the wind force coefficients. While both the current speeds and current force coefficients occupy the analogous wind data categories, this method effectively replicates the current forces experienced by the vessels in the tsunami event by applying the current speeds from the time-history to the current force coefficients.

The input of wind force coefficients would be extraneous to the tsunami event analysis, as wind forces are not considered in conjunction with the tsunami event. Therefore, the duplication of the current force coefficients in the analogous wind data category is acceptable for this analysis.

Furthermore, the current forces resulting from drag between the vessels and the water during vessel translations are accounted for by the definition of the current coefficients in their conventional data category.

5.4 FSRU Analysis Criteria

The FSRU mooring arrangement was assessed for adequate response to mooring forces in the lines and fenders. For the tsunami events, FSRU mooring lines were evaluated for limits of both 60% and 80% of their minimum breaking load (MBL). These limits assume the FSRU winch brakes will perform within the range of the manufacturer's specifications. All fenders are required to not exceed the reaction ratings supplied by the manufacturer.

5.4.1 FSRU Analysis Cases

The best-match case that corresponds to the Q10 threshold conditions was applied to the FSRU mooring arrangement for 1.5 hours. The maximum current in the Q10 case is 3.86 m/s.

5.4.2 Mooring Line Tensions

Figure 9 presents the maximum FSRU mooring line tensions for the Q10 event. All of the line tensions remained below the criteria of 60% MBL and 80% MBL. Figure 10 provides the mooring line tension time series. These line tensions include the additional line tension resulting from changes in water surface elevation. There are two main peaks in the line tension. The first peak occurs when the vessel is being pushed directly off berth at approximately 2,950 s into the simulation. This also corresponds to the largest change in water surface elevation. The second peak, which is larger in magnitude with a line tension of 559 kN, occurs at 3,255 s into the simulation. At this time, the current reaches its largest speed at 3.85 m/s and pushes the stern 12 degrees off berth. This causes Lines 20, 21, and 22 (all stern breasting lines) to experience the highest line tensions. However, during the first 90 minutes of the Q10 tsunami, all mooring lines remained with SWL.

5.4.3 Vessel Motions

Figure 11 presents the surge, sway, roll, and yaw motions throughout the 90-minute Q10 exceedance simulation. The Q10 exceedance plots show that the maximum motions occur around 3,260 s when the vessel is being pushed directly sternward. This time corresponds to the largest current speed of 3.85 m/s and when the stern is being pushed 12 degrees off berth. The maximum surge and sway motions are 0.9 m and 1.1 m respectively while the roll and yaw are moderate, below 0.5 degrees.

5.4.4 Fender Forces

In the Q10 exceedance case, none of the fenders exceed the fender's rated reaction of 3,325 kN. Figure 12 shows the fender load time series. Fender 1 (fender closest to bow) experiences the largest fender load of 1,583 kN. This peak load occurs when the vessel is pushed off the berth at time 3000 s and then pushed back on berth beginning at 3,463 s.

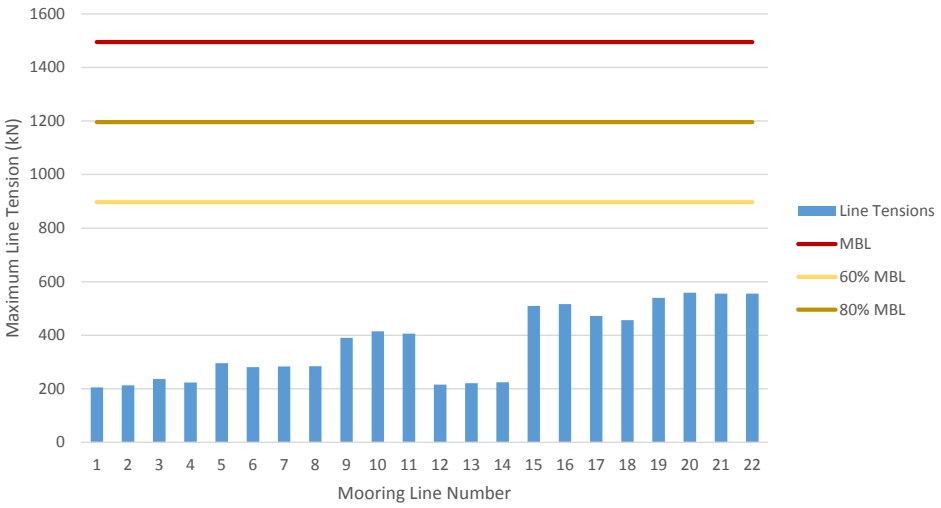

Figure 9: Q10 Maximum Line Tensions

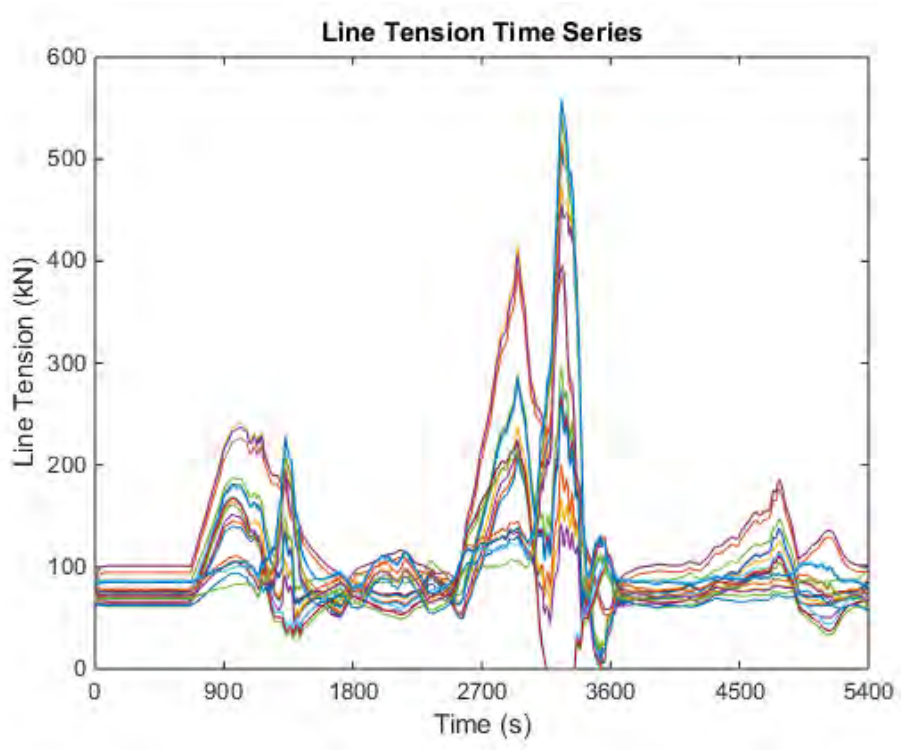

Figure 10:Q10 Line Load Time Series

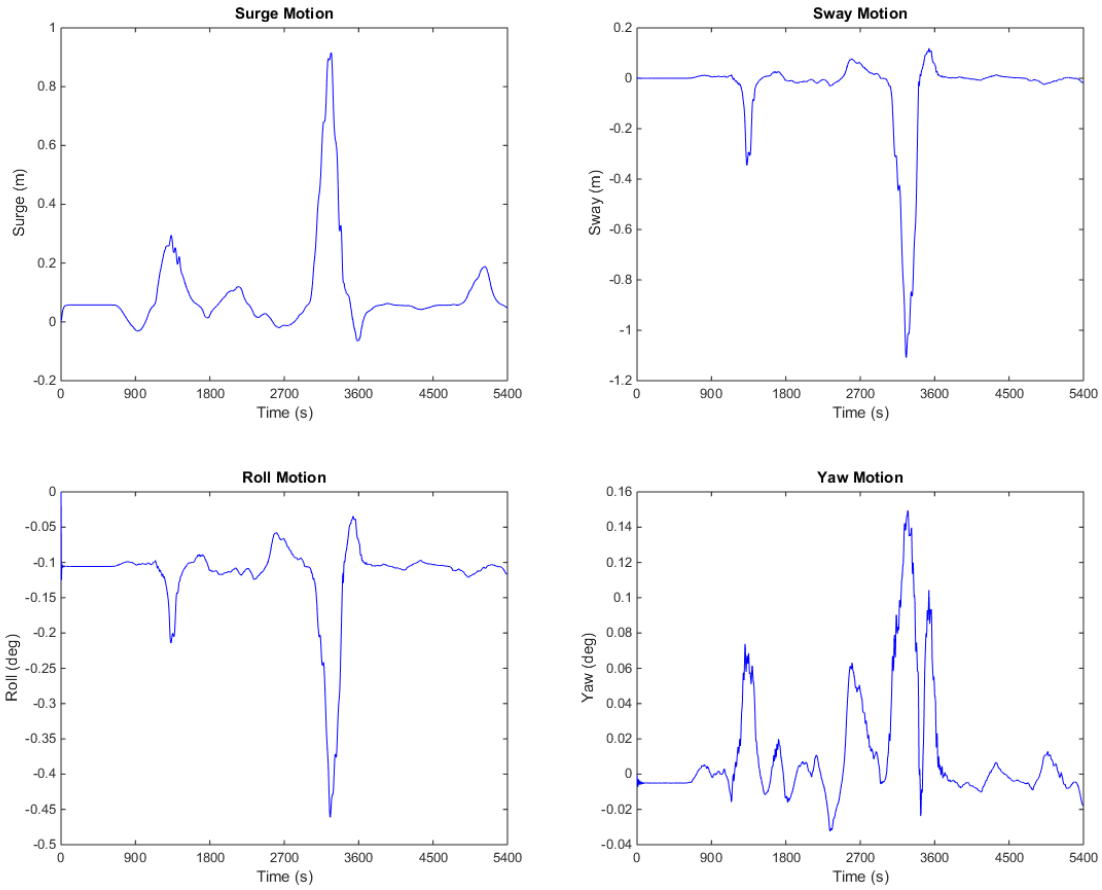

Figure 11: Q10 Surge, Sway, Roll, and Yaw Motion Time Series

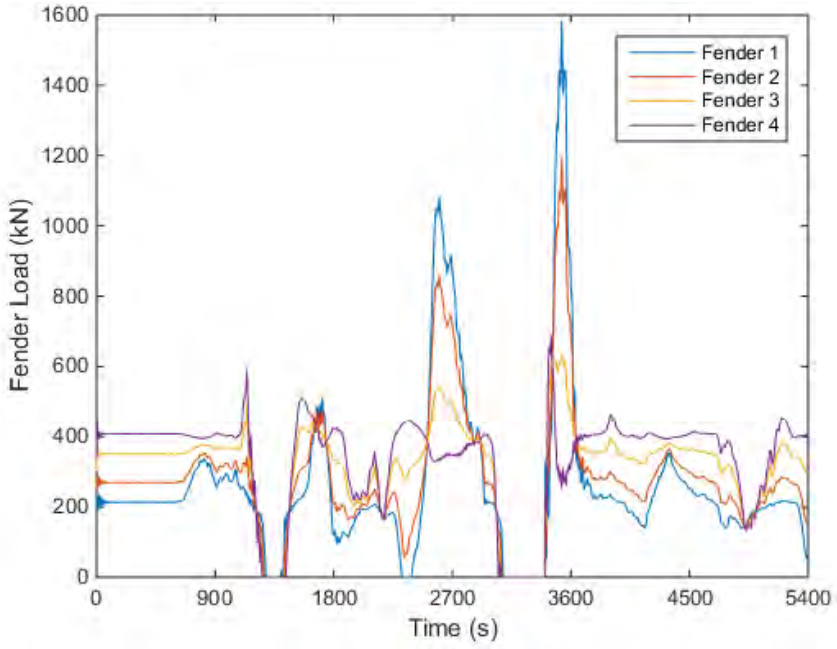

Figure 12: Q10 Fender Load Time Series

5.4.5 Water Elevation Changes

The effect of water elevation changes on mooring line tensions during the tsunami event was examined at 5 second intervals throughout the analysis. For each 5 second interval, mooring line elongations due to the vertical change in water elevation were calculated. The water surface elevations that occur during the Q10 tsunami event are presented in Figure 13. This time-series data is produced during the tsunami simulation process, in addition to current speeds and directions. The corresponding increases in tension due to the fluctuations in water elevation were then calculated and added to the current-force induced tensions to yield the total tension in the system. Note that the maximum total tensions presented in Figure 9 already include both current induced and elevation induced currents.

Figure 13 and Figure 14 show the relationship between the water surface elevation changes and the corresponding increases in tensions for a single spring mooring line. The maximum additional tensions due to water surface elevation change are on the order of 300 kN. These results prove that it is necessary to calculate and add the additional line tension due to water surface elevation changes to the total line tension.

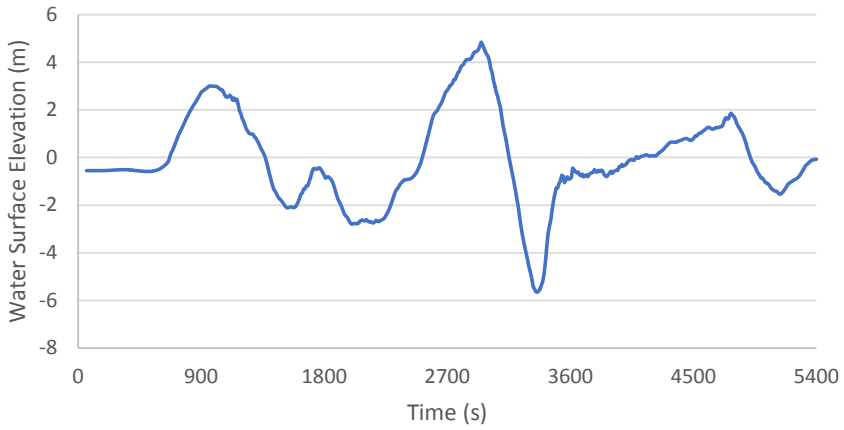

Figure 13: Water surface Elevation of the Q10 Tsunami Event

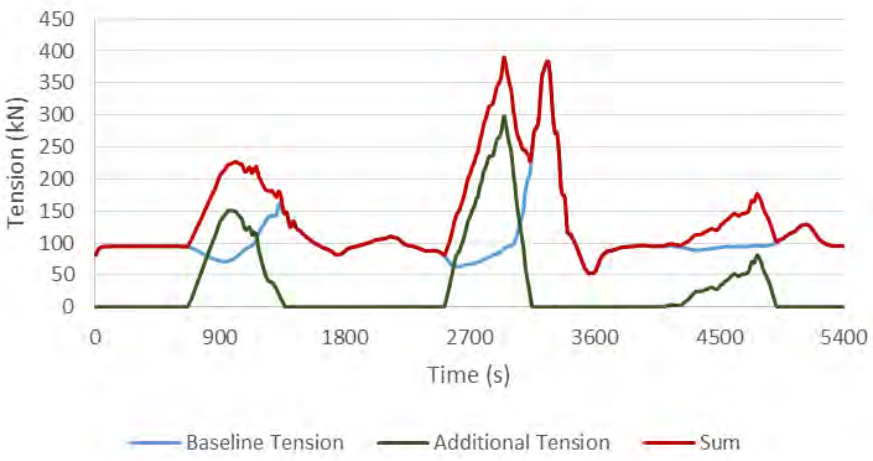

Figure 14: Q10 Superposition of Baseline Tension with Additional Tension Due to Water Surface Elevation Change in Mooring Line 9

5.5 STS Analysis Criteria

For ship-to-ship mooring, the LNGC occupancy will be low (few calls a month and few hours at berth) , therefore the joint probability of both ship being at berth during a tsunami is low. The 50% exceedance (Q50), one hour tsunami event was considered the baseline for the STS analysis.

5.5.1 Q50 Exceedance Tsunami Event

The four design LNGC vessels were analyzed for the Q50 tsunami event for under two mooring arrangements, under both ballast and loaded draft conditions (for analysis cases where the LNGC was modeled as ballast, the FSRU was modeled as loaded, and vice-versa). A total of 16 analysis cases were run for the Q50 tsunami event (4 cases per Design LNGC). Each analysis case yielded time-history data that includes mooring line tensions, vessel motions, and fender compression forces.

5.5.1.1 Mooring Line Tensions

As shown in Figure 15 and **Error! Reference source not found.**, all mooring line tensions remain within the established criteria for all of the FSRU and LNGC mooring lines for the Q50 event. The values depicted represent the maximum mooring line tensions that occur in each line for each Mooring Arrangement, across all FSRU/design LNGC combinations and conditions. Furthermore, these values include the effects of water surface elevation change.

Peak FSRU line tensions (Lines 1-22) appear to be relatively insensitive to mooring arrangement are well below limiting criteria line tensions. This is expected, as the FSRU mooring lines are sized to resist more onerous exceedance FSRU only cases. The LNGC lines, which are connected ship-to-ship tend to be less optimally placed and therefore more sensitive to the tsunami forcing.

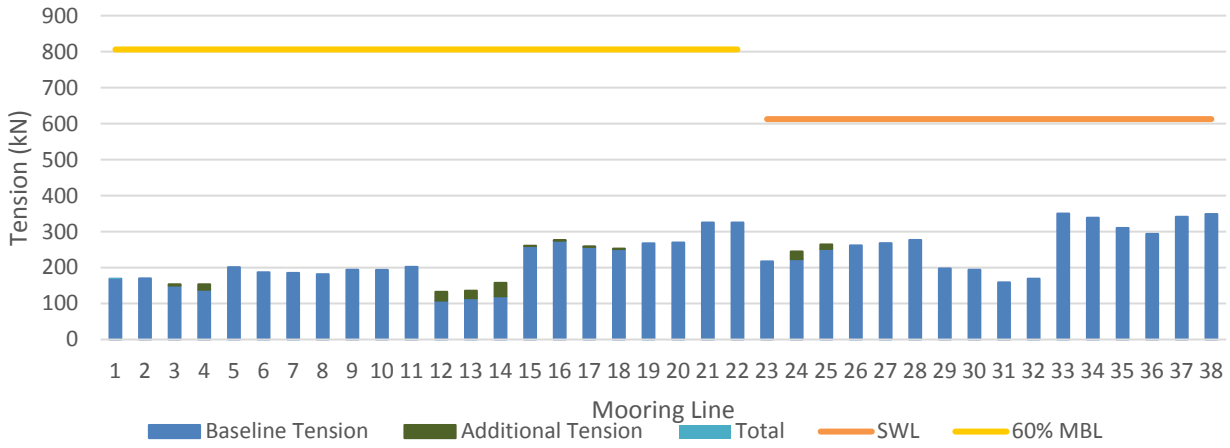

Figure 15: Proportion of Mooring Line Tension Induced by Currents (baseline) and Water Surface Elevation Change (additional)

Maximum LNGC line tensions for both mooring arrangements were below the 50% MBL criteria. The tsunami currents for the Q50 event are approximately aligned with the berth at the peak current speeds, during the initial 60 minutes of the event. Due to the 60 minute tsunami duration used for the FEED analysis and the refined statistical analysis of the tsunami events performed in the FEED tsunami study, the expected yaw motions are reduced due to the relatively narrow angles of peak current loads observed for the Q50 event.

5.5.2 Vessel Motions

The relative vessel motions between the FSRU and LNGC are presented in Figure 16 and Figure 17. These values represent the largest motions of the vessel center of gravity (COG) that occur in any of the 16 analysis cases examined for the Q50 tsunami event. Maximum surge and sway excursions are less than 1.0 m. Note that heave is excluded from the figures. Due to the assumed quasi-static response of the vessels in heave, it is assumed that the COG motions in heave are equivalent to the water surface elevation changes determined by the tsunami event simulation.

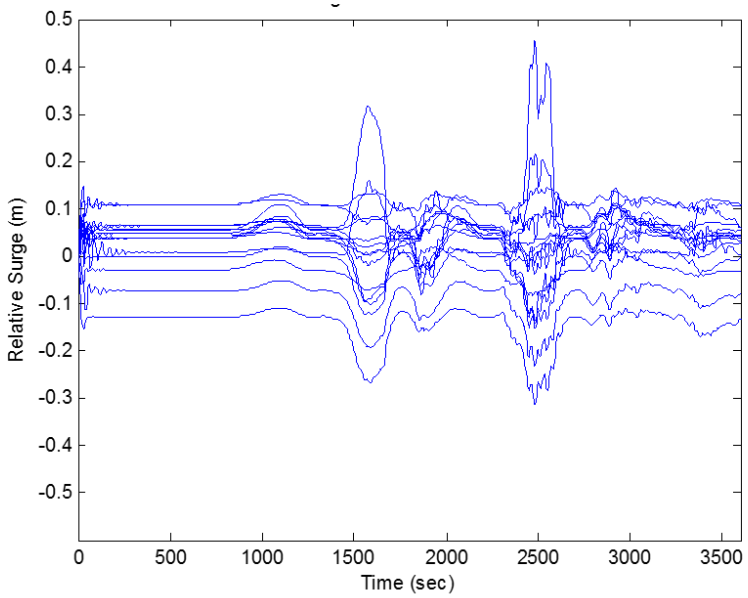

Figure 16: Relative Surge Motion between Vessel COGs; All Q50 Analysis Cases Represented

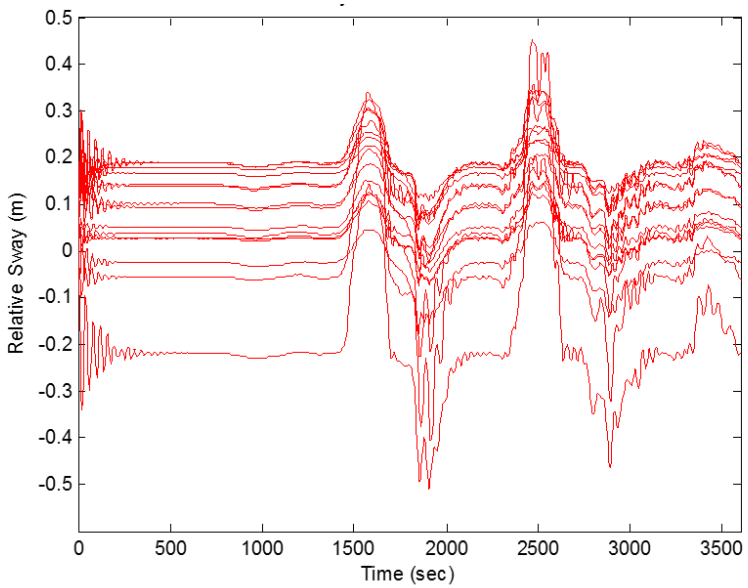

Figure 17: Relative Sway Motion between Vessel COGs; All Q50 Analysis Cases Represented

6 CONCLUSIONS

By combining the tsunami probability evaluation with generation of mooring loads, the mooring performance during tsunami event was predicted to develop an approach for incorporating tsunami mooring loads into the marine structural design.

The tsunami hazard from five different earthquake scenarios was assessed. The numerical tools used for the study include two coupled models, one for the open ocean propagation and another for the site-specific hydrodynamics. The site-specific simulation resolves complex bathymetric features and the associated currents at a horizontal resolution of 10 meters. First, the numerical models are tested against ADCP data measured at the site during the recent 2015 earthquake and tsunami. Although the site is located well north of the rupture zone, a tsunami wave height, or total crest-to-trough distance, of roughly one meter was recorded by the ADCP. The numerical recreation of this event agrees reasonably well with the measured elevation data, with errors between 10-20% in the maximum and minimum elevations. The ADCP recorded no clear velocity signal associated with the tsunami, likely due to under-sampling of the velocity by the instrument.

As expected, the local 1922 source produces the greatest impact at the design location among the five scenarios studied. Measurable waves reach the site just minutes after the earthquake, and the leading crest, which is also the largest predicted for this event at 2.9 m above MSL, arrives 14 minutes post-earthquake. There is very little variation of tsunami elevation along-vessel, less than 10 cm during peak elevation conditions. The speed predictions near the site show considerably more spatial and temporal variation. Maximum predicted speeds along a possible vessel length vary from 2.0-2.6 m/s, and are associated with large eddies (whirlpools) in the immediate vicinity of the site. Due to these eddies and their large spatial changes in flow speed, along-vessel speed gradients may reach 0.5 cm/s per meter of vessel length for periods up to five minutes.

With the simulation of historical tsunamis, it is clear that the 1922 earthquake represents the largest tsunami in the recent past in this area, and is there considered to be the design earthquake for tsunami. To understand the potential variability in the tsunami impacts from this design earthquake, internal parameters of the earthquake are varied and a statistical tsunami analysis is performed. The report provides recurrence periods of the tsunami hazard based on this statistical analysis, which can be used in a mooring line analysis to design to a target reliability consistent with other hazards. The FSRU mooring (without LNGC) meets the allowable mooring criteria for the Q10 level tsunami event during the first 90 minutes of the event. This exceedance level event corresponds to a return period of 1000-2500 years.

Performance results of both the LNGC and FSRU mooring are predicated on departing berth within 60 minutes and 90 minutes, respectively, of the earthquake-generated tsunami event. In the Q10 case, none of the mooring lines reached 60% of their MBL. All of the fenders also stayed below their rated reaction with the maximum fender load (1583 kN) at less than half of the fender's rated reaction. The STS analysis confirmed that the STS mooring arrangements are sufficient in resisting the forces associated for the Q50 threshold tsunami event during the first 60 minutes of the event. This exceedance level event corresponds to a return period of 200-500 years. All FSRU mooring line tensions remained below the criteria of 60% MBL, and all LNGC lines remained below their SWL (50% MBL) with fenders remained within their rated reaction capacity.

This methodology for tsunami impacts on semi-permanently moored structures shows promise for application to other marine terminals in areas with severe tsunami exposure.

7 ACKNOWLEDGEMENTS

The authors wish to thank the engineers Patricio Monardez and Alejandro Pérez, from the Andes LNG team, for their valuable contribution to the development of this work, who through their technical comments and innovative spirit, made it possible to complete the tsunami hazard assessment for this liquified natural gas facility using the approach that was exposed in this document.

8 REFERENCES

Comte, D. and Ortega, F., 2015, Caracterización Sísmica de la Zona de Ruptura Asociada al Terremoto de 1922 Y Al Terremoto de 1943.

Lynett, P., 2006, Nearshore wave modeling with high-order Boussinesq-type equations: Journal of the Waterways and Harbors Division, A.S.C.E., v. 132, p. 348-357.

Lynett, P., 2007, The effect of a shallow water obstruction on long wave runup and overland flow velocity: Journal of Waterway, Port, Coastal, and Ocean Engineering, v. 133, p. 455-462.

Lynett, P., Melby, J., and Kim, D.-H., (2010) "An Application of Boussinesq Modeling to Hurricane Wave Overtopping and Inundation." Ocean Engineering, v. 37, p. 135-153. doi: 10.1016/j.oceaneng.2009.08.021

Okada, Y., 1985. Surface deformation to shear and tensile faults in a half-space. Bull. Seismol. Soc. Am. 75, 1135–1154

Son, S., Lynett, P., and Kim, D.-H. (2011) "Nested and Multi-Physics Modeling of Tsunami Evolution from Generation to Inundation." Ocean Modelling, v. 38 (1-2), p. 96-113, doi: 10.1016/j.ocemod.2011.02.007

Titov, V. V., & Synolakis, C. E. (1995). Modeling of breaking and nonbreaking long-wave evolution and runup using VTCS-2. Journal of Waterway, Port, Coastal, and Ocean Engineering, 121(6), 308-316.

Titov, V. V., & Synolakis, C. E. (1998). Numerical modeling of tidal wave runup. Journal of Waterway, Port, Coastal, and Ocean Engineering, 124(4), 157-171.

Seven Key Words

- Maritime port planning and operations
- Container handling
- Solid bulk handling
- Precast deck system
- Seismic design
- Capacity protection deck design
- Top-down construction system

SEISMIC DESIGN AND CONSTRUCTION OF PILE-SUPPORTED CONCRETE WHARVES FOR CONTAINER AND BULK-HANDLING TERMINALS

By

Jyotirmoy Sircar, PE[1]; Carlos E. Ospina, PhD, PE[2]; and V.K. Kumar, PE, SE[3]

ABSTRACT

The paper describes the seismic design and construction of two adjacent wharves in greenfield terminals off the Pacific coast of Colombia. The wharves include two quays totaling 850 meters and two individual access trestles serving container-handling operations and bulk and breakbulk cargo-handling (coal exports/grain imports) operations, respectively.

The projects started with the intent of providing waterfront infrastructure capable of handling modern post-Panamax ship-to-shore (STS) quay cranes, mobile harbor cranes, and operations of bulk-handling equipment in a remote and high-seismic area of Colombia.

The design adopted a modular and repeatable open-wharf system consisting of high-capacity steel pipe piles supporting a high-capacity precast concrete deck system. Due to heavy rainfall and the remoteness of the site, a deck system consisting primarily of precast concrete elements was implemented in order to delink construction progress and quality control with site constraints. Deck elements needed to have adequate weight and sufficient reinforcement to resist the 35 kPa operational and STS crane loads under service conditions; however, given the high-seismic activity in the region, the overall design also needed to limit seismically induced lateral deflection.

State-of-the-art performance-based and capacity protection seismic design and detailing for pile-supported wharf structures per ASCE/COPRI 61-14 were adopted for the design of the quay and the access trestles. A key component of design was the development of an innovative precast concrete pile plug providing a practical connection between the steel piles and the concrete superstructure. The plugs were designed to provide significant inelastic rotation capacity without penalizing the deck design. The paper will elaborate on important serviceability and seismic design considerations and explain how these challenges were overcome in design and construction. A significant portion of success in meeting the aggressive schedule was attributed to the innovative construction methods adopted in the project. A linear top-down construction approach was adopted wherein previously installed piles were used to install future piles and deck elements. Due to this, precast element design details had to be made compatible with the top-down system.

Construction of both the wharves was completed in late 2016, and they are currently in operation.

INTRODUCTION

The remote Aguadulce peninsula off the Pacific coast of Colombia now hosts one of largest marine terminal complexes in Latin America. The complex includes the 30-hectare Sociedad Puerto Industrial de Aguadulce (SPIA) container terminal and the 4-hectare Boscoal bulk-handling terminal. The construction of the entire marine complex was divided up into multiple contracts; both the container wharf and bulk-handling wharf construction contracts were awarded to design-build (D-B) teams with BergerABAM as prime designer. Both the wharves were constructed by a consortium consisting of Soletanche Bachy Cimas, Conconcreto, and Soletanche Bachy International. The projects were realized after a period of intense value engineering (VE) evaluations by the designer that included evaluation of multiple alternatives. It is to be noted that the configuration of both the wharves, including location and orientation, was defined in previous studies.

The marine structures for the container- and bulk-handling terminals consist of offshore quays connected to the uplands with individual access trestles. The SPIA container terminal consists of a T-shaped pile-supported wharf comprising a 600-meter-long quay connected to a 160-meter-long access trestle and a 25-meter-long platform. The wharf is designed to support super post-Panamax gantry cranes capable of loading 23-wide 12,500-TEU (twenty-foot equivalent unit) container vessels. The wharf design also accounted for berthing of small 300-TEU feeder vessels. The marine structures for the Boscoal bulk-handling terminal is an L-shaped pile-supported wharf, comprising a 250-meter-long quay connected to

[1] Senior Project Engineer, BergerABAM, email: jyotirmoy.sircar@abam.com
[2] Vice President, BergerABAM, email: carlos.ospina@abam.com
[3] Senior Principal, BergerABAM, email: vk.kumar@abam.com

a 186-meter-long access trestle and a 15-meter-long platform. The wharf was designed to support Handymax bulk-handling vessels and conveyor belt supports for coal exports and grain imports.

The site is located in one of the highest reported seismically active regions in the world and experiences heavy rainfall all year long with tidal fluctuations of up to 5 meters. Due to the remoteness of the site and the tight cost and schedule constraints, the D-B team adopted an innovative precast (PC) wharf deck system supported on all driven steel plumb pile substructure system.

To accelerate construction, the D-B contractor for both the projects decided to build the wharves using a top-down construction system. This linear construction approach relies on previously installed steel pipe piles as supporting elements of a platform that rapidly installs future piles and PC deck elements and then moves forward to continue with the construction. One of the big drivers of the accelerated schedule was the fact that the design for both the wharves was made very similar despite it serving two different operations; i.e., container handling and solid bulk handling. This was due to the versatile and modular design that allowed repeatability to the maximum extent possible.

This paper describes the structural analysis and design/construction process of the wharf with emphasis on the seismic design of the wharves. The paper also summarizes how the different PC concrete elements forming the wharf deck system were conceptualized, designed, detailed, erected, and interconnected.

LAYOUT AND FRAMING

Figures 1, 2, 3, 4, and 5 present the layout and typical cross sections of the container- and bulk-handling wharves, respectively. Table 1 presents salient features of the container- and bulk-handling wharves. The site is characterized by the presence of thick layers of soft marine sediments overlying relatively stiff strata of clay and mudstone (Mallorquín formation). From the available laboratory testing, the mudstone showed evidence of weathering as we head onshore. The boreholes showed the presence of mudstone at elevations between -35.0 to -40.0 meters mean sea level (MSL) along the quay, overlaid by 10 to 20 meters of soft (CL, ML type) soil. Across the quay width, the thickness of the soft overburden decreased towards the land. A combination of soil conditions and schedule led to the selection of ***driven open-ended plumb steel pipe piles*** as the preferred piling option for the project. The piles were predominantly friction piles with some contribution from end bearing. To prevent premature plugging of piles while driving, a decision was made early in the project to use driving shoes. For corrosion protection, piles were provided with a polyethylene coating extending 1 meter below mudline.

The quay and trestle structures consist of a concrete deck at Elevation +5.05 meters MSL supported by steel pipe piles. Pictures 2 and 3 indicate the typical quay framing for both the wharves. The trestles in both the container- and bulk-handling wharves consisted of two pile bents. Bents were spaced at 7.5 meters in the longitudinal direction, with no intermediate pile(s) between bents along crane beam grids.

The deck for both the wharves implemented a predominantly ***PC system composed of PC capped pile plugs (champagne-cork type) inserted in pipe piles; PC transverse beams, PC longitudinal crane beams and PC fender beams positioned over pile plug caps, and interconnected via cast-in-place (CIP) closure pours; PC pretensioned deck panels spanning from bent to bent; and a CIP topping.***

For both the container- and bulk-handling wharves, the quay was separated from the trestle by means of expansion joints designed and detailed for operational and seismic loading cases considering movement in similar and opposite directions.

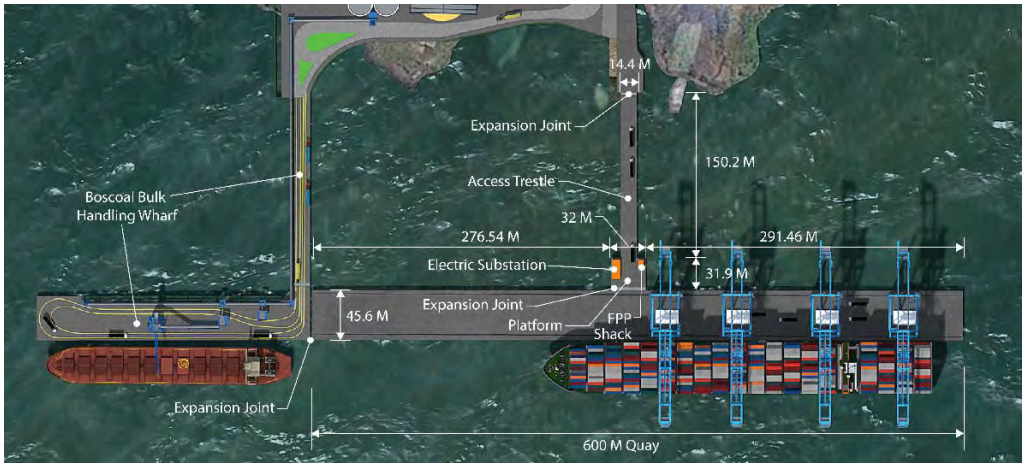

Figure 1. SPIA Container Wharf and Boscoal Bulk-Handling Wharf Layout

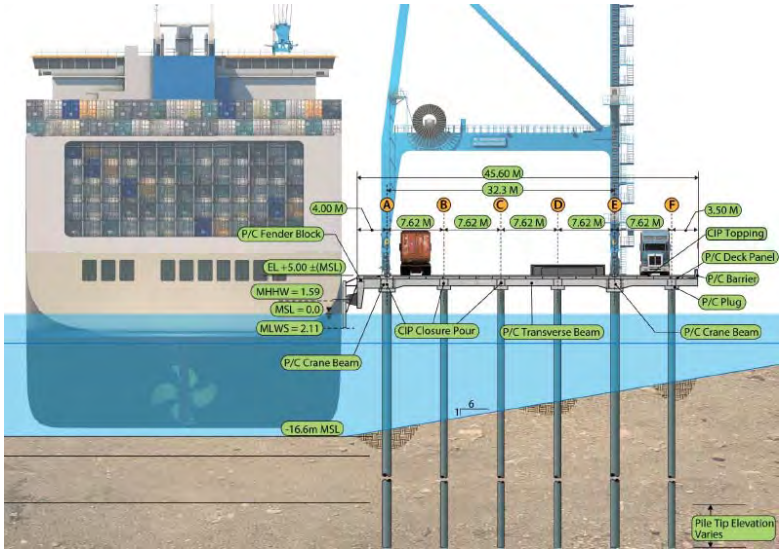

Figure 2. Container Quay Cross Section

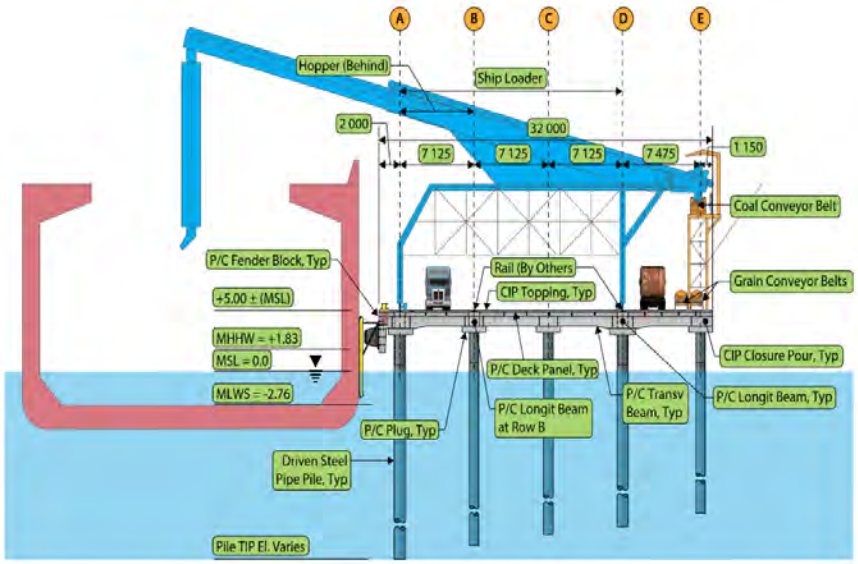

Figure 3. Bulk-Handling Quay Cross Section

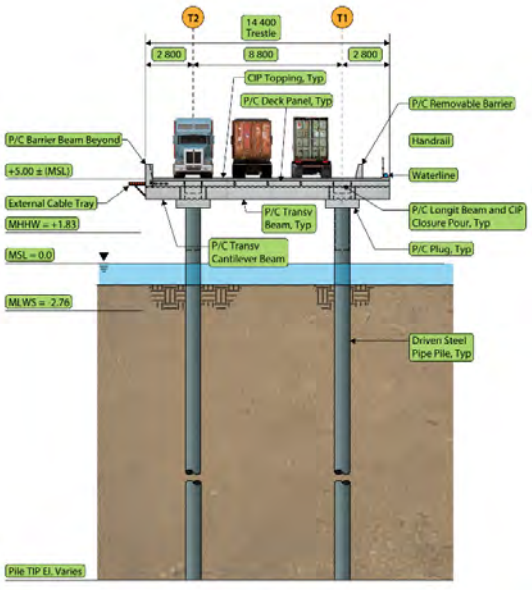

Figure 4. Container Trestle Cross Section

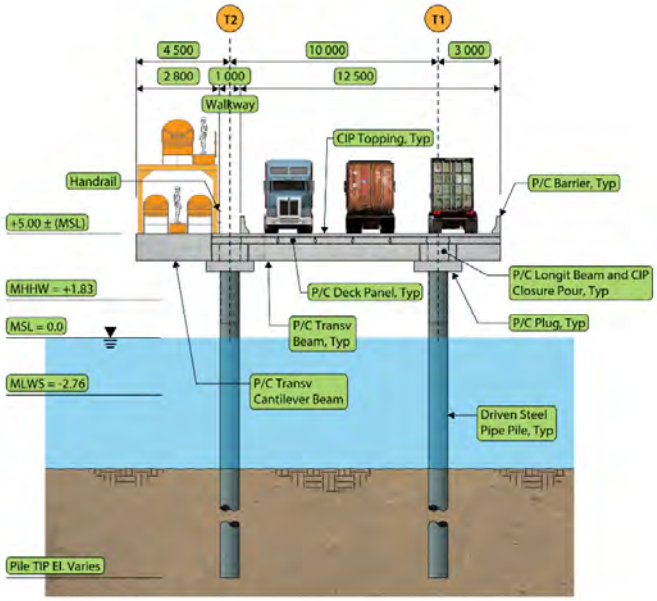

Figure 5. Bulk-Handling Trestle Cross Section

Parameter	Container Wharf	Bulk-Handling Wharf
Quay Dimensions	600 m x 45.6 m	250 m x 40 m (max)
Platform Dimensions	32 m x 32 m	15 m x 30 m (max)
Trestle Dimensions	150.15 m x 14.4 m	185 m x 17.5 m
Dredge Depth	-16.6 m, 1:3 slope	-15.0 m

Table 1: Key Layout Parameters of Container and Bulk Handling Wharves

OPERATIONAL LOADS

Container Wharf

The container wharf design, as well as the framing for the quay portion, was dictated by an owner-specified Basis of Design (BOD) and design, respectively. In addition to self-weight, the deck elements were designed for a uniformly distributed live load of 3.5 tons per square meter and operational crane wheel loads of about 70 tons per meter. A 1.5–meter-wide safety zone was defined at each crane beam row. The controlling operational load case for the trestle deck design was the passing of an unloaded rubber-tired gantry (RTG) crane, representing the case of RTGs being transferred from the wharf to the container yard. The container wharf was also designed to resist lateral berthing and mooring loads from servicing a 12,500-TEU 150,000-DWT (dead weight tonnage) post-Panamax vessel.

Bulk Handling Wharf

The design criteria of the bulk handling wharf were developed by the D-B team in conjunction with the owner. In addition to self-weight, the deck elements were designed for: 1) uniformly distributed live load of 2.0 tons per square meter; 2) operational loads from the shiploader of 28.13 tons (waterside, three wheels per corner); 3) 32.6 tons (landside, two wheels per corner); 4) conveyor belts for coal/cement exports (15 tons every 7.5 meters); and 5) grain imports (4.6 tons every 6.0 meters). In addition, the wharf had to be designed for an LHM 420 Mobile Harbor Crane (MHC) operating anywhere over the quay deck except the cantilever areas and a transiting MHC over the trestle deck. The bulk-handling wharf was also designed to resist lateral berthing and mooring loads from servicing an 80,000-DWT bulk-handling carrier.

SEISMIC DESIGN CONSIDERATIONS

Seismic design was an important component of the D-B team's responsibility for the project because the wharves are located in a high seismic region. The following explains some of the components.

Multilevel Seismic Design

The design had to provide adequate deformation capacity and strength in piles, deck, and pile-deck connections for two design level earthquakes: the Operational Level Earthquake (OLE) with a return period of 72 years and the Contingency Level Earthquake (CLE) with a return period of 475 years. The BOD called for CLE acceleration spectra constructed using A_a=0.45g and A_v=0.45g per Colombian Code NSR-10. Amplified spectral accelerations for the clayey site are shown in Figure 3. Spectral acceleration ordinates for OLE correspond to the damage threshold event prescribed by NSR-10. In general, CLE-based effects controlled design of the primary structural elements. ASCE/COPRI 61-14 also calls for checking the structure for a third event called Design Event (DE) that has a return period for 2475 years. However, the design team decided to adopt a "less stiff" design without sacrificing operational performance – this resulted in design for DE not being a consideration because for periods of vibration greater than 0.6 second, the structure experiences the same acceleration for both CLE and DE. Figure 6 presents the seismic spectra used in design.

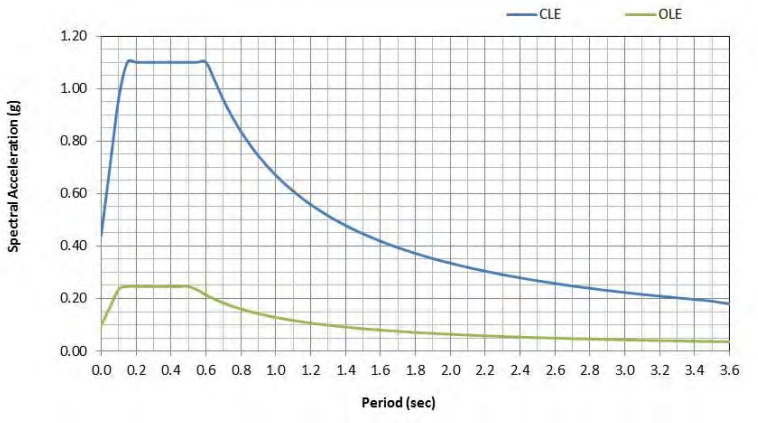

Figure 6. Spectral Accelerations for OLE and CLE

Seismic Weights

A key consideration in design was to limit the seismic weights of the structure as it has an impact on the seismically induced deflections and hence strains in critical members. Earthquake loads were combined with dead and live loads assuming the full dead load and 10 percent of the live load for both the wharves. The same percentage of live load was assumed for the definition of the seismic mass in the dynamic analysis. The container wharf was essentially an “offshore quay” and had a trestle connecting it to land. Due to the limited width of the quay, stacking loaded containers on the quay was deemed an inefficient and ineffective operation and hence the 10 percent value of live load contribution was justified. For the bulk-handling wharf, the most critical component was to include the self-weight of the conveyor belts and hoppers in the seismic mass.

Wharf Seismic Design Philosophy

As in typical horizontal construction for marine/waterfront structures, seismic design followed the “weak column-strong beam” design principle. Capacity protection principles were applied for the shear design of piles, shear design of pile-deck connections, and the shear and flexural design of the deck elements. For the design of capacity-protected members and actions, the calculated demand was based on 125 percent of the calculated plastic strength of the yielding member, which was the pile-deck connection.

Seismic Strains

For practical purposes, the upper end of the steel pipe piles was designed as a confined reinforced concrete (RC) element, with the ability to develop a hinge, with ductility provided by the spiral provided in the PC pile plug, benefitting by confinement provided by the encasing steel pile shell. Pile plug dowels were ASTM A706 steel. Strain limits in dowels complied with ASCE/COPRI 61-14 requirements. The pile-deck connections were detailed per ACI 318-14. Shear design of piles considered the overstrength capacity of the pile-deck connection. The overstrength moment demands at top (deck soffit) and bottom (in-ground hinge) of the pile were calculated from moment-curvature analysis using expected material properties specified by ASCE/COPRI 61-14. The moment-curvature modeling of the plug end of the piles accounted for the impact of potential plug cover spalling. At the in-ground hinge end, the shear capacity of the pile was calculated per AISC Load and Resistance Factor Design (LRFD). P-Delta effects due to seismic loading were considered.

Deck Capacity Protection

Capacity-protection design of the deck was challenging because of the large magnitude of seismic moments in piles applied over an optimized deck with only crane beams in the longitudinal direction. The problem was accentuated by the presence of large diameter piles along crane and longitudinal beams. Due to these being the stiffest elements of the substructure system, these piles attracted a larger portion of the seismic moments. Strictly speaking, full capacity protection of the deck implied it had to resist the sum of seismic moments (factored by 1.25) from all the piles all the way across without undergoing damage.

The sum of pile moments per bent will be resisted by the deck across areas tributary to each pile, with the main tensile contribution coming from the crane beam reinforcement and outside crane beam zones from the top deck reinforcement and bottom deck panel bars. The latter were extended and terminated in 90 degree hooks to enable proper tension force development during earthquake reversals. Refer to Figure 7 for a conceptual idealization of capacity protection design of deck.

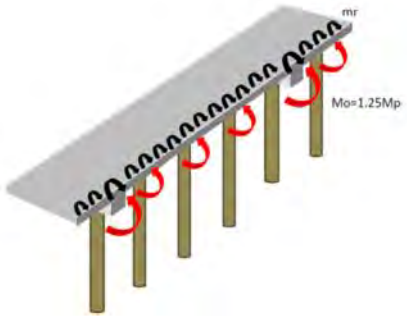

Figure 7. Deck Capacity Protection Design Concept

SUBSTRUCTURE DESIGN

All piles for both the container and bulk-handling wharves had to develop necessary axial and lateral capacities. Because the wharf framing consisted of an all plumb-pile system and the under-wharf slope was very gradual, the design had to make sure that the piles penetrated sufficiently into the weathered mudstone to develop full pile fixity and capacity for operational conditions and provide sufficient ductility for seismic conditions. The D-B team decided to adopt API 5L steel pipe piles for the wharves and adopted a 60-ksi yield strength pipe pile material in order to limit deflections within the elastic regime of the pipe material.

Parameter	Container-Handling Wharf	Bulk-Handling Wharf
Pile Type	Open-Ended Tip-Reinforced Driven Plumb Steel Pipe Pile API 5L Grade 60 ksi	Open-Ended Tip-Reinforced Driven Plumb Steel Pipe Pile API 5L Grade 60 ksi
Quay Working Axial Compression Demand	750 Tons (Waterside Crane) 560 Tons (Landside Crane) 310 Tons (Internal)	310 Tons (All)
Quay Pile Size	1219 mm x 25.4 mm, 914 mm x 19 mm	1067 mm x 25.4 mm, 914 mm x 19 mm
Quay Pile Quantity	486 piles	176 piles
Platform Working Axial Compression Demand	200 Tons	200 Tons
Platform Pile Size	914 mm x 19 mm	914 mm x 19 mm
Platform Pile Quantity	20 piles	7 piles
Trestle Working Axial Compression Demand	200 Tons	200 Tons
Trestle Pile Size	914 mm x 19 mm	914 mm x 19 mm
Trestle Pile Quantity	40 piles	50 piles

Table 2: Key Pile Design Parameters of Container- and Bulk-Handling Wharves

Table 2 summarizes critical pile axial compression loads under service conditions. Due to the owner-specified framing for the container wharf, which did not include intermediate piles under the long-span crane beams, the critical crane beam piles required high capacity. In addition, the offshore container wharf piles had to be designed for a future dredge depth of -16.6 meters. On the other hand, the reasonably modest shiploader loads for the bulk-handling wharf resulted in significantly lower pile axial capacities. Anticipated dredge depth for the bulk-handling wharf was limited to -15.0 meters; therefore, the design team was able to optimize the size of piles. See Figure 8, schematic detail of the driven pile.

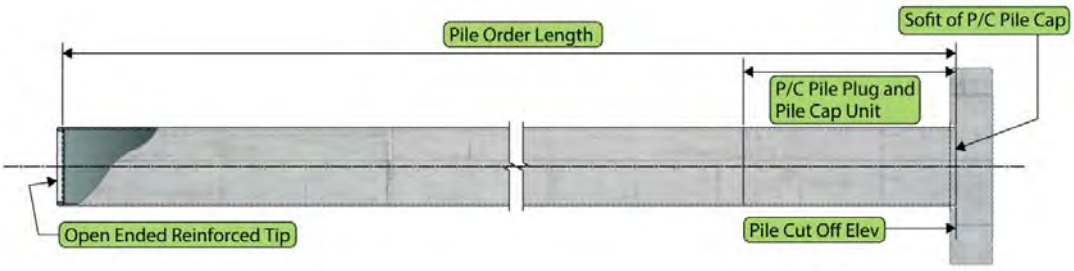

Figure 8. Driven Open-Ended Tip-Reinforced Plumb Steel Pipe Pile

Geotechnical Considerations

The container wharf piles were the first production piles for the marine projects. Due to the variability at the beginning of the job and the varying, yet high, magnitude axial load capacity requirements for the container quay piles, the D-B team decided to adopt the criterion based on

- Providing a pile tip elevation at or below the estimated depth of fixity
- Driving the pile to a specific resistance criteria defined by a specified blow count for a given penetration

However, for the bulk-handling quay, the D-B team decided to drive the piles to grade based on an estimated pile length computed based on providing full fixity at the bottom. The construction of the bulk-handling wharf piles also had the advantage of information gained from installing the container-handling wharf piles.

Structural Considerations

Slenderness effects on axial and bending moment capacity of piles under gravity loads had to be first considered appropriately given the wharf consisted of an all plumb-pile system. For load cases involving operational lateral loads due to berthing or mooring of vessels, analysis and design involved the final configuration of the deck. For seismic analyses, the D-B team had two considerations.

- Minimizing pile top moments for the “flexible” quay piles
- Limiting pile shell strains in the “flexible” quay piles and “stiff” trestle piles to ASCE/COPRI 61-14 recommended seismic strains with the intent of minimizing the possibility of global and local buckling

SUBSTRUCTURE TO SUPERSTRUCTURE CONNECTION DESIGN

A precast reinforced plug connection between the steel pipe piles and the PC superstructure was conceived by BergerABAM and implemented by the contractor team for the project. This is the first instance in which such a system has been implemented on a major scale in marine construction. The PC pile plug was designed and detailed to provide performance equivalent to its traditional CIP counterpart that is identified by ASCE/COPRI 61-14 as a ductile design detail. The PC capped pile plug includes a rectangular reinforced pile cap cast integrally with a cylindrical reinforced plug, the dimensions of which are defined by the inner diameter of the piles. The PC plug transfers all vertical loads to the pile through the cap that was detailed to provide direct bearing over the pile shell. The annulus between the PC pile plug and the steel pile was filled with a cementitious grout carefully selected to minimize shrinkage. The basic concept behind the PC pile plug for lateral load transfer is that it only needs to contact the steel casing at two points to develop a couple that can transfer the moment from the pile top to the deck. The contact points were ensured by the tight-fit size of the plug and overall behavior of pile-deck system when subjected to lateral loads. Load transfer through the PC plug was provided by a seismically detailed connection consisting of longitudinal and transverse confining reinforcement, which is not very different from its CIP plug counterpart. Figure 9 presents details of the PC plug and a typical moment-curvature curve for the same. Note that a stiffness reduction factor of 0.9 was considered for the PC plugs in design to account for the innovativeness of the system.

Parameter	Container Wharf	Bulk-Handling Wharf
Plug Size	1135 mm, 845 mm	985 mm, 845 mm
Plug Reinforcement	24#10, 18#10	20#10, 16#10

Table 3: Key Pile Plug Design Parameters of Container and Bulk Handling Wharves

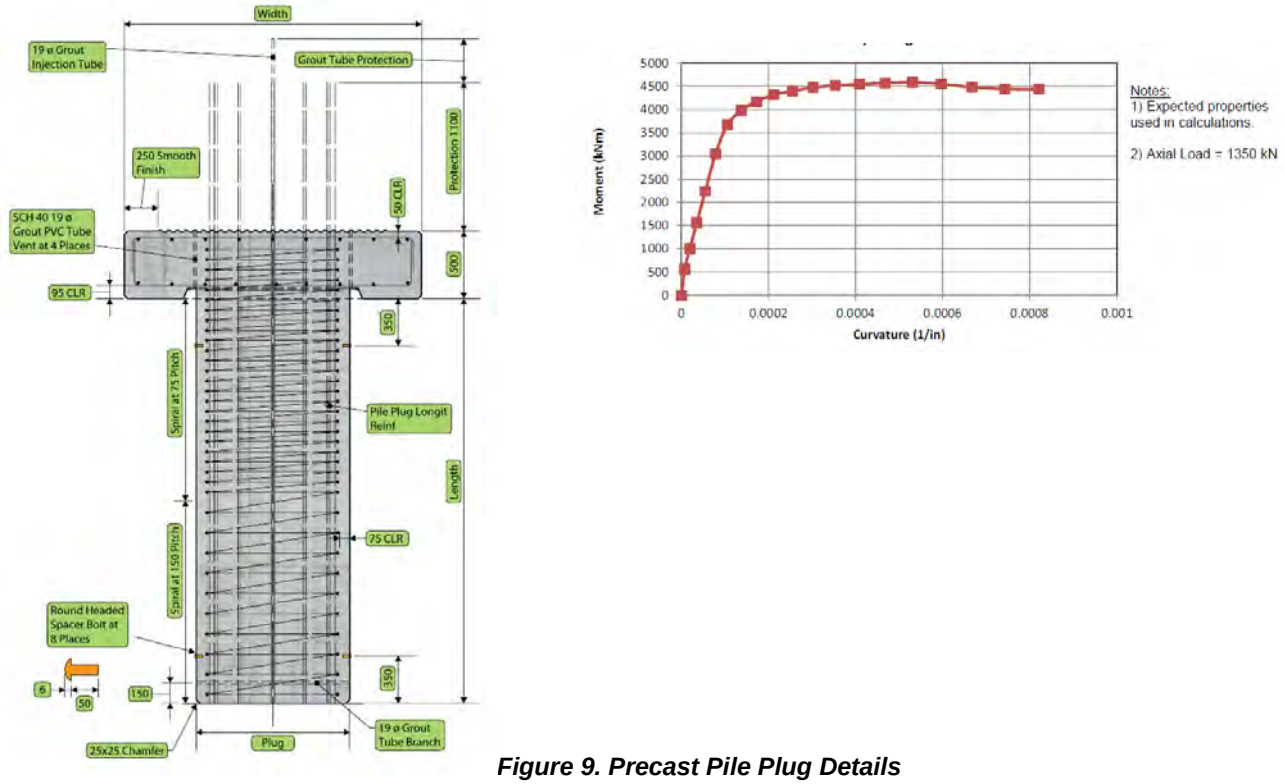

Figure 9. Precast Pile Plug Details

SUPERSTRUCTURE DESIGN

The design team adopted a predominantly precast deck system consisting of precast reinforced transverse and crane/longitudinal beams, precast pretensioned deck panels, and CIP reinforced closure pours and topping. The precast beams and deck panels had projecting top and bottom mild steel reinforcing to provide strength during construction/installation, as well as seismic conditions. The beams framed into seismically detailed CIP closure pours that provided strength, confinement, and continuity to the entire system. In order to provide necessary early and long-term strengths, as well as marine performance, a marine concrete mix consisting of innocuous aggregates, low in permeability and chlorides and rich in cement, was provided. The concrete mix typically had a minimum 28-day compressive strength of 42 MPa. For providing desired ductility, ASTM A706 Grade 60 ksi reinforcing steel was used for the beams. ASTM A416 Grade 270 ksi was used for the pretensioned strands.

Though the owner-specified BOD for the container wharf deck did not include any serviceability requirements, the D-B team decided to adopt a crack-control design philosophy given the design life and marine environment. The same philosophy was adopted for the bulk-handling wharf deck. This was based on our experience that marine structure deck design is typically controlled by meeting service rather than strength design requirements. Structural performance of the structure under service loads was verified through control of cracking and deflections in precast deck elements. Maximum allowable width of flexural cracks at the surface of structural concrete elements under service loads was limited to values presented in Table 4 below. Precast pretensioned concrete deck panels were designed so that any net tension under normal service load conditions did not exceed the limits stipulated in ACI 318. Crack widths in reinforced concrete members were then verified per the recommendations of AASHTO LRFD 2012. Maximum deflection in longitudinal deck elements under normal uniformly distributed service live load was limited to L/500 typically and L/300 for cantilever members.

Non-prestressed concrete elements (beams, topping)	Bottom face	$w \leq 0.25$ mm
	Top face	$w \leq 0.25$ mm
Precast pretensioned concrete deck panels	Bottom face	max $f_{tension} \leq$ ACI 318 limit (normal service loads)

Table 4: Service Design Criteria for Container- and Bulk-Handling Wharf Decks

The deck components had to be designed accounting for the following construction sequence.

1. Beams simply supported on capped pile plugs
2. Beams made continuous through closure pours at joints
3. Self-weight of deck panels on transverse beams
4. Weight of wet topping over continuous deck panels
5. Full design loads applied on the final configuration of the deck

Structural Considerations

1. Precast Reinforced Crane/Longitudinal Beams
   The container quay crane beam vertical load design was controlled by serviceability requirements. These elements were designed to resist the imposed crane loads given the lack of intermediate pile in container quay and yet maintain a reasonable stress level in steel reinforcement for crack control considerations consistent with marine construction practice. The shiploader and internal longitudinal beams in the bulk-handling quay were designed to transfer the operational vertical loads. The beams also needed to have adequate projecting reinforcement to meet the seismic capacity protection requirements.

2. Precast Reinforced Transverse Beams
   The precast transverse beams had to be designed to resist the dead loads from self-weight, as well as weight of deck panels and topping. In order to mitigate cracking, the D-B team developed a construction scheme that minimized loading the bare precast beams before the ends were integrated. The beams also had projecting reinforcement to meet the seismic capacity protection requirements.

3. CIP Reinforced Closure Pour
   The CIP reinforced closure pours included a series of vertical and horizontal stirrups detailed to provide adequate confinement and shear capacity. The closure pour also served to provide space for developing the capacity of the projecting flexural reinforcement.

4. Precast Prestressed Deck Panels
   The deck consisted of precast pretensioned deck panels placed longitudinally. Due to the high magnitude of pretensioning needed for resisting deck operational loads, the panels had top mild steel reinforcing to minimize cracking during the strand stressing process. In order to provide sufficient longitudinal deck capacity protection, the panels had projecting bottom reinforcement hooked into the closure pour.

5. CIP Reinforced Topping
   The deck panels were topped with a bidirectionally reinforced concrete topping. The reinforcing in the topping was designed for not only operational loads but also seismic deck capacity protection.

Figure 10 presents a schematic detail of the precast beams and the reinforcing in the CIP closure pours at the end of beams.

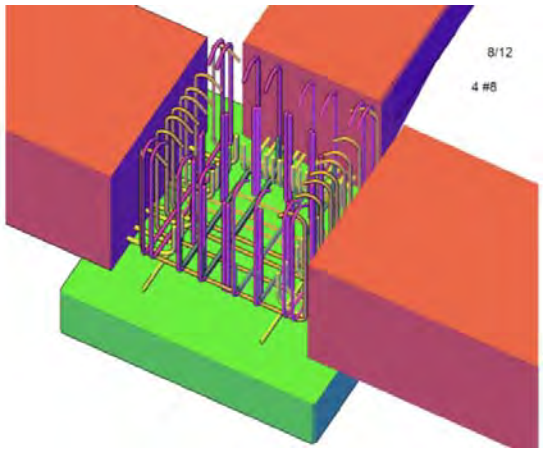

Figure 10. Precast Pile Plug Details

SEISMIC ANALYSES AND DESIGN METHODOLOGY

Seismic load effects were analyzed through displacement-based procedures using non-linear pushover techniques with soil properties derived from the geotechnical investigations. The results were verified with traditional linear response spectra modal analysis. The linear response spectra analyses provided upper bound estimates of displacements that helped in “bracketing” the structural performance. The non-linear pushover analyses incorporated the following features:

1. Full-length structural model with appropriate bent spacing and pile locations
2. Steel pipe piles built out of “expected properties” of API Grade X60 base limit lateral mud and soft rock P-y, skin friction T-z, and end bearing Q-z springs to model lateral and axial stiffness provided by mud and soft rock layers for the two pile types along the length
3. Nonlinear axial-moment interaction hinge (P-M hinge) and plastic hinge lengths for pile section above the estimated fixity points to simulate in-ground hinging effects on all piles
4. Pile-to-cap connection modeled as frame members with stiffness modifier of 0.35 per Reference 4 and built out of “expected properties” of concrete, including design longitudinal reinforcing bars and transverse spacing made of “expected properties” of ASTM A706
5. Nonlinear axial-moment interaction hinge (P-M hinge) and plastic hinge lengths of defined on the plug at the pile-to-deck connection to simulate pile top hinging on all piles
6. Concrete transverse beam section modeled as frame member with stiffness modifier of 0.35
7. Concrete longitudinal beam section modeled as frame member with stiffness modifier of 0.35
8. Concrete deck simulating the 350-mm PC panel and 150-mm CIP topping modeled as shell elements everywhere except over the longitudinal beam section with stiffness modifier of 0.35
9. Pile caps modeled as point loads acting on top of the piles
10. Dead load of all components and 10 percent of live load (1.5 kPa) is incorporated as seismic mass and in period calculations

See Figures 11, 12, and 13 for typical pile springs adopted in seismic analyses and snapshots of the full 3-D finite element model for the container quay and trestle. Note that all the modeling was done on the commercially available software SAP2000 and was verified through hand-checks using spreadsheets. Consistent with ASCE 61/COPRI 61-14 guidelines, analyses were performed for three values of springs – a base value, a lower bound value (less stiff), and an upper bound value (more stiff). Figure 14 presents

a typical pushover curve for the structure with the anticipated performance point for the container quay. Table 5 presents typical analyses results for the container quay assuming baseline spring stiffness. In general, the seismically induced forces, deflections and strains were more onerous for the container quay when compared to the bulk-handling quay given the greater unsupported length, higher seismic mass and live load.

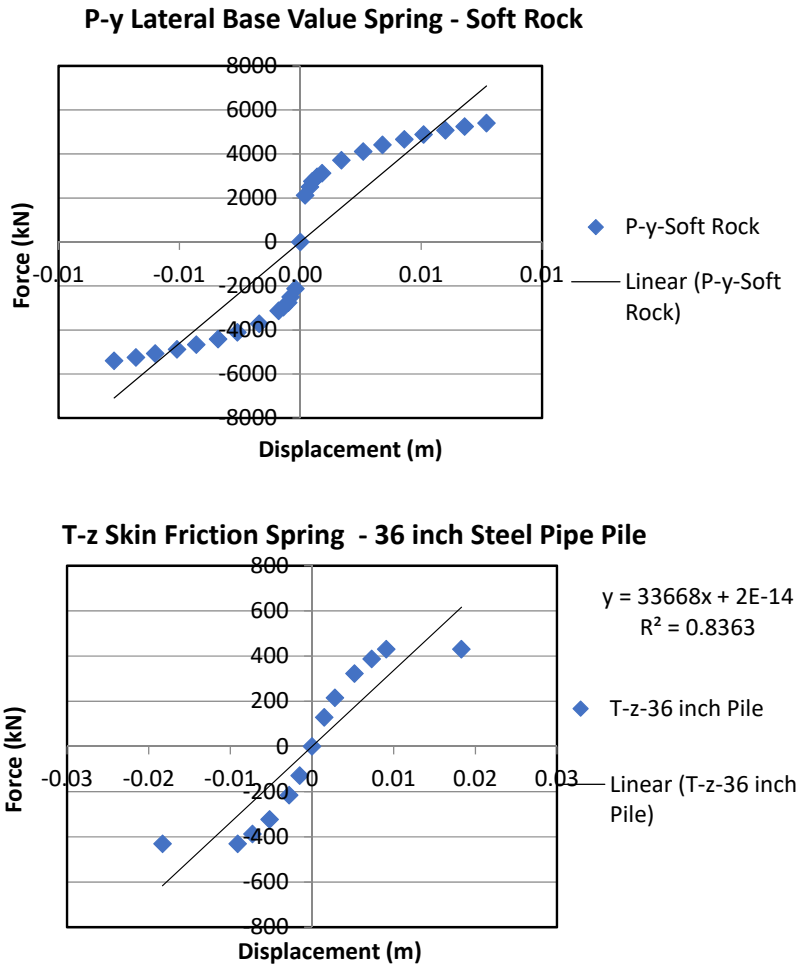

Figure 11. Typical Pile Springs

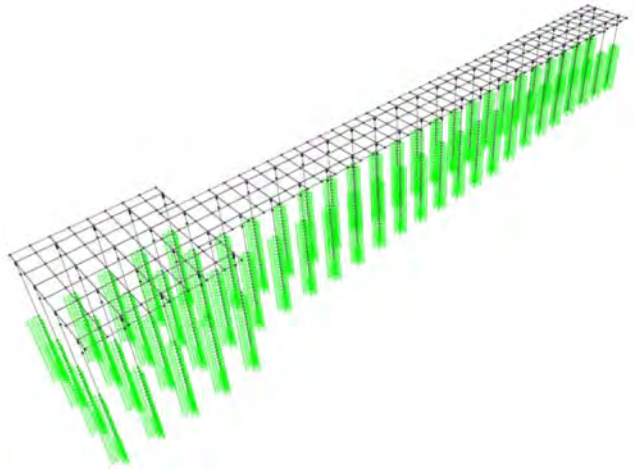

Figure 12. Full Model for Container Trestle and Platform

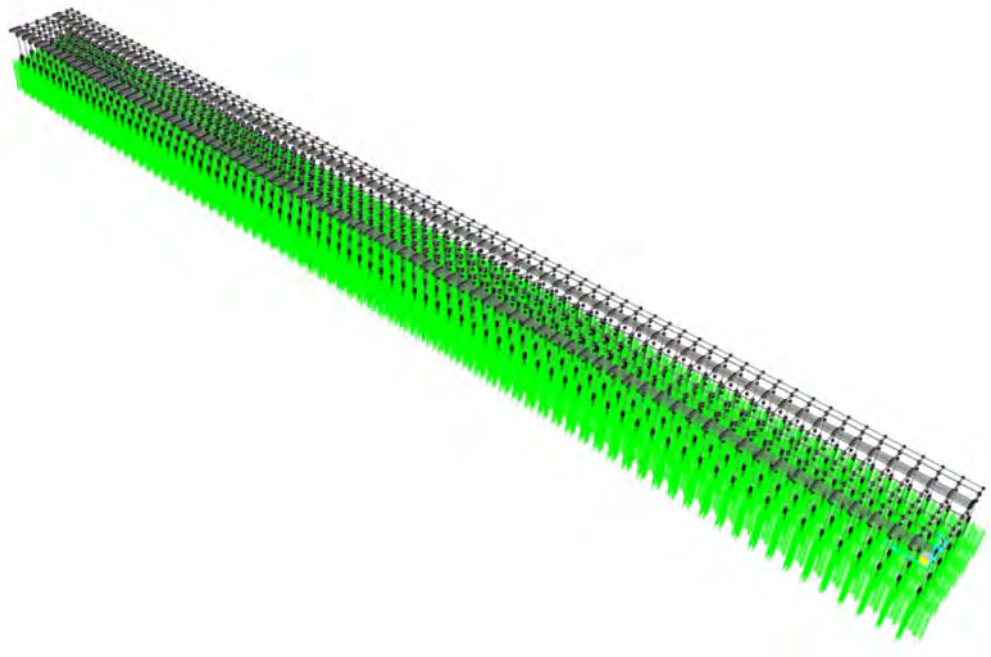

Figure 13. Full Model for Container Quay

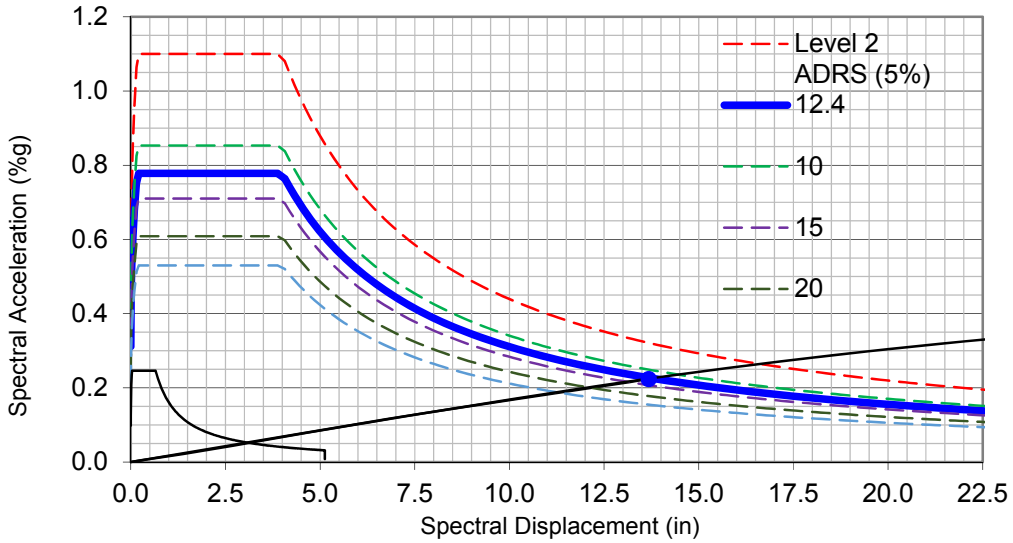

Figure 14. Performance Point Example - Container Quay Transverse Direction

Parameter	Analysis Result
Seismic Mass	Approx. 667,250 kN (150,000 kips)
Performance Point for OLE transverse to quay (x-direction)	Approx. 70 mm (2.8 inches)
Performance Point for OLE parallel to quay (y-direction)	Approx. 75 mm (3.08 inches)
Performance Point for CLE transverse to quay (x-direction)	Approx. 335 mm (13.28 inches)
Performance Point for CLE parallel to quay (y-direction)	Approx. 355 mm (14.08 inches)

Table 5: Service Design Criteria for Container- and Bulk-Handling Wharf Decks

CONSTRUCTION

For both the quays and the trestle for the bulk-handling wharf, the contractor used a top-down construction system to install the piles and deck. The methodology applies a linear construction approach that uses previously driven and cut off steel pipe piles as supporting elements for the “piling platform” (two-bents wide) that installs future piles and PC pile plugs followed by a “deck-works platform” (two-bents wide) that installs the PC deck components. The latter is supported on PC pile plugs previously installed in piles driven and cut off. Once the PC pile plugs were installed, the deck-works crane installed the PC beams over the pile plugs, cast the closure pours at beam intersections, installed pretensioned precast deck panels, and cast topping concrete. PC elements were supplied via floating barges. The interaction between the piling and deck-works platforms required coordination of PC deck elements to be installed per movement. The sequence of construction for the container quay is shown in Figure 15 whereas sequence of construction for the bulk-handling wharf is shown in Figure 16.

Figure 15. Top-Down Container Quay Construction

The trestle piles for the container quay were installed differently. Trestle piles near the abutment were installed with a crane operating from a temporary fill embankment whereas piles located near the platform were installed with the same crane over floating equipment. See Figure 17.

In terms of production, the piling platform managed to install up to six piles (one bent for the container quay) in a 24-hour-long shift. Dismantling and resetting of the platform took two extra days. Figure 18 shows the installation of a PC-capped pile plug. All PC elements, including capped pile plugs, crane beams, transverse beams, fender beams, and deck panels, were fabricated near Medellín. PC elements were trucked to a staging yard in Buenaventura and then barged over to the peninsula. Erection of fender beams was particularly challenging because of weight and asymmetric nature of these elements. Special lifting and temporary strapping elements had to be designed and installed to provide stable support for their Stage 1 erection prior to integration with adjacent crane and transverse beams. See Figure 19 for photographs indicating sequential deck construction.

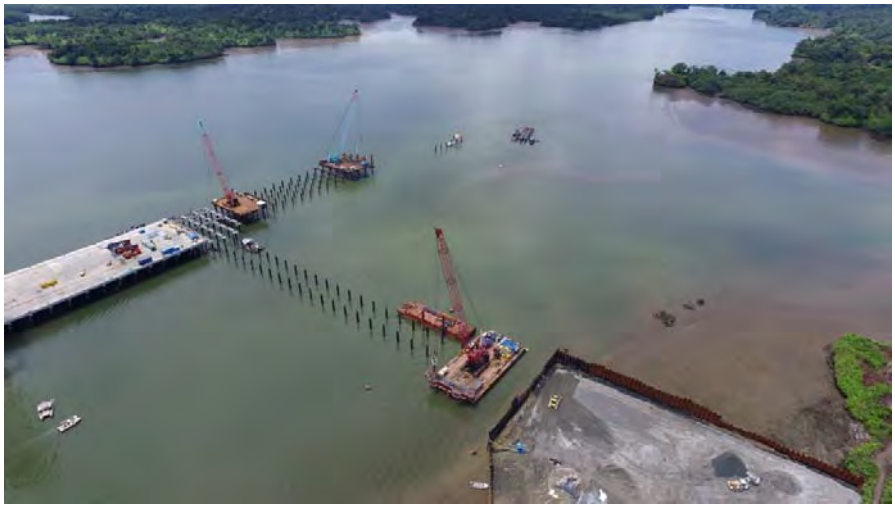

Figure 16. Bulk-Handling Wharf Construction

Figure 17. Container Trestle Construction

Figure 18. PC Pile Plug Installation

Figure 19. Sequential Deck Construction

CONCLUSIONS

The design and construction of the container- and bulk-handling wharves in Aguadulce, Colombia, represent a prime example of extraordinary coordination between the D-B team members. Despite challenging site and environmental conditions, tricky design situations, and a highly compressed schedule, both the wharves were constructed in record time. In fact, wharf construction preceded the upland yard construction by a significant margin, which was inconceivable when the project was being conceptualized. The design adopts the state-of-the-art recommendations for seismic performance as envisioned by ASCE/COPRI 14 and implements a displacement-based design approach that does not penalize the structure despite it being located in a region of high seismicity. The design also maximized

the use of precast elements that not only provided necessary quality for marine performance but also provided the contractor with a way to minimize site logistics and construction. A modular yet versatile approach allowed the wharves with different uses to adopt a consistent design that further reduced construction time. Figure 20 presents an aerial view of the completed projects.

Figure 20. Completed Container- and Bulk-Handling Wharves

ACKNOWLEDGMENTS

We acknowledge technical input from Karim Cheniour (Project Director), Jordan Lagnado (Engineering Manager), Romain Brieu (Construction Specialist), Alejandro Mejía (Construction Manager), and supporting staff of Consortium SBCC and Consortium Aguadulce. Aerial pictures are courtesy of the aforementioned consortia.

REFERENCES

1. Carlos E. Ospina, PhD, PE; Jyotirmoy Sircar, PE; and Viswanath K. Kumar, PE, SE, “Container Wharf with Innovative Precast Deck in High Seismicity Area,” ASCE Ports 2016
2. “Seismic Design of Piers and Wharves (61-14),” American Society of Civil Engineers
3. “The Port of Los Angeles Code for Seismic Design, Upgrade, and Repair of Container Wharves,” City of Los Angeles Harbor Department, May 2010
4. “Building Code Requirements for Structural Concrete, ACI 318-08,” American Concrete Institute
5. AASHTO 6th Edition (2012 with 2013 and 2014 revisions) LRFD Bridge Design and Specifications Manual

METHODOLOGY TO ANALYZE THE MOORED SHIP BEHAVIOUR DUE TO PASSING SHIPS EFFECTS

by

Jose R. Iribarren [1], Ignacio Trejo[2], Carlos Cal[1], Lourdes Pecharroman[1]

ABSTRACT

This paper describes the studies carried out and the methodology developed to analyze the feasibility of a new solid bulk terminal from an operational point of view. The aim of the study is to analyze the effects of passing ships, selected from traffic data in the area, on moored vessels at the new terminal.

The study starts with the determination of the expected passing speed and passing distance to moored vessels in the new terminal of those vessels operating in the nearby berths for different wind conditions (direction and speed) using a fast-time ship manoeuvring software. The results (speed and distance) are used as input data to determine the suction forces and moments generated by the passing vessel on the moored vessels.

The dynamic response of the moored vessels under different weather conditions together with lines and fender forces generated by the passing vessels are also simulated by using specific software. In view of all the previous results, different alternatives are proposed in order to improve the conditions obtained in the analysis and raise the operation limits. The final phase of the study includes real-time manoeuvring simulations in order to verify the results obtained along the process in a realistic working environment.

A complete set of simulation tools is applied sequentially in order to develop a global and precise analysis and elaborate a clear picture of the safety level of the operations. Fast-time manoeuvring simulation (SHIPMA), passing ship effects (ROPES), dynamic response of moored vessels (SHIP-MOORINGS) and Real-time shiphandling simulator. AIS data (Automatic Identification System) covering the vicinity of the new terminal were also considered and analyzed to define manoeuvring strategies executed by the current vessels in the area. The methodology is explained and developed based on a real case in the Port of Barcelona (Spain).

Because of the increase in traffic and the presence of larger ships in port areas, interference between sailing and moored ships is becoming more and more, causing situations where the loading/unloading processes are hindered and safety might become threatened. It is necessary to deal with these scenarios using complete and accurate information in order to ensure safety and efficiency in port operations.

1. INTRODUCTION

A new solid bulk terminal is planned to operate in the Port of Barcelona (Spain). Before it starts operating, the Port is interested in the analysis of the operation of different reference vessels using the facilities under the effects of passing ships expected to operate in the nearby berths.

The new facility is located in a narrow area (210 m width approx.) which gives access to one of the inner areas of the Port. Moored vessels at the new terminal might be affected by the passing ship effect. The design vessels to operate in the terminal are two bulk carriers 186 m and 230 m Loa respectively. These ships will be moored at the berth simultaneously and might be affected by hydrodynamic interaction forces.

[1] Siport21 siport21@siport21.com
Chile, 8. 28290 Las Rozas (Madrid, SPAIN) +34-916307073

[2] ENRED www.enred.com

Figure 1: Location of the new bulk terminal in the Port of Barcelona

The passing ships considered in the study have been selected using the traffic data in the different areas of the port and have the maximum size of those expected to operate in the nearby terminals. A car carrier 265 m Loa and a tanker 200 m Loa have been selected among the passing vessels.

Tanker 200 m LOA	
Length over all	200.0 m
Length between perpendiculars	192.9 m
Beam	32.2 m
Draft fully laden	11.5 m
Draft ballast	8.8 m
Displacement fully laden	60 410 t
Displacement ballast	44 100 t

Table 1: Passing vessel. Tanker 200 m

Car carrier 265 m LOA	
Length over all	265.0 m
Length between perpendiculars	216.6 m
Beam	32.2 m
Draft fully laden	10.5 m
Dead weight	43 878 t

Table 2: Passing vessel. Car carrier 265m

Bulk carrier 230 m LOA	
Length over all	230.0 m
Length between perpendiculars	222.0 m
Beam	32.2 m
Draft fully laden	13.5 m
Draft ballast	7.0 m
Displacement fully laden	71 910 t
Displacement ballast	43 470 t

Table 3: Moored vessel. Bulk carrier 230 m

Bulk carrier 186 m LOA	
Length over all	186.0 m
Length between perpendiculars	181.3 m
Beam	28.7 m
Draft fully laden	10.5 m
Draft ballast	7.9 m
Displacement fully laden	36 450 t
Displacement ballast	30 000 t

Table 4: Moored vessel. Bulk carrier 186 m

2. AIS DATA ANALYSIS

AIS data (Automatic Identification System) covering the vicinity of the new terminal have been considered to define manoeuvring strategies executed by the current vessels in the area.

The available AIS data include one year of recorded data and a total number of 740 vessels. They mainly focus in bulk carrier and tanker vessels that have navigated in the vicinity of the new terminal. They cover 1330 operations. For the aims of the study the following information is extracted:

- Track of the vessels. Different positions of each vessel during the manoeuvre.

- Passing distance. This value is between one ship beam (B=32) and 2 beams (2B=64 m), taking a Panamax vessel as a reference.

- Sailing speed. Reference speed for access manoeuvres is 4-5 knots and for departures 5-6 knots. Speed does not depend on the length of the vessel.

Figure 2: AIS data considered for analysis

3. MANOEUVRES WITH FAST-TIME SIMULATION PROGRAM (SHIPMA)

In order to meet the objectives of the study, the first step is to know the **minimum speed** of each selected vessel to maintain control during the whole manoeuvre as well as the **minimum passing distance to moored vessels**. This phase of the study is developed using a **fast-time simulation** program **SHIPMA**.

This tool simulates the manoeuvring behaviour of a ship. The mathematical model computes the track and course angle of a vessel, taking into account the influences of external forces (wind, waves, currents, shallow water, and bank suction).

The manoeuvres are developed under the local conditions in the Port, which include 3 different wind directions and 3 wind speeds (10, 15 and 20 kts). The strategy for the manoeuvres developed with SHIPMA is defined using the AIS data available, in terms of vessels track, distances, courses, ... The main factor affecting the vessels during manoeuvres in the port is wind. Therefore, different wind directions and intensities are considered for evaluation. The analysis of the manoeuvres includes the occupation of the nearby berths by two bulk carriers 230 m and 186 m Loa respectively. Fully laden condition is considered for both passing ships: tanker 200 m Loa and car carrier 265 m Loa.

Simulation runs are developed in order to define the minimum speed to maintain the vessel controlled using the ship's manoeuvring means. It should be noted the large change of course required for the vessels to access the inner harbour. For the analysis and evaluation of results a maximum course deviation of 5º and 15 m deviation from the reference path are considered valid. Next figure shows one of the approach manoeuvres of the tanker using fast-time simulation (SHIPMA).

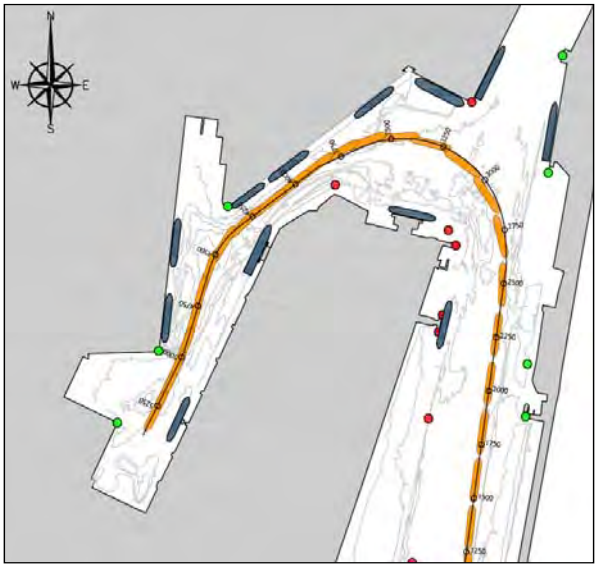

Figure 3: Fast-time simulation (SHIPMA). Access manoeuvre of a tanker 200 m Loa

The results are very similar to those obtained from AIS data. For departure manoeuvres the AIS values are 2 knots above the speed obtained with SHIPMA. One conclusion is that the minimum speed to be controlled highly depends on the intensity and direction of the wind. For strong cross wind, the vessels need to sail with higher speed to keep under control. The following figures show the results:

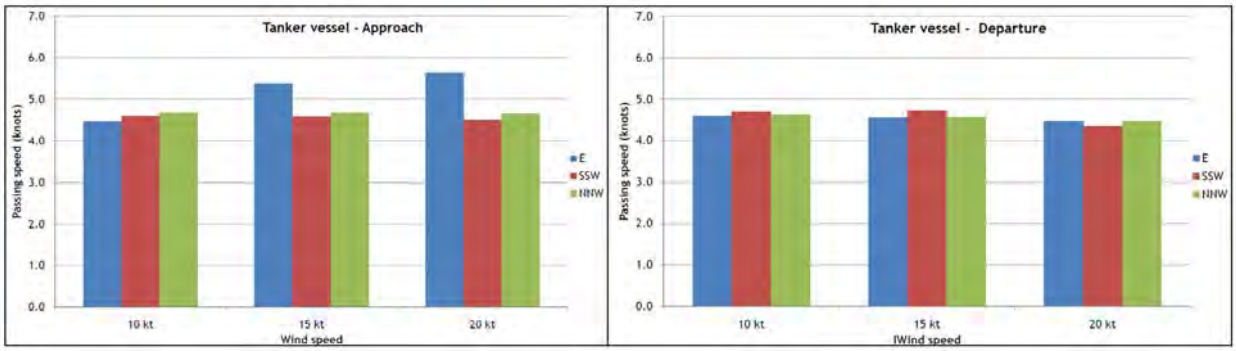

Figure 4: Passing speed - Wind (direction and intensity). Tanker 200 m Loa

4. SHIP TO SHIP INTERACTION FORCES. PASSING SHIP EFFECTS

The traffic in the area, vessels sailing in front of the new terminal, generates passing ship forces on the moored ships. This phenomenon is produced through hydrodynamic interaction between both hulls and induces dynamic loads in lines and fenders. A suction force is generated between vessels caused by the speed and the pressure field variation. This flow variation also depends on the load condition, channel depth and channel cross section.

The interaction effects between a moored ship and one or more passing ships can be computed by means of methods based on 3-D potential theory. The flow is assumed to be inviscid and incompressible and the passing ships are travelling at low speed. In such cases the so-called “double-body solution” can be applied. The solution assumes that the free-surface effects are negligible. This has been shown to be applicable in many cases of large vessels travelling slowly. When the fairway geometry has discontinuities (i.e., docks and harbours openings onto the fairway) the disturbances caused by passing ships can set up seiche-like fluid motions in the basin which can produce important loads on ships moored.

PMH BV (Pinkster Marine Hydrodynamics BV, The Netherlands), Svašek Hydraulics, MARIN and Deltares coordinated the JIP (Joint Industry Project) ROPES which resulted in a numerical model tool. This program allows the user to obtain the calculation of the ship to ship interaction forces and moments

on shallow waters, considering the effects of bathymetry changes and lateral restrictions (navigation channels, vertical structures, slopes, ...). The system calculates the forces and moments on the vessels in all 6 degrees of freedom (surge, sway, heave, roll, pitch and yaw) and on the structures in time-domain. The tool considers the influence of the mooring terminal geometry in the water movements induced by the “Passing Ship” effect of vessels, and also the hull forms of each vessel.

The output of the computations are time-domain records of the 3 forces and 3 moments acting on the vessels, as well as other structures (slopes, vertical quays, …). Results are given in table and graphic format.

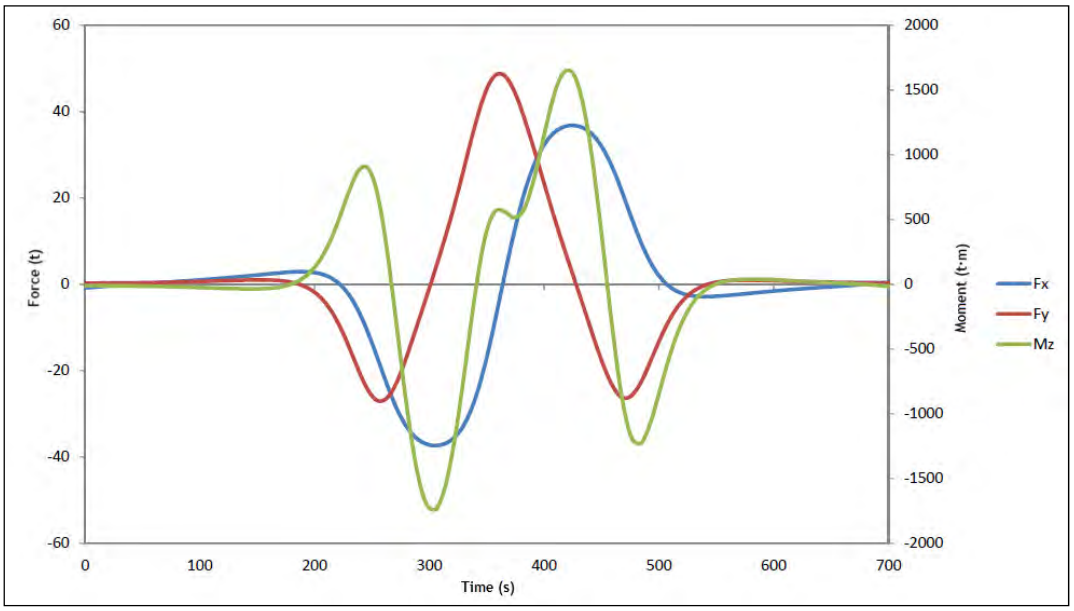

Figure 5: Time series of interaction forces obtained from ROPES

The following factors define the interaction forces and are taken into account in the numerical model: hydrodynamic characteristics of the vessels, speed of the passing ship, course with respect to the centreline of the moored vessels, depth of the channel, distance between vessels and cross-section of the channel (vertical walls, side-slopes, etc.).

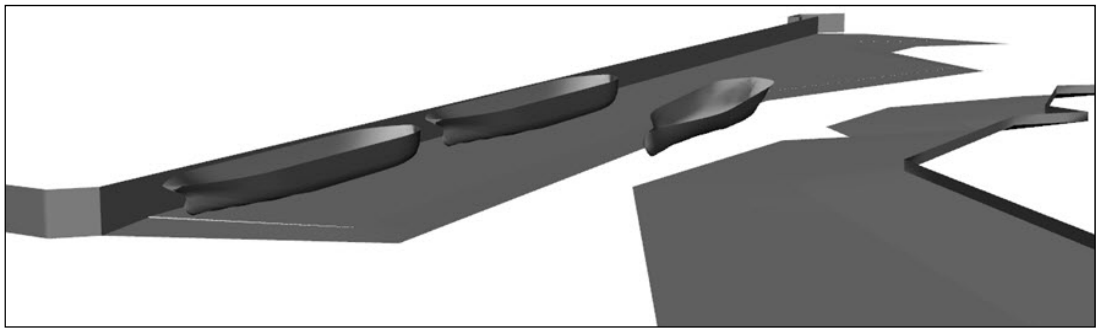

Figure 6: 3D model of the channel with moored and passing vessels

For this phase, different cases (24) are analyzed considering, among others, two moored vessels berthed simultaneously (Panamax bulk carrier 230 m Loa and bulk carrier 186 m Loa), two passing vessels (car carrier 265 m Loa and tanker 200 m Loa) as well as different passing speeds and 2 passing distances (32 m and 48 m, equivalent to 1.0 and 1.5 Panamax beam). The matrix of cases includes both access and departure manoeuvres.

Different suction forces and moments on the moored ships are obtained for each case. The time series of suction forces and moments on the moored vessel clearly depicts a very characteristic situation that varies with the sailing distance of the passing vessel. The following graphs show the variation of interaction forces on moored vessels (surge and sway direction) for access and departure manoeuvres of the car carrier and the tanker according to different passing speeds and passing distances. Blue line is for the moored bulk carrier 230 m Loa and the red one is for the smaller bulk carrier 186 m Loa.

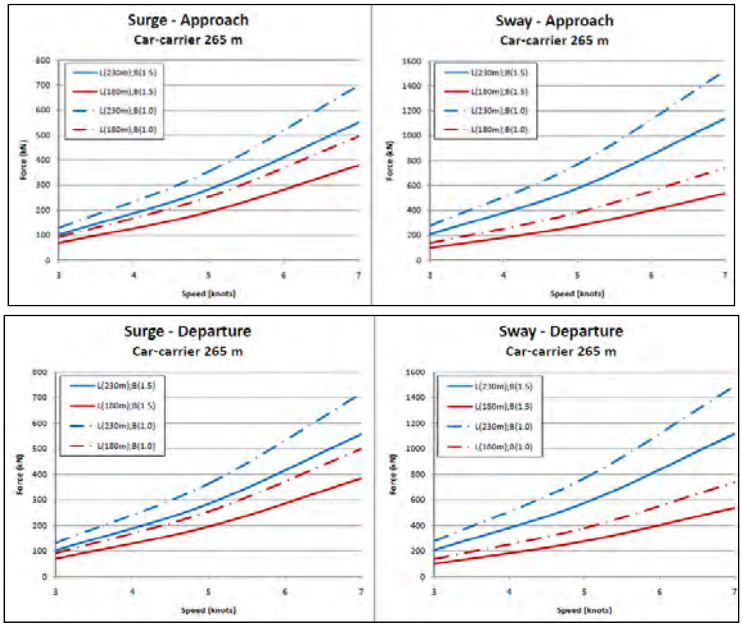

Figure 7: Forces on the moored vessels produced by the passing car carrier

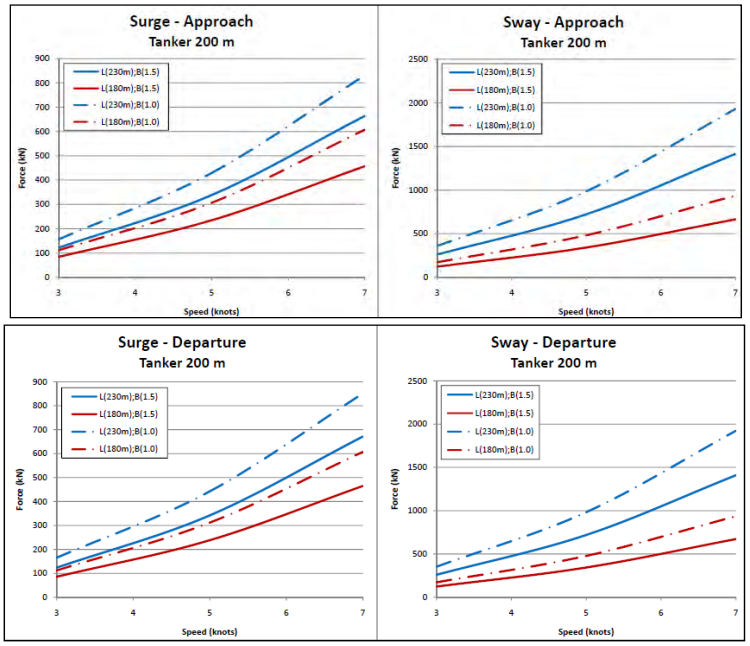

Figure 8: Forces on the moored vessels produced by the passing tanker

The following conclusions can be can be drawn from the analysis:

- The tanker generates suction forces and moments on moored vessel higher than those generated by the car carrier for the same speed and passing distance. These differences are up to 20-30% for suction forces and 20-40% for moments. This is due to the higher displacement, draught and block coefficient.

- Loads on the Panamax bulk carrier 230 m Loa are higher than those on the smaller bulk carrier 186 m Loa. This result does not depend on the passing vessel.

- Forces and moments on moored vessel have a quadratic dependence with the speed of the passing vessel and are inversely proportional to the passing distance.

5. DYNAMIC MOORING ANALYSIS

ROPES results are used as input data to calculate the dynamic response of the moored vessels. The response of the moored vessel is simulated by using the numerical model **SHIP-MOORINGS** developed by Alkyon-Arcadis (Hydraulic Consultancy & Research, Netherlands). This model reproduces the behaviour of a specific ship at berth under the combined action of wind, waves, currents and external forces (such as passing effects). The system solves the equations of ship motion in 6 degrees of freedom (surge, sway, yaw, heave, pitch, roll) in the time domain, without limitations on the motion amplitudes. The simulation results have assessed the motion amplitudes of the ship and the loads transmitted to the fenders and the mooring lines under the combined action of environmental factors typical for the location (wind).

Using the time series of forces and moments obtained from **ROPES** as input for **SHIP-MOORINGS** model, the **movements of the moored ships** and the resulting **loads** on **mooring lines** and **fenders** are calculated. It is then possible to determine the relevant forces and displacements. The calculation includes the interaction between the two vessels combined with wind from the most adverse direction.

The mooring arrangements for the two moored vessels consider their dimensions and the mooring equipment on board as well as the mooring facilities on the berth. The vessels are berthed port side alongside in a bow out position. The initial mooring arrangement comprises 10 lines: 0 head lines (forward) + 3 breast lines (forward) + 2 springs (forward) + 2 springs (aft) + 3 breast lines (aft) + 0 stern lines (aft).

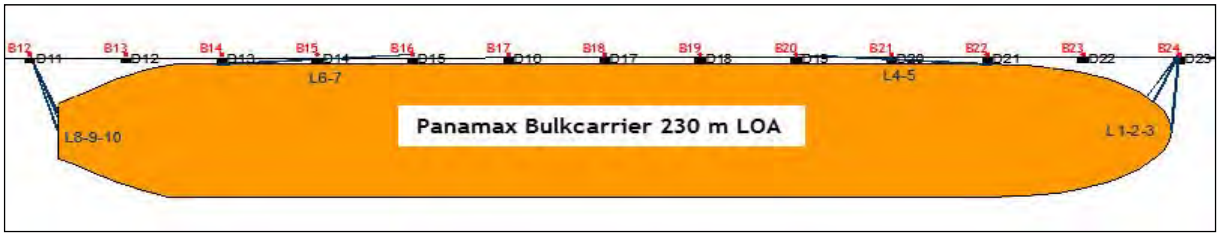

Figure 9: Mooring layout. Bulkcarrier 230 m Loa

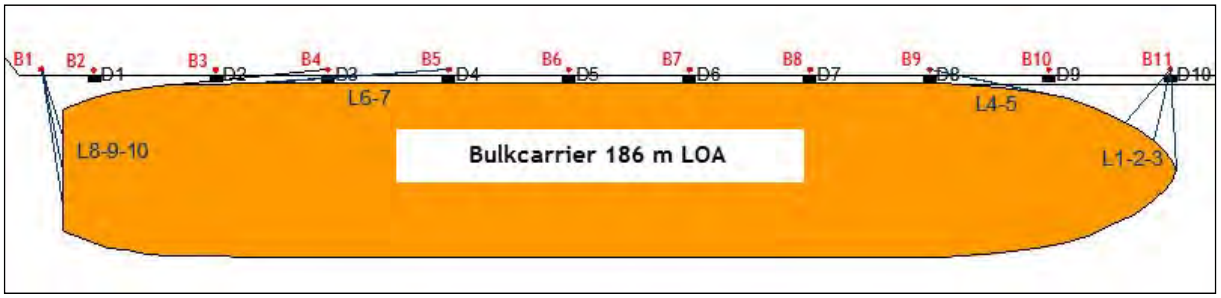

Figure 10: Mooring layout. Bulkcarrier 186 m Loa

The dynamic analysis, response of the moored vessel and line and fender forces, is focused on the bulk carrier 230 m Loa as it showed higher loads than the smaller bulk carrier. A sensitivity analysis regarding wind intensity was done, showing that the effect of the wind on the moored vessel is much less significant than the passing ship effect.

The analysis is focused on defining the operating limits in terms of maximum speed and passing distance for which the mooring system does not exceed acceptable values. The reference wind speed for the analysis is 20 knots with the vessel in loaded condition under the interaction of passing ships for a reference passing distance of 32 m.

Some conclusions of the analysis are as follows:

- The maximum load on lines and fenders does not exceed the defined limits (safe working loads).

- The speed limit for the passing vessels depends on the dimensions of the passing vessel, the loading condition of passing and moored vessels, and the mooring arrangement.

- Conservative values are obtained, as the analysis considers a passing distance of only one beam (32 m), the most adverse wind direction and maximum occupation of the nearby berths.

- The maximum recommended passing speed is above the reasonable speed obtained with the fast-time simulation program.

- From this evaluation different alternatives are proposed in order to obtain less restrictive limits such as: modified manoeuvring strategy, reinforcement of the mooring arrangement and analysis of the dimensions of the passing vessels.

6. ANALYSIS OF ALTERNATIVES

In order to increase the limits of passing speed and passing distance while keeping safety and operability in the terminal, the following alternatives are proposed for analysis:

- **Limit the passing speed in front of the new terminal to maximum values obtained from the dynamic analysis of moored vessels**

For the evaluation of this alternative, fast-time simulation manoeuvres are considered (approach and departures) including the assistance of two tugs with special propulsion and a bollard pull of 75 t. These tugs are similar to those available at the Port. The main conclusions from the evaluation are:

- The use of tugs allows to reduce speed in front of the new terminal under strong cross wind and limits the passing ship effects, as they can keep control the vessel even with engine stopped.

- These results should be verified using advanced analysis tools such as the real-time simulator. This tool allows to assess the possibility of reducing speed under the limit in detail, including the human factor.

- **Different mooring arrangements**

After the analysis of the dynamic behaviour, different mooring arrangements are considered: 2 for the bulk carrier 230 m Loa and 1 for the bulk carrier 186 m Loa. For the larger bulk carrier, the first alternative comprises 12 lines (0-4-2-2-4-0) and the second one includes 14 lines (0-5-2-2-5-0). For the smaller bulk carrier, the new mooring configuration comprises 12 lines (0-3-3-3-3-0).

The main conclusion is that the maximum passing speed for the sailing vessel could be increased (above 0.8 knots) as long as the mooring arrangement for the bulk carrier 230 m Loa has 14 lines and 12 lines for the bulk carrier 186 m Loa respectively.

- **Assess the operating limits for a different loading condition, passing distance and size of the passing vessel**

A sensitivity analysis of the response of the moored vessels is developed for different Loa of the passing vessels, different drafts of the tanker vessel (passing ship) and different passing speeds. The results are shown in the following figures:

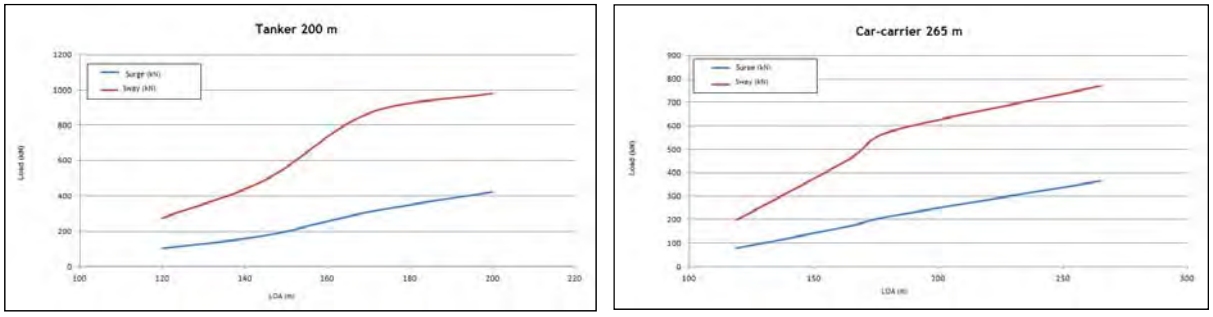

Figure 11: Loads on moored vessels for different Loa of the passing vessel

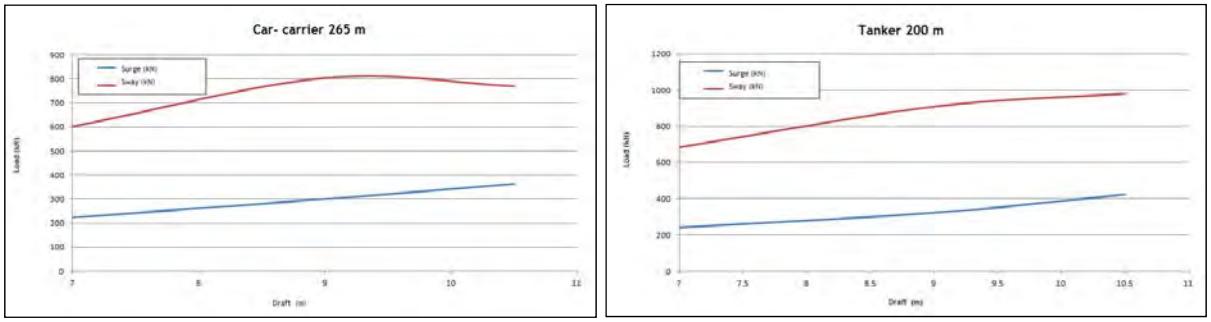

Figure 12: Loads on moored vessels for different draught values of the passing vessel

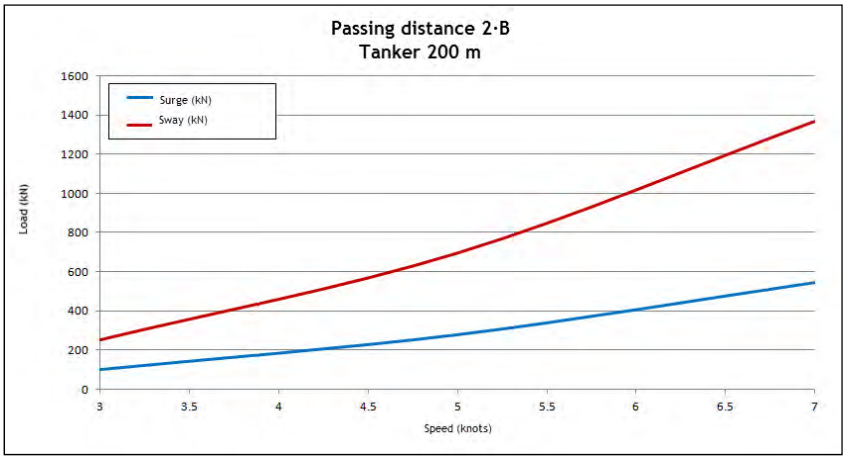

Figure 13: Loads on moored vessels for a passing distance of 2B (64 m) and different passing speeds

From the previous figures it is observed that the interaction forces on the moored vessels decrease significantly when the draught is below 7.0 m and the length below 160 m.

7. REAL-TIME SIMULATOR ANALYSIS

The objective of this final phase of the study is to verify the results and conclusions obtained using the fast-time manoeuvring model (SHIPMA). For this purpose, a real-time ship bridge simulator is used as it is an advanced tool adequate for this type of detailed analysis.

Siport21 real-time ship bridge simulator (MERMAID 500 model developed by MARIN-MSCN (The Netherlands)) reproduces the behaviour of a specific ship while manoeuvring in port areas under the effects of environmental agents (wind, current, waves, limited depth, bank suction, etc.). A Captain or Pilot operates in a main bridge mock-up with real instruments and a radar screen, so human factor is included. The motions of the ship are seen on a 260º wide screen 12 m diameter and sounds (engine, wind, horns) are also perceived.

The ship manoeuvring mathematical model handles 6 degrees of freedom models, with horizontal and vertical motions, and reproduces the ship's behaviour under the action of the following forces: hydrodynamic forces on the hull, propulsion, rudder forces, bow/stern thruster forces, variable depth, wave, wind and current forces, bank suction effects, “squat”, collision forces and hull interaction between ships. Tug operation in the simulator is very detailed, and either conventional or special units are properly modelled.

Figure 14: Siport21 real-time simulator in operation

A total number of 11 manoeuvres were carried out including approach and departure manoeuvres with a tanker 200 m Loa and a car carrier 265 m Loa. These manoeuvres were developed under the most frequent conditions in the port and 2 wind speeds (10 and 15 knots - mean value). The scenarios included the occupation of the nearby berths to restrict the space available for manoeuvres. Some manoeuvres included the use of two tugs of 75 t bollard pull. The objective was to verify that the speed and passing distance were below the limits defined in previous phases.

Figure 15: Real-time simulator manoeuvres: approach manoeuvre of the car carrier and departure manoeuvre of the tanker

From the manoeuvres executed in the real-time simulator the following conclusions were drawn:

- For the tanker 200 m Loa, the passing speed in approach manoeuvres could be reduced below the limits defined in previous phases for 15 knots winds with the assistance of 2 tugs. It is also possible to obtain passing speeds below the limit without tug assistance up to 10 knots wind speed. Results show passing distance to moored vessels increases compared with previous results using SHIPMA.

- In departure manoeuvres of the tanker using 2 tugs, passing speed could also be reduced below the limits and the passing distance increased up to 1.6·B.

- For the car carrier 265 m Loa in approach manoeuvres, the tugs control the vessel with passing speed below the limits for 15 knots wind speed and distance to moored vessels even more than 60 m (2·B). Without tug assistance, passing speed increases above the limits and passing distance decreases down to 1.0-1.6 ·B. The passing speed for departure manoeuvres of this vessel could be reduced below the limits defined. Under this condition the passing distance is 1.6·B, above the results obtained in the fast-time manoeuvres.

- The tugs maintain the vessel controlled when a low passing speed is required which guarantees the safety for the moored vessels at the terminal.

8. CONCLUSIONS

This paper presents the methodology developed to analyze the moored ships behaviour due to passing ship effects with the aim to guarantee a safe operation of moored vessels in a new bulk terminal located in a narrow area of the Port of Barcelona. The analysis combined calculations with four different numerical models: fast-time simulation (SHIPMA), ship-ship interaction (ROPES), dynamic mooring analysis (SHIP MOORINGS) and real-time manoeuvring simulator (MARIN Mermaid).

After a first analysis of AIS data available to know the type of vessels in the area and their manoeuvring strategy (track, course, passing distance and passing speed) a fast-time simulation analysis was developed with the selected design vessels to obtain the minimum passing speed and passing distances. These results (passing distance and passing speed) were used as input data for calculation of ship to ship interaction: effect of passing vessel on the moored vessels in the new terminal using ROPES. Interaction forces and moments on the moored vessels obtained with ROPES were included as an input in the dynamic mooring analysis to define the operational limits using the mooring analysis program SHIP MOORINGS.

A sensitivity analysis was also developed to assess different alternatives which allow a safe operation of the moored vessels in the berth. The final phase of the study consisted of manoeuvres in a real-time simulator with the aim to conduct a detailed analysis of manoeuvres including the human factor in order to verify the previous results obtained during the analysis.

9. ACKNOWLEDGEMENTS

The authors wish to thank the Port Authority of Barcelona (APB), especially Mr. Miguel A. Pindado (Project Manager) and Capt. Jose M. Rovira (Maritime Operations Manager) for their support and help during the project and contribution to this paper.

10. REFERENCES

PIANC Report WG20 “Capability of ship maneuvering simulation models for approach channels and fairways in harbors” (1992)

PIANC Report WG24 “Criteria for Movements of Moored Ships in Harbours” (1995)

PIANC Report 121 “Harbour Approach Channels Design Guidelines” (2014)

OCIMF “Mooring Equipment Guidelines (MEG3)” (2010)

ROM 3.1 “Maritime Recommendations for the Design of Port Access and Manoeuvring Areas” (1999). Spanish Port Authority

SIPORT21 “Análisis del Comportamiento Dinámico de Buques Atracados Bajo la Influencia del Paso de Buques (“Passing Ships”) en el Muelle Álvarez de la Campa del Puerto de Barcelona” (“Analysis of Moored Ship Dynamic response under the Influence of Passing Ships in Alvarez de la Campa Dock, Port of Barcelona”) (2014)

Port Development to Support Offshore Petroleum Exploration and Production

Joseph E. Berlin[1]

ABSTRACT

Offshore petroleum exploration and production is a relatively young and rapidly growing industry which has impacted and benefited ports worldwide. This industry operates much differently than maritime trade and has specific channel requirements to operate efficiently. This presentation describes the channel requirements and port facilities needed to support offshore petroleum exploration and production. The combination of channel requirements and infrastructure needs can be used to determine the best port configuration for ports near offshore petroleum exploration sites.

Offshore platform fabrication requires deep and wide channels to move large platforms. Offshore supply vessels do not need the deep and wide channels that offshore platform fabrication does, but they require reliable channel access because they make frequent trips with short loading cycles. Offshore petroleum exploration ports also require a significant landside infrastructure to provide water, fuel, drilling mud, deck equipment, and supplies to offshore platforms.

INTRODUCTION

Ports that support offshore petroleum exploration and production are essential to the success of the industry. Within the United States, offshore petroleum exploration and production began in Louisiana in the 1930s, with rapid expansion beginning in the 1950s as technology improved. Technological advances are allowing petroleum exploration and production in very deep waters, and as the industry has focused on deep water exploration, the offshore platforms and the offshore supply vessels that support them have become much larger. The large capital investment required for the operation of offshore platforms during exploration is what focuses all supporting businesses, including ports, on efficiency.

Ports that support offshore petroleum exploration and production do so either by harboring a fleet of offshore support vessels (OSVs), or by servicing offshore rigs and platforms. Ports that harbor OSVs to support offshore petroleum exploration are also known as shore bases. Larger navigation channels are needed to service offshore rigs and platforms, as these ports need shipyards with dry docks. An important attribute of the offshore petroleum industry worldwide is that during its short history it has been highly cyclical.

Offshore petroleum exploration has expanded worldwide, including new regions without a history of supporting the industry. This highly technical industry has many experts with deep knowledge of specific subjects. The Bureau of Ocean Energy Management within the U.S. Department of Interior has conducted extensive historical research on the development of the offshore petroleum industry in the Gulf of Mexico. Nevertheless, literature that analyzes the attributes of an efficient offshore petroleum exploration and production port is limited. This presentation is intended to provide an overview for that purpose.

Figure 1 shows an aerial photo of the largest shore base in the United States for supporting offshore exploration and production. OSVs from Port Fourchon supply rigs throughout the U.S. Gulf of Mexico.

[1] **AECOM**, 7389 Florida Blvd., Suite 300, Baton Rouge, La 70002, PH (225) 231-6396; email: joseph.berlin@aecom.com

Figure 1: Aerial Photo of Port Fourchon, Louisiana, USA

Figure 2 shows an aerial photo of the one of the largest shipyards constructing and servicing offshore rigs in the United States. The Keppel-Amfels Shipyard has constructed jack-up rigs and serviced semi-submersible floating rigs.

Figure 2: Aerial Photo of the Keppel-Amfels Shipyard in Brownsville, Texas, USA

OFFSHORE SUPPORT VESSELS

Decisions regarding supplies for offshore petroleum exploration and production are based upon economics and the drive for efficiency. Ports are always managed based upon economics and the need to move cargo as efficiently as possible. The difference with offshore petroleum exploration and production is that the investments in facilities and operating costs are very high. The cost of operating a semi-submersible offshore drilling platform in deep water can exceed $1,000,000 per day. Therefore, the reliability of shipments is very important as platform operators do not want to disrupt operations because of supply problems. Offshore platforms have limited storage capacity, so their ability to cope with supply disruptions is limited.

The industry's emphasis on logistical efficiency favors port locations near offshore petroleum exploration sites with transportation infrastructure and sufficient utilities. Transportation networks are a key factor in determining the viability of a port for supporting offshore petroleum exploration. The availability of barge or ship transportation allows efficient transportation of bulk materials such as drilling mud and fuel. Fuel is most efficiently transported by pipeline. Highway access should be sufficient for trucks to transport equipment and supplies efficiently if equipment and supplies are provided from inland sources. Sufficient waterworks capacity to provide potable water to offshore platforms is essential for an OSV port.

The expenses incurred during exploration, and the limited space for supplies, require highly reliable delivery of supplies. By weight, the bulk of these supplies are potable water, fuel, and drilling mud, which are carried by offshore supply vessels in tanks below deck from stockpiles onshore. Supplies and equipment are generally carried above deck on the same OSVs. Ports that support offshore petroleum exploration usually have liquid bulk storage capacity for fuel and drilling fluids. Supplies and equipment stored at shore bases are loaded as efficiently as possible onto OSVs. Some OSV ports have sufficient laydown space for pipe, anchors, chain, and wire to be stored and inspected.

Offshore Support Vessels primarily serve exploratory and developmental drilling rigs and production platforms and support offshore construction, installation, maintenance, repair, and decommissioning activities. Platform Supply Vessels (PSVs) are the "workhorses" of the offshore support fleet. PSVs generally have a large open deck for dry bulk and internal tanks for liquid bulk. PSVs in the U.S. generally range from 180 feet to 260 feet in length, but can be over 400 feet in length. PSVs leave the port heavier than they enter the port, but they do carry waste and rented equipment back from the offshore structures, so they do not return to port completely empty. Offshore Tug/Supply Ships can be used to assist in rig movements and anchor handling operations or to supply offshore structures similar to PSVs. Table 1 shows OSV types.

Ship Type	SeaWeb Ship Type
OSV	Offshore Support Vessel
	Offshore Tug/Supply Ship
	Pipe Carrier
	Platform Supply Ship
AHTS	Anchor Handling Tug Supply
Construction Vessel	Diving Support Vessel
	Offshore Construction Vessel, jack up
	Pipe Burying Vessel
	Pipe Layer
	Pipe Layer Crane Vessel
	Production Testing Vessel
	Research Survey Vessel
	Trenching Support Vessel
	Well Stimulation Vessel

Table 1: Offshore Support Vessel (OSV) Types

Anchor Handling Tug Supply Vessels (AHTS) have winches and cranes and are used to set and lift anchors used by certain types of offshore structures and to tow and position movable offshore structures. AHTS often enter and leave a port at the same depth because they haul anchors into port for inspection and then back out to offshore structures. Unlike supplies carried by other types of OSVs, such as water or drilling fluid, anchors are not divisible, so the tonnage carried by these vessels is less easily adjusted to account for changes in channel depth. Crew Supply Vessels transport crew to and from offshore structures, but generally have some capacity for deck cargo and internal tank space for liquid bulk. Crew Supply Vessels are generally smaller than other offshore vessels, and are therefore less important when considering channel requirements for an offshore supply operation.

Seismic vessels are larger than most OSV's and are the first vessels involved in exploration of a potential offshore petroleum field. These are among the most complex and technically advanced vessels and are operated by specialty firm from specialized facilities. Since these vessels are the first deployed to a potential field, before the potential petroleum production is known, bunkering of seismic vessels is done from the nearest port facility. Once shore bases are constructed, seismic vessels may call for supplies and bunkering, but they will likely remain based at their owner's home port as these vessels are typically deployed worldwide based upon available contracts. Exploration is likely to continue in and offshore petroleum field after production begins, but the deployment of seismic vessels will not be continual.

A channel closure at an OSV port could result in a significant economic impact to the operators of offshore platforms. Channel depth restrictions impact the efficiency of OSV operations and are an important consideration when OSV operators determine where to base OSVs. The tables below show OSV dimensions for the world fleet based upon year of build. As offshore petroleum exploration has move further offshore into deeper water, OSVs have become larger and more complex.

Year of Build	Design Draft	Length	Beam
1960	3.6	51.5	10.1
1970	3.2	49.5	11.1
1980	3.0	48.8	11.5
1990	3.9	62.9	13.3
2000	4.4	61.8	14.5
2010	5.2	70.6	16.0
2014	5.8	81.1	17.7

Table 2: Dimensions based Upon Year of Build (meters)

Offshore logistics is a complex system involving efficiency and productivity, inventory control, and supply reliability. Exploratory platforms require many more supplies than production platforms, since they are constantly using drilling mud, pipe, and fuel while drilling. This greater need for supplies drives the need for more OSV calls. The scheduling of OSV calls for exploration platforms is also much more uncertain than for production platforms, because drilling conditions and needs constantly change.

Offshore support vessels are generally operated by specialized charter operators. These operators are responsible for loading the vessels, maintaining the vessels, and providing crews. The vessels are used as directed by the petroleum exploration companies, which specify what cargo to carry and what offshore locations to serve. The routing of OSVs is complicated because they sometimes serve multiple platforms, but this task remains the responsibility of the petroleum companies. Offshore vessel operators design the new vessels and sometimes operate shipbuilding companies as subsidiaries. Having the most marketable fleet is important for OSV operators in this competitive market. As offshore petroleum exploration has moved further offshore into deeper water, OSVs have become larger.

An OSV port needs a channel depth of 24 feet for larger OSVs, barge access or deep draft ship access for liquid bulk, proximity to offshore exploration and production areas, highway access for equipment and supplies, and adequate water and power supply. Rail access, which is a major requirement for most commercial ports, is not generally used for offshore supply vessel ports. Most ports contain bunkering facilities, but the scale of bunkering operations for a port serving OSVs is much greater. Infrastructure availability – water, power, fuel – is vital for supporting the offshore petroleum industry.

OSVs are typically piloted by pilots employed directly by the OSV operators. Some OSV operators have company-specific rules regarding under keel clearance. In deep draft ports with channel depths over 24 feet deep these constraints are not an issue, but in shallow draft ports serving OSVs these constraints can impact operations.

Specialized services and facilities can be expected to develop around an offshore support port. The development of these facilities requires sufficient land adjacent to channels. The anchor handling tug facilities are an example of facilities requiring significant waterside land. Anchor handling tugs are used to relocate semi-submersible structures, and transport large amounts of chain and cable on each trip, which needs to be sorted and inspected at the facility. Pipe suppliers also require a significant amount of laydown land, especially if they are inspecting pipe at the facility.

OFFSHORE PLATFORM FABRICATION

Offshore platform fabrication is a highly specialized and integrated market and is the only internationally competitive type of shipbuilding in the United States. Platform fabrication is complex and performed by a limited number of specialized shipyards. Platform structures are constructed in pieces, integrated either on location or at large, deep water facilities. Platforms must be inspected, repaired, and refurbished in port based upon classification society (ABS) schedules. The inspections and refurbishments of existing offshore structures is a major portion of business and revenue for all shipyards in the industry, including those shipyards fabricating new offshore structures. Table 4 describes the different types of offshore platform structures.

Offshore Structure	Mobile (Yes/No)	Self-Propelled (Yes/No)	Exploration / Production	Maximum Depth (ft.)
Drill Barge	Yes	No	Exploration	30
Drill Ship	Yes	Yes	Exploration	12,000
Floating Production, Storage, and Offloading System (FPSO & FSO)	Yes	Yes	Production	12,000
Jack-up	Yes	No	Both	500
Platform Rig				
Fixed Platform	No	No	Production	1,300
Compliant Tower	No	No	Production	3,000
SPAR	Yes	No	Both	8,000
Tension and Mini-Tension Leg Platforms	Yes	No	Production	6,000
Semi-submersible	Yes	No	Both	8,000
Submersible	Yes	No	Both	30
Tender	Yes	No	Both	8,000

Table 3: Types of Offshore Structures

Offshore platform fabrication requires much more capital investment in facilities and equipment than a typical maintenance shipyard. Offshore platform fabrication and repair must meet international standards, as published by classification societies. A highly skilled labor force is needed and a specialized supplier network must be established. Some components of offshore platforms, such as topsides, are shipped hundreds of miles from an inland port to a platform fabricator at a coastal port.

Pilots from the harbor pilots association typically supervise the movement of offshore platforms through harbors. These slow moving structures can impact other vessel traffic as they are maneuvered through the harbor channels. Sometimes simulators must be used to ensure that the offshore platforms can safely transit the harbor channels. This significant effort and cost is incurred because the revenue to the platform fabricators can range from $2 million for inspection and minor repairs to $50 million for major repairs and upgrades. Likewise, the cost to platform operators of finding another available fabricator and transporting the platform an additional distance to that facility is very high. For each day the offshore platform is unavailable for charter, it is losing its charter rate and incurring the cost of the several ocean going tugboats needed to transport the platform.

Labor force skill and training has been a difficult issue for offshore platform fabricators. A skilled workforce takes time to develop and is difficult to maintain during industry downturns. This problem is not unique to offshore structures, but is prevalent through all aspects of the petroleum industry. During the past several decades, employment in this cyclical industry has been volatile. Skilled workers tend to disburse to other industries in need of their skills, and are not necessarily available when fabrication work increases. For this reason, platform fabricators tend to be located near cities with a large enough skilled labor force to allow increased production. Sufficient skilled labor in a cyclical industry is always a difficult issue and platform fabricators have avoided remote locations where obtaining sufficient labor is more difficult.

Ports with facilities capable of constructing & servicing jack-up structures and semi-submersible structures have at least 30 feet of channel depth. The average transit draft of semi-submersibles in the Gulf of Mexico is 31 feet. These facilities should have a reasonable proximity to open water as structures can disrupt normal ship channel traffic. At the same time, facilities should have sufficient elevation and protection from storm surge.

The depth of water for offshore drilling determines to type of structures likely to be employed, which also impacts the type of offshore supply vessel employed. Jack-up platforms are used in water up to 300 feet deep. Semi-submersible structures are prominent in deep water to 8000 feet and require a fleet of anchor-handling tugs. Drill ships are a relatively recent development, and are used for drilling in ultra-deep water. Jack-up platforms can be transported through smaller channels than semi- submersible platforms. Drill ships are more maneuverable than either jack-up platforms or semi-submersible platforms, and are also the most costly vessels to charter and operate.

Although sufficient depth is important, channel width can be just as important. The beam width of these structures can be several hundred feet wide. Table 5 shows the average beams of selected types of offshore structures in the U.S. Gulf of Mexico.

Offshore Structure Type	**Average**	**Median**
Drill Ship	39.3	38.1
Jack-up	49.7	52.1
Platform Rig	NA	NA
Semi-submersible	82.9	78.0
Submersible	54.9	54.9
All	**56.4**	**53.7**

Table 4: Average and Median Beam Size of Offshore Structures in the U.S. Gulf of Mexico (meters)

The channel dimensions required to move offshore structures are not absolute. There are steps the structure operators can take to reduce the transit dimensions, such as removing the thrusters offshore. These steps have a cost that operators must consider when determining where to service an offshore structure.

OPERATIONS AT OSV PORTS (SHORE BASES)

Drilling fluids, also described as drilling mud, is produced by mixing barite and betonite with other chemicals and water, and is most efficiently done at shore bases near offshore petroleum exploration. Much of OSV capacity is used for drilling fluids during offshore petroleum exploration, and the drilling fluids are returned to shore bases for recycling. The drilling fluids are usually prepared for use by each supply company as the mixtures are proprietary.

Ports serving the offshore petroleum industry must fuel and supply the OSVs. This is typically done at a central facility that serves multiple fleets operating from the port.

Offshore petroleum ports sometimes have associated heliports that transport crews and urgent supplies offshore. There are benefits to having these facilities adjacent to port serving the offshore petroleum industry, where supplies and expertise are readily available.

As offshore petroleum fields shift from exploration to production, pipelines may be built to bring petroleum ashore. Offshore petroleum production does not require pipelines to shore as FPSO (Floating Production and Offloading vessels are now often used to transport crude oil to distant refineries. Offshore natural gas production requires either pipelines to shore or FLNG (Floating Liquefied Natural Gas) vessels. The decision to lay pipelines to shore from new offshore petroleum fields is based upon several factors, including the distance from the offshore field to storage facilities on shore, the expected longevity of the offshore field, and the market for the petroleum within the region. Since many of the more recent offshore fields are more than 100 km from shore

The construction of pipelines from production platforms to shore is facilitated by OSVs operating from shore bases. However, construction of pipelines to shore requires specialized vessels that are much larger than PSVs, and spooling facilities that require a large area that is not always available at a shore base. Within the United States there are two major spooling facilities in Galveston, TX and Theodore, Al

that prepare spool pipelines for the entire U.S. Gulf of Mexico. These facilities have access to channels 14 meters deep.

Processing waste from offshore and transporting to appropriate disposal sites is an important shore base function. Offshore rigs and platforms have limited storage space for waste. Waste from rigs is typically retrieved by OSVs when returning to port after delivering supplies. The environmental laws of the receiving nation and the business practices of the company managing the offshore exploration determine the storage methods for the waste, whether incineration, or landfills. The waste is sorted based upon hazard level before disposal and hazardous waste is sorted out and disposed of separately. The sorting and disposal is usually performed by specialized logistics firms with facilities at shore bases.

Much offshore exploration equipment must be inspected after each use including drill pipes, chains, and risers. The inspections require specialized equipment, skilled labor, and sufficient land area. The inspection of drilling pipes and risers requires specialized equipment. The efficiency of performing the inspections at shore bases rather than transporting the equipment to centralized facilities may be sufficient to warrant the investment in inspection equipment and a facility, depending upon the amount of exploration drilling in the region.

OPERATIONS AT INLAND PORT FACILITIES

The supplies and equipment needed for offshore petroleum exploration are varied and are managed by many different types of specialized businesses. Petroleum companies rely upon long term relationships with suppliers. Within the U.S., the complex machinery and equipment used on offshore rigs and platforms is assembled and maintained where skilled labor is available which is not necessarily at shore bases.

Some operations, such as spooling of pipelines, require significant land. Spooling is the manufacturing process of joining pipes together to lay offshore. These facilities must be located dock side to allow the loading of specialized vessels where pipelines are spooled onto the vessels for delivery offshore.

CONCLUSION

The reason that new petroleum exploration ports will be needed is that transportation costs for supplies to offshore platforms are very high, and the cost of transporting structures is also very high. Larger semi-submersibles platforms have a charter rate of $300,000 to $400,000 per day, and require towing vessels at an additional cost as they transit long distances at slow speeds. The investment in building a shipyard capable of servicing these platforms is substantial. Therefore, these investments are only made in a continental region after petroleum exploration findings indicate that exploration and production in the region will continue. There are many specialized businesses that support the offshore petroleum industry, and as a port develops sufficient land is needed to allow these businesses to open and expand.

REFERENCES

Aas, Bjornar, and Halskau, Oyvind and Wallace, Stien (2009) The Role of Supply Vessels in Offshore Logistics, Maritime Economics and Logistics, Vol. 2-3

Jayawardana, Jay and Hochstein, Anatoly (June 2004) Supply Network for Deepwater Oil and Gas Development in the Gulf of Mexico: An Empirical Analysis of Demand for Port Services, Final Report, Department of the Interior, Mineral Management Service 2004-047, New Orleans, Louisiana

Kaiser, Mark, J. and Snyder, Brian (February 2010) An Empirical Analysis of Offshore Service Vessel Utilization in the Gulf of Mexico, International Journal of Energy Sector Management

Kaiser, Mark, J. and Snyder, Brian (2010) Mobile Offshore Drilling Newbuild and Replacement Cost Functions, Maritime Economics and Logistics, Vol. 12-4

Koske, Rose, and Robin, Sebastion (February 2011) Future Characteristics of Offshore Support Vessels, Massachusetts Institute of Technology, Cambridge, MA

U.S. Army Corps of Engineers Galveston District (December 2010) Draft Freeport Harbor, Texas Channel Improvement Project Feasibility Study, Galveston, Texas

U.S. Department of the Interior (May 2012), Oil and Gas Utilization, Onshore and Offshore, Updated Report to the President, Washington D.C.

The development of Aberdeen Harbour Expansion Project, UK

Ian Cruickshank, HR Wallingford,
Aurora Orsini, HR Wallingford
Peter Hunter, HR Wallingford
Tom Young, Arch Henderson
Keith Young, Aberdeen Harbour Board,

Abstract

One of Europe's largest greenfield port capital investments projects over the next few decades will be the Aberdeen Harbour Expansion Project. (Figure 1). It has a project investment of over £300 million, the project involves the construction of two new breakwaters each 600m long, quay lengths of over 1.5km, 2 million m^3 of dredging including 0.25 million m^3 of rock dredge and approximately 1 million m^3 of reclamation. The harbour is situated on the east coast of Scotland and is subject to severe wave climate where design waves exceed Hs~8m requiring single layer concrete armour units of up to 16m^3 to protect the Southern Breakwater.

This paper sets out the elements of the development of the port masterplan including the key engineering design and environmental constraints and operational requirements using many of the principles set out in the forthcoming PIANC WG185 guide to site selection and masterplanning of greenfield ports. The paper presents the context and background of the project, the masterplanning process, numerical and physical wave modelling studies, navigation simulation, aspects of the engineering design and the procurement process. The construction contract was awarded on 20 December 2016 with the project due to be complete in 2020. The construction is now fully underway.

Introduction - Background and context

King David 1st of Scotland, first established Aberdeen Harbour as a business in 1136 and is, according to the Guinness Book of Business Records, the oldest existing business in Britain, with a history that has spanned almost 900 years. Over the last 50 years Aberdeen Harbour (Figure 1) has undergone substantial development, primarily as a result of the growth in the northeast oil and gas industry. The growing trend for new, larger, multi-purpose vessels and the oversubscription of the existing harbour combined with the potential for new business streams, large cruise ships, renewable energy sector and oil and gas decommissioning, indicated there was a case for growth outside the existing harbour infrastructure. Aberdeen Harbour Board therefore proceeded with a series of technical, studies, economic and masterplanning studies (HR Wallingford, 2012) culminating in the Case for Growth (AHB, 2012) and then the Direction for Growth (AHB, 2013) to address these future challenges.

The masterplanning process

The HR Wallingford masterplanning studies applied many of the principles set out in PIANC *'Working Group 185 Ports on greenfield sites – guidelines for site selection and masterplanning (PIANC (2018))'*. When the masterplanning process began in 2000, these guidelines were not available and the masterplanning process drew on a number of publications and good practice including The Maritime Code, BS6349 Part 1 (now superseded by Part 1.1) PIANC 158 and experience. However,

the process helped seed, formulate and develop many of the masterplanning principles now being set out in the PIANC guidelines.

The high level process for masterplanning a greenfield port is illustrated in Figure 2. The PIANC process starts with identifying the *future needs and vision* (high level objectives) for the port drawing upon the business case scoping report, which sets out opportunities from future markets. For the Aberdeen project this was undertaken by a joint team culminating in the publication of the Case for Growth (AHB 2012) setting out the markets and the need for development. The next step is to establish the *performance and functional requirements* and constraints based on these future business needs.

Figure 1: Aberdeen's existing harbour

This was followed by establishing key *spatial requirements* for land, water and access allowing the existing port and potential sites to be screened against these requirements. A number of potential development sites (over 20) were identified and matched against these requirements. The next step was to collect data and *develop, evaluate and screen* these sites (undertaken during the prefeasibility/feasibility stage) before identifying the preferred option. A range of drivers and constraints (including performance and environmental drivers) were considered right through the masterplanning process and these were integral to the decision making process.

The results were collated into the Technical Feasibility Study prepared by HR Wallingford and the wider planning document Directions for Growth (AHB 2013) prepared by Barton Wilmore. Directions for Growth considered the wider social impacts, the planning constraints and city's growth agenda.

After initial screening four potential options were considered for detailed review. These were:

- The Existing Harbour
- North Beach
- Nigg Bay
- South of Cove Bay

The three new sites beyond the existing harbour are illustrated in Figure 3. In addition, the existing port operations underwent a business case to assess whether improvements would enable an improved existing harbour to be a viable option. It was established that limiting operations to the existing harbour would mean acceptance of Aberdeen Harbour as a fully mature business, with future development focussed solely on its current estate in a programme of consolidation and internal adjustment. This option remained under consideration as a "Low/No Growth Option" in the event that others could not proceed. The process of identifying and subsequently characterising the three potential sites considered:

- Marine: Bathymetry, metocean data, currents, sediments geology and geotechnical constraints
- Terrestrial: Road and rail connections, material sources, utilities

- Environmental Constraints: Legislative framework, local planning issues, constraints and consultation. The chosen site included a Site of Special Scientific Interest (SSSI) and was adjacent to a Special Area of Conservation (SAC)

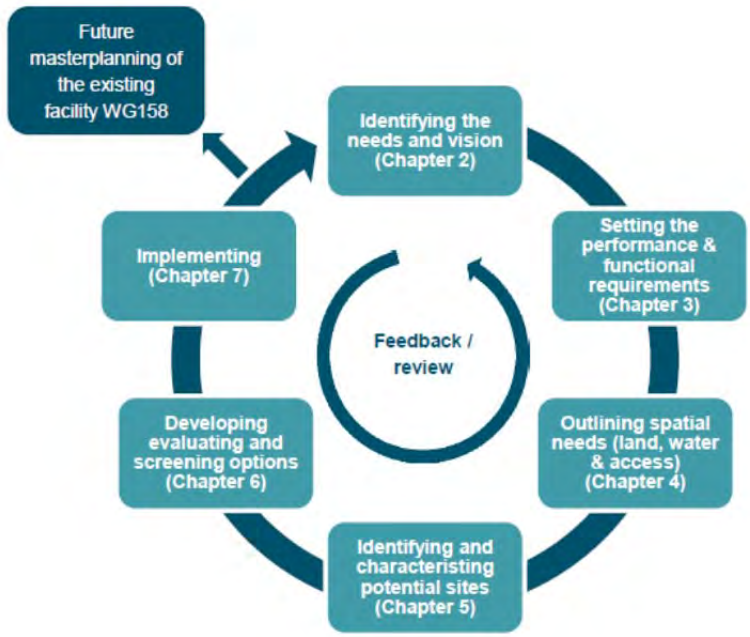

Figure 2 PIANC Outline masterplanning process for greenfield ports (PIANC 185)

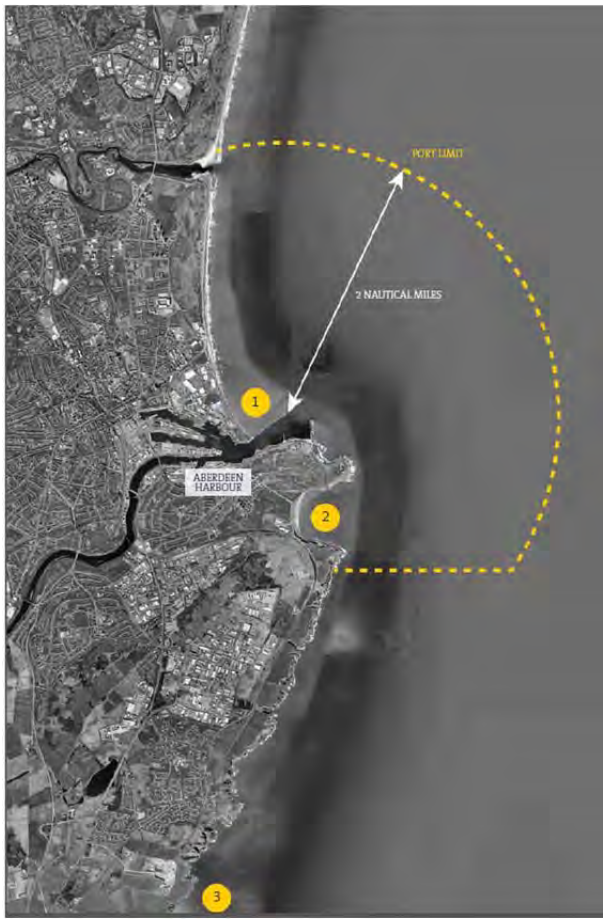

Figure 3 Site options considered

Figure 4 Hinterland links and constraints

Through this process Nigg Bay was identified as the preferred direction for growth. It was apparent that for a facility at South Cove, the lack of natural shelter meant that the costs associated with the creation of extensive new breakwaters, land reclamation and dredging, were greater than at both North Beach and Nigg Bay. The construction costs alone meant that a development at Cove was not financially viable. In addition, due to topographical constraints along this stretch of coastline, accessibility from land to the harbour facility would be challenging.

North Beach offered some greater scope to create the required berthing space but this came with traffic and environmental impact which would have proved problematic to mitigate against. The development of this area would offer little in the way of community benefits and would result in adverse impact upon the amenity of the city centre and local residents.

Nigg Bay offered the greatest scope to accommodate a new deep-water facility with potential for the lowest environmental and traffic impact. The facility will be constructed with little to no impact upon the operations of the existing harbour with considerable potential for regeneration of nearby communities. At the same time the site was close enough to the existing harbour to ensure that the logistical and operational management aspects could be efficiently addressed. The natural topography means that landside access was relatively straightforward. These combined to make the overall construction and operational costs of Nigg Bay the most commercially attractive option with the lowest environmental impact.

For all sites landside storage area was limited. More port area could be created through providing greater areas of reclamation albeit at a cost premium. The required areas were reviewed in with the port to ensure future flexibility. The present and expected future operations required little storage area and the proposed facility provided greater storage area behind the quay than the harbour had at present. The final Reference Design layout is shown Figure 5.

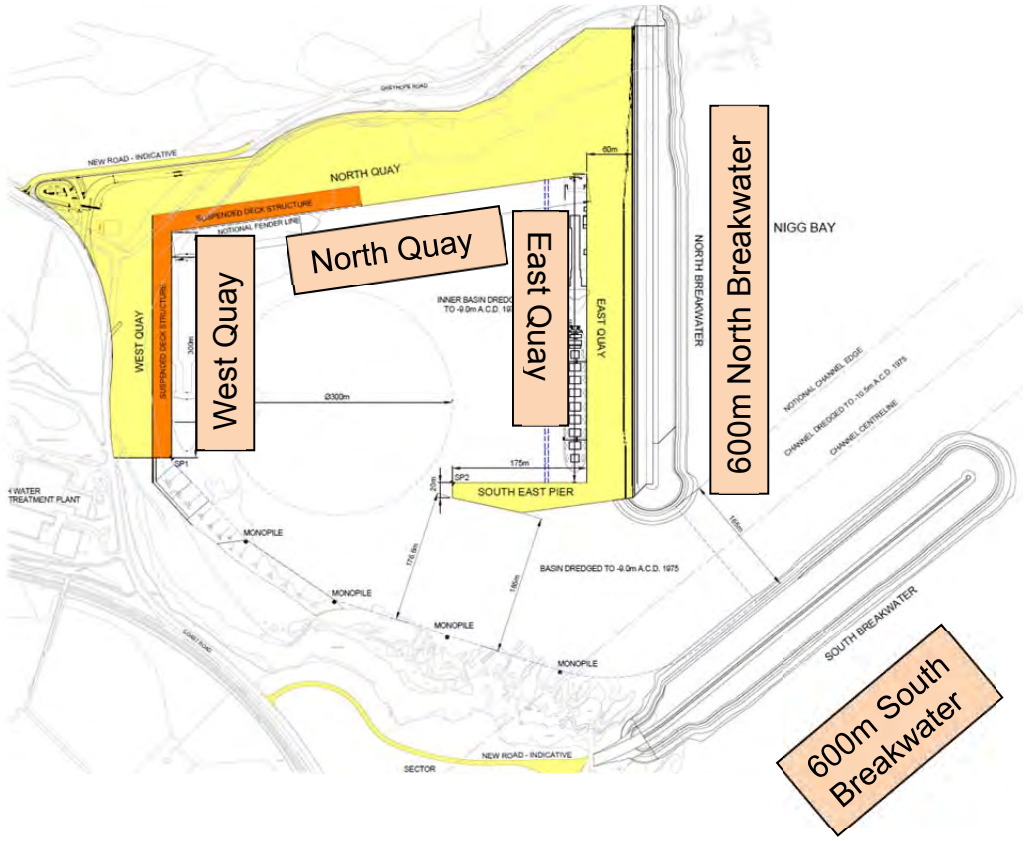

Figure 5 Overall port masterplan (Reference Design)

Simulation and modelling studies

Existing bathymetry and ground conditions

The existing bathymetry slopes steeply within the bay from the rock outcrops to the north and south and the boulder, cobble and sand beach in the west to approximately -7mCD at the entrance to the bay. Outside the bay the seabed slopes quickly to -20mCD within 600m of the entrance.

The superficial sediments within the survey area are sands, underlain by horizontally bedded silts, sands and gravels. However, Nigg Bay is a former (geological) channel of the River Dee, which has been partially infilled with glacial tills and sediments associated with the last Ice Age. The channel is carved into the underlying bedrock and descends to up to 40 m below sea-level. Part of the upper cliffs in the SE corner of Nigg Bay is an area classified as a Special Site of Scientific Interest (SSSI) due to the glacial sediments within the surrounding cliffs, some of which have been transported from as far as Scandinavia.

The bedrock which encircles the bay comprises of Dalradian Psammites and Semipelites, originally formed in shallow seas as sedimentary rocks and transformed by low grade metamorphism, with igneous intrusions having subsequently altered the sequence. The igneous rock within the survey area is unnamed but is estimated as Archaean to Silurian in Period. It was originally formed by silica poor magma. Subsequently these rocks have undergone metamorphism associated with the Caledonian Period.

Rock levels rise at the north and south of the bay. The masterplan layout was optimised to reduce the founding depth of the breakwaters but this meant in turn that it was necessary to dredge some 250,000 m^3 of hard rock, although this rock would be reused in the works.

Metocean – Waves, currents and sediments

Figure 6 Wave condition at the existing South Breakwater, Aberdeen Harbour 7 January 2016

a) Nearshore wave conditions

The project used MetOffice and ReMap data sets. Aberdeen is characterised by severe waves conditions (Figure 6) from three primary sectors, 60 degree, 90 degree and 120 degrees. The extreme waves from all three sectors are similar, but the 90 degree sector, followed by 120 degree produce the largest waves.

a) Tidal currents
The tidal currents were generally weak (approximately <1m/s) flowing north south across the bay.

b) Sediments
The seabed consists of fine to coarse sand. The combined waves and currents mean that there is significant potential for sediment transport just outside Nigg Bay with potential for significant sedimentation inside and at the entrance to the proposed harbour.

Table 1 Predicted all direction wave heights at the -19mCD contour for a water level of 5.1mCD at the entrance to the bay

Wave RP (years)	Hs (m)	Tp (s)
50:1	3.1	8.8
10:1	4.2	10.2
1:1	5.3	11.5
1:10	6.2	12.5
1:50	7.3	13.5
1:200	8.2	14.3

Numerical and physical modelling of wave disturbance

ARTEMIS numerical modelling was initially undertaken to define, refine and optimise the harbour layout. Due to the significant wave energy present at Nigg Bay, providing a suitably sheltered environment inside the harbour was challenging and required substantial engineering design to block much of the wave energy, using the north and south breakwaters, before it could access the harbour. In addition, features were incorporated within the proposed harbour to dissipate the residual energy from waves that did enter the harbour. Wave absorbing features were included; revetment under the west quay and along the north quay to reduce the wave energy. Following the numerical modelling, 3D physical modelling was undertaken (see below) to confirm the wave conditions and refine the design. In the physical model, it was clear that the southern cliff area was particularly sensitive regarding wave reflection during numerical modelling and a lot of attention was placed into refinement of this feature in the physical modelling.

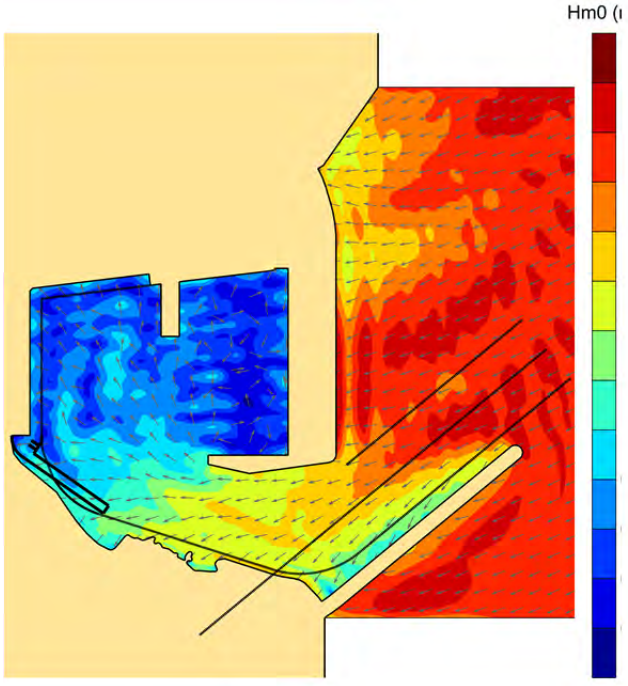

Figure 7: Initial ARTEMIS Wave modelling

Navigation simulation

Real time navigation simulation was undertaken (Figure 8 and 9) to prove the navigability of the proposed layout, refine and optimise the design and examine operational limits. This was particularly important to ensure safe navigation was possible, whilst keeping the entrance width to a minimum due to the severe wave conditions at the site. The navigation simulations showed that the design vessels could safely navigate the entrance, identified the operational limits, the tug requirements and the navigational aids. It also showed that the South East Pier could be extended to provide a longer berth and more sheltered conditions. The simulator was also used later to confirm an anticlockwise rotational change the SE pier could be adopted.

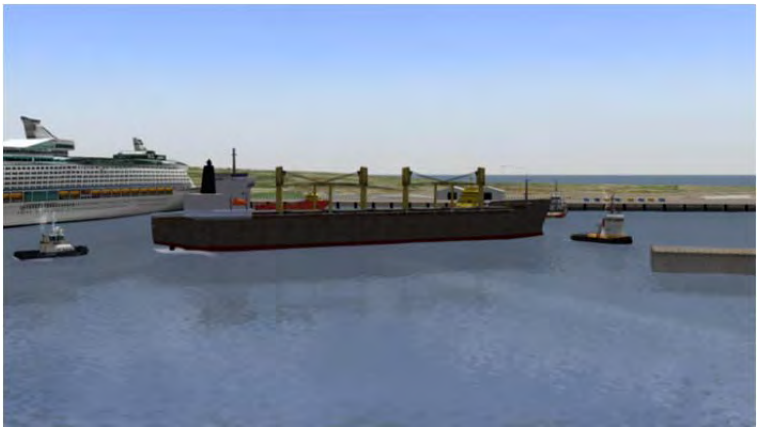

Figure 8: Real time navigation simulation

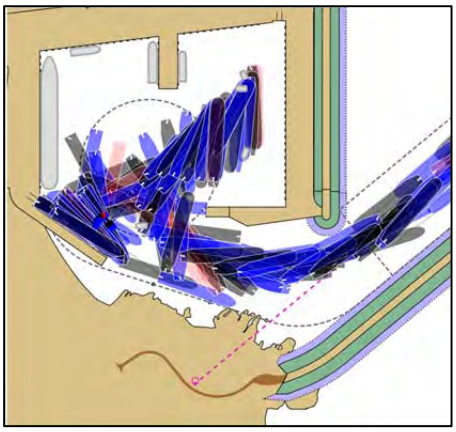

Figure 9: Real time navigation simulation track plots

Design development of the breakwater

The breakwater construction was the single biggest cost element in the project. Various options were considered including rubble mound with crown walls and caissons. The final Reference Design breakwater design solution adopted a lower crested breakwater concept to reduce cost. There was a need to minimise wave overtopping and protect the quays. The adopted design concept allowed significant wave overtopping of the breakwater where the residual overtopping water was collected in a drainage channel at the rear of the breakwater. It also provided the residual benefit of lower visual impact.

Physical modelling

2D Physical modelling of the northern breakwater

Initially 2D Physical modelling of the northern breakwater (Figure 10) was undertaken to prove project concept. The design was refined and the design of the drainage trench improved.

3D physical modelling of breakwater stability, waves and vessel motions

3D physical modelling to test breakwater stability, wave disturbance within the harbour and vessel motions with monitoring of mooring line and fender loads (Figure 11) was then undertaken. The physical modelling compared relatively well to the previous numerical modelling although the physical modelling showed that some improvements were necessary. The 3D physical modelling showed that the harbour, particularly underlining the make-up of the southern cliff shore, was sensitive to wave conditions. As the wave conditions outside the harbour were very severe and there was a need to provide calm conditions at the quay it was necessary to implement as much wave absorption as possible into the layout. Thus the profile in this key area was engineered to provide additional wave absorption by providing shallow slopes and revetments.

During and following the tender period the Contractor (Dragados) elected to undertake additional modelling to optimise and validate the design. In particular the SE pier was rotated anticlockwise to help reduce the wave conditions in the harbour and a crown wall was introduced on the north breakwater (see below) as the contractor considered this change would produce a cost saving, whilst delivering the required performance

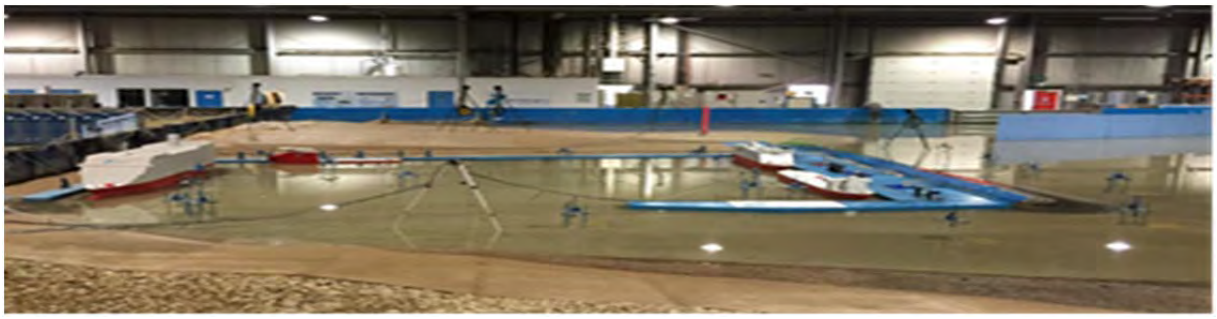

Figure 10: 2D Physical modelling of breakwater performance

Figure 11a (top)and b (right): 3D physical modelling of armour stability, waves and ship motion.

Environmental impact

The environmental drivers were considered right through the masterplanning process and these were integral with the decision to develop a new harbour and site selection. The independent Environmental Impact Assessment (EIA) was undertaken, led by Aberdeen Harbour Board, to identify the potential for the development to cause significant effects on a range of physical, biological and human receptors. The results are presented in the Environmental Statement (ES) which accompanies the consent applications. Where the EIA identified significant adverse effects on the environment (e.g. loss of green space (local amenity) and habitat (intertidal and subtidal sands and gravels), mitigation measures have been proposed to reduce the significance of the effects. These mitigation measures, which were brought together in an Outline Environmental Management Plan forming part of the ES, will be developed into a Detailed Environmental Management Plan by the appointed contractor. The key environmental impacts identified in the EIA were underwater and airborne noise during construction, visual impacts, construction traffic, and loss of habitat. The mitigation measures proposed (for example, the use of bubble curtains during blasting to reduce propagation of underwater noise) enabled the regulatory bodies to determine that the environmental impacts were acceptable and to grant consent for the development. Consents have been obtained with respect to the Harbours Act 1964, Town and Country Planning (Scotland) Act 1997 and Marine (Scotland) Act 2010.

Development of the engineering design

HR Wallingford and Arch Henderson were responsible for developing the design of the new harbour, with HR Wallingford taking responsibility for the design of the overall harbour layout and breakwaters and Arch Henderson leading the design of the quays, dredging, reclamation, paving, drainage and other quay ancillaries. Due to the nature of the project a wholly collaborative approach was required with significant overlap in roles.

The breakwater design

Following the physical modelling testing described above, the adopted Reference Design (Figure 5) incorporated the use of $8m^3$, $10m^3$, $12m^3$ and $16m^3$ concrete armour units with crests at +12.6mCD and toes founded at levels reaching -11mCD and founded deeper in places (Figure 12). The Contractor maintained a similar deign for the southern breakwater, but elected to reduce the overall width of the northern breakwater by incorporating a large crown wall (+16mCD) at the crest instead.

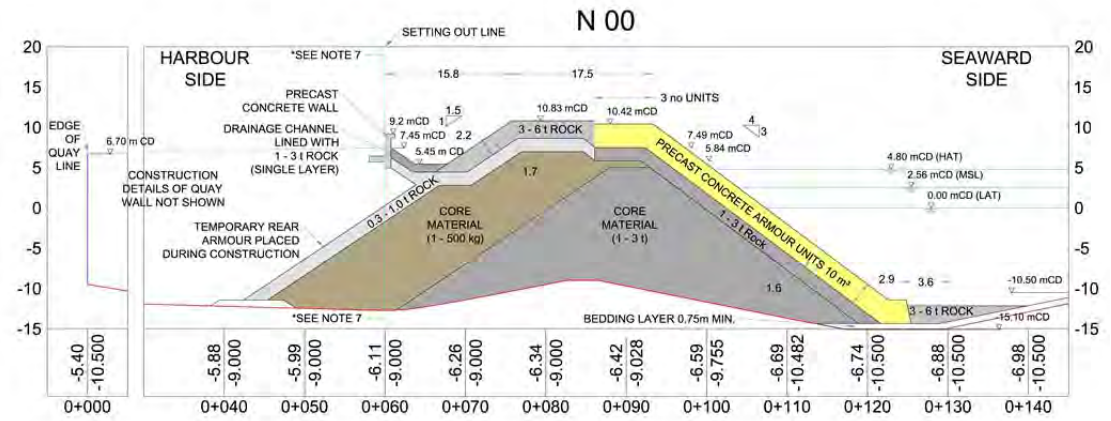

Figure 12 Breakwater (Reference) design

The quay wall design

Various forms of quay construction were developed incorporating the client's operational requirements and preferences whilst taking cognisance of the differing ground conditions and the performance criteria associated with limiting the wave disturbance within the harbour. To allow Aberdeen Harbour to best cater for modern Offshore Supply Vessels (OSV) solid un-fendered quays were adopted where possible. However, due to the requirements to mitigate wave agitation within the harbour, open piled quays with wave absorbing rock armoured revetments below were introduced. Thus solid quays were adopted at the northeast quay, east quay and southeast pier with open piled quay structures being adopted at the west and northwest quays. The channel side of the southeast pier, due to its increased exposure to wave impact, was further developed such that increased durability was achieved at this location. All quays were designed to accommodate a range of design vessels which are included within Table 2.

Table 2 Design vessels used in master planning and quay wall design

Range of Bulk Carriers	
Smallest Vessel	Largest Vessel
Deadweight Tonnage (DWT) 5,000 t	Displacement Laden 48,000 t
Overall Length 95 m	Overall Length 185 m
Range of Cruise Ships	
Smallest Vessel	Largest Vessel (West Quay Only)
Gross Tonnage (GT) 2,100 t	Displacement 54,500 t
Overall Length 70 m	Overall Length 290 m
Range of Offshore Supply / Construction Vessels	
Smallest Vessel	Largest Vessel
Gross Tonnage (GT) 1,500 t	Gross Tonnage (GT) 14,000 t
Overall Length 60 m	Overall Length 150 m

Dredging design

The ground conditions at the site vary considerably. The dredging will involve removing sand and gravels from the surface layers and glacial till at depth accompanied by drilling and blasting of hard rock prior to removal. The works will require, as a minimum, utilisation of both cutter suction dredgers (CSD) and backhoe dredgers (BHD). Dredging will be performed 24 hours a day, 7 days a week. The TSHD will most likely utilise its own hopper for storage and transportation of material, whereas the BHD will place dredged material into self-propelled dump barges. The material will then be transported for offshore disposal where not suitable for re-use within the works. A licence has been obtained from Marine Scotland to dispose of all dredged material at an existing sea disposal site; however, both from a commercial and environmental respect, an emphasis has been placed on the beneficial re-use of suitable material within the site. An extensive sediment sampling campaign has determined that the material is chemically suitable for disposal at sea or to be used in the reclamation. Where possible, physically suitable material (i.e. gravels and sands) will be used in the reclamation or inside the caissons. All dredged rock will be reused (and cannot be disposed offshore).

3D Visualisation

Several fly through 3D visualisations of the proposed works have been produced to enable the client and stakeholders to understand the nature and scope of the works being proposed (Figure 13).

Procurement strategy

Key to achieving best value in procuring the marine construction was configuring the design to suit the operational limitations of a tendering contractors' plant and equipment, the construction method, the environmental constraints and possible sources of available material. It was seen that significant optimisation could be achieved if the tendering contractors were empowered to refine the design to suit their preferred method of construction. Hence, the procurement strategy was configured to enable this goal and a Design & Build form of contract was adopted using the NEC3 Engineering and Construction Contract with a Reference Design forming the basis of the tender. Key parts of the tender package were:

- Definitive drawings setting out the fundamental project requirements
- Reference drawings setting out design development of the scheme
- Illustrative drawings setting out how the clients' requirements may be achieved
- Detailed reference design reports
- Design and performance requirements
- Construction and material requirements
- Environmental Impact Assessment
- Site information and ground investigation.

Figure 14: Visualisation of the project

Construction update

The works are well underway with the north breakwater expected to be complete in 2018 and the rest of the project in 2020.

Figure 14: North breakwater under construction

Conclusions and lessons learnt

The Aberdeen Harbour Expansion Project is to be one of Europe's largest greenfield port capital investments projects over the next few decades and has developed from realisation of a need for growth through to conception and start of construction in just over only 6 years. The masterplanning process helped seed, formulate and develop many of the masterplanning principles now being set out into the PIANC Working Group 185 Ports on greenfield sites – guidelines for site selection and masterplanning. This project, like all port projects, benefitted from early engagement with the consultees and the planning framework and careful technical, and iterative, evaluation of the technical issues. These principles have been integrated into the PIANC guide.

It is still too early a stage to set out lessons learnt with the benefit of hindsight, but it is clear that a combination of detailed technical assessments and early and clear communication to stakeholders of the vision was essential to enable development of the project and progress it through the planning

process. In terms of technical aspects, whilst it was always known that the severe wave climate would dominate the design, ensuring the target wave conditions were met through the design process of computation then physical modelling whilst at the same time optimising the design has been challenging.

Acknowledgements

The authors would like to thank wider project team for providing information in this paper including those at Aberdeen Harbour Board, HR Wallingford, Arch Henderson, Doig & Smith, Barton Wilmore, Fisher Associates, Harris Holden Ltd, Arup and Dragados and in particular, , Colin Parker, Ken Reilly, Katherine Harris, Ian Taylor, Stephen Cork, Jamie Holmes, Keith Powell, Mark McBride, Jonathan Woodhams, Nigel Bunn and Stephen Grey, Jim Clarke, Vince Crockett, Tim Pullen, Martina Melas, Ian Chandler, Ross Matthews, Tom Matthews, Richard Rankine and Grant Alexander.

References

PIANC 158 Masterplans for the development of existing ports, Report of MarCom Working Group 158.
PIANC 185 (Planed to be published 2018), Ports on greenfield sites – guidelines for site selection and masterplanning, Report of MarCom Working Group 185.
AHB (2012) Case for Growth, Aberdeen Harbour Board, Barton Wilmore, September 2012
AHB (2013) Directions for growth, Aberdeen Harbour Board, Barton Wilmore,
HR Wallingford (2012) Aberdeen harbour expansion, Technical feasibility report, DKR4708-RT001-R03-00.

SHIP MANOEUVRE PATTERNS TO PREVENT PROPELLER SCOURING EFFECTS

by

Castells, M.[1], Mujal-Colilles, A.[2], Llull, T.[2], Gironella, X.[2,] Martínez de Osés, F.X.[1], Martín, A.[1], Sánchez-Arcilla, A.[2]

ABSTRACT

Nowadays, vessels are bigger in size and are forced to operate in relatively smaller harbour areas. The propulsion systems of Ro-Ro and Ro-Pax are getting closer to the soil of the docks, due to their increase in ship and propulsion capacity and generating erosion and stability problems to harbour's structures. Moreover, Ro-Ro and Ro-Pax vessels, which serve regular services, have high docking frequencies. The most significant effect from propeller induced current can be found during manoeuvring situation in restricted waters due to the magnification caused by harbour structures. Therefore, the combination of docking frequencies along with the increase in ship dimensions can cause severe damages both to docking structures and basin manoeuvrability. The main problem is not only the damages to harbour structures but also the reduction in harbour basin depth caused by the sedimentation of the eroded sediment, with important consequences on the operability of the basin. This paper further analyses manoeuvre patterns to understand the effects of the resulting eroded sediment using Automatic Identification System (AIS) data. Results of scouring processes caused by manoeuvres of a particular Ro-Pax vessel without the help of a tugboat are described. The aim of this contribution is to analyse ship manoeuvre patterns and design new manoeuvres of a regular maritime service to minimize their effects on erosion and sedimentation and avoid adverse impacts resulting from ship manoeuvring. We can conclude that the used method, based on the study of a particular case starting from the reproduction of the manoeuvre, becomes adequate to establish the relation between the scouring forcing and its generator, which is the ship's manoeuvre near the docking.

1. INTRODUCTION

According to United Nations Conference on Trade and Development (UNCTAD) annual report (2017), over 80 per cent of global trade by volume and more than 70 per cent of its value is being carried on board ships and handled by seaports worldwide. The evolution of shipping industry over the last decades has led to growing structural and operational problems, in particular, for quays and harbours designed to host ships with lower drafts. Nowadays, port authorities are seeking ways to adopt existing infrastructures to meet the changing demand of the market. The increase in capacity, size, power and propulsion of vessels linked to high docking frequencies of regular services are the main causes of morphodynamic sea bed changes in harbour basins. This is producing two different effects: scouring effects near the structures affecting their stability and, on the other hand, sedimentation of the scoured material in other areas of the basin. This reduces the average depth and may affect vessel's

[1] Department of Engineering and Nautical Sciences, Universitat Politècnica de Catalunya, BarcelonaTech, Spain, mcastells@cen.upc.edu

[2] Marine Engineering Laboratory, Department of Civil and Environmental Engineering, Universitat Politècnica de Catalunya, BarcelonaTech, Spain

manoeuvring capabilities (turning and stopping abilities) due to the change of hydrodynamic forces. Moreover, new range of propulsion types (e.g. propellers, bow-thrusters, podded propulsors, azimuthing thrusters, waterjets) can also increase the scouring action. Several ports present problems related to the scouring and sediment deposition (e.g. BERG & MAGNUSSSON, 1987; CHAIT, 1987; FUERHRER, POHL & RÖMISH, 1987; HAMILL, JOHNSTON & STEWART, 1999; HAMILL, RYAN & JOHNSTON, 2009; MUJAL COLILLES, 2017; STHOKKING, JANSSEN & VERHAGEN, 2003). DOMINGO (2014) concluded that the highest erosion problem comes from regular vessels, excepting tugboat and pilot operations. Ro-Ro and Ro-Pax vessels, due to their characteristics and operational needs, are especially relevant when talking about scouring action. These vessels usually perform short voyages, so they berth and unberth frequently, at the same harbours and quays.

Most of the research published about the prediction of the maximum scouring action produced by ships propellers has been carried out in laboratories, using physical models with a single propeller at bollard pull condition (CHIEW & LIM, 1996; HAMILL, 1987; HONG, CHIEW & CHENG, 2013; MUJAL-COLILLES, 2018; SCHOKKING, JANSSEN & VERHAGEN, 2003; STEWART, 1992). MUJAL-COLILLES et al. (2017) use all the pre-existing formulations to compare their results with a real case and conclude that most of them are far from reality when applied to a particular real case. Therefore, further investigations using twin propellers, more similar to the real Ro-Ro or Ro-Pax stern configuration and different manoeuvers assessment is clearly needed in order to give harbour authorities tools to prevent this increasing problem.

A particular case of study was performed by LLULL et al. (2018) who used an Acoustic Doppler Velocimetry fixed close to the docking area combined with Automatic Identification System (AIS) data and found that it is possible to obtain the geographical position and orientations of the vessel when the current is maximum and, consequently more harmful. LLULL et al. (2018) concluded that, although the existing formulae to predict scouring actions yield results far from reality, they can still be used as a qualitative tool to know where the maximum scouring depth will occur. The propeller action can be studied as a consequence of the manoeuvring patterns, which, in turn, can be obtained through AIS data analysis (AARSATHER & MOAN, 2009; CASTELLS et al., 2017). Therefore, the study of the manoeuvre and its reproduction can be used to obtain the evolution of parameters directly related with the scouring action for every particular case depending on vessel type, ship location during the berthing and unberthing manoeuvres and met-ocean conditions. From the simulation of specific manoeuvres, main parameters of the propellers can be obtained (thrust power, speed propeller and pitch/diameter ratio propeller). Considering these parameters and the existing formulae in maritime engineering proposed by PIANC (2015) and R.O.M 2.1-11 (2012), the efflux velocities, the axial velocities along the propeller and the maximum bed velocities can be calculated.

The present contribution aims to reproduce a set of manoeuvres from AIS reports of a real Ro-Pax vessel, analyse ship manoeuvre patterns and design new manoeuvres of a regular maritime service. Results will help harbour authorities and ship's masters to reduce the impact on erosion and sedimentation resulting from ship manoeuvring.

2. METHODOLOGY

This study combines different set of data. First, the use of the AIS data from the vessel of the selected harbour area. AIS data is obtained to reproduce ship manoeuvres and identify manoeuvring patterns. Once the data is obtained, it is analysed with the bathymetric surveys to establish the relation between the manoeuvring patters and the scouring and sedimentation effects of the harbour basin. Considering the formulae from literature, new alternative manoeuvres are proposed with the aid of Transas NTPro 5000-v-5.35 simulator to reduce the scouring action.

2.1 Automatic Identification System

The AIS is an automatic tracking system for identification and location of vessels by exchanging data via VHF communication to other nearby vessels (IMO, 2003). The use of AIS data permits to understand the effect of changes to the fairway and vessel manoeuvring. The Automatic Identification System is a valuable source for ship manoeuvring information and analysis. The analysis of this data can be employed to generate statistics of patterns during the docking and undocking manoeuvring and estimate scouring induced by vessel propeller in harbour basins. Scarce work has been done to apply AIS to analysis on the scale of manoeuvres in a constrained area. The trace of a vessel position obtained from

AIS can be transformed into a digital image. The AIS data frames are stored in an Excel database for easy management and extraction. Excel file is converted to KML. KML is a file format used to display geographic data in applications such as Google Earth or Google Maps.

For research purposes, The Port Authority provided AIS data reports for the period of June 2016 and January of 2017 for the selected area. The AIS information received contained mainly, time, latitude, longitude, speed over ground (SOG), and course over ground (COG) and Rate of Turn. The presented data will be, therefore, anonymized as much as possible.

2.2 Bathymetric surveys

Periodic bathymetric surveys were carried out with a multibeam system SeaBeam1185, Elac Nautik, Germany in the selected area. The blanking distance from the floating line was 0.65m and data was recorded at 180 kHz with a ship speed ranging from 3 to 5 knots. The data acquisition average error was around 0.1m due to an upper layer of mud within the harbour basin of an estimated thickness of 0.5m. Geological studies performed by the harbour authorities yield sediment characteristics below the mud layer of d_{50} =0.3mm and d_{90} = 1.0 mm, normal sizes for a harbour located in a deltaic zone. Figure 1 plots bathymetric data of a real harbour basin with a mean depth of -12m above sea level (asl) where the evolution of berthing depth and profiles of the harbour basin from June 2015 to March 2017 (last bathymetric survey carried out by the harbour authority).

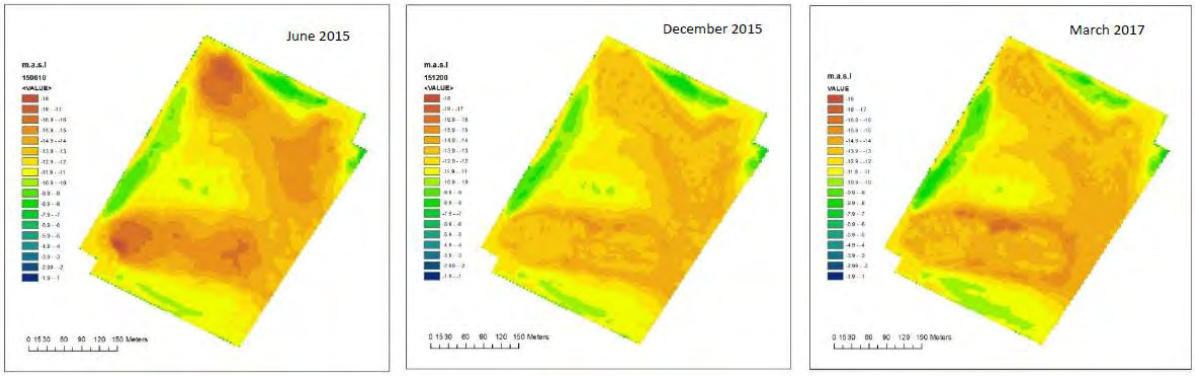

Figure 1: Evolution of the bathymetry along the harbour

As can be seen in Figure 1, the profiles in the North and West quays (see Figure 2) show holes of up to 5 m compared to the mean depth of -12m asl. Parallel to the scouring action, a sedimentation is of the order of 2 m in the west, north and south quays and in the middle of the harbour. In June 2015, harbour authority decided to dredge the areas with a lower depth in the harbour basin. As can be observed, a new hole is generating in the SW area of the harbour.

2.3 Manoeuvre simulator

The use of a manoeuvre simulator is useful to both reproduce the manoeuvre and test alternative manoeuvrings in a simulator with controlled conditions. The aid of real-time full mission bridge simulator Transas NTPro 5000-v-5.35 identifies the main parameters of a manoeuvre with positioning data obtained from AIS of the same area and can identify which manoeuvring behaviour is acceptable to reduce the effect of the toe scouring induced by vessel propeller.

3. CASE STUDY

The effects of ship manoeuvring are analysed in a specific area. A detailed study of the docking and undocking manoeuvres is conducted considering one Ro-Pax vessel which serve regular service at the same dock. Vessels particulars are very common among the Ro-Pax vessels, regarding both dimensions and propulsion. The dimensions of the case study vessel are: 225 m of length, 30 m of beam

and 55000 GT. The vessel has two controllable pitch propellers and two bow-thrusters. The engine power of four main engines is 55440kW and the power of each bow-thruster is 1850 kW. The draft of the vessel is 7 m. To know the effect of propellers in the harbour basin it is important to know the AIS position with respect the propellers position (150 m forward).

The location (case study area selected) of the Ro-Pax vessel with a daily frequency is at the SW corner (West Quay) (see Figure 2). The effect of other vessels docking and undocking in the same area is not considered. With the aim of being conservative, this research is focused only with the manoeuvrings of this Ro-Pax vessel.

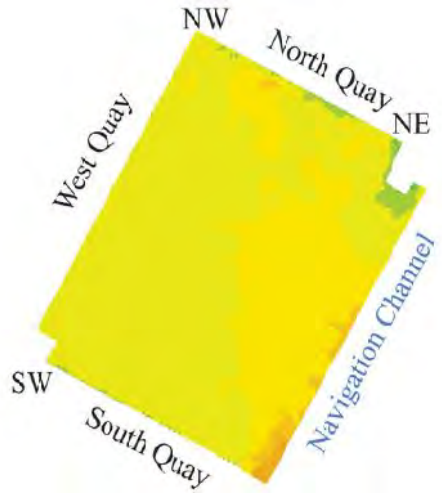

Figure 2: Case study docking area

The total AIS manoeuvres reports are 20 during June 2016, July 2016 and January 2017. Figure 3 shows an example of the AIS information: speed, rate-of-turn and position with an accuracy of about 30 seconds.

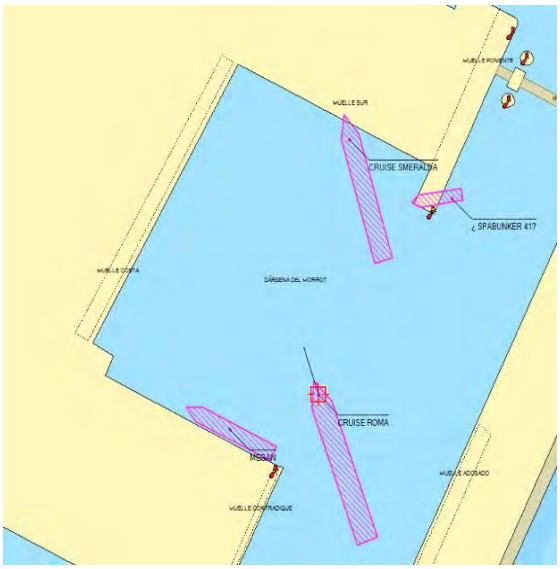

Figure 3: Case study area with AIS position information (1st July 2016)

In order to analyse manoeuvres, expected weather conditions must be known. In the present research two different weather conditions are considered: calm weather conditions (June and July 2016) and bad weather conditions (January 2017) (see Table 1).

Manoeuvre/Data	Wind speed (knots)	Wind direction	Significant wave height, Hs (m)
Docking. 08/06/16	6.5	205	0.3
Undocking. 08/06/16	2.1	280	0.19
Docking. 17/06/16	7.7	222	0.51
Undocking. 17/06/16	5.4	248	0.49
Docking. 19/06/16	4	142	0.37
Undocking. 20/06/16	4.3	231	0.24
Docking. 01/07/16	6	211	0.43
Undocking. 01/07/16	4.1	296	0.36
Docking. 06/07/16	6	222	0.44
Undocking. 06/07/16	2.6	249	0.26
Docking. 12/01/17	5.3	269	0.78
Undocking. 13/01/17	21.1	303	0.75
Docking. 14/01/17	12.1	304	0.37
Undocking. 15/01/17	14.3	299	0.34
Docking. 17/01/17	1.1	273	1.62
Undocking. 18/01/17	6	23	1.42
Docking. 20/01/17	23	47	2.7
Undocking. 20/01/16	21.8	54	2.58
Docking. 23/01/17	12.3	32	2.42
Undocking. 23/01/16	10.5	307	1.59

Table 1: Outside port weather information of selected manoeuvrings obtained from Puertos del Estado website (http://puertos.es)

As can be seen in Table 1, from coastal buoy information, in calm weather, the maximum wind speed is 7.7 knots with a significant wave height of 0.51 (17th June) and in bad weather, the maximum wind speed is 23 knots with a significant wave height of 2.7 m (20th January).

3.1 Manoeuvres description

The ship manoeuvring process is represented as a sequence of basic manoeuvres, being the basic subdivision of manoeuvre patterns between constant course and course changing manoeuvres. The ship manoeuvres pattern in calm and heavy weather has been identified. From AIS data, track manoeuvres can be displayed in the docking area.

Figure 4 shows tracked arrival manoeuvres during calm and bad weather conditions. The starting point of the entrance manoeuvre pattern is the track line in the middle of the navigational channel with a vessel's course of 20º and speed of 6.5 knots. At the harbour entrance of the docking area, the speed is reduced to 5 knots and the vessel alter the course to her port side (320º). When the vessel is in the middle of the docking area, the speed is slow and vessel is turning about its own centre of rotation until 40º. At this point, the vessel starts to go astern and the bow thrusters are used to position the bow with a degree precision.

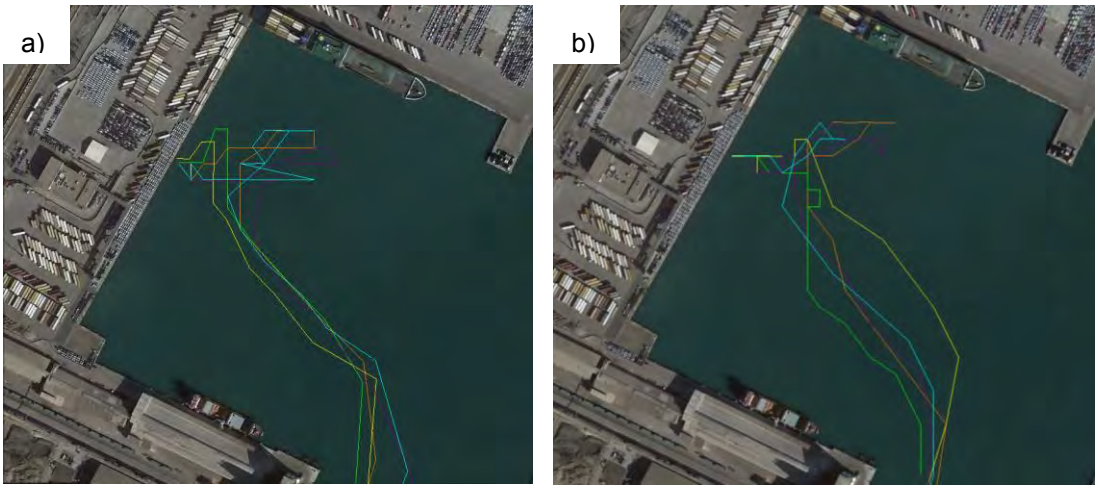

Figure 4: West quay docking manoeuvres scenario (a) Calm weather (8th June (blue), 17th June 2016 (orange), 19th June 2016 (purple), 1st July 2016 (yellow) and 6th July 2016 (green)). (b) Heavy weather (12th January 2017 (blue), 14th January 2017 (orange), 17th January 2017 (purple), 20th January 2017 (yellow) and 23th January 2017 (green)

All entrance manoeuvres follow the same pattern with some variations. In calm weather, the turning circle around its own centre of rotation in the middle of the docking area is smaller during approaching manoeuvres of 1st and 6th of July and the manoeuvring period takes less time than the others (16 minutes and 14 minutes respectively). Only one manoeuvre (20th January 2017) required tug assistance due to bad weather.

Figures 5 and 6 show the Course over Ground and Speed over Ground of ten arrival manoeuvring considered in calm weather and bad weather. Only the manoeuvre of 1st of July varies compared with the rest of manoeuvres.

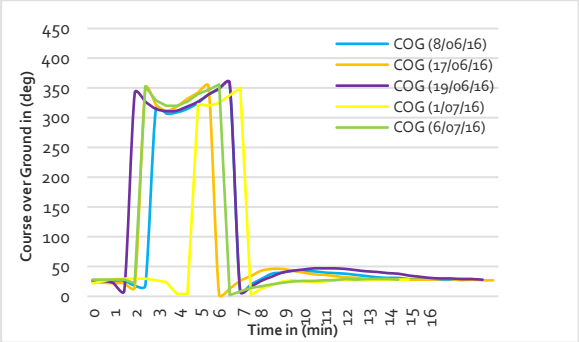

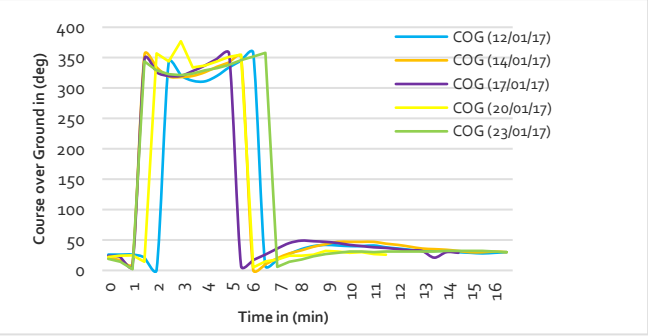

Figure 5: Course over Ground (COG) for entrance manoeuvrings considered in calm (left) and bad (right) weather

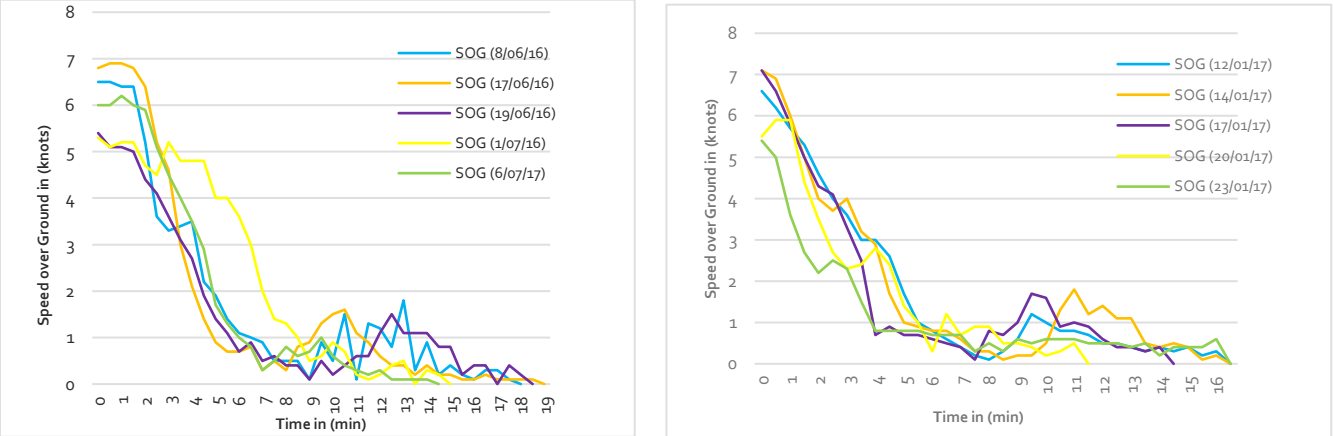

Figure 6: Speed over Ground (SOG) for entrance manoeuvrings considered in calm (left) and bad (right) weather

The departure manoeuvres pattern in calm and bad weather is easier and faster than the arrival manoeuvres (see Figure 7). When departing from the west quay, vessel has to move away from the quay while initially remaining in parallel with the quay. Such a movement is produced by the bow thrusters and the main propellers. When the vessel has moved away 30 m, the vessel starts to turn to starboard and speed increases to 2 knots. At the end of the turn, the new and steady course is 200º and the speed of the vessel will reach 6 knots at the navigational channel.

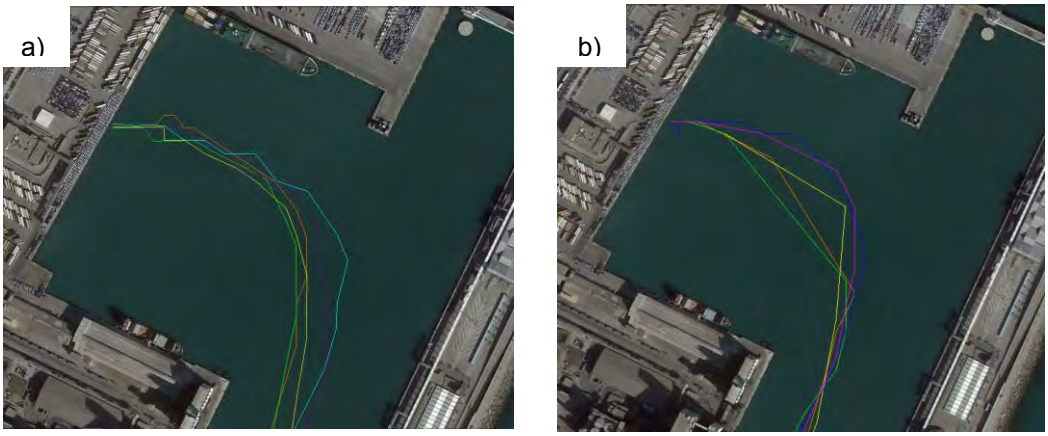

Figure 7: West quay undocking manoeuvres scenario (a) Calm weather (08/06/16-blue, 17/06/16-orange, 20/06/16-purple, 01/07/16-yellow and 06/07/16-green) (b) Bad weather (13/01/17-blue, 15/01/1- orange, 18/01/17-purple, 20/01/17-yellow and 23/01/17-green)

Figures 8 and 9 show the Course over Ground and Speed over Ground of ten departure manoeuvring considered in calm weather and bad weather. Only the manoeuvre of 1st of July varies compared with the rest of manoeuvres.

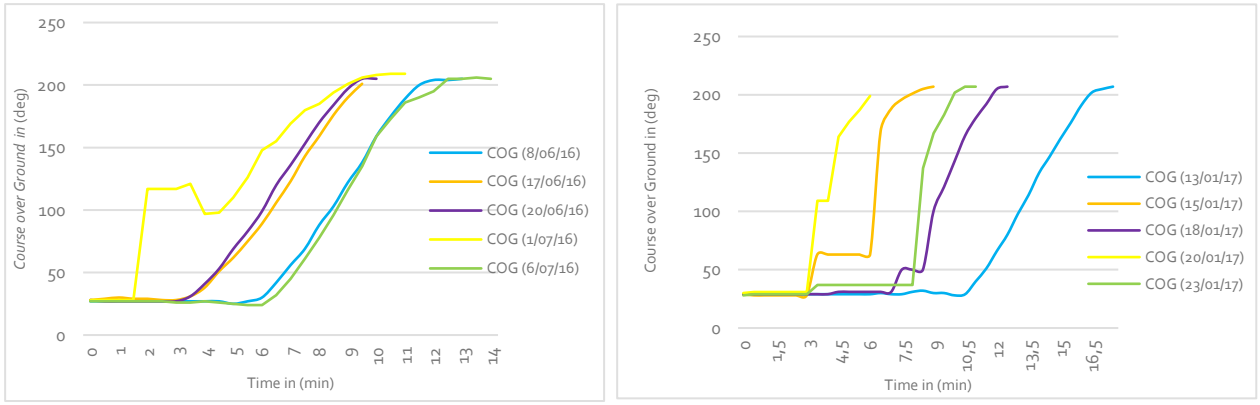

Figure 8: Course over Ground (COG) for departure manoeuvrings considered in calm (left) and bad (right) weather

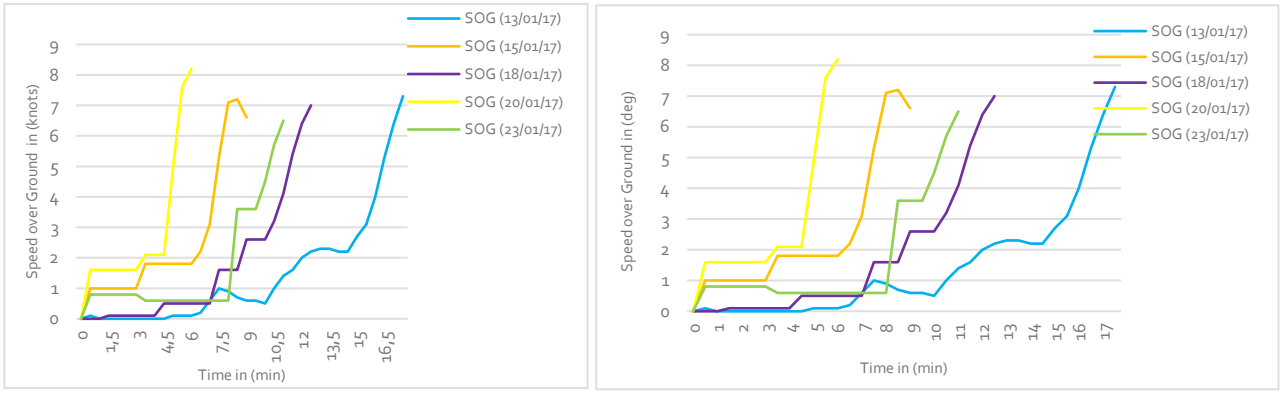

Figure 9: Speed over Ground (SOG) for departure manoeuvrings considered in calm (left) and bad (right) weather

4. RESULTS

The analysis of ship manoeuvres is important to understand the effect of changes of course and speed to prevent propeller scouring effects and to assess harbour authorities. This section will identify the main parameters (approach/departure course angle (COG), number of turning manoeuvres, approach/departure ship's speed (SOG) and period of time) of a manoeuvre using the positioning data obtained from AIS of the same ship and in the same area.

4.1 Entrance manoeuvring

Figure 10 shows mean parameters of docking manoeuvring (COG and SOG) in both conditions, calm and bad weather. The approach to harbour is modelled as a section with constant course followed by a Rate of Turn manoeuvre to change the course for the entry into the harbour.

The total average entrance manoeuvring period takes about 16.2 minutes. After 2 minutes of manoeuvre, the speed is reduced drastically and takes 7 minutes to reach 1 knot. The time of the turning manoeuvre is around 5 or 6 minutes and the period of time to reach the quay is about 8 minutes.

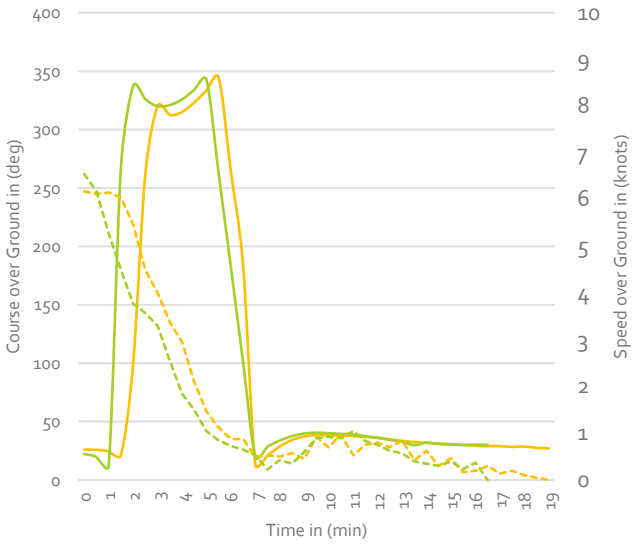

Figure 10: Mean Course over Ground (COG – continuous line) and Speed over Ground (SOG – dashed line) for ten arrival manoeuvrings in calm weather (yellow) and bad weather (green)

Bad weather manoeuvres are shorter (around 1.5 minutes) compared with calm weather ones due to the orientation of the quay and the direction of the wind considered. The manoeuvre with tug takes 9.5 minutes. Even though the speed is very similar in both cases, the course of the vessel in bad weather conditions turns before to the port side.

4.2 Departure manoeuvring

Figure 11 shows mean parameters of undocking manoeuvring (COG and SOG) in both conditions, calm and bad weather. The departure to harbour is modelled as a parallel movement to the quay followed by a Rate of Turn manoeuver with final straight course on the navigational channel.

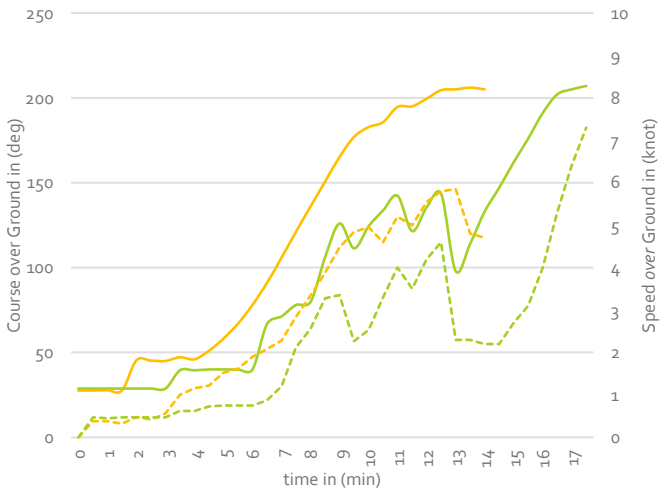

Figure 11: Course over Ground (COG - line) and Speed over Ground (SOG – dashed line) for ten departure manoeuvrings in calm weather (yellow) and bad weather (green)

In calm weather, manoeuvres are more stable compared with bad weather due to the influence of wind at low speed. The departure manoeuvre is shorter than the arrival manoeuvre and is around 8 minutes. The period of time to move away from the quay is around 3.5 minutes and then starts with the evolution

circle. The total average entrance manoeuvring period in calm weather takes about 7.8 minutes and in bad weather is 9.6 minutes. The manoeuvre with tug is shorter and takes 5.5 minutes.

The results from the AIS data processing showed the vessel entering the harbour with two turn approaches and the vessel departing only with one turn.

4.3 Influence of manoeuvring to scouring processes

To identify the influence of the manoeuvring described in the previous section with the scouring processes, it is necessary establish the relation between scouring forcing (observed in the bathymetric surveys) and its generator, which is the ship's manoeuvre pattern near the docking. Figures 12 and 13 show bathymetric surveys in the west quay and in the north quay of the harbour during the period between years 2015 and 2017.

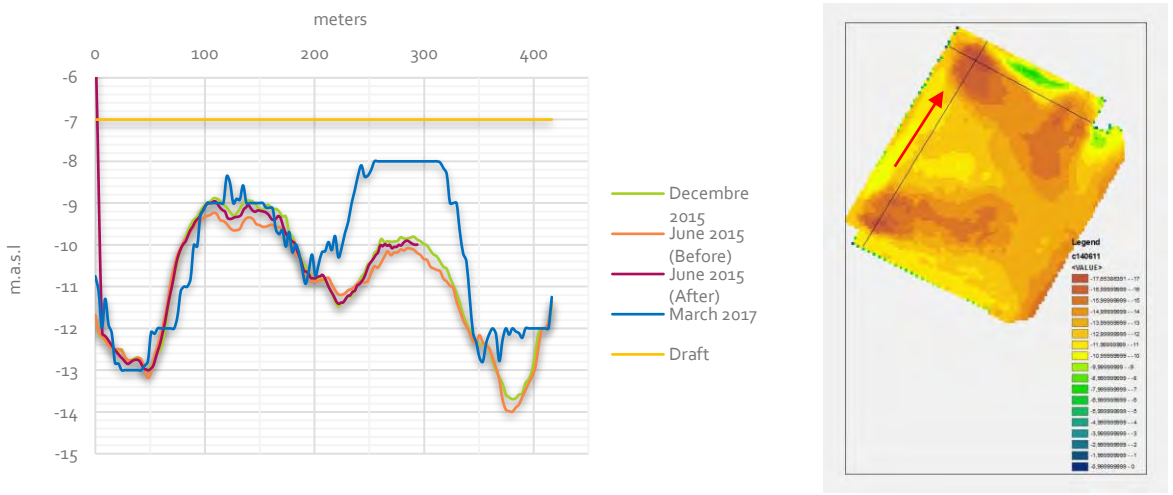

Figure 12: Evolution of the bathymetry along a section parallel to the west quay, from south to north

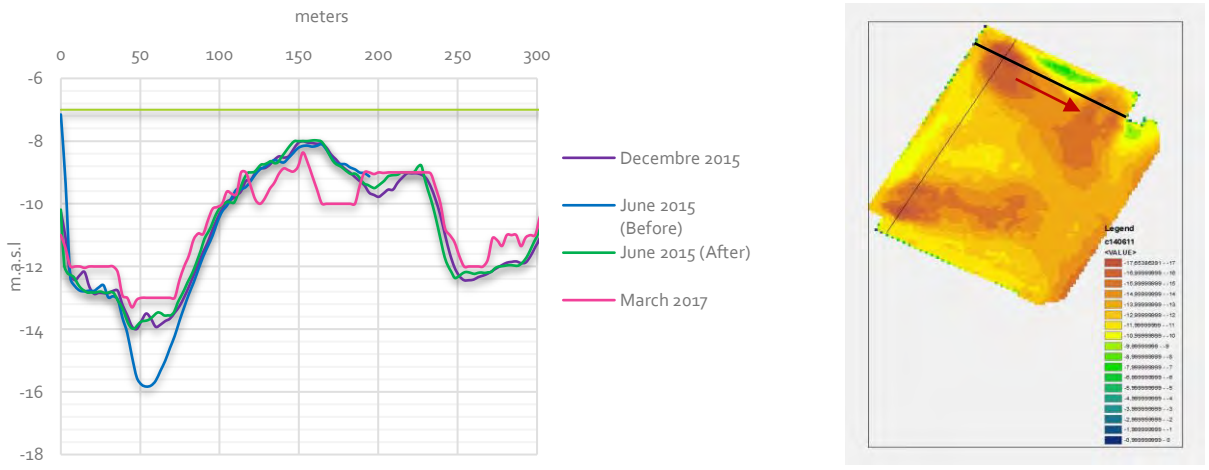

Figure 13: Evolution of the bathymetry along a section parallel to the north quay, from west to east

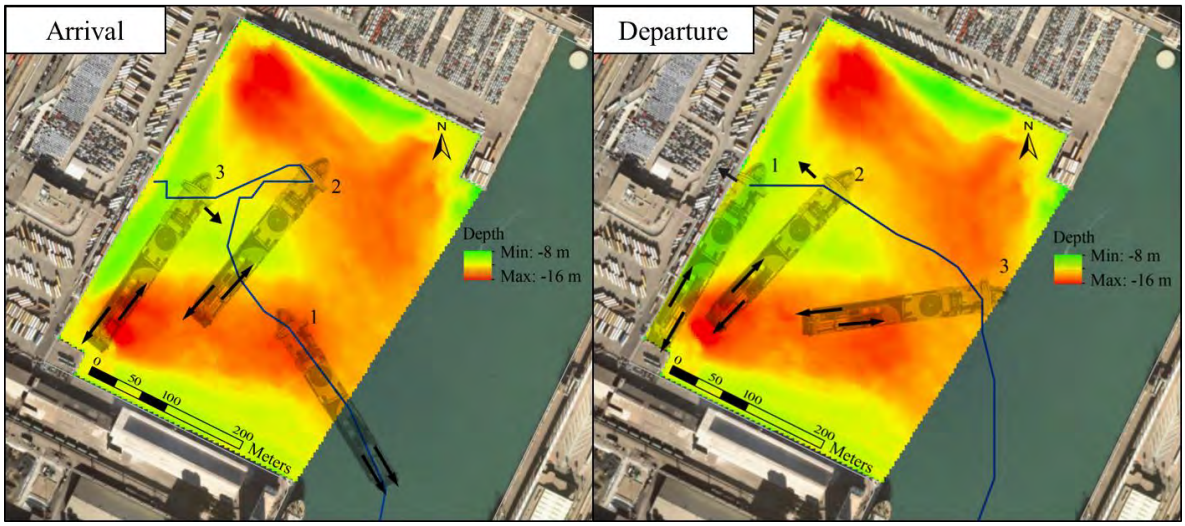

Figure 14: Representation of the arrival and departure manoeuvres

Figure 14 shows the representation of the manoeuvring patterns described in the above section. There is a clear influence of the manoeuvring with the scouring process when the vessel is berthing (Figure 14 left). When the vessel is turning around its own centre of rotation, the position of port propeller is ahead and the starboard propeller is astern (the first generating a wash towards the aft and the second, generating it inversely). It can be seen that the propellers track follows the scouring area in the SW harbour area. In addition, the bow thrusters are generating wash outwards. The reproduction of the unberthing manoeuvre (Figures 14 right) shows that the vessel moves parallel to the quay with the starboard propeller ahead (generating wash towards the aft) and the port propeller astern (generating a wash towards the bow) and the bow thrusters are generating wash inwards. The maximum scouring effect is when the main propellers are located near the SW corner, with holes of up to 5 m compared to the mean depth of -12 asl. Additionally, the sedimentation area is located below the bow thruster.in the west quay.

4.4 Influence of shallow waters

Shallow waters can seriously affect navigation and manoeuvring in these areas. Manoeuvring properties are particularly important in shallow water. Due to squat caused by increased velocities under the vessel, a combination of a mean bodily sinkage plus a trimming effect can produce unstable motion and decrease of course keeping ability. According to QUADVELIEG & COEVORDEN (2003) the vessel should have enough course stability and tuning ability to fulfil the IMO requirement (IMO 1993) with respect the overshoot angles and turning circle dimensions in shallow water. The criteria should be fulfilled in water depths above sea level (asl) larger than 1.3 times the draught (T) of the vessel ($Depth_{asl}/T>1/3$). If the draft of the vessel considered is 7 m, considering the IMO criteria, the water depth should be higher than 9m. From Figure 1, there are some critical areas closer to the West, North and South quays and in the middle of manoeuvring area, where the water depth-draught ratio could be lower than 1.3 (green areas).

In the section parallel to the west quay (Figure 12), there is a clear area situated between 80 and 110m from the SW corner where the $Depth_{asl}/T$ ratio is lower than 1.3 in several bathymetries analysed. Moreover, in March 2017 another shallow water can be found between 230 and 330 m from the SW corner. It could be the effect of wash generated by bow-thrusters.

In the section parallel to the north quay (Figure 13), there is a clear area situated in the middle of the quay, between 90 and 160 m from the NW corner where the $Depth_{asl}/T$ ratio is lower than 1.3 in bathymetries analysed.

A critical green area can be observed in the middle of the harbour area, see Figure 1. In this area, the vessel is manoeuvring at slow ahead or slow astern speed and shallow water can produce unstable motions and can disturb the course turning ability of the vessel.

4.5 Alternative manoeuvres

In order to reduce the effect of the toe scouring induced by vessel propeller, alternative docking and undocking manoeuvres with the same ship and in the same navigation area are assessed. Due to the vessel characteristics and the manoeuvring harbour area, there are some limitations to define new alternative manoeuvres. Thanks to the relative large clearance of tugs, the berthing and unberthing manoeuvres for larger vessels will often use tug assisted (HAWKSWOOD et al., 2014). Authors have reproduced alternative manoeuvres with the aid of Transas NTPro 5000-v-5.35 simulator. Two alternative berthing manoeuvres and two alternative unberthing manoeuvres are proposed.

The alternative berthing manoeuvres are: one manoeuvre with the assistance received from two tugs (without ship propulsion system) and one with the assistance of one tug. Two tugs assistance manoeuvre is shown in Figure 15 (left). When the vessel is in the central area of the harbour, the first tug is pushing at the starboard bow and the aft tug is on the port side. This will enable the vessel to complete a swing with a bow to port (anticlockwise). When the vessel is just off the berth, the tugs are pushing the ship onto the berth. Sometimes, the use of two tugs is impractical, in such cases, other alternative manoeuvre is proposed with the assistance of one tug at the aft part with the help of bow-thruster, see Figure 15 (right).

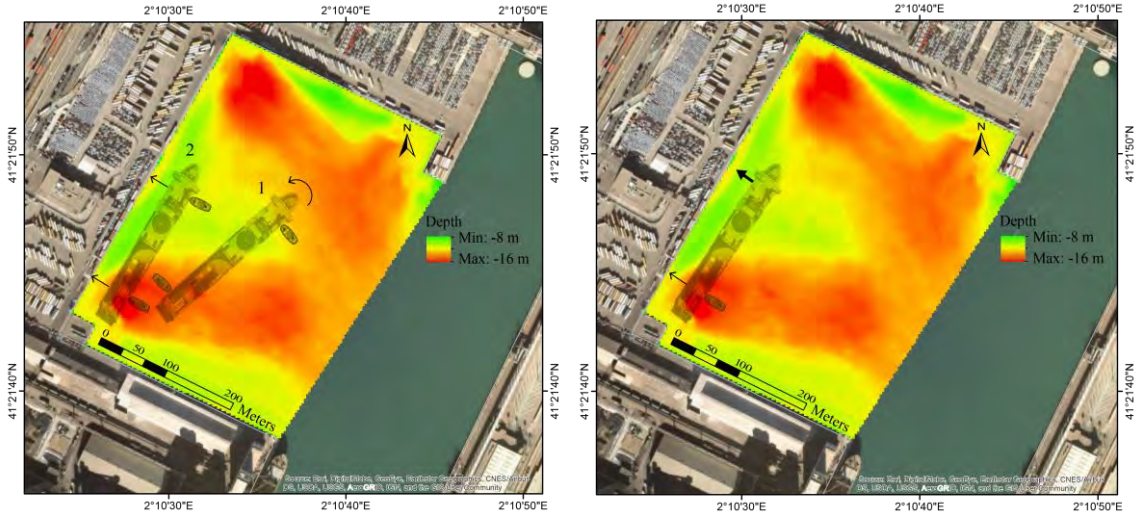

Figure 15: Representation of alternative berthing manoeuvres with tugs

The main objective of alternative undocking manoeuvres is seek to move the vessel from the quay walls so that the vessel does not get sucked onto the quay with the ahead movement. Two means of manoeuvring the vessel while moving her away from the quay are proposed: producing the transverse force by tugboats external to the vessel or using one tug and the bow thruster. Two tugs assistance manoeuvre is shown in Figure 16 (left). When the vessel is unberthing with the assistance of two tugs, these are used to pull the ship off the berth. The vessel will be pulled nearly parallel to the berth to avoid either end from making contact with the berth. Once the vessel is safely clear form the berth, swing movement will start. Alternatively, with the help of bow-thruster, one tug aft can be sufficient for unberthing, see Figure 16 (right).

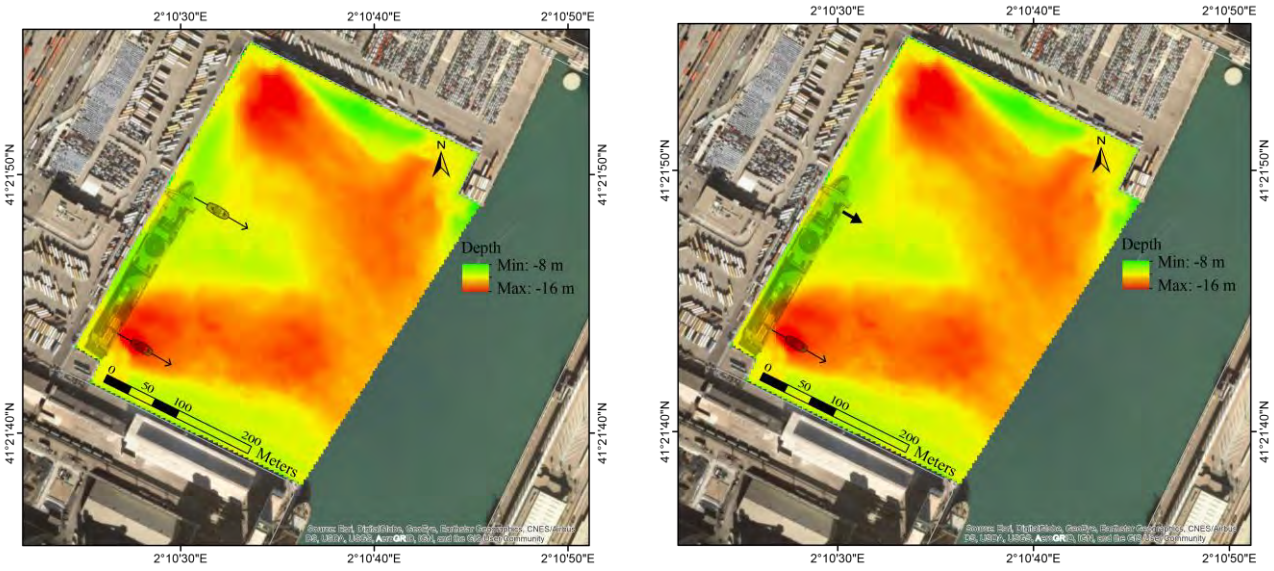

Figure 16: Representation of alternative unberthing manoeuvres with tugs

The manoeuvre without tugs, controlling the speed of the main engine and using mooring lines is difficult. Speeds analysed in the above section are adequate, because the vessel requires a minimum powering. Lower speeds should affect the manoeuvrability abilities, because the rudder is not effective.

5. CONCLUSIONS

The use of AIS is an easily available source of information about the manoeuvring vessel behaviour and a useful tool to prevent propeller scouring effects. Results obtained in this paper show that AIS data can be used to obtain the identification of statistical manoeuvring parameters and patterns of docking and undocking manoeuvres in both calm and bad weather. Manoeuvres analysed show similar patterns in docking and undocking manoeuvres with some variations when bad weather conditions are considered.

The combination of AIS data together with bathymetric surveys of the same harbour basin shows an evident relation between the manoeuvers and the scouring depth patterns. When the vessel is unberthing, the influence of the wall is clear, causing higher damage to the structure for both the localization of the deeper point in the scouring hole and its magnitude. Moreover, the sediment eroded can settle at different locations reducing the total depth in the harbour basin and produce operational problems in the particular basin. Some critical zones have been detected.

In order to reduce the effect of the toe scouring induced by vessel propeller, alternative docking and undocking manoeuvres with the same ship and in the same navigation area are assessed and proposed. From the point of view of navigation, the use of mooring lines controlling the speed of the main engine and bow thrusters is quite difficult and the manoeuver using tug assistance is the best option. When two tugs are used, scouring action is the lowest because tugs have a relatively low drafts and the vessel propeller and bow thrusters are usually not used. However, due to the high cost, a single tug can be used reducing the scouring action as well.

The use of the bridge simulator allows to reproduce any manoeuvre of any ship in any harbour basin with any met-ocean conditions, so the results obtained can help to port authorities to make decisions to improve port management and minimise the scouring problems.

ACKNOWLEDGMENT

This research has been supported by MINECO (Ministerio de Economía y Competitividad) and FEDER (Unión Europea- FondoEuropeo de Desarrollo Regional "Una Manera de hacer Europa") from Spanish Government through project BIA2012-38676-C03-01 and TRA2015-70473-R.

REFERENCES

Aarsæther K.G. & Moan T. (2009). Computer vision and ship traffic analysis: Inferring maneuver patters from the automatic identification system. Marine Navigation and Safety of Sea Transport, vol. 4, no. 3, pp. 303-308.

Berg, H., & Magnusson, N. (1987). Propeller erosion and protection methods used in ferry terminals in the port of Stockholm. Bulletin of the Permanent International Association of Navigation Congress (PIANC), 58, 112–120.

Castells, M, Martínez de Osés, X., Martín, A., Mujal, A. & Gironella, X. (2017). Tools for evaluation quay toe scouring induced by vessel propellers in harbour basins during the docking and undocking manoeuvring. Marine Navigation and Safety of Sea Transport. 61-66, ISBN 9781138001053

Chait, S. (1987). Undermining of quay walls at South African ports due to the use of bow thrusters and other propeller units. Bulletin of the Permanent International Association of Navigation Congress (PIANC), 58, 107–110.

Chiew, Y., & Lim, S. (1996). Local scour by a deeply submerged horizontal circular jet. Journal of Hydraulic Engineering, 122(9), 529–532.

Domingo, J. (2014). Avaluació de l'erosió en els fons portuaris generada per la propulsió dels bucs [Harbour basin erosion due to ships propulsion system] (Masters thesis).UPC-Barcelona Tech, Barcelona

Fuehrer, M., Pohl, H., & Römish, K. (1987). Propeller jet erosion and stability criteria for bottom protections of various constructions. Bulletin of the Permanent International Association of Navigation Congress (PIANC), 58, 45–56.

Hamill, G. A. (1987). Characteristics of the screw wash of a manoeuvring ship and the resulting bed scour (PhD thesis). Queen's University of Belfast, Belfast.

Hamill, G. A., Johnston, H. T., & Stewart, D. (1999). Propeller wash scour near quay walls. Journal of Waterway, Port, Coastal and Ocean Engineering, 125(4), 170–175.

Hamill, G. A., Ryan, D., & Johnston, H. T. (2009). Effect of rudder angle on propeller wash velocities at a seabed. Proceedings of the ICE – Maritime Engineering, 162(1), 27–38.

Hawkswood M. G., Laveger, F.H., Hawkswood, G.M. (2014). Berth scour protection for modern vessels. PIANC World Congress San Francisco, USA.

Hong, J.-H., Chiew, Y. M., & Cheng, N.-S. (2013). Scour caused by a propeller jet. Journal of Hydraulic Engineering, 139(9), 1003–1012.

International Maritime Organization (IMO). (2003). Guidelines for the installation of a shipborne automatic identification (AIS)

Llull, T., Mujal-Colilles, A., Castells M., Gironella, X., Martínez de Osés, X., Martín, A. & Sanchez-Arcilla, A. (2018). Hybrid tool to prevent ship propeller erosion. Proceedings of the ASME 2018, 37th International Conference on Ocean, Offshore & Arctic Engineering, OMAE2018, Spain.

Mujal-Colilles, A., Xavier G., Sanchez-Arcilla A., Puig Polo C., and Garcia-Leon, M. (2017). “Erosion Caused by Propeller Jets in a Low Energy Harbour Basin.” Journal of Hydraulic Research 55 (1). Taylor & Francis: 121–28. doi:10.1080/00221686.2016.1252801.

Mujal-Colilles, A., Llull, T., Castells, M., Gironella, X. Martínez de Osés, X., Sánchez-Arcilla, A. (2018). Ship Manoeuvring effects on propeller induced erosion. Proceedings of the 7th International Conference on the Application of Physical Modelling in Coastal and Port Engineering and Science (Coastlab18), Spain.

PIANC. 2015. Guidelines for Protecting Berthing Structures from Scour Caused by Ships. Report N° 180. The World Association for Waterborne Transportation Infrastructure.

Puertos del Estado. (2012). "Obras de Atraque y Amarre: Criterios generales y Factores del Proyecto" (R.O.M. 2.0-11).

Quadvlieg, F.H.H.A. & van Coevorden, P. (2003). Manoeuvring criteria: more than IMO A.751 requirements alone. MARSIM International conference on marine simulation and ship manoeuvrability.

Schokking, L. A., Janssen, P. C., & Verhagen, H. J. (2003). Bowthruster-induced damage. Bulletin of the Permanent International Association of Navigation Congress (PIANC), 114, 53–63.

Schokking, L. A., Janssen, P. C., & Verhagen, H. J. (2003). Bowthruster-induced damage. Bulletin of the Permanent International Association of Navigation Congress (PIANC), 114, 53–63.

Stewart, D. P. J. (1992). Characteristics of a ship’s screw wash and the influence of quay wall proximity (PhD thesis). Queen’s University of Belfast, Belfast.

United Nations Conference on Trade and Development (UNCTAD) Annual Report (2017).

DEVELOPMENT AND EXPANSION OF PSA's PANAMA HUB PORT AT THE FORMER RODMAN NAVAL BASE

By

Manfred Zinserling, PE, SE, MASCE[1]; David Taylor, MICE CEng[2]; and Jyotirmoy Sircar, PE[3]

ABSTRACT

The opening of the new, third lane of the Panama Canal, and the projected increase in shipping traffic in the region, presented PSA with the opportunity to expand their single berth facility at the former Rodman Naval Base. Two new, deep-draft berths (-18.5 meters mean low water spring [MLWS]) were built to accommodate the largest future container vessels. However, the planning did not stop there. A new high-capacity/high-volume container yard for transshipment was developed using rail-mounted gantry (RMG) cranes. There are 12 container blocks (4,200-TEU [twenty-foot unit] ground slots) fitted with 20 semi-automatic RMG cranes. The RMG cranes can later be converted to fully automatic, self-stacking cranes (ASCs), as cargo throughput increases. There are also six container blocks (990-TEU ground slots) fitted with rubber-tyred gantry (RTG) cranes to service refrigerated containers (reefer) and import/export container cargo. Other improvements included advanced information technology (IT) services and multiple redundancies to allow the facility to operate seamlessly and continuously.

The benefits of the former Rodman Naval Base are that it is 'across the bridge' from Panama City and hence does not present the same restrictions and traffic conflicts experienced at the other port facilities and also provides easy access to the hinterlands in the rapidly growing western provinces of Panama.

The terminal was developed rapidly on a site with difficult and diverse geology. This terminal sets new standards for modern container terminals in Panama and the region.

1.0 PROJECT DEVELOPMENT OBJECTIVES AND TIME LINE

A decision was taken in 2013 to expand the current terminal to accommodate New Panamax (or Neopanamax) vessels. When completed, the PSA Rodman Terminal will be one of the most modern terminals in Latin America and will include semi-automatic RMGs and an extensive data collection system (fiber optics and Wi-Fi) to provide information for the terminal operating system.

2.0 DESCRIPTION OF THE TERMINAL

2.1 Overview

PSA Panama International Terminal (PPIT) is located at the Pacific entrance to the Panama Canal on the west bank (the opposite side to Panama City). Figure 1 shows the location. The terminal operates under a concession with the Panamanian government, via the Maritime Authority (AMP). The initial concession was granted in 2008.

Planning, design, and construction of the terminal took place over a three-year period with the first cargo handled in 2011. The design was based on a single Panamax berth of 330-meter length, three quay cranes, and an operating area of 14 hectares, including container yard, gate, maintenance workshop, and administrative and customs buildings.

Figure 2 shows the operating Phase 1 terminal, with a large container vessel on the berth and well-utilized container storage yard. The administration building, gate complex, and equipment workshop are in the right-hand corner and clearance has started for the Phase 2 construction area.

[1] Senior Project Manager, BergerABAM, manfred.zinserling@abam.com
[2] Head of Civil Engineering Latin America, PSA, david.taylor@globalpsa.com
[3] Project Engineer, BergerABAM, jyotirmoy.sircar@abam.com

Figure 1: Location of PSA Panama

Figure 2: Completed PPIT Phase 1 Terminal

2.2 Phase 1 Construction

Construction of the quay deck was carried out partially in the dry, with the rock slope at the rear of the quay wall being constructed in a bunded area. Figure 3 shows the initial excavation of the slope at the rear of the quay deck, together with a later photo showing the ongoing quay deck construction, including piling operations, placing of the grillage of concrete beams to tie the piles together. Figure 4 shows further construction photos during the piling and quay deck construction.

Figure 3: Phase 1 Quay Deck Construction

Figure 4: Phase 1 Quay Deck Construction

3.0 EXPANSION OF THE TERMINAL

3.1 Shipping Line and Container Vessel Dynamics

In the period from the planning and negotiation of the concession in the mid-2000s, there have been many significant changes in the shipping world. There has been a dramatic increase in the size of container vessels (see Figure 5), the opening of the expanded Panama Canal, and major consolidation of container shipping lines and alliances (see Figure 6).

The dimensions of the locks in the original Panama Canal restricted vessel dimensions such that the maximum capacity of container vessels was approximately 3,500 TEUs (twenty-foot equivalent units—the standard measure of container volumes and capacities, with 1 TEU being a single ISO 20-foot-long container).

The enlargement of the canal, which was completed in 2016, now enables vessels of up to 13,500 TEUs to transit the canal, greatly changing the economics of container vessel operations. In combination with this, there has been a huge increase in ship sizes, and the quantity of these large ships, as shipping lines have sought to reduce the shipping costs per container. The injection of capital needed for these new build campaigns and the need for revenues and capacity has resulted in dramatic consolidation of individual shipping lines and shipping line alliances to the point where there are now only three global alliances. Figure 6 illustrates this rapid consolidation starting from the mid-1990s to the present day.

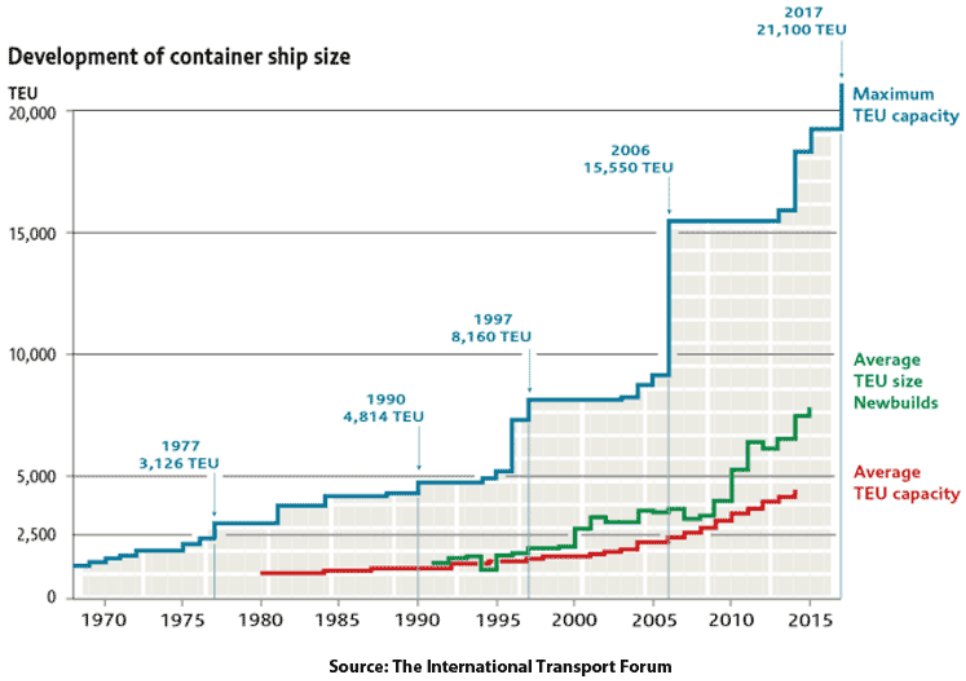

Figure 5: Evolution of Container Vessels Sizes

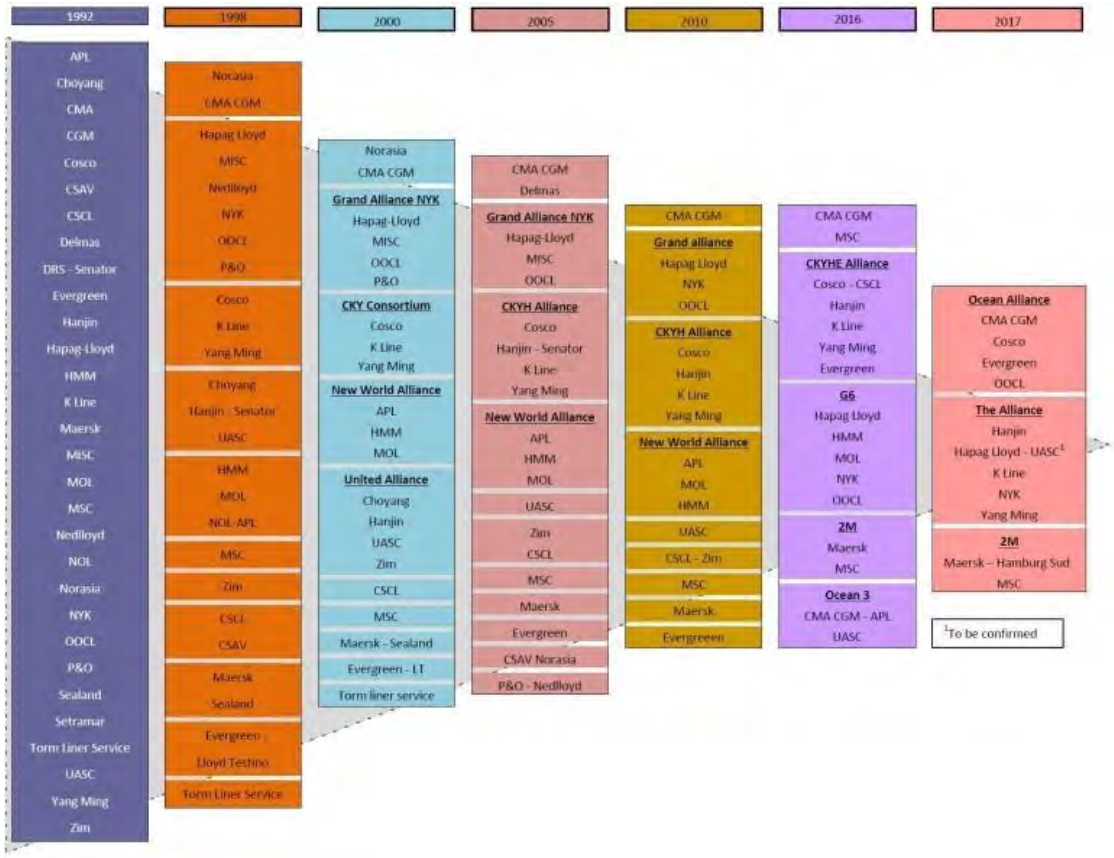

Figure 6: Consolidation of Container Shipping Lines and Alliances

Source – Ricardo J. Sanchez (UN-ECLAC)

3.2 Expanding PSA Panama

Taking account of the dynamics of the shipping industry, it was clear that Phase 1 was not sufficient for future needs and thus planning for an expansion of the terminal was commenced. The main criteria adopted were 800 meters of additional berthing for large vessels, plus sufficient yard to support an annual throughput of 2 million TEUs, based on knowledge of the market and estimated demand in the region.

Options were identified for expansion and discussions held with adjacent concession holders/land owners, with an option to lease a parcel of land between the Canal and the Phase 1 yard from ACP being the preferred option.

The next stage in the process was to carry out vessel navigation studies to determine the optimum alignment of the new berth with respect to the Panama Canal. This was carried out locally using the SIDMAR navigation simulation centre in Panama and with Panama Canal pilots.

Once the berth alignment was established, then it was possible to design the terminal layout to suit the operational goals, including vessel sizes, terminal capacity, etc.; thus enabling preliminary engineering design and site investigation works to be carried out.

4.0 CONTAINER YARD PROJECT SCOPE

The new terminal will have three berths; two Neopanamax and one Panamax, and 5,190-TEU grounded slots and 1,350 refrigerated container plugs. See Figure 7 below.

Figure 7. Reconfigured Rodman Terminal (Phase 2)

Construction of the new Phase 2 terminal includes reconfiguration of the existing Phase 1 container yard and utilities; however, the existing Phase 1 terminal continued to operate during the reconfiguration process.

The design and construction of the civil works for the Phase 2 expansion project was divided into three major packages; the new quays and basin dredging, the new container yard, and electrical and IT services. Yard and quay equipment was procured separately by PSA. The new quays, basin dredging, electrical, and IT services were procured through FIDIC Yellow Book contracts; the new container yard was procured through the FIDIC Red Book process. The equipment order was placed in 2015 in conjunction with the award of the contracts for the quay and dredging, but well in advance of container yard civil works construction. This necessitated a fast-track process to complete the civil works in time. This goal was generally achieved; however, the overlap in equipment deliveries, commissioning, and operator training did produce some conflicts with the civil works.

5.0 DESIGN CHALLENGES – PAVEMENT SECTION

The project was developed on the site of the former Rodman Naval Base (Rodman). The northerly portion of the Rodman site includes the PSA concession. The southerly portion is a separate concession to receive refined petroleum products and provide berthing for the Panamanian naval forces, visiting warships, and product tankers.

The terminal is a greenfield project; however, the site was previously used for dredge disposal and military support activities. The site also hosts navigation towers for the Panama Canal, which have been adjusted to suit the new land use of the site.

The site geology provided challenges to the design team. The underlying soils consisted of imported fill (the “American fill”) and dredge spoils of various depths overlying Pacific Muck (organic materials) and finally the La Boca rock formation. The rock formation was very irregular; in some places, it was located very close to the existing surface of the site, particularly in the future berth area. Over the course of the design program, multiple geotechnical investigations were undertaken, including a geophysical survey in the quay/berth area. The goal of the investigation programs was to refine the ground improvement program and develop the most cost-effective pavement section that could be rapidly built.

Design long-term settlements, after completion of the ground improvement program, were estimated to be on the order of 300 millimeters (mm); and differential settlements were estimated to be 20 mm within the container stacking areas. The containers are stored on discrete reinforced concrete bases in order to mitigate the impact of differential settlements on operations, and the other travel surfaces are portland cement concrete (PCC) pavements. Relatively shallow excavations and a soil replacement program with crushed rock were employed throughout the new container yard area. The Phase 1 container yard used similar methods and no further measures were required in this area,

In consideration of the fast-track schedule and construction cost, the designer investigated various strategies to minimize the pavement sections across the site. The general pavement section consisted of geotextile, crushed rock subbase, and base topped with concrete. The final solution was to implement three different pavement sections according to the intended use. This resulted in deeper subbase levels in the container stacking areas and reduced subbase levels elsewhere. General details are shown in Figure 8 below.

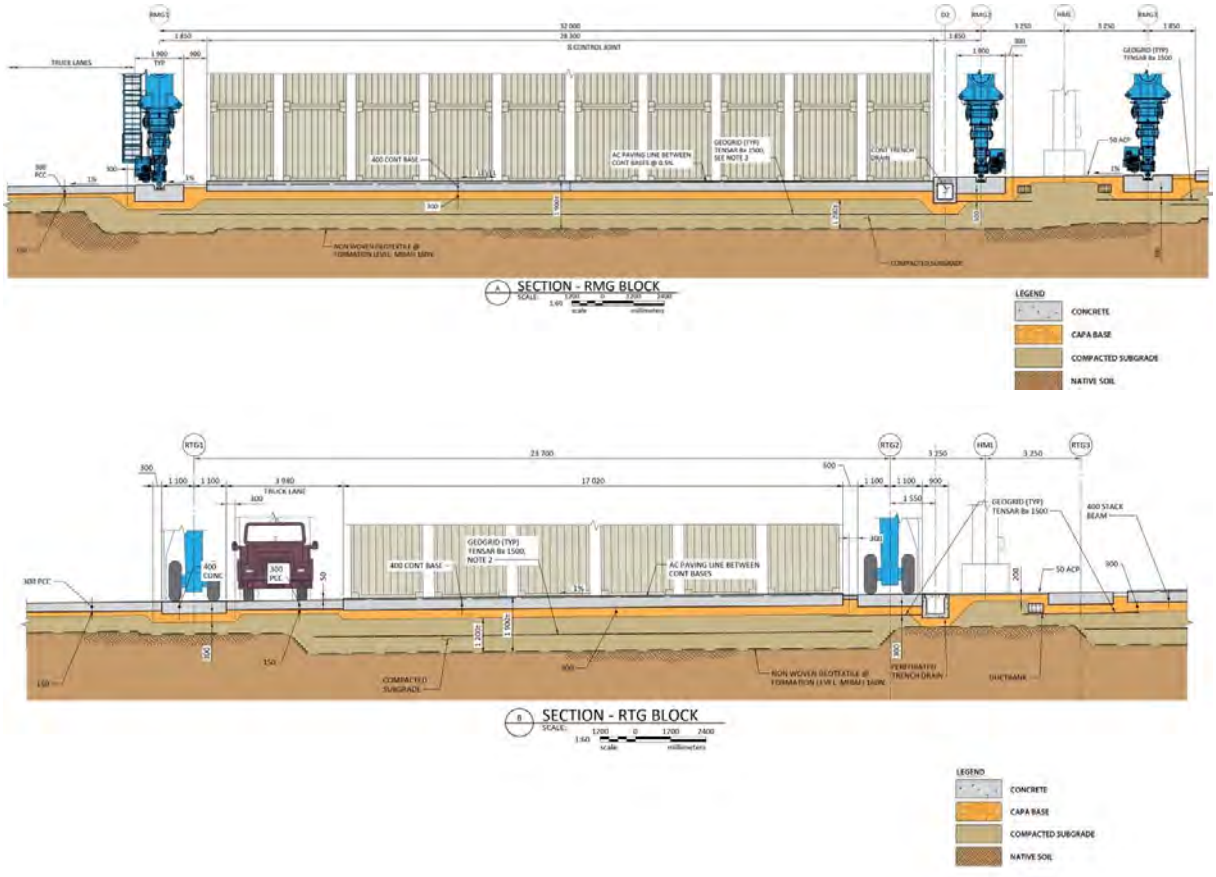

Figure 8. General Pavement Section

6.0 DESIGN CHALLENGES – ELECTRICAL SYSTEMS

The reconfiguration of the terminal had to take into account the existing electrical power distribution system, switchgear, Phase 1 quay cranes, Phase 1 refrigerated container facilities, and the terminal administration buildings. The eventual goal was to develop a new main power center and use the Phase 1 substation to support only legacy equipment from Phase 1. The Phase 1 substation is rated at 5 megavolt amperes (MVA). Feeder line voltage is 12 kilovolts (kV) in from the power company and 6.6 kV out to the terminal. The new Phase 2 main substation (power center) is rated at 16 MVA. Feeder line voltage is 12 kV in from the power company and 12 kV out to the terminal. The local power company, GNF, is constructing a new district substation rated at 16 MVA, with future expansion to 32 MVA. The feeder line voltage will be 44 kV in and 12 kV out to the PSA Phase 2 substation. Emergency power on the new terminal is provided by two 2.5-MVA diesel gensets.

The Phase 1 substation provided power for the entire site/terminal until the new power center was completed. Because the Phase 2 main substation could not be built early in the project, a temporary power feed was required from the Phase 1 substation to the new quay substations powering the new quay cranes, RMG cranes, and refrigerated containers. This temporary system required new duct banks and manholes, which were not envisaged in the original container yard civil works contract.

The new terminal also includes a latest state-of-the-art terminal operating system with extensive fiber-optic cabling and Wi-Fi transmission facilities. The terminal has multiple redundant systems for electrical power, IT services, CCTV, and sensors. The systems design and equipment specifications were not fully developed until after the award of the new container yard civil works contract. This fact required extensive design engineering and close coordination with the contractor throughout the construction period to relocate duct banks and add new duct banks and electrical manholes.

7.0 CONSTRUCTION CHALLENGES

The overall Phase 2 development plan included an early works program to clear the site, install wick drains, and surcharge the future Phase 2 container yard area. Surcharge was removed prior to start of the Phase 2 civil works, and the sand drain blanket material was stockpiled on site for future use.

Construction commenced with rough grading and excavation of near surface weak soils and Pacific Muck to the design contours for the subbase formation level, and then was followed by installation of the stormwater drainage system, which was generally located below the subbase formation level. Following the rough grading operations, the prepared site was proof rolled and tested. Soft spots and areas that did not achieve a minimum CBR=2 (California Bearing Ratio) were over excavated for an additional depth of 600 mm and backfilled with crushed rock; or if the area was very small, crushed rock was spread and rolled into the soft spot. After inspection and acceptance, geotextile fabric was spread over the area and backfilling with crushed rock commenced. The crushed rock was placed in layers and compacted to achieve a relative density of at least 95 percent. The above-described operations were straightforward; however, the site was handed over to the container yard contractor in smaller segments as the quay contractor finished his work that led to inefficiencies and eventually resulted in double shifting of some of the works. Water utilities, electrical duct banks, RMG and RTG runways, container bases, and PCC pavement construction followed.

Resident engineering services were provided in two phases; the first phase was for the new quay construction and basin dredging, the second phase was for the new container yard and electrical and IT services. The start of new quay and basin construction preceded the container yard construction by about 15 months; however, there were still conflicts due to site, schedule, and logistic issues. Therefore, the resident engineer for the second phase had the responsibility to coordinate the new container yard construction with all of the remaining contracts, which included completion of the new quay, equipment deliveries, electrical and IT services, and staged handover of the completed Phase 2 construction.

The coordination process was challenging; requiring continuous oversight of different major contracts, contractors, and subcontractors. A coordination meeting was held every morning between all contractors working on the site; the day's work area priorities were then established for each contractor. The process worked smoothly except for delays in completion of tasks within the first phase works and the electrical contract; and finally the delivery of new quay and yard equipment to the site. The new container yard civil works contractor was impacted several times during the construction process, as he had to give way to the quay contractor, and then the equipment deliveries and commissioning. At numerous occasions, civil works for the container yard were performed out of sequence until the quay contractor completed his work and demobilized. In order to meet schedule, the designer had to develop numerous temporary solutions for the civil works and electrical connections, as the civil facilities housing the

electrical components could not be built. This posed both design and safety issues that were handled admirably by the entire project team.

8.0 CLOSING STATEMENT

The extremely short construction schedule for the new container yard, including reconfiguration of the existing Phase 1 terminal, compounded by coordination with other contracts and major design changes during construction, presented some interesting challenges to the design and construction team. The close collaboration between the PSA engineering teams and the designer, together with the cooperative spirit of the civil works contractor, resulted in the successful delivery of a high-quality and very complex terminal project.

Figure 9 shows the current progress of the Phase 2 development being readied for the first trial vessels in anticipation of the start of full commercial operations.

Figure 9. Overview of the Phase 2 Development Nearing Completion

ANALYSIS OF PIANC GUIDELINE AND ROM STANDARD IN DESIGN OF APPROACH CHANNEL AND HARBOR BASIN

by

Cui Jianghao[1] *and Dou Degong*[2]

ABSTRACT

For the harbor waterway and coastal engineering the approach channel and harbor basin play an important role. It will be dangerous for the sailing vessel to make the channel too shallow and the basin too narrow, in turn it will be to thriftless if the channel is over deep and the basin is over wide, which means the project cost will increase. A moderate size of channel and basin is recommended. In order to find out this moderate size, several primary standards in the world have respective calculation methods. PIANC is short for Permanent International Association of Navigation Congresses, and it has a well-rounded system and criterion for the design work of harbor engineering. ROM is the standard system in Spain, and it becomes more and more prevalent in waterborne transportation industry, especially in South America and Caribbean nations. PIANC's design guidelines and ROM standard have different methods in calculating the depth and width of approach channel and harbor basin in port project, which are caused by diversity of designing factors. In order to analyze the respective results and summarize the characteristics of these two standards, this article analyzes the factors and methods in the designing of approach channel and harbor basin and takes a project as an example. An appropriate suggestion of channel and harbor basin in design phase is proposed after comparing the results in using these two standards and real-time manoeuvring simulation study of the vessel, which can be safer and economical for the project and supply technical support in designing works.

1. INTRODUCTION

This paper analyzes the PIANC guideline and ROM standard of 3 dimensions in harbor engineering, which are width of channel, depth of channel and width of harbor basin. The calculation method of these 2 standards is not same. Combining with a actual project and Real-Time simulator analysis, this paper gives a result of these 3 dimensions in PIANC guideline and ROM standard.

2. Width of approach channel

2.1 PIANC guideline

In the PIANC guideline, the width of straight channel can be calculated in the following modern method, which should provide adequate navigational safety in the concept design phase. In detail design phase, local conditions may require an optimization with respect to cost, operational conditions and environmental aspects.

For the overall width bottom width of an access channel with straight sections, i.e. **Figure 1: Channel and fairway definition** is given by:

$$W=W_{BM}+\sum W_i+W_{BR}+W_{BG} \quad \text{(One-way channel)} \tag{1}$$

$$W=2W_{BM}+2\sum W_i+W_{BR}+W_{BG}+\sum W_P \quad \text{(Two-way channel)} \tag{2}$$

Where:

W_{BM} =width of basic manoeuvring lane as a multiple of the design ship's beam B, given in Table 1.

$\sum W_i$=additional widths to allow for the effects of wind, current etc, given in Table 2.

[1, 2] CCCC First Harbor Consultants Co., LTD, China

W_{BR}+W_{BG}=bank clearance on the 'red' and 'green' sides of the channel, given in Table 3.
ΣW_P=passing distance, comprising the sum of a separation distance between both manoeuvring lanes W_M (shown in **Figure 2: Elements of channel width**) and an additional distance for traffic density, given in table 4.

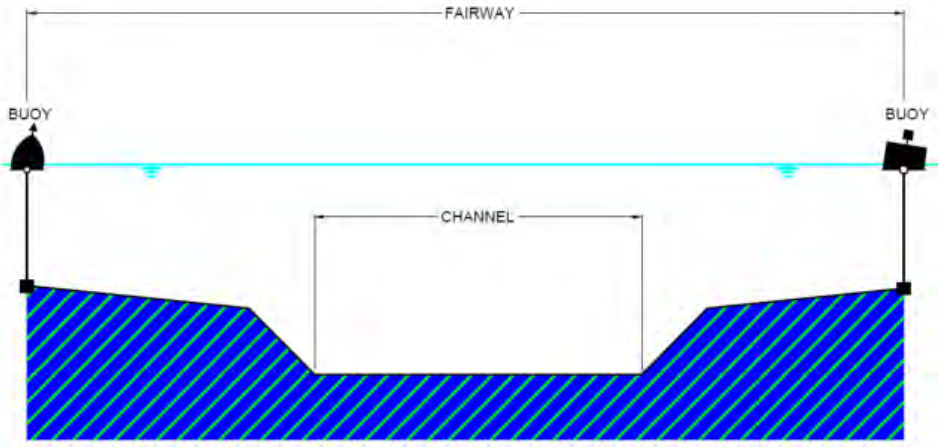

Figure 1: Channel and fairway definition (PIANC)

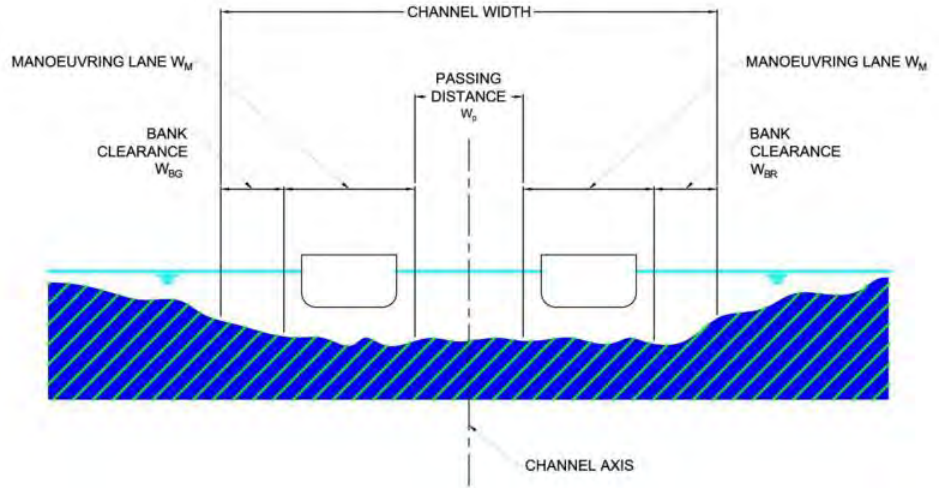

Figure 2: Elements of channel width

Ship Manoeuvrability	Good	Moderate	Poor
Basic manoeuvring Lane, W_{BM}	1.3*B*	1.5*B*	1.8*B*

Table 1: Basic manoeuvring lane W_{BM}

Width W_i	**Vessel speed**	**Outer channel (open water)**	**Inner channel (protected water)**
(a) Vessel speed V_S (kts, with respect)			
$V_S \geq 12$kts	Fast	0.1 *B*	
$8\text{kts} \leq V_S < 12\text{kts}$	Mod	0	
$5\text{kts} \leq V_S < 8\text{kts}$	Slow	0	
(b) Prevailing cross wind V_{CW} (kts) -mild	Fast	0.1 *B*	

V_{CW}<15kts	Mod Slow	0.2 *B* 0.3 *B*	
-moderate 15kts≤V_S<33kts	Fast Mod Slow	0.3 *B* 0.4 *B* 0.6 *B*	
-strong 33kts≤V_S<48kts	Fast Mod Slow	0.5 *B* 0.7 *B* 1.1 *B*	
(c) Prevailing cross current V_{CC} (kts) -negligible V_{CC}<0.2kts	All	0.0	0.0
-low 0.2kts≤V_{CC}<0.5kts	Fast Mod Slow	0.2 *B* 0.25 *B* 0.3 *B*	0.1 *B* 0.2 *B* 0.3 *B*
-moderate 0.5kts≤V_{CC}<1.5kts	Fast Mod Slow	0.5 *B* 0.7 *B* 1.0 *B*	0.4 *B* 0.6 *B* 0.8 *B*
-strong 1.5kts≤V_{CC}<2.0kts	Fast Mod Slow	1.0 *B* 1.2 *B* 1.6 *B*	- - -
(d) Prevailing longitudinal current V_{lC} (kts) -low V_{CW}<1.5kts	All	0.0	
-moderate 1.5kts≤V_{lC}<3kts	Fast Mod Slow	0.0 0.1 *B* 0.2 *B*	
-strong V_{lC}≥3kts	Fast Mod Slow	0.1 *B* 0.2 *B* 0.4 *B*	
(e) Beam and stern quartering wave height H_S (m) H_S≤1m 1m<H_S<3m H_S≥3m	All All All	0.0 0-0.5 *B* 0-1.0 *B*	0.0 - -
(f) Aids to Navigation Excellent Good moderate		0.0 0.2 *B* 0.4 *B*	
(g) Bottom surface Depth $h \geq 1.5T$		0.0	

Depth $h < 1.5T$ -Smooth and soft -Rough and hard		0.1 *B* 0.2 *B*			
(h) Depth of waterway		$h \geqslant 1.5T$ $1.5T > h \geqslant 1.25T$ $h < 1.25T$	0.0 *B* 0.1 *B* *0.2 B*	$h \geqslant 1.5T$ $1.5T > h \geqslant 1.25T$ $h < 1.25T$	0.0 *B* 0.1 *B* *0.2 B*

Table 2: Additional widths W_i for straight channel sections

Width for bank clearance	Vessel speed	Outer channel (open water)	Inner channel (protected water)
Gentle underwater channel slope (1:10 ro less steep)	Fast Moderate Slow	0.2 *B* 0.1 *B* 0.0	0.2 *B* 0.1 *B* 0.0
Sloping channel edges and shoals	Fast Moderate Slow	0.7 *B* 0.5 *B* 0.3 *B*	0.7 *B* 0.5 *B* 0.3 *B*
Steep and hard embankments structures	Fast Moderate Slow	1.3 *B* 1.0 *B* 0.5 *B*	1.3 *B* 1.0 *B* 0.5 *B*

Table 3: Additional width for bank clearance W_{BR} and W_{BG}

Width for passing distance W_P	Good	Moderate
Vessel speed V_S (knots)		
- **Fast: $V_S \geqslant 12$**	2.0 *B*	1.8 *B*
- **Moderate: $8 \leqslant V_S < 12$**	1.6 *B*	1.4 *B*
- **Slow: $5 \leqslant V_S < 8$**	1.2 *B*	1.0 *B*

Table 4: Additional width for passing distance in two-way-traffic W_P

2.2 ROM standard

In ROM standard, the width of straight channel can be calculated in following term (shown in **Figure 3: Channel and fairway definition**).

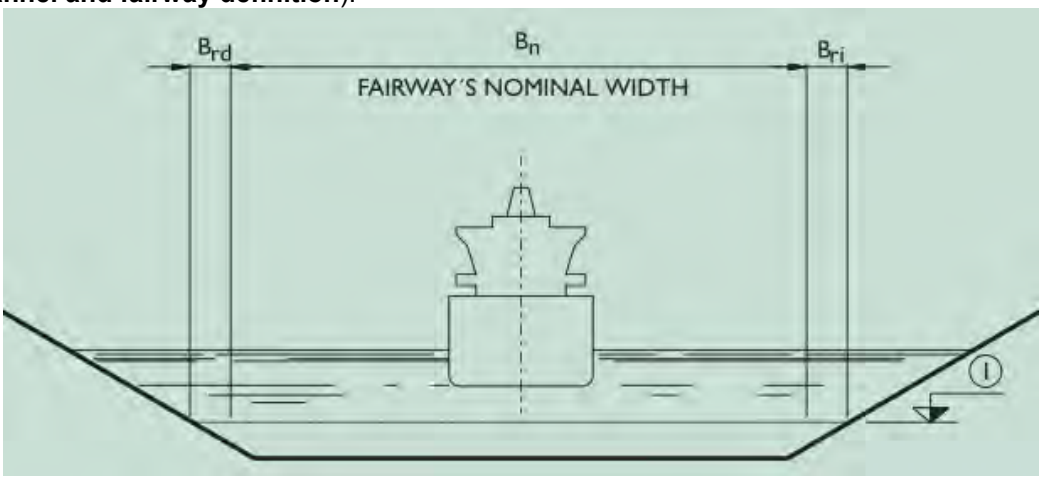

Figure 3: Channel and fairway definition (ROM)

$$B_t = B_n + B_r \quad (3)$$

Where:

B_t= The fairway's overall width.
B_n= The fairway's nominal width or clear space which must remain permanently available for vessel navigation, including safety margins.
B_r= An additional reserve width for taking into account boundary.
The bottom width B_n of straight channel can be calculated in the following method.

$$B_n=B+b_d+2(b_c+b_r+b_b)+(rh_{sm}+rh_{sd})_i+(rh_{sm}+rh_{sd})_d \text{ (One-way channel)} \quad (4)$$

$$B_n=2[B+b_d+2(b_c+b_r+b_b)]+b_s+(rh_{sm}+rh_{sd})_i+(rh_{sm}+rh_{sd})_d \text{ (Two-way channel)} \quad (5)$$

Where:
B=Maximum beam of vessels which will sail over the fairway.
b_d=Additional width of the vessel's swept path produced by navigation with a certain angle–drift angle to the fairway's axis, in order to correct the vessel's drift caused by the wind, wave, current or tugboat effect. The additional width necessary (b_d) will be calculated with the following formula:

$$b_d=L_{pp}*\sin\beta \text{ (for evaluating water spaces)} \quad (6)$$

$$b_d=L*\sin\beta \text{ (for evaluating above water spaces)} \quad (7)$$

where:
L_{pp} = Length between the design vessel's perpendiculars.
L= Design vessel's length overall.
β =Angle of drift, which can be determined with the following formulas.

$$\sin\beta =\sin\beta_1+\sin\beta_2+\sin\beta_3+\sin\beta_4 \quad (8)$$

where:
β_1 is drift caused only by wind action.
β_2 is drift caused only by current action.
β_3 is drift caused only by wave action.
β_4 is drift caused only by tug-boat action.

$$\beta_1=\arcsin[(K_v*C_v*V_{sr}*\sin\alpha_{VT})/V_r] \quad (9)$$

where:
K_v =Coefficient depending on the ratio h/D between the site's water depth (h) and the vessel's draught (D) and the angle α_{vr}, shown in table 5.

h/D	K_v			
	$\alpha_{vr}\leqslant 10^\circ$	$\alpha_{vr}\leqslant 30^\circ$	$\alpha_{vr}\leqslant 60^\circ$	$\alpha_{vr}\leqslant 90^\circ$
$\leqslant 1.2$	0.0243	0.0161	0.0130	0.0121
2.0	0.0255	0.0168	0.0136	0.0127
$\geqslant 5.0$	0.0259	0.0171	0.0139	0.0129

Table 5: Coefficient K_v

$$C_v=(A_{LV}/A_{LC})^{0.5} \quad (10)$$

A_{LV}=Windage of the vessel's longitudinal projection.
A_{LC}=Vessel's longitudinal submerged area projected onto the centre line plane.
V_{vr}=Wind speed relative to the vessel being analyzed.
V_r=Vessel's speed relative to the water.
α_{vr}=Angle between the relative wind direction (incoming) and the vessel's centre line plane.

$$\beta_2=\text{arctg}[(V_c*\sin\alpha_{CV})/(V+V_c*\cos\alpha_{CV})] \quad (11)$$

where:
V_c =Absolute current speed considered as the fairway's operating limit.
V =Absolute vessel speed relative to the seabed.
α_{CV}=Angle between the absolute current direction and the vessel's absolute speed.

$$\beta_3=\arcsin e[K_w*(g/D)^{0.5}*(H_s/V_r)] \quad (12)$$

where:

K_w =Coefficient depending on the ratio h/D between the site's water depth (h) and the vessel's draught (D) and the angle α_{vr}, shown in table 6.

h/D	K_w						
	$\alpha_w \leqslant 10^\circ$	$\alpha_w \leqslant 30^\circ$	$\alpha_w \leqslant 60^\circ$	$\alpha_w \leqslant 90^\circ$	$\alpha_w \leqslant 120^\circ$	$\alpha_w \leqslant 150^\circ$	$\alpha_w \leqslant 170^\circ$
$\leqslant 1.2$	0.0296	0.0512	0.1067	0.1323	0.1183	0.0725	0.0418
2.0	0.0310	0.0537	0.1118	0.1387	0.1240	0.0760	0.0439
$\geqslant 5.0$	0.0315	0.0546	0.1137	0.1410	0.1261	0.0772	0.0446

Table 6: Coefficient K_w

α_w= Angle between the wave propagation direction and the vessel's centre line plane.

g= Acceleration of gravity

D= Draught of the vessel under analysis.

H_s= Significant wave height of the waves considered as the fairway operating limit for the vessel being analyzed.

V_r= Vessel's speed relative to the water.

$$\beta_4 = \arcsin e[K_r * ((g * F_{TR})/(A_{LC} * \gamma_w))^{0.5} * (1/V_r)] \quad (13)$$

where:

K_r =Coefficient depending on the ratio h/D between the site's water depth (h), shown in table 7.

h/D	K_r
$\leqslant 1.2$	0.45
2.0	0.47
$\geqslant 5.0$	0.48

Table 7: Coefficient K_r

F_{TR} = Component of the force resulting in the vessel's transverse direction from tug-boats acting on it.

γ_w = Specific weight of water.

b_c =Additional width through positioning errors, shown in Table 8.

	Operation without a pilot or captain experienced in site being considered	**Operation with a pilot or captain experienced in site being considered**
Visual positioning in open estuaries,without navigation marking	100m	50m
Visual positioning referred to buoys or beacons in approach ways	50m	25m
Visual positioning between buoy or beacon alignments marking the fairway's limits	20m	10m

Table 8: Additional width b_c

b_r = Additional response width which assesses the additional deviation that may occur from the moment when the vessel's deviation from its theoretical position is detected and the instant when the correction becomes effective.

$$b_r = (1.5 - E_{max}) * b_{ro} \quad (14)$$

Where:

E_{max} = Maximum Risk admissible determined with the criteria.

b_{ro}= Additional response width, given in table 9.

Vessel's manouvrability	b_{ro}	
	$h/D \leqslant 1.2$	$h/D \geqslant 1.5$
Good	0.1 B	0.1 B
Medium	0.2 B	0.15 B

Bad	0.3 *B*	0.2 *B*

Table 9: Additional response width

b_b = Additional width for covering an error which might derive from the navigation marking systems.

$$b_b = D*\sin 0.5^\circ \quad (15)$$

Where:

D= The distance between 2 buoys along the channel direction.

rh_{sm}, rh_{sd}=Additional safety clearance which should be considered on each side of the fairway to enable the vessel to navigate without being affected by bank suction or rejection effects, shown in Table 10..

	rh_{sm}	rh_{sd}	$rh_{sm}+rh_{sd}$
Fairways with sloping channel edge and shoals($V/H \leqslant 1/3$)			
Vessel's absolute speed$\geqslant$6m/s	0.6 *B*	0.1 *B*	0.7 *B*
Vessel's absolute speed between 4 and 6 m/s	0.4 *B*	0.1 *B*	0.5 *B*
Vessel's absolute speed$\leqslant$4m/s	0.2 *B*	0.1 *B*	0.3 *B*
Fairways with rigid slopes($V/H \geqslant 1/2$) or with rocky or structural banks			
Vessel's absolute speed$\geqslant$6m/s	1.2 *B*	0.2 *B*	1.4 *B*
Vessel's absolute speed between 4 and 6 m/s	0.8 *B*	0.2 *B*	1.0 *B*
Vessel's absolute speed$\leqslant$4m/s	0.4 *B*	0.2 *B*	0.6 *B*

Table 10: Additional response width

b_s = the passing distance between the two lines, given in Table 10

	b_s	
	Fairway in exposed areas	Fairway in sheltered areas
Vessel's absolute speed$\geqslant$6m/s	2.0 *B*	-
Vessel's absolute speed between 4 and 6 m/s	1.6 *B*	1.4 *B*
Vessel's absolute speed$\leqslant$4m/s	1.2 *B*	1.0 *B*
Traffic density: 0-1 vessels/hour	0.0 *B*	0.0 *B*
Traffic density : 1-3 vessels/hour	0.2 *B*	0.2 *B*
Traffic density: $>$3 vessels/hour	0.5 *B*	0.4 *B*

Table 11: Passing distance b_s

3. Depth of approach channel

3.1 PIANC guideline

In PIANC guideline, the depth of channel can be calculated in Table 11

Description	Vessel speed	Wave conditions	Channel Bottom	Inner channel	Outer channel
Ship Related Factors					
Depth	$\leqslant$10kts	None		1.10*T*	
	10-15kts			1.12*T*	
	$>$15kts			1.15*T*	
	All	Low swell ($Hs<1$m)			1.15*T*-1.2*T*
		Moderate swell (1m$<Hs<$2m)			1.2*T*-1.3*T*
		Heavy swell ($Hs>2$m)			1.3*T*-1.4*T*

	Add for channel bottom type				
	all	all	Mud	None	None
			Sand/clay	0.4m	0.5m
			Rock/coral	0.6m	1.0m

Table 12: Channel depth components estimates

3.2 ROM standard

In ROM standard the factors taking part in determining water depths in navigation channels and harbor basins are shown in **Figure 4: Factors of water depths in navigation channels and harbor basins.**

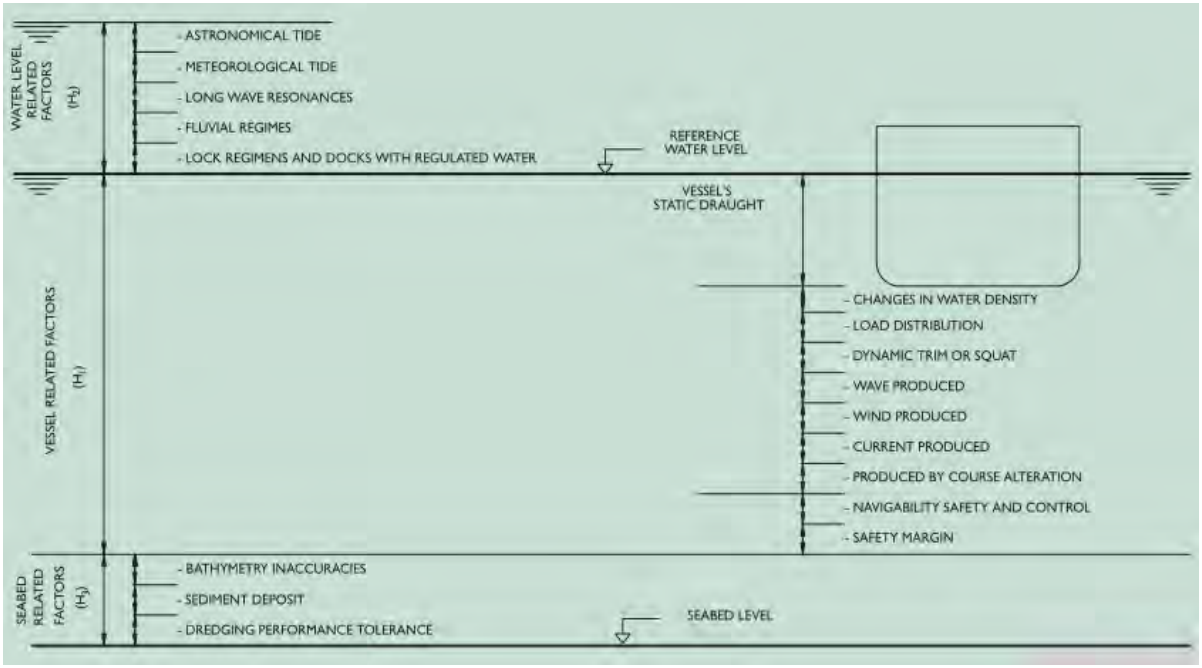

Figure 4: Factors of water depths in navigation channels and harbor basins

Where:
H_1 is the depth caused by the static draught of vessel, dynamic environment and other natural conditions element.
H_2 is the design water level, which is determined by the tide, wave, fluvial, requirement of navigation.
H_3 is the margin depth cause by seabed related factors.

The vessel related factors H_1 is constituted by the following factors:

$$H_1=D_e+d_s+d_g+d_t+0.7d_w+rv_{sm}+rv_{sd} \quad \text{(vessel's centerline)} \quad (16)$$

$$H_1=D_e+d_s+d_g+d_t+d_w+d_v+d_c+d_r+0.7rv_{sm}+rv_{sd} \quad \text{(vessel's port and starboard sides)} \quad (17)$$

Choose the max of value of H_1 above.

D_e is the static draught of the maximum design vessel.
d_s is the change in vessel's draught caused by changes in the density of the water. 3% of the vessel's static draught of increase is applied when the vessel moves from salt water to fresh water.
d_g is the additional draught due to cargo distribution.
d_t is the dynamic trim or squat which is taken to be the additional increase in relation to the water's static level.

$$d_t = 2.4*(\nabla/L_{PP}^2)*(F_{nh}^2/(1-F_{nh}^2)^{0.5})*K_s \quad (18)$$

Where:
d_t =Maximum value of dynamic trim (m)
∇=Vessel's volume of displacement (m^3)
L_{PP} =Vessel's length between perpendiculars

F_{nh} =Froude number, $F_{nh} = V_r/(gh)^{0.5}$
V_r =Vessel's speed relative to the water,excluding local effects (m/sec.)
g=Acceleration of gravity
h=Depth of water at rest,excluding local effects
K_s=Non-dimensional correction coefficient

d_w is the increase of vessel's draught caused by waves, shown in Table 12.

	Wave height (m)							
	0.5	1.0	1.5	2.0	2.5	3.0	3.5	4.0
Vessel's length overall (L_{pp} in m)	Vertical displacement (m)							
75	0.10	0.17	0.34	0.58	0.76	1.02	1.30	1.58
100	0.05	0.14	0.28	0.46	0.65	0.87	1.12	1.36
150	0.00	0.09	0.20	0.34	0.51	0.69	0.87	1.08
200	0.00	0.05	0.15	0.26	0.40	0.57	0.72	0.92
250	0.00	0.03	0.10	0.21	0.33	0.48	0.63	0.80
300	0.00	0.00	0.07	0.16	0.25	0.39	0.56	0.68
400	0.00	0.00	0.04	0.11	0.18	0.31	0.51	0.58

Table 13: increase of vessel's draught cause by wave

d_v is the increase of vessel's draught caused by wind.

$$d_v = (B\sin\theta_{TV})/2 \quad (19)$$

$$\tan\theta_{TV} = (F_{TV} * d_{vd})/[\gamma_w (I - \nabla d_{bg})] \quad (20)$$

Where:
θ_{TV}=Vessel's rolling angle cause by cross wind action
F_{TV}=Component of the resultant wind action force on the vessel in its transverse direction.
d_{vd}=Vertical distance between the F_{TV} line of action for the case of vessels underway and the centre of drift.
γ_w=Specific weight of water
I=The area moment of inertia of the water plane of constant displacement about its longitudinal axis.

$$I = (\pi * L_{pp} * B^3)/64 \quad (21)$$

∇= Vessel's displacement expressed in units of volume.
d_{bg}=Vertical distance between the mass centre of gravity and the centre of buoyancy (centre of the submerged volume) of the vessel being analyzed.

$$d_{bg} = KG - D[0.84 - (0.33 * C_b)/(0.18 + 0.87 * C_b)] \quad (22)$$

Where:
KG = Height of the mass centre of gravity above keel
D =Vessel's mean draught under the load conditions considered
C_b =Block coefficient at the foregoing draught D

d_c is the increase of vessel's draught caused by current.

$$d_c = (B\sin\theta_{TC})/2 \quad (23)$$

$$\tan\theta_{TC} = (F_{TC} * d_{cg})/[\gamma_w (I - \nabla d_{bg})] \quad (24)$$

Where:
θ_{TC}=Vessel's rolling angle cause by cross current
F_{TC}=Component of the resultant current action force on the vessel in its transverse direction.
d_{cg}=Vertical distance between the F_{TC} line and the vessel's centre of gravity.

d_r is the increase of vessel's draught caused by alterations of approach channel.

$rv_{sm}+rv_{sd}$ is the clearance for the vessel's manoeuvrability and control (rv_{sm}), and safety margin (rv_{sd}), , shown in Table 13..

	rv_{sm}	rv_{sd}	$rv_{sm}+ rv_{sd}$

Large displacement vessels (>30,000 t)			
- Navigation over silty or sandy seabed			
Unlimited vessel speed (> 8 knots)	0.6	0.3	0.9
Limited vessel speed (≤8 knots)	0.3	0.3	0.6
Vessel at rest (quays, berthing, etc.)	0.0	0.3	0.3
- Navigation over rocky seabed			
Unlimited vessel speed (> 8 knots)			
Limited vessel speed (≤8 knots)	0.6	0.6	1.2
Vessel at rest (quays, berthing, etc.)	0.3	0.6	0.9
	0.0	0.6	0.6
Vessels with a medium and small displacement (≤10,000t, except small, recreational and fishing boats)			
- Navigation over silty or sandy seabed			
Unlimited vessel speed (> 8 knots)	0.3	0.3	0.6
Limited vessel speed (≤8 knots)	0.2	0.3	0.5
Vessel at rest (quays, berthing, etc.)	0.0	0.3	0.3
- Navigation over rocky seabed			
Unlimited vessel speed (>8 knots)			
Limited vessel speed (≤8 knots)	0.3	0.6	0.9
Vessel at rest (quays, berthing, etc.)	0.2	0.6	0.8
	0.0	0.6	0.6
Vessels with displacements between 10,000 and 30,000 t -Linearly interpolate as a function of the displacement given in sections 1 and 2			
Small, recreational and fishing vessels			
- Navigation over silty or sandy seabed			
Unlimited vessel speed (> 8 knots)			
Limited vessel speed (≤8 knots)	0.2	0.2	0.4
Vessel at rest (quays, berthing, etc.)	0.1	0.2	0.3
- Navigation over rocky seabed	0.0	0.2	0.2
Unlimited vessel speed (>8 knots)			
Limited vessel speed (≤8 knots)			
Vessel at rest (quays, berthing, etc.)	0.2	0.4	0.6
	0.1	0.4	0.5
	0.0	0.4	0.4

Table 14: Clearances for the vessel's manoeuvrability safety and control and safety margin

H_3 is the margin depth cause by seabed related factors.
The first factor is margin for bathymetry inaccuracies, which in shown in Table 14

	With wave compensation system	Without wave compensation system
Outer waters	1% of the water depth	0.25m+1% of the water depth
Inner water	1% of the water depth	0.1m+1% of the water depth

Table 15: Margin for bathymetry inaccuracies

The second factor is sediment deposit between two dredging campaigns.
The third factor is dredging performance tolerance, the adoption of tolerances of 0.30 m for soft ground and 0.50 m for rocky ground are recommended.

4. Width of harbor basin

4.1 PIANC guideline

In PIANC guideline, the nominal diameter of the turning basin should be more than 2 times of the vessel's length.

4.2 ROM standard

In ROM standard, the shape of turning basin is a irregular round area, which is shown in **Figure 5: Turning basin in ROM standard.**

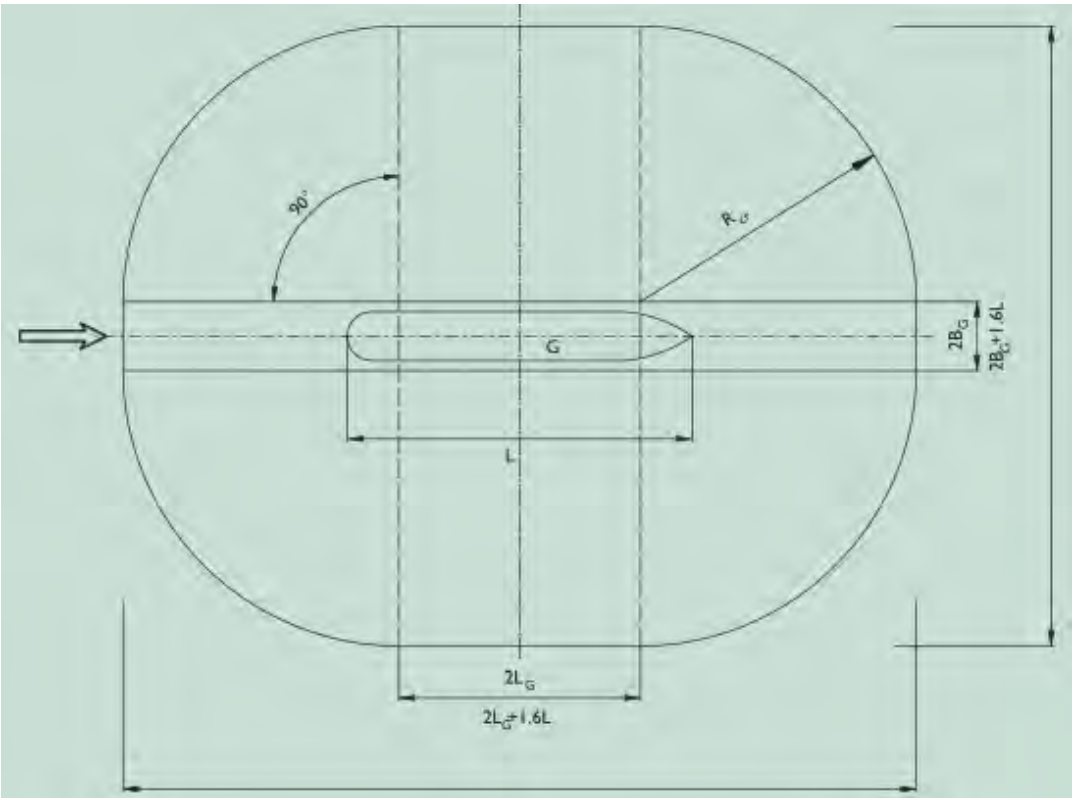

Figure 5: Turning basin in ROM standard

Where:

$B_G \geqslant 0.10L$

$L_G \geqslant 0.35L$

$R_{cr} \geqslant 0.80L$

L is the overall vessel's length.

5. Project example

A cruise terminal project in Panama is located in Panama Bay, face to the Pacific Ocean, nearby Panama Canal. The parameters of design vessels are shown in Table 15.

Design vessel	LOA	Beam	Draught	Passenger
Oasis of the Seas	360m	47m	9.3m	5400
Brilliance of the Seas	293m	32.2m	9.5m	2501

Table 16: Design vessel

The calculation results by using PIANC guideline and ROM standard are shown in Table 16.

	PIANC guideline	ROM standard
Width of channel	170m	200m
Depth of channel	12.1m	12.3m
Width of harbor basin	720m X 720m	760m X 580m

Table 17: Calculation result

The proposed water area layout of the project in shown in **Figure 6: General layout of project**.

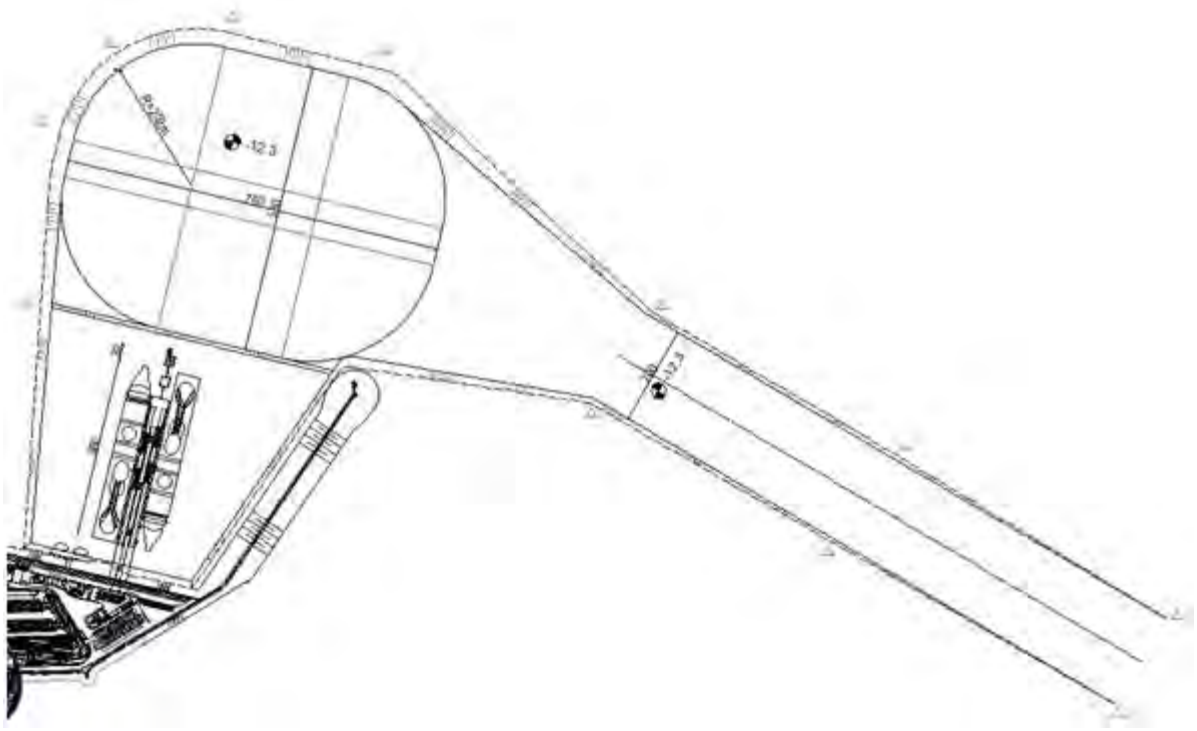

Figure 6: General layout of project

In order to make compare of the design (in ROM standard) and actual manoeuvre operation, a Real-Time simulator analysis was made, the result is shown in **Figure 7: Safe manoeuvre space.**

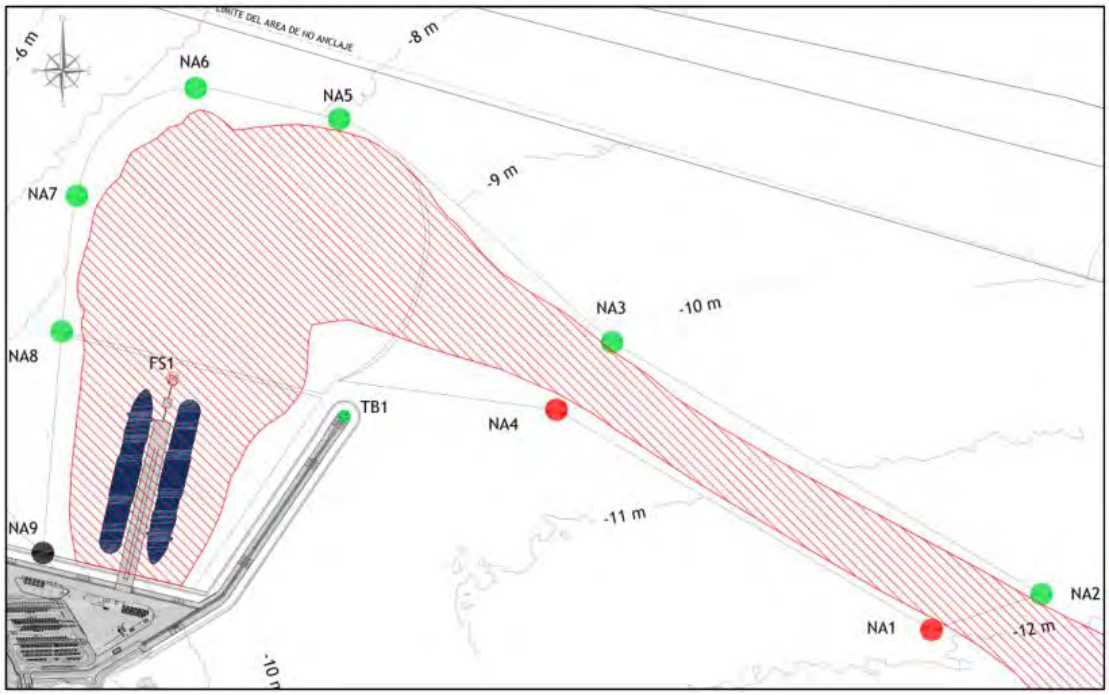

Figure 7: Safe manoeuvre space

This result shows that the shadow area of the vessel track is completely contained inside the water area. The shadow area of harbor basin is nearly an oval, so the design method of ROM standard is more closely aligned with actual manoeuvre operation. And at the corner of the harbor basin, the boundary of water area can be reduced. As for the width of channel, the design result of ROM

standard is more conservative, and the design result of PIANC guideline is on the risky side, the Real-Time simulator analysis shows that the ROM standard is more suitable in this project.

6. CONCLUTIONS AND RECOMMENDATIONS

1. The PIANC guideline and ROM standard has respective characteristics and scope of application. For the width of channel, the design method of PIANC guideline is more dangerous and the ROM standard is more conservative.
2. For the depth of channel, the design result of PIANC guideline and ROM standard are almost same.
3. For the shape and width of the harbor basin, the design method of ROM standard is a irregular oval and PIANC guideline is a regular round, the ROM standard is more closely aligned with actual manoeuvre operation.

7. REFERENCES

PIANC (2014) Report n°121-2014 Harbour approach channels design guidelines, PIANC, Brussels.

PIANC (1997) Approach Channels A Guide for Design, PIANC, Brussels.

ROM 3.1-99: 2007. Recommendations for the Design of the Maritime Configuration of Ports, Approach Channels and Harbour Basins, Spain.

ASCE (2005). Manuals and Reports on Engineering Practice No. 107: 2005. Ship Channel Design and Operation, USA.

ASCE (1993). Manuals and Reports on Engineering Practice No. 80: 1993. Report On Ship Channel Design, USA.

Carl A. Thoresen. (2010) Port designer's handbook (Second edition) . British: Tomas Telford 2010: 91-144.

EM (2006). Coastal Engineering Manual, USA.

OCDI (2009). Technical Standards and Commentaries for Port and Harbour Facilities in Japan, OCDI, Japan.

BS 6349-1-1 (2013). Maritime works – part 1-1: General – Code of practice for planning and design for operations. BSI Standards Publication British.

8. COPYRIGHT

CHARACTERIZATION ANALYSIS ON HARBOUR SILTATION IN JAPAN

by

Yasuyuki Nakagawa[1], K. Zen[2], M. Takayama[3] and T. Umeyama[3]

ABSTRACT

The purpose of the present study is to review the current situation of the dredging activities for navigation channels around Kyushu district in Japan and to elucidate the siltation mechanism and sedimentary characteristics especially soft mud environment around a navigation channel. By the collection of the dredging volume data for access channels in the study area, the relationship between required depth for the channel and dredged volume is presented with the discussion of the dependency of dredging volume on the topographic conditions of the area of access channels.

By the analysis of the field data to elucidate the characteristics of sediment transport process around a navigation channel, the contributions of several factors for transport process were estimated and the result shows the dominant factor of tidal current in the present study site. Furthermore, field data of muddy sediment structure around the navigation channel is also presented to examine the applicability of the nautical depth concept in a Japanese port, though the fluid mud layer with the thickness of around 10 cm in the present case study site.

1. INTRODUCTION

Port and harbors have been constructed more than one hundred for commercial use around Japanese coast and developed and utilized for the local and national economic activity. Several ports locate at the area of shallow coasts and estuaries, where back siltation may occur in dredged navigation channels and turning basins. Minimizing harbor siltation, therefor, is key factor for the efficient port operation by reducing the cost of maintenance dredging and the environmental impacts of the damping of dredged sediments as is often the case in ports and harbors all over the world (e.g. PIANC,2008).

The purpose of the present study is reviewing the current situation of the dredging activities for navigation channels around Japan, especially in Kyushu district, and characterizing the siltation mechanisms and sedimentary conditions around a navigation channel through the field data analysis. The present study discusses on the results from 1) a data analysis of historical records of dredging volume for several ports and 2) field data analysis for understanding the siltation mechanism and fluid mud formation, considering the applicability of the nautical depth concepts for the ports.

1 Kyushu University, Professor, y.nakagawa@civil.kyushu-u.ac.jp
2 Kyushu University, Professor Emeritus
3 Kyushu Regional Development Bureau of Ministry of Land, Infrastructure, Transport and Tourism

2. DREDGING VOLUME FOR ACCESS CHANNELS

2.1 Study Area and Data Source

In order to characterize the dredging activity for access channels to the port in the Kyushu district in Japan (Figure 1), the dredging records for fifteen years since 2002 through 2017 were collected from the Kyushu Regional Development Bureau of Ministry of Land, Infrastructure, Transport and Tourism (MLIT). The location of the target ports in the present study are indicated also in Figure 1 and several ports locate in the shallow muddy coast surrounded by the intertidal mud flat, where should suffering from back siltation by sediment transport from surrounding area under the natural forces such as current and waves. The study examines, as a fundamental analysis, the relationship between the dredging activities for developments of navigation channels and natural sedimentary condition around the port area qualitatively.

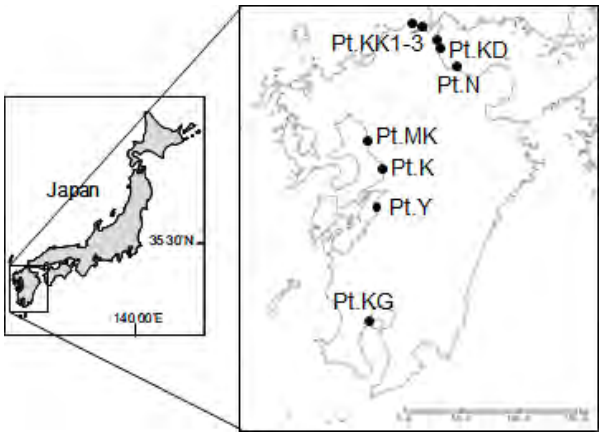

Figure 1: Map of Study Site

2.2 Dredging Volume

The total volumes of dredging for development of navigation channels at the ports are calculated as shown in Figure 2. The figure demonstrates the relationship between the designated depth of the navigation channel and dredged volume for the recent 15 years. The data for the turning basin was excluded in the present analysis because the dredging volume may depend on the size of harbour basin. The dredging volume for the navigation channel, however, mainly depends on the bathymetrical condition and the length of the channel to approach the required depth at the offshore.

The dredged volume, therefore, does not have proportional relationship with the required depth or designated depth, showing the case with relatively smaller dredging volume for deeper navigation channel at Port KK2, where the bathymetry condition is suitable for deeper access channel with natural deeper basin. On the other hand, the Port K required the relatively larger dredging volume in spite of

the channel depth is less than 8 m, since the port locates in the shallow coast as demonstrated in the following chapter.

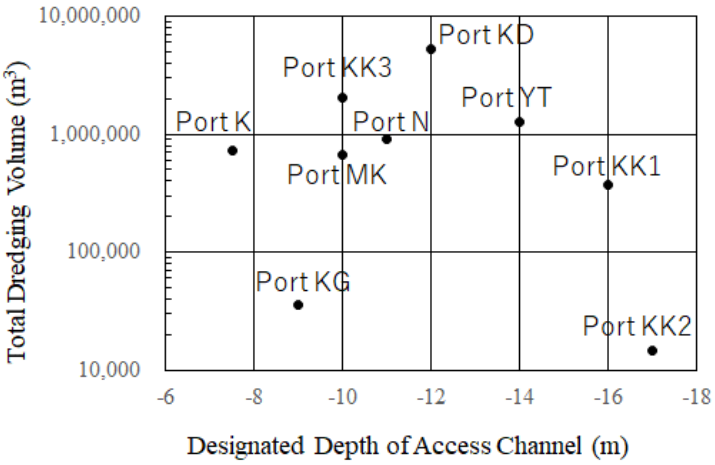

Figure 2: Total Dredging Volume for Access Channels

3. SEDIMENTATION PROCESS AROUND ACCESS CHANNELS

3.1 Study site

As a case study for elucidating the siltation process, sediment transport processes around navigation channel were studied and analyzed with the field data monitored at the Pt K in figure 1 or the port of Kumamoto in the Ariake Bay (Figure 3). The field monitoring campaign during the two weeks captured key processes of sediment transport dynamics, including resuspension of the bottom sediment due to the currents and waves. The sediment fluxes around the port were estimated with the field measured data and it provides the dominant effect of the storm event on the redistribution of bottom sediments. Another specific finding from the monitoring is that the wave induced by the ferry boat cause the suspension of the sediment in the area.

3.2 Field monitoring and results

Field monitoring were carried out at the offshore of the port of Kumamoto including the deployment of bottom mounted instruments for current and turbidity measurements as shown in Figure 4 for two weeks between Aug. 10 and Aug. 25 in 2013 (Takashima et al. 2015). The wave data was collected at the wave monitoring station operated by the MLIT.

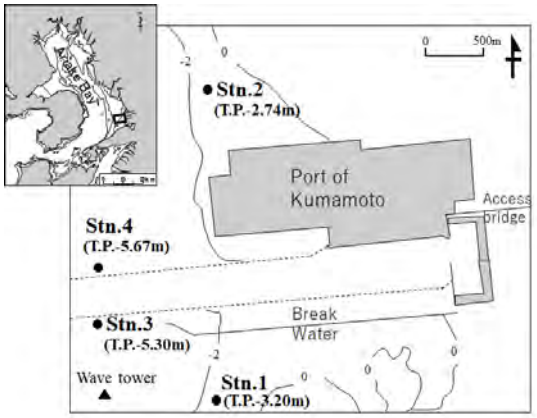

Figure 3: Monitoring Site for Sediment Transport Study

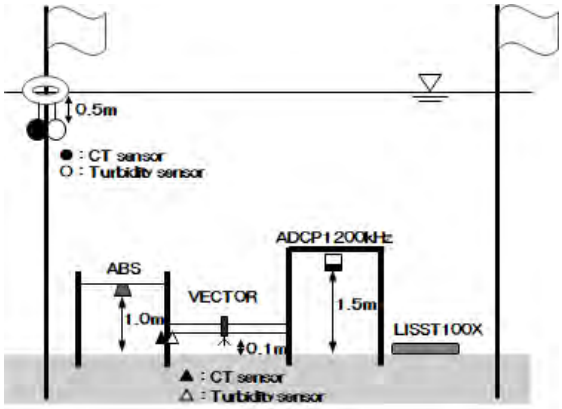

Figure 4: Instrumentation Layout for Current and Turbidity Measurements (Stn.1 in Figure 3)

Measured data during the observation period is shown in Figure 5, where flow velocity near the bottom surface at Stn.1 and Stn.2 are measured at 10 cm above the bottom surface, SS concentration at the bottom layer was measured at 10 cm above the bottom. During the observation period, the wind speed increases periodically in the day time with the increase of significant wave height. In the latter half of the observation period, there was a storm event with the highest wave in the observation period and the maximum suspended sediment concentration (SSC) was also observed during the storm period.

Another characteristic point of SSC fluctuation is shown in Figure 6 and they are compared with temporal variations of wave height and current velocity. The figure shows periodical increase of SSC at relatively shorter intervals than the tidal period and the occurrence of these periodic SSC increase matches when the higher speed car ferry boat enters the port. Besides the period of service of the regular high-speed ferry, increase of SSC is observed also due to the tidal current as indicated by the red circle in Figure 6. The boat traffic often become a factor for the sediment transport in estuarine system with navigation channel (e.g. Verney et al. 2007)

By using the observed current and SSC data set, suspended sediment flux was also analyzed with the estimation of contribution by several factors including tidal current and wave event to the total flux. According to this estimation, dominant transport at the measurement point of Stn.1 was eastward (blue

line in Figure 7) and 91% of the flux was due to tidal current, 9% was due to waves (wind wave) and boat traffic waves, respectively. Contribution of SS concentration due to waves (wind waves) and boat traffic is relatively small but the tidal current during the spring tide period is dominant factor of SS transport.

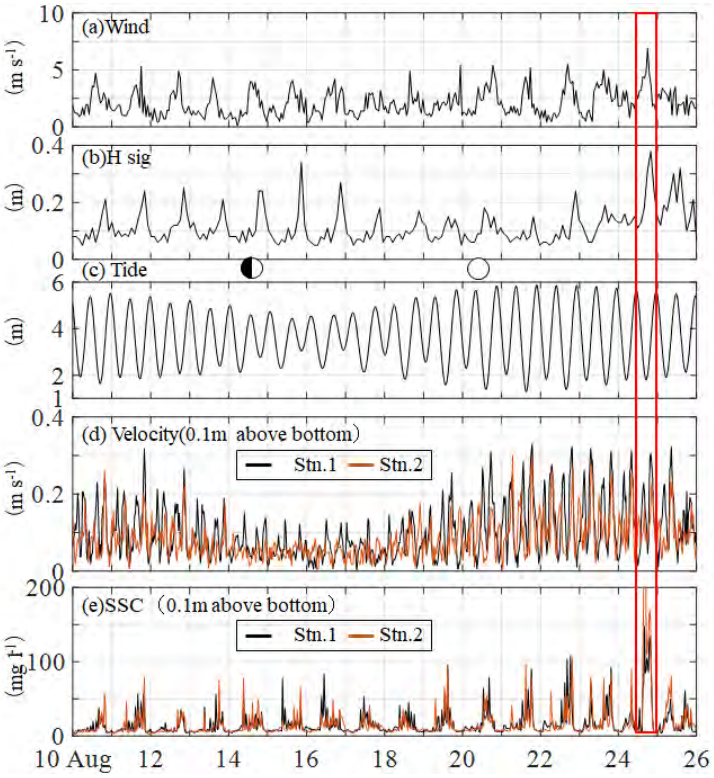

Figure 5: Measured Data during the Monitoring Period

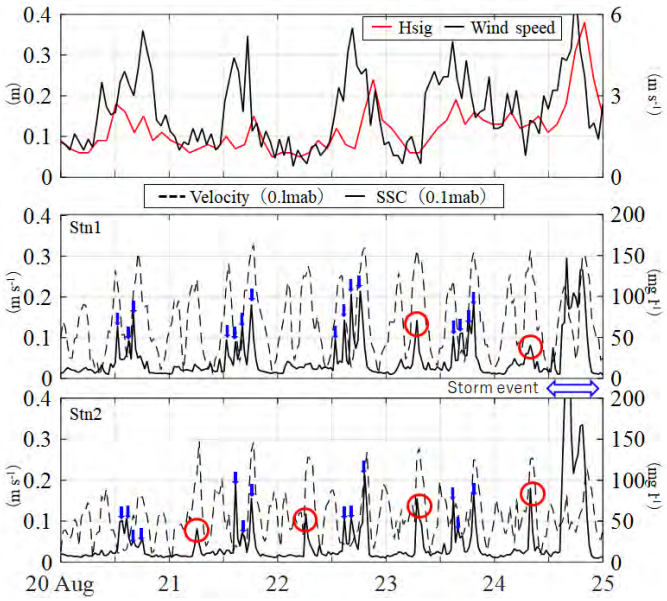

Figure 6: Measured Data during the Spring Tide Period (Red circle means increase of SSC due to tidal current and Blue arrow means ferry boat traffic)

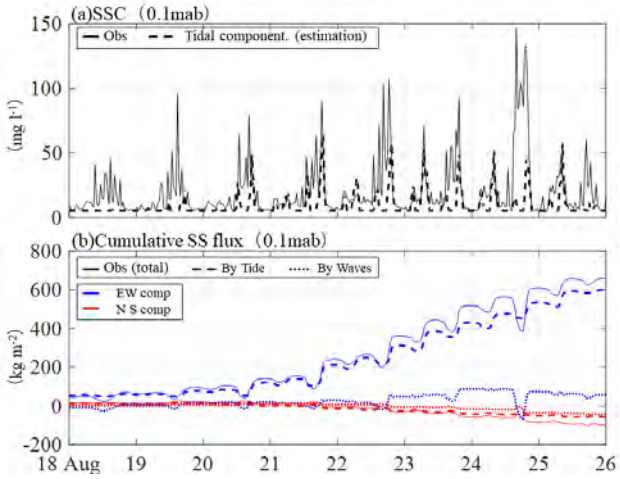

Figure 7: Estimated Suspended Sediment Flux

4. FIELD SURVEY FOR CHARACTERIZING VERTICAL STRUCTURE OF MUDDY SEDIMENT

4.1 Field survey for mud density measurement

As shown in the previous section, the fine sediments are transported by the current and waves and they may be accumulated in the deeper channel. We also have the field data of the bottom sediment around the navigation channel of the port of Kumamoto as shown in Figure 8. The data shown here was taken during the field survey on December 11 and 12 in 2002. For the density measurement, the tuning folk type densimeter was used and the instrument consists of the mono folk type sensor with the length of 10 cm and the diameter of 1.5 cm (Figure 9). The measurement system detects the vibration frequency of the sensor that varies with the density of the surrounding medium. Total weight of the sensor unit is 5 kg in the air and 4 kg in the water. It is connected through a cable with a PC and both measured depth and density data are logged at the same sampling rate of 1 Hz. The measurement range of density is 0.9-1.5 g/cm^3 and the resolution is 0.001 g/cm^3. For the measurement, the sensor was taking the data at the vertical interval of 10 cm above the bottom level. The density can be measured until the sensor is settle with the own weight in the consolidated mud layer.

Besides the data acquisition of bulk density, sediment samples were taken with core samplers with the diameter of 43 mm and they were sliced with the thickness of 10 cm and analyzed for sediment properties such as bulk density, particle size distribution, dry density, etc. Soundings were also carried out by an acoustic sounding with the frequency of 200 kHz and a lead line also.

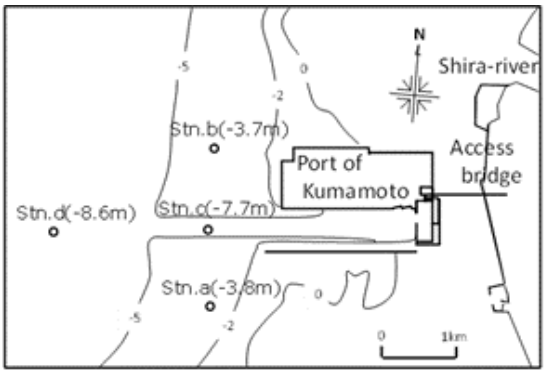

Figure 8: Monitoring Locations for Muddy Sediment Sampling

Figure 9: Instrument for In-situ Bulk Density Measurement

4.2 Results and discussion

Analyzed results for the bottom surface sediments at the all stations are shown in Table 1. Most the surface sediments at the stations consists of fine sediments with the median grain size of less than 2.5 micrometer and with the mud content (sum of silt and clay fractions in weight) of over 97 %, except the Stn.a where sand fraction is relatively higher and mud content is less than 80 %. The higher mud content correlates with the higher water content, *Wc*, which is defined as following equation.

$$Wc=100w_w/w_s \qquad (1)$$

where w_w: mass of water and w_s: mass of sediment grains. The highest value of the water content in the monitoring stations is around 220 % at Stn.c. The dry density of the sediment particles are almost same values around 2.6 g/cm^3. However, the bulk density is ranging from 1.11 through 1.51 g/cm^3 and it decreases less than 1.2 g/cm^3 in the higher water content environment, which is classified as the fluid mud, eg. PIANC(2008), at Stn.c and d.

At the Stn.a with the relatively higher sand content, the bulk densities near the bottom surface are over 1.4 g/cm^3 all through the sliced layers of sediment core sample showing rigid sediment condition as shown in Figure 10 (a). The density profile measured by the in-situ densimeter shows rapid increase in the bulk density at the interface between the sea water with the density of around 1.02 g/cm^3 and the consolidated sediment with the density of over 1.4 g/cm^3. In case of muddy sediment with relatively

lower water content at Stn.b (Figure 10(b)), the densities obtained by the core sample analysis shows almost uniformly distribute in vertical around 1.3-1.4 g/m^3, which is categorized as consolidating mud. The in-situ bulk density measurement result shows rapid increase at the interface between the sea water and the mud layer. The difference between the detected bed levels by the acoustic device and the lead method is around 15 cm both for Stn.a and Stn.b.

Table 1: Sediment Properties at the Monitoring Points

	Stn.a	Stn.b	Stn.c	Stn.d
D50 (μm)	24.9	2.5	2.0	<1.0
% of Sand (> 75 μm)	24.8	4.7	3.6	2.6
% of Silt (5 < d < 75 μm)	46.5	37.3	33.3	30.0
% of Clay (d < 5 μm)	28.7	58.0	63.1	67.4
Density of particles (g/cm^3)	2.697	2.682	2.662	2.674
Water content (%)	81.4	159.6	222.6	179.8
Bulk density (g/cm^3)	1.513	1.357	1.180	1.114

The data shows the highest water content and fluid mud at Stn.c and Stn.d. It should be noted that Stn.c is in the navigation channel dredged up to -7.7 m from the original depth of less than 4 m. This fact indicates that fine particles accumulates in the dredged deeper channel with so high concentration that fluid mud layer may be formed.

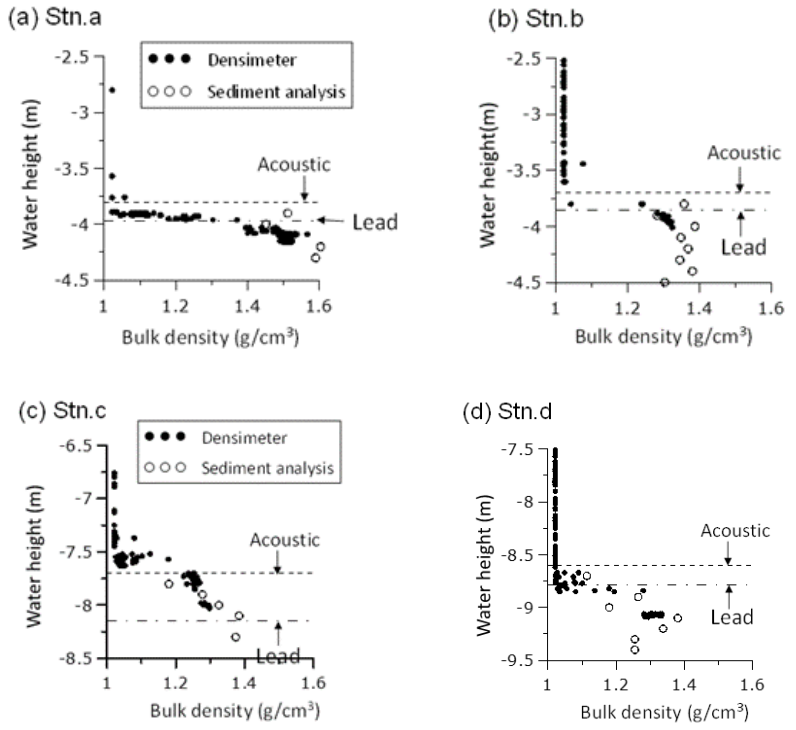

Figure 10: Measured density profiles by sediment core analysis and in-situ densimeter. (The vertical scale is relative to D. L.)

In the cases of the mud with higher water content at Stn.c and Stn.d, the structures are different from the above two stations and they shows gradual increase on bulk density into the depth as shown in Figure 10(c) and (d). The measured profile of the bulk density by the in-situ densimeter for these stations shows the transition layer with the thickness of around 10 to 20 cm where the bulk density is between 1.02 and 1.2 g/cm3. The detection of the density range with the thickness around 10 to 20 cm means the existence of fluid mud layer at these stations. Although the present study area under the monitoring condition is relatively small amount of fluid mud layer as much as 20 cm, this information is critical for the maintenance of navigation channel depth under muddy environment and some ports applying the nautical depth approach (e.g. Mehta et al. 2014) and the present monitoring techniques can be applied for better understanding of the fluid mud dynamics around the port and harbors in estuarine environment.

5. CONCLUSIONS

Maintenance of navigation channel is crucial topics for the of port and harbors, which are suffering from back siltation of access channel. By the analysis of total amount of dredging volume to develop access channels for Japanese port, the relationship between the required cannel depth and dredging volume showed non-linear relation and dependency of the dredging volume on bathymetry condition.

As a case study at the port, which is surrounded by shallow intertidal flat area, the analysis results of the field data for the measurement of current and turbidity were presented and it shows several factors of resuspension forces such as tidal current, wind waves and waves generated by ferry boat traffic, though the tidal current is most dominant for the horizontal transport among them in the present study site. Furthermore, field data of muddy sediment structure around the navigation channel was also presented and the data shows fluid mud layer with the thickness of around 20 cm in the present case study site. Although it does not require to apply the nautical depth concept in the study site with the fluid mud thickness, the monitoring technique can be applied for a maintenance of navigation channel in soft muddy sediment environment.

References

PIANC (2008), Minimizing harbor siltation, World association for waterborne transport infrastructures, Report No. 102, 75p.

Mehta, A., Samsami. F., Khare, Y.P. and Sahin, C. (2014). Fluid Mud Properties in Nautical Depth Estimation, Journal of Waterway, Port, Coastal and Ocean Engineering, 140, ASCE, pp210-222.

Takashima, N., Nakagawa, Y., Matsuo, T., IKKI, Y. and Matsumoto, H. (2015). Effect of Current and Wave Forces on Sediment Transport Processes at Shallow Coast Water around Tidal Flat, Journal of Japan Society of Civil Engineers, Ser. B2 (Coastal Engineering). Vol. 71, Issue 2, pp.I_547-I552 in Japanese

Verney, R., Deloffre, J., Brun-Cottan, J.-C., and Lafite, R.: The effect of wave-induced turbulence on

intertidal mud-flats: Impact of boat traffic and wind., Continental Shelf Re-search., Vol.27, No.5, pp.594–612, 2007.

SHIP SIMULATION – IMPORTANT ASPECTS FOR CONSIDERATION

by

Neil Lawson[1] and Captain Rory Main[2]

ABSTRACT

Full bridge ship simulation systems have developed significantly over recent years to the extent that they now present with very high levels of realism. However these high levels of realism cannot be taken as a proxy for accurate results. There are three factors that need detailed consideration to ensure that the results of the simulation series will be realistic. These are human, environmental and model factors. This paper discusses the importance of these factors and how, if given due attention, they can ensure high quality simulation results. If they are not given the proper attention then the results from the simulation series will be believed due the high levels of realism but will be inaccurate because of lack of attention to these factors.

1. INTRODUCTION

Ship handing simulators have been available in many forms since the 1980's and earlier. Since then simulators have developed significantly in realism and in the underlying model mathematical formulation to the extent now that they present to a pilot as being very realistic.

However, when an engineer is considering the use of simulation for detailed design of a port or, as is often the case, whether a larger ship can use existing port infrastructure then it is incumbent on the engineer to address a number of matters before and during simulation. Otherwise realism becomes a proxy for truth but the results of the simulation may be inaccurate or even misleading. Realism is only one part of what is required to make a simulations series successful.

This paper explores the main factors that need to be considered when preparing and undertaking a simulation series. It does not discuss the methods that should be used to analyse the simulation data to support the outcome decisions from the simulations.

In this respect this paper only considers a small portion of the matters that will be covered by PIANC WG171 *Ship Handling Simulation Dedicated to Channel and Harbour Design* which is expected to be published in 2018-2019.

There are, however, a number of factors that still need to be considered when using these tools, whether as pilot training, scenario testing or for engineering design.

These factors can be generally divided into the following categories: -

1. Human factors
2. Environmental factors and
3. Modelling factors

This paper has been written from the perspective of a simulation that is being used as an engineering tool to carry out a detailed design of a new port or to look at a change of use of an existing port.

The use of simulators in the design of shipping channels and basins is described in PIANC WG121. WG 121 considers both **concept** and **detailed** design (simulation). PIANC WG171 will be updating the WG in relation to detailed design using ship simulation.

2. HUMAN FACTORS

All three factors are important but human factors are perhaps the hardest to assess. All pilots have their own personalities and pilotage preferences and not all pilots can easily move into a full bridge simulator and feel comfortable. The success of full bridge simulations relies on the pilot feeling comfortable within the simulation environment and for them to behave in exactly the same way as they do during actual pilotage.

The aim of a full bridge simulator is to put the pilot into an environment that closely matches the actual bridge of a ship with views out of the bridge that look very much like the port that they work in. This will ensure that the mental model of the Pilot is accurately recreated, which is necessary for the Pilots to be fully immersed in the simulation. Thereby ensuring the pilots information processing and recall is close to reality. Situational engagement is dependent on providing the same cues utilised by Pilots in reality to the simulated environment.

Consequently full bridge simulators are built to be as close as possible to real life and the bridge view is also modelled to be as close to real life as possible. All the visual aids that pilots use need to be realistically presented in the out of the bridge view. These visual aids are usually more than just the channel markers and lead lines for the port. They will include prominent features along the shoreline.

However the simulator presents a 2D view of the surroundings and the depth of view perception is not always easy to assess in the simulator. It is important to have at least a 180 degree view to allow the pilot to visually recognise their position in a 3D world.

Bridge protocol is also important. A helmsman should be provided in the simulations and pilot orders and responses should take the same form as if it is a real pilotage. A common mistake is to use the another pilot as the helmsman which has 2 problems:

1. It results in discussion between the pilots during the simulation and
2. Does provide independant views when the helmsman becomes the pilot

When tugs are being used not only is it important that the tug models are correctly prepared but also that tug masters are available for simulation (or for tug simulators which are part of the simulation). The tug masters comments provide practical input to the simulations.

So in summary the human factors that need to be considered are ensuring that each pilots are not influenced by a previous pilots experiences and ensuring that the out of the bridge view contains all the information that a pilot uses for a pilotage. This additional information may vary from pilot to pilot. And of course it is important that pilots who use the simulator feel comfortable in the simulations environment.

Research findings support the notion that simulation exercises are stressful activities regardless of experience, and that even well-trained pilots can overlook key information that is critical to the passage plan. At present, the evidence base regarding the utility and effectiveness of ship simulation is in its infancy, yet the available results are promising. High-fidelity simulators can seemingly fill the increasing void in

maritime engineering by enabling an experienced pilot to competently perform the role under a diverse array of conditions (e.g., poor weather, mechanical issues).

3. ENVIRONMENTAL FACTORS

Usually bathymetry may be seen as the most important input data for the model. Bathymetry is important and usually it is available without having to carry out any specific additional work. But of equal importance is the preparation of the environmental data.

A conclusion from a simulation series can be misleading if the metocean conditions presented for simulation are inaccurate.

The preparation of the environmental data for simulation can take some time to prepare, particularly if measurements need to be collected and/or hydrodynamic modelling is required to better understand the environment.

But often a simulation series might be requested with insufficient time being allowed to carry out the necessary studies which may them compromise the outcomes from simulation.

Some of the issues that need to be considered when preparing environmental conditions include: -

1. The wind speed that is generally used for simulation is the 10min average 10m height wind speed over water. A pilot will usually have access to this wind speed before and during pilotage but can also be influenced by the gust speed or the wind speed displayed on the bridge of the ship. The bridge wind speed is invariably sampled at a greater height than 10m and can be impacted by the ship itself. In addition wind in real life has gustiness and fluctuations in wind direction. Depending on the levels of these fluctuations they can impact on the simulation and create more uncetainty in the mind of the pilot than a steady state wind speed being applied to the ship. It does need to be noted however that a large ship is a big integrator of winds and very short fluctuations only have small impacts on the progress of the ship.
2. Currents are usually measured in depth cells (acoustic current meters) or as single depth measurements. The characterestics of the currents at the location of the port are very important. Are the currrents 3 dimensional? Are currents driven primarily by tides or winds? Or are both tides and winds important? Answering these questions takes skill and time. And, or course, it is the currents in the upper layers that are important. As with winds, currents can also have a degree of instability and also display gustiness.
3. Waves can also play an important part in simulations. Vertical ship motions can place the ship in close proximity to the bottom and horizontal motions can increase the swept path of a manoeuvre thereby impacting on channel width. Usually wave spectra will change over the simulation path. Typically waves are well known at one location along the pilotage path and this will be used to calibrate a wave model to translate waves over the simulation area.

If the currents need to be modelled, because there is insufficient measured data, then an appropriate model must be selected. All the considerations that need to be covered for a quality hydrodynamic model including 2D vs 3D and grid scale size to define the features can impact the quality if the modelled results and need to be resolved. Often an existing hydrodynamic model that was prepared for some other purpose, without due consideration to the above, can produce misleading information. Often the

information that has being prepared for an existing port will be challenged by pilots if it does not match their expectations.

The preparation of environmental data for simulation needs to be managed by someone who understands the technical requirement of ship simulation.

Pilots develop a good understanding of the impact of metocean conditions on pilotage without necessarily having a knowledge of the magnitudes of the currents, waves or winds. This knowledge is really important in ensuring that the environmental data prepared for the model is accurate. However if currents and winds in the model are estimated based on current port users experience then the metocean parameters will usually be overestimated. When the force on the ship exerted by currents or wind is a function of the velocity squared then the importance of good quality metcean data can be appreciated.

4. MODELLING FACTORS

There are a number of different ship simulation modelling systems that provide for full bridge simulation. If simulation is being used to assess a greenfields port or whether it is being used to assess the acceptance of larger ships into existing ports a decision has to be made on which ship/ships are going to be used in simulation to make the assessment.

The mathematical model of the ship can be prepared a number of ways from scaling from a similar ship to specific scaled model tests in a basin and wind tunnel. Full scale sea trials are almost always available which help in validing a mathematical model of the ship. Often, however, a new ship will be prepared by simply scaling up or down from an existing ship without due consideration to differences in engines, rudder or perhaps hull form. These situations usually occur when a quick decision needs to be made about a new (larger) ship that is going to visit a port and commercial pressures result in corners being cut. This may compromise the outcomes from the simulations.

In addition to the ship model there is the simulation model. Every model uses best available mathematical descriptions to model all the components of ship simulation including shallow water effects, bank effects etc. There are areas of ship interaction with the environment where the theory is still being actively developed. An example where active development is underway at the moment is ship/bank interaction. Another example is dynamic adjustment of Cd where a ship is moving in constrained waterways. An example of this is where a ship in swinging is a constrained waterway with low underkeel clearance. An specific example was the swinging of a large container ship in a constrained waterway where in the extreme condition the ship blocked about 75% of the cross sectional area. The harbour was at the bottom of a significant estuary and tidal flows would exert forces on the ship. Normal simulation systems do not dynamically adjust the Cd to model the increased forces on the ship in this condition.

5. CONCLUSIONS

The increase in realism of modern ship simulation systems has provided mariners and managers increased confidence that the results that come from simulation systems closely represent real life pilotage of ships. For this confidence to be justified there are a number of matters that need close attention to allow the clients to make this assessment.

The paper categorises the matters that need close attention into human, environmental and model factors. If due attention is given to all these factors then the user will have justified confidence that the simulations

closely follow real life pilotage. However if due regard is not given to all of these factors then the confidence in the simulation which flows from the high quality realism will be miss placed.

6. REFERENCES

PIANC (2014) WG 121, Harbour Approach Channels, Design Guidelines, PIANC, Brussels.

T P Chambers, R Main (2016), The Use of High-Fidelity Simulators for Training Maritime Pilots.

EVALUATION OF MARINE STRUCTURES FOR KINEMATIC EFFECTS

by:

Julie A. Galbraith[1], M. Ali Naeem[2], William M. Bruin[3]

ABSTRACT

In performance-based seismic design, a marine structure is designed for inertial loading effects associated with the dynamic response of the structure. Some waterfront structures also experience seismically induced kinematic effects, associated with soil liquefaction and lateral spreading. This paper explores some of the approaches for incorporating these kinematic effects into the seismic design and analysis of marine structures.

Although most performance-based design provisions for piers and wharves require that kinematic effects be considered in seismic design, there is generally not detailed guidance on how these effects should be considered analytically. In addition, there are various opinions and practices across the industry in accounting for these soil-structural demands. Considerable judgement is required by the design professional in deciding how to include the kinematic loads into the structural analysis.

Combination of inertial and kinematic earthquake effects is one of the major decisions that needs to be made in the analysis and design process. Determination of the coupled load combination can be done with analytical methods or by engineering judgement and experience. Further, how to practically combine the kinematic and inertial loading is also an important decision. This paper discusses three analytical methodologies; including, superposition of results, post-inertial kinematic response, and post-kinematic inertial response. This paper will provide commentary on how these approaches can be implemented, and the advantages and shortcomings of each method.

Important analysis parameters are also discussed; including application of the kinematic loading, soil structure interaction, and modeling of nonlinear structural behavior using pile hinges.

[1] Simpson Gumpertz & Heger, Inc., Oakland, CA, USA, jagalbraith@sgh.com
[2] Simpson Gumpertz & Heger, Inc., Oakland, CA, USA, manaeem@sgh.com
[3] Simpson Gumpertz & Heger, Inc., Oakland, CA, USA, wmbruin@sgh.com

1. INTRODUCTION

Although most performance-based design provisions for waterfront structures require that kinematic effects be considered in seismic design, there generally is not detailed guidance on how these effects should be considered analytically. In addition, there are various opinions and practices across the industry in accounting for how to incorporate these soil-structural demands. Considerable judgement is required by the design professional in deciding how to include the kinematic loads into the structural analysis.

1.1 Description of Kinematic Effects

Kinematic effects in the context of marine and waterfront structures occur when lateral soil movements, typically associated with liquefaction-induced lateral spreading of marine slopes during seismic shaking, load the foundation elements of the structure. A less common occurrence is associated with cyclic plastification of clay-type soils that results in loss of stiffness. Kinematic loading of marine structures, and its effect on seismic performance, has been observed and its significant impact on waterfront infrastructure has been documented following recent earthquakes in Haiti (TCLEE 2012), Japan (COPRI 2014), Chile (COPRI 2013), and New Zealand. Marine structures like marginal wharves or pier landings, which are often founded on marine slopes, are particularly vulnerable to this hazard. For many structures, kinematic displacements can often be the governing seismic load condition, especially when combined with inertial demands. This seismic load condition is dynamic, occurring when a liquefiable layer is mobilized by ground shaking. The magnitude and characterization of the kinematic movement is dependent on project specific factors such as foundation pile density, slope angle, soil layering, cyclic behavior of sloped soils, as well as surcharge loading conditions. Structural response is dependent on the magnitude and depth of soil movements, relative soil layer stiffnesses at the slip plane, stiffness of the non-liquefied or crust layer, as well as inertial response. Because of the influence of these factors, kinematic soils are typically addressed on a project-by-project basis.

1.2 Code Design Requirements

At present, performance-based seismic design standards for marine and waterfront structures (ASCE 61-14, CBC 2016, POLA 2010, POLB 2014) require the consideration of seismically induced kinematic loading in the design of foundation systems. These standards to some degree imply that coupling of the inertial and kinematic loads should be performed, but no specific guidance is provided. Exact phasing of the kinematic slope mobilization with respect to the inertial shaking is not well known nor is there a professional consensus about how to combine these conditions. As is reported in Dickenson et al. (Dickenson 2016), scaling factors for combining the uncoupled inertial response with the uncoupled kinematic response range from 20% to 100%, provided by various guidelines, for surface transportation applications. Dickenson also concludes that the selection of weighting factors for combining kinematic and inertia loads should be done judiciously.

2. COMBINATION WITH INERTIAL RESPONSE

As noted, deciding whether and how to combine kinematic effects with inertial demands is a complicated issue, with minimal research, and currently no specific standard for waterfront structures. The first consideration for the design professional is how the occurrence of liquefaction correlates with ground shaking during the earthquake event. Generally, some level of strong ground motion must occur to initiate kinematic soil displacements, but the level of shaking required is variable and dependent on site-specific conditions. Additionally, the ground deformation from liquefaction is typically not an instantaneous motion, but rather a ramping up of movement to the maximum displacement as the earthquake shaking continues. The responses can be coupled, but generally not in a manner where the maximum magnitudes of both effects occur simultaneously.

Figure 1 illustrates the development of kinematic ground displacement over the duration of a typical earthquake time history. The dark smooth line in the displacement curve reflects the kinematic portion of soil movement. This example shows how the peak ground acceleration (at approximately 23 seconds) is not concurrent with the peak kinematic displacement.

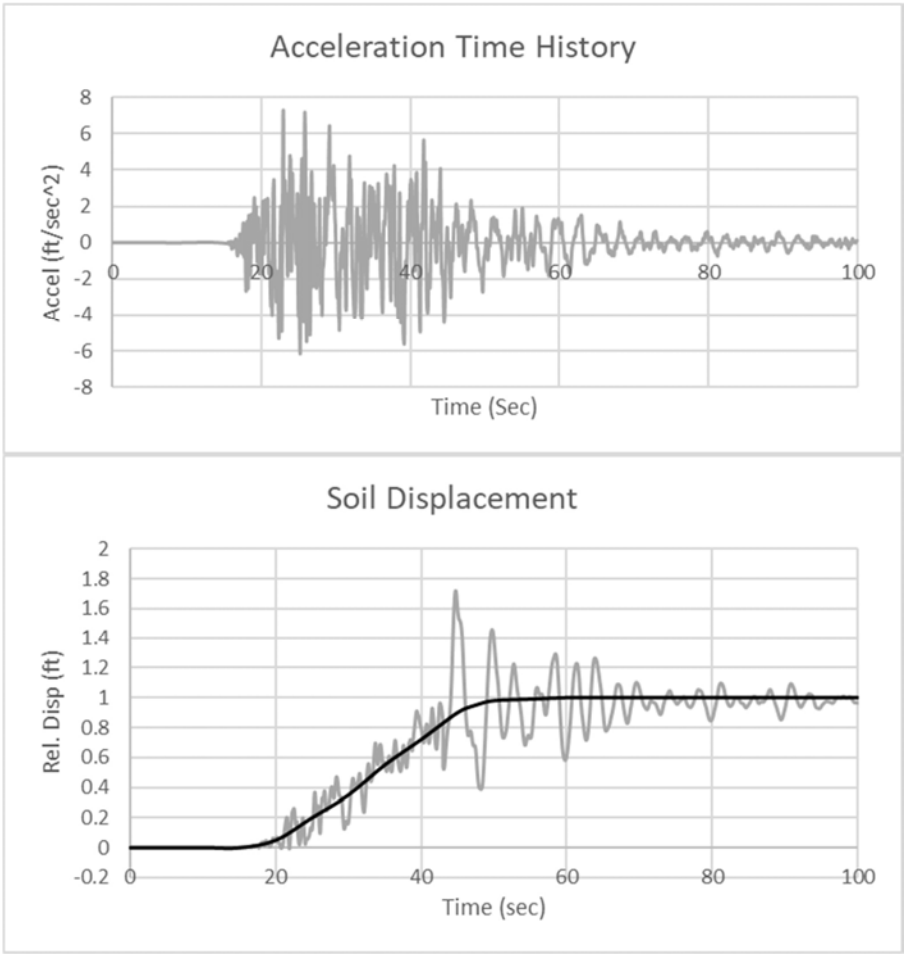

Figure 1: Example Soil Displacement During Acceleration Time History

Most design standards acknowledge some coupling and recommend that a combination of kinematic and inertial earthquake effects be considered. However, what percent of the full inertial demand and what percent of the full kinematic demand to be used in combination is open for interpretation and typically addressed on a project-by-project basis.

Performing time-history analyses on a soil profile model is one method for understanding the degree of coupling and the determination of combinations. The geotechnical and structural engineer can identify combinations by comparing a time history acceleration to the resulting kinematic motion, in terms of a percentage of the simultaneous maximum of each. Common points to identify are at the peak acceleration as well as at the peak kinematic displacement. Intermediate combinations may be worth consideration as well. For example, referring again to Figure 1, a combination of 100% inertial plus 20% kinematic could be interpreted at approximately 23 seconds; and 100% kinematic plus 30% inertial at approximately 50 seconds. A third combination of 75% inertial plus 80% kinematic at approximately 42 seconds may also be relevant for this ground motion. This process could be completed for multiple earthquake ground motions or based on an average of a ground motion set.

These time-history comparisons would be used only for determining the coupled load combinations; a nonlinear static pushover analysis and response spectrum curve would still be used for calculating inertial demand displacements and assessing structural performance. This procedure, although a very credible approach for estimating load combinations, is not commonly used, mainly because of the significant level of effort in performing these time histories. More commonly, geotechnical engineers may provide load combinations based simply on engineering judgement, with knowledge of soil type

and probable earthquake scenarios. Some designers may simply choose to combine 100% kinematic and 100% inertial demands, recognizing that this is the most conservative assumption of load coupling.

The second consideration for the design professional in developing combined kinematic and inertial load combinations is recognizing that the damage from each loading type often does not occur in the same location of the foundation structure. For example, under inertial earthquake demands, the pile hinge is typically at the deck connection and/or the mudline elevation, as shown in Figure 2. Under kinematic loading, the hinge usually forms in the soil just below the liquified layer, where the stiffness of the underlying soil is significantly higher than the liquefied layer. For this configuration, it is rational to not combine the two effects; the maximum loading and inelastic hinging for each condition is occurring at completely different locations on the pile, suggesting not much coupling of response with respect to global seismic performance.

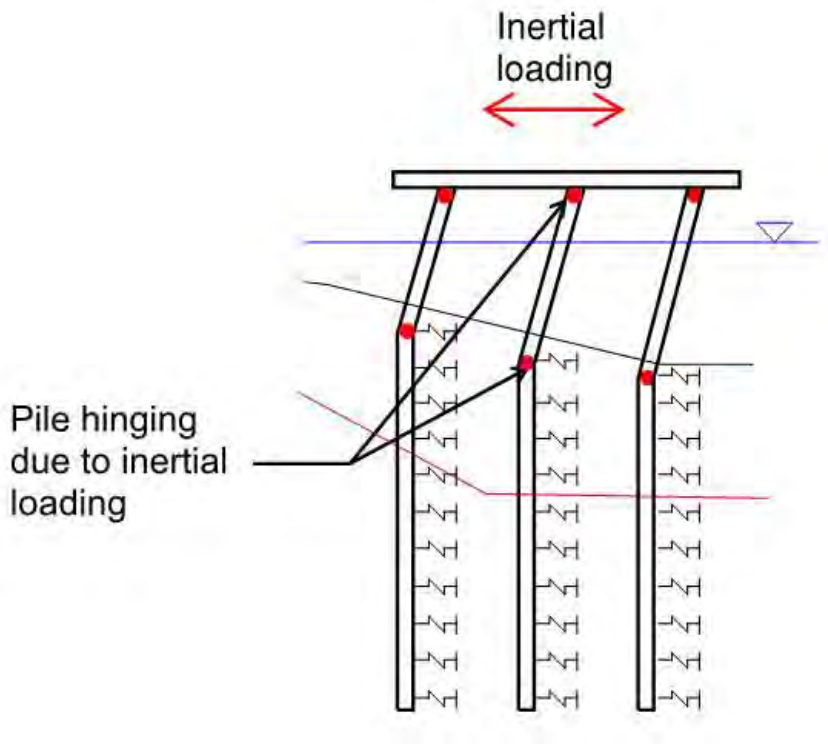

Figure 2a: Typical Pile Hinge Locations for Inertial Loading

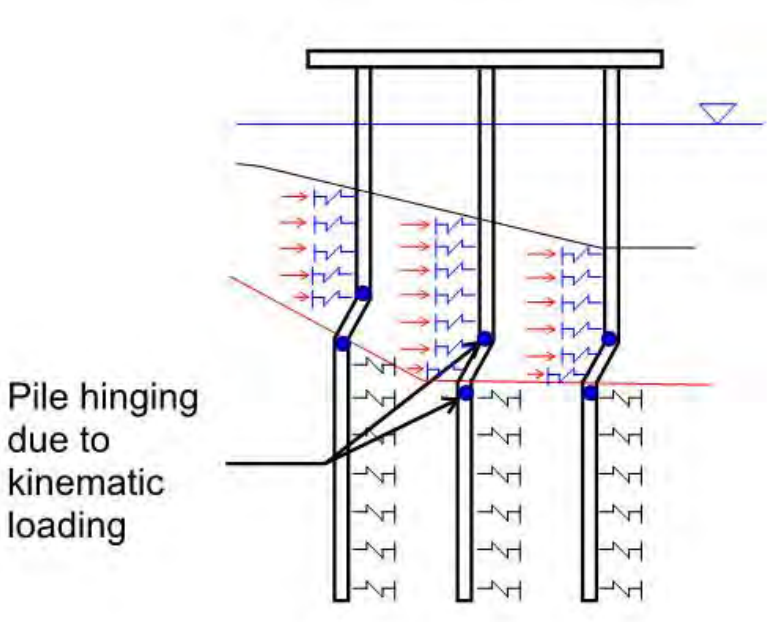

Figure 2b: Typical Pile Hinge Locations for Kinematic Loading

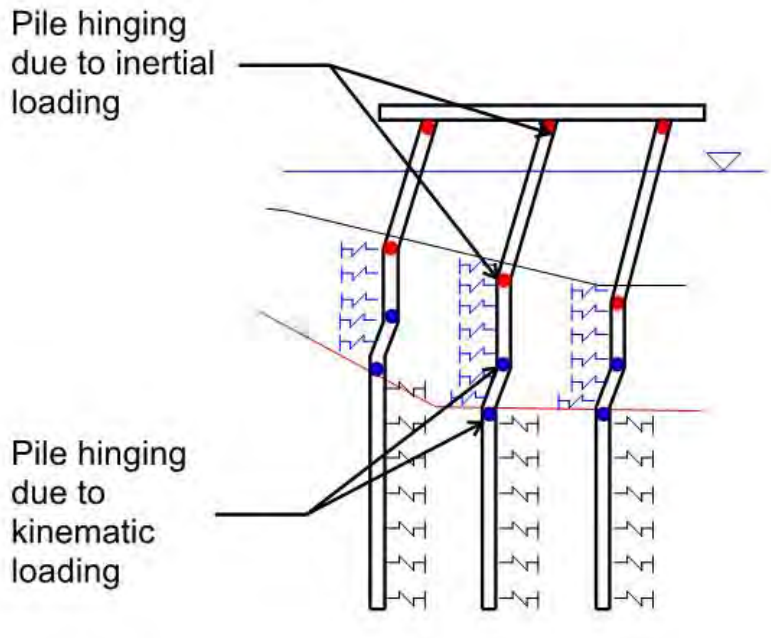

Figure 2c: Combined Pile Hinge Locations for Inertial and Kinematic Loading

When choosing to combine kinematic and inertial responses, there are multiple methods with varying capabilities and limitations. The concepts behind each of these methods, and the advantages and disadvantages of each, are discussed in the following subsection.

2.1 Superposition Method

The superposition method is the easiest method for combining inertial and kinematic effects, from an analytical standpoint; but it is also the least accurate, and generally provides very conservative results. This method allows the design professional to perform independent, uncoupled analyses for inertial loading and kinematic loading conditions. The results, in terms of component demands, are then combined additively. This typically results in an overestimation of pile flexure because each analysis starts from zero displacement, ignoring the preloaded wharf state that is accounted for in the other methods, and therefore moving the pile up the elastic portion of the moment-curvature response twice, versus the lower slope of the secondary stiffness portion of the curve.

Also, with this approach, the inertial demand is based on a non-liquified, or static, soil stiffness. For many wharf structures the soil stiffness is significant in computation of the demand displacement (which is a function of the effective period squared and the spectra acceleration at the initial stiffness). In some cases, the difference between static soil stiffness and liquified soil stiffness can result in significant differences in computed demand displacement.

For structures that remain elastic, the superposition of element forces is a reasonable approach. However, in most cases marine structures experience nonlinearity during the design earthquake; and this method will overpredict demands for those piles. Typically, the authors do not use the superposition method in practice, and instead opt for a combined analysis approach.

2.2 Post-Inertial Combination

This method follows the premise that significant ground shaking will occur prior to the liquefaction of the soil. However, this method is somewhat complicated to model, and requires a bit of uncertainty in the assumptions. Soil springs used to represent lateral stiffness of the soil change between initial ground shaking and after entering a liquefied state. This behavior can be accounted for in a more sophisticated structural model that includes staged loading (sometimes called ‘construction staging’) and changes in the support restraint conditions. An inertial demand can be applied with one type of soil spring active, imparting loads and displacements on the structure. This requires the engineer to have already determined the demand displacement. Then, the soil springs can be changed, and kinematic displacements added to the already displaced structure.

The fundamental issue with this method is that calculated inertial demand displacement is not a residual displacement, but an estimate of max displacement during a design seismic event. Applying the kinematic demands to the inertial demand displacement can be quite conservative. A better implementation of this method would be to apply kinematic displacement to the residual inertial displacements, but the residual displacement is typically not calculated in a pushover type of analysis. Due to the complicated nature, and uncertainties involved, the authors generally do not use this approach. The preferred approach of applying inertial demands to a post-kinematic analysis is described in the next section.

2.3 Post-Kinematic Combination

In a broad sense, this method involves application of kinematic demands prior to inertial demands. This method is commonly used in the industry and provides results that best represent actual behavior, short of performing numerous dynamic time-history models. This approach utilizes a single structural model with soil springs representative of a liquified condition. The kinematic displacements (or pressures) are first applied to the structure as a nonlinear static analysis. This will result in a structural displacement that preloads the foundation. The inertial pushover is then started from the end of the kinematic load case. Demand displacements are calculated from the pushover curve using either the Substitute Structure approach (ASCE 61-14 and CBC 2016) or the Coefficient Method (CBC 2016), just as would be done for a site without kinematic effects, except that an initial displacement is present at the start of the pushover. The calculation of displacement demand is simply adjusted to account for that initial displacement associated with the kinematic effects. An illustration of this pushover analysis is shown in Figure 3. Inertial demand displacement is calculated as a function of effective stiffness (K_{eff}) and is added to the kinematic displacement to determine the total demand displacement. For further information on the pushover procedures, refer to the relevant standards.

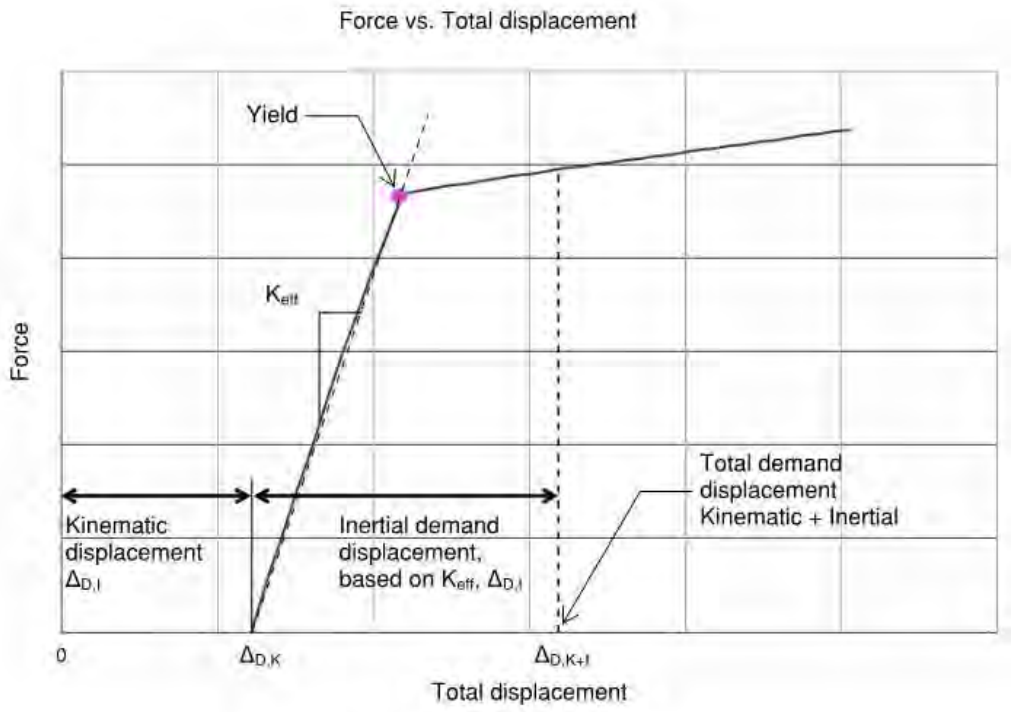

Figure 3: Pushover Curve for Kinematic plus Inertial Analysis

This method also allows for easy adjustments to the magnitude of either kinematic or inertial forces. The percent of inertial demand can be adjusted simply by scaling the response spectrum within the pushover demand procedure. The percent kinematic demand can be adjusted by the magnitude of force or displacement applied in the initial step. For example, if the geotechnical engineer has recommended combining 100% kinematic plus 50% inertial demand; the response spectrum acceleration is multiplied by 0.5 within the demand displacement equation. The actual percentages used in these combinations is determined based on considerations of the site-specific parameters and engineering judgement, as discussed earlier in this paper.

3. MODELING FOR KINEMATIC ANALYSIS

This section has general recommendations for analyzing seismic inertial and kinematic loading.

3.1 Soil Spring Definitions

Soil-structure interaction on a pile supported structure is typically modeled with multilinear springs. The spring properties depend on several factors including soil type, pile cross section, depth, and loading scenario. The geotechnical engineer provides the soil spring stiffness parameters and accounts for the uncertainty of the soil when developing the springs. Seismic inertial analysis is typically performed with both upper bound and lower bound sets of soil spring parameters, whereas kinematic analysis only requires median or best-estimate soil springs.

The best-estimate springs are used for the kinematic condition as they generally are the upper bound stiffness for the liquified soil condition, which is responsible for initiating the lateral spreading and kinematic loads. Stiffer springs (or the inertial upper bound ones) are considered to be an unrealistic load condition as these stiffer soils are not likely to liquefy and produce kinematic load conditions. Lower bound springs are generally not considered in the kinematic analysis despite predicting larger slope movements as these softer springs tend to also have less resistance, resulting in lower demands on foundation elements.

Horizontal (P-Y) soil springs provide lateral resistance to plumb piles. Battered piles, which resist lateral loads primarily through tension and compression are modeled with axial (T-Z) springs that represent skin friction on the circumference of the pile. End bearing resistance can either be modeled with a one-directional (Q-Z) spring or a simple vertical support, as recommended by the geotechnical engineer.

Analysis can be sensitive to soil spring spacing and element discretization. Spring spacing should be reduced near locations of anticipated pile hinging such as the mudline elevation and the interfaces of soil layer changes to improve discretization of the foundation system analytical model.

3.2 Application of Kinematic Loads

Kinematic loads can be applied indirectly as fluid pressures or as support displacements on soil springs, as illustrated in Figure 4 and Figure 5, respectively. Both approaches require modification to the soil springs from their static condition, within the liquified soil layer. If soil displacements are expected to exceed the plasticity of the soil, it is a reasonable simplification to apply the soil pressure as the maximum fluid pressure from the liquified layer (and any material above it) and remove soil springs completely within that layer.

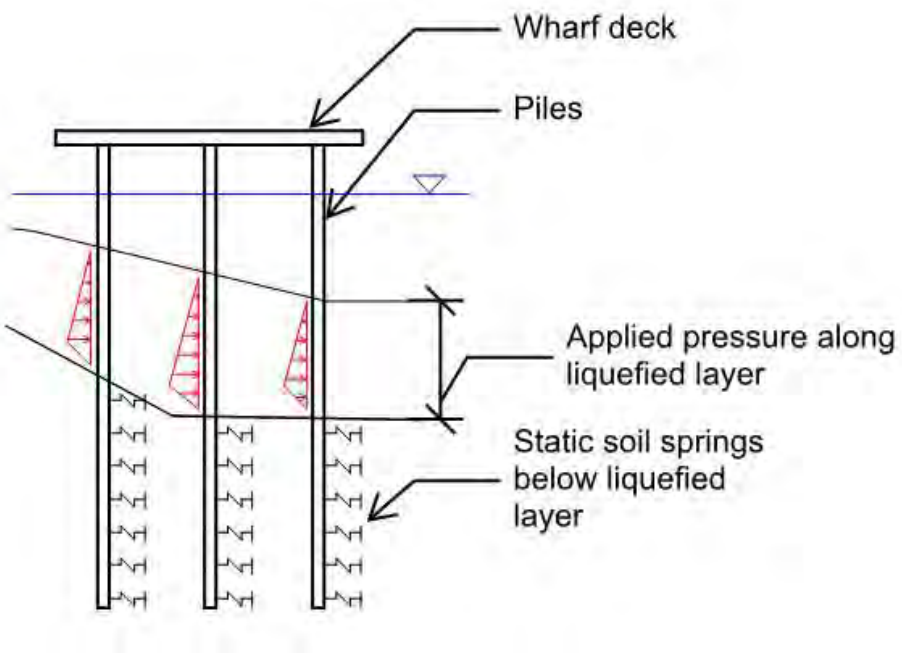

Figure 4: Kinematic Load Applied as Fluid Pressure

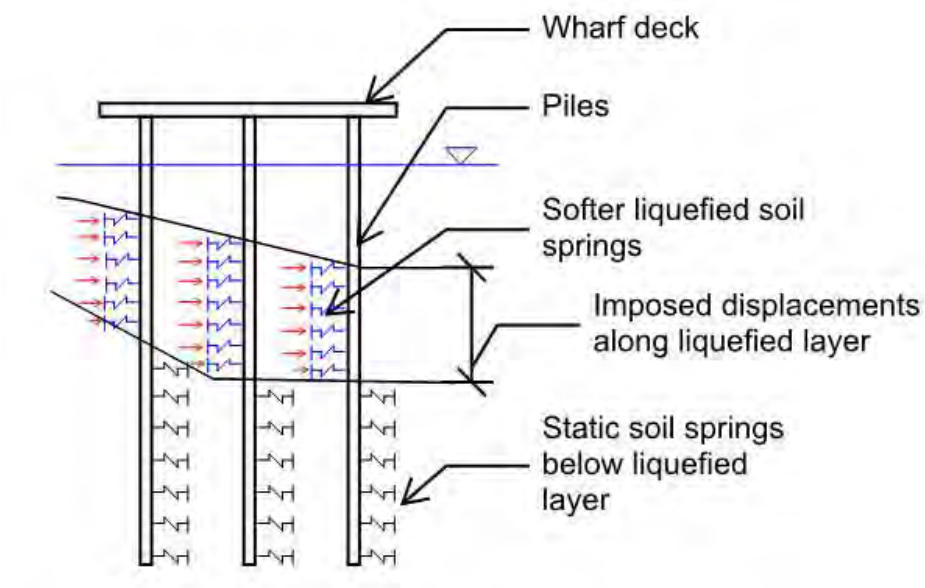

Figure 5: Kinematic Displacement Applied at Softened Soil Spring

The geotechnical engineer provides the kinematic load effects and the recommended soil spring parameters. Their geotechnical analyses may provide complex soil displacement profiles, but these are commonly simplified to a multi-linear profile. Similarly, soil springs are typically modeled as a symmetric tri-linear curve.

3.3 Pile Hinges

Pile hinges are applied consistent with general practice for inertial loading. Hinges are recommended at locations of anticipated damage such as the pile-deck connection, mudline location and soil layer changes. Pile hinges are developed based on cross sectional moment curvature response at relevant axial loads. Performance points can also be defined within the hinge to monitor performance. The limit states are defined by code prescribed material strain limits to represent different damage criteria, such as immediate occupancy, life safety, and collapse prevention. Based on project criteria, these hinge states can also be compared to different demand displacements using corresponding levels of seismic response spectra. An example would be checking “life safety” strain limits for the high intensity but low probability earthquake but limiting strain limits to “immediate occupancy” for moderate intensity but more frequent earthquakes. The recurrence interval that corresponds to each limit state is typically defined in code criterion.

A recommended approach is to first perform separate inertial and kinematic analyses to determine the location of hinging and overall utilization under separate seismic effects As noted above and shown in Figure 2, the first instance of hinging typically occurs in different locations. The compound effects of the kinematic and inertial combination depend on the relative proximity of the expected hinges. In many instances there is only a minor impact of combining inertial and kinematic effects due to the separation of hinge points. However, there are also cases where the in-ground inertial and kinematic hinges occur at close proximity and thus the combination has a more significant impact.

3.4 Non-ductile elements

Non-ductile components such as pile caps, decks and shear in piles should account for over-strength in pile flexural hinge capacity. The over-strength of the pile in flexure is calculated using upper bound expected material strengths instead of design strengths. Piles can have significant over-strength in flexure, which increases the demands on non-ductile components. This approach is consistent with capacity design where the goal is to have a ductile response mechanism instead of a brittle or sudden failure. Piles with a short freestanding height, and piles which penetrate a suddenly dense layer, such

as a rock dike are more susceptible to shear demands from either inertial ground shaking or kinematic soil displacement.

4. CONCLUSION

This paper describes some rational approaches for analyzing waterfront structures for kinematic effects, as well as presents some tips for modeling this behavior using a finite element analysis program.

Kinematic load conditions are coupled with inertial loads and need to be considered in combination. To better predict an appropriate degree of coupling, a geotechnical time history analysis may be used to estimate load combinations for various earthquake ground motions for a specific site. However, since this approach involves significant time and resources, a combination is often selected by engineering judgement and experience considering the specifics of the project site.

Three methods of combining the kinematic and inertial effects are discussed herein. The preferred approach is a post-kinematic inertial combination, which involves an inertial pushover analysis using a starting displacement reflective of kinematic effects.

Kinematic effects can be incorporated into a finite element analysis as either displacements or fluid pressures. Some other key modeling parameters, discussed herein, are soil springs, pile hinges, and the consideration of non-ductile components.

5. REFERENCES

1. ASCE 61-14 (2014) Seismic Design of Piers and Wharves, American Society of Civil Engineers (ASCE/COPRI), Reston, VA.

2. California Building Code (CBC 2016), Chapter 31F, Title 24, Marine Oil Terminal Engineering and Maintenance Standards (MOTEMS), California State Lands Commission, Sacramento, CA.

3. “Chile Earthquake and Tsunami of 2010: Performance of Coastal Infrastructure”, Edited by Billy Edge, Prepared by the Port and Harbor Facilities Field Survey Team of the Coasts, Oceans, Ports, and Rivers Institute (COPRI) of the American Society of Civil Engineers. 2013.

4. Dickenson, S., Yang, S., Schwarm, D., and Rees, M., “Design Considerations for Kinematic Loading of Piles”, Proceedings of Ports '16: 14th Triennial International Conference, June 2016.

5. “Haiti Mw 7.0 Earthquake of January 12, 2010, Lifeline Performance”, Edited by Curtis Edwards, ASCE Technical Council on Lifeline Earthquake Engineering (TCLEE), TCLEE Monograph No. 35. 2012.

6. “Tohoku, Japan, Earthquake and Tsunami of 2011: Survey of Port and Harbor Facilities, Northern Region”, Edited by Marc Percher, Prepared by the Port and Harbor Facilities Field Survey Team of the Coasts, Oceans, Ports, and Rivers Institute (COPRI) of the American Society of Civil Engineers. 2014.

7. Port of Long Beach Wharf Design Criteria, POLB WDC Version 3.0, February 29, 2012.

8. Port of Los Angeles Code for Seismic Design, Upgrade and Repair of Container Wharves, City of Los Angeles Harbor Department, May 2010.

Ship Handling Simulation in Approach Channel and Harbour Design

by

Carl-Uwe Böttner[1]

ABSTRACT

Ship handling simulation became a basic and vital part of training of seafarers all over the world. Along with the ever increasing fidelity of the simulators available, they were used more and more regularly for other purposes like feasibility studies, whereas the aspect of no risk for life and environment is paramount. Nevertheless, the demands and requirements of proofs of concept and approachability checking on the simulation and simulator technology differ from those of training and education. There is a huge overlap, which makes use of full mission bridge installations at nautical schools and training centres for approachability checking so widespread and common, but also some substantial differences. This contribution discusses the strengths and weaknesses of full mission bridge simulation applied to channel approachability and harbour layout checking.

1. INTRODUCTION

Ship handling simulators are part of the education schedule of mariners and nautical personal. Training is mandatory according to the STCW-95 convention adopted by the IMO and there is a procedure of certification installed by the classification societies. For instance the Norske Veritas alone lists 164 Simulators world-wide, certified to their standard “2.14 Maritime Simulator Systems”. There is a long history of constant development and improvement before the simulators in the training centres reached the level of fidelity today’s full mission bridge installations offer. It started with small heading control handles and a radar screen for radar training and later on followed the development and improvements of computational power and instrumentation installation aboard ocean going ships. A major step towards enhanced training experience was the availability of full integrated bridge installations together with recognizable pilotage areas in the display system of the environment. The fast development and tremendous efforts of the gaming industry was helpful to gain ever better and deeper levels of virtual reality, also for this kind of so called serious games. The viewing systems of today’s ship handling simulators display spray of water at the bow, shadows, reflections on water, different colouring according to solar altitude, starry sky at night, moon phases, glare of deck lights and lantern ashore and the like.

It is well accepted from simulator training research that the level of immersion into the scenery and the exercise requires a certain degree of realistic, which is easily interrupted or even abruptly destroyed by any disturbance from outside and/or an unexpected and unrealistic appearance in the virtual reality. An unnatural behaviour experienced by the trainee abruptly changes his perception from being in the scenery to being part of a computer game – which obviously has to be avoided as far as possible.

With the availability of full mission bridge simulators and well recognizable displays of the environment, the use of these assets for approachability and harbour layout checking started. It is an alluring offer to approach a channel or a complete harbour with all buildings before breaking ground.

In the past decade there was a trend towards tailored and specifically developed simulators in the maritime field. Today, there are simulators available for training of very specific skills, to name a few: manoeuvring in ice, offshore and harbour tug operations, emergency salvage tugging, crane handling

[1] Bundesanstalt für Wasserbau, Hamburg, Germany. carl-uwe.boettner@baw.de

on board, offshore supply vessel operations, ship to ship operations and lightering, dynamic positioning, search and rescue, firefighting and so on.

Some of the specific task simulators required additional and/or refined manoeuvring and ship dynamic models to reach the required level of reality. Each further development of dynamic models is a gain in capabilities also for using the simulator in terms of layout checking. This is important since the demands on a ship handling simulator differ for training to checking of approach channels and harbour layout design.

2. DIFFERENT DEMANDS OF TRAINING AND CHECKING

Training at the ship handling simulator aims at gaining experience and application of freshly acquired knowledge. Usually there are scenarios and sceneries prepared to specifically answer to this need. The simulator's hardware needs to provide every single instrument and handle the student needs to fulfil the particular task. Furthermore it is required that the simulated environment including the vessel under command acts realistic, but it is not necessarily precisely a certain ship and channel.

As for training and education purposes, the aim of the simulator study needs to be defined first when a ship handling simulation is considered for checking of channel and harbour design. After the aim is precisely defined, there are many significant differences to a simulation for training. It is mainly the level of detail of almost every aspect which has to be higher or go deeper.

Based on the gist the scenarios to be examined are chosen, this is a general habit. For training purposes reasonable and regular conditions of wind and visibility, sea state and so on are chosen suitable to the task. In the case of a definite pilotage area and location, the selection of environmental conditions requires careful consideration in terms of specific local peculiarities and demanding or risky nautical situations. At the best the decision on the environmental conditions is based on the statistical analysis of long term measurements in the particular area and agreed on by all parties involved.

The next step consists of proper tuning of the ship dynamics in the simulator. For training it is usually sufficient to match a typical behaviour of a ship of the particular size and type. If the simulation is the basis for later authoritative decisions, usually on speed or size limits, the conformance of the modelled ship dynamics with the particular ship in operation in the area needs to be satisfactory high. This is a demanding task; on the one hand results of sea trials are rare and usually not performed at recommended weather conditions. On the other hand even if reliable sea trials are available, the adaptation of the simulator's manoeuvring model to match the data is not trivial.

In the vast majority the pilotage areas, approach channels and harbours constitute shallow water conditions to the ships sailing there. This is further demanding for the simulator's mathematical model of ship dynamics, especially since sea trials in shallow water are scarce to not existent. Shallow water effects are more or less prominent, depending on the proportion of under keel clearance to the ship's draft. For small values the shallow water effects become dominant and alter the deep water manoeuvring characteristics of the particular ship completely. There is ongoing research in generalized mathematical modelling of shallow water effects, but for the time being the tuning of the simulator model still relies on the experience and knowledge of the personal in charge.

In approach channels the waterway is not only restricted in water depth, but also in width by side walls or banks. Amongst other effects the shallow water conditions include ship to bank interactions, which shall serve as an example for illustration. The ship to bank interaction may lead to unsafe situations or cause accidents if the ship gets close to bank's side at higher speed. The effect is a combination of a sucking force towards the bank accompanied by a bow-out moment changing ships heading. Therefore the occurrence and the intensity of the effect are eminent for a channel to be approachable for a particular ship, and accordingly the model's tuning gets a dominant role in the

set-up of the simulation. A sophisticated and sufficiently accurate mathematical model of this effect in combination with careful calibration is essential for the simulation's success if this effect is considered prominent for the approach channels width declaration.

It is a quarter of a century ago, that recommendations on set-up of ship handling simulations and evaluation of mathematical models were felt missing and according reports were assembled by specialists groups in the US [Webster (ed.) (1992)] and international [PIANC (1992)]. Today, 25 years later, there is a further report in progress which shall update the latter one as well as serve as kind of a handbook and reference for use of ship handling simulation to approach channel and harbour layout checking.

3. HUMAN ELEMENT IN SIMULATION

Basically the human element is the reason for setting up a scenario and using a full mission bridge simulator when checking an approach channel or a harbour layout. Otherwise, pure geometrical considerations supplemented by mathematical-physical calculations were sufficient.

Besides this elementary premise, the human element is inherent in almost all steps of a simulation. One of the most important parts of the simulation process is the validation of the existing conditions. Experienced pilots familiar with the pilotage area judge the simulator's ship behaviour and environmental effects calibration based on their expertise to be as realistic as considered necessary.

Another part consists of the experience and psychological effective acting of the instructors of the simulation. Mainly their expertise keeps the level of immersion in the simulation at the required level and to gain meaningful results. This especially includes the ability to spontaneously react on difficulties and incidents of misbehaviour of the simulator by work-arounds they can find due to their deep knowledge of the facility.

Even more difficult is to balance the typical gap between the expectations which result of a properly set-up simulation and the actual level of mathematical-physical modelling. A careful and experienced prepared simulation, even more in combination of today's display systems and their photo-realistic capabilities, creates the impression of a perfect virtual reality. This often leads to unrealistic and excessive expectations on the results of the simulation by the spectators not directly involved. But also the pilots may experience similar impressions and conclusions and ending up with a less reflected judgement of the nautical situations based on the fact that it worked easy in the simulator.

The most important and the most difficult part of a simulation to check a new and nautically unknown harbour layout or approach channel is the evaluation of the experience in the simulation performed. To harvest the first impression and first thought, it is essential to have sufficient debriefing after each exercise or run. But the complete judgement can only be done after the whole figure of situations is simulated and checked. The challenge consists in a proper division of individual experience and opinions to get an honest, appropriate and reliable judgement of the nautical situation which is the basis to draw correct conclusions.

Therefore, the success of such a simulation basically depends on the ability and the honest support of each participant, especially the pilots on the simulator's bridge to bring in their expertise to properly evaluate each run. It is essential that the pilots compare the result of a simulation, how deep and close to perfection the immersion into the virtual reality has ever been, with their experience and reflect openly and with good grace what they have experienced in the simulation some minutes ago on their knowledge of the particular pilotage area and experience in ship handling.

4. SUMMARY

Ship handling simulators equipped with full mission bridges and fitted with real instruments are the only and a very efficient tool to judge and check new approach channels and harbour designs before being build. Continuous development and improvement of mathematical-physical models together with increasing computing power and photo-realistic displays make the SHS paramount to any other approach, as long as the flaws, drawbacks and imperfections of this virtual reality are known to the involved parties and are considered in the evaluation phase of the results. The report of the PIANC WG 171 aims at spreading the knowledge on the actual performance of state of the art ship handling simulator technology as well as providing recommendations on further development and improvements by scientific research on ship hydrodynamics as well as of the software and hardware available for full mission bridge ship handling simulators.

References

PIANC (1992) Capability of ship manoeuvring simulation models for approach channels and fairways in harbours. Report of Working Group No. 20 of Permanent Technical Committee II. Brussels, Belgium: General Secretariat of PIANC (Supplement to Bulletin no. 77 (1992))

Webster, W.C. (ed.) (1992), Shiphandling simulation. Application to waterway design. National Research Council (U.S.). Washington, D.C: National Academy Press. Online available: http://search.ebscohost.com/login.aspx?direct=true&scope=site&db=nlebk&db=nlabk&AN=14163.

EXPERIMENTAL INVESTIGATION ON SUBMERGED REEF

Rahul Dev Raju[1], Sakthivel S[3], Saikat De[2], Sundaravadivelu R[2], Anbazhagan K[4], Ramanamurthy M.V[5] , Panneer Selvam R[2]*

ABSTRACT

Submerged artificial reef have multipurpose benefits. They have great potential for environmental and recreational benefits in addition to shoreline protection and stabilisation. One such reef was proposed along the southern coast of Indian peninsula. As a part of studies experiments were performed to measure wave transformation and breaking over the physical model of the submerged reef with triangular steel wedge connected to shore and with a scale of 1:10. Experimental studies have been carried out to study the details of wave transformation and breaking over the submerged reef for regular wave in head sea condition and influence of water levels on breaking and wave transformation. The effect of design parameters like wave height, wave period and submergence depth of the reef were assessed from experiments. The results show that the relative water depth over the reef crest is a major factor influencing the breaking and transformation characteristics. The paper also covers the impact of submerged reefs on the waves and generation of secondary waves when the incident wave period is large and seaward slope of the reef is gentle. It is inferred from the experiment that waves break over the submerged reef dissipating most of the wave energy.

Keywords: Submerged artificial reef, Wave transformation, Wave breaking, Transmission coefficient, Steel wedge reef, Submergence depth.

1. INTRODUCTION

Coastal areas are subjected to geomorphological changes due to natural and manmade activities. Artificial reef is considered an effective way in preventing coastal erosion due to its multipurpose benefits as compared to other shore protection methods. Artificial reefs are manmade underwater structure built to promote marine life, coastal protection, shoreline stabilisation and recreational activities. Due to increased use of artificial reefs in coastal environment, it is necessary to study the various design parameters of these reefs as the behaviour of waves and beach in presence of these artificial reefs is not well established. Also there is no fixed model or design of these reefs available.
Wide crested submerged reefs dissipate the incoming wave energy by forcing waves to break on top of the reef thereby drastically reducing the wave energy reaching the shore. Wave attenuation also occurs due to turbulence and nonlinear interaction between the reef and the incoming waves. Waves in the leeward side will be shorter and smaller and help in accumulation of sediments. These types of offshore reefs are custom-designed to trap sediment for each unique zone for different application. Due to various complexities associated with wave attenuation, breaking and refraction, numerous physical and numerical model tests were performed to determine the reef configuration.

Beji et al. (1993) did experimental studies to observe the various process of refraction, diffraction, shoaling and breaking of wave propagating over an offshore bar. The generation of higher harmonics in wave propagating over a submerged obstacle has been long known but the investigation aimed at the phenomenon of de-shoaling and wave decomposition which takes place for both non-breaking and breaking waves passing over a bar. Masselink (1997) conducted a field investigation to study generation of secondary wave during wave propagation over an offshore bar. The results of the experiment showed the decomposition of breaking incident swell into smaller and shorter waves upon entering the deeper water across the bar.

---

[1]Department of Ocean & Mechanical Engineering, Florida Atlantic University, Florida, USA
[2]Ocean Engineering Department, IIT Madras, Chennai, India
[3]Ocean Engineering & Consultancy Private Limited, Chennai, India
[4]Hitech Civil Engineers Private Limited, Port Blair, Andaman & Nicobar Islands, India
[5]National Institute of Ocean Technology, Chennai, India
[*]Presenting author email:pselvam@iitm.ac.in

The generation of secondary wave drastically reduced the wave energy hitting the beach. Blenkinsopp et al. (2008) performed experiments to show that wave transmission and breaking is affected by the water depth over the crest of the offshore reef. There was considerable increase in wave breaking, decrease in wave transmission and reflectance observed with the reduced crest submergence. Harris (2009) elucidates two mechanisms of wave attenuation and wave refraction by which submerged breakwaters assist with shoreline stabilisation. Kamath et all (2015) stimulated wave propagation over a bar and compared numerical results with the experimental data. The wave transformation was clearly observed as the wave propagated over the upward slope of the submerged bar.

In this paper the experimental investigation of wave transformation and breaking over the submerged reef with triangular steel wedge connected to shore is carried out. The submerged reef was tested for regular and random wave at different water levels in Shallow Wave Basin at IIT Madras, India. The reef is designed for conditions of South East Coast of India. The reef makes an angle of 13° with respect to the shore line and envisaged to trap the sediments from the long shore sediment transport. The submerged reef has a triangular wedge-shaped steel structure with armour stones and concrete cubes, the first of its kind in India. The main part of the submerged reef is triangular shaped steel wedge weighing 900 t (in prototype) with dimensions 60 m × 50 m × 2.5 m with slope on either side resting on stone bed. The model studies were carried out in 1:10 model scale for head sea condition with wave heights 5 cm to 15 cm with wave period 1.9 s to 3 s. The present paper describes the experimental study details of wave transformation and breaking over the submerged reef for regular wave in head sea condition. The influence of water levels on breaking and wave transformation is also studied.

2. EXPERIMENTAL SETUP

2.1 Test Facility

The experiments were carried out in the Shallow Wave Basin of the Department of Ocean Engineering, Indian Institute of Technology Madras, India. The basin has length of 19 m, width 15 m and height 1 m. Experiments were carried out for three different water levels i.e 50 cm, 54 cm and 58 cm.

The Shallow Wave Basin is equipped with a wave maker with five piston type paddles operating at one end, through a servo actuator with a remote-control system, used to generate both regular and random waves. This is executed with a personal computer connected to the servo activator and another computer is dedicated for data acquisition of the signals from the wave probes and run-up meter through an amplifier. An artificial beach (wave absorber) on the other end is provided with the combination of parabolic perforated Fiber-Reinforced Polymer (FRP) sheet and rubble mound to absorb the waves. The top view of the shallow wave basin with the test model is shown in Figure 1.

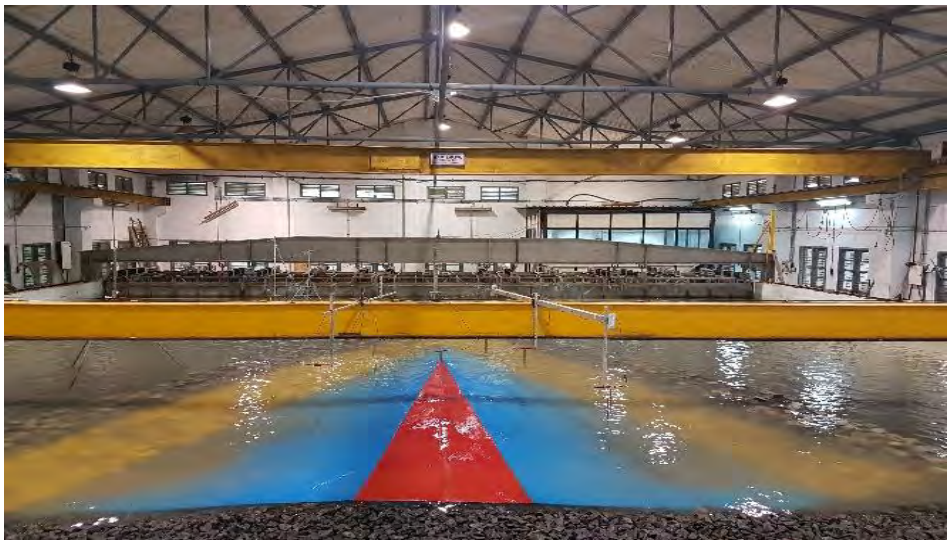

Figure 1: Top view of the experimental set-up in the shallow wave basin of IIT Madras

2.2 Test model

A submerged triangular reef is constructed using 2.5 mm thick IS 2062 grade steel sheets with base length 5 m and base height 6 m. The steel wedge consisted of top horizontal plate of base 1 m and length 4.5 m. The top horizontal plate is followed by slope of 1:0.8 on both the sides. The steel wedge has a height of 0.25 cm and installed in the basin with the toe of the wedge 7.3 m from the wavemaker. The horizontal crest of the steel wedge was at the water level for 50 cm water depth. Around the steel wedge at the opposite end of the wave generator in the basin, a beach with a 1:20 slope was made using 20 mm aggregate. The experimental setup inside the shallow wave basin is shown in Figure 2.

Armour stones of average size 5 cm was placed all around the steel wedge for a length of 1 m. Stones were placed for a depth of 10 cm(in vertical direction 2 layers) to prevent toe scour. Additional concrete cubes of size 10 cm with 2cm holes on all the six sides was place all around the armour stone for a length of 0.5 m. Concrete cubes with holes were placed in random for a depth of 20 cm to dissipate the wave energy and prevent scour erosion as shown in Figure 3.

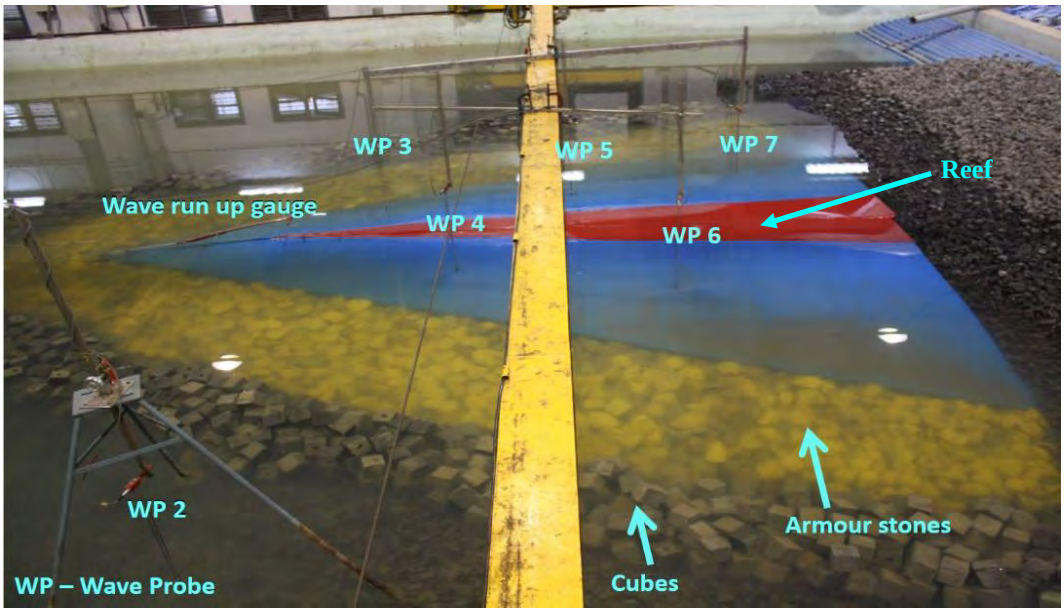

Figure 2: Experimental set up (1:10 scale) at shallow wave basin at IIT Madras

Figure 3: Armour stones and concrete cubes with holes

2.3 Instrumentation

A total of seven wave probes and a run-up meter was used during the experiment. The first wave probe (WP 1) was installed in front of the submerged reef structure at 5 m from the wavemaker to measure the incident wave. The second wave probe (WP 2) was placed over the beach at 11 m from the wave maker and 3.7 m away from the centre of the steel wedge. A further of five wave gauges (WP 3 to WP 7) were installed over the submerged reef to measure the transmitted waves in the water section near the beach end of the basin after breaking. The run-up meter (WP 8) was installed on the tip of the steel wedge to register the run-up. Location of various wave probes and runup meter is shown in the Figure 4.

The wave probes were calibrated before installation. The signatures from seven wave probes and one run-up meter, were simultaneously acquired and recorded by a personal computer loaded with data acquisition software. The signals from the measurements were recorded with a sampling interval of 0.02 s. For the present study, one personal computer connected to servo actuator was used to give the required wave height and wave period to the wave generator. Another personnel computer was used for data acquisition with application software package.

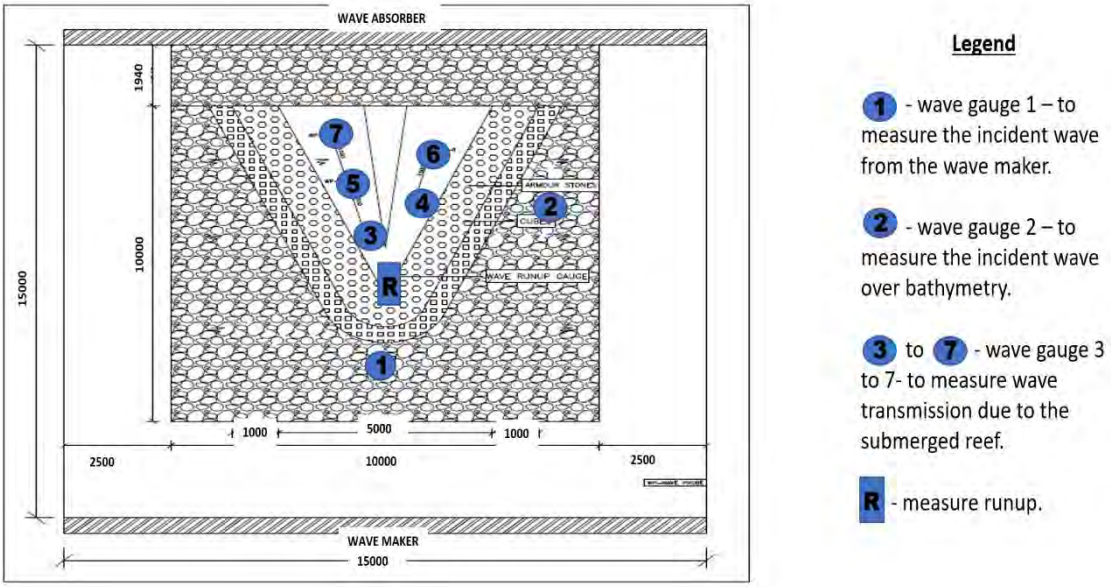

Figure 4: Location of various wave probes and runup meter at shallow wave basin

2.4 Experimental program

During the experiment the test were conducted for three different water levels i.e 50 cm, 54 cm and 58 cm considering both the situation with and without storm surge. Regular waves with different wave heights of 5 cm, 8 cm, 10 cm, 12 cm and 15 cm were generated with various wave period of 1.9 s, 2.2 s, 2.5 s, 2.8 s and 3 s. A total of twenty-five different combinations were realised for the regular wave: five different wave heights and five different wave periods. The tests were conducted for all three different water levels. Thus, a total of seventy-five runs were performed for regular wave.

3. RESULTS AND DISCUSSION

During the experiment typical wave elevation were measured over the submerged reef subjected to regular wave field characterised by input wave height H= 5 cm, and 15 cm; wave period T=1.9 s, 2.5 s, 3 s at various water depth of 50 cm, 54 cm and 58 cm. Visual observation during the experiments and from inspection of chart elevation we concluded that submergence depth, wave height and wave period greatly influence the breaking and transformation of the wave over the submerged reef.

3.1 Submergence depth

Figure 5 and 6 depicts the wave elevation over the reef at various points for H=5 cm, T=1.9 s and H=15 cm, T=3 s for various water depth respectively. The transformation of the wave as it propagates over the submerged reef is computed using the wave probes fixed at various places over the reef. The incident wave on the submerged reef is measured by wave probe(WP1) as shown in Figure 5. The wave is deformed as it moves up the slope of the submerged reef due to shoaling as seen in wave probe 3 (WP3) in Figure 5 (a). The wave reaches the crest of the reef and propagates. The decomposition of wave begins at wave probe 5 (WP5) in Figure 5 (a). The formation of secondary crest after the primary crest is observed. As the wave propagates further over the reef towards wave probe 7 (WP7), the amplitude of wave reduces drastically and secondary and tertiary crests are seen. It is clearly seen that the intensity of wave breaking increases as the water depth and submergence depth of reef crest is reduced. Shallower depth of submergence of the reef, results in greater portion of water column becoming turbulent due to higher air entrapment and energy dissipation. Hence the breaker type of the wave is strongly influenced by the water level over the reef crest.

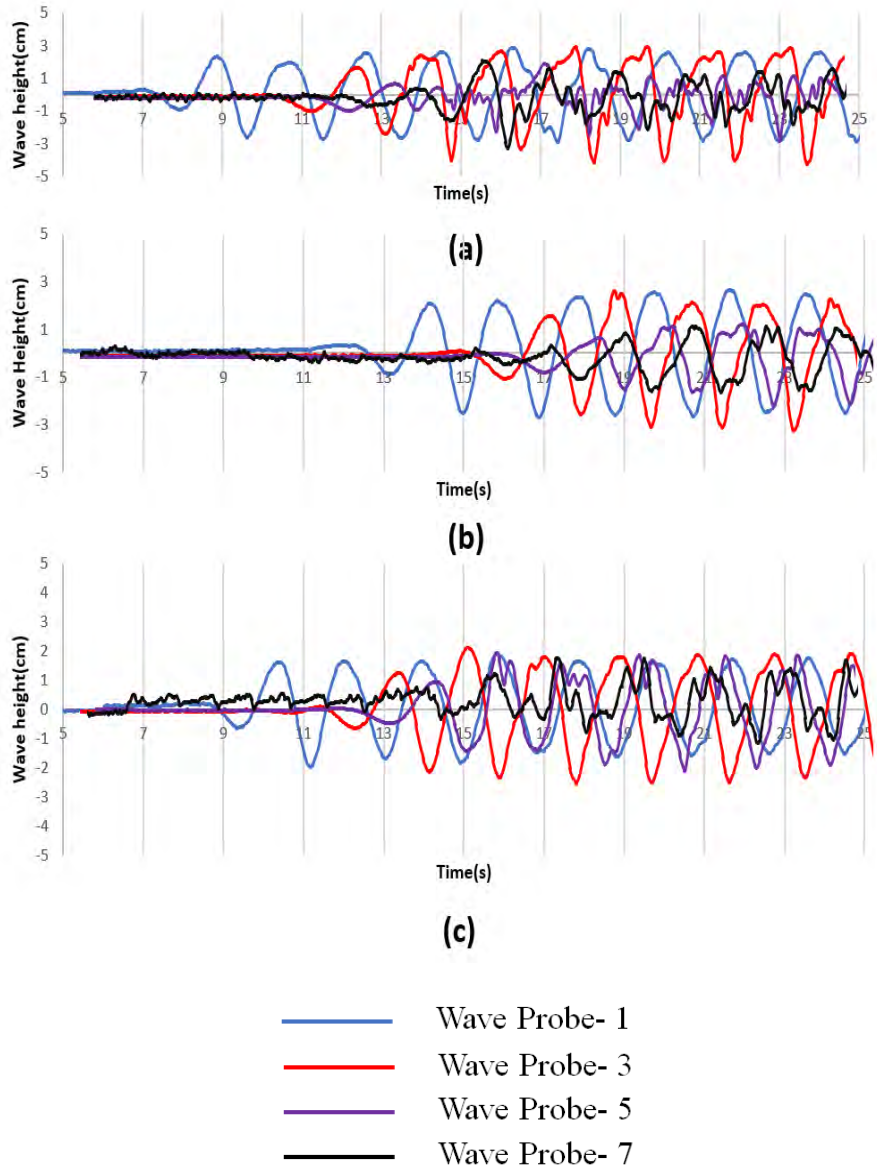

Figure 5: Surface elevation records for wave height 5 cm and wave period 1.9 s for water depth (a)50 cm (b)54 cm (c)58 cm.

3.2 Wave height and wave period

In Figure 5 and 6 it is seen that at wave probes 5 and 7, waves propagating across the reef is predominantly breaking as indicated by observation and suggested by their asymmetric shape. But the wave breaking does not alter the characteristics of the wave form completely; hence it is comparable with its unbroken counterpart.

The pattern of wave transformation in Figure 5 for H=5 cm and in Figure 6 for H=15 cm are similar but with few differences in the transformed wave. There is formation of sharp secondary peaks at WP 5 in Figure 5 as compared to Figure 6. Also the secondary peak is much lower than the primary peak in Figure 6.

Long waves (T=3 s), as they travel upslope of the reef, lose their vertical symmetry and assume saw toothed shape due to generation of primary secondary harmonics. In these waves a very rapid flow of energy begins from the primary wave to higher harmonics which generates dispersive tail waves travelling at nearly the same celerity as the primary waves as mentioned in study reported by Beji et all (1993). Short waves (T=1.9 s) do not develop tail wave as they grow in amplitude but keep their vertical symmetry and appear as higher order Stokes waves.

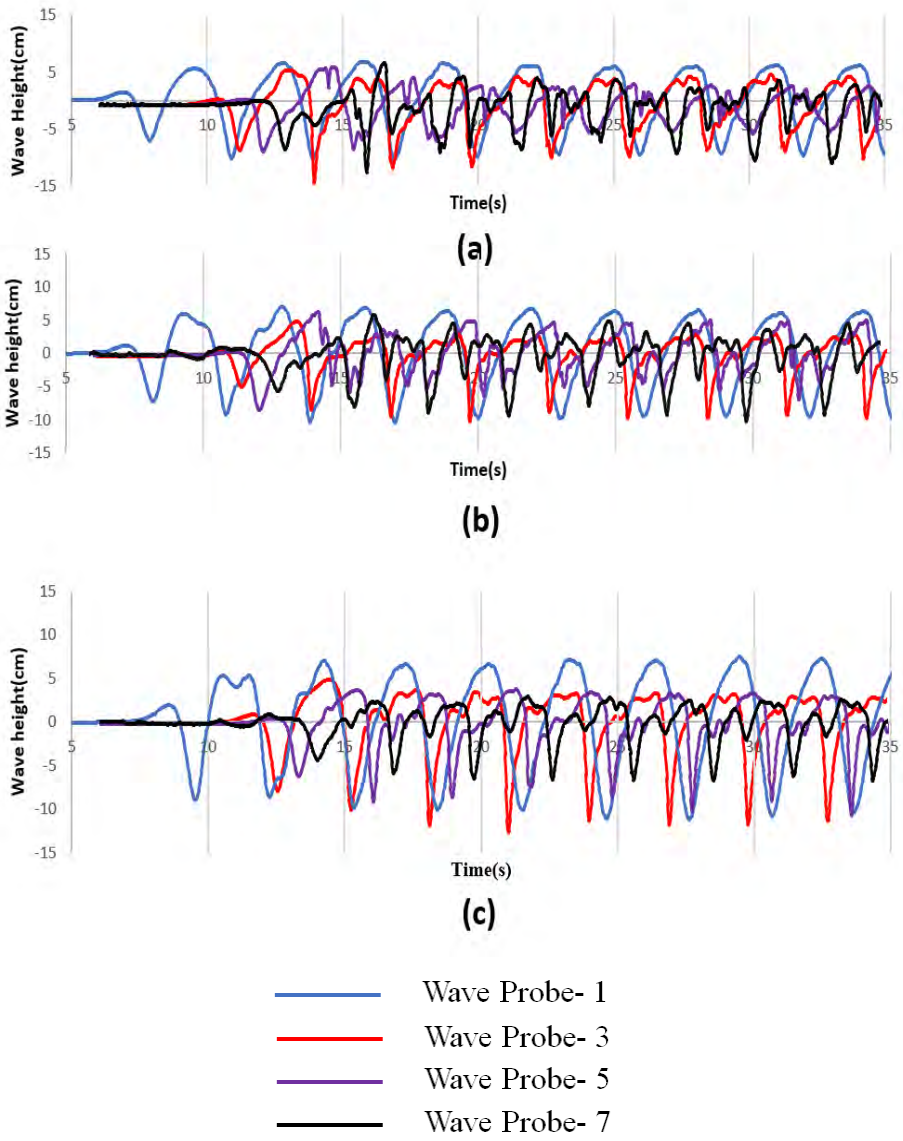

Figure 6: Surface elevation records for wave height 15 cm and wave period 3 s for water depth (a) 50 cm (b)54 cm (c)58 cm.

3.3 Transformation coefficient

Study of wave transformation characteristics of submerged reef is important for calculation of near shore currents, beach evolution and effect of wave forces on the shoreline structures. The transformation coefficient (the wave height(Ht) at different locations (WP3 to WP7) on the reef divided by the incident wave height (Hi), WP1) was found to be influenced by the incident wave conditions (wave height and wave period) and the submergence depth of the reef.

The different locations of the probe from tip of wedge on the reef (D_P) is normalized with the ratio of water depth to height of reef (d/h_r) and the transformation coefficient, H_T/H_i plotted Vs D_P/L_r in Fig7 to Fig10. The transformation coefficient increases from 1 to more than 1.5 as the wave propagates from WP1 to WP3 and then decreases. The non-dimensional parameter submergence depth, d/h_R (h_R is 50 cm and is equal to the total height of reef) and relative wave steepness H/L (L is wave length) are used to study the effect of submergence depth of reef and wave period. The submergence depth of 1,1.08 and 1.16 corresponds to 50 cm, 54 cm and 58 cm water depth respectively. The relative wave steepness varies in the range of 0.056 to 0.038 and the non-dimensional wave height, Hi/d varies in the range of 0.086 to 0.1 for lower wave height and 0.25 to 0.3 for higher wave height. The influence of each wave height and each wave period with all three water depth in the same plot have been evaluated.

Figure 7 and Figure 8 shows the result for lower input wave height (Hi/d), wave period of 1.9 s, 2.5 s and 3 s subsequently for all three submergence depth. Similarly, Figure 9 and Figure 10 shows the result for higher input wave height (Hi/d), wave period of 1.9 s, 2.5 s and 3 s subsequently for all three submergence depth. From Figure 7 to Figure 10, it is concluded that transformation coefficient reduces from as the wave propagates over the reef.

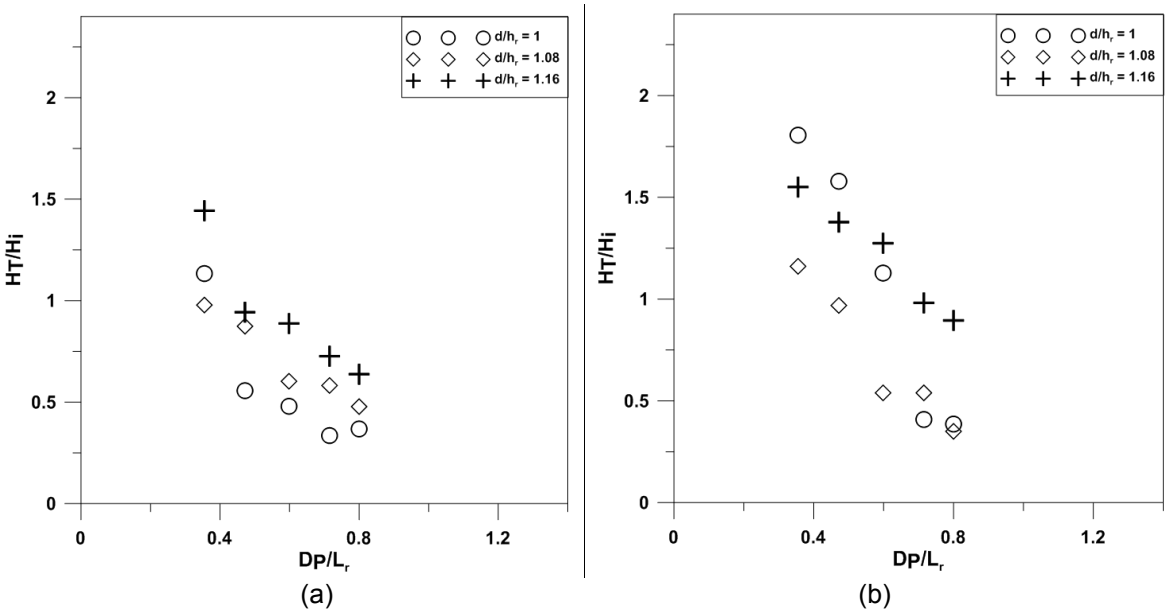

Figure 7: Wave Transformation for L_r/L = 1.48 to 1.56 & H/d = 0.086 to 0.1 (a) and Wave Transformation for L_r/L = 1.4 to 1.48 & H/d = 0.086 to 0.1 (b)

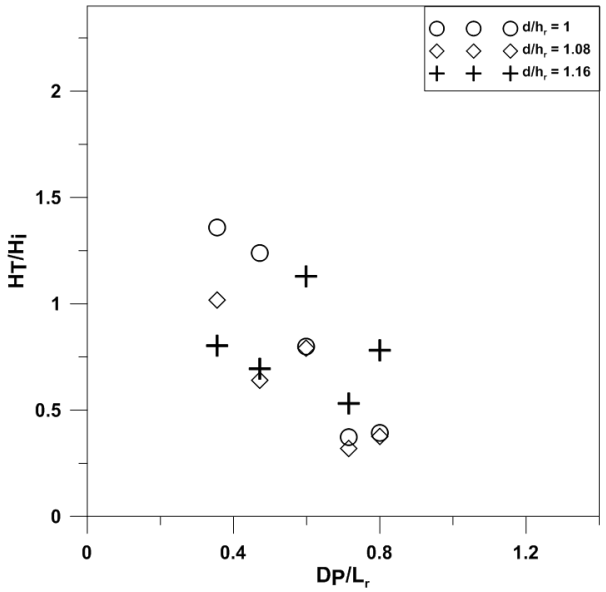

Figure 8: Wave Transformation for L_r/L = 0.88 to 0.93 & H/d = 0.086 to 0.1

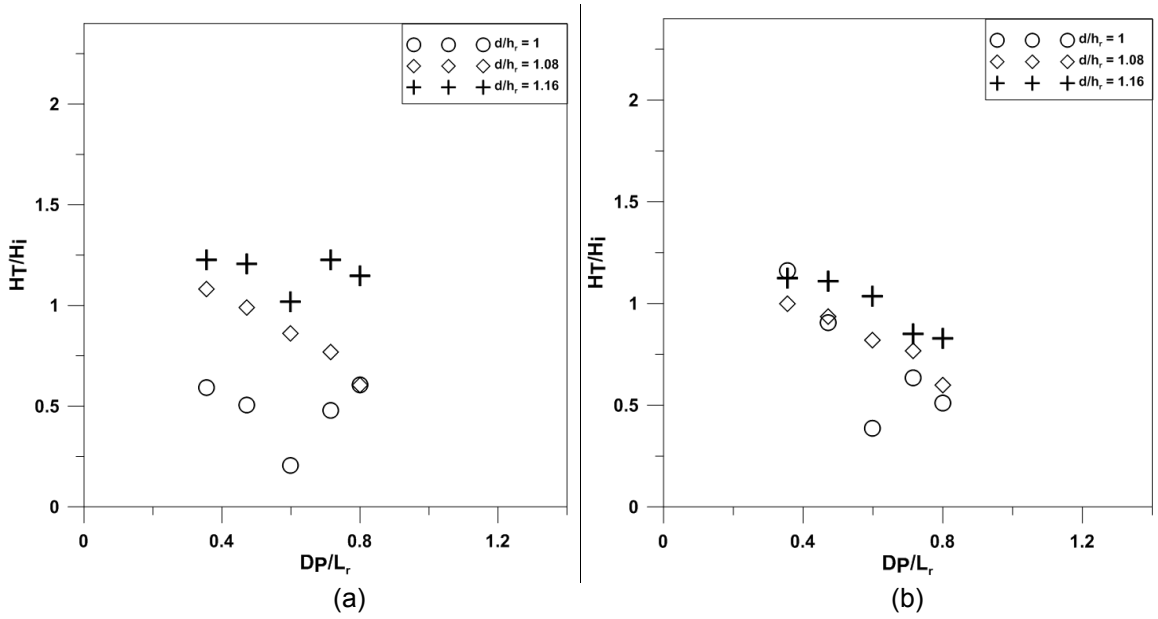

Figure 9: Wave Transformation for L_r/L = 1.48 to 1.56 & H/d = 0.25 to 0.3 (a) and Wave Transformation for L_r/L = 1.4 to 1.48 & H/d = 0.25 to 0.3 (b)

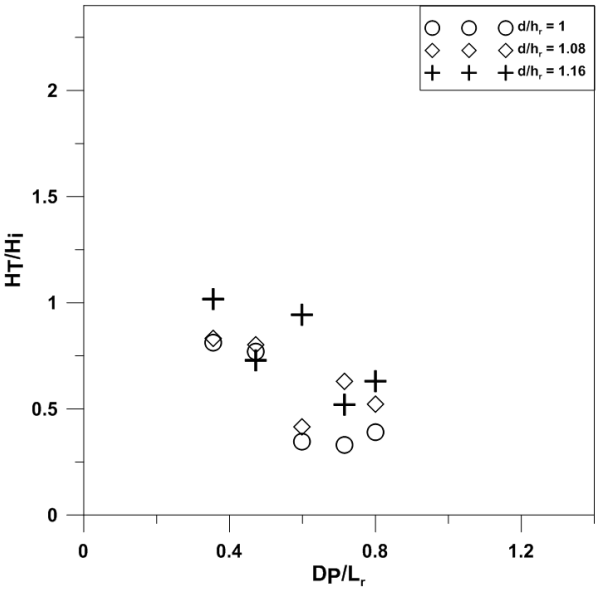

Figure 10: Wave Transformation for L_r/L = 0.88 to 0.93 & H/d = 0.25 to 0.3

Where,

H_T = Transformed wave height
Hi = Measured incident wave height
L_r = Length of the submerged Reef
D_P = Position of wave probe from tip of the wedge
h_R = Total height of reef
d = water depth
L = Wave length

4. CONCLUSIONS

The main findings for regular wave in head sea condition on the reef being installed in India are given below.

1. Intensity of the wave breaking increases as the submergence depth of the reef crest is reduced.
2. When crest of reef is submerged long period waves get attenuated and generate dispersive tail wave.
3. The wave with higher incident height shows more shoaling on the upward slope of the submerged reef as compared to the lower incident wave height. Hence wave transformation depends on the incident wave height.
4. Transmission coefficient increases with increase in submergence depth and wave period and decreases with increase in wave height.
5. Wave breaking is enhanced by the submerged reef.

5. REFERENCES

Beji, S. and Battjes, J.A. (1993). Experimental investigation of wave propagation over a bar. Coastal Engineering19:151-162.

Blenkinsopp, C.E. and Chaplin, J.R. (2008). The effect of relative crest submergence on wave breaking over submerged slopes. Coastal Engineering. 55:967-974.

Harris, L.E. (2009). Reef Journal Vol. 1 No. 1:235-246.

Kamath, A., Bhis, H., Chella, M.A. and Arntsen, O.A.(2015). CFD Stimulations of Wave Propagation and Shoaling over a Submerged Bar. Proceedings of the International Conference on Water Resources, Coastal and Ocean Engineering, Trondheim, Norway.

Masselink,G. (1998). Field investigation of wave propagation over a bar and the consequent generation of secondary waves. Coastal Engineering. 33:1-9.

Strategic Port Planning and its associated Management A Guide for Port Authorities

Authors: Maria Natalia Urriza, Pablo Arecco, Carlos Ginés, Pedja Zivojnovic, Ricardo Schwarz, Eric van Drunen, Vincent Besson, et al

Contact Information:
- ✓ **Company:** Consorcio de Gestión del Puerto de Bahía Blanca and Port Consultants Rotterdam
- ✓ **Business Address:** Avda. Mario Guido S/N
- ✓ **Phone:** 5492915705674
- ✓ **Email:** nurriza@puertobahiablanca.com

Topic: Maritime Port Planning and Operations

Key words: planning, port, vision, strategy, process

ABSTRACT

Ports will undoubtedly face some tough challenges in an ever more competitive environment. Although there will be pressures on our daily activities, there are also many opportunities for us to build on our strengths and diversify our activities into new areas. We have the capability to contribute more to our community, the region and the world's economy, .through our business engagement as well as to grow our international profile.

Planning will help ensure that the port continues to provide the highest quality service for domestic and international traffic and for import and export cargo.

That is why it is so important to have a shared and common vision of our future priorities, and why it is ineludible to debate the changing shape of the port over the next 20 years. In working towards this exciting future and while undergoing so much change, it is necessary not lose sight of our values, visión and mission.

Having a good strategy stablishes "how" you travel the road you have selected and effective execution makes sure you are checking in along the way.

In order to facilitate the strategic planning process, this paper proposes a methodology that helps port to organize the work, dreaming and building the future.

INTRODUCTION

This paper is focused on the aim of answering these two questions:
1- Is it a utopia to prepare our port for future uncertainties?
2- How can we design a specific methodology for developing port authorities´ strategies?

The core of this work is to provide a practical Port Planning Guideline to support ports on how to accomplish their strategies, and more importantly, on how to manage them for achieving realization.

In the following pages, the reader will not find a magical recipe, instead of it, a cooperative method to guide ports that want to succeed in preparing for the exciting future, exceeding the port authority members involvement and trying to build an engaged port community that foresees the future. The possibility to benefit from new perspectives is the added value: work consultatively and collaboratively

FROM GENERAL BUSSINESS MANAGEMENT TO PORT MANAGEMENT: the strategic planning process.

Thinking globally, for every kind of organization, strategic planning consists in an integrated process of five big blocks:

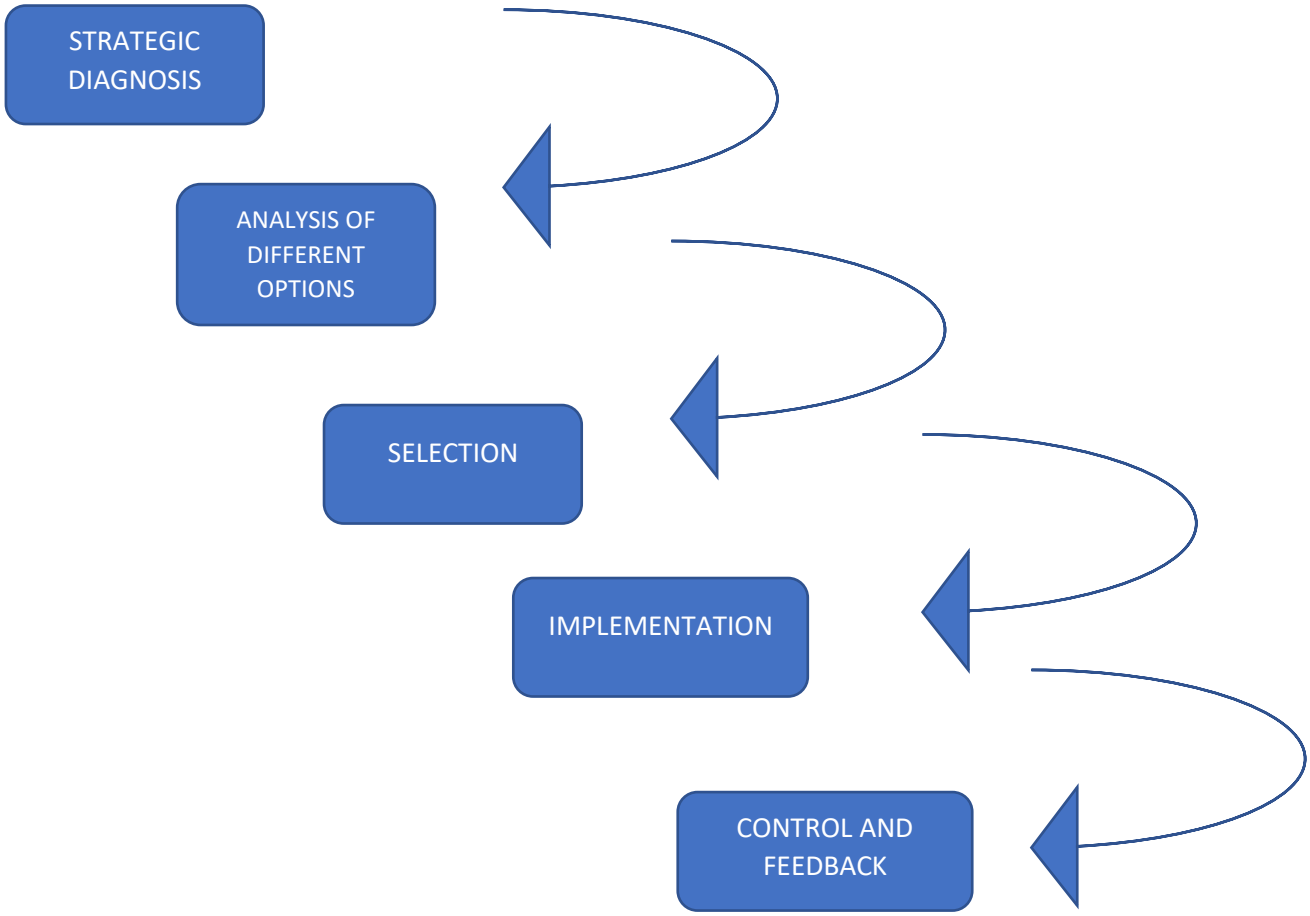

FIGURE 1: STRATEGIC PLANNING PROCESS.

If the reader wants to deepen about this topic, a great variety of authors dedicate their studies and investigations to this matter, a field focused on having access to greater productivity, culture, empowerment, and overall effectiveness, giving the directors of complex organizations a key to improve their performance. Among the authors, Johnson and Scholes (2006) will provide a quick and exhaustive view about strategy.

In accordance with this general organization of the planning process, if we focus on Ports, this is a scheme of our proposal: a Port Planning Guideline:

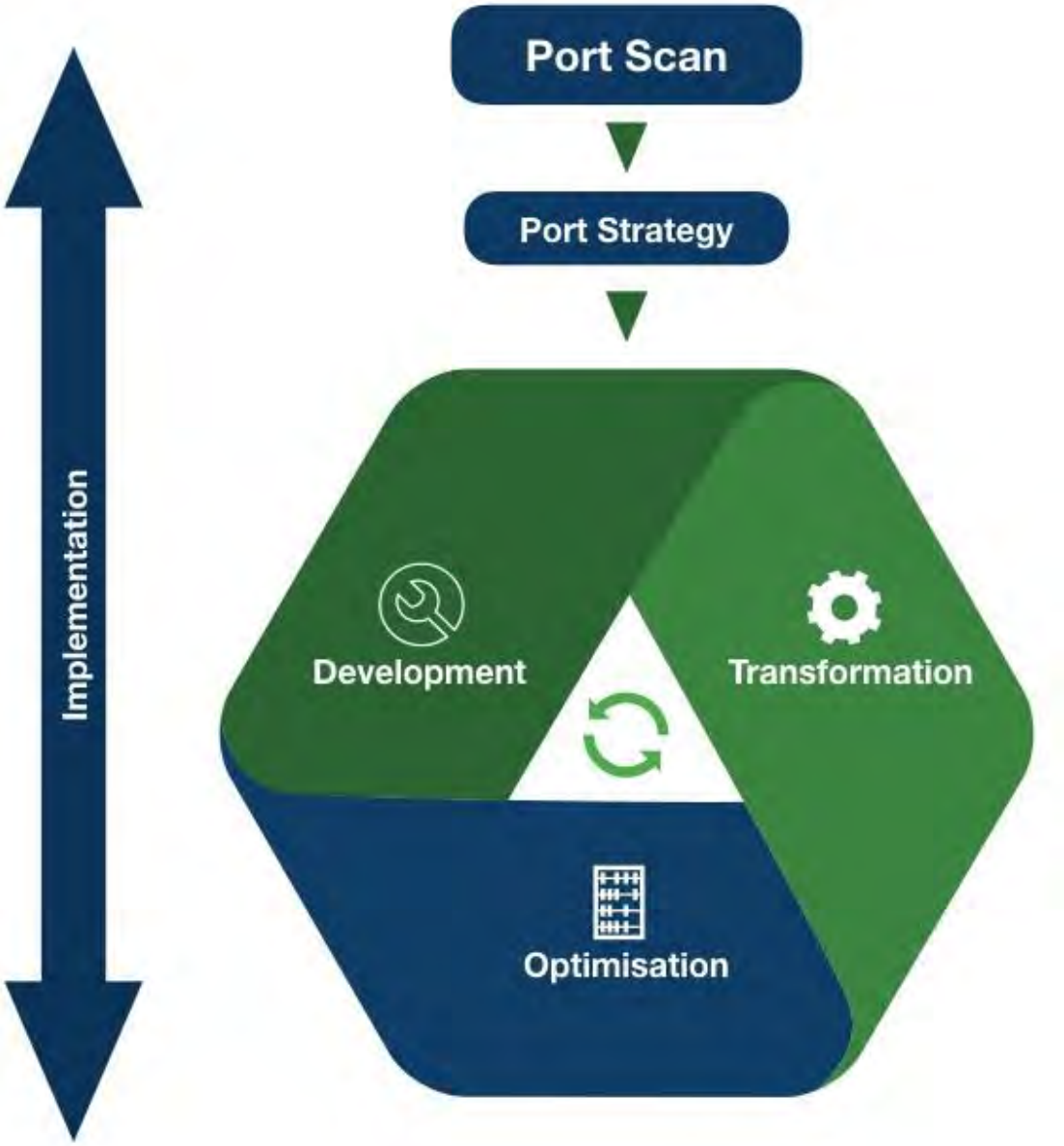

FIGURE 2: PORT PLANNING GUIDELINE

,
This focused technique is developed in the following five steps:

1-perform a comprehensive analysis of the current situation of the port,
2-build a long-term Port Vision with the participation of every stakeholder,
3-prepare/draft a joint action plan with strategic stakeholders based on the Port Vision,
4-turn the Port Vision into a Commercial Plan and
5-develop a sustainable and flexible Masterplan.

The first three steps are usually known as Strategic Planning while the last two steps are usually categorized as Technical Planning.

In addition to the mentioned steps, it is important to emphasize two of the core values of this methodology. Every phase is thought in a participative basis promoting the collaboration of all the

stakeholders involved in the port community who are not restricted to the port area itself. Some of the strategic stakeholders that can be listed are: the National Government, the Provincial Government, the Municipality, all the companies and industries within the port and nearby areas, NGOs, educational and research institutions, environmental protection organizations, et cetera. Besides, within this process, sustainability is the other core value taken on board from the very beginning in order to anticipate the needs of future generations and the prosperity of the region served by the port. In summary, this approach adopts PIANC Working with Nature Philosophy and PIANC Sustainable Ports Approach to promote ports as one of the key drivers for reducing inequality and enhancing the quality of life within their areas of influence.

In these next pages, we explain in detail the phases that allow the company to traduce the strategic planning in action.

STEP ONE: perform a comprehensive analysis of the current situation of the port: Port Scan

The first step is the “Port Scan”, a tool developed by Port Consultants Rotterdam for the elaboration of a high-level assessment for a terminal and/or a port complex. Following this holistic approach, the performance of a terminal and/or a port complex can be understood, the bottlenecks identified, the potentials recognized and the priorities set throughout a SWOT analysis. Furthermore, this diagnosis focuses on four specific topics:

Layout and insfraestructure

Operations & logistics

Organization & finances

Environmental & social aspects

FIGURE 3: PORT SCAN FOCUS

By covering the afore-mentioned topics, the current internal and external situation can be systematically addressed.

This first step ensures that a Port Authority will be able to answer:

- ✓ What is our starting point? And to reply this question, this methodology proposes the sweep of the general situation by the analysis of the following issues:
- ✓ What is the general condition of port infrastructure?
- ✓ What are the most important indicators that allow the port/terminal to show its level of activities and performance?
- ✓ Are nautical and land accesses adequate for actual activity and future expansion?
- ✓ Which are the ways of transportation to join the port/terminal with its cargo? How is the general condition/maintenance of them?
- ✓ Which are the drivers that conduce to competitiveness in port areas?
- ✓ Is the environment of the port/terminal growing in accordance with the port?
- ✓ Who are the stakeholders? Can you map them using high/low interest in the organization and high/low power in order to organize the strategies toward them?
- ✓ What are the economic, cultural, and political trends, in our region/country/world?
- ✓ … and a lot of other questions regarding the local situation, that will give the planner the best diagnosis of the port.

STEP TWO: build a long-term Port Vision with the participation of every stakeholder,

The second step is the elaboration of a long-term Port Vision which uses as starting point all the collected and processed data for the “Port Scan”. This step tries to set the future ambitions for developing a terminal and/or a port complex. Consequently, it is interlinked with a second question: Where do we want to go?

The process for elaborating a Port Vision can become a topic on its own; however, it is important to highlight the most relevant characteristics. A Port Vision is of importance for promoting an investment climate and license-to-operate (SLO) by giving confidence to policymakers, companies and stakeholders in the future, by allowing the alignment of strategies between the port authority and stakeholders and by facilitating the cooperation among all the involved parties. Moreover, a Port Vision sets the course for future developments, as it is a public document of easy access made with the contributions of all related stakeholders. Usually, it is composed by some core visions which are based on key success factors.

The Port Vision aspires to be a base guide for the successful advancement of a port complex/terminal, in the long term, and its objective is to set out the ambitions for the future. In this documentation, the trends and perspectives, the dreams, and the port indicators identified within the four groups of the "Port Scan" will be made comprehensible to all stakeholders
The main objective of the documentation (report, brochure, presentation, etc.) that is generated is to take the first steps to achieve consensus with all the actors of the sector towards a sustainable development of the port complex/terminal. Due to this, the methodology proposed is, again, working together with the stakeholders to delimit their wishes, expectations and aspirations towards their mental image or the port/terminal 20 years ahead, through workshops, meetings and interviews, to collect the prospects and forecasts and in a subsequent opportunity to validate the conclusions or change them in order to feel represented by the high lines of the vision.

After building the vision, it will be useful to edit and print it, to encourage the organization and its stakeholders to work in order to guide the future actions towards the fulfillment of it.

It is recommended to present the vision to society with a public meeting, as a way of obtaining the support of the community. Afterwards, it is useful to publish it in order to allow everyone to reach and download the vision.

As an example, we can read the Port of Rotterdam´s vision 2030 in this link: https://www.portofrotterdam.com/sites/default/files/upload/Port-Vision/Port-Vision-2030/files/assets/basic-html/index.html#1, and the Port of Bahia Blanca´s vision 2040 in this link: http://puertobahiablanca.com/vision_portuaria_2040/.
.

The authorities of Port of Rotterdam consider something that is crucial and fundamental: The Port Vision is like a compass: ambitions are a spot on the horizon, even when circumstances change. Flexibility is the keyword. It is exactly the aim of the process of building a vision.

STEP THREE: prepare/draft a joint action plan with strategic stakeholders based on the Port Vision

The third step is the definition of strategic objectives and an action plan for accomplishing the ambitions set in the Port Vision. Corporate performance objectives must be defined to fulfill these characteristics: Specific, Measurable, Achievable, Reasonable and Time-bound, just to let the port to measure success along time.

The agenda includes actions to be done by the port and combined actions with some of the strategic stakeholders in order to implement the set goals and objectives. This step ends up with all the information related to the defined actions that allow the ulterior high-level control of the performance of the port through KPIs to monitor the successful progress of the Strategic Plan.

With this step we can close the circle of the strategic planning: the diagnosis, our Port Scan, the expectations and ambitions, our Port Vision, and the concrete actions to implement our dreams, the Action Plan.

How can we settle an action plan to bring the Vision back to earth and don't let the strategic process only be a nice path of theoretical ideas that never can be done?

This proposal is based on the idea of setting strategic goals, with the essential characteristic of being measurable over the course of time. The possibility to quantify a goal lets us measure within 3 months or more if we can achieve it or we need to modify our behavior in order to reach the fulfillment of the goal. (Believing that not only the port/terminal is the owner of the vision, it is necessary to get the community involved in the commitment to obtain real changes by the allocation of different actions to the organization and the stakeholders. With this activity, you will get the compromise of changing the future, having in your boat a lot of internal and external members, all with the same compass: doing a change possible.

Another step concerning the Action Plan is the Revision Plan, that consists in a periodical review of the evolution of the actions in order not to lose productivity. To track the progress, the port stablishes actions for short, medium and large term, identifying the period of time while the actions is going to be held and the results will be reported annually to the board of Directors.

This step, that is critical viewing the strategic plan with a concrete and practical eye, the outcomes determine the success of the plan, and can be resumed as:

How can we bring the vision back to earth? A quick summary:

VISION

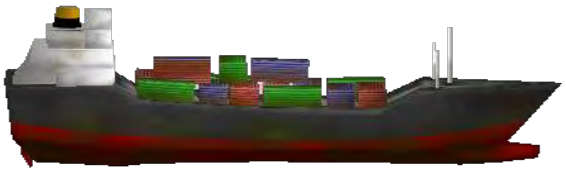

OBJETIVES (LONG TERM)

GOALS (CUANTITATIVES)

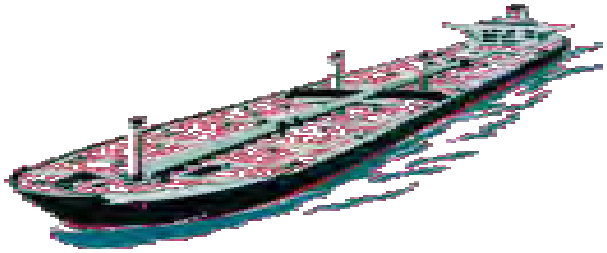

ACTIONS

PRIVATE (PORT AUTHORITY)

PUBLIC (THE COMMUNITY)

INDICATORS

ANNUAL REPORT

FIGURE 4: TURNING THE VISION INTO ACTION

STEP FOUR AND FIVE: turn the Port Vision into a Commercial Plan and develop a sustainable and flexible Masterplan.

The fourth and fifth steps are closely interrelated as the formulation of the Commercial Plan directly influences the elaboration of the Masterplan and, to the same extent, the other way round. This can be easily explained by the proposed approach of developing a Masterplan which is always centered around the financial feasibility of the Masterplan itself.

The objective of preparing a Masterplan is to define the best territorial order according to the strategy and the market. It helps to clarify and communicate the port vision and it constitutes with the vision a critical part in a ports' 'licence to grow'. They also provide a strategic framework for port authorities to consider a range of internal and external factors that may impact on current and/or future operations

It is not only a matter of technical feasibility, the financial model must be used to fine-tune and improve the Masterplan: different layouts, designs or phasing will generate different financial effects. The idea is that the financial model is used to generate the optimal choice. Thus, the Masterplan is only acceptable if it is also financially feasible, under various scenarios and following the Adaptive Port Planning Framework (Taneja, 2013) meeting many other criteria such as social, environmental and legal requirements, towards a sustainable growth.

A conscious masterplan requires placing filters, which will be transferred only by the best options:

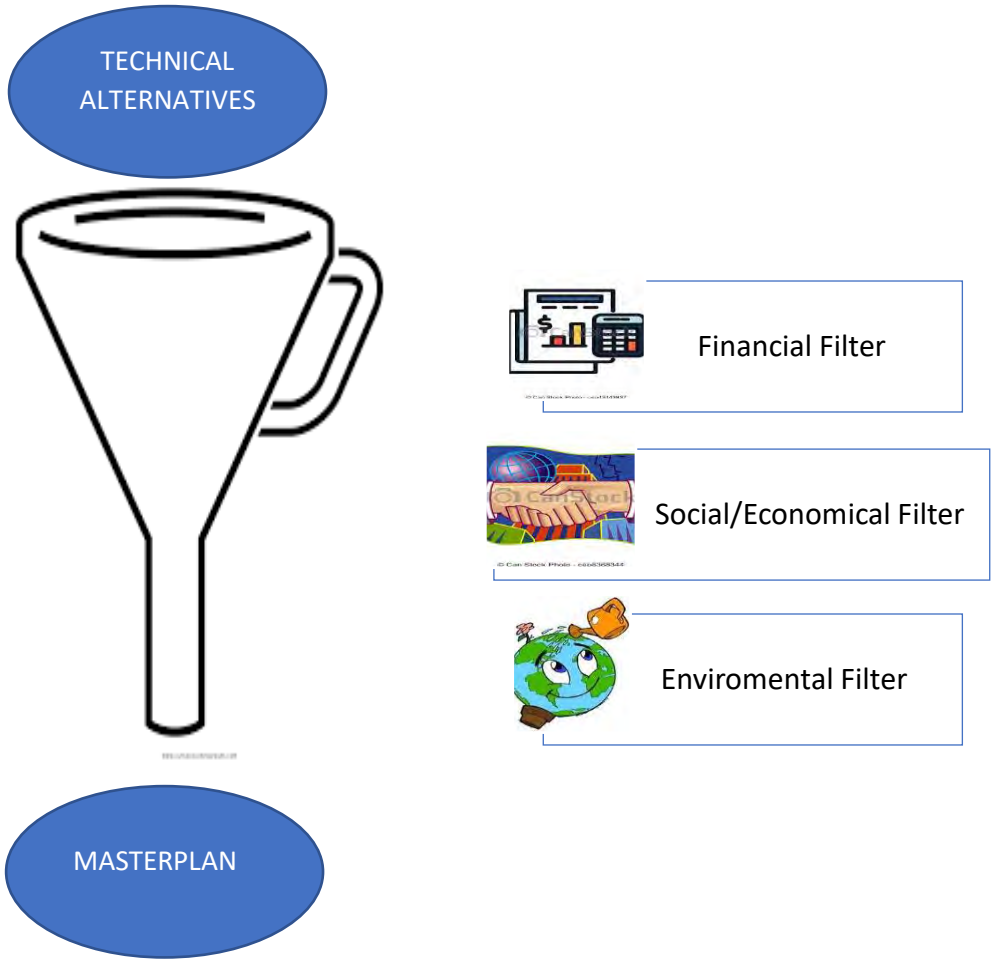

FIGURE 5: FILTERING THE TECHNICAL ALTERNATIVES TO BUILD A MASTERPLAN

Additionally, a strategic managerial process is also needed as the abovementioned steps require a regular cycle for reviews and updates based on the feedback obtained through the defined KPIs, the commercial trends and developments and the many associated uncertainties considered during the Port Planning process.

To conclude, and with no need to highlight the importance of sharing the knowledge gained during the implementation of this Port Planning Guideline for the Port of Bahía Blanca in Argentina, the spirit of this paper is to encourage Port Authorities to develop their own long-term Port Visions, Commercial Plans and Flexible Masterplans, based on a meaningful use of stakeholder engagement and the identification of win-win options towards a continuous improvement of the ports.

REFERENCES

Gerry Johnson; Kevan Scholes; Richard Whittington (2006). Exploring Corporate Strategy (7ª ed.). Pearson Ed. ISBN: 9788420546186

Taneja Poonam (2013). The Flexible Port. Next Generation Infrastructure Foundation. ISBN 9789079787470

PIANC – World Congress Panama City, Panama 2018

FUTURE PORTS AND PILOTING IN PANAMA

by

Tommy Mikkelsen [1]

INTRODUCTION

With so much talk about automation and data, and how they will impact ports, terminals and vessels in the future, this paper will be of particular interest to attendees as it takes a more practical, sober look at the technologies that are available now, how they can be used in practice and how they might evolve going forward. It calls on real life case studies and examples to highlight how the future is already arriving, and could offer huge efficiencies and savings for ports and vessels alike.

Shipping and ports are ripe for disruption, as big data, artificial intelligence and automation force a drastic change in the business models of today.

The shipping industry value chain will be driven toward 'hyper-collaboration'.

'The future won't be about doing one thing the best, it'll be about connecting to everybody else, who's doing adjacent things the best.'

The benefits of landside automation of port operations, must be extended to the shipside: with a need to improve safety, efficiency and sustainability of operations from vessel approach, to when it is moored.

This paper will discuss how ports and vessels will be shaped by data and smart technologies, through current case studies, while highlighting new technical innovations the company is evolving to support data-driven best practices.

Some of the pratical problems ports have handle every day are:

- that 45% of all container vessels are delayed by more than 8 hours
- High maintenance costs
- Larger vessels / deeper drafted
- Berth space
- Expansion problems
- Increasing environmental focus

In this paper we will highlight how we have a very pratical approach to solve these problems in a scalable and sustainable way.

VISION

The 'Port of the Future' or SmartPort vision sees vessels, ports and hinterland transport becoming part of a connected eco-system. This will require collaboration throughout the supply chain, which necessitates a common platform for communication and data sharing, with shared standards and processes.

As our industry faces globalization of operators, increasing scale and utilization of vessels, and expectation of ever-improving efficiencies, shipping and port operators must work smarter, together to address and deliver against these expectations.

[1] Managing Director - Trelleborg Marine Systems Denmark - tommy.mikkelsen@trelleborg.com

SmartPort realizes the now critical interface between ship and port, on land and at sea. Via engineering ingenuity, data capture and management, and technology-driven insight, SmartPort is accelerating performance through optimized operations, improved safety, reduced costs, greater sustainability and increased revenue return.

SmartPort is setting the true course for consistent commercial success, now and for the future.

FROM THE VIEWPOINT OF THE OPERATION

Taking a birds eye view of the complete vessel turn around process allows us to do a segmentation of the operations needed (Figure 1) to do vessel turn around. Allowing us to look in more details on each operation and how to improve, both on efficiency and safety. But even more importantly the bird's eye view allows us to see the interactions between processes and stakeholders in the various operations.

At sea: At sea, smart technology has a key role to play in ensuring shipping efficiency, optimizing fuel efficiency and improving sustainability.

Approach: As the vessel moves from the relatively unrestricted waters of the coastal phase into more restricted and busier waters near and within a bay, river, or harbor, the navigator is confronted with a requirement for more frequent position fixing and manoeuvring the vessel to avoid collision with other traffic and grounding dangers. Pre-berthing coordination is key to a smooth and efficient approach.

At berth: Once a vessel reaches berth, it's critical that personnel on-board the vessel, and on shore are able to communicate quickly, effectively and comprehensively informed by access to common data. A common approach to coordination and communication is required to avoid confusion and delays.

Transfer: When transferring hazardous materials such as oil and gas, safety is absolutely paramount. All parties require the correct data at the optimum time to stay informed and act quickly in an emergency.

Departure: From leaving berth to navigating the channel, it's essential that the vessel completes a controlled, safe and efficient procedure.

This allows us to look at models that will enhance collaboration across operations and systems.

The problem with today's systems is that they take a "systems" approach, not a data driven one. For example, if the need arises for controlling the entry to the port area, an access system will be purchased and put in place. This is a shielded off system that only does what it was made for - controll access. But looking at it from a data driven perspective, the same data (entry and exit of specific people) could be used for time billing / work hour registration and emergency coordination.

It is widely accepted that the way forward is to take a data driven approach to systems.

THE SMARTPORT PORT AND VESSEL INTERFACE OPERATING CYCLE

So, how do we manage that critical interface between vessel and port to best empower both? The SmartPort platform is designed to continuously capture, manage and present data to both quay side and vessel stakeholders, to ensure consistent communication between the two, improve operational decision making, and eliminate inefficiency in the port and vessel interface. But importantly, the platform is also engineered to build these data points into longitudinal strategic insights, to enable process refinement and business improvement.

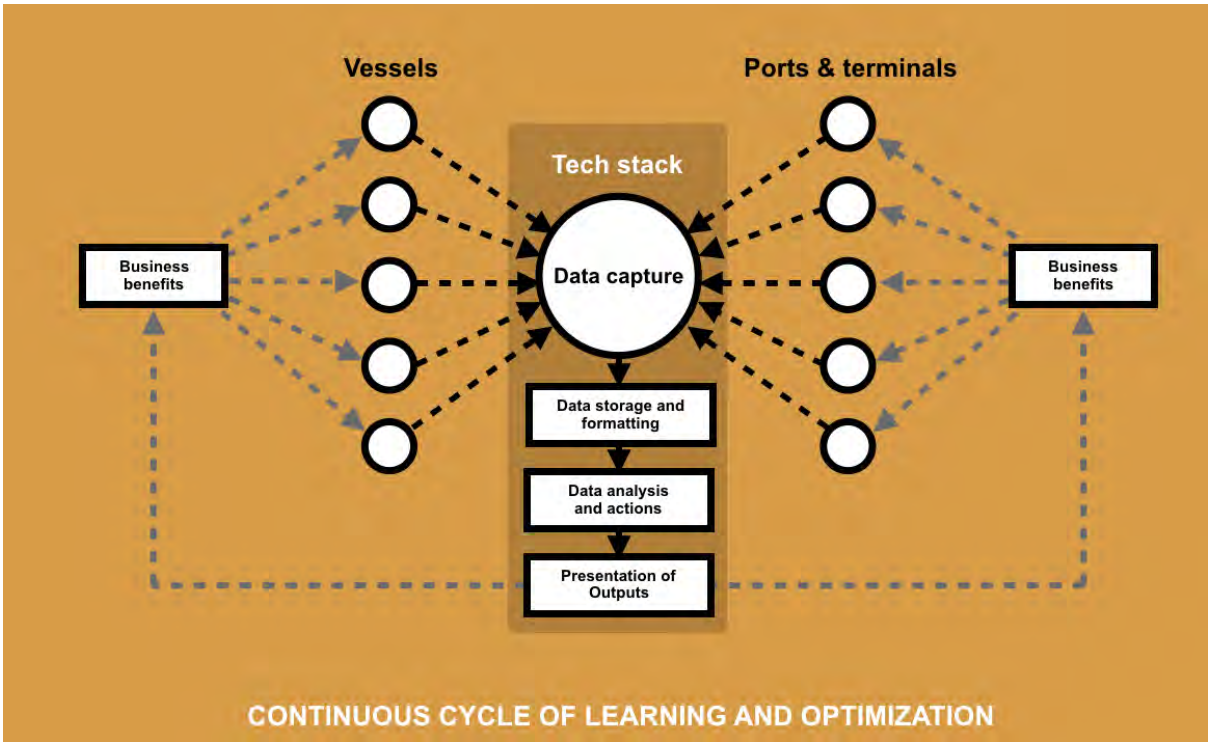

Figure 1: Port and Vessel Interface Operating Cycle

Data capture points, assigned to various assets across both vessels and within the port environment, feed the information they collect into a cloud solution. Data is standardized and analyzed, and useful insights are generated and presented back to the stakeholders that need them.

This presentation of data can be customized, so it is extremely relevant to the person viewing it. All viewed enjoy a clear picture of operations, to help them make quick and effective decisions, whether operational or strategic.

Ultimately, the outputs generated inform board level strategic decision making for the greater benefit of the business.

The ideas implemented, in turn, can be closely monitored and adapted where necessary, fueling this continuous cycle of learning and optimization, constantly improving the overall facility to help meet strategic drivers, and smoothing operations on an ongoing basis.

SmartPort connects port operations, allowing operators to analyze performance and use data to improve decision making (Figure 1). The system integrates Trelleborg, client and third party infrastructure by connecting a network of assets like fenders, mooring equipment, ship performance monitoring, and navigation systems through a network of sensors, across a common platform.

COLLABORATION AND THE TECH STACK

The majority of major ports in the world are looking at transforming the way they do business in order to adopt a ‘smarter’ approach. This paper looks at the importance of an open system to help the industry achieve a standardized way to collect, store and thereby benefit from data in its myriad forms. To achieve exactly that, the technology platform must be built around an API structure that enables collaboration with third party systems and third party assets, a step towards achieving a common platform for the industry. This openness allows customers to make more effective decisions through deeper, accurate insights across all operations, irrespective of supplier.

To be truly collaborative, technology solutions must have the ability to work across different aspects of the supply chain, whether that's within ports and terminals, on board vessels or as they get into the landside logistics.

By adopting smart technology built around open system architecture, any port or terminal asset can be brought under one cloud based system. This enables the development of custom apps to access asset data, interrogate it and present it across a wider range of users, enabling more effective decision-making through deeper, accurate insights. Multi collaboration is at the heart of these kinds of systems as they use data from many different suppliers of different equipment, to develop informative services that are as useful to the customer as possible. This requires all available data to be formatted, collected and stored in a common way, making it easier to analyze, identify and implement measures that enhance safety, efficiency and productivity.

Fundamental to the SmartPort architecture is the tech stack (Figure 2). The tech stack describes the architecture and operation of the SmartPort platform.

Performance data is captured through sensors and transmitters located on assets in the port and vessel environment. This data is standardized and stored, to enable seamless interrogation when it is accessed. Sector knowledge and engineering expertise inform the analysis of this data to present the most relevant and robust insights and recommendations.

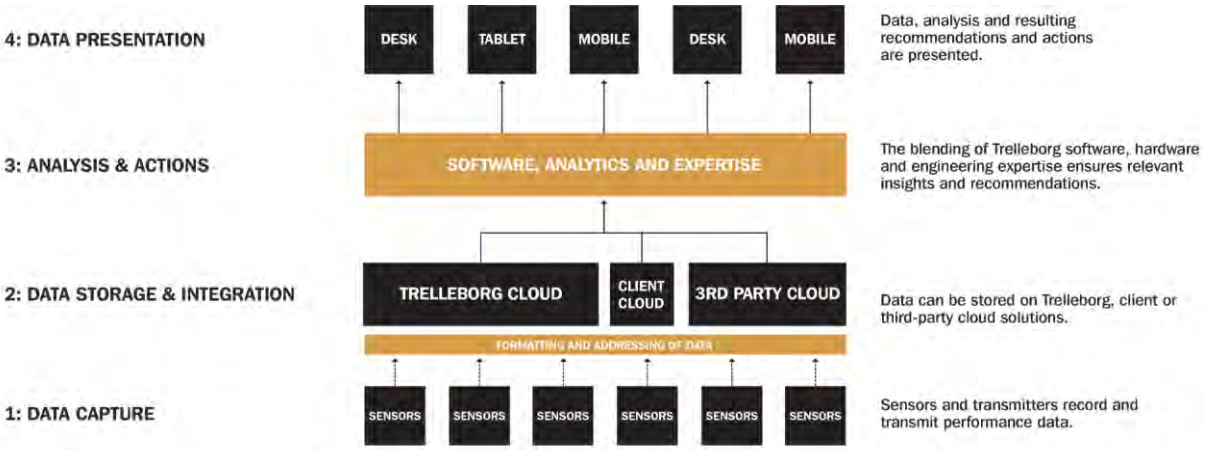

Figure 2: the Tech Stack

Data capture: Sensors and transmitters are attached to vessels and port assets to record and transmit a holistic range of performance data.

Data storage and integration: Data can be stored on any cloud solution, as the solution has been developed to enable standardized formatting and addressing to enable seamless interrogation of data.

Analysis and actions: The blending of software, hardware and engineering expertise ensures the data analysis focuses on the most relevant and robust insights and operational recommendations.

Data presentation: Data, analysis and resulting recommendations and actions are presented in an easy to access format, consistently across device-types: ensuring operational value is easily implemented.

Finally, consistent data is presented in an easy to access format to relevant stakeholders, across a range of device types.

A look at the layers

The core framework consists of three layers. The cloud layer manages intelligent data collection, transfer and storage. The application layer provides access to unique product functionality and data insights from within the cloud.

The cloud layer includes cloud connectors that enable data to be collected from remote devices, installed on specific SmartPort enabled products or assets such as fenders. In addition to data collected through

such devices, an API provides access to an open architecture that enables third party partner or client systems and data to be integrated with a data cloud.

The application layer delivers specific product functionality and business logic, to enable data to be easily accessed and visualized, and real-time decisions to be made. Dedicated Apps ensure easy deployment and provide remote access via connected devices. As the SmartPort enabled product portfolio expands, individual products and data clouds can be integrated to provide a connected view of all port operations: unlocking even greater efficiencies and empowering operational excellence.

The devices layer is the collected sum of all the devises / sensors / systems, i.e.: assets a port has. Each of these assets provides important realtime data to the cloud system. By nature these assets are all very different by different suppliers and providing access to their individual data points can be a challenge.

Therefore a critical point, upon purchase, is to be made about openness of sensors/systems to data interrogation. It is critical that the procurement process insures that new systems can indeed be integrated with third party system.

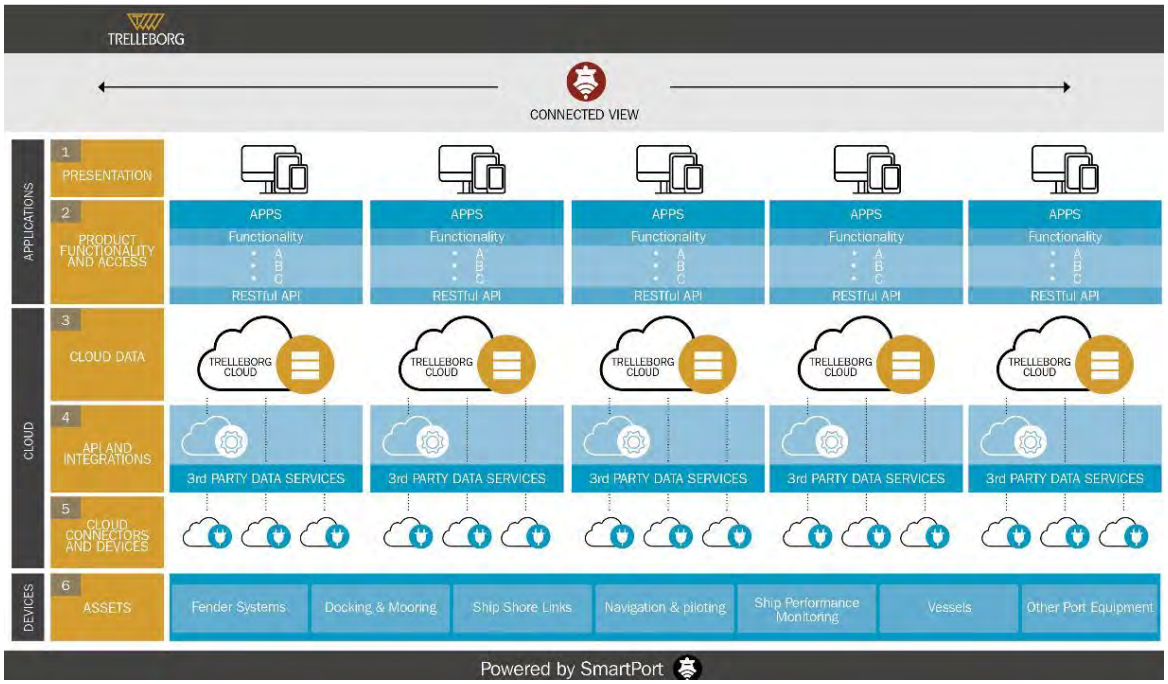

Figure 3: Tech Stack Details

CONCLUSION

So how do we help our customers to navigate their way through the vast sea of data (figure 4) in order to help their business grow?

Figure 4: the Vast Sea of Data

Answer:

- Evolve from product bundling to integrated solutions provider
- Develop consultancy style sales skills
- Support the most progressive customers with their “Port of the Future” challenge
- Act as an integrator when the customer wants it
- The smarter the equipment/product is, the more attractive it gets to the customer
- A wide spectrum of services is a competitive advantage

We are doing this already with help from the core components of the SmartPort sytem, the Tech Stack.

Following are two case stories and a technology systems description that will highlight the value of a data driven approach.

CASE STUDY - SMART NAVIGATION WITH AMP

The technology platform is designed to empower decision making and communication during port approach, docking and deberthing. A key part of this process is the piloting and navigation operation.

The Association of Maryland Pilots (AMP) are utilizing their Portable Pilot Units (PPUs) and a Port System server solution to facilitate consistent, real-time information sharing between almost 70 pilots.

The AMP serves the Chesapeake Bay, the longest pilotage route on the East Coast of the United States, with its nearly 200 miles of waters. The scale of the waters put demands on the operational battery time the piloting equipment requires. Vessels of almost 48 feet draft transit the narrow channels of the bay, which themselves are only 50 feet deep.

The PPU combines a Rate of Turn sensor with a GNSS high-accuracy positioning sensor. It is used in paired units, with one connected to the ship's AIS pilot plug and power adaptor for continuous charging. The other is located on the bridge wing, running on a built-in battery. When the battery is flat, the pilot simply swaps the two units, allowing a continuous operation.

All data is visualized on an iPad overlaying a sea chart. The iPad is continuously in connection with the cloud to exchange vital data.

The technology platform system server solution synchronizes data between pilots. Updates to information are made on shore, and distributed in real time to ensure accurate decision making during the piloting operation. Recordings of all operations are stored for future review and pilot devices backed up in the data cloud, enabling the data storage and sharing that will offer real insight for future operations, a key element required within the Smart Port model.

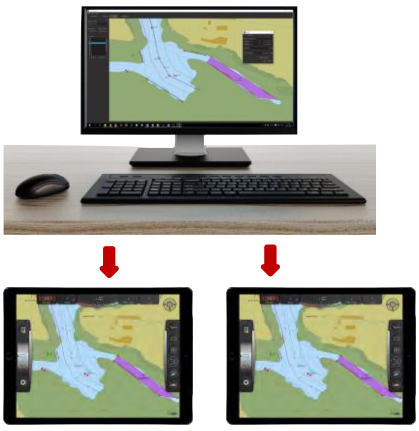

One of the main drivers for the AMP is the real time data exchange. From shore all valuable information is geographical added to the system, automatically uploaded to the cloud and distributed to all clients. That could be essential information like notes to mariners about missing sea marks or weather warnings. Furthermore, the precise navigation of the piloted ships is shared, allowing everyone to see the precise movement of each vessel.

Collaboration with NOAA on the integration of the NOAA ports system, means that realtime weather information is present at anytime on all screens.

The combination of sensors, integration of 3rd party systems, cloud data and intelligent apps for data display gives AMP a unique advantage and added safety when navigating the Chesapeake Bay waterways.

The add on possibilities are endless. By adopting a data driven SmartPort solution, AMP is ready for future demands.

TECHNOLOGY SYSTEM - ADAPTIVE UNDER KEEL CLEARANCE (AUKC)

As ship sizes grow and many waterways become more constrained, the need for precision tools increases. Under Keel Clearance (UKC) systems is one such tool used for describing the amount of water from the ship's keel to the seabed. This is mostly used in the planning phase, to be able to determine the optimum time for passing the constrained waterway, sometimes called the tidal window. The output from the planning phase is a passage plan that describes the voyage waypoint, speed, time, etc.

There is a number of challenges associated with determining UKC.

- Ships motion affects displacement
- Accuracy of seabed survey
- Prediction of weather / tide / sea state
- Realtime conditions might changed from the prediction

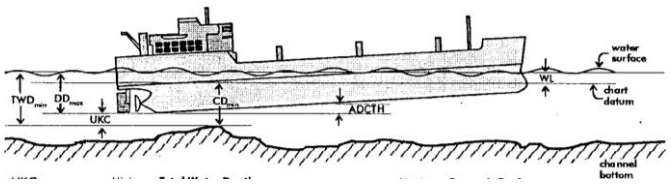

Adaptive Under Keel Clearance (AUKC)

The AUKC system uses third party integrated data to overcome these challenges, by providing a planning tool to develop a Passage Plan that is specific to the vessel and its journey. It will then provide real-time measurement to ensure that the plan is still valid throughout the approach, updates when conditions change and alert if there is a risk that the AUKC will be too small further down the route.

The AUKC system will potentially enable ships to carry more cargo, save on dredging cost and increase safety.

There are three phases of AUKC: Plan, Monitor and Analyze. Each has an important role to play in supporting real-time collaboration and decision making, and optimization.

The Adaptive Under Keel Clearance system will:

- Provide a planning tool to develop a Passage Plan for the specific vessels visit/journey
- Provide realtime measurements to asses if the plan holds.
- Provide realtime updates on No go areas when conditions changes.
- Alert if there is a risk that UKC will be too small further down the route.

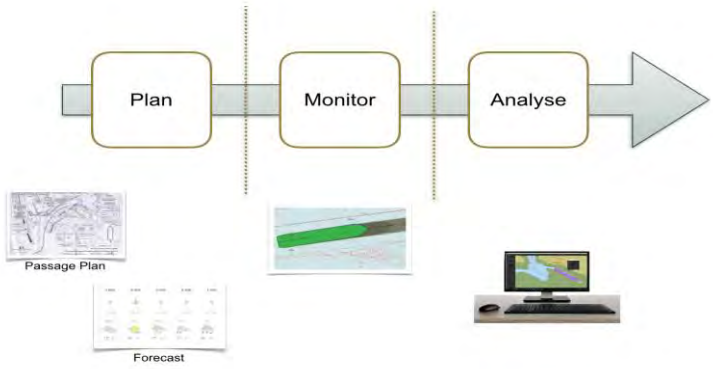

Planning

There are many different planning / prediction tools available, some ports use these today. But most don't. There is great value in doing passage planning and prediction of tidal windows. But of cause the benefit varies from location to location. But going from a paper plan to a digital one is a big step forward, and allows for integration of weather forecast and ship model calculation to better predict the tidal

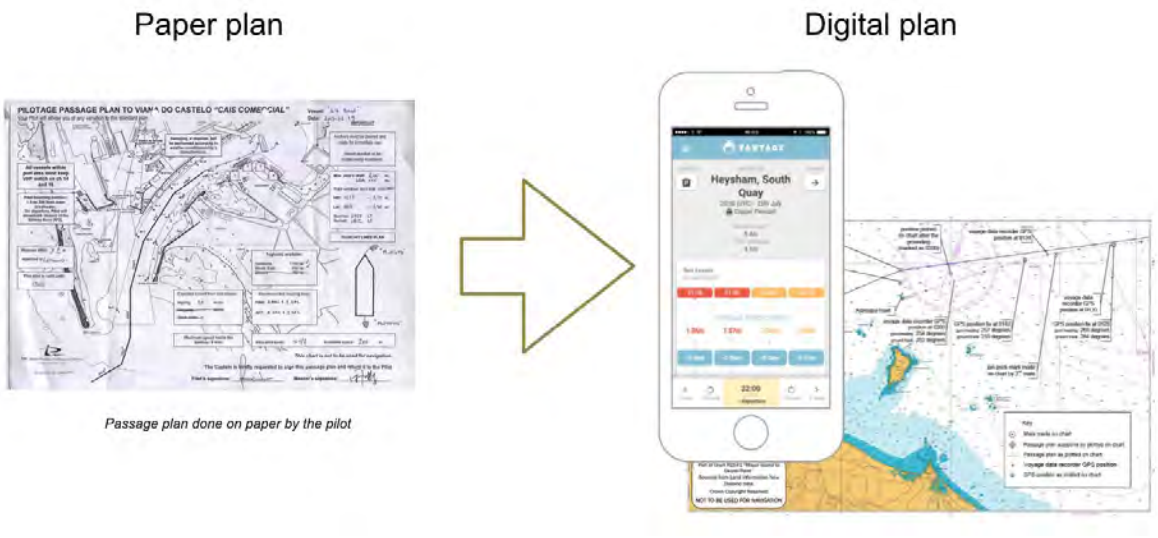

Passage plan done on paper by the pilot

window.

Monitoring

On the vessel the pilot uses his precise navigation tool. To accurately monitor his exact location, and equally important, measure the ship's motion. By utilizing precise survey of the seabed synchronized from the cloud whenever there is new data, a very accurate under keel clearance can be calculated along the route.

As the ship moves through the water, a number of hydrodynamic effect occur. These are captured using realtime accelerometers, gyros and RTK GPS. All embedded in a carry along package (PPU) the size of a loaf of bread.

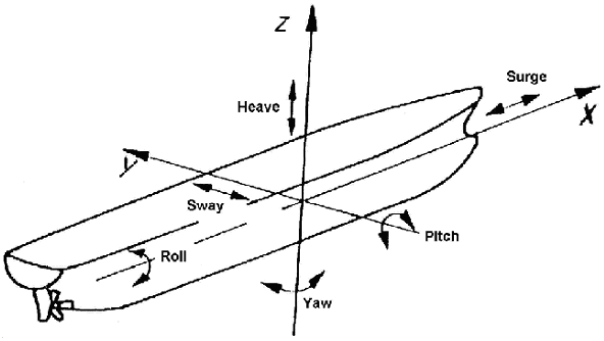

Ship Motion and PPU System

The data is then compared in realtime, by sending measurement data back to the cloud to see if the prediction from the passage plan still is within the safe tidal window. If not the pilot will be warned.

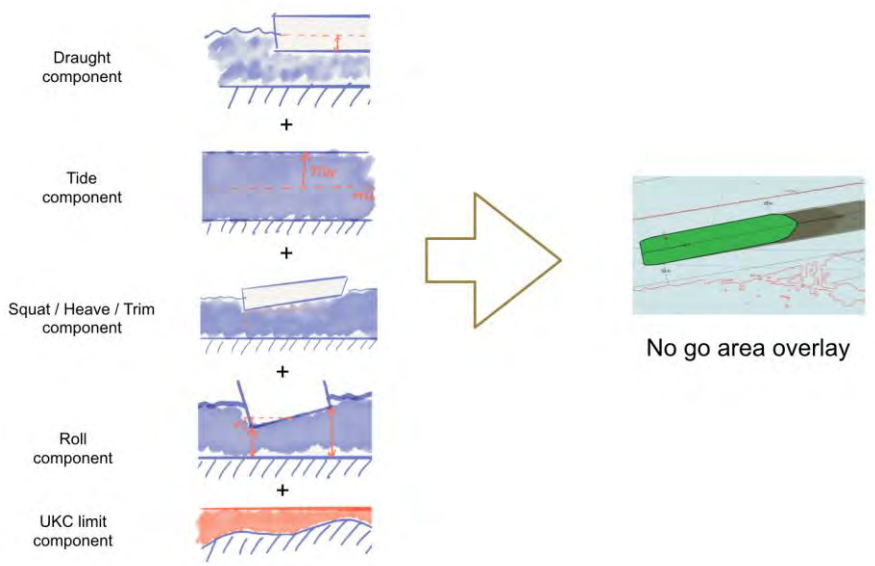

The cloud system then reassesses and provides an updated prediction. Consisting of no-go areas marked on the sea chart.

Analysis

All the data measured by the sensors are sent back to the cloud and can be used for analysis. Several different usages are possible, among others:

- Identifying areas of need for dredging
- Feedback into passage plan for future voyages
- Increasing allowed draft
- Increasing port throughput

The Adaptive Under Keel Clearance (AUKC) will allow for a predicted and realtime adaptive under keel clearance, and indication of NO-GO areas.

CASE STUDY - PANAMA CANAL

Trelleborg has supplied the ACP - The Panama Canal Authority and the Panama Canal Pilots with state of the art navigational and piloting systems for the new canal expansion.

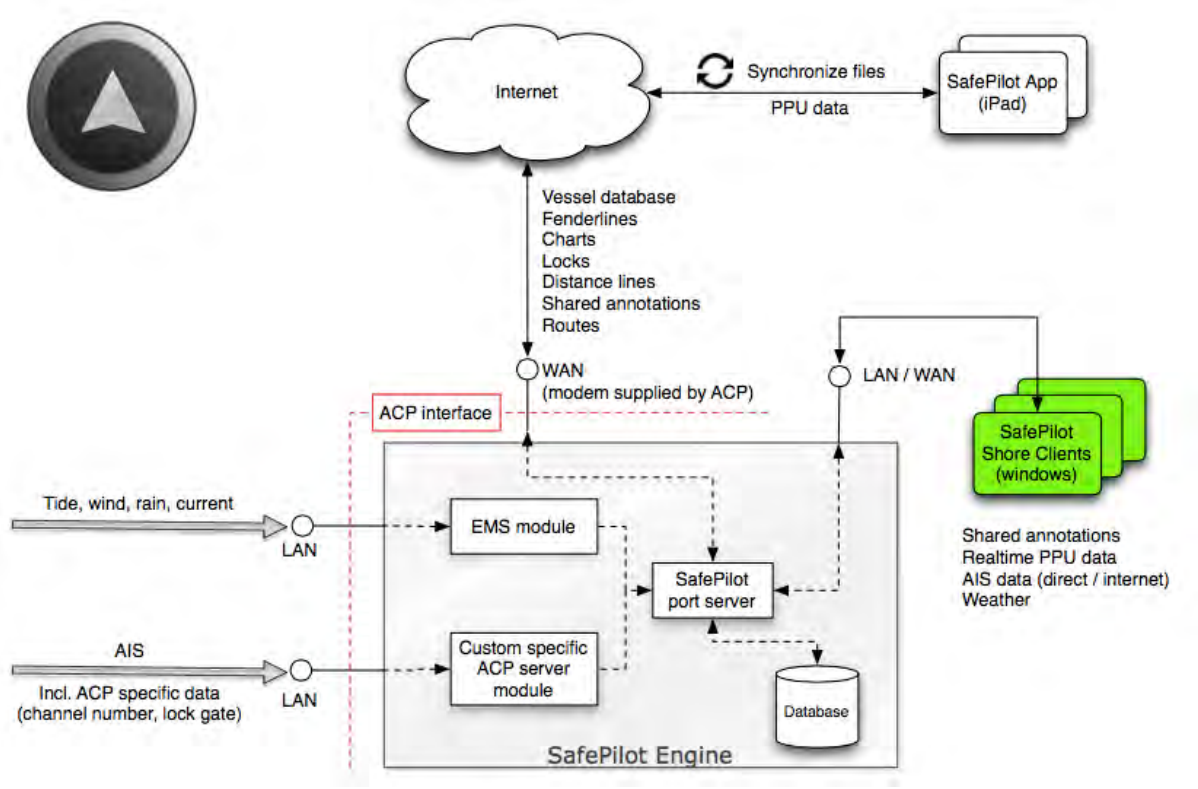

A specific ACP module was developed. This module replaces the name of ships with schedule numbers, and color coding for different types of ships.

Integration with ACP systems are managed by the Cloud system, specifically the SafePilot Engine. The Engine binds together pilots and port administration during operation with all information and data needed for efficient piloting and port management. It allows personnel, data, schedules and subsystems to be linked together.

The SmartPort Engine is the brain of the SafePilot system, synchronizing data between pilot, port and subsystems. It is a complex server set-up that gathers, structures, stores and communicates data in real-time.

Recordings of all operations can be stored and pilot devices backed up in the Engine.

The system consist cm accuracy RTK GPS portable Pilots Units (SafePilot Cat III) for the new locks and sub-meter accuracy SafePilot Cat ROT/1 system for the old locks.

For both the new and the old locks, the pilots are using SafePilot app for data monitoring and precise navigation.

Further weather sensors, AIS repeater stations and admin data are all updated to the cloud on a realtime basis. Even sensors on the lock gates allow the pilots to monitor the open/closed state on the gates directly on the Safepilot app.

A built-in alarm system allows a pilot to set his ship in an alert state to notify his colleagues on the water that his ship is in trouble. This alert will show up on all screens both on the water and on shore, quickly identifying and marking the troubled ship.

The pilots also utilize the advance built-in meeting point calculations function. This allows the the pilots to quickly access when and where they will meet an oncoming ship in the canal, allowing them to adjust speed accordingly. They can get a recommend speed for meeting the oncoming ship in a select location, allowing for safe passage.

Future of pilotage in the Panama Canal

There are a lot of potential benefits of building on top of the existing system. Fortunately, ACP have chosen a data driven approach that gives them the advantage of easily adapting new innovations. These innovations could be third party systems, but Trelleborg also has a range of Smart products that could enable an even smarter system in Panama. To mention a few:

SafePilot: already being used as a navigational tool, it also offers an overview of planned as well as ongoing port and piloting operations by intelligently integrating relevant schedules.

AutoMoor: a rope-free, automated mooring system. Created for efficiency and safety, it uses vacuum technology to rapidly attach to and secure a vessel at berth. The need for mooring lines is eliminated, and safety is greatly improved.

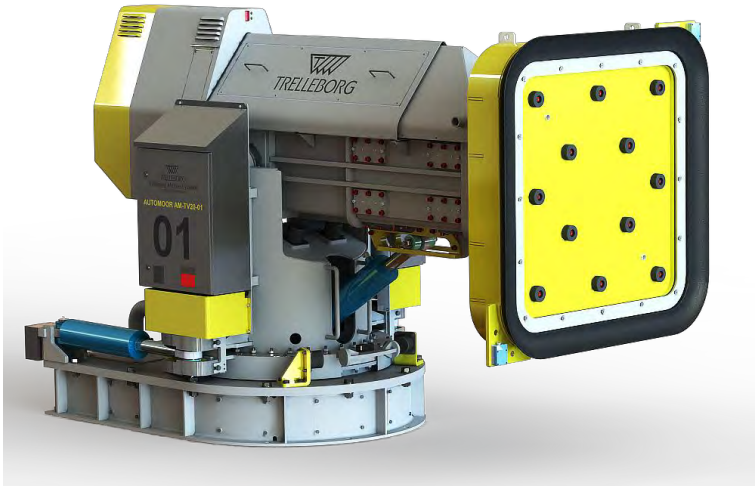

Pneumatic fender monitoring: sensors fitted to fenders to monitor pressure, temperature and position. Data is shared through the cloud

SafeTug: tugs carry a SafePilot system. This allows both Pilot and Master to see the position of each tug as they are working with on the Pilot's system, increasing situational awareness and safety. The Pilot will also be able to see the tug's realtime power reserves.

Ship-Shore Link Service App: collates all service history data for SSL shore and terminal systems, including spares purchasing, to allow proactive interaction for service contracts. Tracking of equipment and purchasing behavior will also allow product and training issues to be identified.

Smart bollards: Bollards don't provide line monitoring, berths are exposed to overload conditions or slack lines which can result in;

- Mooring line failure.
- Injury from line recoil in the event of a mooring failure.
- Successive mooring line failure from transfer of forces to adjoining lines.
- Vessel damage
- Significant down time and demurrage fees.
- Slack lines lead to uncontrolled vessel drift off.
- The ability to provide real time monitoring and alarm conditions is fundamental to safe mooring.

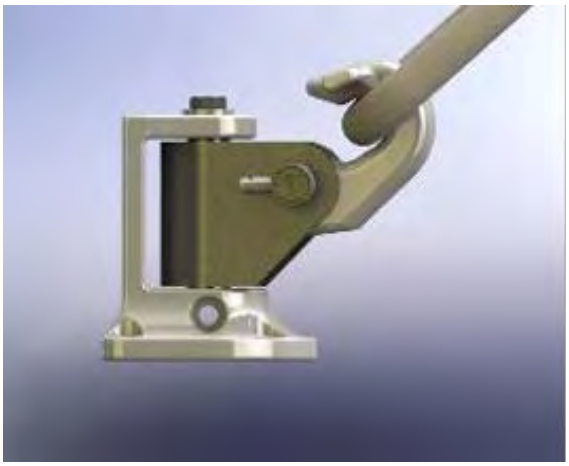

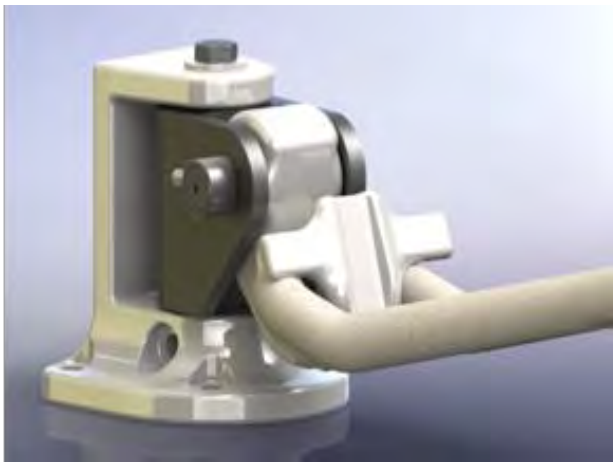

With the Smart Bollard system all this information is shared and available to the reliever personnel.

CHALLENGES AND CONSIDERATIONS IN SELECTION, ANCHORAGE DESIGN, AND INSTALLATION OF QUICK-RELEASE MOORING HOOKS ON EXISTING STRUCTURES

by

William M. Bruin PE, D.PE[1], Rune Iversen, PE[2] and Julie A. Galbraith, PE[3]

ABSTRACT

Quick-release mooring hooks have become increasingly popular for use in design of new mooring systems, especially for larger vessels. Hooks offer several operational and safety benefits over the standard bollards or cleats. Such benefits include the abilities to release mooring lines without de-tensioning the lines, release mooring lines remotely from a distant control location in possible emergency situations, as well as monitoring of tension in the mooring lines while a vessel is at berth. In addition, mooring hooks are increasingly being required for new installations by local rules or regulations. This paper discusses the challenges and solutions for designing and installing quick-release mooring hook at existing marine facilities. Examples of successful installations and typical technical challenges are presented.

1. INTRODUCTION

Selection, design, and installation of quick release mooring hooks follow a relatively straight forward path when applied in design of new mooring structures. Several institutions and authorities offer standards or guidelines to aid in this process, such as Unified Facilities Criteria (UFC 2017), British Standards in the UK (BS 2014), the Marine Oil Terminals Engineering and Maintenance Standards – MOTEMS (CBC 2016) in California, as well as the recently released PIANC Working Group MarCom 153 “Recommendations for the Design of Marine Oil Terminals” (PIANC 2017).

Quick-release mooring hook installations for new designs in a best practice scenario adhere to a hierarchy of failure modes that attempt to maximize safety and minimize economic impact if the mooring system is accidentally overloaded (See **Figure 1**). PIANC Working Group MarCom 153 has identified that the successive modes of failure should be as follows: winch brake tending, mooring line failure, mooring hook failure, and finally, mooring structure failure. While the concept is simple for new designs, ensuring that the progression of failure adheres to this hierarchy can be difficult to accomplish when any changes are made to an existing mooring system. These changes can occur at different levels, including change in mooring line strengths or types that are carried by vessels calling at a terminal, upgrades of mooring hardware at a terminal due to regulatory requirements, or upgrades of mooring hardware due to changes of service at a terminal. The question will then arise as to how a possible break in the hierarchy of failure modes can best be handled and at what point in the chain the break should be implemented. In addition, existing marine terminals may have mooring systems and structures that were not designed to these standards, making possible upgrades of the mooring system even more challenging.

[1] Senior Principal, Simpson Gumpertz & Heger Inc., USA, wmbruin@sgh.com
[2] Staff Consultant, Simpson Gumpertz & Heger Inc., USA, riversen@sgh.com
[3] Senior Staff II, Simpson Gumpertz & Heger Inc., USA, jagalbraith@sgh.com

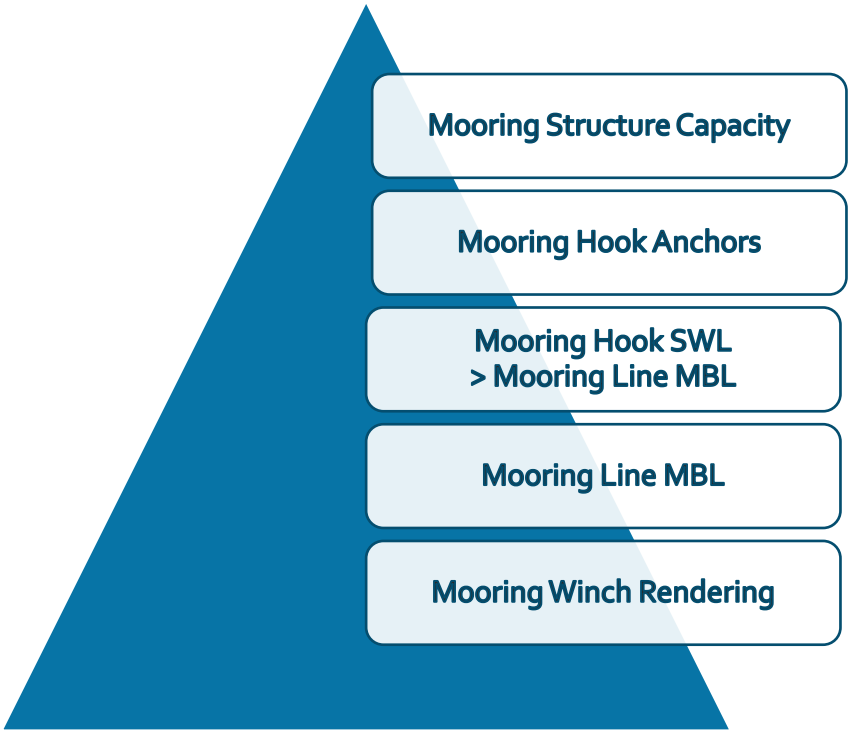

Figure 1: PIANC Working Group MarCom 153 Hierarchy of Failure for Mooring System Design (PIANC 2017)

2. DESIGN CHALLENGES

Installation of new quick-release mooring hooks at an existing terminal as either a replacement or upgrade require careful thought and attention by the design profession. The design professional must review the entire mooring system, not just the specific hook assembly, to ensure a design that is appropriate for the site, safe, and not overly conservative in terms of capacity (Iversen 2014). Blindly following the available design standards geared for new terminal installations may lead to impractical, unsuitable, and/or unnecessarily expensive designs.

For new installations at existing terminals, the design professional must consider the location of the mooring points, the number of mooring hooks at each mooring point, the appropriate Safe Working Load (SWL) for the individual hooks and the hook assembly, the type and design of the anchorage system, as well as the available structural capacity of the existing mooring structure. All these factors can greatly influence the size and scope of the design. Further challenges faced by the designer include developing a design that will work with operational expectations that the terminal will remain open or minimally impacted by installation of the new work. A successful design needs not only to consider the structural aspects of the installation, but also the order of installation as well as methodologies to speed up installation. A discussion of these common challenges and some successfully implemented solutions is presented below.

2.1 Selection of Mooring Line Strength for Design

Most mooring hook design guidelines state that for new construction, mooring hooks should be selected based on the anticipated maximum mooring line strength for vessels calling at the terminal. At first, this seems to be a reasonable approach to ensure that the mooring lines are the weakest link in the hierarchy of failure chain for the mooring system, but there are several pitfalls associated with this approach for installing new hooks on existing structures.

Firstly, the design professional may find it difficult to anticipate what this mooring line strength would be. Some of the references noted above provide good estimates for typical mooring line strengths for various vessel sizes and types. However, there will always be vessels carrying stronger lines than the normal range. A common observation is that many vessel owners tend to increase line strengths of their vessel during refitting or to accommodate a specific terminal with higher environmental loads. The motto of "stronger is better" often prevails in these situations. If a vessel with unusually strong lines be considered to size the new mooring hooks, the hooks are likely to be unnecessarily oversized compared to actual mooring loads and the corresponding demands on the supporting structures will be even larger, possibly exceeding available capacity, without a real increase in safety.

Overly conservative designs may be avoided by sizing the mooring hooks using a more reasonable line strength that is selected after careful review of all vessel types and sizes expected to call. The designer should carefully review the vessel inventory to understand actual line sizes and types calling at the terminal for the entire fleet, with the intend to identify vessels with unusually high line strengths. Line strength outliers may be considered an exception and ignored for the purposes of mooring hook sizing.

2.2 Selection of Number of Mooring Hooks

Selection of the number of mooring hooks should be done to provide the terminal operator with the maximum possible flexibility of vessels they can accept. For new terminals, the mooring analysis strives to establish the minimum mooring line strength needed to provide for safe mooring arrangements for the selected vessel types and environmental conditions. For existing terminals, the mooring analysis may focus on ways to limit hook or hook assembly loads by considering additional hooks or even additional mooring points. Overly conservative designs may be avoided by introducing more hooks or mooring points to the facility to spread mooring loads or reducing the load experienced by a single mooring structure. Introducing additional hooks is likely to be significantly cheaper than strengthening or rebuilding existing marine structures.

2.3 Selection of Hook Safe Working Load (SWL)

Following the hierarchy of failure, the hooks themselves are the next link in the hierarchy of failure chain. The Maximum Breaking Load (MBL) of the mooring lines is usually compared to the Safe Working Load (SWL) of the hooks for size selection. Mooring hooks are manufactured with a stated SWL from the manufacturer. The SWL is typically the capacity referenced by guidelines when recommendations are made for sizing of mooring hooks. However, the SWL is usually well below any real failure limits of the hook. The proof, yield, and ultimate loads of the hook are generally at least 1.5, 2, and 3 times the SWL of the hook, respectively. By inspection, the designer can see that the proof load of the hooks will be close in value to the anticipated MBL of the mooring lines if the SWL of the hooks are selected to match the MBL of the mooring lines. Based on this observation, there remains a significant margin of safety built into the design of the hooks themselves when hooks with lower SWLs are considered.

2.4 Hook Assembly Anchorage Design

In general, anchor bolt capacities are rarely a limiting factor in the capacity of new mooring hook assemblies on new structures. This is not the case for new installations on existing structures. Existing anchor bolts are frequently too corroded, too small, or an insufficient number for reuse. New bolts of larger size and number are almost always required. Installing new large diameter, embedded anchors into concrete structures can be a challenge. There are very post-installed anchorage systems (adhesive or mechanical) rated for bolt diameters between 46 and 90 mm, typical for most hook assemblies. Most manufacturers simply do not test anchors at these sizes because of their infrequent use. Allowable design capacities, when provided, tend to be very conservative as they are not supported by large test data sets. In addition, for concrete installations, the situation is made even more challenging by common design guidelines for post-installed anchorages, such as Appendix D of the American Concrete Institute (ACI) Standard 318, which heavily penalize mechanical anchorage

installations in existing concrete. Existing reinforcing details, often non-conforming to modern code requirements, tend to be conservatively treated as being unreinforced for concrete pullout failure modes, potentially underestimating available capacity.

One successful solution for avoiding the concrete failure penalties is to install new anchor bolts that pass completely through the concrete deck of the supporting structure. In this case, the capacity of the anchors in uplift will be determined by the bearing capacity of washers and bearing plates in the deck soffit in conjunction with global bending of the deck. This approach can be an efficient design where the full tension capacity of the bolt can be more easily developed. Coring anchorage holes up to 155 mm in diameter through 2 m of reinforced is not an especially difficult practice. Issues such as conflicting deck reinforcement, interfering piles, as well as other obstructions can often be addressed by ordering custom hook assembly bases that allow placing the anchor bolts in desirable locations. Specifying custom bases will impact hook procurement times, but typically do not significantly increase the cost.

Another advantage of the through bolt design is that a hole pattern can be selected that is outside the footprint of the existing mooring hook as shown in **Figure 2**. This placement can allow coring work to be done before the old hook is pulled from service, greatly reducing the time to swap out an old hook for new during a terminal shutdown.

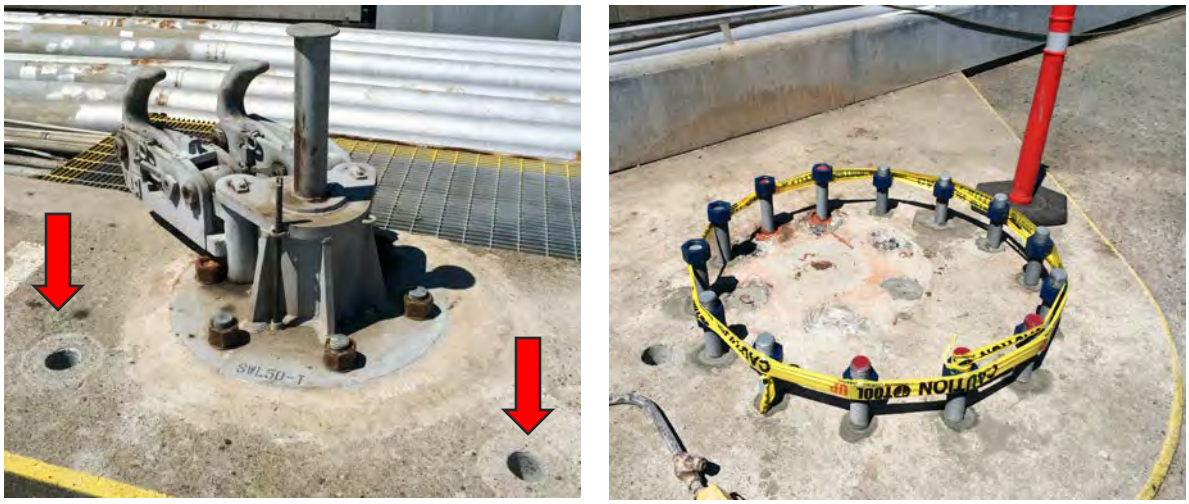

Figure 2: New mooring hook installations showing preinstalled coring for anchor bolts (left, arrows) and new bolt pattern prior to setting the new hook assembly (right).

2.5 Supporting Structure Capacity

Generally, the mooring structure has sufficient capacity to support an in-kind hook replacement. When the hook is upgraded with a larger SWL or additional hooks, the supporting structure might not have sufficient local or global capacity to support the new larger hook demands. In this case, a decision will need to be made to determine the proper path forward. While local strengthening is often feasible, global strengthening of the mooring structure can often prove to be too costly. In addition to local or global strengthening, it might be an option to reduce the potential loads on the structure. This can be done by limiting the size of the vessels that call at the terminal or limiting acceptable operating wind conditions.

2.6 Operational Considerations

Replacing mooring hooks often occurs at one time and may require weeks of terminal shutdown to install. For multi-berth facilities, this is not a big concern. However, for smaller, highly used terminals, this can be a significant disruption to service with business losses far exceeding project costs. In these cases, the hook installations can be timed to fit around vessel schedules, can be split up to install one hook at the time, and careful planning of the installation can minimize downtime. If the vessel schedules are known, mooring locations that will not be used during the upcoming arrivals can also be scheduled for replacement with no impact on operations.

2.7 Global Mooring System Considerations

Hook replacement projects are always at risk of ignoring overall mooring system performance with respect to the new work. The design professional can easily overlook the global aspects of the system and just jump into hook design, which is often the task assigned. This limited approach, when narrowly following the hierarchy of failure, may result in inefficient designs with an uneven distribution of the safety margin in the system. This uneven distribution is a characteristic often associated with over conservative and unnecessarily costly designs.

To avoid these situations, a detailed mooring analysis of the entire mooring system with the actual vessel fleet calling on the terminal and real environmental loads should be done by the design professional to understand the real demands in the system. Only by comparing these demands with actual capacities of the various components of the mooring system can the designer comprehend the force flow and margin of safety in the system. Careful evaluation of the results of this system analysis will make apparent if there is an unreasonable margin of safety for any individual component. Ultimate capacities of each component should be compared in this analysis with actual working loads to determine the relative safety margin. For cases where mooring structures are require strengthening or replacement, alternative mooring arrangements should also be considered, including the addition of new mooring points.

3. DESIGN EXAMPLES

A few design examples highlighting the lessons learned from successful mooring hook unit installations at existing terminals are provided in this section.

3.1 Selecting the Best Mooring Line Strength for Design

A California marine oil terminal serving vessels up to 188,000 DWT was in the process of replacing some of their mooring hooks to mitigate mooring arrangements that utilize two lines per hook, as well as to install tension monitoring at all mooring points. At this terminal, the existing mooring dolphins support double hook mooring assemblies, with each hook having a SWL of 45 MT. While this size of mooring hook can appear to be undersized for the size of vessels calling at this terminal, a comprehensive mooring analysis confirmed that operations were safe even under the combined loads of maximum currents and survival level wind speeds.

By using the available guidelines for mooring hook design, the size of the hooks would have to increase considerably as would the supporting mooring dolphins at significant cost beyond that of new hooks. In this case, it was therefore decided to not use the vessel MBL as a guideline for selecting hooks and new hooks were installed with a SWL that matched the original installation.

3.2 Selecting the Right Number of Mooring Hooks

In the example above, before the installation of the new hooks, the terminal would commonly tie up vessels with three lines to one double hook assembly, thereby often driving two thirds of the load to

the assembly into just one hook. To improve operations, the terminal owner decided to go with triple hooks instead of the existing double hook arrangement. By installing just one additional hook, selecting a triple hook assembly instead of a double hook assembly, the actual maximum load seen by one hook was reduced by 50%. The load on the total assembly did not change.

3.3 Anchorage Design

In the example above where double hooks were replaced by triple hooks, the selected hook SWL was much lower than what would have typically been selected for a new terminal design. As mentioned, comprehensive mooring calculations were performed to ensure that this approach was feasible. As the ultimate capacity of the hooks are so much higher than the SWL, there were concerns that the anchorage to the mooring dolphin might not be strong enough. The anchorage itself was therefore designed based on the MBL of the strongest line. Anchor bolts were installed as through-bolts to ensure that full tension capacity of the bolts could be developed.

3.4 Selecting the Best Hook Safe Working Load (SWL)

For the example, while the existing mooring arrangements worked safely, with additional safety factors on both the SWL of the mooring hooks as well as the capacity of the supporting marine structures, the goal of the upgrade was not to increase the mooring capacity of the berth, but to improve operations by avoiding the need for two lines per hook mooring arrangements as well as to install tension monitoring. The operator decided that it was important to not install mooring hooks with more capacity than the existing ones to avoid driving more loads into the supporting structures and requiring significant strengthening.

The decision was made to install mooring hooks with the same SWL as the existing ones, but to replace the double hook units with triple hook units. This way the mooring dolphins would see the load from the same number of lines, but with similar safety factors in place when tying up the lines. While the new mooring hooks will not have a SWL larger than the MBL of the anticipated strongest mooring line, their proof load is larger than the MBL, as are both the yield and ultimate loads. The mooring hardware was also checked against actual loads, with proper load factors applied, with resulting acceptable factors of safety. This rational approach avoided unnecessary upgrades to the terminal that would not necessarily increase terminal safety.

3.5 Supporting Structure Capacity

Through the process described above, no strengthening of the existing supporting structure was needed. The selection of mooring hooks with the same SWL as the existing hooks in combination with the increase form double to triple hooks ensured safer operations, but with no increased chance of overloading the structure.

At another terminal site, local strengthening of the deck was required to provide sufficient capacity for support of the hooks. In this case, the deck was strengthened locally by thickening the section immediately around the hook anchorage from above or below to achieve the requisite bending capacity. This is shown in **Figure 3**. Although much easier to install from above, deck thickening also needed to consider hook access and use. It was needed to provide sufficient space around the hook for an operator to work without falling off the transition and to not elevate the integrated capstan too by the thickening, potentially making use difficult.

Figure 3: An example of localized deck strengthening in preparation to support a new quick-release mooring hook on an existing wharf deck.

3.6 Rapid Installation Considerations

For one California terminal replacing old mooring hardware, the installation time to install eight new quick-release hook units at once was determined to be too disruptive to terminal operations and would possibly conflict with a berth availability agreement with a major client. The terminal was too small and located in a relatively exposed site to allow multiple construction barges to operate to speed installation and reduce terminal downtime. To reduce the impact of the project, a piecemeal installation scheme was developed in cooperation with the owner and construction contractors, requiring only three days of berth shutdown to replace the mooring hook units at each mooring point. With only three days of closure, the operator felt confident the work could proceed within the normal gaps in the berth schedule.

To allow for this rapid installation, the anchorage at each mooring point would have to be installed with the existing hook assembly in service. The mooring structures at this terminal were too small to accommodate a parallel installation where a new hook assembly could be installed adjacent to the in-service hook. Rather, a new anchorage had to be installed around the existing, requiring the specification of custom bases for the new hooks with a bolting pattern outside the footprint of the existing.

By ordering the custom base, the contractor could core the marine structure deck and install the anchor bolts prior to new hook placement. A three-day window was left the pull the old hook, cut the old anchor bolts flush with the existing deck, place the new hook, and grout the new base. By the time the 6th hook was installed, only a two-day window was required. Most new hook units are immediately operable without installation of tension monitoring instrumentation and power. These systems were added later with the new hooks in service, greatly reducing berth downtime.

4. CONCLUSIONS

Unlike new installations, design new mooring hooks require more attention by the design professional to prevent overly conservative and costly installation schemes. Blindly following new design guidelines for retrofit or replacement project may result in impractical designs. Care must be used to carefully consider whether maintaining the hierarchy of failure is necessary or appropriate to maintain a sufficient margin of failure.

5. REFERENCES

British Standard (BS 2014), “Maritime Works: Code of Practice for Design of Fendering and Mooring Systems”, BS 6349-4:2014. 2014.

California Building Code (CBC 2016), Chapter 31F, Title 24, Marine Oil Terminal Engineering and Maintenance Standards (MOTEMS), California State Lands Commission, Sacramento, CA. 2016.

Iversen, R. (Iversen 2014), “Structural Considerations for Selection of Quick-Release Mooring Hooks”, Proceedings of the PIANC World Congress, San Francisco USA. 2014.

PIANC (PIANC 2017), “Recommendations for the Design of Marine Oil Terminals”, PIANC Working Group MarCom 153, PIANC, Brussels. 2017.

Unified Facilities Criteria (UFC 2017), “Design: Piers and Wharves”, UFC 4-152-01. January 2017.

CASE STUDY: ENGINEERING OF A EPC 3KM JETTY FAST TRACK PROJECT

by

***Hubert Vander Meulen*[1]**

Keywords: Jetty, EPC, In-house engineering, tight schedule, remote location, seabed reefs

1. INTRODUCTION

Arab Petroleum Pipelines Company (SUMED) has developed a refined product terminal hub at Ain Sukhna, Suez Egypt, adjacent to the existing crude oil terminal, to include the services of storage, loading, unloading and send out of Fuel Oil, LPG and Natural Gas. In addition, SUMED's aim is to make the facilities expandable for future expansions including other refined products.

The BESIX-Orascom Joint Venture has constructed a 3 km F-shaped jetty. The project consists of three berths, including berthing furniture and M&E works. The construction time was less than one year.

The paper will consist in a case study about the fast track engineering study in the framework of a challenging EPC contract with limited information at start of the detailed design. The mains challenges of the project have been:

- Extremely tight construction schedule
- Absence of trustable geotechnical investigation at start of the works
- Top side equipment and layout not fully defined at the start of the detailed design

2. JETTY LAYOUT

Owner considered no dredging for this project. Following constraints have governed the layout of the jetty:

- Vessels sizes, under keel clearance, turning basins requirements
- Exclusion zones between the different berths
- Presence of reefs at the seabed
- Existing SPMs and corresponding pipelines

The adopted layout consists in an “F-shaped” jetty with two Product Berths at the deepest arm and a LNG FSRU Berth at intermediate water depth. The berth orientation matches with the currents while the trestle is perpendicular to the shoreline.

The range of vessel being wide, each berth is fitted with four berthing dolphins and six mooring dolphins. One mooring dolphin has been added to the LNG FSRU berth during construction to cope with the unexpected position of the first FSRU vessel at the loading platforms. The loading platforms are equipped with fenders as well to allow safe berthing of the smallest vessels of the range.

[1] BESIX Engineering Department Belgium, hvandermeulen@besix.com

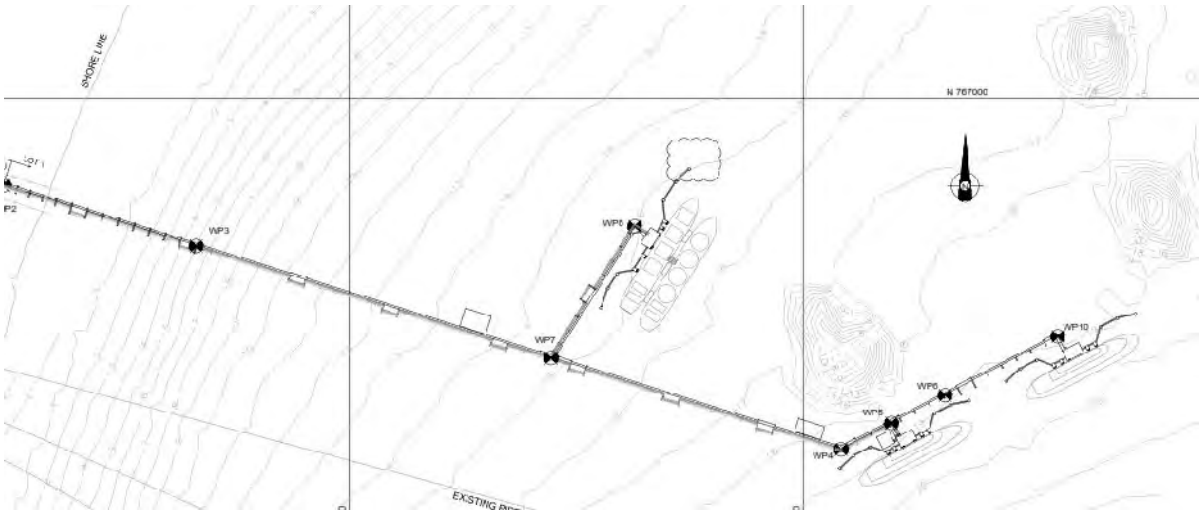

Figure 1: Jetty Layout

3. DESIGN VESSELS

At both Product Berths, the design vessels are ranging from 160,000 DWT Suezmax Fuel Oil to 5,000 m³ LPG Carrier. The FSRU Berth is designed to host a 170,000m³ FSRU vessel hosting a guest 216,000 m³ LNG Carrier in Tandem configuration. This berth is also design for LPG carriers ranging from 82,000 m³ to 5,000 m³

4. ENGINEERING SCHEDULE

The engineering schedule being very tight, a basic design stage with some tangible targets has been prepared immediately after kick-off. Its results with the associated limitations was provided to the procurement team to enable market enquiries while the detailed design was progressing.

5. GEOTECHNICAL INVESTIGATION AND CONSEQUENCES ON DESIGN

A soil investigation campaign was part of the detailed design package. In order to compensate the time required to mobilize a floating equipment in this remote area, the campaign has started with land-based equipment operated from a temporary bund. It has allowed the early identification of a liquefiable layer in the first 300meters of the jetty where a permanent causeway was originally planned. The stability of a traditional rubble mounted causeway was jeopardized by the presence of this layer. Hence, it has been proposed to cast vertical concrete piles through a temporary bund with land-based equipment.

The marine CPTs preformed by the JV indicated a soil profile constituted of alternating weak sand and soft clay layers. The interpretations of the results of the soil investigation lead to very long steel piles to be installed for the jetty (up to 75m). Two static load pile test at two different locations have confirmed the design. At each location, 4 piles where installed: two reaction piles, 1 compression test pile and 1 tension test pile. A spreading beam allowed to test in compression and tension with the same reaction piles.

6. STRUCTURAL DESIGN

The paper will describe structural design of the trestle, platform and dolphins. Pile design was mainly governed by geotechnical bearing capacity and by the combination of axial force and bending moment. The installation of the very long piles with jack-up barges was also carefully designed. The very long stick up portion of their length above the driving gates before start of driving leads to high localized

stress. Finite 3D models where undertaken to check the risk of local buckling inside the gate supports under the combined effects of: self-weight of the pile; weight of the driving equipment and compression wave during driving.

The crosshead beams joining the piles have been designed to work properly in absence of piperack, with 1 or with 2 piperacks. As the jetty has a particular F shape, piperacks are crossing the roadway at some locations. Particular crossheads have been designed to support the piperack bridges at these locations. The roadway spanning from Crossheads to crossheads has been designed as simply supported on a 36m span. It is made of a composite deck. On top ow welded steel beams, precast planks are installed which are connected to the main beams via in-situ concrete and pockets of shear studs. This choice of structural solution has allowed procurement near the site, ensuring guarantee on the delivery.

The loading platforms are supported on a mixture of vertical piles and raked piles, to resist horizontal loads from fenders. Services platforms are supported on vertical piles.

Figure 2: View from Product Berth 2: Product Berth 1 and FSRU berth

7. M&E REQUIREMENTS

In order to allow early exploitation of the terminal, during design to support water piping and gas piping along the jetty. Extension of the bracings of the main roadway girders at the outer side has been designed as support for the piping.

8. CONCLUSION

This case study demonstrates how the detailed design by an in-house engineering department of an EPC contractor has allowed building the jetty in the required period with the selected equipment. Focus has been set on the constructability of the different parts of the project, showing the interconnections between: design; procurement and construction, resulting in a safe and efficient project.

BENDING VIBRATIONS OF THE AFSLUITDIJK GATES SUBJECTED TO WAVE IMPACTS: A COMPARISON OF TWO DESIGN METHODS

O.C. Tieleman[1,2], B. Hofland[1], S.N. Jonkman[1]

ABSTRACT

This paper describes a first case study of the application of a newly developed fluid-structure interaction model to the design of flood gates. The gates in the Afsluitdijk, that will be replaced in the coming years, are considered. Due to the presence of a concrete beam in front of the gates breaking wave can occur, leading to high impact pressures acting on the gate. For this case both a quasi-static approach and a more detailed semi-analytical model representing the dynamic behaviour including fluid-structure interaction are applied to determine the maximum deflection of the gate. Results show the capability of the model to efficiently quantify flood gate vibrations while considering the involved fluid-structure interaction. For the Afsluitdijk case this leads to a slightly lower maximum deflection of the gate, and therefore potentially allows a more economical design.

INTRODUCTION

A vast amount of flood defence structures contribute to the safety and water regulation in coastal areas. Gates form essential parts of these systems as they regulate the discharge between bodies of water. During storm conditions these structures are often subjected to high water levels and waves. When breaking waves impact on a gate, this generally involves high peak pressures of short duration in the order of a few milliseconds (Bagnold, 1939; Hofland et al., 2011; Ramkema, 1978). Such impulsive loads lead to vibrations of the structure, potentially amplifying internal stresses compared to the static situation.

From 2018 to 2022 the Afsluitdijk in the Netherlands is being renovated, including the replacement of 25 steel flood gates in two discharge sluice complexes. Due to the presence of the overhanging monumental concrete defence beam as shown in Figure 1, inpacting waves were expected to result in high impact pressures. This was confirmed in physical scale experiments performed in the Deltares Scheldegoot (Hofland, 2015), where peak pressures were measured corresponding to 32 times the significant wave height related pressure, $\rho g H_{m0}$. The gate strength required to withstand these pressures lead to a gate design with high weight, having consequences for the lifting mechanism and towers as well. The decision was therefore made to remove the monumental defence beam.

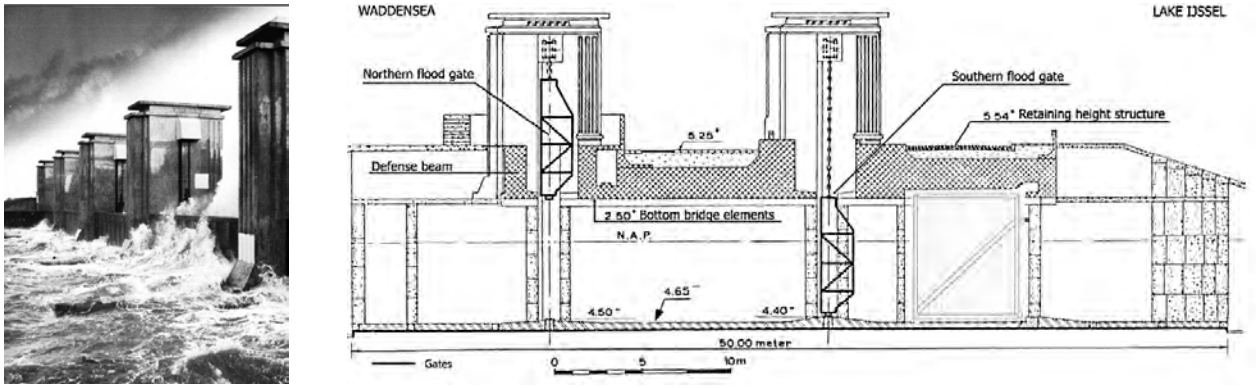

Figure 1: Wave impacts on the defence beam (left) (Thijsse, 1972) *and a cross-section of one discharge sluice at Den Oever (right)* (Tieleman, 2016)

[1] Delft University of Technology, Faculty of Civil Engineering and Geosciences
[2] Corresponding author, email address: o.c.tieleman@tudelft.nl

Due to the two-way interaction between the structure and fluid, detailed prediction of these dynamic interactions can become very complex. Advanced numerical methods exist, but are still computationally expensive for three-dimensional problems (Erdbrink, 2014). For this reason in common engineering practice a quasi-static approach is often used in which an amplification factor is applied to the time-varying load to account for dynamic behaviour of the gate (Kolkman & Jongeling, 2007a, 2007b, 2007c). Such an approach however lacks behind in accuracy and resolution compared to design standards in other fields, and gives little insight in the actual behaviour of the structure. For this reason, a semi-analytical model using fundamental theory of dynamics of continuous systems was developed (Tieleman, 2016)In the present study, a comparison is made between outcome of the common design method and the semi-analytical model for the case of the Afsluitdijk flood gates. It is shown that explicitly predicting the dynamic behaviour of gates including the fluid-structure interaction may lead to different outcomes and more economic designs.

CASE DESCRIPTION

After the renovation of the Afsluitdijk the seaside gates in the discharge sluices will retain the water during storm conditions; the other gates are for water regulations during daily conditions. The gates are required to withstand the net hydrostatic force due to the water level difference and the wave impact force corresponding to 1/10,000 year return frequency hydraulic boundary conditions. In the present study the latter is considered.

A gate design was made by an engineering firm as shown in Figure 2. The design wave impact pressures have been determined in scale experiments and are considered to be acting simultaneously over the full width of the gate. The spacing between the horizontal girders is reduced towards the top of the gate to increase its resistance at the location where the wave impact leads to the highest pressures.

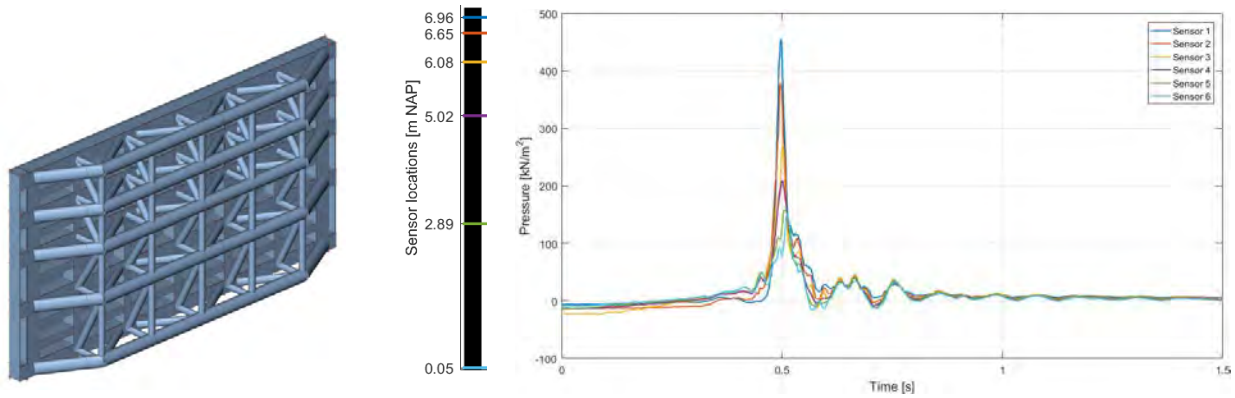

Figure 2: Conceptual flood gate design for the Afsluitdijk (Witteveen+Bos, 2016) *(left), and the governing wave impact pressure as measured in scale experiments at 6 locations with z = 0 at the bottom of the gate (right). Data:* (Hofland, 2015). *In this study the gate is represented by a thin plate.*

In the present study, the gate is represented by a thin plate with equal total mass. The stiffness is chosen such that the fundamental dry frequency of the thin plate is equal to that of the realistic gate design. The thin plate is expected to be a reasonable approximation when considering the deflection of the gate. However, it does not give correct insight in the occurring stresses in the realistic gate design. In contrast to the real gate design, the mass and stiffness are equally distributed over the uniform plate. The gate is simply supported at both vertical sides and is stress-free at its top and bottom. The sluice is assumed infinitely long, which simplifies the derivation of the hydrodynamic response to gate vibrations. The gate is slightly wider than the sluice due to sockets at this location. An overview of the model geometry is shown in Figure 3. All case parameters and their values are summarised in Table 1.

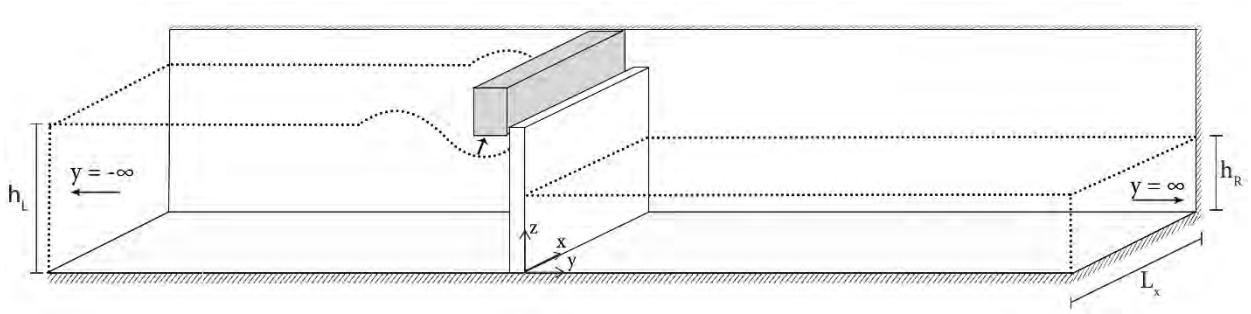

Figure 3: Three dimensional overview of the model geometry

Table 1: Case parameters

Structural parameters	Symbol	Value	Unit	Fluid parameters	Symbol	Value	Unit
Gate width	L_x	12.5	m	Sluice width	L_x	12	m
Gate height	L_z	7.25	m	Water level sea	h_L	7.25	m
Plate thickness	t	0.64	m				
Bending stiffness	D	$4.36 \cdot 10^9$	Nm^2	Water level lake	h_R	3.35	m
Distributed mass	ρ_s	929	kg/m^2	Fluid density	ρ_f	1025	kg/m^3
Modulus of elasticity	E	$2 \cdot 10^{11}$	Nm^2	Fluid sound velocity	c	1500	m/s
Moment of inertia	I	$2.17 \cdot 10^{-2}$	m^4	Gravitational constant	g	9.81	m/s^2
Poisson's ratio	v	0.3	-				
Yield strength (steel)	f_y	$355 \cdot 10^6$	N/m^2				

MODEL APPROACH

The motion of the plate is solved analytically in the frequency domain by a so called modal analysis, including the effect of the surrounding fluid. The motion of the homogeneous and isotropic thin plate is described by the following equation:

$$\rho_s w_{tt} + D[w_{xxxx} + 2w_{xxzz} + w_{zzzz}] = -f_L + f_R + f_e \quad (1)$$

in which w denotes the displacement of the mid-surface of the plate, f_e the time signal of the external force on the plate, and f_L and f_R define the fluid pressures at either sides acting on the surface of the gate. The external force is in this case the measured wave impact pressure signal. As the plate is considered thin, shear deformation is neglected in equation (1). The boundary conditions of the plate are as follows:

$$w(0,z) = M_x(0,z) = w(L_x,z) = M_x(L_x,z) = 0 \quad (2)$$

$$V_z(x,0) = M_z(x,0) = V_z(x,L_z) = M_z(x,L_z) = 0 \quad (3)$$

in which M_x and M_z are the bending moments in x- and z-direction respectively, and V_z is the net shear force in z-direction.

The fluid is described as a compressible potential flow with a boundary condition that accounts for the generation of surface waves. At the moment, the effect of the defence beam on the responsive fluid pressures is excluded, i.e. the free boundary condition of the fluid is not altered at this location. The equation of motion and boundary conditions for the fluid domain at the right side of the gate are:

$$\nabla^2\phi - \frac{1}{c_p^2}\phi_{tt} = 0 \quad (4)$$

$$\phi_{tt}(x,y,h_R,t) + g\phi_z(x,y,h_R,t) = 0 \quad (5)$$

$$\phi_x(0,y,z,t) = \phi_x(L_x,y,z,t) = \phi_z(x,y,0,t) = 0 \quad (6)$$

$$\phi_y(x,0,z,t) = w_t(x,y,t) \quad (7)$$

in which ∇ is the Nabla operator, ϕ is the fluid potential, and c_p is the sound velocity in water. Further, the radiation condition at $y = \infty$ should be satisfied at all times. The boundary conditions for the left side of the gate are similar with $y = -y$.

An analytical solution to this system can be derived by describing both the structure and fluid as a summation of their modal shapes (W_{km}, Φ_{pr}) multiplied by yet unknown modal constants (A_{km}, B_{pr}):

$$w = \sum_{k=1}^{\infty}\sum_{m=1}^{\infty} A_{km} W_{km} \tag{8}$$

$$\phi = \sum_{p=1}^{\infty}\sum_{r=1}^{\infty} B_{pr} \Phi_{pr} \tag{9}$$

in which k and m denote the modal shapes of the structure in x- and z-direction, and p and r those of the fluid. The modal shapes and corresponding natural frequencies can be found either analytically or numerically. Subsequently, the following semi-analytical solution can be obtained by describing the motion of the entire fluid-structure system fully in terms of the modal coefficients of the structure:

$$\sum_{k=1}^{\infty}\sum_{m=1}^{\infty}\left[\rho_s(\omega_{km}^2 - \omega^2)\delta_{kl}\delta_{mn}\Gamma_{ln} + L_{km,ln} + R_{km,ln}\right] A_{ln} = F_{ln} \tag{10}$$

in which ω_{km} are the natural frequencies of the plate modes, δ_{kl} and δ_{mn} are Kronecker deltas, Γ_{ln} is the result of the surface integration $\iint_S W_{km}\, W_{ln}\, dx\, dz$, $L_{km,\mathrm{ln}}$ and $R_{km,\mathrm{ln}}$ are the the fluid impedances at both sides of the gate, S is the surface area of the plate or fluid in the x,z-plane, the modal force $F_{ln} = \iint_S \hat{f}_e\, W_{ln}\, dx\, dz$, and $\hat{f}_e$ is the representation of the wave impact force in the frequency domain. For an extensive derivation and description of the fluid impedances is referred to (Tieleman et al., 2018; Tsouvalas & Metrikine, 2013).

To solve the system of equations, the summation should be truncated to a finite number of structural and fluid modal shapes. The obtained frequency domain solution can be transferred to the time-domain by an inverse Fourier transform.

QUASI-STATIC ANALYSIS

The existing design analysis for the flood gates is based on a quasi-static approach by means of a finite element model. This analysis includes several assumptions that cannot be translated when regarding the dynamic response of the gate to the measured full time signal of the occurring wave pressures. Secondly, the uniform thin plate will change the static behaviour compared to the actual gate design. In this section, a similar quasi-static design approach is therefore applied by means of the analytical plate model to allow for a good comparison with the results of the dynamic analysis in the following section. Regular load and safety factors are excluded for clarity. Only the deflection of the gate is considered for the comparison, internal stresses are not quantified, but can be obtained from the model.

Amplification of the deflection due the dynamic response of the gate was considered based on the theory of (Kolkman & Jongeling, 2007b) for impulsive loads and single degree of freedom systems. The duration of the impulsive part of the vertically integrated pressure signal was estimated to be τ = 30 ms. This value is based on a scale model, so could be prone to scale effects. The fundamental period of the gate in dry condition is approximately T = 45 ms. The ratio τ/T is in this case close to the point where according to Figure 4 maximum amplification of $1{,}85 * \pi/4 = 1{,}45$ occurs. This factor was therefore applied to the maximum wave force to obtain the design load, and will be included in the present analysis as well.

It must be noted however that the theory of (Kolkman & Jongeling, 2007b) allows one to consider the hydrodynamic mass when estimating the resonance frequency of the gate. The hydrodynamic mass increases the resonance period of the gate, leading to a different amplification factor.

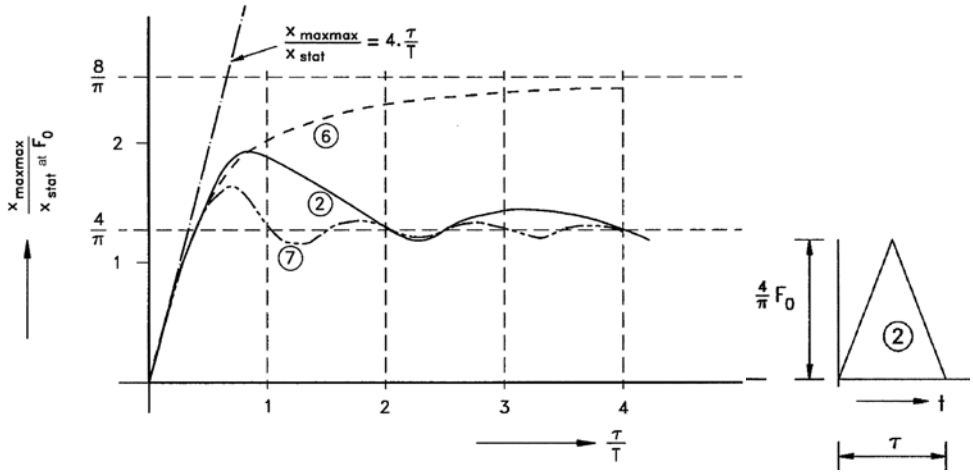

Figure 4: Amplification of a single degree of freedom structure to a triangular-shaped impact force signal (Kolkman & Jongeling, 2007b)

The applied wave pressure force including amplification factor and the determined static response of the gate to this force are shown in Figure 5. The deflection is found with equation (10), excluding the fluid impedance which is zero in the static situation. The maximum static deflection of 21.8 mm is found at the top middle of the gate. The maximum stress in the plate occurs at the same location and equals 84.8 N/mm^2. The static response of the gate to the hydrostatic force (difference) is an order of magnitude smaller, and not considered further. The modal decomposition and the static response predicted by the analytical model have been validated by FE software.

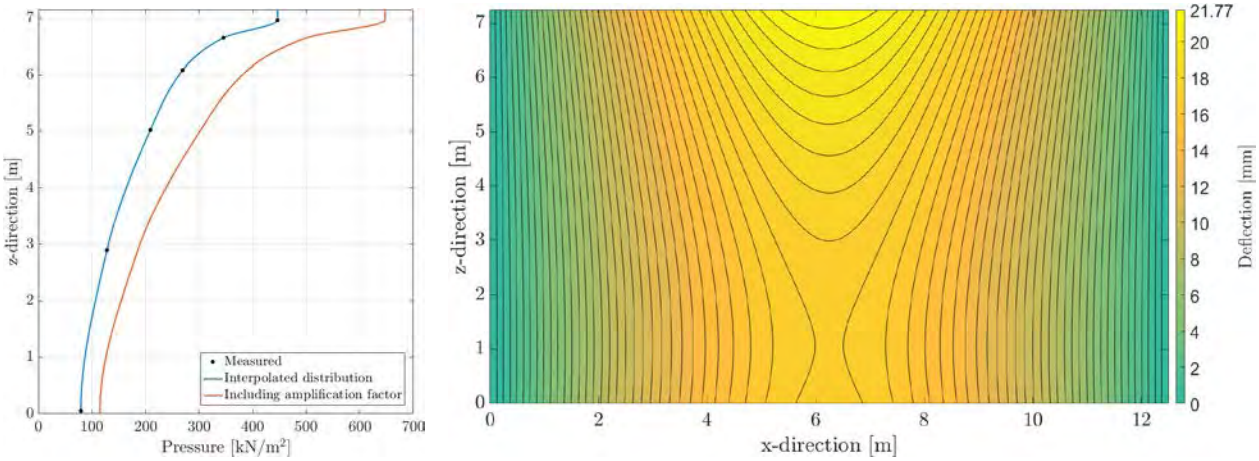

Figure 5: Maximum measured wave pressures with and without amplification factor (left) and the static response of the gate to the wave force including amplification factor (right)

DYNAMIC ANALYSIS INCLUDING FLUID-STRUCTURE INTERACTION

In the following analysis the dynamic behaviour of the plate is solved by means of the analytical solution in eq. (10), which implicitly takes into account the effect of the hydrodynamic pressures resulting from the motion of the gate. The full time-domain wave pressure signal is applied, which varies over the vertical of the gate, and is assumed constant over the width. For the present analysis the summation of 25 structural modal shapes is considered. The first four modal shapes are shown in Figure 6.

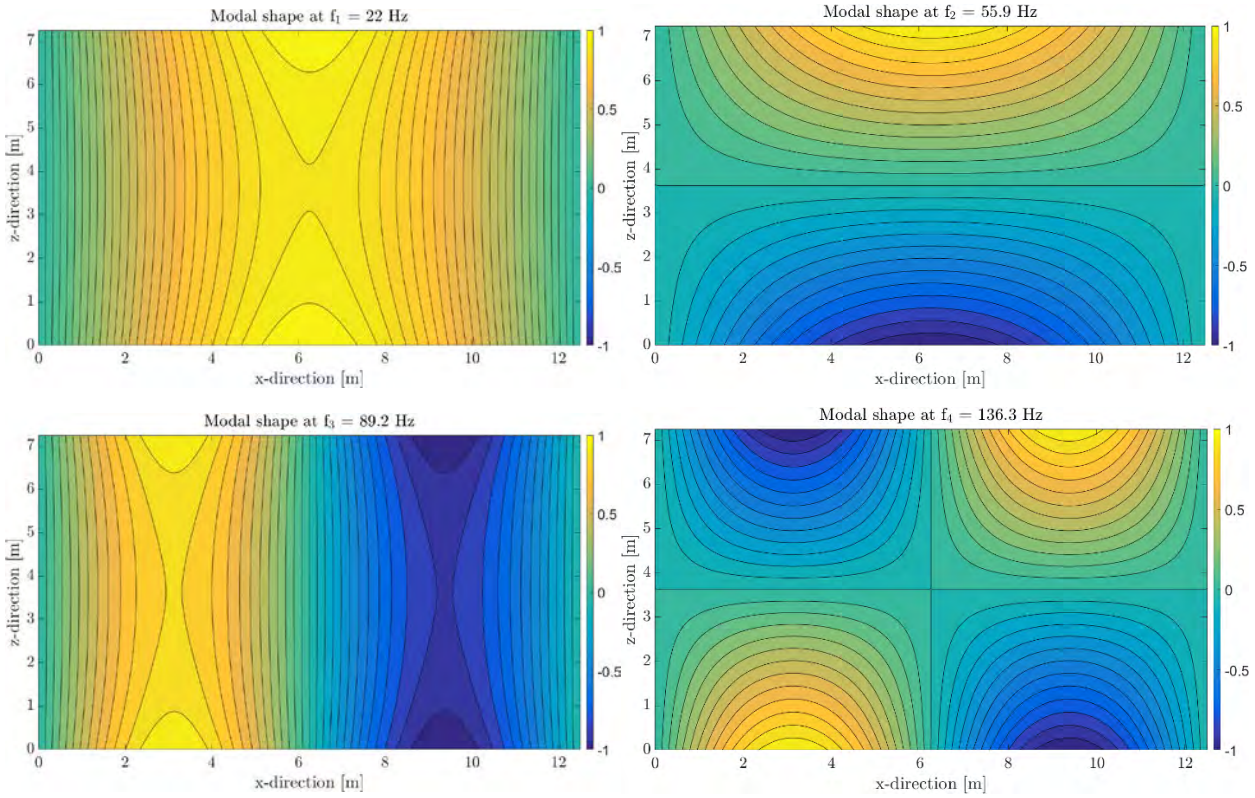

Figure 6: First four natural frequencies of the plate in dry condition

Due to the hydrodynamic pressures the resonance shapes and frequencies of the gate-fluid system are different from those of the gate in dry condition. The hydrodynamic mass significantly reduces the resonance frequencies, as shown in Table 2. Since the wave pressure acts simultaneously over the entire width of the gate in this case, the antisymmetric modes in this direction are not excited.

Table 2: Resonance frequencies of the gate in vacuo and in submerged condition

Condition	f_1	f_2	f_3	f_4	f_5	f_6
In vacuo [Hz]	22	55.9	89.2	136.3	189.8	201.9
Submerged [Hz]	10	32	44.2	83.1	108.2	116.2

To obtain a stable time signal after application of the inverse Fourier transform, a small amount of material damping is introduced in the model by applying a complex bending stiffness $E = (1 + \eta i)\, E$ with damping coefficient $\eta = 0.01$. In Figure 7 the deflection of the mid bottom and mid top of the gate are shown in time. The maximum deflection now occurs at the bottom of the gate, contrary to what was found with the quasi-static approach. Decreasing the strength of the gate towards the bottom as was done in the gate design of Figure 2 might therefore not be beneficial. The maximum deflection equals 19.9 mm and the maximum stress at this location is 79.4 N/mm^2. The relatively difference between stress found in the quasi-static and dynamic analysis is slightly less than for the deflection, as higher modal shapes result in larger stresses for the same deflection.

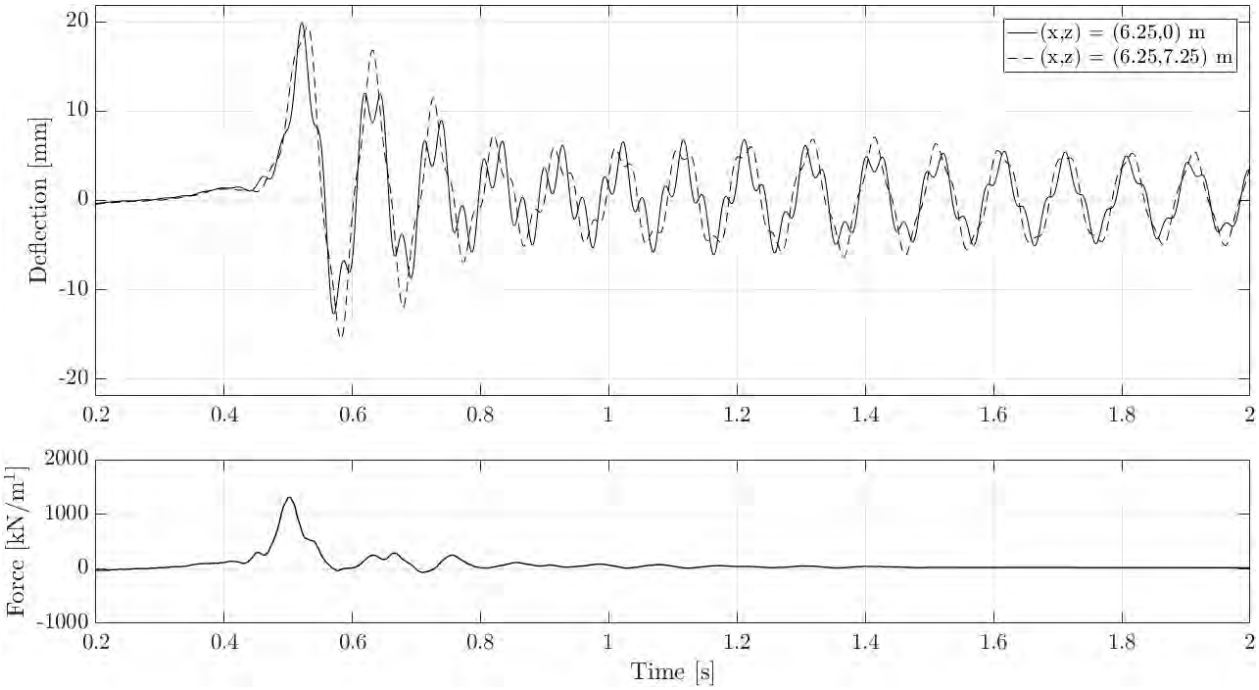

Figure 7: Deflection of the middle top and bottom of the gate as a result of the wave impact

The maximum deflection obtained at the top of the gate is 19.47 mm, which is about 11% lower than what was found in the quasi-static analysis. The second modal shape of the plate is amplified the most, while the first modal shape does not amplify as much as the quasi-static approach assumes. Due to the domination of the first mode in this case, the net effect is relatively small compared to the quasi-static approach. This is however not given for other designs or wave signals.

Table 3: Deflection at the top of the gate in mm as found by both methods compared to the static deflection without amplification

Structural mode	Deflection (static)	Amplification (quasi-static)	Deflection (quasi-static)	Amplification (dynamic)	Deflection (dynamic)
1	13.45	1.45	19.50	1.29	17.30
2	1.60	1.45	2.32	1.39	2.22
3 to 25	-0.04	1.45	-0.06	1.25	-0.05
Total	15.01	1.45	21.76	1.30	19.47

DISCUSSION

The semi-analytic model describes the dynamic behaviour of the gate-fluid system including the involved fluid-structure interaction. Further validation of the model is still required. Small scale model tests are planned to obtain this validation.

The effect of the defence beam on the hydrodynamic response to the motion of the gate was neglected in the analysis. This simplification is expected to significantly change the fluid pressure distribution. For a more accurate analysis the boundary conditions imposed by the defence beam should therefore be included when determining the modal shapes of the fluid. This can be accomplished by including a separate fluid domain with closed boundary condition at the top of which the modal decomposition is matched to the domain seaward of it. Additionally, when determining the fluid modal shapes the water level is considered to be constant. In reality, over a certain distance the free surface is altered due to the incoming breaking wave.

The comparison between the two design approaches was based on the representation of the gate by a thin plate. Although this may give a good indication of the relative difference between the two design methods, this does not accurately represent the deflection and internal stresses of a more realistic gate design. With the presented semi-analytical model it is possible to apply modal shapes of the gate found by FE software.

In this way, it is possible to utilise the precision of the FE model to determine the gate deflection and internal stresses while including the fluid-structure interaction in a computationally efficient manner.

In reality a storm consists of thousands of waves, and the impact with the highest impact does not necessarily give the largest response. Hence, in a real case, more or all impacts need to be considered. As the duration of impacts is prone to scale effects (the total impulse is expected to be scaled well), some variation in the duration of the impacts is to be taken into account as well.

CONCLUSIONS

The semi-analytic model represents the dynamic behaviour of the gate more precisely than the common quasi-static approach on several aspects. First of all, the interaction with the surrounding fluid is taken into account. As expected, the hydrodynamic mass is shown to have a substantial effect on the natural frequency of the designed gate, leading to a different response and in case of the Afsluitdijk a lower amplification of the first modal shape of the gate. The method allows to determine the effect of the temporal and spatial distribution of the measured wave impact signal on the gate's response. Finally, multiple gate vibration modes were included in the analysis. For the Afsluitdijk case, the second modal shape of the gate was significantly excited as well. The net result was a slightly lower deflection and internal stress.

Compared to application of the maximum dynamic amplification factor to the entire measured wave force signal, it is expected that more detailed inquiry into the dynamic behaviour of the gate will generally result in better gate designs.

ACKNOWLEDGMENT

This research was supported by Rijkswaterstaat (contract RWT31120028).and NWO grant AL-WTW.2016.041.

REFERENCES

Bagnold, R. A. (1939). *Interim Report on Wave-Pressure Research. (Includes Plates and Photographs). Journal of the Institution of Civil Engineers* (Vol. 12). https://doi.org/10.1680/ijoti.1939.14539

Erdbrink, C. D. (2014). *Modelling flow-induced vibrations of gates in hydraulic structures*. PhD thesis.

Hofland, B. (2015). *Modeltesten golfkrachten spuisluizen Afsluitdijk*. Technical report. *Deltares*

Hofland, B., Kaminski, M., & Wolters, G. (2011). Large Scale Wave Impacts on a Vertical Wall. *Coastal Engineering Proceedings*, *1*(32), 15. https://doi.org/10.9753/icce.v32.structures.15

Kolkman, P. A., & Jongeling, T. H. G. (2007a). Dynamic behaviour of hydraulic structures - Part A. *Delft Hydraulics*, 304. Retrieved from http://repository.tudelft.nl/view/hydro/uuid:057be929-11e8-4da0-93cd-7df8c59d1d4d/

Kolkman, P. A., & Jongeling, T. H. G. (2007b). Dynamic behaviour of hydraulic structures - Part B. Retrieved from http://repository.tudelft.nl/view/hydro/uuid:057be929-11e8-4da0-93cd-7df8c59d1d4d/

Kolkman, P. A., & Jongeling, T. H. G. (2007c). Dynamic behaviour of hydraulic structures - Part C. *Delft Hydraulics*, 304. Retrieved from http://repository.tudelft.nl/view/hydro/uuid:057be929-11e8-4da0-93cd-7df8c59d1d4d/

Ramkema, C. (1978). A model law for wave impacts on coastal structures. *Coastal Engineering Proceedings*, *16*(Figure 7), 2308–2327.

Thijsse, J. T. (1972). *Een halve eeuw Zuiderzeewerken 1920-1970*. HD Tjeenk Willink.

Tieleman, O. C. (2016). *The dynamic behaviour of pump gates in the Afsluitdijk*. Delft University of Technology.

Tieleman, O. C., Tsouvalas, A., Hofland, B., & Jonkman, S. N. (2018). A three dimensional semi-analytical model for the prediction of gate vibrations. *To Be Published*.

Tsouvalas, A., & Metrikine, A. V. (2013). A semi-analytical model for the prediction of underwater noise from offshore pile driving. *Journal of Sound and Vibration*, *332*(13), 2283–2311. https://doi.org/10.1016/j.jsv.2013.11.045

Witteveen+Bos. (2016). *Herbeschouwing systeemontwerp noordelijke hefschuiven van spuicomplexen Den Oever en Kornwerderzand naar aanleiding van schaalmodelproeven Deltares*.

HYDRODYNAMIC ASPECTS OF WATERWAY DESIGN AND OPERATION

by

***T.J.P. Sellers*[1]**

ABSTRACT

As a ship sails through a waterway there are many considerations that influence the path of the ship. Obvious culprits include the bathymetry of the waterway, the presence of waterborne traffic, the availability of maneuvering devices, such as tugs and thrusters, and the environment. The less obvious, factors include the hydrodynamic effects acting within confined waterways. Hydrodynamic phenomena including shallow water effects, forces from passing vessels and confined water forces such as bank suction can be significant and can be the dominant force contribution on a vessel in a waterway. To assess all of the hydrodynamic effects, a combination of simulation tools is required. Model tests, potential flow codes, and complete Navier-Stokes CFD methods are used to develop high fidelity numerical models that can accurately predict the hydrodynamic forces acting on vessels operating in ports and waterways. To study in detail all the hydrodynamic effects present on a vessel during a specific maneuver or operating area is not a cost effective option for most simulation studies. Fortunately, software programs are available that use hydrodynamic databases to predict the motions of vessels in response to confined water hydrodynamics. A combination of software packages is required to assess the full cycle, from transit to berthing, of a vessel in a waterway. Linear potential flow software such as diffraction codes can be used to gain an initial insight into the effect of shallow water on vessel motions and maneuvering software or model tests can be used to determine maneuvering coefficients. Using a set of hydrodynamic databases allows the numerical models of vessels to switch to the most appropriate coefficients for the given surrounding area. Programs such as SHIPMA utilize combinations of depth-to-draft dependent numerical models, that include multiple sets of maneuvering models, first order wave responses, drift forces and interaction models. SHIPMA also allows for the inclusion of maneuvering devices (propellers, thrusters, tugs) combined with an autopilot in order to assess the accessibility of waterway designs for a variety of vessels and environments. In addition to the environmental and area forces acting on in-port vessels, forces from passing ships can be of significant importance when analyzing the limitation of vessels within a port. The ROPES software can be used to predict the effect of a passing vessels on a moored vessel and programs such as aNySIM XMF can be used to study mooring systems and vessel response to environmental and mechanical loading. The hydrodynamic effects experienced in waterways can greatly influence the behavior of vessels, however, it is also important to address the operational feasibility of the maneuvers and operations being simulated. Real-time bridge simulations combined with sophisticated maneuvering models can be used to assess the operational feasibility of maneuvers with input and feedback from operators such as pilots, captains and tug masters. This allows for operational input to be considered in the design process. The models produced at each stage of a study can be used in combination to produce a numerical model that can be used in time domain simulation software in both real-time and fast-time. This type of encompassing model can be efficiently transferred between simulation platforms to allow for accurate and consistent results between tools.

This paper will discuss the use of software to aid and improve simulations of vessels operating within waterways. Cases will be discussed to demonstrate the importance of modeling the complex hydrodynamic effects experienced by vessels in confined water. The utilization of simulation tools and model tests can assist waterway designers and operational personnel with engineering and operational design. This paper focuses on the software and processes used to assess the feasibility and limitations of ports, waterways, mooring systems and operations.

1. INTRODUCTION

U.S. ports are responsible for 4.5 trillion in economic activity, approximately 26% of the U.S. economy (ASCE, 2017). Globalization and the rise of large economies such as China and India are causing ship builders to rapidly scale up the size of vessels. Since 1970, container ships have increased in size 15 fold, with a doubling occurring in the last ten years. Due to the rapid increase in vessel size, ports are encountering new requirements for larger channels, deeper berths and new terminals. The recent expansion of the Panama canal to a depth of 50 feet is passing container ships beyond the capacity of most U.S. ports. Currently, only seven ports in the U.S. can accept vessels with drafts between 45 and 50 feet. In addition to the container ship trade, the U.S. has started exporting liquefied natural gas (LNG) resulting in a demand for new LNG export terminals. LNG vessels have a shallower draft than the large container ships, but have a wide beam and stringent safety requirements that require a maneuvering space greater than most U.S. ports can offer. The culmination of the expanding shipping sector, the increase in vessel size and the expansion of the Panama canal has spurred a “race to the bottom” among U.S. ports.

The U.S. Army Corps of Engineers is tasked with the challenging job of maintaining all U.S. ports and waterways with a limited budget. A large part of improving the waterways of the U.S. includes the work to deepen and widen ship channels and inland waterways. In order to efficiently utilize the limited improvement resources, efficient analysis techniques and tools are required. Organizations such as the Permanent International Association of Navigation Congresses (PIANC) and International Association of Maritime Aids to Navigation and Lighthouse Authorities Maritime Buoyage System (IALA) were established to provided design guidelines for ports and waterways. The PIANC guidelines utilize empirical methods to determine the required depth and width of waterways based upon safety factors applied to considerations such as vessel size, maneuverability, access to tugs and environmental considerations such as wind, wave and current. The outcome of this type of calculation alone can often air on the side of caution creating a costly design that is beyond the system’s requirements. For this reason, American ports have not adopted PIANC guidelines in the way that major European and other international ports have. The lack of design guideline implementation in U.S. ports combined with a vessel control center lacking routing authority has lead to a high frequency of vessel collisions when compared to European and other international ports. With the recent desire to expand U.S. ports, port designers should make use of simulation programs in order to design efficient, optimized and cost effective ports and waterways. With tools that can accurately predict the effect of confined water, engineers can effectively design waterways to the vessel requirements. In order to model these scenarios correctly, the software and maneuvering models must account for the complex hydrodynamic interactions between vessels and their surroundings including both the surrounding area and the applied environment.

Several options are available to study the response of a vessel to confined water. Frequency domain programs can provide an initial insight into the response of vessels in shallow water, however frequency domain programs can miss the non-linear effects associated with shallow water vessel response. Combining frequency domain software with time domain software allows for a better estimate of the response of vessels to non-linear wave effects and allows for the study of different environments, external systems and maneuvers. Fast-time simulations programs, such as SHIPMA, Dolphin and aNySIM XMF can be used to study a variety of cases. SHIPMA can simulate the maneuvering behavior of vessels in ports and fairways and is particularly useful for comparative studies to evaluate several different design possibilities. aNySIM allows for multi-body simulations with the inclusion of mooring systems, thrusters, and other external forces. Advances in CFD are now allowing engineers to study the complex viscous forces at work in confined water hydrodynamics. The use of these programs and the hydrodynamic effects to consider for vessel behavior in ports and waterways is discussed in this paper.

This paper addresses the hydrodynamic aspects of waterway design. The design of a port, harbor or channel can greatly influence the behavior of the ships operating within the waterway. A poorly designed waterway can lead to an increase in downtime, reduced operability and unsafe operating conditions. Hydrodynamic effects such as shallow water effects, bank suction and passing vessels are a few of the challenges facing waterway designers and potentially the captains of vessel’s operating within confined waterways. Predicting the effects of confined water and allowing port pilots to experience a waterway design at an early stage can help engineers and designers to improve design, efficiency and safety of waterway designs. To effectively achieve this, high fidelity

hydrodynamic software must be used to capture the complex hydrodynamic aspects of waterway design.

Several cases studies will be presented to provide examples of how simulation software can be used for cases of ship design, operation design and waterway design. The cases will demonstrate the effect of hydrodynamics in confined waters. The first topic discusses the importance of considering the effect of shallow water on the response of vessels operating within ports and confined waterways. This section will demonstrate the effect shallow water has on the hydrodynamic coefficients for a vessel. Second, the effect of a passing vessel on a moored vessel will be discussed through the description of a case study. Finally, a maneuvering study will be presented that presents the importance of including shallow water interaction effects in maneuvering models.

2. CONFINED WATER HYDRODYNAMICS

2.1 Effect of shallow water on vessel motions

Wave exciting forces such as added mass and potential damping depend upon wave frequencies and are influenced by the boundary conditions of the area. Figure 1 shows the added mass for three depth to draft ratios of a 175m loaded bulk carrier with a draft of 11.5m. The considered depth to draft ratios are shallow (h/T=1.1), intermediate (h/t=2) and deep (h/t>5). For shallow water cases, the reduced water depth and the resulting low under keel clearance creates a restricted area that limits the flow of the water surrounding the hull. The added mass and potential terms can be calculated by the pressure distributions on a hull mesh. The added mass plays a significant role in determining the natural periods of the vessel's motion and is known to increase significantly as the under keel clearance decreases. The added mass is also used in the equations of motions and can therefore influence the response of the vessel. The most noticeable differences in added mass as the seabed approaches are observed in the vertical degrees of freedom. Comparing the added mass for the bulk carrier with a 10% under keel clearance (h/T=1.1) to the deepwater case (h/T>5), Figure 1 shows that the added mass (left side figure) can be more than three times greater for the horizontal motions and 8 times greater for the vertical motions. The differences in the horizontal added mass are most noticeable for low frequency waves, below 0.8 rad/s, since for higher frequencies the dispersive relation becomes negligible. In general, greater added mass decreases the motion response of the vessels since more force is needed to move the vessel. However, potential damping also increases as the seabed approaches which reduces the vessel response.

In addition to the added mass, the potential damping also varies considerably over different depth to draft ratios. The potential damping for the low depth to draft ratio is greatest due to the increase in radiated waves for shallow water cases. More radiated waves are produced for shallow water cases for two reasons, the close proximity of the seabed and the increase in free surface fluctuations.. The right figure in Figure 1 shows the potential damping of the same bulk carrier. Similar to the added mass, the potential damping is greatest for the vessel with the 10% UKC. The range in potential damping is also greatest for the lower frequency waves.

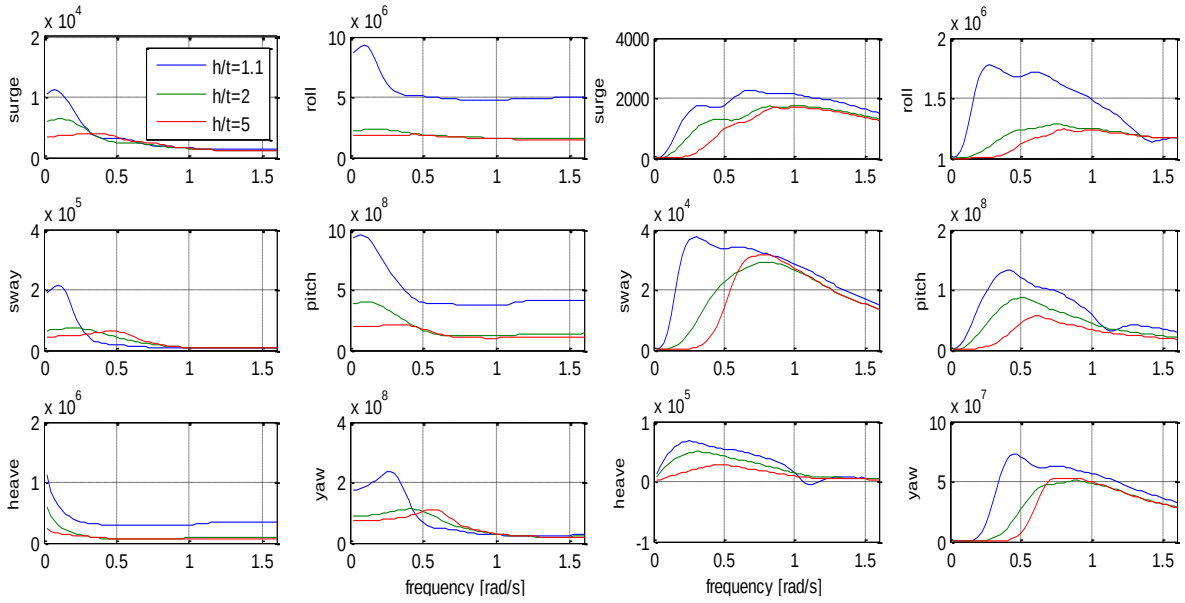

Figure 1: Effect of UKC on added mass and potential damping (mt, kNms)

Due to the differences in added mass and potential damping, the same vessel operating in varying water depths will exhibit different motion characteristics. Vessel motions are usually calculated in frequency domain from potential theory programs such as DIFFRAC. These programs give a initial approximation of the vessel response considering the incoming wave is linear and non-breaking. The motion amplitude and phase shift of the vessel can be written in proportion to the wave amplitude through transfer functions known as response amplitude operators (RAO)s. Figure 2 shows the response amplitude operators for the bulk carrier for the three depth to draft ratios. The response is shown for a short, 4 second wave of 1 m height encountering the vessel at 35 degrees off the bow. The response in the vertical plane is greatest for the depth to draft ratio of 1.1. The maximum resonance dominated roll response and the maximum excitement dominated pitch response shifts towards a lower frequency for the vessel in shallow water due to the additional added mass. For mooring simulations, all degrees of freedom can greatly influence the results, however, for maneuvering simulations, the horizontal motions are of greatest importance.

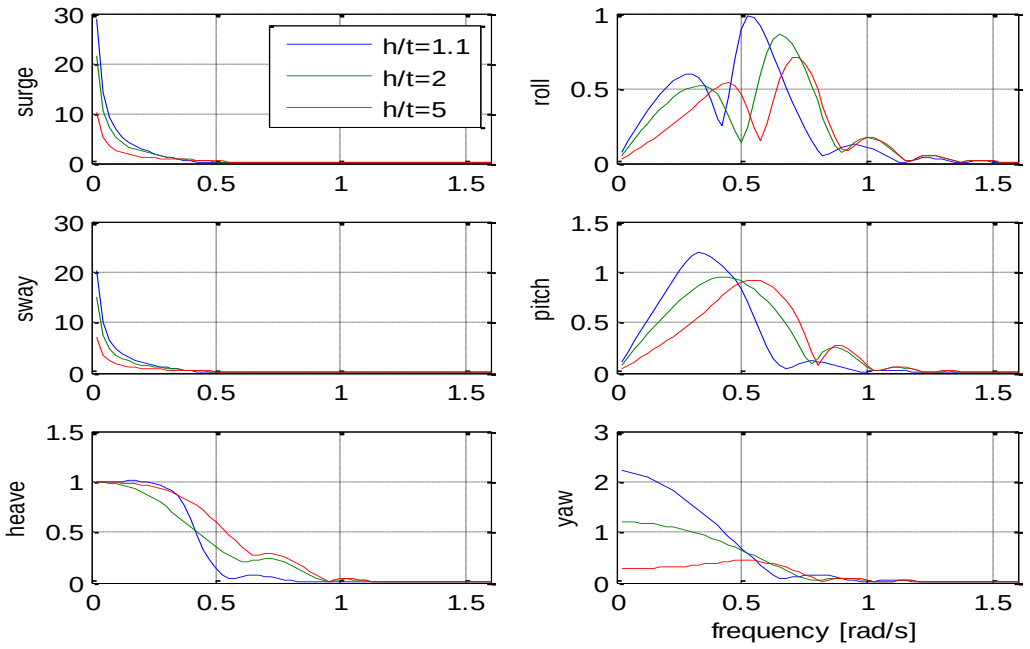

Figure 2: Effect of UKC on RAO (motion [m, deg]/m wave)

Second order difference frequency drift forces are also affected by water depth. The difference frequency drift forces can increase significantly due to the second order velocity potential. For an undisturbed, second order wave, the second order component of the wave group is known as the “set down”. For shallow water, the set-down effect plays an important role for the slowly varying drift forces, but less noticeable in the mean drift forces. It is therefore important to consider the difference frequencies and compute the full quadratic transfer functions (QTF)s in order to predict the effect of the shallow water wave drift forces. Figure 3 shows the wave drift forces from the main diagonal and from an off diagonal with a difference frequency of 0.1rad/s. The differences in drift forces between the deepwater and shallow water cases is most prevalent in the off-diagonals.

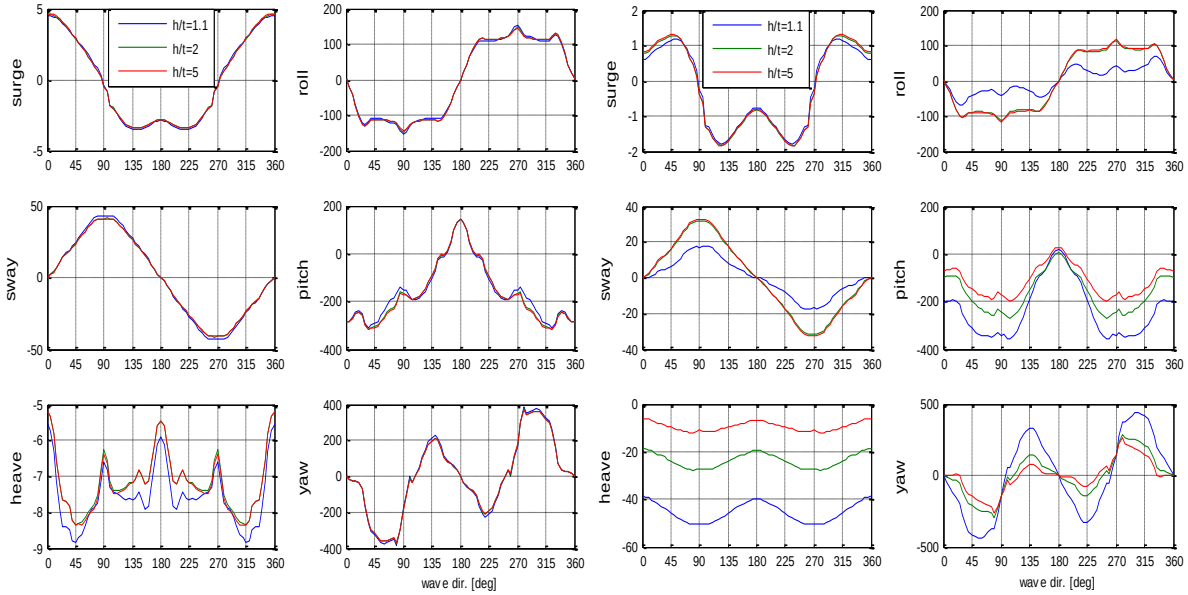

Figure 3: Effect of UKC on drift forces(mean on left, difference frequency on right [kN, kNm])

Figure 1 –Figure 3 demonstrate the importance of using a numerical model that correctly describes the vessel and the area surrounding the vessel. This is especially important for simulations within confined waterways due to the interaction of the vessel with the seabed.

2.3 Passing vessels

Passing vessels generate large suction forces which can influence the motions of moored vessels. The effect of the passing vessel on the moored vessel increases with the size and speed of the passing vessel. The force from a passing vessel in a restricted waterway can often be responsible for some of the largest excitation force contributions on the moored vessel. MARIN investigated the effect of passing vessels during the ROPES JIP through a series of monitoring trials in the port of Rotterdam, model tests and CFD experiments. As a result of the JIP, a fast and reliable tool was developed to calculate the excitation of moored vessels caused by passing vessels. The tool couples results from the RANS code ReFRESCO, which is used to predict the viscous effects associated with the passing vessel in a restricted waterway with the linear diffraction code, DIFFRAC, which is used to describe the resulting forces on the moored vessels. The tool was validated with data from model tests and full scale monitoring programs. This section discusses a case study of a large sailing vessel in a restricted waterway passing a large moored ship with a bunker vessel moored alongside.

The hydrodynamics associated with a vessel moored at a quay can be complex due to the interaction effects of the vessel with the quay. Waves reflect from the quay, water between the vessel and the quay can experience amplification due to resonance, interaction occurs between the vessel and the quay and the shallow water influences all the hydrodynamics. For the sailing vessel, viscous effects can be of importance to the flow of the water around the sailing vessel in a restricted waterway, especially for vessels sailing at drift angles or at high speeds.

The moored vessels in this case are a large cruise ship with a small bunker moored on the port side. The passing vessel and the moored vessel are both the same ship model and have an Lpp greater than 300m. The side-by-side bunker vessel is much smaller with a Lpp of 110m. The large cruise vessels have a depth to draft ratio of 1.2. The goal of the study was to determine the maximum speed vessels could sail at in the waterway without disturbing port operations. Figure 4 shows the mesh file used to describe the set up of the moored vessels in the channel.

The mesh files are used in the diffraction and second order drift force software packages Diffrac and Driftp. The Diffrac and Driftp software packages create a hydrodynamic database for the vessel and bunker that describe the added mass, potential damping and first and second order wave forces acting on the vessels. The interaction effects between the vessels and the quay are described in the hydrodynamic database. The vessel meshes are also used along with a larger port mesh for the passing vessel simulations. The port mesh is larger for the passing vessel simulations in order to capture the effect of the passing vessel as it moves through the waterway. Long sailing periods can be required to allow for the start-up effects to dissipate prior to the passing vessel arriving at the point of interest. The lower figure in Figure 4 shows the passing vessel mesh including the area and the moored vessels

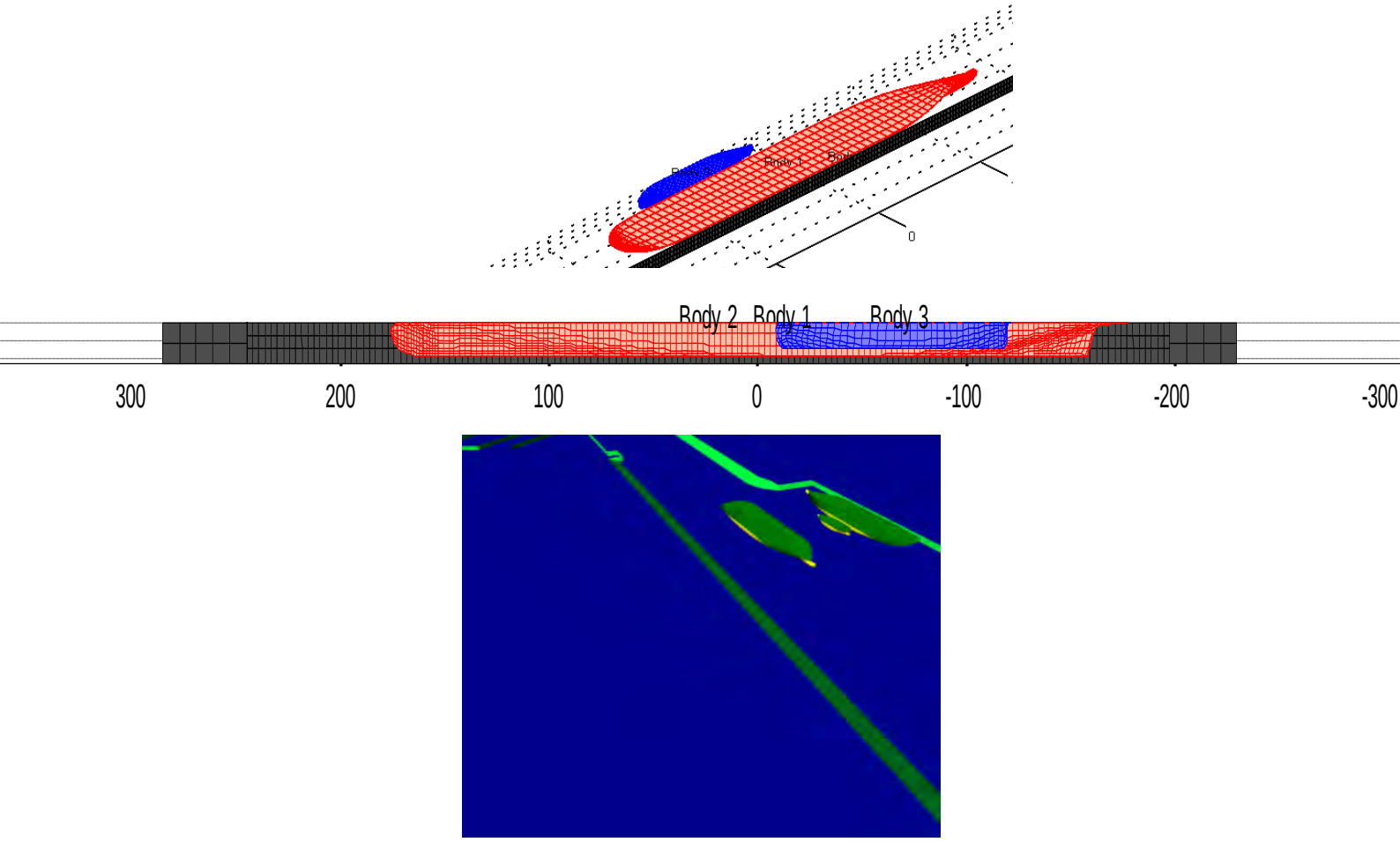

Figure 4: mesh files for motion/mooring analysis (top) and passing vessel analysis (bottom)

Passing vessel cases are run to examine the effect of the passing vessel speed on a moored vessel within a port. The port speed limit is used first and the passing speed is decreased until the moored vessel motions and mooring systems are within acceptable criteria. The first cases considers the passing vessel moving at 7 knots and the second case considers the passing vessel at 6 knots. For both passing vessel cases, no environmental forces are included. The passing vessel simulations consider the moored vessels as captive vessels in a force frame as the sailing vessel passes by. The forces exerted by the passing vessel on the captive moored vessels are determined by a double body potential flow method and stored as a 6 DOF time trace that can be input into time domain simulation

software to assess the impact of passing vessels on a mooring system or maneuver. The passing vessel forces for both passing speeds are shown in Figure 5. The forces shown are the forces exerted on the moored cruise ship and bunker.

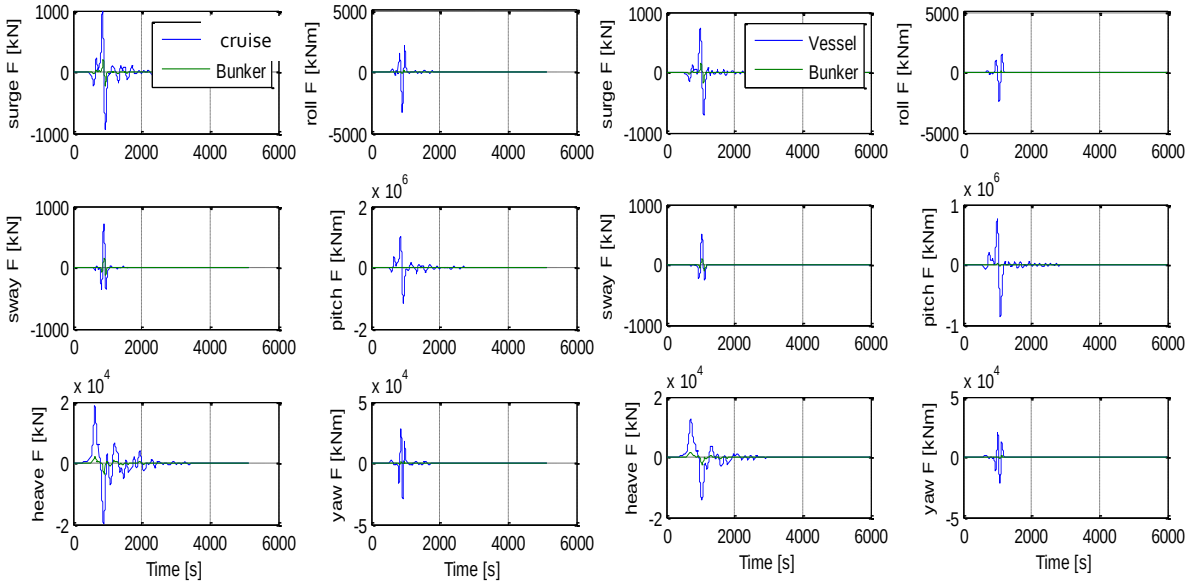

Figure 5: passing vessel forces (7kn right, 6kn left)

As Figure 5 shows, the forces from a passing vessel are substantial, horizontal surge forces for the cruise ship in this 7 knot passing case can reach 1000kN, the equivalent force of a 20knot beam wind for the larger vessel. The passing vessel force time trace is fed into time-domain simulations in order to assess the motions of the vessels and the limits of the mooring systems.

The time domain simulations are run to determine the speed limits for sailing vessels with respect to the moored vessels within a port. The simulations included a current running parallel to the channel and a wind speed of 25 knots for every 45° starting from North. It was quickly determined that the forces generated from the 7 knot passing vessel were beyond the limits of the bunker vessel mooring system despite the additional presence of an environment. The imparted forces from the passing vessel result in increased motions of the bunker and cruise vessel. The bunker vessel and bunker mooring system is especially impacted by the passing vessel due to its small size. The surge motions are most impacted for two reasons, first the mooring system springs are smaller in the surge direction than in the sway direction and second, the fenders limit the sway motions. As a result of the large surge motions, high tensions occur in the bunker vessel's spring lines. The wind directions that come from the port-aft side of the bunker vessel contribute to the positive surge forces from the passing vessel and result in the most critical cases. Wind from the starboard-aft side of the bunker vessel is shielded by the moored cruise ship and the total force acting on the bunker is therefore reduced. A time trace of the surge motions and the mooring line tensions for the north wind case and a 7 knot passing vessel speed is shown in Figure 6. The red lines in Figure 6 indicate the safe working load of the mooring lines for the bunker mooring system, 225kN. The motions and mooring system forces for the moored cruise ship were within the set criteria.

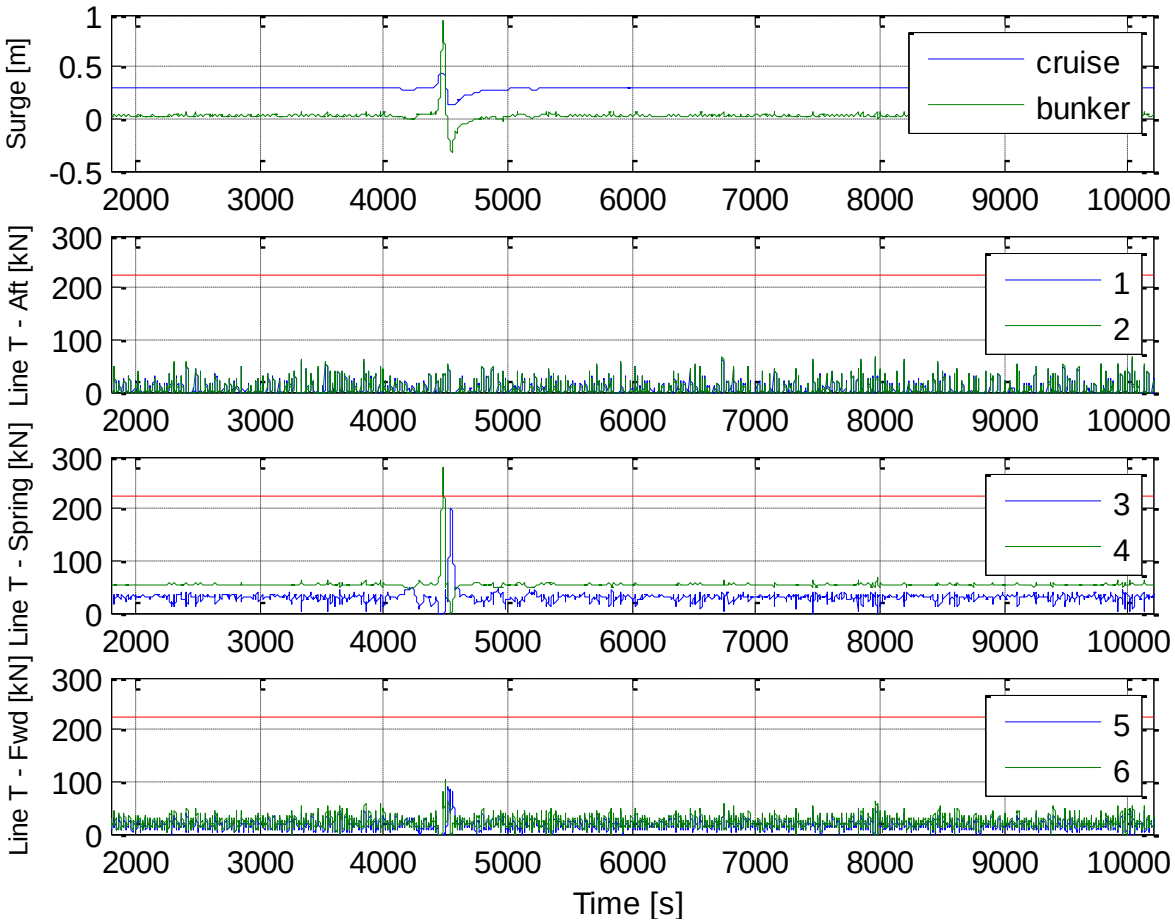

Figure 6: Time traces of motions and mooring forces for bunker vessel – N windw/ passing speed of 7 knots

Figure 6 shows that the maximum forces in all the mooring lines occur at the time of the passing vessel event. The maximum motions and mooring forces for all simulation cases always occurred at the time of the passing vessel for both the passing speeds studied and all environments considered. Both the cruise ship and bunker vessel mooring systems and motions were within the set criteria for all cases with the 6 knot passing vessel forces.

This case involved three phases, the passing vessel simulations, the time domain simulations and finally real-time bridge simulations. The passing vessel simulations were initially run to determine the passing vessel forces. Once the forces were determined, the force time-traces were run in the fast-time simulation program aNySIM to determine the environmental and passing speed limitations as a function of the moored vessel limitations. Once the limitations were determined, real-time simulations on a bridge simulator were run to assess the maneuvering limitations of the waterway. The effect of the moored vessels on the maneuvering ship were assessed through a real-time double body potential flow software coupled to the maneuvering model of the cruise ship.

Figure 7: MARIN Houston real-time bridge simulator

2.4 Confined water effects for maneuvering cases

To study the effect of confined water during maneuvering, the mathematical vessel models need to account for the effect of the depth to draft ratio on the maneuvering ability of the vessels. To account for this, the numerical models have multiple sets of hydrodynamic coefficients available that can be used for the different depths and waterways encountered while maneuvering within a port. Fast-time software (SHIPMA, aNySIM) and real-time bridge simulation software (Mermaid Dolphin) are used to assess the feasibility of in port maneuvers and the spatial limitations of waterways. These programs solves a set of differential equations to obtain the behavior of the ship within a particular area. Within the simulation these maneuvering software accounts for:

- Hull forces
- Propeller forces through KT/KQ diagrams
- Rudder forces, including side forces
- Shallow water effects
- Current forces, through relative velocity substitution
- Wind wave drift forces
- Bank suction, through Norrbin model
- Tug assistance and other maneuvering devices

All simulation programs designed to predict vessel motions as the vessel sails through the water must use a hydrodynamic databases as input. Most simulation models use frequency domain diffraction programs based upon linear potential theory to build the wave response hydrodynamic databases used in the vessel's numerical model. This approach works well for stationary vessels (FPSO's, Semi-submersibles, Moored ships), vessel's operating in deep water, or vessel's operating within an area with a constant water depth, however, most in port simulations involve varying water depths as the ship moves in and out of channels and harbors. To account for the variation in water depths, numerical models use multiple sets of hydrodynamic coefficients to accurately describe the changes in depth to draft ratio. The coefficients are used to describe forces from the maneuvering model, the second order wave drift forces and first order wave response. For fast-time maneuvering simulations, the horizontal motions of the vessel are most important since the spatial limitations of the waterway are dependent upon their accuracy. The required maneuvering area of the ship is assessed by the swept path of the vessel along the defined track, and the maximum deviations from the track definition. The required maneuvering space of the vessel is compared to the guidelines from PIANC and the effective width of the channel. The vessels ability to maneuver in the waterway is of great importance and the maneuvering model needs to account for the effect of depth to draft variability. Figure 8 shows the effect of depth to draft ratio on the turning circle characteristics.

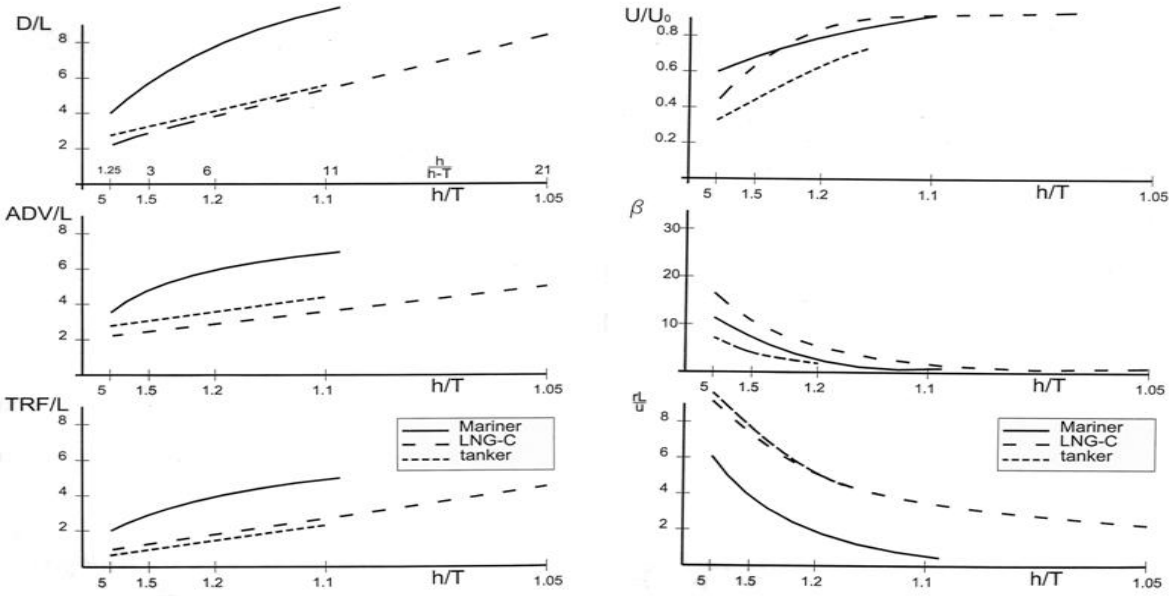

Figure 8: Effect of depth to draft ratio on turning circle characteristics

The ships interaction with the surrounding area such as channels and quays is also of consequence to the maneuvering behavior. Many complex non-linear, viscous dominated factors contribute to interaction effects such as bank suction and ship-to-ship interaction. To fully understand and model these effects, detailed CFD and model test studies are required. This type of study can be very costly and is often not a feasible option for smaller scale mooring or maneuverings studies. Fortunately, more generic and simplified methods can be used in numerical models to account for force contributions from vessel-to-area and vessel-to-vessel interactions. One such method is the Norrbin bank suction method. The Norrbin model makes use of a set of vessel specific coefficients that are used to calculate the additional surge, sway and moment forces applied to the vessel from bank suction. The Norrbin model uses a parameter based upon the relative distance from the vessel to a specified depth on the channel bank. The X, Y and N coefficients used in equations 1 through 3 below are used with the velocity of the vessel and the relative distance of the vessel to the bank to determine the additional suction forces acting on the vessels.

$$X_{suc} = \frac{X_{uuu/brh}U^3}{(a1+a2).h} + X_{u|v|B/br}\frac{U|V|B}{(a1+a2)} \quad (1)$$

$$Y_{suc} = Y_{uvx}uvx + Y_{aaauu}a^3u^2 + Y_{aauv}a^2uv \quad (2)$$

$$N_{suc} = N_{uvx}uvx + N_{aaauu}a^3u^2 + N_{aauv}a^2uv \quad (3)$$

Where,

$$x = 0.333 - \frac{0.33(a1+a2)}{B} \quad \text{and} \quad a = \frac{B}{a2} - \frac{B}{a1} \quad (4)$$

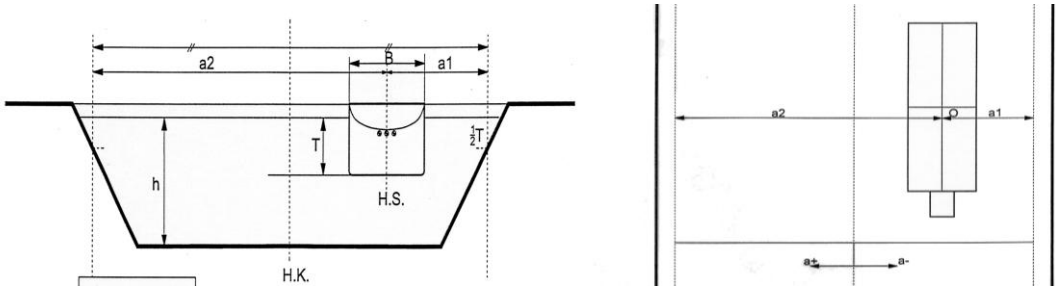

Figure 9: Dimensions used in the Norrbin bank suction model

The effect of bank suction can be of critical importance to assessing channel width requirements and limitations for maneuvering vessels in channels. Figure 10 below shows the swept path of a vessel with and without the bank suction forces calculated with the Norrbin bank suction effect included. The swept path of the vessel from the simulation without bank suction considered is over 20m less than the simulation considering bank suction. Shallow water and bank suction greatly influence the maneuvering characteristics of vessels and must be included correctly to obtain a reliable assessment of a waterway.

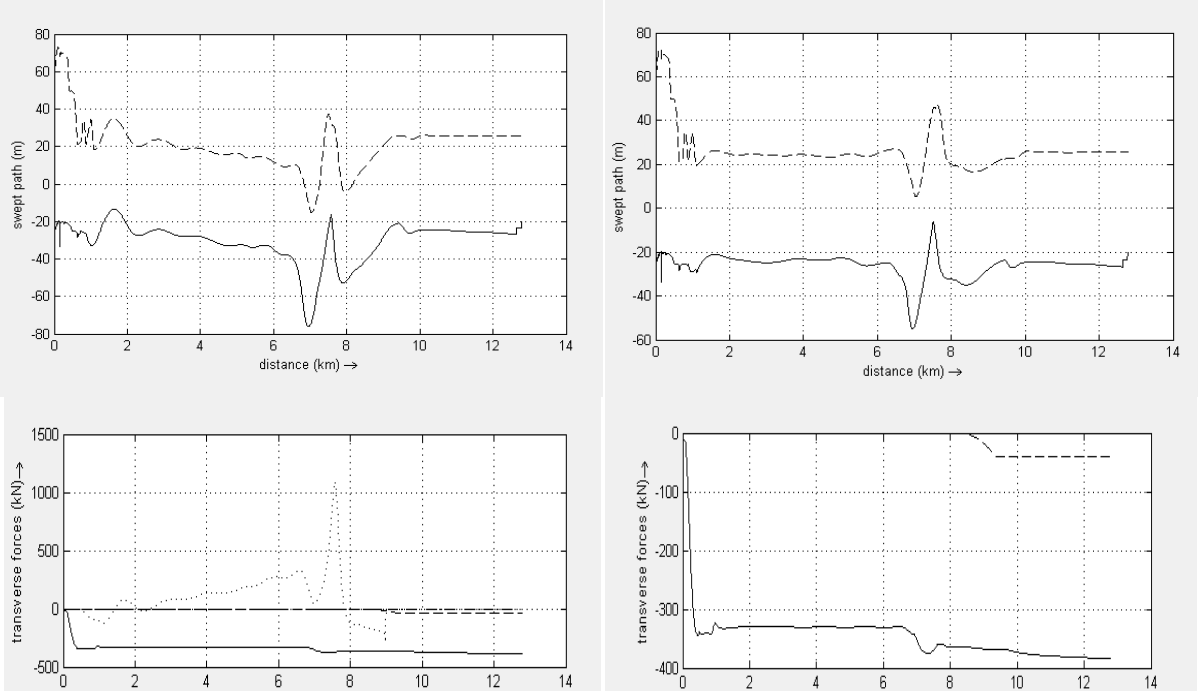

Figure 10: Effect of bank suction on swept path

3. CONCLUSION

United States ports and waterways are in need of improvements to accommodate the increasing size of future vessels. To analyze how vessels interact with the design of these ports numerical tools and model tests can be applied. Studying the interaction of vessels with ports and waterway designs allows engineers to understand the limitations of the waterways at an early stage. Combining hydrodynamic simulation models with real-time bridge simulators provides port pilots and tug boat captains a means to practice maneuvers and operations with large vessels in advance, thereby including operational feedback into the design at an early stage. For these tools to accurately assess the feasibility of waterways, the tools must realistically predict the behavior of vessels in confined water.

With the advancement of hydrodynamic knowledge, testing facilities, computational tools and computational capacity, engineers can now give detailed information on the behavior of ships in open as well as confined waters before designing waterways. The hydrodynamic models describing sailing and maneuvering in waves provide new insights into the relation between waterway design, ship design and downtime. New computational tools such as computation fluid dynamics and advanced bridge simulators give the option to optimize the hull for special environmental conditions and to train the crew for specific operations such as maneuvering in confined areas, ship-ship interaction, berthing and mooring. Large computer clusters have opened the opportunity to systematic variation studies and extensive time domain simulations for optimizing hulls, choosing sailing routes, scheduling operations or assessing the number of ships needed for a specific task while bridge and voyage simulations tools can give insight in the critical sections of a channel.

[1] Maritime research Institute Netherlands MARIN, MARIN USA, t.sellers@marin.nl

4. REFERENCES

PIANC (2014), Report No.121, Harbour Approach Channels Design Guidelines, PIANC, Brussels.

ASCE (2017), Infrastructure Report Card 2017, ASCE, Washington D.C.

5. KEYWORDS

Hydrodynamics, Vessel response, shallow water effects, passing vessels, vessel maneuvering, bank suction, vessel-to-vessel interaction, computational fluid dynamics, CFD, model tests, bridge simulations, time domain simulations, port design, waterway design, ship channels, motion analysis

Multi-Use Offshore Platform on the Guiana Shield

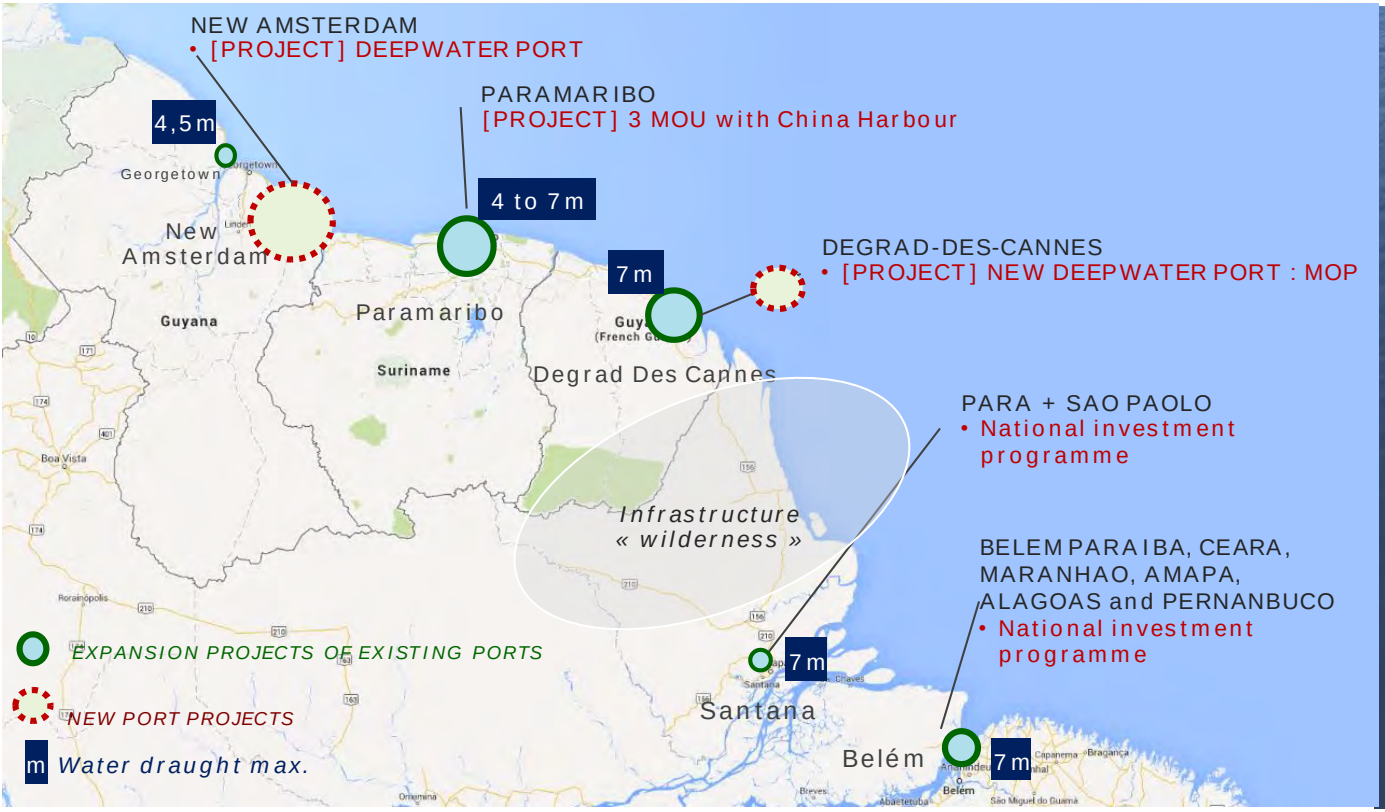

thomas.lockhart@gican.asso.fr
CORICAN: French national council for maritime industry research and innovation orientation

Multi-use Offshore Platform challenges

- TRADE requirements

Water draught < 7m

Trend

Water draught > 15m

DEPTH AND SPACE LIMITS

+ Opportunities related to the Panama Canal

With favourable met-ocean conditions

- RESOURCES opportunities

O&G resources

- Fishing
- Aquaculture

Ocean Energies
Especially tidal & OTEC

SUSTAINABLE VALORISATION OF BIO-RESOURCES

Multi-use Offshore Platform Markets

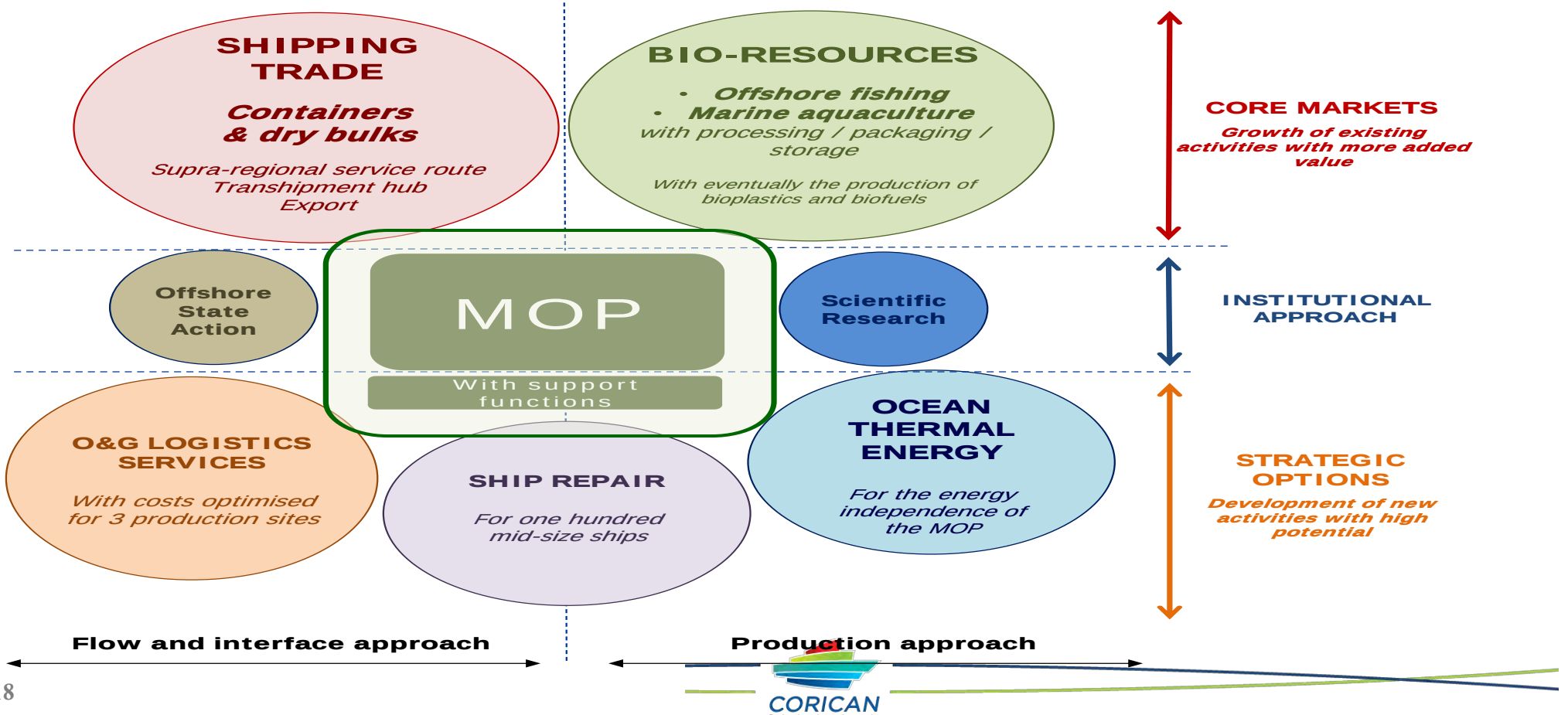

Multi-use Offshore Platform Concept

Towards a « maritimisation » of the global economy

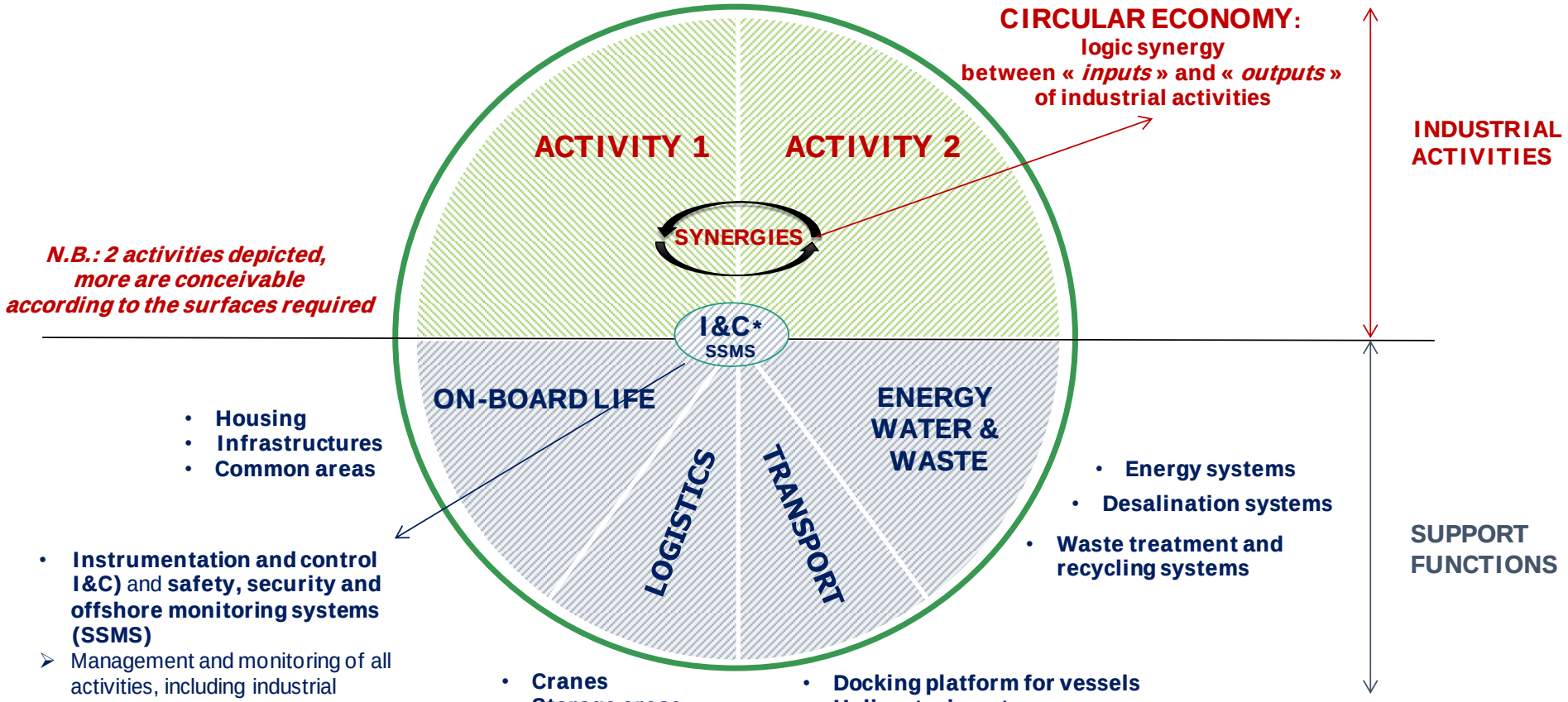

Multi-use Offshore Platform
Value proposition

Logistic

- facilitate Panamax 2016 container ships stop & act as a **distribution hub** for the area
- provide a **barge system** for container feedering & semi-**automated container transfer** system
- **reduce dispatch times** and **transportation costs** for shipping and oil & gas companies

Offshore aquaculture

- enabler for aquaculture farmers to **exploit 800km²of nutrient rich waters,** around the platform **without conflict of interest**
- ballast tanks on the floating platform will provide a location to **hatch and grow juveniles**
- **shorter distance** between aquaculture farms and seafood workshops
- **increased safety and quality**

Two identified scenarios, One Floating MOP and One Gravity Based MOP

Gravity based MOP:

- *In the TTW, at **12 nm** North East off Mahury River Mouth, by **22m depth, on sand soil***
  - ☺ Enough water depth to host any Container ship (even over Panamax)
  - ☺ In vincinity of Degrad des Cannes
  - ☹ Very limited biomass production and transformation possibilities

Floating MOP:

- *In the EEZ, Close to continental shelf edge, at **70 n** au Nord Nord Est de Cayenne, by **75m depth, on sand soil***
  - ☺ Close to offshore O&G platform, to minimize supply permanent ship number
  - ☺ Favourable place for offshore aquaculture and OTEC
  - ☹ 4 Hours sailing from Cayenne

Offshore French Guyana weather

Conditions météo clémentes

			In operation	Extreme conditions
Weather conditions	**Swell**	Significative Height	Below 1m	3.9 m
		Period	8.5s	12s
		Orientation	SW	SW
	Current	Vitesse	1 m/s	2 m/s
		Orientation	NW	NW
	Vent	speed	9 m/s	19 m/s
		Orientation	ENE (NE /ESE)	ENE (NE /ESE)
Environnment	**Water depth**	100 m		
	seabed	sand		

MOP reference scenario

- **3 major activities:**
  - **container hub**
  - **O&G logistical activities**
  - **support services for aquaculture and fisheries**

- **2 step pilot:**
  - **Step one in 2026,** a 14 ha platform to deal with:
    - 150 00 TEU per year
    - logistic support for 2 O&G platforms
    - 5000t/yr of aquaculture fish
  - **Step 2 in 2030,** a 20 ha platform to deal with:
    - 300 00 TEU per year
    - logistic support for 3 O&G platforms
    - 5000t/yr of aquaculture fish

The floating MOP will be located 75 nm North-East of Cayenne, by 75m depth on sand soil

- *for fish farming*
- *close to Shelf Break for OTEC*

Power source:

- Step1: diesel or already OTEC
  - Consumption : 25'000MWh/yr
- Step2: OTEC 5 / 10 MW
  - Consumption : 35'000MWh/yr
  - Diesel as backup

Project Financial attractiveness demonstrated

Item	Value	Unit
CAPEX	1436	€million
OPEX	2030	€million
DECEX	6	€million
Cost of finance	1384	€million
Container hub revenue	60	€million/year
O&G support revenue	86	€million/year
Aquaculture revenue	37	€million/year
Levelised cost, FLW_WAV	110%	-
Simple payback	12.1	Years
Discount rate of WACC	*5.0%*	-
Operating for	40.0	Years
Payback	**20.7**	Years
NPV (yr -4)	15.0	€million
NPV (yr 0)	19.0	€million
NPV (yr 0)/CAPEX	1.2%	-
IRR	5.1%	-

- **Project funding**

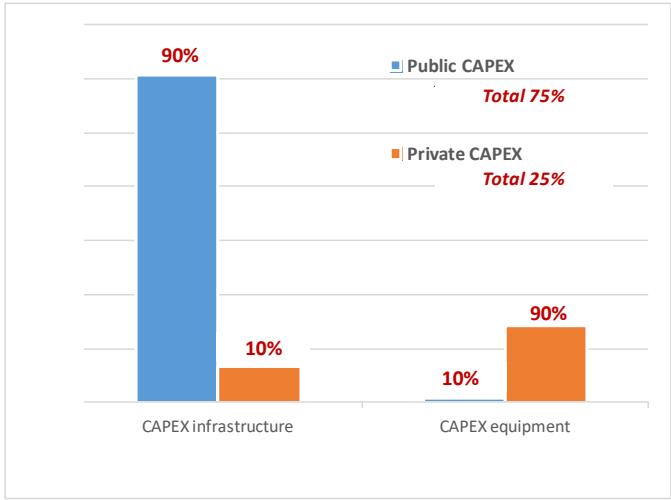

Reference financial plan:

- **75% from public financial vectors**
- **25% from private investment**

  - The share of financing related to infrastructure would be mostly public (90% public vs. 10% private)
  - While the one related to equipment would be mainly private (10% private vs. 10% public)

Project Evaluation of socio-economic benefits

An infrastructure of over 20 hectares to accommodate logistics services and activities of sustainable industrial production

A new secure marine area of over 800 km²

n investment of round 1,500M€ *rovided by the public State, Regions, public banks)*

onomic potential of than 150 M€/year *eding under certain itions the economic eness threshold of the project*

A potential impact of around +3% of GDP in French Guiana

4,000 jobs for the construction phase *(4 years)*

3,300 jobs for the operations phase *(30 years and beyond)*

- **Construction phase** (estimated duration: 4 years) peak load difficult to capture in French Guiana
  - Limited industrial capacities and time of a significant increase in local demand (concrete and steel production, equipment manufacture and complex subassemblies assembly, offshore integration…)
- Recommendations :
  - Focus on **the operations phase, which refers to activities and long-term jobs**
  - over 40 years at least (MOP lifetime: about 100 years)

Compliance with the requirements of sustainable development by controlling environmental impacts

In the end an offshore circular economy

shore transhipment hub of 300,000 TEU/year
Including 150,000 TEU for sub-regional access
Including 150,000 TEU for interlining transfer

Guiana shield offshore aquaculture farms
with industrial support and value-creation capacities on the mooring axis

nfrastructure for regional exports of dry bulk commodities: 4 Mt/year
(Brazilian Iron ore, bauxite from the Shield, …)

An O&G logistics base supplying 3 production platforms
to meet costs adapted to their needs in logistics

CORICAN Recherche et innovation navale

STEP 2 GENERAL ARRANGEMENT
MOP 8*8

The 8x8 MOP, below, will host the 300 000 EVP container hub and the O&G logistical base.

It is composed of 73 modules, 62 similar elementary modules 63m(x43mx15m), plus 10 wave breaker modules.

Total outdoor surface totale: 19.1 Ha / Dimensions : 567m /: 430m

3400 m3 of concrete per module

220 000m3 of concrete for the platform

Lessons learnt from Total Nkossa FPSO
and EC FP7 TROPOS project

ZOOM ON ELEMENTARY MODULE

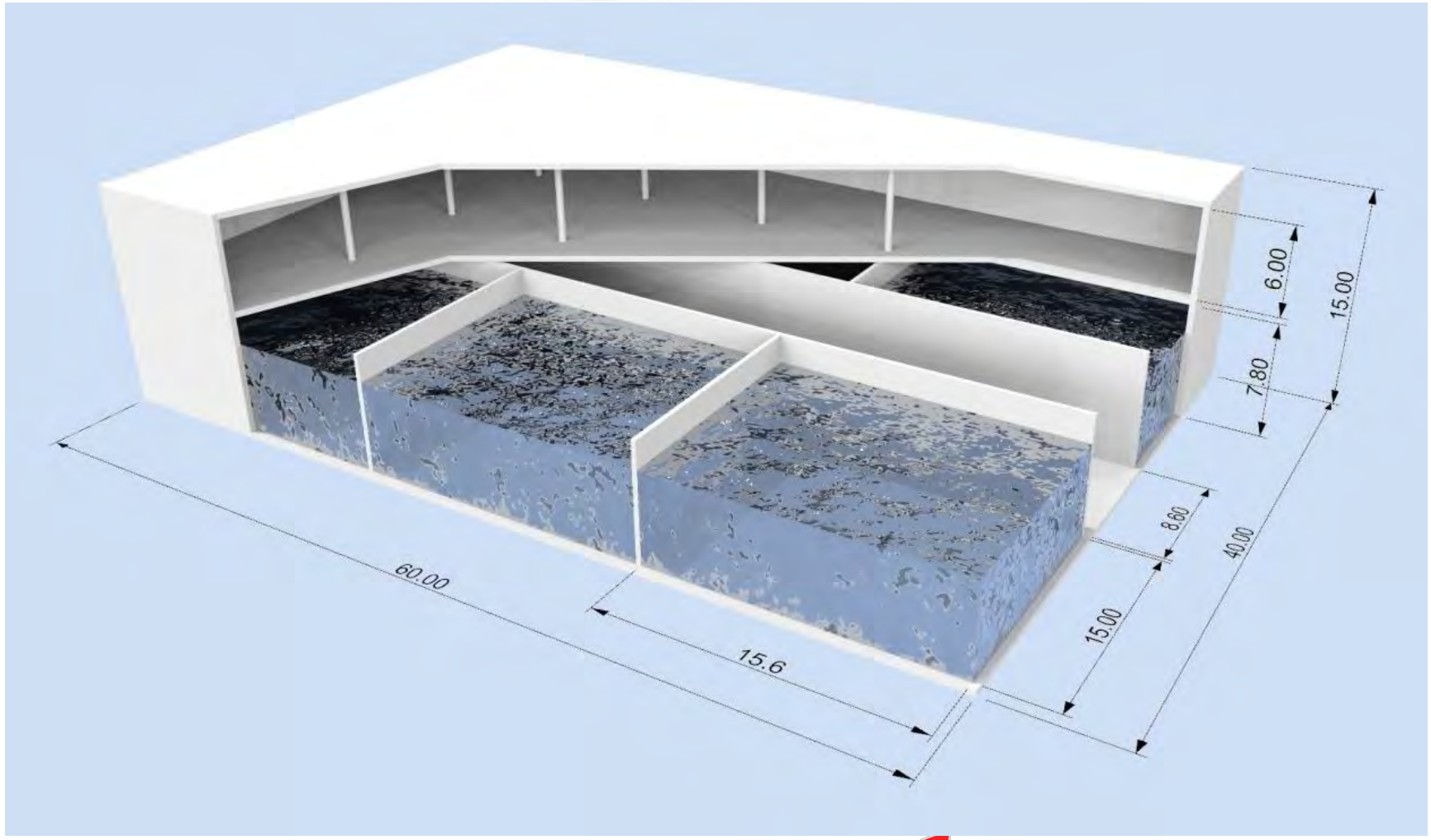

MODULAR STRUCTURE

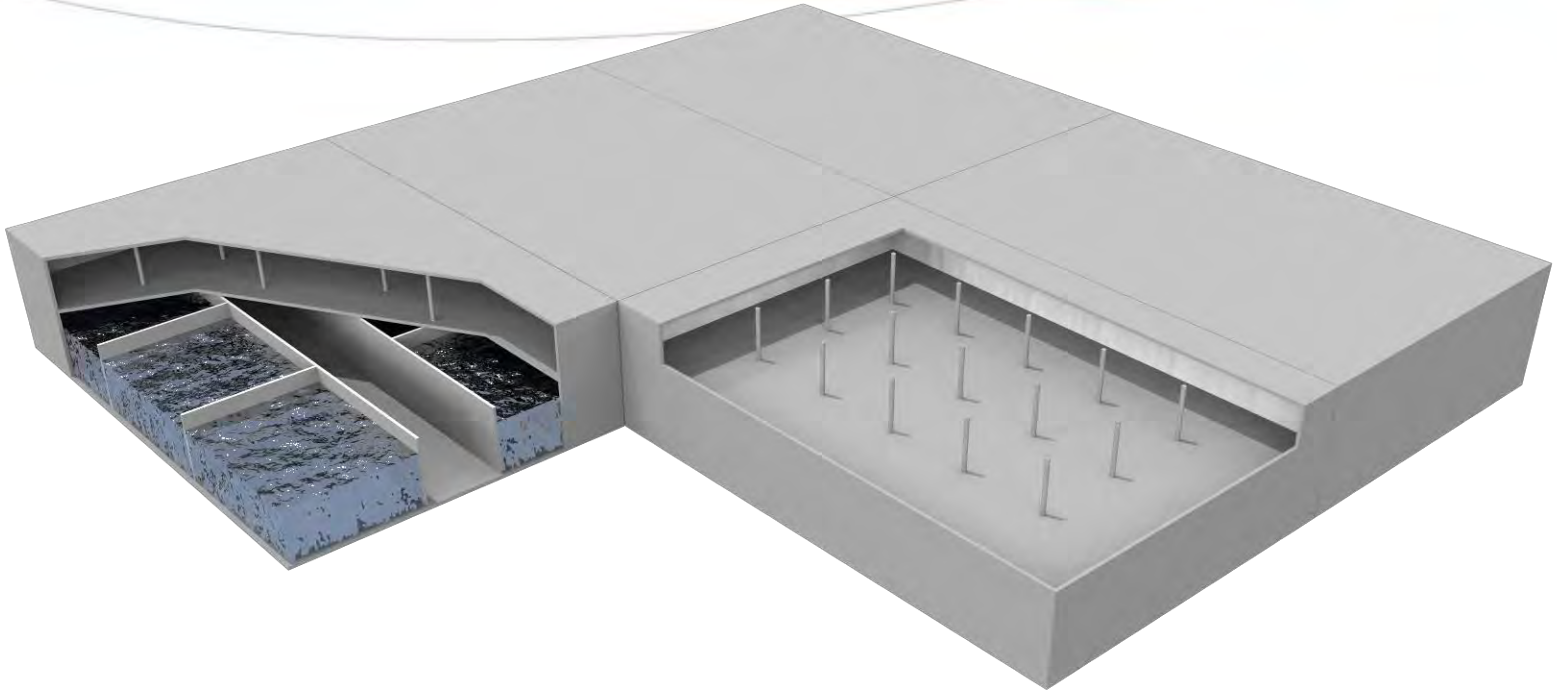

Technical studies to be conducted

- **Modular Platform production, transport, assembly and anchorage methodology**
  - **in cooperation with Oil & Gaz EPCI companies**
- **Inter Modules connection constraint analysis and solution development**
- **Module anchorage constraint analysis and solution development**
- **Platform protection against waves and storm surges,**
  - **in connection with costal protection projects**

FRENCH GUIANA VISION 2028

To build with the MOP a sustainable industrial future
looking towards the maritime space, inter-regional integration and marine resources

Trelleborg Marine Systems

PIANC Congress 2018

Full paper submission

Theme / topic: Maritime port planning and operations

Name: Mishra Kumar

Company: Trelleborg Marine Systems

Business address: 4 Jalan Pesawat, Singapore 619362

Phone: +65 6265 0955

Email: mishra.kumar@trelleborg.com

Introduction

Marine rubber fenders provide a critical role in the operations of ports. They allow several thousand tonne vessels to berth against vital infrastructure without damaging the wharf or the vessel. Use of fenders also allows the structural engineer to know the expected berthing loads which are critical to the design of the wharf as they are the products which turn vessel kinetic energy into known reactions when they absorb the vessel's energy.

Prior to PIANC publishing the document "Guidelines for the Design of Fender Systems" in 2002 [PIANC 2002] there was a lack of uniformity in how fender systems were designed, specified, and tested. Extensive reference to this publication will be made throughout this paper.

For a fender system to be designed and procured properly the consultant must perform each the following steps.

1. Determine the expected normal berthing energy of the vessel and then apply an appropriate factor of safety to establish the abnormal berthing energy requirement.
2. Select an appropriate fender inclusive of all correction factors that affect the nominal performance of the fender.
3. Verify from testing that the fenders produced for the project actually meet the performance requirements specified.

While most consultants understand the first step in this process many have only a vague understanding how to address the last two steps. Probably no other subject results in more

requests for assistance from fender manufactures than how to properly apply correction factors. Without a doubt there is no more misunderstanding or lack of oversite than of performance verification testing. This paper attempts to clarify each of these steps with a focus primarily on the topic of verification testing.

Why Use fenders?

It is important that the user have a clear understanding of why marine fenders are even used if the selection and verification process is to be performed correctly. There is one primary reason fenders are used and several secondary reasons.

- Absorb vessel kinetic energy (primary reason for using fenders)
- Provide a known reaction load for the design of the wharf
- Protect the vessel as well at the wharf
- Provide an easily replaceable component between the vessel and the wharf

Selection of Fenders

After a fender designer determines the estimated abnormal berthing energy it is time to select a fender equal to or greater than that energy. While doing so would seem straightforward it can be confusing for consultants or owners who are not specialist in fendering. Prior to PIANC 2002 the only factors typically considered in the fender selection process were the effects compression angle had on the fender's performance and sometimes the manufacturing tolerance, usually +/-10% of a fender's catalog performance. Two other important factors were being ignored, that being the speed at which the fender was being compressed and the temperature of the rubber fender at that time.

How to Select the Right Fender

The following equations can be used to determine a fender's corrected performance. The manufacturing tolerance is assumed to be +/-10%. Additional details can be found within the published whitepaper "Applying the right correction factors" [Trelleborg 2015].

Energy

$$(E_{nom})(AF)(VF)(TF_{High})(0.9) >= Ed \times Cab$$

Where:

E_{nom} is the nominal catalog energy capacity of the fender, or RPD if following PIANC methods.

AF is the manufacturer specific angular correction factor for the effective angle at which the vessel is berthing, or in the case of multiple fender contact, the highest angle at which any single fender is being compressed.

VF is the manufacturer specific velocity correction factor for the speed at which normal berthing occurs.

TF_{High} is the temperature correction factor at the highest expected service temperature.

Ed is the nominal calculated berthing energy (PIANC 2002 Section 4.2.1)

Cab is the factor of safety used to determine the "abnormal energy". (PIANC 2002 Section 4.2.5)

Reaction

$(R_{nom})(VF)(TF_{Low})(1.1) = R_{des}$

R_{nom} is the nominal catalog reaction of the fender selected that meets the E_{nom} calculated above.

VF is the manufacturer specific velocity correction factor for the speed at which the berthing occurs.

TF_{Low} is the temperature correction factor at the lowest expected service temperature.

R_{des} is the design reaction after accounting for all modifications to the fender's nominal performance. This is the estimated reaction used in the design of the wharf structure. It is also the suggested reaction used to design the fender panel system and its components.

PIANC 2002, Appendix D details two cases that demonstrate in more detail how to calculate the resulting energy and reaction values when using correction factors.

Performance Verification Testing

Performance verification testing, sometimes referred to as a Factory Acceptance Test, is a test performed on the actual fenders produced for a project. Rubber fenders are almost always manufactured to order as there are too many models, sizes, and grades to stock. To ensure the fenders were produced correctly and according to the particular specification of the intended project, some quantity are tested, usually 10%. These tests differ from the scale model testing performed to establish catalog rated performance values, RPD, or for determining the various correction factors which are described in PIANC 2002, Appendix A, sections 1 through 5. Verification testing is testing of "your" fenders, not prototype fenders. This is described in Appendix A, section 6.

How to Perform the Verification Test

Performance verification testing is usually performed in a large press or test frame with either load cells or pressure transducers, which are installed in the hydraulic circuit of the press, measuring the load and a displacement transducer for measuring the deflection. Consideration must be given to the sheer size of even a mid-sized rubber fender. Besides the large specimen size, testing or rubber fenders requires more stoke, or deflection capability, than most frames can produce. There are a limited number of publically available test frames around the world capable of testing rubber fenders. For this reason performance verification testing is almost always performed at the manufacturer's facility. There are significant reasons that should cause pause with the user when he elects to test their fenders at the manufacturer's factory. These reasons will be discussed later.

Break-In Cycles

Before a fender's performance can be verified it must first be subjected to a number of break-in cycles. When the fenders were molded a number of weak or temporary bonds are formed in the rubber that must be broken so that the fenders performs in a repeatable fashion. The first two or three deflection cycles on a newly molded fender are not indicative of the fender's performance in service. The first cycle in particular can be as high as 30% greater than its actual performance. Once the fender is broken in it will never achieve these high levels of reaction again.

Constant Velocity vs. Decreasing Velocity

PIANC 2002 allows for performance verification testing to be performed using either the Constant Velocity, CV, or Decreasing Velocity, DV methods noted in PIANC 2002 Appendix A, section 4. A few manufacturers have built full scale dynamic test frames that can simulate actual berthing speeds during the testing of fenders, but most have not. This is not a problem as PIANC 2002 was written specifically to address the fact that most manufacturers can only perform verification testing using the CV method. If available, testing using the DV method has the advantage that the results do not need to be velocity corrected which leads to more accurate results.

How Correction Factors Apply to Verification Testing

The correction factors mentioned earlier actually serve another purpose [Figure 1]. They may be necessary to correct the performance established during performance verification testing if the fender is tested outside of the required test speed or temperature range.

Correction factors used to specify the fender are to account for site conditions such as temperature and berthing velocity that vary from the nominal performance of the fender. Correction factors applied to the performance varication tests are to account for testing conditions that exist at the time of the test. These are usually limited to the effects of temperature and velocity during testing. Few fender test frames are located in climate controlled facilities. Even fewer are capable of testing at the actual velocities used to determine the berthing energy.

- When selecting a fender correction factors are used to account for the conditions under which the fender must operate that differ from the nominal catalog rated performance.
- When performing verification testing of a fender the correction factors are used to modify the test results so that the fender's nominal performance can be determined.

PIANC 2002 requires that performance testing using the CV method be performed at a speed of 2 to 8 cm/min and with a temperature range of 23°C +/-5°. If the performance verification test is completed outside of either of these parameters then the results must be corrected so that the results reflect the fender's nominal performance. How the test results are corrected depends on how the fenders were rated.

If the fender's catalog rated performance is published using PIANC RPD values based on the recommended 150 mm/s compression speed then the results must be velocity corrected to determine the catalog rated nominal performance within tolerances. If the fender's catalog

rated performance is based on CV test results, then no velocity correcting is necessary as long as the verification test velocity was between 2 to 8 cm/min. If the corrected performance verification test results meet the nominal performance of the fender within manufacturing tolerances then the fender is assumed to have passed the test.

Fender selection and performance verification test procedure based on CV catalog rating and CV performance verification testing

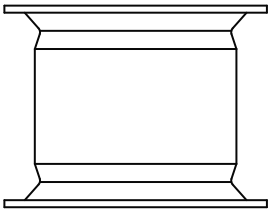

Selecting a fender for use

- Calculate berthing energy
- Use VF based on berthing velocity to correct both Reaction and Energy values
- Use TF based on site low temperature to correct Reaction value
- Use TF based on site high temperature to correct Energy value
- Use AF based on the effective berthing angle to correct Energy value
- Use +10% manufacturing tolerance to correct reaction value
- Use -10% manufacturing tolerance to correct energy value
- If corrected fender reaction is below allowable for the structure AND the corrected fender energy is above calculated abnormal berthing energy THEN the selected fender is acceptable for the design

Performance verification testing

- Stabilize fender temperature as recommended by PIANC 2002
- Break-in fender with a least 3 cycles to design deflection or greater
- Wait a minimum of one hour
- Test fender and record load vs. deflection data
- If fender test speed is outside of 2 to 8 cm/min. use VF to correct both Reaction and Energy values
- If fender test temperature is outside of 23°+/-5° use TF to correct Reaction and Energy value to standard test temperature
- Test at 0° angle so no angular correction necessary
- After correcting for test speed and test temperature fender Reaction shall be less than 110% of catalog reaction
  Energy shall be greater than 90% of catalog energy

Figure 1 - Fender Selection and Verification Testing Workflow.

Ramifications of Out of Specification Fenders

Little thought is given by the fender designer as to the consequences of installing an out of specification fender. There are two primary concerns if the fender specified is not the one being installed.

Energy absorption below specified value

> When the fender is incapable of absorbing the specified energy it is very likely the wharf will experience loads much higher than anticipated. The kinetic energy of the vessel must go somewhere, it can't simply disappear. When a fender does not have adequate energy capacity it will undergo an extreme increase in reaction with very little additional deflection. Since energy is defined by the product of reaction and deflection, the additional energy absorbed is very little when the fender is compressed beyond its design reaction. In that instance something else must deflect, either the vessel hull or the wharf itself, to absorb the excess energy. Since neither the vessel hull nor the wharf itself is intentionally designed to deflect there is little chance they will do so in the elastic range.

Reaction above specified value

> When the fender being installed is above the specified reaction there is the possibility that the wharf will see unacceptable reactions. A high stiffness fender can have as much as twice the reaction of a low stiffness fender of the same size. Given that live load factors are usually 1.6, it is quite easy for the fender to produce reactions far in excess than that anticipated. This has very serious consequences for load sensitive structures such as fenders installed on monopiles.

The Problems with Current Industry Testing Practices

There are several serious concerns with the way fender performance verification testing is currently performed. Some of these concerns mainly involve the authenticity of the reported performance as very little thought is given to the need for independent certification of the reported test results.

Why Verification Testing Cannot Be Left to the Manufacturer

When testing is performed at the factory the fender being tested can easily be selected especially for the test and not randomly selected. Manufacturers can build special test fenders that will pass the test and build the remaining production run with substandard materials.

Testing results can also be manipulated for commercial reasons. It is much less expensive to build a low quality fender that does not meet performance requirements and just manipulate the test results than to build it to the requirements.

An Inconvenient Truth About Witnessed Testing

Common practice in the industry has relied on factory testing with witnessing by either a 3rd party or by the consultant. There are several reasons why this is inadequate with the primary reason being there is no easy way for a witness to verify the results independently of what

the manufacturer is reporting. Modern data acquisition methods rely on computers to interpret the data and produce a report. The witness rarely has any understanding of how the data acquisition system functions. There is little difficulty in manufacturer adjusting the recorded data inside the computer without the witness's knowledge.

Many project specifications require a 3rd party inspection agency witness the test. It should be absolutely clear that they are indeed only doing just that, witnessing a test. They do provide any oversight on how the test data was acquired or if the report they are asked to stamp is even from the test they just witnessed. The inspection agencies are not in any way guaranteeing the validity of the data they are stamping. If the data being stamped and presented to the customer for acceptance cannot be guaranteed then what useful purpose does the test serve?

Independent construction materials testing is a common practice in the construction business. Why is it not standard practice in the verification of fender performance when it has such a critical effect on safety and protection and valuable assets?

"Trust But Verify" But how?

Independently verifying fender performance during the performance verification test is not easy, but it is critical if the intended performance of the fender is to be guaranteed.

Independent verification testing is possible with one of two methods.

- Testing at an independent structural laboratory
- Testing at the manufacturer's factory using their test frame but independently recorded performance data.

Each of the two methods has its advantages and disadvantages

Independent Laboratory

Testing at an independent structural laboratory is the easiest method to verify performance. These laboratories have large test frames capable of generating high loads on large specimens.

The advantages of independent laboratory testing include:

- The laboratory is a 3rd party testing laboratory that has no incentive to manipulate the results.
- No purchase of additional equipment is usually needed to perform the test.
- The laboratories are often located in climate controlled buildings eliminating the need to accommodate changing temperature conditions or having to deal with weather. Therefore, no temperature correction of the results is necessary.
- The results, including raw data, can be available for review by the consultant or the end user.
- Laboratories are often nationally accredited

The disadvantages of independent laboratory testing include:

- There are a limited number of these test laboratories available around the world.

- Time must be allowed in the schedule for the fender test specimens to be delivered to the testing laboratory which may be some distance from the jobsite.
- The fenders to be tested should be from the full lot delivered to site to avoid the manufacturer attempting to prepare special fenders for testing purposes.
- There is a cost associated with testing, but the costs for a reasonably size project are usually only 2% to 4% of the value of the fender contract.
- There is a limit to the amount of stroke on any test frame and fenders, with their unusually high deflection requirements, can exceed the abilities of even the largest test frames.

Manufacturer's Facility

Manufactures are accustomed to the specific needs for fender testing and they are already setup to easily test fenders at their factories.

The advantages of factory testing include:

- The large test frame needed to compress the fender is available.
- Convenient in that the fenders are usually made in the same factory, so no logistics to consider.
- Other inspections of the fenders such as build quality and dimensions can occur during one inspection visit.

The disadvantages of factory testing include:

- The consultant or independent inspector has no way to verify that the data being generated during the test is authentic. There are numerous ways in which a manufacturer can manipulate the results without raising any suspicion.
- The factories are almost all located in faraway foreign countries where even getting there can be problematic. There is potential foreign language difficulties to deal with including the specific language on each of the pieces of equipment used for the test as well as the computer used to collect the data.

It is time for the fender industry to accept that performance verification testing needs to be done independently, or at least outside of the manufacturer's control. There is simply too much an incentive for the manufacturer to just "make it pass" when such large contracts at high dollar amounts are at stake.

Ways the Industry Could Offer True Independent Testing

While the industry moves towards true independent testing and not just witnessed testing the simplest way to get trustworthy results is to use an independent laboratory. This is assuming there is one convenient for your use available and you dedicate the funds and time to carry out the test at an independent laboratory.

The long term goal for the industry should be for manufacturers to offer testing at their own facilities but with results guaranteed to be independently recorded and guaranteed by an inspection agency. Doing this will require the industry to adopt standards and methods that are easy to implement, cost effective, and easy to understand by independent inspectors and consultants.

The industry should develop a PIANC or ISO working group to write a specification on how 3rd party inspection companies can verify performance, not just witness it.

Recommendations

It is recommended that the user not rely on simple witness testing to determine performance. The person witnessing the performance verification test probably knows less about fenders than you.

A way needs to be established to verify the load vs. deflection data outside of the control of the fender manufacturer. The real time data should be shown on an external display and the results printed in real-time so the witness has direct access to the data. This method is only useful if the load sensing system is calibrated by an independent agency just prior to the performance verification testing.

PIANC needs to establish methods and procedures that give confidence in the performance verification results being reported.

Consult with well-known 3rd party inspection agencies to determine the feasibility of offering certified inspectors that understand how to use the independent test equipment that will be made available for performance verification purposes. The agency should be able to certify the results, not just serve as a witness to the testing.

Summary and Conclusions

The subject of specifying fender systems and verifying performance is not a difficult subject to master if proper attention is given to the subject. Given the importance of fenders in protecting the wharf and vessel it is difficult to understand how little attention some users give to the procurement of fenders. No matter how well the designer understands the fender specification process it will hardly matter if the performance verification testing is not independently verified.

References

PIANC 2002, *Guidelines for the Design of Fender Systems: 2002, Report of Working Group 33 – MARCON, PIANC, Brussels, Belgium.*

Trelleborg 2015, *Applying the Right Correction Factors, Trelleborg Marine Systems, www.trelleborg.com/marine.*